NREL/CP-470-6431 • UC-1360 • DE94011835

Proceedings of the 1994 DOE/NREL Hydrogen Program Review

April 18–21, 1994
Livermore, California

Hosted by the National Renewable Energy Laboratory

Sponsored by the Advanced Utility Concepts Division, Office of Energy Management, U.S. Department of Energy

National Renewable Energy Laboratory
1617 Cole Boulevard
Golden, Colorado 80401-3393

A national laboratory of the U.S. Department of Energy
managed by Midwest Research Institute
for the U.S. Department of Energy
under Contract No. DE-AC36-83CH10093.
Prepared under Task No. HY411010

July 1994

NOTICE

Foreword

The U.S. Department of Energy has conducted programs of research and development in hydrogen and related technologies since 1975. The current program, conducted in accordance with the DOE *Hydrogen Program Plan FY 1993 - FY 1997* published in June 1992, establishes program priorities and guidance for allocating funding. The core program, currently under the Office of Energy Management, supports projects in the areas of hydrogen production, storage, and systems research. At an annual program review, each research project is evaluated by a panel of technical experts for technical quality, progress, and programmatic benefit.

This *Proceedings* of the April 1994 Hydrogen Program Review compiles all research projects supported by the Hydrogen Program during FY 1994. For those people interested in the status of hydrogen technologies, we hope that the *Proceedings* will serve as a useful technical reference.

Thomas Cawthon
Hydrogen Program Manager
National Renewable Energy Laboratory
Golden, Colorado

TABLE OF CONTENTS

HYDROGEN ENERGY SYSTEM STUDIES

Joan M. Ogden, John W. Strohbehn, and E. Dennis
Center for Energy and Environmental Studies
Princeton University
Princeton, NJ 08544

Abstract

Our previous research suggests that beginning in the early part of the next century, renewable hydrogen could become competitive as a low polluting energy carrier. Our current work is focussed on the near term role of natural gas in a transition toward use of renewable hydrogen. There are a number of reasons why natural gas could be attractive as a transitional source of hydrogen: it is currently the least expensive source of hydrogen and natural gas is widely distributed via pipelines.

In Task 1, we assess various possibilities for producing hydrogen from natural gas for use in hydrogen vehicles. We consider several options including: 1) hydrogen produced in a large, centralized steam reforming plant and distributed via pipelines or truck to refueling stations, and 2) hydrogen produced at the refueling station via small scale steam reforming of natural gas. Conceptual designs for hydrogen refueling stations based on small scale reformers are presented, and preliminary cost estimates are made.

Task 2 involves assessment of the feasibility of using hydrogen blends and pure hydrogen in the existing natural gas transmission and distribution system. This study is being done in collaboration with researchers at the Institute of Gas Technology and Southern California Gas Company.

In Task 3 we continue our earlier work on fuel cell systems, assessing the use of PEM fuel cells for dispersed residential cogeneration systems producing electricity, space heat and domestic hot water. A model of a small scale PEM fuel cell cogeneration system is being developed, and performance of the system in various types of buildings is estimated. The value of the electricity to an electric utility is estimated based on utility demand curves and saved transmission and distribution costs for distributed generation.

Introduction

For several years, we have carried out technical and economic assessments of hydrogen energy systems (Ogden and Williams 1989, Ogden 1991, Ogden and DeLuchi 1993, Ogden and Nitsch 1993, Ogden 1993). The objective has been to understand the potential for producing hydrogen from various sources and using it in low polluting, efficient end-use devices such as fuel cells. To assess alternatives for producing and using hydrogen we consider 1) the cost and performance of hydrogen production systems, 2) the levelized hydrogen production cost, 3) the cost of delivering hydrogen for various end-uses, 4) the cost and performance of hydrogen end-use equipment, 5) the consumer's lifecycle cost of energy, 6) environmental effects (e.g. emissions), 7) resource constraints, and 8) infrastructure issues.

Much of our previous research has assessed the long term potential of hydrogen energy systems based on renewables (including solar, wind, and biomass). These studies indicate that beginning in the early part of the next century, renewable hydrogen could become competitive as a low polluting energy carrier (Ogden 1993, Ogden and Nitsch 1993). Our current work is focussed in the nearer term, asking how a transition toward renewable hydrogen might begin. Our earlier assessments and those of other analysts suggest that natural gas could play an important near term role as a transition fuel leading toward a hydrogen energy system, based on renewable sources (Birk 1992, Blazek 1992, Lynch 1992). There are a number of reasons why the expanded use of hydrogen from natural gas is likely to be the first step toward a renewable hydrogen energy system:

* Most industrial hydrogen today is derived from natural gas. At present, steam reforming of natural gas is the least expensive way of producing hydrogen over a wide range of plant sizes (Ogden 1993, Moore and Nahmias 1991, Katofsky 1993).

* The natural gas infrastructure is vast and widespread. In the US about 300,000 miles of high pressure pipelines (Cialone 1984) and 650,000 miles of distribution mains serve 45 million customers (Blazek 1992), delivering 20 EJ per year of energy. [In contrast, the present hydrogen distribution infrastructure consists of a few hundred miles of industrial pipelines, plus fleets of trucks delivering compressed hydrogen or liquid hydrogen. Although about 1 EJ per year of hydrogen is consumed in the US, most of this is produced and used onsite for chemical processes. Merchant hydrogen (hydrogen which is distributed) amounts to about 0.5% of the total.] There are several ways the natural gas infrastructure could be used to bring hydrogen to consumers. First, it is possible to produce hydrogen onsite from natural gas using steam reforming, even at relatively small scale. Since most large users of hydrogen currently produce it onsite from natural gas, this is in essence how most hydrogen is distributed today. Alternatively, hydrogen could be blended into natural gas at concentrations of 15-20% by volume without major changes in the gas distribution system or in consumer appliances (Blazek 1992). Blending could be done at the gas utility plant, with hydrogen produced from natural gas, biomass or other sources. Under certain combustion conditions, hydrogen/natural gas blends would produce lower emissions of CO or NOx than pure natural gas, when used directly as "hythane" in modified compressed natural gas vehicles (Lynch 1992, Foute 1992). If pure hydrogen were needed for fuel cell vehicles, it might be possible to separate out the hydrogen at the point of use (Mezzina 1992). It has also been suggested that the existing natural gas distribution system might be used with pure hydrogen with only minor changes (Blazek et. al. 1992, also see Task 2 below).

* Use of natural gas in vehicles is growing rapidly, and the technologies for natural gas refueling stations are being demonstrated and improved. This experience could be valuable for hydrogen vehicles as well,

since vehicles using compressed hydrogen gas would require similar equipment.

Two tasks are now underway which assess the role of natural gas in the development of a hydrogen energy system. A third task continues our earlier work on fuel cell systems.

In Task 1, we assess various possibilities for producing hydrogen from natural gas for use in low polluting hydrogen vehicles. We consider several options including: 1) hydrogen produced in a large, centralized steam reforming plant and distributed via pipelines or truck to refueling stations, and 2) hydrogen produced at the refueling station via small scale steam reforming of natural gas. Conceptual designs for hydrogen refueling stations based on small scale reformers are presented, and preliminary cost estimates are made. The best option for providing hydrogen transportation fuel depends on the type of demand.

Task 2 involves assessment of the feasibility of using hydrogen blends and pure hydrogen in the existing natural gas pipeline system. This study is being done in collaboration with researchers at the Institute of Gas Technology and Southern California Gas Company. Drawing on earlier work by IGT we are looking at how the natural gas system would have to be changed as the concentration of hydrogen in natural gas was increased.

In Task 3 we assess the use of PEM fuel cells for dispersed residential cogeneration systems producing electricity, space heat and domestic hot water. A model of a small scale PEM fuel cell cogeneration system is being developed, and performance of the system in various types of buildings is estimated. The value of the electricity to an electric utility is estimated based on utility demand curves and saved costs transmission and distribution costs for distributed generation.

Task 1: Assessment of Alternative Methods of Producing Hydrogen Transportation Fuel from Natural Gas

One of the first uses of hydrogen fuel is likely to be in low polluting hydrogen vehicles. Hydrogen internal combustion engine vehicles have been demonstrated by automotive manufacturers including BMW, Daimler-Benz and Mazda (DeLuchi 1989, DeLuchi 1992). Several groups are developing experimental hydrogen fuel cell vehicles (DeLuchi 1992, SAE 1993). A bus based on a PEM fuel cell was demonstrated by Ballard Power Systems (Prater 1993) last year and several other fuel cell vehicles are scheduled for demonstration over the next few years. Recently, hybrid hydrogen internal combustion engine/electric vehicles have been proposed as another low polluting, high efficiency alternative (Smith 1993). After initial tests in the 1990s, hydrogen vehicles might be ready for use in larger fleets. If hydrogen fleet vehicles are successful, the next step might be to bring hydrogen vehicles into the California zero emission vehicle market, offering hydrogen to the public in hydrogen refueling stations.

In this task we look at a range of issues, focussing on the introduction of hydrogen as a transportation fuel for zero (or near zero) emission vehicles. Because the first use of hydrogen vehicles will probably be in Southern California, we are planning to use data from this area where possible.

A variety of options exist for producing hydrogen transportation fuel. (Some possibilities are sketched in Figure 1, where the production method, distribution system, refueling station and end-use are shown.) In the early stages of developing a hydrogen transportation fuel infrastructure, hydrogen will probably come from natural gas. This could be done in several ways.

* Hydrogen could be produced in a large steam reforming plant and distributed to refueling stations via gas pipelines or truck (as a compressed gas or liquid).

* Hydrogen could be produced at the refueling station site via small scale steam reforming of natural gas.

To compare these alternatives, we plan to address the following questions:

* What is the delivered cost of hydrogen transportation fuel derived from natural gas for various supply options and levels of demand (ranging from small demonstration fleet to city supply)?

* What would a hydrogen refueling station look like for various options? Under what conditions does it make sense to produce hydrogen at the refueling station?

* How does hydrogen from natural gas compare to other hydrogen sources in terms of resource size and environmental impacts?

* In the longer term, a range of renewable hydrogen supply options might be phased in. What are the synergisms between renewable systems and natural gas hydrogen systems?

Clearly, the type of hydrogen storage used on the vehicle has a major impact on hydrogen distribution and refueling station design. For this study, we have chosen high pressure gaseous hydrogen as the storage method, both at the refueling station and onboard the vehicle (we look at a range of vehicle pressures from 3600 to 8000 psia). Although gaseous hydrogen storage systems have a lower energy density than those for liquid hydrogen, the simplicity, similarity to compressed natural gas (CNG) vehicle technology and

speed of refueling are attractive features. Moreover with high efficiency vehicles such as fuel cell or hybrid IC/electric vehicles, a reasonable range could be achieved even with onboard compressed gas cylinders (DeLuchi 1992, Ogden and DeLuchi 1993).

Designing the total hydrogen energy system to give the lowest delivered hydrogen cost generally involves a tradeoff between production costs (which would decrease with plant size) and transmission and distribution costs (which could increase significantly if a larger transmission and distribution network were needed). The best solution depends on the total hydrogen demand (which determines the total production capacity needed) and the geographical location of the demand (which determines what kind of transmission and distribution system is needed).

Production of hydrogen at the refueling station via small scale reforming of natural gas

A gaseous hydrogen refueling station based on small scale reforming of natural gas is sketched in Figure 2. The refueling station consists of a natural gas reformer, with a pressure swing absorption unit to produce fuel cell quality, high purity hydrogen (99.999% pure), a hydrogen compressor, pressure cylinders for hydrogen storage, and a hydrogen dispenser.

To look at various possible designs for hydrogen refueling stations:

* Cost and performance data were gathered on the major components of the station: small scale steam reformers, hydrogen purification equipment (pressure swing absorption units), hydrogen compressors, hydrogen storage cylinders, and hydrogen dispensing systems.

* We estimated the daily hydrogen production needed to serve various types of hydrogen vehicle demand. From this we were able to estimate the approximate size of the reformer needed.

* For several hydrogen hourly demand profiles, we estimated the amount of hydrogen storage which would be needed to meet peak station demands. The rest of the station equipment was sized for various refueling strategies.

* Using ASPEN-PLUS software, we simulated the performance of the reformer and hydrogen compressor.

* We estimated the hydrogen refueling station cost and the delivered cost of hydrogen transportation fuel.

In Figure 3a, onboard hydrogen requirements are shown for vehicles as a function of vehicle range and energy efficiency. Depending on the conditions, about 0.15 - 1.1 GJ of hydrogen (or about 400-3000 scf) must be stored onboard. Figure 3b shows the hydrogen demand for a refueling station in standard cubic feet per day (scf/day) as a function of station size (in number of vehicles refueled per day) and vehicle energy efficiency (in equivalent miles per gallon gasoline). In discussions with vendors, we found that the minimum size for commercially available steam reformers is about 0.1 million scf/day. Below this size, the capital cost decreases very little and other sources of hydrogen (truck delivery or electrolysis) would be less expensive. Thus, refueling stations based on commercially available reforming technology would require a fairly large demand (a hundred cars per day or more).

Manufacturers' cost data for small scale steam reforming plants in the range 0.1-1.2 million scf/day are shown in Figure 4. We see that there are strong scale economies, and that the reformer is an expensive piece of equipment, costing about $1-3 million installed. To achieve good performance, low emissions

and long equipment lifetime, reformer manufacturers indicated that the reformer should be run continuously at constant output (King 1994). The reformer start-up time is 4-6 hours, so that following a variable hydrogen demand would be difficult.

We considered two hourly demand profiles. For a fleet application, the hydrogen demand might be scheduled to be approximately constant (Figure 5a). For a public refueling station with a pattern similar to today's gasoline stations, there would probably be peak periods in the morning and afternoon (Figure 5b).

We explored several different strategies for refueling hydrogen vehicles. As a starting point we considered adapting refueling systems commonly used for compressed natural gas vehicles. Several configurations are used in CNG stations (Figure 6):

* In a "booster compressor" system, hydrogen is stored at high pressure. As vehicles are refueled from storage, the storage pressure drops, and is "boosted" back to a higher pressure for vehicle refueling. The advantage of this type of system is that most of the hydrogen could be recovered from storage. The disadvantage is that compressor costs are higher.

* In a "cascade" storage system, a series of pressure vessels are connected. Initially, hydrogen in all the vessels is above the desired vehicle storage pressure. When the first vehicle is refueled, the pressure in the first storage cylinder drops. The next vehicle then refuels from storage cylinder 1 until it reaches the maximum possible pressure. If this is lower than the desired storage pressure, it switches to vessel 2. The next vehicle starts with the lowest pressure storage cylinder and moves to the highest pressure cylinder until the desired vehicle storage pressure is reached. This system has the advantage of saving on compressor costs. However, the total recovery from the system is typically 40-60%, so that more storage capacity is needed than with a booster compression system.

* "Direct compression" systems are sometimes used with CNG vehicles. Here the compressor follows the demand for fuel. However, this would not work with hydrogen produced via onsite reforming, since the reformer must be run continuously.

We examined both booster compressor and cascade storage designs. We find that the design considerations are rather different for CNG and hydrogen. In a hydrogen refueling station, the reformer is the dominant capital cost. Moreover, the reformer has a long start-up time (several hours). Thus, the best strategy appears to be running the reformer continuously, both from an operational and economic viewpoint, and storing any hydrogen produced during off-peak demand hours. For a refueling station with an hourly demand profile similar to a public gasoline station (Figure 5b), this means that the hydrogen storage system must be sized to hold the nighttime hydrogen production. A storage system this size should be able to meet the peak hydrogen demand with capacity to spare. This contrasts with a CNG station where storage is generally sized on the basis of meeting peak demand.

Data on hydrogen storage vessels and compressors were collected, and based on this information, we calculated the station performance and cost for several cases (Tables 3 and 4). We assume the station serves 300 cars/day, each with 0.4 EJ of gaseous hydrogen stored onboard at 8000 psia. The daily station demand is 0.366 million scf/day. The capital cost of the reformer can be estimated at $2.24 million (King 1994). Depending on the refueling strategy (cascade or booster compressor) and the hydrogen storage and vehicle pressures, the capital costs for compressors and storage cylinders vary from about $730,000 to $1.6 million. (In the two cases shown the total capital cost is about $730,000.) The total station cost for our

two best cases was about $3.0-3.1 million (Figure 7). In both cases, the reformer dominates the capital cost of the station, accounting for 75% of the capital cost. For our assumptions, the design with cascade storage is slightly less expensive than the best booster compressor design.

In Figure 8, the delivered cost of hydrogen transportation fuel (in $/GJ) is shown, based on the information in Tables 3 and 4. The largest single factor is the reformer capital cost, which contributes almost 40% of the total cost of hydrogen. Natural gas costs are also large, roughly 25% of the total (assuming natural gas costs $4/MBTU). The sum of compression and storage costs accounts for about 20% of the delivered cost of hydrogen. The delivered cost of hydrogen transportation fuel is found to be about $18/GJ (equivalent in energy terms to about $2.35/gallon gasoline).

The results shown here are still preliminary. Next we plan to look at design tradeoffs in more detail. For example, we would examine how the station design is effected by the vehicle storage pressure, and the station size, and make a more thorough comparison of cascade and booster compressor designs. We will also examine the sensitivity of the delivered cost to changes in the technical and cost assumptions.

It is clear, however, that the reformer capital cost is an important factor. If this could be reduced, the cost of hydrogen from onsite reforming might be significantly lower.

Production of hydrogen via large scale reforming of natural gas

The cost of producing hydrogen via large scale steam reforming has been estimated by various authors (Katofsky 1993, Moore and Nahmias 1992, Steinberg 1988) as about $6-9/GJ. Industrial hydrogen suppliers in Southern California indicate that truck delivered compressed hydrogen gas or liquid hydrogen would cost about $15-20/GJ for a demand of 0.5 million scf/day (Kerr 1993).

The next phase of this study will be to gather better data on the cost of distributing gaseous hydrogen via a local gas distribution system or via truck (as a compressed gas or liquid). We would also examine refueling station designs based on hydrogen delivered to the station by truck or pipeline.

Task 2: Assessment of the Feasibility of Using Hydrogen Blends and Pure Hydrogen in Existing Natural Gas Pipelines

One of the key challenges facing hydrogen is the lack of infrastructure. Unlike electricity and natural gas, there is currently no widespread transmission and distribution system for hydrogen. Experience in the petrochemical and chemical hydrogen industries has shown that it would be possible to build and safely operate long distance pipelines and local distribution systems designed for gaseous hydrogen. However, building a new system for hydrogen would be a costly undertaking. If pure hydrogen or hydrogen blends could be used in all or part of the existing natural gas system, this might save a huge capital investment.

In this task we examine how existing natural gas long distance transmission, distribution and end-use systems might have to be changed to allow the use of hydrogen/natural gas blends and pure hydrogen. [Note: in this paper the term "transmission system" refers to long distance, large pipelines operated at typical pressures of up to 1000 psia. "Distribution system" refers to a gas utility type local distribution system operated at pressure of between 50 and 500 psia. "End-use systems" are gas using equipment (heaters, gas engines, etc.)]

In particular, we are interested in how an increased percentage of hydrogen might impact:

* the materials used for pipes, seals, etc.

* compatibility of existing natural gas pipeline and distribution system equipment including compressors, meters, etc.

* compatibility of existing natural gas end-use equipment.

* the energy flow rate and leak rate from the system

* safety

This study is being conducted in collaboration with researchers at the Institute of Gas Technology (IGT) who have done work on a number of these issues for hydrogen distribution and end-use systems.

Since many studies have been done on the use of hydrogen and hydrogen blends in the existing natural gas system, we began our work with a survey of the literature. We summarize the results of some previous studies below, and indicate questions for further investigation.

Use of hydrogen in natural gas distribution systems

Much of the published work on using hydrogen and hydrogen blends in the natural gas distribution system was done by IGT starting in the 1970s. Their results to date were summarized in a recent paper (Blazek et. al. 1992). It was found that it would be possible to use hydrogen in natural gas distribution systems with minor changes. Some key results from this study are listed below.

* With the possible exception of meters, existing components and piping should be adequate for hydrogen service. Larger capacity meters may be needed.

* Short term (6 month) exposure to hydrogen did not effect the metallic components of the distribution system. There are some indications that plastic components and adhesive might be effected. More testing is needed to resolve this question.

* Assuming that the distribution system pressures are the same, the energy flow rate for hydrogen would be similar to that for natural gas.

* Depending on the type of materials used, the volumetric leak rate for the distribution system would be about 2.9 to 3.5 times that of natural gas. The energy loss would be about the same as that for natural gas.

Use of hydrogen in natural gas end-use systems

The feasibility of using hydrogen and hydrogen blends in end-use systems designed for natural gas has also been investigated by researchers at IGT (Blazek 1993, Jasionowski 1993). Here it was found that no changes in end-use equipment would be necessary at hydrogen concentrations up to about 15-20% by volume. Above this level, major changes in burners, metering equipment and seals would be necessary. End-use equipment designed for hydrogen has been demonstrated for transportation, power

and heating applications.

Use of hydrogen in natural gas long distance pipeline systems

The suitability of existing long distance natural gas pipelines to hydrogen service is more problematic. This is true because higher pressures are present (up to 1000 psia for long distance pipelines) which may make hydrogen embrittlement a serious issue.

The term hydrogen embrittlement is used to refer to several materials effects of hydrogen on metals. Three types of hydrogen embrittlement have been identified (Louthan and McNitt 1977):

* Internal hydrogen embrittlement (I-H) can cause delayed failure in cases where hydrogen has been absorbed into the metal during plating or direct contact with gaseous hydrogen or from reactions with water during melting, casting, or welding operations. In order for embrittlement to take place, hydrogen must diffuse from within the metal to the vicinity of a crack. I-H embrittlement is most severe near room temperature.

* Hydrogen reaction embrittlement (H-R) where a chemical reaction takes place between hydrogen and the metal. This type of embrittlement is seen in refineries. Increased temperatures and pressures accelerate the reaction rate.

* Hydrogen environment embrittlement (H-E) is the degardation of mechanical properties which takes place while the metal is exposed to a hydrogen environment. H-E embrittlement occurs when the metal is under stress and cracks are present. Unlike I-H embrittlement, there is no time delay. Embrittlement occurs once a stress level greater than the yield strength is reached. Interactions of hydrogen with the metal surface are the likely cause of H-E embrittlement.

For hydrogen pipelines, H-E embrittlement is thought to be the most important mechanism (Cialone 1984).

The basic materials science of hydrogen embrittlement has been investigated, and many of the physical mechanisms are well understood (Flis 1991, Fullenweider 1984, Gibala 1984, Raymond 1989, Beachem 1977). However, applying this knowledge to practical situations is complex because several competing effects may be present. It is not possible to predict a priori the degree of embrittlement in a given material from first principles. Embrittlement will be effected by the pipeline construction (type of welds, etc.) However, data has been gathered on the effects of hydrogen on a variety of materials, including steels commonly used in natural gas pipelines.

Following unexpected problems with high pressure gaseous hydrogen storage vessels, NASA sponsored numerous studies on hydrogen embrittlement, particularly by Rocketdyne (Jewett et.al 1973). The Rocketdyne study gives a large data base on hydrogen reaction with metals. The American Petroleum Institute also publishes data on materials for hydrogen service (API 1990).

The only published work we found on the possible effects of hydrogen on existing natural gas pipelines was carried out by researchers at Brookhaven National Laboratory and Battelle Columbus Laboratories (Holbrook et. al. 1982, 1986, Cialone 1984.). These studies indicate that several types of steel commonly used in natural gas pipelines would experience serious embrittlement from pure hydrogen at 1000 psia. Embrittlement might be reduced to low levels with various gas additives (e.g. oxygen, ethylene, carbon sulfide, sulfur dioxide, nitrous oxide, carbon monoxide, and ethane). Adding a few percent oxygen or

sulfur dioxide to pure hydrogen essentially eliminated embrittlement, but posed safety problems.

Summary and Future Research Directions

In summary, our understanding at present is:

* It appears that hydrogen blends and pure hydrogen could be used in existing natural gas distribution systems with only minor changes.

* Existing natural gas end-use systems could be used with blends of up to 15-20% hydrogen by volume. Above this level significant changes in the end-use equipment and metering equipment would be needed.

* Because of the higher pressures used in long distance pipelines, hydrogen embrittlement could be a serious problem for natural gas pipelines carrying pure hydrogen. The situation for hydrogen blends has not been examined explicitly.

Although the outlook for using hydrogen in the distribution system and end-use systems is well studied, the situation for hydrogen in long distance natural gas pipelines is less clear. We hope to answer several questions with regard to hydrogen in natural gas pipelines:

* Various remedies for embrittlement have been proposed including gaseous additives (small percentages of oxygen or sulfur dioxide strongly inhibit embrittlement), coating pipelines with plastic, testing pipeline sections and replacing those having materials susceptible to embrittlement, and replacing the entire pipeline with hydrogen compatible steels. How feasible are these measures and what would they cost?

* What would be the effect on long distance pipelines of blending hydrogen with methane at various concentrations? At what percentage of hydrogen would embrittlement become a problem?

* Although natural gas pipelines typically have a long life (in excess of thirty years), they will eventually need replacement. Are there pipeline steels which would be appropriate for both natural gas and hydrogen service at a cost comparable to present pipelines? If not, how much would it cost to make new natural gas pipelines hydrogen compatible?

The product of this task will be an updated summary of the feasibility of using hydrogen and hydrogen blends in existing natural gas distribution, transmission and end-use systems.

In the future we would like to explore the implications of this study for building a gaseous hydrogen infrastructure. The relative ease of changing local natural gas distribution systems to hydrogen suggests that hydrogen might be produced locally from natural gas or renewable resources as needed and introduced into local distribution systems. Because the United States has a wealth of widely distributed renewable resources (solar, wind, biomass), it may not be necessary to transport hydrogen long distances via high pressure pipeline, even in the long term. It would be interesting to do a case study, examining the issues involved in changing the local distribution system in a particular site.

Task 3: Assessment of PEM Fuel Cells For Residential Cogeneration

Proton exchange membrane (PEM) fuel cells are attractive candidates for residential cogeneration. They are compact, quiet and could potentially reach low costs at sizes of 5-10 kW. Fueled with hydrogen and air, PEM fuel cells fueled based on near term technology could convert about 45% of the energy value of hydrogen to electricity and 40% to heat in the form of hot water at 70° to 100°C. The PEM fuel cell can produce domestic hot water, space heat and electricity.

In this task, we consider PEM fuel cells for residential cogeneration applications.

We are currently collecting data on PEM fuel cell performance from manufacturers. In parallel a model of a PEM fuel cell cogeneration system is being developed.

We plan to estimate the performance of the fuel cell cogeneration system for energy demands in various types of buildings (for example: conventional and superinsulated houses). The value of the electricity to an electric utility would be estimated, based on utility demand curves and saved transmission and distribution costs for distributed generation.

Future Research Directions

In the future, we would like to conduct further research on how a hydrogen infrastructure might develop.

We would continue studies of how a hydrogen transportation fuel infrastructure might evolve. We would like to assess electrolysis from off-peak power as an option for small scale onsite hydrogen production and look at the infrastructure issues for hydrogen transportation fuel at specific sites (for example, Southern California or the Northeastern US).

We would explore the implications of our ongoing assessment of using hydrogen in the existing natural gas system. It would be interesting to do a site specific study of converting a local natural gas distribution system to hydrogen.

Finally, we would plan to continue our studies of fuel cell systems for transportation and power generation.

Acknowledgments

The authors would like to thank Bart Munro (Princeton U. mechanical and aerospace engineering department) for assistance in hydrogen refueling station design calculations. We would also like to thank Jeff Chen, Eric Larson, and Robert Williams (all of Princeton CEES) and Mark Delucchi (UC Davis) for useful comments. Chris Blazek (IGT) and Carol Bailey (Southern California Gas Company) helped frame the scope of our studies on hydrogen distribution and transmission systems. We would also like to thank Walt Jasionowski (IGT), David Crain (Southern California Gas Company), Gary Fenner (Praxair), Robert Moore (Air Products), Michael Kerr (Praxair), David King (Howe-Baker Engineers), R. Dowling (Christy Park Industries), Keith Prater (Ballard Power Systems and Frano Barbir (Energy Partners), B.D. Savidge (RIX Industries), engineers at Hydrochem and Al Mezzina (consultant) for useful conversations.

References

American Petroleum Institute April 1990. "Operating Limits and Fundamental Data for Steels Operating In Hydrogen Service," Publication 941, Fourth Edition.

Beachem, Cedric D. 1977. Hydrogen Damage, Naval Research Laboratory, American Society for Metals.

Birk, J.R., Mehta, B., Fickett, A., Mauro, R., Serfass, J. June 22-25 1992. A bridge to the future hydrogen-electric economy, Additive to the Proceedings of the 9th World Hydrogen Energy Conference, Paris, France.

Blazek, C.F., Biederman, R.T., Foh, S.E. and Jasionowski, W. March 18-20, 1992. Underground storage and transmission of hydrogen, Proceedings of the Third Annual Meeting of the National Hydrogen Association, Washington, DC.

Bochow, D. 1994. Howe-Baker Engineering, private communications.

Cialone, H.J., P.M. Scott, J.H. Holbrook, K. Sieradzki and N. Bandyopadhyay 1984. "Hydrogen Effects on Conventional Pipeline Steels," in Hydrogen Energy Progress V, Pergamon Press, p.1855-1868.

DeLuchi, M.A. 1989. Hydrogen vehicles: An evaluation of fuel storage, performance, safety, environmental impacts and cost, International Journal of Hydrogen Energy, 14:81-130.

DeLuchi, M.A. 1992. Hydrogen fuel-cell vehicles, Institute of Transportation Studies Research Report No. UCD-ITS-RR-92-14, University of California, Davis.

Dowling, R. 1993. Christy Park Industries, private communications.

Electric Power Research Institute, September 1987. Technical Assessment Guide, Volume 2: Electricity End Use; Part 1: Residential Electricity Use--1987.

Flis, Janusz, ed. 1991. "Corrosion of metals and hydrogen-related phenomena," Materials Science Monographs, 59, Elsevier.

Foute, S. et. al. March 18-20, 1992. The Denver hythane project, Proceedings of the Third Annual Meeting of the National Hydrogen Association, Washington, DC.

Fullenweider, Malcom A. 1983. Hydrogen Entry and Action in Metals, Pergamon Press, TN690.F78, 123 pp.

Gibala, R. and R.F. Hehemann, eds. 1984. Hydrogen Embrittlement and Stress Corrosion Cracking, American Society for Metals, Case Western University.

Gregory, D. P., Tsaros, C. L., Arora, J. L. and Nevrekar, P. 1980. The economics of hydrogen production, American Chemical Society Report, 0-8412-0522-1/80/47-116-003.

Holbrook, J.H., E.W. Collings, H.J.Cialone and E.J. Dragulis 1986. "Hydrogen Degradation of Pipeline Steels," Final report BNL-52049, Battelle Columbus Laboratories.

Holbrook, J.H., and H.J.Cialone 1982. "The Effect of Hydrogen on Low Cycle Fatigue Life and Subcritical Crack Growth in Pipeline Steels," Final report BNL-35589, Battelle Columbus Laboratories.

Jewett, R.P., R.J. Walter, W.T. Chandler and R.P. Frohmberg 1973. "Hydrogen Embrittlement of Metals," NASA CR-2163, Rocketdyne.

Katofsky, Ryan June 1993. Production of Fluid Fuels from Biomass, Princeton University Center for Energy and Environmental Studies Report No. 279.

Kerr, M. 1993. Praxair, private communications.

King, David 1994. Howe-Baker Engineering, private communications.

Larson, E.D., Katofsky, R.E. July 1992. Production of methanol and hydrogen from biomass, Princeton University Center for Energy and Environmental Studies Report No. 271, Princeton, NJ.

Larson, E.D., Katofsky, R. May 11-15, 1992. Production of hydrogen and methanol from biomass, in Advances in Thermochemical Biomass Conversion, Interlaken, Switzerland.

Louthan, M.R. and R.P. McNitt, eds. 1977. Environmental Degradation of Engineering Materials, College of Engineering, Virginia Tech.

Lynch, F. March 18-20, 1992. Near term pathways toward hydrogen energy, Proceedings of the Third Annual Meeting of the National Hydrogen Association, Washington, DC.
Mezzina, A., 1994. Private communication.

Moore, R.B. and D. Nahmias 1991. "Gaseous Hydrogen Markets and Technologies," Proceedings of the First Annual Meeting of the National Hydrogen Association, Palo Alto, CA, EPRI Report GS-7248.

Ogden, J. M., Williams, R. H. 1989. Solar Hydrogen: Moving Beyond Fossil Fuels, Washington DC:World Resources Institute. 123 pp.

Ogden, J.M. 1991. Cost and performance sensitivity studies for solar photovoltaic electrolytic hydrogen systems, Solar Cells, 30: No. 1-4:515.

Ogden, J.M., DeLuchi, M.A. 1993. Solar hydrogen transportation fuels, to appear in Proceedings of the Conference on Transportation and Global Climate Change, American Council for an Energy Efficient Economy, Washington, DC.

Ogden,J.M. and Nitsch, J. 1993. Solar hydrogen, in T. Johannson, H. Kelly, A.K.N. Reddy and R.H. Williams, eds. Renewable Energy: Fuels and Electricity from Renewable Resources, Island Press, Washington DC.

Ogden, J.M. June 24, 1993. Renewable hydrogen energy systems studies, final report for NREL subcontract No. XR-2-11265-1.

Prater, K. 1992. Ballard Power Systems, North Vancouver, British Columbia, "Solid Polymer Developments at Ballard," Journal of Power Sources, v. 37, pp. 181-188.
Prater, K. 1994. Ballard Power Systems, private communications.

Raymond, Louis 1989. "Evaluation of Hydrogen Embrittlement," Metals Handbook, Ninth Edition, Vol. 13, Corrosion, AMS International, pp. 283-290.

Savidge, B.D. 1994. RIX Industries, private communications.

Steinberg, M. and H.C. Cheng 1988. Assessment of Hydrogen Production by Conventional and Advanced Processes, Brookhaven National Laboratory Report, Washington, DC, US Department of Energy.

Tables

Figures

Table 1. Conversion factors

1 EJ = Exajoule (10^{18} Joules) = 0.95 Quadrillion BTUs

1 GJ = Gigajoule (10^{9} Joules) = 0.95 Million BTUs

1 million standard cubic feet H2/day = 28,300 Nm^3 H2/day = 362 GJ/day (HHV)

1 gallon gasoline = 0.1304 GJ (higher heating value)

$1/gallon gasoline = $7.67/GJ = $8.09/MBTU

Table 2. Economic assumptions

All costs are given in constant 1993 US dollars.

For hydrogen production plants, compression, storage and transmission systems owned by utilities levelized costs were calculated in constant dollars assuming (EPRI 1987):

Real discount rate = 6.2%
Corporate income tax rate = 38%
Annual insurance = 0.5% of installed capital cost
Annual property taxes = 1.5% of installed capital cost

For hydrogen refueling stations it is assumed that:

Real discount rate = 9.9% for equity
Real discount rate = 6.2% for debt
Corporate income tax rate = 44%
Annual insurance = 0.5% of installed capital cost
Annual property taxes = 1.5% of installed capital cost

All hydrogen costs are based on the higher heating value of hydrogen

TABLE 3. ALTERNATIVE DESIGNS FOR HYDROGEN REFUELING STATIONS BASED ON SMALL SCALE STEAM REFORMING OF NATURAL GAS

CARS FUELED PER DAY : 304 (assumes 0.4 GJ/vehicle for range of 400 km @75mpg)

REFORMER			
Operating temperature	845-870°C		
Outlet pressure from PSA	200 psig		
Capacity	0.366 million scf H2/day		
Installed Capital cost	$2.24 x 10^6		
Natural gas consumption	0.400 MBTU/1000 scf H2		
Energy conversion effiency	86% (HHV)		
Electricity consumption	220 kwh/day		
Water consumption	1023 gallons/day		
O&M cost	$16,000/yr		
Equipment lifetime	20 years		
Land area	30 ft x 30 ft		
		Booster	Cascade
HYDROGEN STORAGE CYLINDERS			
Storage pressure (psia)		5000	8400
Total Storage capacity (scf hydrogen)		335,500	305,000
# vessels		35	52
Vessel capacity (scf H2)		9600	6050
Capital cost ($)		367,500	534,240
O&M costs ($/yr)		3500	5200
H2 recovery (%)		54.7%	59.9%
Equipment lifetime (yr)		10	10
STORAGE COMPRESSOR			
Flow rate (scf H2/min)		260	260
Inlet pressure (psia)		200	200
Outlet pressure (psia)		5000	8400
Installed Capital cost ($)		170,000	190,000
O&M Cost ($/yr)		3000	3000
Compressor power (kW)		82	99
Electricity consumption	(kWh/1000 scf H2)	5.37	6.49
	(kwh/kwh H2)	0.053	0.065
Equipment lifetime (hr)		100,000	100,000
BOOSTER COMPRESSOR			
Max Flow rate (scf H2/min)		1590	
Inlet pressure (psia)		2000	
Outlet pressure (psia)		8400	
Installed Capital cost ($)		200,000	
O&M Cost ($/yr)		3000	
Compressor power (kW)		228	
Electricity consumption	(kWh/1000 scf H2)	2.39	
	(kwh/ kwh H2)	0.024	
Equipment lifetime (hr)		100,000	
HYDROGEN DISPENSER (4 bays @10,000 each)		40,000	
LABOR COSTS ($/yr)		131,400	

TABLE 4. DELIVERED COST OF HYDROGEN TRANSPORTATION FUEL

	BOOSTER	CASCADE
INSTALLED CAPITAL COSTS (million $)		
Reformer	2,240,000	2,240,000
Storage cylinders	367,500	534,240
Storage compressor	170,000	190,000
Booster compressor	200,000	-
Dispenser	40,000	40,000
TOTAL	3,107,500	3,000,420
OPERATING COSTS ($/yr)		
Natural gas (NG @ $4/MBTU)	213,744	213,744
Reformer O&M	16,000	16,000
Storage cylinder O&M	3500	5200
Compressor electricity (@6 cents/kwh)	62,200	52,020
Compressor O&M	6000	3000
Labor	131,400	131,400
TOTAL	432,344	421,364
DELIVERED HYDROGEN COST ($/GJ)		
Reformer capital	6.95	6.95
Natural gas feedstock	4.42	4.42
Reformer O&M	0.33	0.33
Storage cylinders	1.14	1.66
Compressor capital	1.15	0.59
Compressor electricity	1.29	1.08
Compressor O&M	0.12	0.06
Labor	2.72	2.72
TOTAL	18.6	18.0

Estimates for reformer performance and cost are based from Howe-Baker Engineers (King 1994, Bochow 1994)

Estimates for compressors are from RIX Compressors (Savidge 1994).

Estimates for hydrogen storage cylinders are from Christy Park Industries (Dowling 1994).

OPTIONS FOR SUPPLYING H2 FROM NATURAL GAS

PRODUCTION	DISTRIBUTION	FILLING STA.	END-USE
NG	NG DISTRIB. SYSTEM	SMALL STEAM REFORMING PLANT NG -> COMP.H2 GAS	H2 VEH.
NG/HYDROGEN BLENDS UP TO 15-20% H2	NG DISTRIB. SYSTEM	COMP.GAS STATION	HYTHANE VEH., H2 VEH.
LARGE STEAM REFORMING PLANT NG -> H2			H2 VEH.
	H2 GAS PIPELINE	COMP. H2 GAS	
	H2 COMP. GAS TRUCK	COMP. H2 GAS	
	LH2 TRUCK DELIVERY	LH2	
LARGE PLANT NG -> MeOH	MeOH TRUCK	MeOH STATION	MeOH FCEVS (ONBOARD REFORMING MeOH -> H2

RENEWABLE OPTIONS FOR H2 TRANSPORT FUEL

PRODUCTION	DISTRIBUTION	FILLING STA.	END-USE
LARGE BIOMASS GASIFIER PLANT BIOMASS -> H2			H2 VEH.
	H2 GAS PIPELINE	COMP. H2 GAS	
	H2 COMP. GAS TRUCK	COMP. H2 GAS	
	LH2 TRUCK DELIVERY	LH2	
LARGE PLANT BIOMASS -> MeOH	MeOH TRUCK	MeOH STATION	MeOH FCEVS (ONBOARD REFORMING MeOH -> H2)
OFF-PEAK PV OR WIND POWER	ELEC. DISTRIB. SYSTEM	ELECTROLYSIS AT FILLING STATION	H2 VEH.
OFF-PEAK, PV OR WIND ELECTROLYSIS	H2 DISTRIBUTION	COMP. H2 GAS	H2 VEH.
		STAND-ALONE PV ELECTROLYSIS	H2 VEH.

FIGURE 1

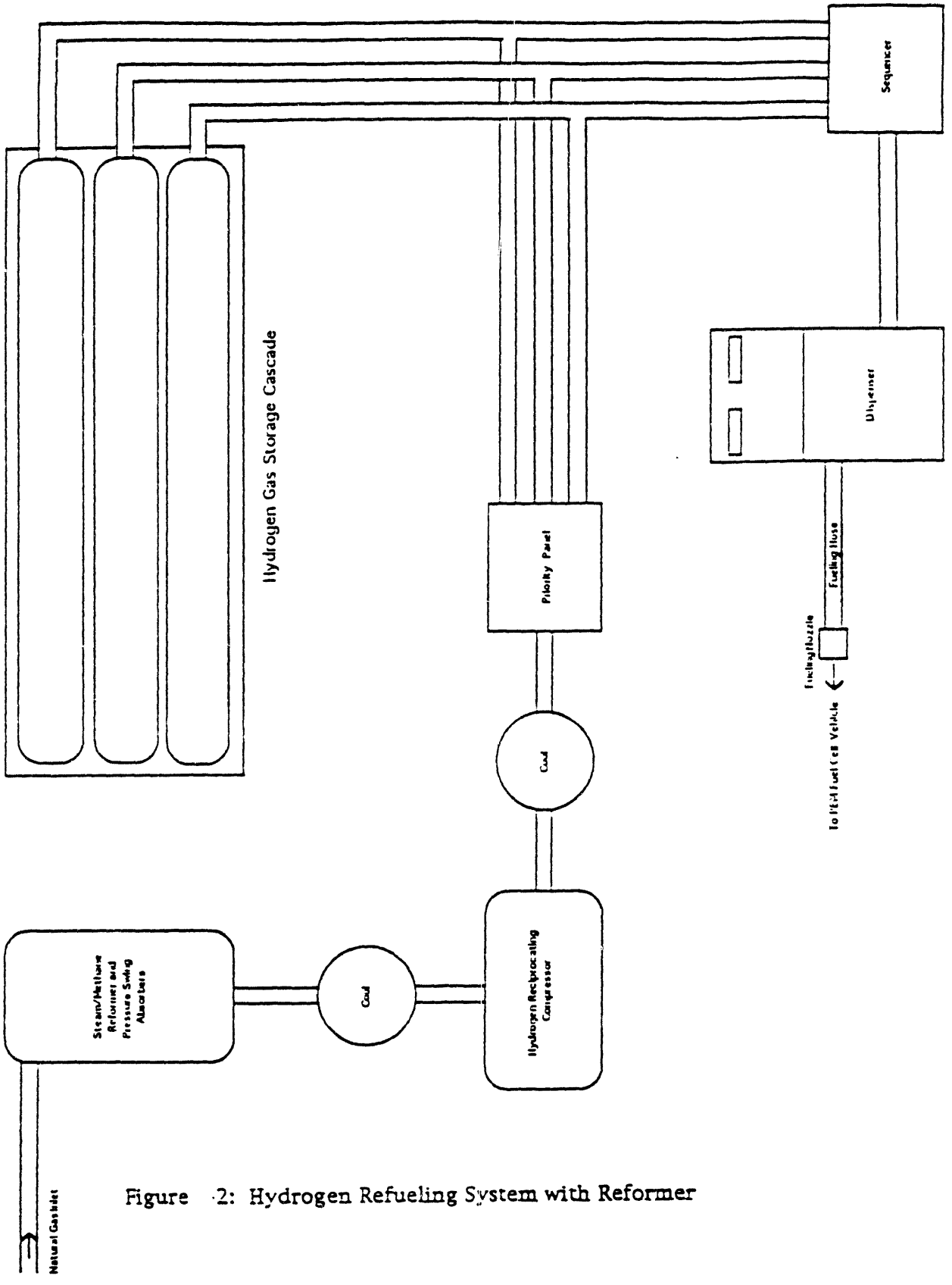

Figure 2: Hydrogen Refueling System with Reformer

ONBOARD ENERGY STORAGE FOR HYDROGEN VEHICLES

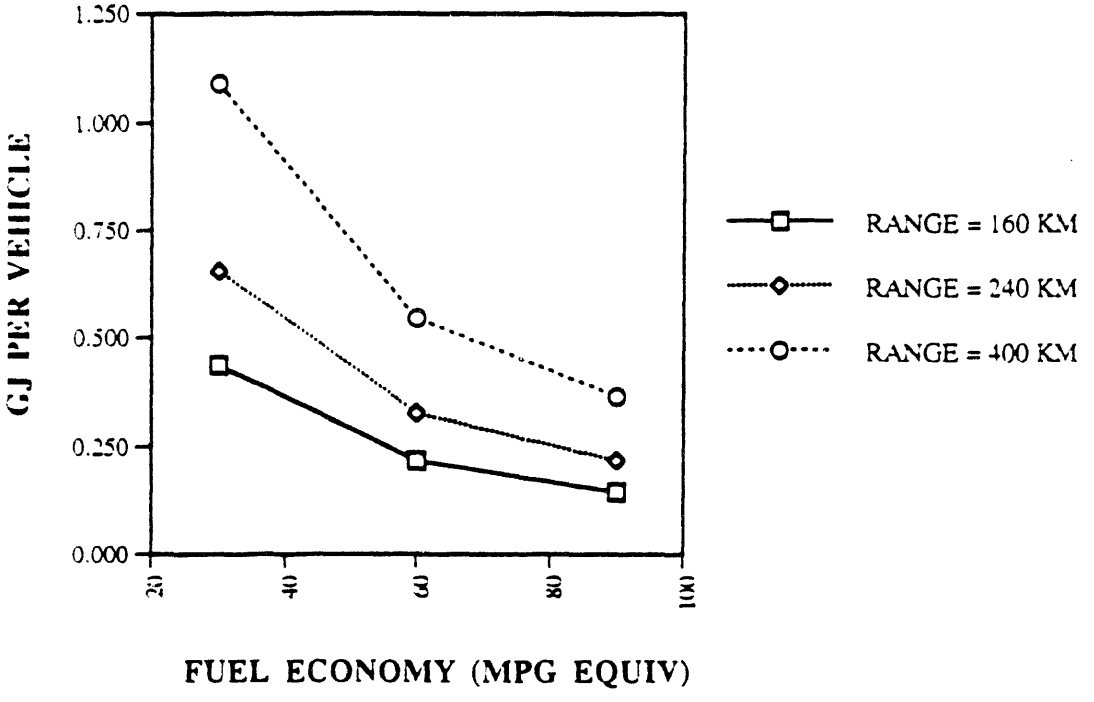

FIGURE 3

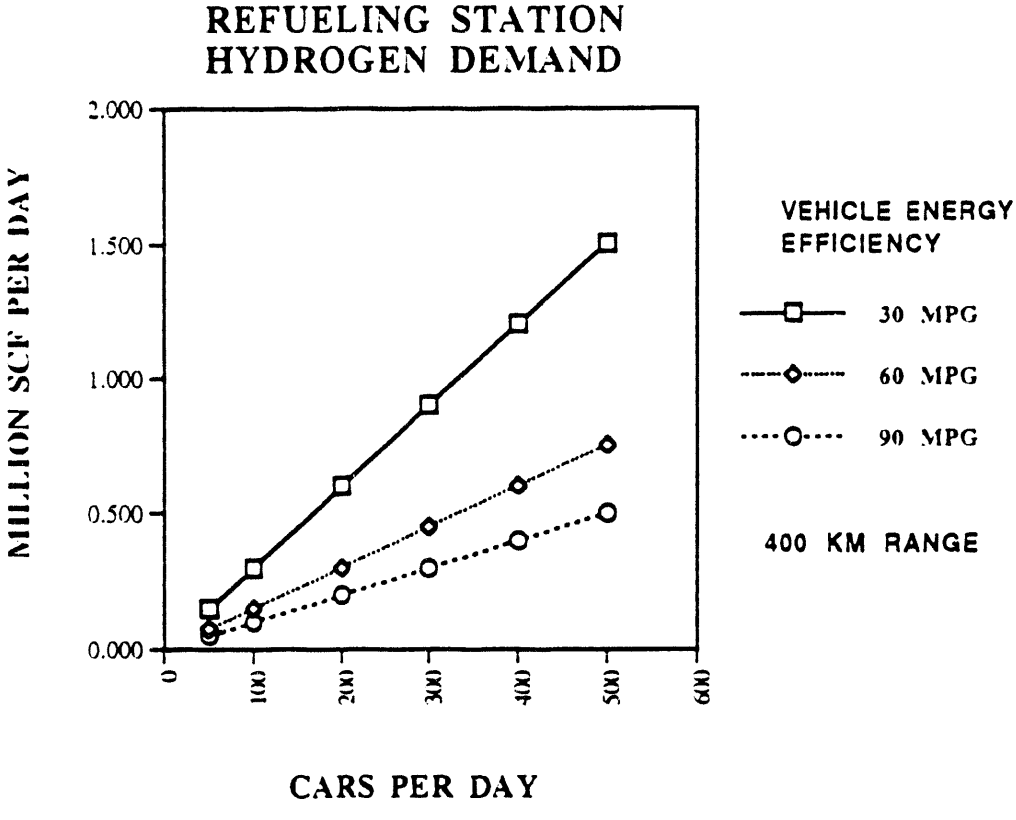
REFUELING STATION
HYDROGEN DEMAND
MILLION SCF PER DAY
2.000
1.500
1.000
0.500
0.000
0
100
200
300
400
500
600
CARS PER DAY
VEHICLE ENERGY
EFFICIENCY
30 MPG
60 MPG
90 MPG
400 KM RANGE

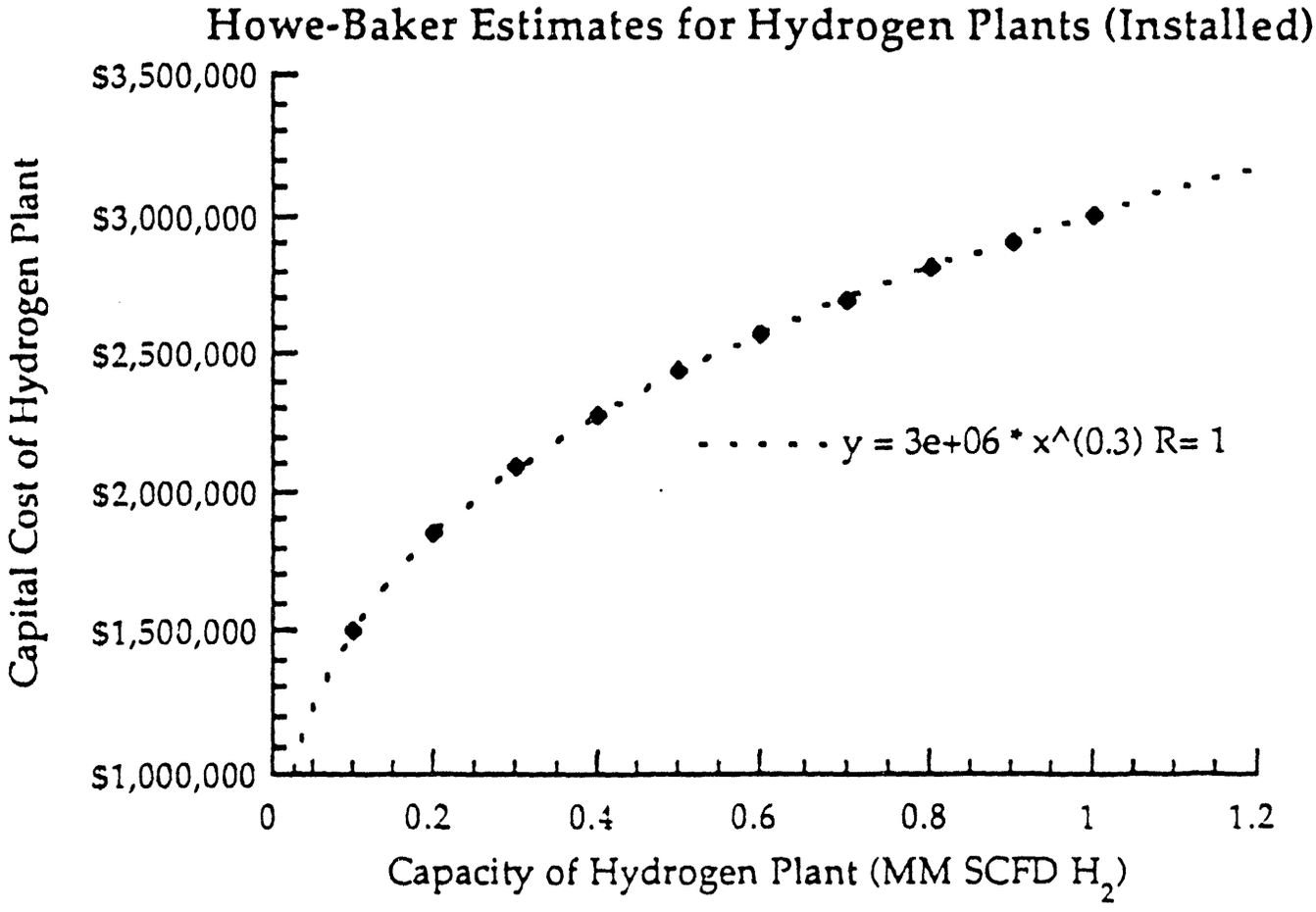
Howe-Baker Estimates for Hydrogen Plants (Installed)
Capital Cost of Hydrogen Plant
$3,500,000
$3,000,000
$2,500,000
$2,000,000
$1,500,000
$1,000,000
y = 3e+06 * x^(0.3) R= 1
0
0.2
0.4
0.6
0.8
1
1.2
Capacity of Hydrogen Plant (MM SCFD H2)

FIGURE 4

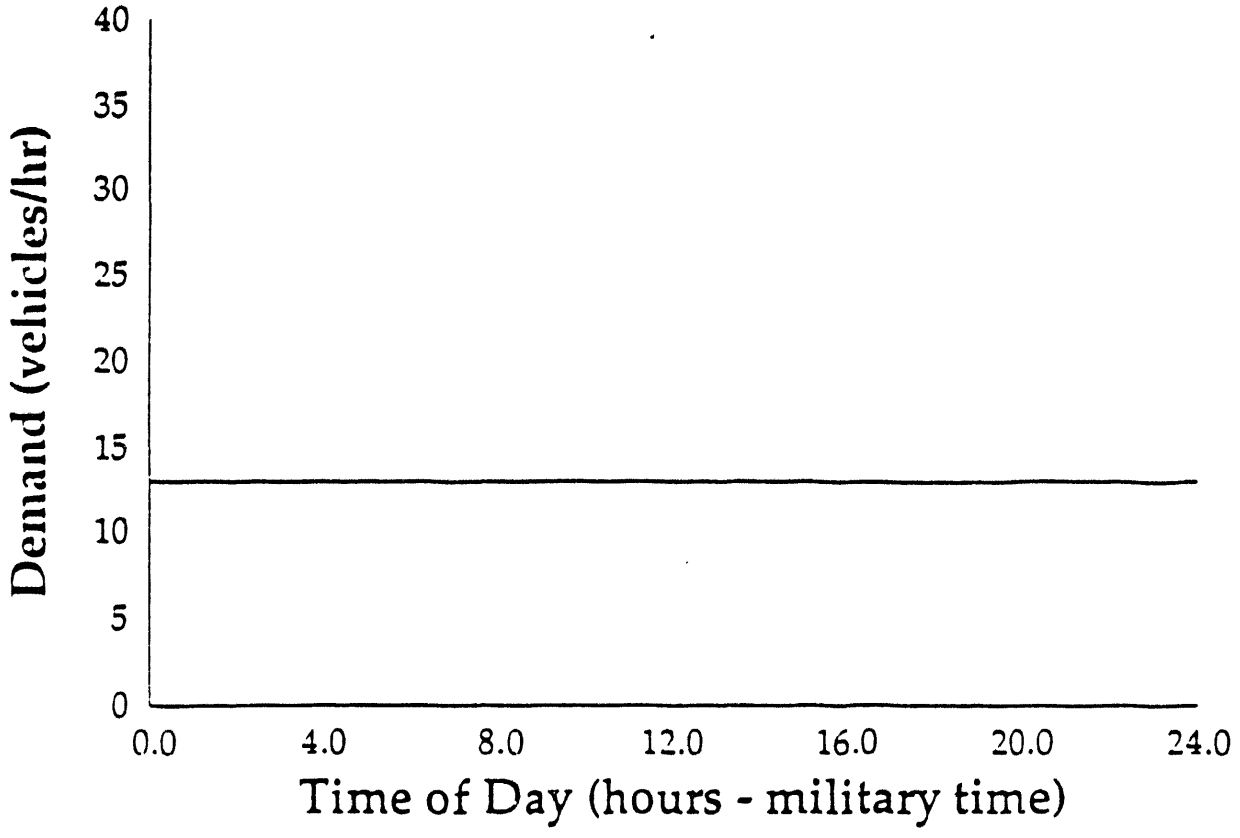
Demand (vehicles/hr)
40
35
30
25
20
15
10
5
0
0.0
4.0
8.0
12.0
16.0
20.0
24.0
Time of Day (hours - military time)

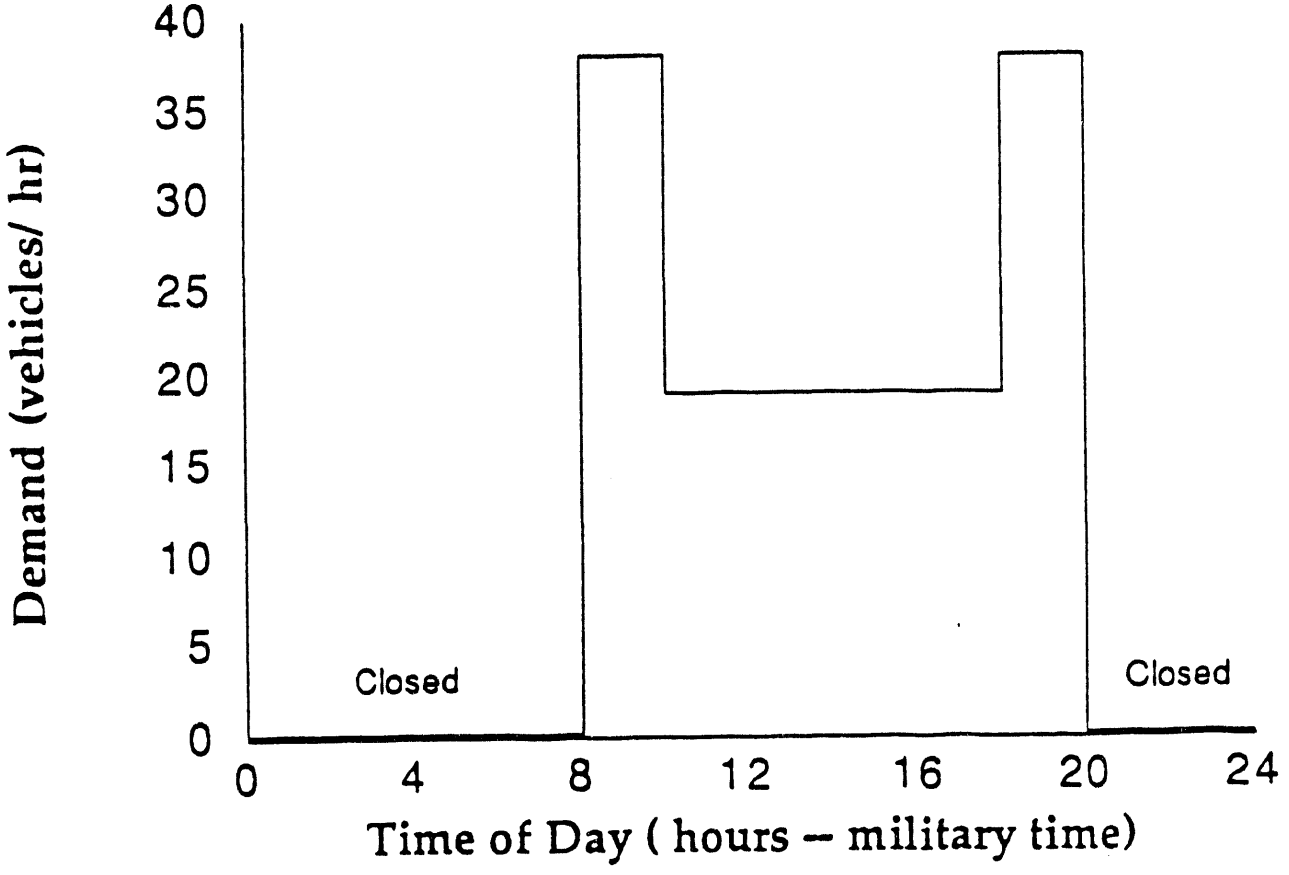
Demand (vehicles/ hr)
40
35
30
25
20
15
10
5
0
Closed
Closed
0
4
8
12
16
20
24
Time of Day (hours -- military time)

FIGURE 5

FIGURE 6

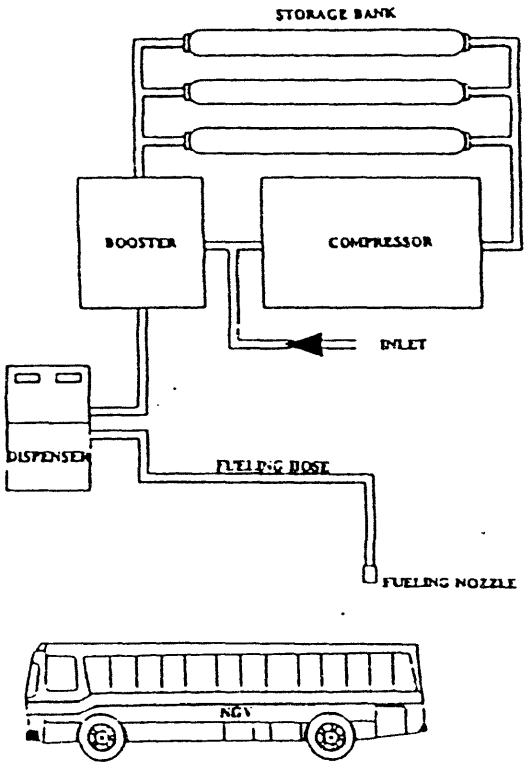

Pressure Booster Refueling (GRI, 1991)

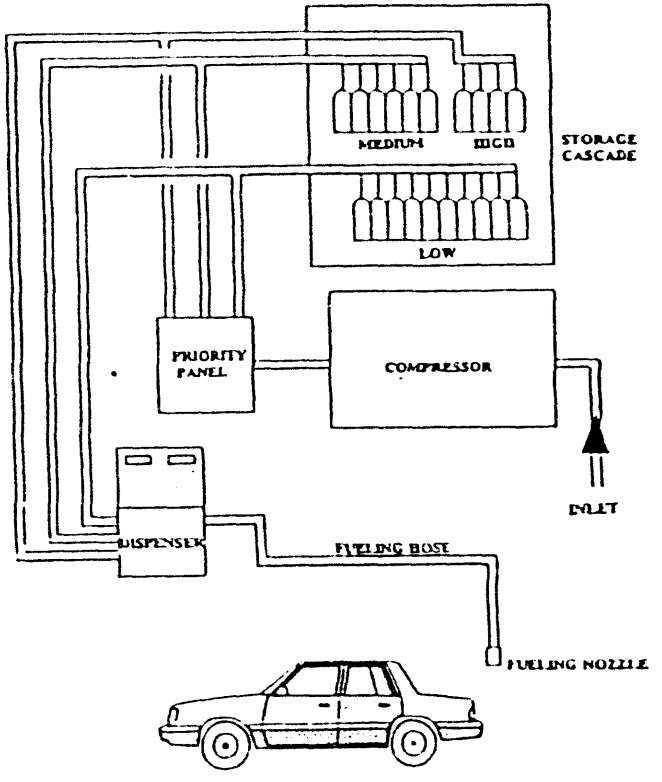

Standard Cascade Refueling System Design (GRI, 1991)

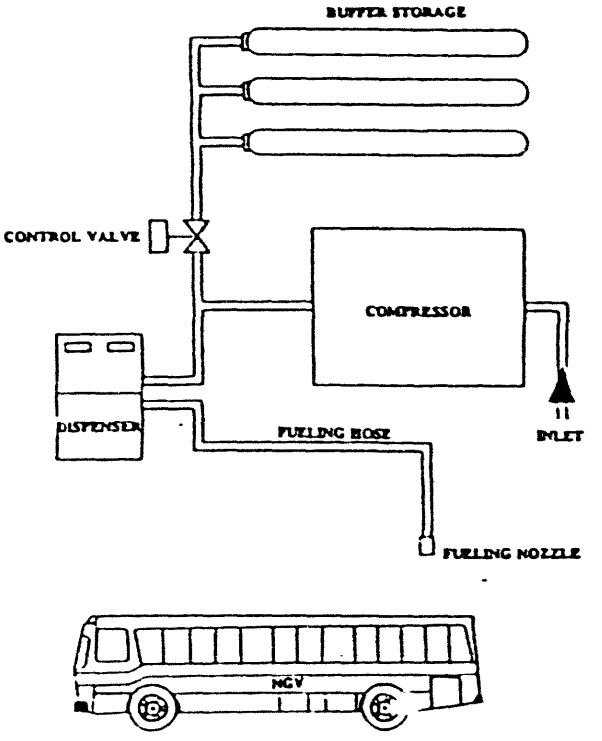

Direct Compressor Refueling (GRI, 1991)

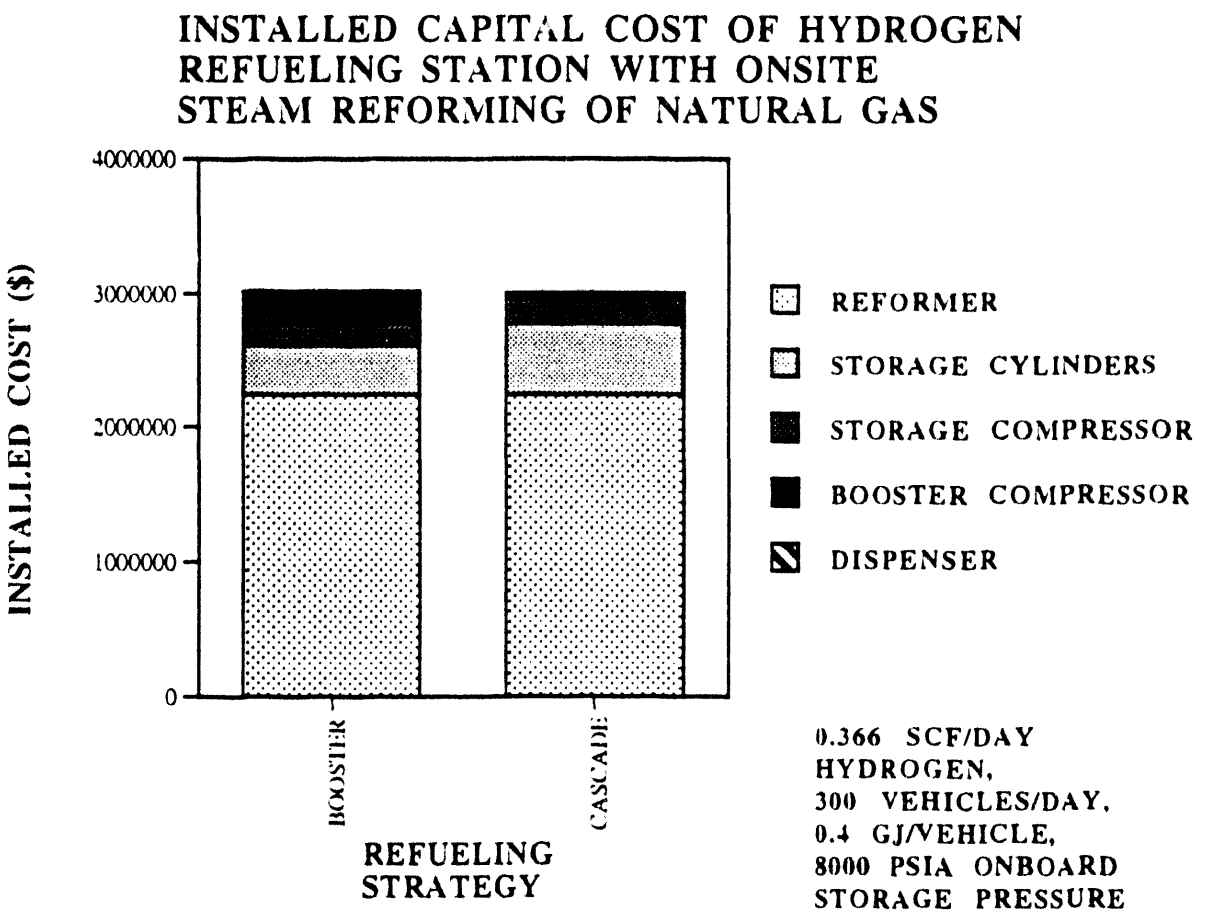
INSTALLED CAPITAL COST OF HYDROGEN
REFUELING STATION WITH ONSITE
STEAM REFORMING OF NATURAL GAS
INSTALLED COST ($)
4000000
3000000
2000000
1000000
0
BOOSTER
CASCADE
REFUELING
STRATEGY
REFORMER
STORAGE CYLINDERS
STORAGE COMPRESSOR
BOOSTER COMPRESSOR
DISPENSER
0.366 SCF/DAY
HYDROGEN,
300 VEHICLES/DAY,
0.4 GJ/VEHICLE,
8000 PSIA ONBOARD
STORAGE PRESSURE

FIGURE 7

DELIVERED COST OF H2 TRANSPORTATION FUEL FROM ONSITE STEAM REFORMING OF NATURAL GAS

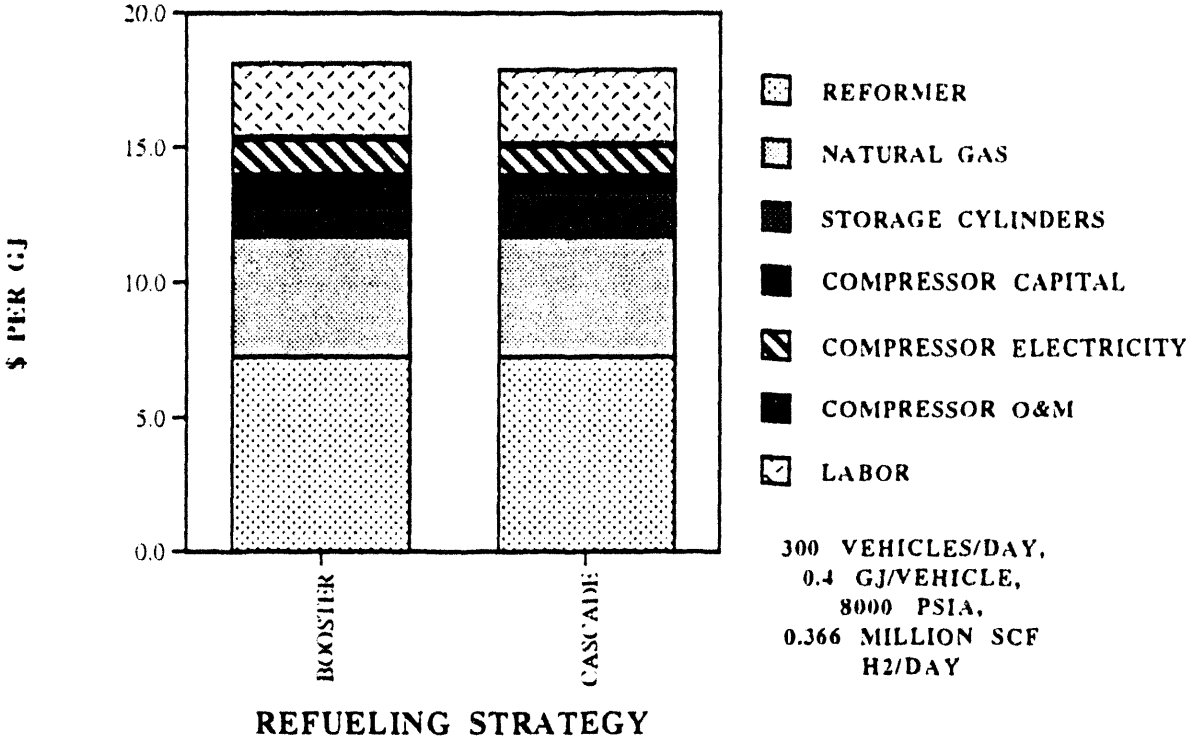

FIGURE 8

Development of Industrial Interest in Hydrogen

Robert L. Mauro and Debbi L. Smith
National Hydrogen Association
Washington, D.C.

Abstract

The project will review, with industry, current and near-term potential uses and opportunities for hydrogen as a fuel. By working through NHA and its members, the project provides DOE with direct access to industry hydrogen activities, interests and reaction to ongoing efforts. The study approach is to work with industry, principally NHA members to:

- Provide aggregate information on production, transport and use of hydrogen by region,
- Identify hydrogen consortia, describe their programs and discuss participants' interests,
- Determine NASA's interest in a hydrogen vehicle demonstration at a NASA site in the Southeast,
- Examine supply of hydrogen from the Southeastern U.S. and demand in Southern California to determine the feasibility of a long distance hydrogen pipeline,
- Determine interest & identify potential DOE role in consortium activities, and
- Categorize the nature of industry interest in hydrogen through broader NHA industrial network.

A successful outcome for these efforts would entail the following:

- Accurate characterization of hydrogen production, transport and use by region,
- Accurate summaries of all major joint hydrogen projects with a proper determination about the appropriate nature and level of DOE involvement,

- Development of NASA interest in a hydrogen vehicle demonstration,
- A preliminary determination on the cost and feasibility of a hydrogen pipeline from the Southeast to Southern California, and
- A summary of the day to day hydrogen issues industry is interested in.

Since the contract has not yet been signed, there are no key findings at this time. Industry will be extensively involved in providing much of the information for this project. All materials for the project will be reviewed by the NHA's Technology Review Committee and the NHA Board of Directors. All NHA members will receive copies of the final report. The project expects to extensively use infrastructure information developed by Dr. Joan Ogden, Center for Energy and Environmental Studies, Princeton University and current production information produced by Barbara Heydorn at SRI. A number of NHA and non-NHA members will be contacted for information and review during the course of this study.

Background

Sometime beyond 2000, hydrogen will be the energy carrier of choice due to its efficiency, environmental benefit, and flexibility. The National Hydrogen Association (NHA) is dedicated to working with industry and government toward rapid implementation of hydrogen technology. Toward that aim the NHA has undertaken this effort with NREL and DOE to identify near term hydrogen opportunities. The purpose of this effort is to identify near-term opportunities for hydrogen production and utilization. These opportunities could include "dump" hydro in the Pacific Northwest, hydrogen as refinery offgas in the Gulf States, byproduct hydrogen production from the chlor-alkali industry, or hydrogen storage and use for enhanced renewable electricity production in Alaska. In this study, the NHA will network with industry, utilities, regulators, and others to identify and evaluate potential sources and opportunities for near-term hydrogen production. Potential venture opportunities will also be described.

For commercialization to succeed, critical issues surrounding hydrogen production, distribution, storage, safety, and infrastructure must be examined from the perspective of those selling, shipping, and using hydrogen in the marketplace. The NHA will assist NREL and DOE in analyzing potential near-term markets and assess the technical, institutional, and regulatory issues that must be addressed before commercial hydrogen energy markets emerge. The evolution of commercial opportunities is a continuing effort on a changing landscape that one study can not adequately address. However, this study can facilitate partnerships, identify barriers, and present industry interests and motivations for engaging in various near-term venture projects that will take hydrogen from a specialized industrial product to a widely available energy carrier. The NHA will recommend to NREL and DOE various venture opportunities with industry that lead to launching commercial-scale deployment of hydrogen production and end-use technologies.

The study is divided into four distinct activities:

- Update hydrogen production and use data,
- Identify and describe near-term venture opportunities,

- Discuss near-term hydrogen supply in Southern California, and

- Public information and education on hydrogen issues.

With the exception of the public information and education activity, the reports on each activity will be reviewed by the NHA Technology Review Committee and the NHA Board of Directors before being sent to NREL. (lists attached)

Survey of Hydrogen Production and Use

The NHA will update and extend information on hydrogen production and use contained in the Chemical Economics Handbook by surveying industrial producers and users in the United States and Canada. In support of this effort, the NHA will survey industry about hydrogen production by industry type and identify yearly output and consumption, quantity of sales, and type of production or use of hydrogen. The hydrogen costs in the *Hydrogen Technology Assessment Report, Phase I* will be updated, and develop cost, performance, and demand information on steam reformed hydrogen. In this effort the NHA will contact producers to obtain information regarding demand for steam reformed hydrogen, cost ranges for steam reformed hydrogen, and average amounts of hydrogen shipped by pipeline annually in the United States. The NHA will not be responsible for supplying confidential information or disaggregated (company by company or plant by plant) data.

The approach toward carrying out this activity is:

Develop a regional hydrogen database. The NHA plans to aggregate the data in SRI's report on hydrogen markets and display the information in an applications-and-use matrix. The categories for the matrix are yet to be determined. Once the matrix has been laid out, hydrogen producers and others will be contacted to fill in the gaps that exist. Prices for steam reformed hydrogen will be obtained from hydrogen producers, most of whom are NHA members. The steam reforming information to be obtained from the producers include: the size of the facility, cost of natural gas, cost of the facility, aggregated cost of O&M, and cost of hydrogen produced.

Update the Hydrogen Technology Assessment Report, Phase 1. The values obtained for steam reformed hydrogen will also be used to update the NHA Hydrogen Technology Assessment Report, Phase 1, and will be compared to those presented in DOE's pathway analysis used in the *Hydrogen Program Plan*. Pipeline costs and operating data will be updated from the base year 1989 to 1993 or latest available year using the wholesale price index for those costs not directly obtained as a result of this study. A copy of the updated report will be produced and provided to NREL.

Review annual hydrogen pipeline shipments by hydrogen producers. This information will be obtained from U. S. hydrogen producers along with specifications on hydrogen pipeline costs and operating data discussed later.

Develop a targeted questionnaire. Producers, whether they are members of NHA or not, will be interviewed about demand for hydrogen by region and industry. The results will be summarized and contained in the task report.

Potential Near-Term Venture Opportunities

This activity focuses on seeking out and describing venture opportunities to produce, store, ship and use hydrogen as an energy carrier. Particular attention will be given to those regions of the country where public/private ventures are being discussed, budgeted, or begun. Since one of the regions of intense hydrogen activity is California, information developed in this activity will be used in other activities within the study. The emphasis in this task is on end-use demand for hydrogen and the necessary hydrogen supply and capacity required to satisfy that demand.

The approach to identify near-term opportunities will be composed of three parts:

- Identify consortia that the NHA and its members know of by talking to NHA members
- Review Press articles, news releases and other periodicals, and
- Speak to non-NHA members identified through contacts with NREL, DOE, NHA inquiry list, NHA member leads.

Once the list is developed, create a list of questions for each venture. Then contact participants and contractors and interview them. For each venture write summaries--*Venture Briefs*--that characterize the project, its purpose, cost, role and interest of the participants. From that, prognosticate hydrogen demand implications of widespread commercialization of as many of these efforts as possible.

Another component of this activity is to identify the flexibility and size of the hydrogen supply in the Southeastern U.S. The NHA plans to apply the data from the Survey of Hydrogen Production & Use Task to the Southeastern U.S., broken down by state. NHA members will verify information accuracy and supplement as it is necessary. In addition, the NHA will produce a listing by industry and state of hydrogen production in the Southeastern U.S.

The final effort in this task is to discuss, with NASA facilities in the Southeastern U.S., their interest in hosting a hydrogen fleet demonstration. The NHA plans to identify contacts at Marshall, Stennis, and Kennedy, (all facilities with extensive hydrogen handling capability), and speak with them about their interest in hosting a hydrogen vehicle demonstration and summarize their responses and level of interest.

Near-Term Hydrogen Supply in Southern California

Almost all of the existing supply of hydrogen is produced from steam reforming natural gas. Taking Southern California as a study area, the NHA will assist NREL in evaluating supply and demand of hydrogen produced in the area, as well as the cost of importing hydrogen from other parts of the U.S., specifically the Gulf States. The NHA will identify and discuss the perspectives, interests, and needs of industry and other hydrogen stakeholders in developing a hydrogen energy industry in the study area. Identification of specific venture opportunities in Southern California will be included in this task.

In this activity, the NHA plans to use the database information to summarize the current supply and demand for hydrogen in Southern California. Once this data is in suitable form, the NHA plans to gain input from members and non-members like Princeton University's Center for Energy & Environmental Studies and SRI, about hydrogen use, infrastructure requirements, and hydrogen demand. Once supply

and demand have been estimated, review literature and contact hydrogen producers that operate pipelines to determine operating pressures, frequency of booster stations, specifications for piping used, installation procedures, pipe cost, quantity of hydrogen shipped as a function of pipe size, overall cost-per-mile of installed pipe, etc. This information will be used to calculate the cost of a hydrogen pipeline from the Southeastern U.S. to Southern California and the incremental increase in the cost of hydrogen due to pipeline transmission. These results will be summarized in a matrix of hydrogen pipeline parameters and costs.

Using the information developed previously on Southern California demonstrations, the NHA will examine in greater depth, three major demonstrations in Southern California that DOE might have an interest in participating in. If three suitable candidates do not exist in Southern California, then one of the demonstrations might be from another region of the United States. As a part of the investigation, each of the participants will be asked about their interest in DOE support for the demonstration, and what, in their view, is the appropriate role for DOE in furthering the commercial development of that technology. A project summary will be prepared that includes: a project description, the roles of the participants, market potential, state of technology, and a recommended role and level of DOE participation in the effort, if appropriate. A report will be prepared on the findings from this activity.

Public Information and Education on Hydrogen Issues

The purpose of this activity is to develop an insight of the interest and issues that industry has with respect to hydrogen. The NHA will be assisting DOE in disseminating information to the public on hydrogen and on the DOE program, such as the *Multi-Year Hydrogen Program Plan* and the *Hydrogen Program Implementation Plan*. The activities associated with this task include responding to industry and other inquiries about hydrogen, categorizing the source and type of inquiry, the nature of the interest, the recommendations made by the NHA, and any actions taken by the NHA as a result of the inquiry. The output from this task is a quarterly report on the summary of the information mentioned above.

Synopsis

This is a broad-based approach to find and take industry's pulse with respect to hydrogen. The effort ranges from passively assessing interest based on industry inquiries to actively pursuing demonstration project participation. It provides NREL with a view of what activities are moving forward with, and without, DOE involvement. It should provide a road map for identifying which hydrogen activities can be enhanced by DOE participation. The next step is to identify which projects should be done, but are not planned. The final project report for the study should be delivered to NREL by October 1, 1994.

Funding: $100,000

NHA TECHNOLOGY REVIEW COMMITTEE

Chairman

Christopher Blazek
Asst. Director, Energy Systems & Applications
Energy Development Center,
Institute of Gas Technology

Mikio Abe
Executive Director
Nippon Sanso

Dr. John Appleby
Director
Center for Electrochemical Systems & Hydrogen Research

Addison Bain
Hydrogen Program Manager
NASA

Dr. Kirk Collier
Director, PV & AT Division
Florida Solar Energy Center

Ray Drnevich
Mngr., Technology Contract Acquisition
Praxair, Inc.

Thomas Cawthon
Hydrogen Program Manager
National Renewable Energy Laboratory

Keith Krause
Mngr., Customer Services/Engineering
Air Liquide Corporation

Ben Mehta
Project Manager, Hydrogen Technology
Electric Power Research Institute

Robert Moore
Senior Manager, Economic Evaluation
Air Products and Chemicals, Inc.

Rhett Ross
Engineer Sales Manager
Energy Partners, Inc.

Neil Rossmeissl
Hydrogen Program Manager
U.S. Department of Energy

Dr. James A. Schwarz
Professor, Chemical Engineering
Syracuse University

Drexel Smith
Director, Program Development
Wyle Laboratories

NHA Board of Directors
1994/1995 Class

Chairman
John Kennedy
AlliedSignal

Vice Chairman
Edward Trlica
Energy Partners

Vice Chairman
Patrick Takahashi
Hawaii Natural Energy Institute

Jim Braselton
Airco Gases

Michael Stimson
Air Liquide America

Frank Frenduto
Air Products & Chemicals

Keith Prater
Ballard Power Systems

Dr. Dieter Volk
Daimler-Benz

Ira Kuhn
Directed Technologies

Elie Shama
Econoden

Sandy Stuart
Electrolyser Corporation

Bradford Bates
Ford Motor Company

Dominique Kluyskens
Hydro-Quebec

Toschiichi Takematsu
Iwatani International

Mikio Abe
Nippon Sanso

Mike Hainsselin
Praxair, Inc.

Bud Beebe
Sacramento Municipal Utility District

Carol Bailey
Southern California Gas Company

Toby Kincaid
Solardyne

Jay Laskin
Teledyne-Brown Energy Systems

Demonstration and Consortium Projects
United States Only

Alaska

Aleutian Islands

Hydrogen as storage for geothermal and wind power. Produced hydrogen will also be used when renewable sources are not optimal and will provide potential export for state. All end users will be remote villages on the Aleutian Island chain.

Players: Alaska Global Hydrogen Corporation*, Alaska State Energy Office, Aleut Energy Company, Electrolyser Corporation*, other parties to be named.

Contact: Jack Wood, Alaska Global Hydrogen Corporation.

California

Sacramento

Solar Hydrogen compressor project to aerate fish tanks in University Marine Laboratories.

Players: Humboldt State University, Sacramento Municipal Utility District*

Contact: Peter Lehman, Chemical Engineering, Humboldt State

[redacted]

Fuel Cell Bus Project using solar produced hydrogen, compressed and stored on board.

Players: Sacramento Municipal Utility District*, Schatz Fuel Cell Lab at Humboldt State University, Center for Electrochemical Systems and Hydrogen Research at Texas A&M University*

Contact: Bud Beebe, Sacramento Municipal Utility District

[redacted]

Livermore

"Helios Project"--unmanned small aircraft powered by fuel cell using hydrogen stored on board.

Players: AeroVironment, United Technologies, Siemens Solar, Lawrence Livermore*

Contact: Jim McElroy, United Technologies

[redacted]

Santa Clara

Groundbreaking on a 2MW molten carbonate fuel cell unit for the City of Santa Clara Utility.

Players: Energy Research Corporation, City of Santa Clara, State of California, Fuel Cell Commercialization Group

Contact: Bill Baker, Energy Research Corporation

Diamond Bar

200kW Phosphoric acid fuel cell demonstration unit operating at the SCAQMD office. Unit was installed and is maintained by Southern California Gas.

Players: SCAQMD*, Southern California Gas.*

Contact: Alan Lloyd, SCAQMD

Phosphoric acid fuel cell locomotive consortium to use on-board hydrogen.

Players: SCAQMD*, Fuel Cells for Transportation†, GM ElectroMotive Div., Burlington Northern, U.S. DOE (OTT)*.

Contact: Alan Lloyd, SCAQMD

Solid polymer fuel cell bus commercialization-scale demonstration using compressed hydrogen storage.

Players: SCAQMD*, Ballard Power Systems*, B.C. Transit, Provincial Government of British Columbia

Los Angeles Residential Project--demonstration using solid polymer fuel cell to supply residential electric power and use iron oxide hydrogen storage.

Players: H-Power, SCAQMD*, Rolls-Royce, Johnson Mathey, Southern California Gas Company*

Contact: Joe Maceda, H-Power

Riverside

IC engine conversions using solar-produced hydrogen stored on-board.

Players: SCAQMD*, University of California Riverside, Electrolyser Corporation*, Hydrogen Consultants, Inc.*

Contact: Jim Heffel, University of California, Riverside.

El Segundo

IC engine vehicle conversions using solar-produced hydrogen stored on-board. Vehicles are part of Xerox facility's fleet and will continue to operate in that environment.

Players: Xerox, Clean Air Now!†, ARPA, Praxair*, United Technologies, Hydrogen Consultants, Inc.*, City of El Segundo.

Contact: Paul Staples, Clean Air Now!

Irvine

Commercialization-scale hydrogen IC vehicles road tested in 1995.

Players: Mazda R&D of North America*, Mazda of Japan, Hydrogen suppliers.

Contact: Vahe Kludjian, Mazda R&D.

Colorado

Denver

IC engine conversion to run on HYTHANE, a blend of 95/5 methane-to-hydrogen by weight. Includes comparison with comparable natural gas and gasoline vehicles, and a HYTHANE refueling station.

Players: Hydrogen Consultants*, Air Products & Chemicals*, City and County of Denver, Public Service Company, Public Technologies' Urban Consortium.

Contact: Deborah Kielian, City and County of Denver.

Michigan

Detroit

Solid polymer fuel cell demonstration vehicle to use on-board compressed hydrogen.

Players: Ford Motor Company*, Directed Technologies*, U.S. DOE (OTT)*, hydrogen suppliers, fuel cell suppliers to be named and others to be named.

Contact: Bradford Bates, Ford Motor Company

New York

White Plains

Construction of commercial production plant using Hytex® technology and air separation to produce hydrogen from various fuel feedstocks.

Players: Praxair* and Texaco

Contact: Michael Kerr, Praxair

Syracuse

Small-scale demonstration solid polymer fuel cell vehicle using advanced carbon as on-board storage.

Players: Niagara Mohawk, Syracuse University*, U.S. DOE (OEM)*, National Renewable Energy Laboratory*, YTi, Inc.

Contact: Karl Young, YTi

Pennsylvania

Erie

IC vehicle conversions using HYTHANE fuel, and HYTHANE refueling station.

Players: Bruderly Engineering, Hydrogen Consultants, Inc.*, Air Products & Chemicals*, Pennsylvania Energy Office, National Fuel Gas Company

Contact: Venki Raman, Air Products

Pittsburgh

Phosphoric acid fuel cell demonstration at the Pittsburgh airport. Will be used for an EV recharging station.

Players: Pennsylvania Energy Office, Westinghouse, Pittsburgh Airport, Mid-Atlantic Regional Consortium for Advanced Vehicles.

Contact: Dan Desmond, Pennsylvania Energy Office

Mid-Atlantic

Mid-Atlantic Regional Consortium for Advanced Vehicles is a large consortium that includes the states of: New York, New Jersey, Pennsylvania, Delaware, Maryland, Virginia, Washington DC and West Virginia. The Consortium also consists of a number of large and small companies and research centers

that combine consortium funds and ARPA funds for various demonstration projects are part of a commercialization plan.

Projects include:

- two hybrid buses and one hybrid taxi to include the following technologies (not necessarily all in one vehicle): atmospheric pressure solid polymer fuel cell with on-board hydrogen storage, advanced flywheel and lithium polymer batteries.
- 15-75 kW multi-gaseous fueled hybrid gen set (gaseous fuels will be hydrogen, hythane, methane and propane).
- "Intelligent battery" diagnostic smart switch technology for EVs.
- Advanced HV/AC hydride heat pump (is CFC-free) for vehicles.

South Carolina

Aiken

Hydrogen refueling facility using steam reforming and hydride storage.

Players: Westinghouse Savannah River Facility, Exxon, others to be named.

Contact: Bill Summers, Westinghouse Savannah River

Georgia

Atlanta

Hydrogen IC Transit Bus using hydride storage to be used at the 1996 Olympics.

Players: Westinghouse Savannah River Facility, Georgia Tech, City of Augusta, Georgia Power.

Contact: Bill Summers, Westinghouse Savannah River

Florida

Cape Canaveral

Hydrothane project in an IC Ford Crown Victoria. This project uses higher hydrogen content methane/hydrogen blend.

Players: NASA*, Florida Solar Energy Center*, Praxair*, City Gas of Florida, EG&G.

Contact: Addison Bain, NASA

West Palm Beach
Known as the PEM fuel cell demonstration using compressed hydrogen storage. Energy Partners Green Car Project.

Players: Energy Partners*

Contact: Rhett Ross, Energy Partners

West Palm Beach
Prototype designs for fuel cell manufacturing facilities.

Players: Energy Partners*, Florida Solar Energy Center*, State of Florida, Florida Atlantic University, Florida Institute of Technology.

Contact: Rhett Ross, Energy Partners

Alabama

McIntosh
Construction of a commercial hydrogen production facility using by-product hydrogen from chlor-alkalai manufacturing.

Players: Praxair*, Olin Chemical

Contact: Michael Kerr, Praxair

Louisiana

Plaquemine
Molten carbonate fuel cell demonstration using coal-derived syngas.

Players: EPRI*, Energy Research Corporation, Destec Energy.

Contact: Bill Baker, Energy Research Corporation

Washington DC

Phosphoric acid fuel cell bus using reformed methanol from on-board reformer will be demonstrated sometime this year.

Players: Georgetown University*, U.S. DOE (OTT)*, H-Power, other players.

Contact: Sam Romano, Georgetown University

[redacted]

Solid polymer fuel cell vehicle bench-scale test using reformed methanol from on-board reformer to be demonstrated in 1997.

Players: SCAQMD*, DOE (OTT)*, Dow Chemical, Ballard Power Systems*, GM (formerly their Allison Division).

Contact: Pandit Patil, U.S. DOE

[redacted]

USCAR and Clean Car Initiative Projects. Among other projects, will include hybrids and fuel cell vehicles using hydrogen.

Players: Initially, Big Three auto companies, Department of Energy (OTT has lead for DOE), Department of Commerce (Mary Goode). Others to be named as projects develop.

* Denotes NHA Member
† Denotes participating membership association of NHA's Colleagal Relationship Information

Answering Hydrogen Inquiries from the Public

Typically, phone call inquiries that come into the National Hydrogen Association are from industries and small business that want to learn more about the NHA and its programs, or use us as a networking tool. All phone calls result in an NHA information packet being sent and adding the caller's name, affiliation, address, phone and fax number to the NHA database.

Often, the caller's questions are aimed at a specific technology, application or method of production, and NHA staff is able to give them general information and an aggregated view of the relevant industry or research group. For very detailed technical information about a specific process, or questions aimed at collaborative efforts, the NHA staff, after making a judgement decision on the level of seriousness and knowledge of the caller, recommends further contact from among its members, colleagues, or network.

The NHA has a policy on handling questions about hydrogen and its enabling technologies: All correspondence results in at least one action item. If the phone call, fax or letter did not generate some reciprocal activity on the part of the NHA, then we did not perform our job of information transfer.

For the quarterly reports that are submitted to NREL, information will be conveyed on the attached form. The reports will include a catalogue, listed alphabetically by organization, and assigned a code indicating the type of organization they are, e.g., industry, small business, membership organization, student, etc. Each name will be added to the NHA's existing database, and one printed copy and diskette copy will be given to NREL at the termination of the contract.

Inquiry Response Form

NAME: _____

COMPANY: _____

ADDRESS: _____

_____

PHONE _____ FAX _____

E-MAIL _____

COMMENTS

ACTIONS TAKEN

NHA DATABASE CODE

CLASSIFICATION TYPE

SUPPORTING ANALYSES AND ASSESSMENTS: HYDROGEN MARKET ANALYSIS

Jim Ohi
National Renewable Energy Laboratory
Golden, CO 80401

Abstract

Supporting analysis and assessments can provide a sound analytic foundation and focus for program planning, evaluation, and coordination, particularly if issues of hydrogen production, distribution, storage, safety, and infrastructure can be analyzed in the context of a competitive marketplace. The overall purpose of this activity is to conduct key analytic tasks—such as market status, opportunities, and trends; environmental costs and benefits; and regulatory constraints—to help establish a long-term and systematic analytic foundation for program planning and evaluation. Within this context, the purpose of the project is to help develop near-term transition strategies to achieve the long-term goal of the Hydrogen Program. In FY94, NREL will develop a cooperative effort with industry, the National Hydrogen Association (NHA), state/regional regulatory agencies, and other federal agencies to identify and evaluate near-term market opportunities for hydrogen utilization. The goal of this project is to identify one or more potential industrial partnerships for near-term hydrogen, production, distribution, and utilization. Activity to date is reported.

Project Rationale

Supporting analysis and assessments can help establish a sound analytic foundation and focus for program planning, evaluation, and coordination. The overall purpose of this activity is to address key issues—such as market status, opportunities, and trends; environmental costs and benefits; and regulatory constraints and opportunities—to help establish a long-term and systematic analytic foundation for program planning and evaluation. One key need under program planning is defining and implementing a transition strategy to achieve the long-term goals and objectives of the Hydrogen Program through near and mid-term initiatives, activities, and projects. This transition strategy must ensure that near-term efforts are part of a cost-effective and coherent path to achieve the strategic and long-term programmatic goals. As part of defining a transition strategy, hydrogen production, distribution, storage, safety, and infrastructure needs should be analyzed in the context of a competitive marketplace. In pursuing near-term efforts as part of a transition strategy, it is particularly important to work closely with industry and to analyze critical technical and non-technical issues within an actual market context. In summary, the project will help identify and develop near-term efforts with industry as part of transition a strategy to achieve the long-term goals of the Hydrogen Program.

Approach

In FY94, NREL has begun to develop a cooperative effort with industry, the National Hydrogen Association (NHA), other industry associations, state/regional agencies, and other federal agencies to identify and evaluate near-term market opportunities for hydrogen production, storage, distribution, and utilization. The NHA will survey the hydrogen industry and provide a status report on existing hydrogen production, storage, distribution, and utilization. The NHA will also obtain the industry's perspective on near-term business opportunities. Based on the NHA survey of industry status and the industry's perception and interest in near-term opportunities, NREL will identify and evaluate potential projects for near-term hydrogen production, storage, distribution, and utilization in the utility, industrial, and commercial energy sectors. Potential near-term opportunities in the utility sector include sources of inexpensive electricity such as "spilled hydro" from the Bonneville Power Authority and other large hydroelectric systems for hydrogen production through electrolysis. In the industrial sector, potential near-term opportunities include higher-value use of hydrogen generated as a by-product of industrial processes, such as sodium chlorate production. In the commercial sector, the potential use of hydrogen as a fuel for mobile and stationary energy needs of eco-tourism facilities will be explored. Based on this inventory and evaluation, NREL will identify potential near-term opportunities, develop evaluation criteria based on industry input and needs, and explore selected opportunities for cost-shared, collaborative government- industry projects that will further the strategic and long-term goals of the Hydrogen Program through co-development of critical near-term technologies for hydrogen production, storage, distribution, and utilization.

Key Results

Progress to date on identifying and evaluating potential opportunities and industrial partnerships for near-

term hydrogen, production, distribution, and utilization are described below by energy-use sector.

Utility Sector

NREL is conducting major analytic activities for the DOE Office of Utility Technologies and for the Office of Planning and Analysis on utility issues. These activities include integrated resource planning involving, for example the National Association of Regulatory Utility Commissioners (NARUC), the Independent Power Producers Association, and the American Public Power Association, and a major project on identifying and assessing the needs of principal stakeholders in renewable energy generation, including major utilities, the DOE Power Marketing Administrations (PMAs), major financial institutions and investors, manufacturers, and all major renewable energy industry associations. NREL is also conducting a major technical, economic, and environmental study of distributed utility generation. These and other complementary efforts at NREL, other national laboratories, and in the public and private sectors will be coordinated with this activity to identify and evaluate near-term market opportunities for hydrogen in the utility sector.

Bonneville Power Administration (BPA)

The BPA is developing a R&D strategy as part of a comprehensive reorganization effort to redefine itself and its role in the Northwest energy market. The BPA is interested in dispersed generation and in hydrogen generation, storage, and use to meet peak seasonal demand. According to the BPA, water flow on the Columbia River will be determined more by the needs of the salmon fishery than by the needs of the BPA system for power generation to meet customer demand. Hydrogen could meet an important need if it can be generated economically during peak river flow in the spring, stored over summer and fall, and used to generate electricity during winter to help meet peak demand. Hydrogen has the potential to enable the BPA to meet both its energy and environmental needs, particularly if seasonal storage can be provided. NREL will work with the BPA (after reorganization) to address the critical generation, storage, distribution, and conversion issues. NREL will assess issues concerning technology, economics, and infrastructure for integrating hydrogen into the BPA system.

Euro-Quebec Hydro-Hydrogen Pilot Project (EQHHP)

NREL will explore opportunities for cooperation and collaboration with the EQHHP, which includes hydrogen storage and transportation, urban transportation applications, and market/distribution studies.

EPRI Utility Interest Group

NREL is exploring a collaborative study and evaluation of hydrogen -enhanced gas turbine combustion for NO_x control with this group. This informal group includes gas and electric utilities and turbine manufacturers. NREL will also explore opportunities for hydrogen-enhanced gas turbine combustion for NO_x control in rapidly urbanizing states with strict emission controls such as Florida and California.

Industrial Sector

NREL is working with industry on a number of cooperative research and development agreements on technologies, ranging from advanced vacuum insulation for thermal management of high-temperature batteries with the US Advanced Battery Consortium to producing ethanol from municipal solid waste with the Amoco Corporation. Based on this experience, NREL will explore opportunities for near-term, cost-

shared technology development with industrial partners. NREL will begin by contacting major industry associations, such as the Compressed Gas Association, the National Petroleum Refiners Association, the American Independent Refiners Association, the National Petroleum Council, and the Chemical Manufacturers Association, to obtain information on potential users of hydrogen in the industrial sector.

By-Product Hydrogen from Chemical Production

NREL will identify industrial by-product hydrogen, for example from sodium chlorate production and evaluate storage, distribution, and higher-value use options for this supply source. Potential industrial collaborators include the Kerr-McGee facility in Mississippi for alternative by-product hydrogen use and a Dow Chemical plant in Louisiana for hydrogen- enhanced natural gas turbine combustion to meet tighter emission controls. NREL is also exploring linkages of this effort with the Texas Sustainable Economic Development Commission, which is interested in hydrogen as a transitional and end fuel for sustainable economic development.

Foster Wheeler/Energy Technology Engineering Center (ETEC)

NREL is exploring a potential collaborative effort with Foster Wheeler and ETEC to develop a small-scale natural gas reformer that would be suitable for decentralized hydrogen fueling stations. NREL will also contact other critical potential participants, such as the Southern California Gas Company, the Gas Research Institute, Air Products, and Oak Ridge National Laboratory to assess the near-term market potential for small-scale, distributed natural gas reforming stations for hydrogen refueling.

Commercial Sector

The near-term focus for this sector will be hydrogen applications in buildings and in business ventures that can take advantage of environmental qualities of hydrogen use and renewable energy sources for hydrogen production. NREL conducts a comprehensive R&D program on energy efficient and renewable energy technologies for buildings, including passive and active heating and lighting technologies and computer-assisted building envelop design. NREL is also involved in a major program in DOE's Office of Transportation Technologies to develop fuel cells for transportation applications. The timely development of a hydrogen fuel infrastructure is a critical issue for this program.

Natural Energy Laboratory for Hawaii (NELH)-Hilton Hotels

In the commercial sector, NREL will explore the potential of hydrogen generation, storage, and use as part of the growing interest in eco-tourism. The Hilton Hotels has expressed interest to the NELH in exploring the use of hydrogen generated locally to fuel vehicles and to fuel boats used for diving and other marine activities on its resort at Kona on the big island. The NELH is interested in exploring a number of hydrogen generation options based on indigenous renewable energy resources.

Definition of Success

The project will be successful if NREL can facilitate partnerships among industry, utilities, and government (local, state, federal) to enter into venture opportunities for near-term hydrogen production,

storage, distribution, and use. A key measure of success will be the willingness of industry to co-develop critical near-term transitional hydrogen technologies with the DOE. The project can then make an important contribution toward linking near-term demonstration efforts with the long-term strategic goals of the Hydrogen Program. Other measures of success include helping to transfer technology and information to industry and other stakeholders.

Proposed Future Work

Proposed future work will depend on the outcome of on-going work, but a number of follow-on efforts are possible. These include:

- A systematic method to identify and screen potential near-term market opportunities, based on existing and projected market trends and industry activity, regulatory constraints and opportunities, regional interests and development patterns, etc.
- Comprehensive criteria to evaluate near-term demonstration opportunities based on industry perspectives and needs.
- A collaborative effort with ETEC to develop a component/system modeling and testing capability for hydrogen production, storage, and dispensing options.
- A comprehensive programmatic benefits analysis to develop quality metrics based on energy, economic, environmental, and equity criteria to help evaluate program strategy, options, priorities, and direction based on projected benefits streams

Technology Transfer

The project embodies technology transfer because its purpose is to identify, evaluate, and propose near-term, cost-shared, venture opportunities to produce, store, distribute, and use hydrogen. Close interaction with industry will be key to the success of this project.

Acknowledgements

The author would like to thank Neil Rossmeissl, DOE Hydrogen Program Manager, for encouragement and guidance on this project and for supporting a comprehensive analysis and assessment effort in the Program; Tom Cawthon, NREL Hydrogen Program Manager for guidance, support, and review of the paper; and Pat Takahashi, Hawaii Natural Energy Institute, for providing key contacts. In acknowledging these people, the author does not relinquish complete responsibility for any errors in the paper.

ENERGY PATHWAY ANALYSIS

Joseph S. Badin, George Kervitsky,
and Stephen Mack
Energetics, Incorporated
Columbia, MD 21046

Abstract

An analytical framework has been developed that can be used to estimate a range of life-cycle costs and impacts resulting from environmentally-driven, market-based, and prescriptive scenarios. This ten month effort has resulted in a comparative normalized analysis of energy pathways that encompass incremental production, storage, transport, and use of different fuels or energy carriers, such as hydrogen, electricity, natural gas, and gasoline. This analytical framework is the result of a series of recommendations of the Hydrogen Technical Advisory Panel after its review of the U.S. DOE Hydrogen Program Multiyear Plan FY 1993 - FY 1997.

The pathways provide DOE with an indication of near-, mid-, and long-term technologies that have the greatest potential for advancement and can meet cost goals. The individual pathways have been linked into a linear programming network model. The methodology and conceptual issues are discussed. Also presented are results for selected pathways from the E3 (Energy, Economics, Emissions) Pathway Analysis Model and from selected scenarios for the E3 Network Analysis Model. The analyses are framed by economic considerations of decisionmaking to select energy pathway or fuel cycle options. To be a competitive energy resource, the environmental, efficiency, and domestic sustainability benefits of utilizing hydrogen must outweigh the total production and delivery cots. The aim of these studies is to identify the pathways that maximize the difference between total consumption benefits and total production costs. When this condition is reached, economic efficiency is achieved. Differential life-cycle costs criteria can be used to judge whether a considered pathway improves economic efficiency relative to the status quo or to some other energy investment.

Pathway results and network scenarios will identify the magnitude of the technical, economic, and societal (infrastructural) challenges which need to be overcome to effect a transition to a hydrogen-electricity economy. Analytical results will suggest various hydrogen energy applications that have early market possibilities. This information can accelerate the development of hydrogen energy systems for market

possibilities. This information can accelerate the development of hydrogen energy systems for market introduction. Future work will consist of the expansion of the models to include: system measures of reliability and safety; a more diverse set of nodal activities; complete update of the Multiyear Plan appendices; coordination with the International Energy Agency Agreement (IEA) Annex 11, Integrated Systems; aircraft applications; and additional scenario development and analysis.

The pathway/network framework will be made available as an analytical tool to screen competing system options for regional or site-specific conditions. For example, candidate systems or strategies are being proposed for Southern California, Alaska, and other sites. Total pathway impacts of each strategy need to be evaluated. Coordination with industry and national laboratories will allow a continuous update of input values and additions to pathway activities that will keep the models relevant and useful. This framework can also be applied in the screening process of candidate demonstration projects. Additionally, this work complements system simulation activities proposed in the IEA Agreement and helps to integrate the results of ongoing projects in the program.

Introduction

Hydrogen has long been envisioned as a desired energy carrier for the future sustainable energy economy. Hydrogen is not a primary resource, but must be manufactured at significant costs and primary energy consumption. To be a competitive energy resource, the environmental, efficiency, and domestic sustainability benefits of utilizing hydrogen must outweigh the total production and delivery costs. The aim of system studies and analyses is to identify the pathways that maximize the difference between total consumption benefits and total production costs. When this condition is reached, economic efficiency is achieved. Differential life-cycle costs criteria can be used to judge whether a considered pathway improves economic efficiency relative to the status quo or to some other energy investment. It is emphasized that our analysis is framed by economic considerations of decision making to select energy pathway or fuel cycle options: this means that financial models are used to structure the organization and scope of the analysis and that the analysis of physical phenomena, such as emissions, reliability, safety, and impacts, is driven by concern for estimating monetary values.

In order to provide answers to the questions posed from considering the multi-dimensional aspects of economic efficiency, the U.S. DOE Hydrogen Program has expanded its System Studies program element. System studies are a broad coordinated set of efforts in the areas of life-cycle cost analysis, market analysis and assessment, environmental analysis, and assessments of system safety and reliability.

Coordinated analyses of the integration of component technologies will ensure that the Federal investment is directed to systems that could actually be deployed. Such activities will identify and quantify estimates of the implications of the transition to the hydrogen energy economy and the actions that could influence its evolution. System studies will identify the magnitude of the technical, economic, and societal (infrastructual) challenges which need to be overcome to effect such a transition. Analytical results will suggest various hydrogen energy applications that have early market possibilities. This will accelerate the development of hydrogen energy systems for market introduction.

Analytical Framework

An energy economy is comprised of a diverse set of energy technologies and pathways serving the needs of the various demand sectors. An energy pathway is a series of source to end-use processes defined by particular technologies. Pathways include primary energy sources, conversion processes, energy storage, methods of delivery, and end-uses, as shown in Figure 1.

The primary objectives of the energy pathway framework are:

- To create a unified conceptual design for organizing the various costs, performance, and physical measures associated with the production and consumption of energy from different fuel types;
- To demonstrate an accounting framework that can be used to estimate measures of costs and impacts along a pathway that result from an incremental use of different fuel types and use this information in a comparative analysis;
- To identify critical trends, impacts, issues, and information needs that will affect the expanded analytical efforts to develop comprehensive assessments of energy pathways for large-scale delivery.

The economic evaluation of technologies is not straightforward because tradeoffs are made between cost, efficiency, and other properties, and different technologies may turn out to be more advantageous depending on the entire scenario or pathway within which they are considered. Thus, different pathways are evaluated by means of a system model. The E3 Pathway Model considers efficiency, capital costs, life-cycle costs, and emissions. The analysis pinpoints targets of opportunities as a result of sensitivity studies. Thus, the analysis leads to guidelines and goals for technology development and provides a framework for decision making.

The structure and data flows of the E3 Pathway Model are shown in Figure 2. The model is run in a relational database environment, PARADOX® 4.0. The model contains libraries of activity nodes (pathway steps) by technology with data for current and advanced scenarios. Also included are libraries for financial data, emission values, and for analyzed pathways. Data libraries are described in more detail in Table 1. Reports can be generated in both tabulated and graphical formats.

Table 1. Description of Data Libraries

Data Set	Description	Parameters
Activities Library	Technology characterization cost and performance data • Current status • Advanced	Capital Cost ($/kW), ($/kWh) O&M; Fixed ($/kW-yr), variable ($/kWh-yr), % of capital ($/yr) Capacity Factor (%) Efficiency (%) Life (yrs) Emissions (g/kWh); CO_2, NO_x, SO_2

Node-Pairs Library (Directly Linked to Activities Library)	Establishes links among energy conversion, delivery, and end-use activities	"To" Node "From" Node Activity Type (technology)
Pathway Library	Saved and completed pathway analyses	Energy IN/OUT Annual Cost ($/Yr) Present Worth ($) Levelized Cost ($/kWh delivered) Emissions (tons/yr)
Financial Library	Discounted cash flow data for life-cycle analysis	Discount Rate (%) Inflation Rate (%) Depreciation (yrs) Tax Rate (%) Property taxes and Insurance (%)

Progress in Pathway Analysis

Much progress in pathway analysis has been accomplished since the U.S. DOE Hydrogen Program Plan FY 1993 - FY 1997 was issued in June 1992. In that document, pathways were compared based on a first cost only screening criteria and on a preliminary screening of emission, as shown in Figure 3. In addition, the economic screening ended at the point of energy delivery without including the consumer segment of the pathway.

A rigorous methodology for estimating life-cycle costs and impacts for each energy pathway or fuel cycle was developed and modeled in the E3 Pathway Analytical Model. The following sections will briefly overview the energy efficiency, economics, and emission valuation approach used in the model.

Energy Efficiency

All pathways in this comparative framework are normalized to provide one kilowatt (kW) of equivalent power to an end-use customer. Energy delivered (in equivalent kilowatt-hours) is based on temporal demands characterized by an annual capacity factor or hours per year operated and dispatched.

Differences among the efficiencies of various pathways are accounted for in component cost, since larger or smaller system components are required to deliver a given amount of power depending on the efficiencies of downstream conversion steps. As shown by the following equation:

$$\text{Capacity } i = \text{Capacity } (i+1)/\text{Efficiency } (i+1) \qquad (1)$$

where (i+1) is the subsequent downstream process step. The required capacity of each component in the technology pathway per kW of delivered power is obtained by dividing the delivered power by the product of all efficiencies downstream. The overall system cost thus incorporates not only the cost of each technology, but also the capacity required in each transfer step.

Economics

The discussion of economic life-cycle cost valuation for pathway analysis highlights conceptual and practical issues that must be addressed to combine impact and economic information. The economic methodology for determining an estimate of life-cycle costs for each process step is represented by the following equations:

$$\text{Capital Recovery Factor (CRF)} = k/(1-(1+k)^{-N}) \quad (2)$$

where: k = real discount rate (weighted average cost of capital)
n = project life

$$\text{Fixed Charge Rate (FCR)} = \text{CRF}\ ((1-T(DPF) - (ITC)/(1-T)) + PTI \quad (3)$$

where: T = income tax rate
DPF = real depreciation factor
ITC = investment tax credit (currently = 0)
PTI = property taxes and insurance

Typical utility applications have a discount rate of 6.1% and a project life of 30 years.

$$\text{Life-Cycle Cost (\$/kWh)} = [P_{pw}(FCR_p) + R_{pw}(FCR_R) + CRF(OC_{pw})]/kWh_{out} \quad (4)$$

where: P_{pw} = present worth of plant capital
FCR_p = fixed charge rate for plant
R_{pw} = present worth of replacement capital
FCR_R = fixed charge rate for replacement
OC_{pw} = present worth of all annual and intermittent operating costs, fuels, and electricity costs, maintenance, and externalities.

Total pathway life-cycle cost is the sum of all the component calculated life-cycle costs. The E3 Pathway Analysis Model also contains an automatic parametric analysis option which forms the basis for sensitivity studies.

Emissions

Energy resources impose a variety of costs on society. Traditionally, the cost of energy resources have included only a portion of these costs such as capital cost, operation and maintenance, fuel/electricity cost, and fixed charges. Other costs, which can be substantial, have not traditionally been included in the cost structure. These costs, typically referred to as externalities, are real costs borne by society in the form of increased health care expense, economic impacts on material and agricultural resources, and reduced quality of life.

In recent years, economists, environmentalists, regulators, and other have debated whether the cost of externalities should be incorporated into the total cost of an energy resource. Economists argue that inefficient economic outcomes result when external costs are not incorporated in economic decisions. The suboptional outcomes can directly effect the quantities of energy that consumers demand and may lead society to pursue the "wrong" types of energy resource options. By accounting for external costs, the selection of energy sources and production of energy products can lead to an equilibrium, where the total

cost of energy and energy products, together with the resulting social costs, can be brought to an economic minimum, thereby reaching the condition of economic efficiency.

A variety of methods have been suggested for internalizing the cost of externalities, including the use of monetized emission costs, estimates, weighing and ranking schemes, fixed percentage production adders, and other approaches. Of these, two approaches, the use of monetized emission costs and fixed percentage production adders have gained a relative acceptance. To date, five states (CA, MA, NV, NY, OR) have adopted the use of monetized emission costs and others, including Wisconsin and Vermont, have adopted the use of fixed percentage production adders. The E3 Pathway Analysis Model allows for either approach to be used and includes representative emission values for CO_2, NO_x, SO_2 that are used by State Public Utility Commissions. Selected values are presented in Table 2. The model has an option to include state-specific or user-defined emission values into the annual operating costs of the life-cycle cost equation.

Table 2. Recommended Emission Values (1989 $/ton emitted)

Emission	Oregon OR	Massachusetts MA	New York NY	Nevada NV	BPA[a]	PACE University Study
SO_2	1,500	1,500	820	1,560	1,500	4,060
NO_X	884	6,500	1,780	6,800	69/884	1,640
CO_2	NE	22	2	22	NE	14

Emission	California[b] SDG&E/SCE CA	California[c] PG&E CA	California[d] CEC-In State CA	California CEC-Out of State CA
SO_2	18,300	4,060	12,460	1,080
NO_X	24,500	7,100	12,560	2,920
CO_2	26	26	7	7

Footnotes:

a. BPA - Bonneville Power Administration
b. SDG&E - San Diego Gas & Electric
   SCE - Southern California Edison
c. PG&E - Pacific Gas & Electric
d. CEC - California Energy Commission

Network Model

Individual pathways share several resources in common. A key limitation of this comparative framework is that there is no simple method to allocate these common resources in a realistic manner. A network model has been developed that interties the individual pathways and utilizes their previously determined cost, capacity, and emission coefficients as shown in Figure 4. The linkage between the E3 Pathway model and the E3 Network model is shown in Figure 5. A linear programming (LP) model, using a set

of reasonable boundary conditions and constraints, will help estimate the optimum mix of primary resource to be applied to hydrogen production. Other impacts can also be estimated. The resulting equilibrium conditions will help establish program priorities and provide information for program planning. Rather than examining energy pathways separately, their components and common resource connections are combined into a network lattice that consists of feasible energy forms and transformation activities generated from the current E3 Pathway activity data sets. They are then analyzed using the E3 Network model.

LP is a technique for finding the least cost solution to a problem which contains many potential alternatives. In this study, the alternatives are the energy transformation steps producing and using both conventional and renewable resources including hydrogen. LP optimization is particularly useful for cases in which several different constraining factors are to be considered. These factors may include limits on resources, minimal performance standard for secondary objectives (e.g. emissions targets), or a forced resource allocation based partly on regulatory or legislative mandates. An LP optimization usually generates an optimal solution that contains only some of the considered activities. Scenario modeling entails defining and optimizing (solving) a parametric set of related problems that are somewhat different in cost, resource limits or externality constraints and then examining their effects on total system cost.

In E3 Network scenario development, an initial base or unconstrained case is first formulated and executed as an LP model. No externalities are considered. The resulting optimal solution set is driven strictly by economic considerations and is therefore the lowest cost possible. All other scenarios will generate optimal solutions greater than or equal to the base case. Therefore the base case acts as a reference point for analysis. One would expect that in the E3 Network, the base case would consist of only non-renewable resources which at current prices, are economically the most attractive. This was found with a test case. By defining model scenarios, alternative or renewable forms of energy, including hydrogen, can be forced into a LP solution by the addition of secondary constraints or limiting non-renewable resources to levels that are exceeded by demand. The effects on total system cost can then be examined. If a scenario with side constraints is globally feasible, it will generate an alternative optimal low cost solution that still satisfies each constraint. Infeasibilities can occur when multiple constraints are formulated that are impossible to simultaneously satisfy. When a series of scenarios are run, cost and utilization solution values can be compared, indicating the renewable and/or environmental strategies that would be most attractive. Scenarios will also indicate the economic choke points of potential pathways by pointing out which energy transformation steps would be the most costly parts of the process. An E3 Network studies the interconnections of energy transformation activities culminating in end-use demands and should predict the actual economic synergies among current and envisioned technologies.

A secondary product of an LP optimization called the reduced cost is a basic mechanism for post-optimum sensitivity analysis. Unique reduced costs exist for each energy transformation activity in a network problem. In an optimal solution to an LP problem, some activities will have positive levels and some will be zero. This linear combination of activity levels is what constitutes the low cost solution to meet end-use demand. In other words, in the process of meeting end-use demands each energy transformation activity will either be utilized to some degree or, for economic reasons, it will not be used at all. For activities with non-zero levels at optimality, their corresponding reduced costs will indicate how much the total system cost could be decreased if one additional unit of the resource were available. The examination of reduced costs will generally indicate which resource activities are candidates for further study. A non-basic (zero level) energy transformation activity with a high reduced cost would be a prediction of substantial economic resistance to the technology's introduction, while a non-basic activity with a relatively low reduced cost would identify an energy technology that may be attractive in the future

after short term improvements in efficiency or else present the least resistance to forced introduction by regulatory or legislative mandates.

Findings

The current and advanced transportation and utility pathways presented in the Hydrogen Program Multiyear Plan were re-analyzed using the E3 Pathway Analysis Model. Results are displayed in Figures 6 presents a side-by-side pathway comparison of the energy ratio (primary energy required/energy output), life-cycle costs ($/km) with and without levelized emission values, and the physical measure (tons) of emissions. It is clear that delivered fuel cost is a relatively small share of total pathway life-cycle costs, with vehicle costs dominating. The values of the emission costs will impact pathway competitiveness. Conventional gasoline/internal combustion engine pathway costs can increase as much as 40 to 75% while the costs of alternatives increase only by about 5%, bringing some into the competitive range. Several conditions can be identified under which hydrogen would become a more competitive energy carrier. Gasification production routes appear to be most cost competitive but emissions and hydrogen purity may be issues. Lower power generation or production costs (and higher efficiencies) would mitigate impacts downstream in a pathway. In addition, R&D should be continued to provide practical direct photolysis production approaches. Efficient low-cost, compact storage is also necessary. In terms of end-use, inexpensive and highly efficient fuel cells would significantly enhance the attractiveness of hydrogen energy applications. Also, cogeneration applications would increase overall system efficiency by taking advantage of hydrogen's thermal energy value.

The results of this study to date are suggestive, not definitive, due to the broad scope of the analysis. Future studies comparing hydrogen, electricity, and other energy carriers would benefit from site-specific analyses. Sensitivity studies have been performed on parameters such as efficiency, capital cost, and capacity factor/storage cycles per year. Figure 7 presents results of a sensitivity study of capital costs and efficiency of photovoltaics (PV) and fuel cells in a utility pathway. Other sensitivity studies for transportation and transmission distances, storage capacity per cycle, cogeneration, time dependent dispatch and end-use values, water requirements and costs, and other applications would be valuable areas of further investigation.

Future Work

The E3 Pathway Analysis Model is in the process of being expanded and updated to include system considerations of reliability and safety in the estimation of life-cycle costs for hydrogen technologies. Future work will also consist of the expansion of the models to include: a more diverse set of nodal activities complete update of the Annex 11, Integrated Systems; aircraft applications; and additional scenario development and analysis. In addition, the ability to convey uncertainty will be a user option. Uncertainty refers to the spread of plausible values for an estimate and the level of confidence placed in a quantitative statement. The pathway/network framework will be made available as an analytical tool to screen competing system options for regional or site-specific conditions. For example, candidate systems or strategies are being proposed for Southern California, Alaska, and other sites. Total pathway impacts of each strategy need to be evaluated. Coordination with industry and national laboratories will allow a continuous update of input values and additions to pathway activities that will keep the models relevant and useful. This framework can also be applied in the screening process of candidate demonstration projects. Additionally, this work helps to integrate the results of ongoing projects in the program.

Acknowledgements

This study was supported by the U.S. Department of Energy and the National Renewable Energy Laboratory under contract no. BC-2-12150.

References

Badin, J. S., Eaton, R., 1993. "Hydrogen Energy Pathways: A Federal Plan for a Sustainable Energy Economy", Intersociety Energy Conversion Engineering Conference.

Badin, J. S., Kervitsky, G., 1993. "Recommendations of Emission Values for the E3 Pathway Analysis Modeling System", Energetics, Incorporated.

Badin, J. S., Mack, S., Kervitsky, G., 1993. "E3 Pathway Analysis Modeling System Users Guide, Version 1.0", Energetics, Incorporated.

U.S. Department of Energy, 1993. "Hydrogen Program Implementation Plan, FY 1994 - FY 1998," Office of Energy Management.

U.S. Department of Energy, 1992. "Hydrogen Program Plan, FY 1993 - FY 1997," Office of Conservation and Renewable Energy, DOE/CH10093-147, DE92010556.

Figures

Typical Pathway:
Generation —> Production —> Transport —> Storage —> End Use

Figure 1. Typical Pathway Elements

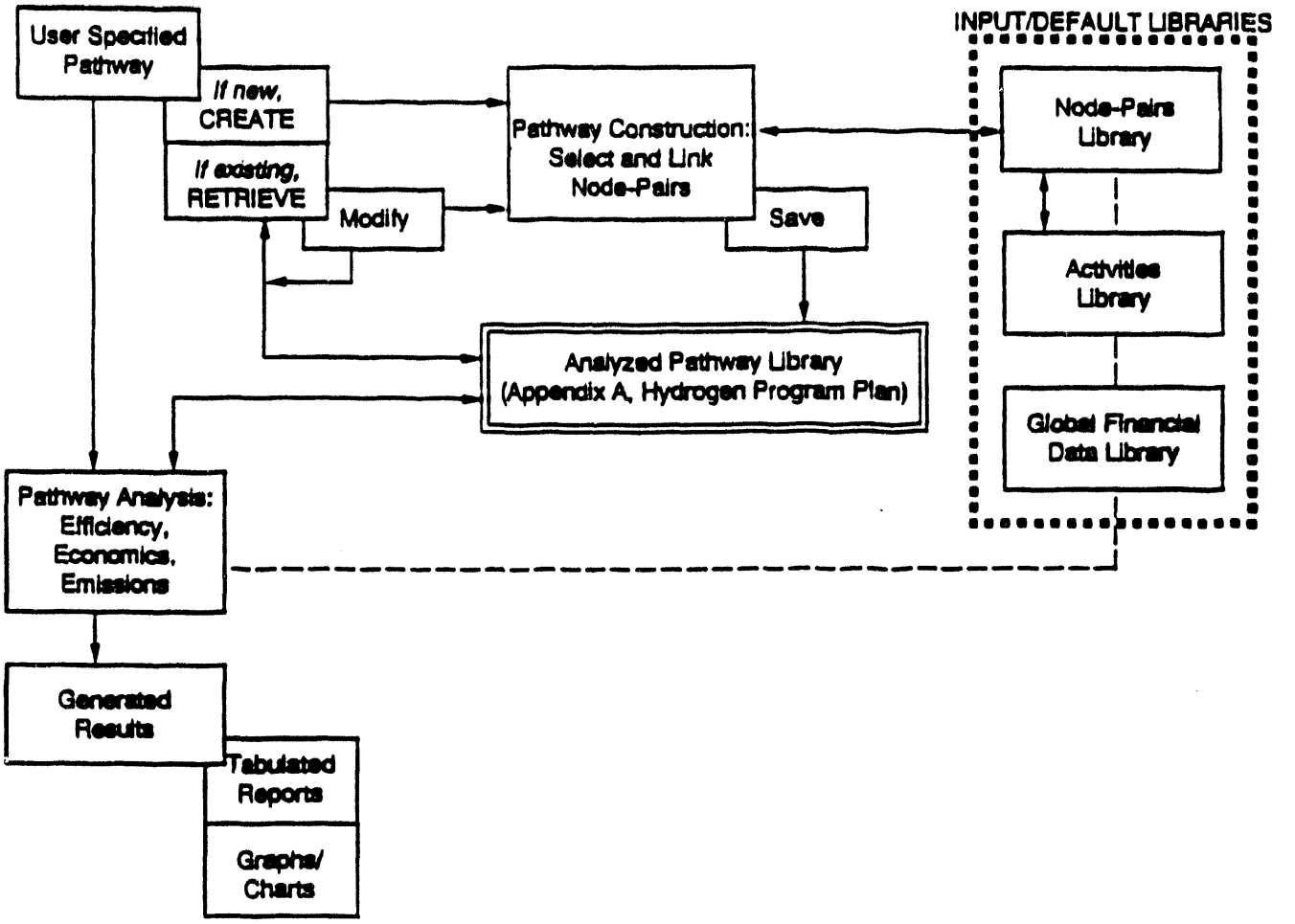

Figure 2. E3 Pathway Model Structure

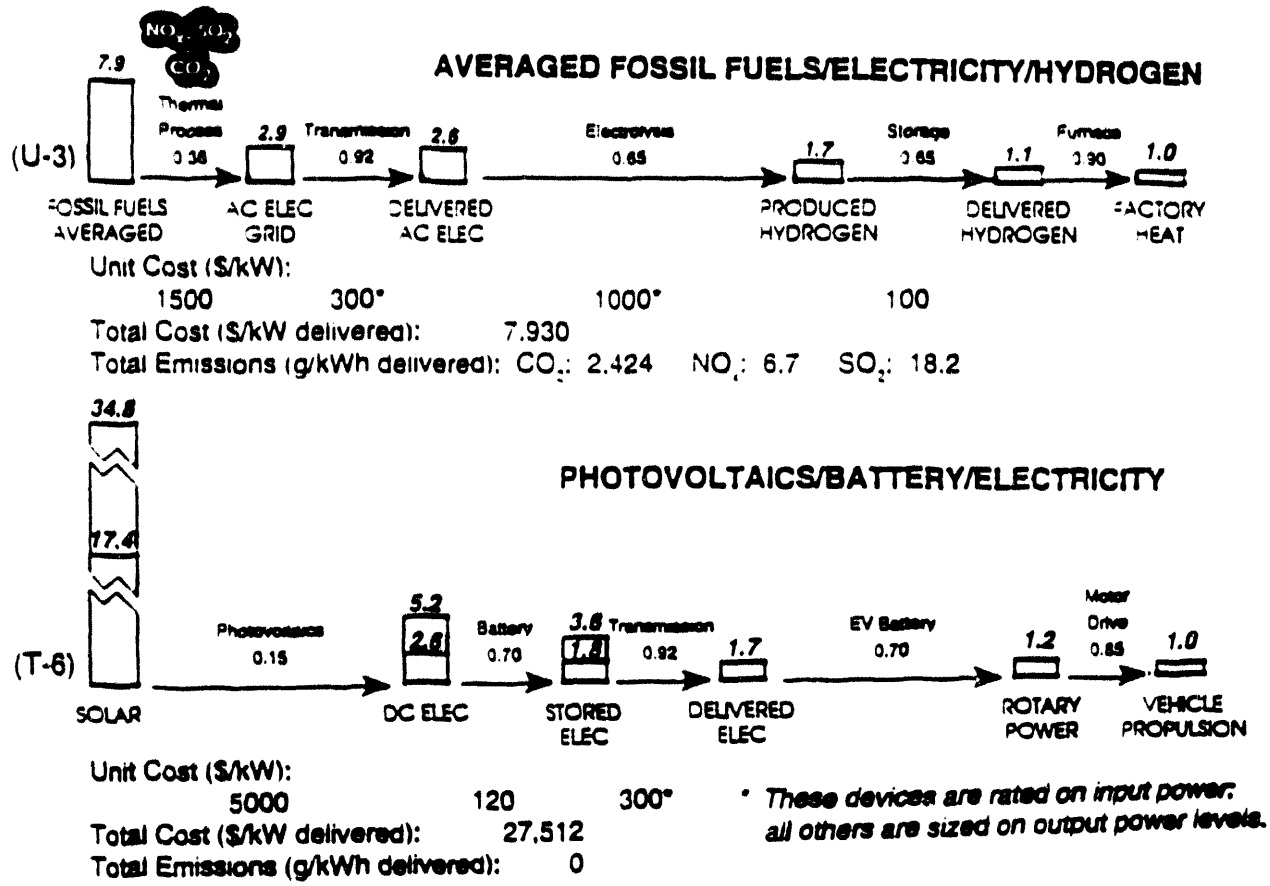

Figure 3. Representative Pathways

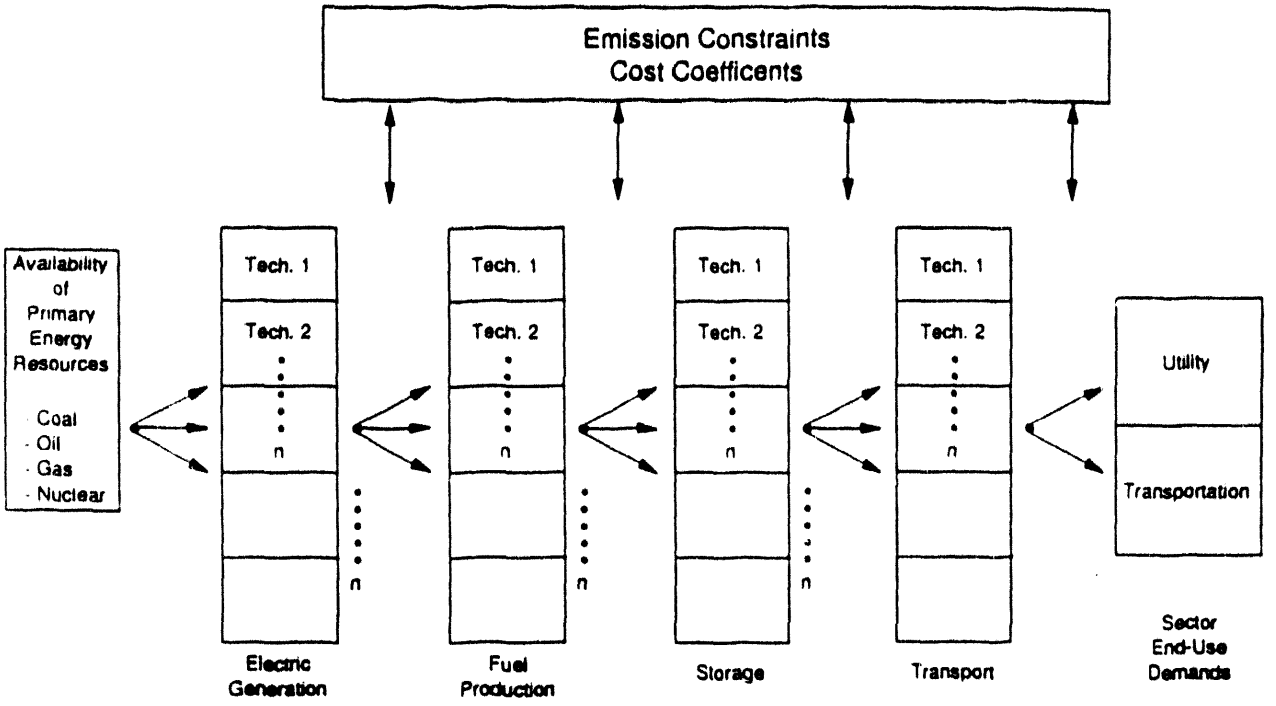

Figure 4. Conceptual Network Structure

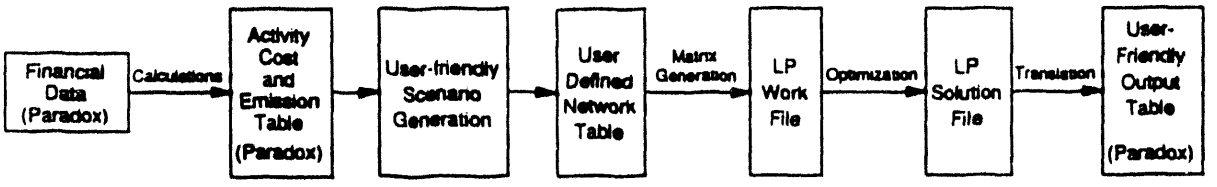

Figure 5. Pathway - Network Linkage

Figure 6: Select Transportation Pathway Results

E3 Pathway Model (Version 2.0)

(Delivery and End-use Segments)

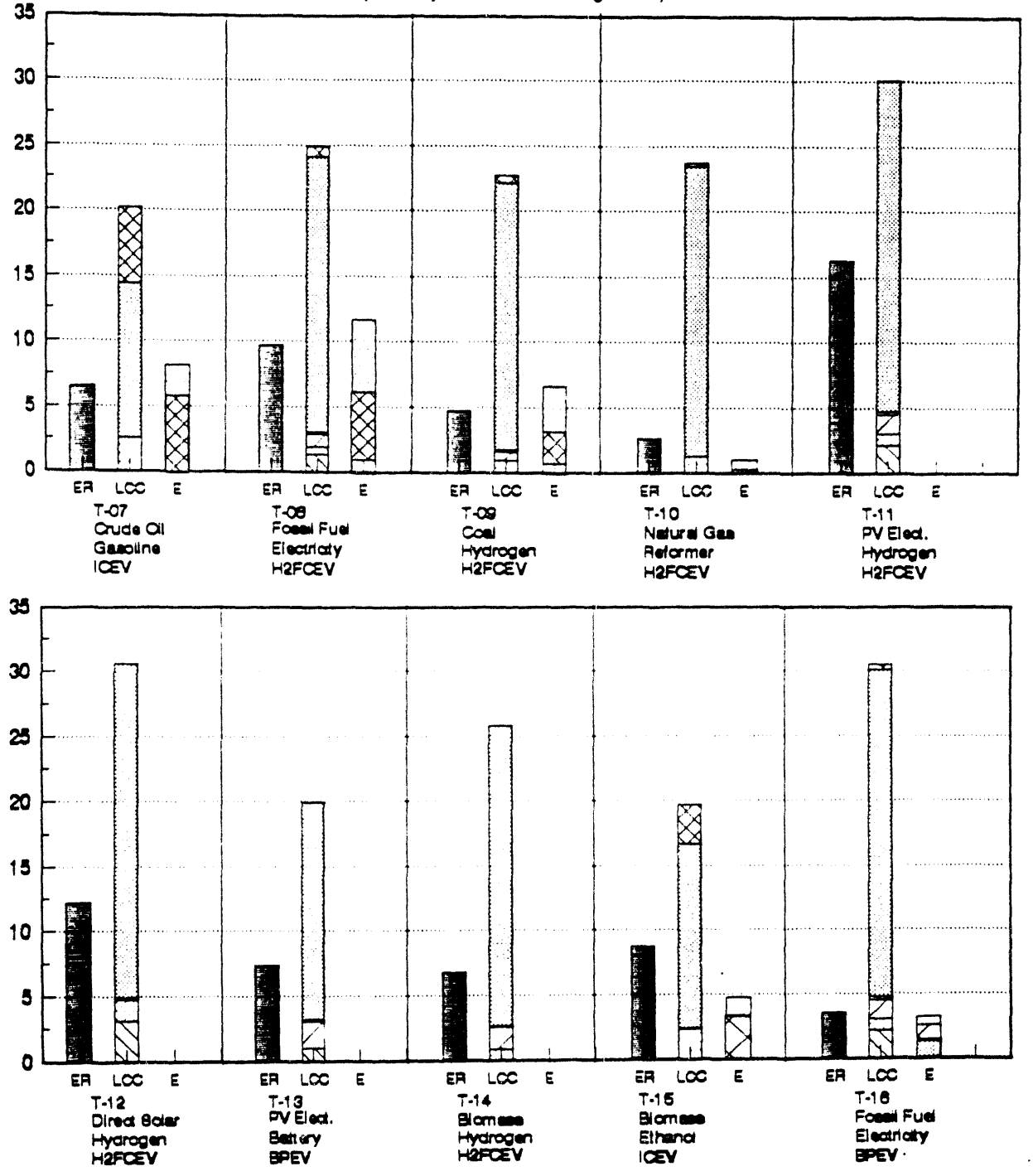

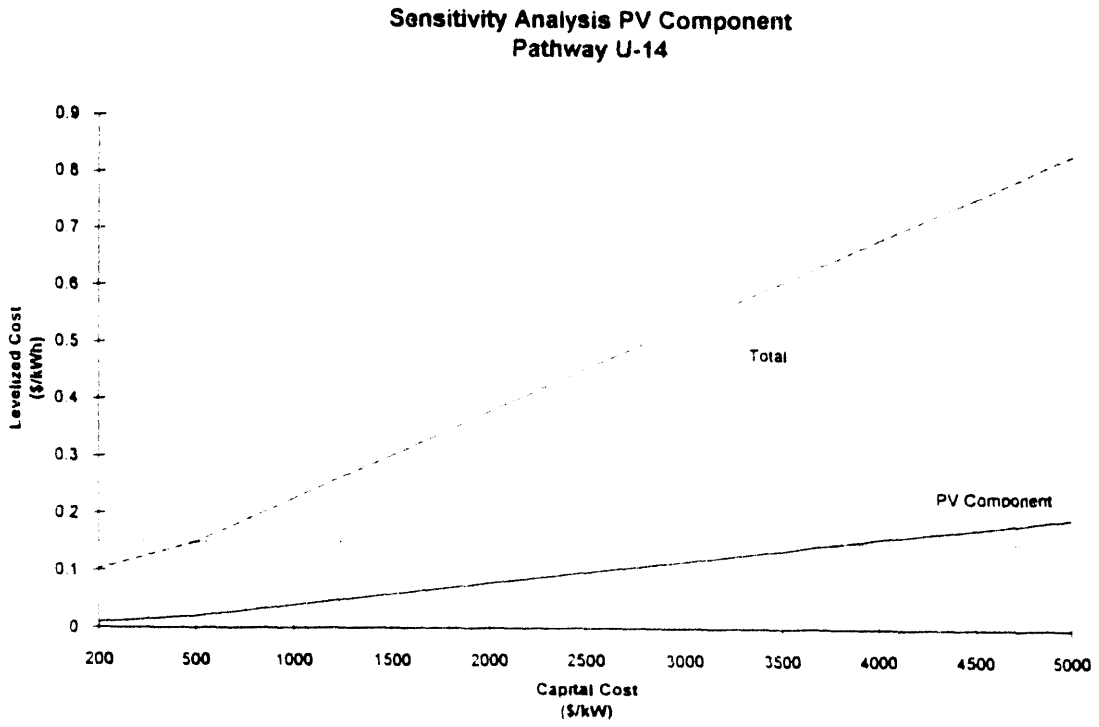

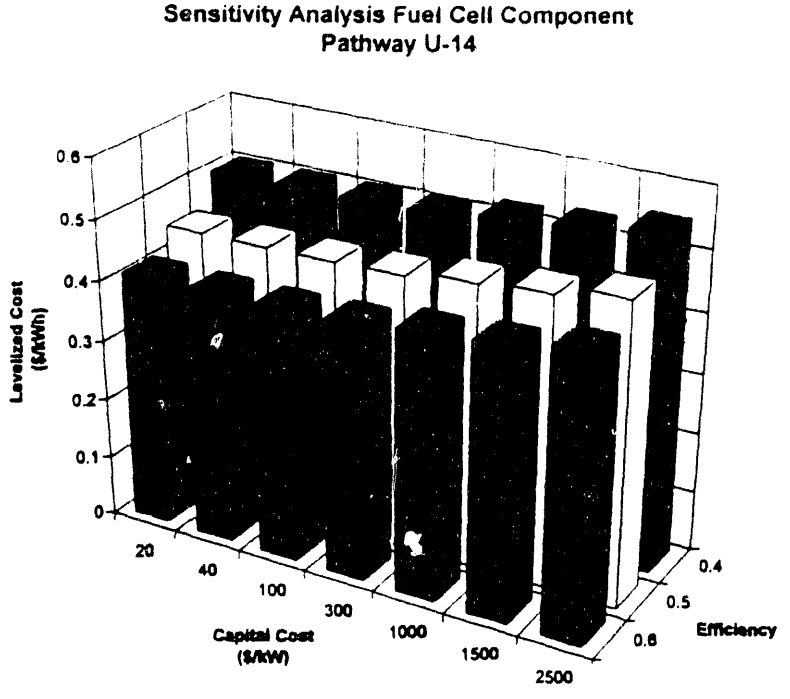

Figure 7. PV/Fuel Cell Sensitivity Case Study - Utility Pathway

PASSIVE VENTILATION SYSTEMS FOR THE SAFE USE OF HYDROGEN

M. R. Swain
University of Miami
P.O. Box 248294
Coral Gables, FL 33124

M. N. Swain
Analytical Technologies, Inc.
14057 SW 140th St.
Miami, FL 33186

Abstract

These are the findings from a computer model study of hydrogen gas leakage in buildings. The gas cloud shape and size was predicted using FLUENT 3.03. This study investigated the influence of building geometry and passive venting on the formation of combustible gas clouds. The intent was to determine under what conditions a "hydrogen safe building" could be constructed. That is to say what leakage rates and for what length of time hydrogen can be vented from properly designed buildings without producing sizable quantities of combustible fuel-air mixtures.

Introduction

Leaks of gaseous fuels inside residential or industrial structures create a risk of accidental combustion. Equipping those structures with properly designed ventilation systems reduces that risk. If there is enough ventilation such that a combustible mixture cannot accumulate, the accidental combustion risk can be eliminated. This study is an investigation into the parameters which effect the accumulation of hydrogen within a structure. Utilizing hydrogen's high buoyancy to drive the ventilation flow was investigated as a means to produce self venting structure (SVS) designs that would prevent the accumulation of a combustible gas mixture.

SVS in this context refers to buildings and rooms which have no fresh air ventilation or have fresh air ventilation rates compatible with ANSI/ASHRAE 62-1989. ANSI/ASHRAE 62-1989 is a standard which was developed taking into account the effect of energy loss in the climate control system due to fresh air ventilation. SVS designs do not have active ventilation systems which detect and evacuate hydrogen if found.

Choice of Ventilation Rates for Modeling

It is important to note that climate controlled structures need some ventilation to promote good health. Accumulation of gases that can be harmful to humans needs to be prevented. Current residential structure designs include various vents. For example, stoves, bathrooms, and fireplaces are vented to the outside. Proper SVS design (positioning and design of vents) using the current level of ventilation flow, will reduce the risk of accidental combustion and may make these structures safe without reducing the energy efficiency of the climate control system.

ANSI/ASHRAE 62-1989 was developed taking into account the effect of energy loss in the climate control system due to fresh air ventilation. The flow rates indicated for various structures in ANSI/ASHRAE 62-1989 were used to choose the ventilation flow rates used in the modeling in this study. ANSI/ASHRAE 62-1989 including Addendum 62a-1990 were developed by the National Voluntary Consensus Standard under the auspices of the American Society of Heating, Refrigerating and Air-conditioning Engineers (ASHRAE). Consensus in this case was defined as "substantial agreement reached by concerned interests according to the judgement of a duly appointed authority, after a concerted attempt at resolving objections. Consensus implies much more than the concept of a simple majority but not necessarily unanimity". The consensus was derived with the participation of ASHRAE's national and international members, associated societies and public review. Though ASHRAE standards are referenced in many building codes, conformance to them is completely voluntary.

The standard must make a compromise. Acceptable indoor air quality and minimizing climate control energy consumption are contradictory goals. High ventilation rates improve indoor air quality but increase energy consumption. Low ventilation rates improve energy consumption but reduce indoor air quality. An interdisciplinary committee of engineers, architects, chemists, physiologists, product manufacturers, and industry representatives was used to determine standards that would adequately balance the two contradictory desires (Bell, 1983; Berg-Munch, 1984; Hicks, 1984; Janssen, 1986; Leaderer, 1983; Raijhans, 1983; and Thayer, 1982).

Figures 1 and 2 show the required ventilation rates for various types of structures given in the ANSI/ASHRAE standard. The ventilation rates are presented in terms of SCFM/ft^2 (L/s-m^2). If the standard did not specify the ventilation flow rate in terms of SCFM/ft^2 (L/s-m^2) then the values of occupancy/floor area were multiplied with ventilation rate/occupant to determine the ventilation flow rate shown in the graph. Ventilation rates of 0.3 SCFM/ft^2 (1.5 L/s-m^2) and 1.5 SCFM/ft^2 (7.5 L/s-m^2) were chosen for the modeling to roughly bracket the range of ventilation rates given in the ANSI/ASHRAE standard and are shown in the figures 1 and 2 as horizontal lines.

Active ventilation systems that use sensors to detect combustible gas and then actively purge the structure by opening vents and/or forcing air through the structure would only create a ventilation flow when combustible gas is present. The presence of combustible gas, which would trigger the active ventilation system, would be very infrequent and would not increase the load on the climate control system under normal circumstances. Unfortunately, the infrequency of use would make active systems subject to reliability problems and they would probably need redundancy and a scheduled maintenance program to be reliable. SVS designs are passive and would not suffer from these reliability problems.

In this work effort passive SVS with and without ANSI/ASHRAE 62-1989 compatible flow rates were modeled. The choice of whether or not to use a SVS or an active ventilating system is a function of the leakage rate for which protection is sought and the length of leak time for which protection is sought.

Description of Model

FLUENT (Creare. X Inc., Hanover, New Hampshire) a computational fluid dynamics software package which models fluid and heat transfer problems with a finite difference scheme; was used to solve the continuity, momentum and concentration equations with the appropriate boundary conditions for this work.

A time dependent analysis of the size and shape of gas clouds formed by hydrogen leaking into a building was conducted using FLUENT.

Description of Problem

A variety of structural configurations for buildings into which hydrogen may leak were modeled. The following parameters were varied:

1. Number of vents
2. Location of vents
3. Size of vents
4. Slope of ceiling (0°, 26.6°, 45°, 63.4°)
5. Rate of forced ventilation (0, 1.5, 7.5 L/s-m^2)
6. Rate of hydrogen leakage (10, 100, 1000 L/min)

Inflow (Leakage)

Measured leakage flow rates (Swain, 1992); for hydrogen, methane, and propane, ranged from 1 ml/min to 2.5 l/min in residential settings. The selection of hydrogen leakage flow rates was based on this

experimental data. In an effort to investigate worst case scenarios, the minimum hydrogen leakage rate used was four times that of the largest measured hydrogen leak from pipe samples routinely removed from natural gas service by Peoples Gas in Miami, FL. This flow rate was then increased by up to 100 times during the course of the modeling.

Lean Limit of Combustion

Convective currents (gas motion due to density differences between cool unburned gas and hot burned gas) can quench a flame (stop flame propagation) by increasing the expansion rate of the burned gases and increasing mixing with the cooler gases. This is particularly true for lean mixtures since there is a relatively small amount of fuel in the mixture. Both the fuel consumption rate and the quantity of heat released per unit of fuel-air mixture are small in lean mixtures. This makes the lean mixture more susceptible to quenching. For example, it is widely accepted that hydrogen-air mixtures at concentrations less than 10% hydrogen will not sustain a flame propagating downward (Strehlow, 1968; Fischer, 1986; Al-Khishali, 1983; Bebelin, 1988; Edeskuty, 1988; Lewis, 1987; Glassman, 1987) and that a flame propagating upward through a 4% to 10% mixture will only consume part of the hydrogen in the mixture (Al-Khishali, 1983; Edeskuty, 1988; and Edeskuty, 1986).

Since the acceptable lean limit of combustion for the conditions inside a building is not clear this study uses the following definition for safety evaluations. Mixtures leaner than 4.1% by volume hydrogen are classified safe and mixtures richer than 10% by volume hydrogen are classified as very dangerous. Mixtures between 4.1% and 10% were noted but not evaluated as safe or unsafe.

Discussion of Results of Computer Model of Indoor Leakage

The study of hydrogen leakage inside buildings was initiated with a parametric analysis of vent location and size. The parameters studied were lower vent (floor vent) position and size, and upper vent (ceiling vent) position and size. This part of the analysis was made without ANSI/ASHRAE 62-1989 compatible fresh air ventilation. Depictions of the findings are displayed in figures 3 and 4. Figure 3 shows the results of hydrogen gas leakage into three single vent rooms. Figure 4 shows the results of hydrogen gas leakage into seven multiple vent rooms. Each room was 8 feet tall, 12 feet long, and 8 feet wide. The leak was located in the middle of the far wall. The leakage rate was 10 liters/min of pure hydrogen. Modeling with no outlet vents was not done because at least one outlet was necessary to keep the room at atmospheric pressure. The concentration at a specific location in the room is plotted as a function of time. A "standard cloud" was used to define this location. The standard cloud is shown in each room in the figures. A "cloud" in this context is a constant concentration surface generated by the computer model. The hydrogen concentration at the boundary of the standard cloud (specifically, the concentration at which the constant concentration surface was generated) was used as a measure of the room concentration. The concentration at the boundary of the standard cloud is not necessarily the average hydrogen concentration in the room but rather the hydrogen concentration at a particular location in the room.

Figure 3 shows the hydrogen gas concentration for the standard cloud versus time in single vent rooms. The room configuration for each curve is shown in small pictorials surrounding the graph. The average

concentration of hydrogen in the room is lower than the concentration depicted in the graph because, as can be seen, the gas cloud is small relative to the size of the room. The hydrogen concentration inside the cloud is larger than the concentration depicted in the graph and the hydrogen concentration outside the cloud (the rest of the room) is lower than the concentration depicted in the graph. The vent configurations producing curves in the upper portion of the graph are less desirable. The findings were as follows:

With a single floor vent (the lower room in figure 3) the standard cloud concentration was 0.91% in 12 minutes. A single roof vent located directly above the leak (the middle room in figure 3) yielded a standard cloud concentration of 0.90% in 12 minutes. Very little difference was seen between the single floor vent and the single roof vent results because the flow rate in the outlet vent was required (by physics) to be the same as the inlet flow rate. The buoyancy of hydrogen could not effect the flow rates in the vents in the single vent room case. It can be concluded that a room with a single vent, whether in the floor or ceiling, accumulates a combustible mixture relatively rapidly. A single vent allows for exit of gas mixture from the room at the same rate that pure hydrogen is entering the room from the leak. The fact that the accumulation rate of hydrogen is only slightly lower when the single vent is in the ceiling rather than the floor can be attributed to the large amount of diffusion of hydrogen into the air before the mixture can reach either vent. This yields relatively small concentration gradients in the rooms.
Figure 4 depicts the results of modeling rooms with more than one vent. The addition of a second vent allowed the buoyancy of hydrogen to effect the flow rate in the outlet vent. As the buoyancy of hydrogen drives the flow out a vent in the ceiling a second vent in the floor can allow fresh air to be drawn in, increasing the total flow rate out the ceiling vent. Again, the room configurations for each curve are shown in small pictorials surrounding the graph.

The room pictorial in the lower right hand corner of figure 4 has a standard vent (1.06 ft by 0.80 ft) (0.324 m by 0.244 m) both above and below the hydrogen leak. This configuration produces a significantly lower hydrogen accumulation rate.

Dividing the area of the lower vent into two vents, one on each side of the room (the first pictorial above the bottom right hand side of figure 4), has little effect on the accumulation rate of hydrogen in the room. The purpose of the lower vent is to provide additional air flow into the room as the buoyancy of hydrogen increases the flow rate of hydrogen and air out of the ceiling vent. The location of this "make-up" air is not as important as the fact that additional air can be added to the room.

Moving the lower vent to the other side of the room and reducing its size by 1/2 (the second pictorial above the bottom right) causes the hydrogen to accumulate slightly more rapidly. This is a further demonstration that the location and size of the lower vent is not important as long as a lower vent is provided.

Moving the upper vent to the other side of the room (the pictorial in the upper right hand corner of figure 4) has a dramatic effect, increasing the accumulation rate to that of the single vent configurations. Comparing the room in the lower right corner of figure 4 with the room in the upper right corner of figure 4 shows the importance of upper vent location. In the room in the upper right corner of figure 4 the hydrogen is so diffused and mixed with air by the time it reaches the ceiling vent that the buoyancy effect has become negligible. The higher concentrations of hydrogen found in the core of the leak cloud are needed to appreciably decrease the hydrogen accumulation rate in the room.

Doubling the upper vent size (the first pictorial to the left of the bottom right hand corner of figure 4) slightly reduces the accumulation rate of hydrogen in the room. The standard vent size chosen for this modeling does not appreciably restrict the flow of rising hydrogen-air mixture.

Moving the lower vent to the opposite side of the room (the second pictorial to the left of the bottom right hand corner of figure 4) has no discernible effect on the accumulation rate. Comparing the room second from the top on the right of figure 4 with the room second from right at the bottom of figure 4 shows the increase in accumulation rate is due primarily to decrease in floor vent size.

Decreasing the upper vent size (the lower left pictorial) significantly increases the hydrogen accumulation rate. Comparing the two rooms at the right and the room on the left at the bottom of figure 4 shows that the standard vent size provides most of the available improvement in hydrogen venting. Doubling the area of the standard vent yields only a small reduction in hydrogen accumulation rate while cutting the standard vent area in half significantly increases the hydrogen accumulation rate.

In summary: Lower vent size had a weak effect on combustible gas cloud size unless the lower vent becomes very small. Lower vent position had the least effect on cloud size. Upper vent size had a stronger effect on cloud size than did lower vent size. The benefit from increasing upper vent size diminishes with large vent sizes. Upper vent position had the strongest effect on cloud size.

The Effect of Ceiling Configuration

Ideally, based on the above analysis, a vent should be placed directly over any potential leak in a structure. This would maximize the effectiveness of the vent but is impractical in most cases. For this reason ceiling configuration was investigated to see if changes to the shape of the ceiling could improve the effectiveness of misaligned ceiling vents. This investigation used a single centrally located ceiling vent as the baseline. It was known from the previous work that with a flat ceiling a single centrally located ceiling vent would be substantially inferior to a single vent located directly over the leak. The floor vent was placed at the base of the wall encircling the room. This was done because floor vent location has little effect on the hydrogen accumulation rate and encircling the room gives no preference to any particular leak location. It was found that a leak at the wall produced a higher accumulation rate than a leak in the center of the room. Therefore the baseline condition was as follows.:

Room size -	10 ft by 10 ft by 7.8 ft (same volume as above)
Floor vent -	encircling the room on the floor along the baseboard
Roof -	flat
Roof vent -	In the center of the ceiling
Hydrogen leak -	in the middle of the far wall at 10 liter/min

Figure 5 shows the standard cloud size and shape for the ceiling shape modeling. Four ceiling shapes were modeled that were peaked in the middle with the angle of each side, measured from horizontal, being 0°, 26.6°, 45°, and 63.4°. In each case room volume was held constant by reducing wall height or, in the case of the 63.4° ceiling, scaling the room down slightly in all dimensions.

Figure 6 is a plot of concentration versus time for all four roof configurations. It can be seen that the shape of the roof had little effect on the accumulation rate of hydrogen in the room even after 5 hours

elapsed time. The 63.4° ceiling did perform the best but the differences were small. The standard cloud concentration for the 0° (flat) ceiling after 5 hours was 13.1%. The standard cloud concentration for the 63.4° (steepest) ceiling after 5 hours was 12.9%. Similar differences were found at elapsed times shorter than 5 hours and the intermediate slopes (26.6°and 45°) produced standard cloud concentrations between those of the 0° and 63.4° ceilings. It was concluded that without ANSI/ASHRAE compatible fresh air ventilation, ceiling slope did not appreciably improve the centrally located ceiling vent performance. This was due to the considerable amount of mixing and diffusion that occurred during the lengthy path from leak to ceiling vent. The low concentration of hydrogen at the ceiling vent did not produce high buoyancy and was not enough to drive large flow rates of hydrogen-air mixture out the vent.

Effect of ANSI/ASHRAE Compatible Fresh Air Ventilation

Figure 7 shows a comparison of the 0° and 63.4° ceilings with the same 10 liter/min hydrogen leak but with ANSI/ASHRAE compatible fresh air ventilation of 7.5 liter/sec-m^2. It can be seen that there is a more noticeable difference in vent performance due to ceiling slope with 7.5 liter/sec-m^2 fresh air ventilation but once again the differences are not appreciable. On the other hand the simple addition of ANSI/ASHRAE compatible fresh air ventilation caused a dramatic reduction in hydrogen accumulation rate. Without fresh air ventilation the room had not reached steady state in 5 hours and was at approximately 13% accumulated hydrogen by volume. This is very dangerous. With fresh air ventilation the concentration reached steady state in 20 min at a level of 0.24% to 0.32% accumulated hydrogen by volume. These are safe conditions. The next question addressed was at what leakage rate would the fresh air ventilated room become unsafe?

Figures 8 and 9 show the effect of increasing leak flow rate with the 0° and 63.4° ceilings and ANSI/ASHRAE compatible fresh air ventilation of 7.5 liter/sec-m^2. Steady state is still reached in 10 to 20 minutes and the results with both ceilings are similar. There is however a substantial increase in hydrogen accumulation rate as leak flow rate is increased. Increasing the leak flow rate an order of magnitude to 100 liters/min raises the steady state concentration to 2.5% for the 0° ceiling and 2.3% for the 63.4° ceiling. These are still safe values though. The steady state concentrations increased approximately linearly with leak flow rate. Increasing the leak flow rate 10 times increased the concentration approximately 10 times. Increasing the leak flow rate an additional order of magnitude to 1000 liters/min increased the steady state concentration to 19.7% for the 0° ceiling and 19.0% for the 63.4° ceiling. This is a very dangerous situation and was reached within 10 to 20 minutes after the leak started. However, this is an extremely high leak flow rate (400 times greater than any that were measured from pipes removed from service by Peoples Gas in Miami, Florida) and would probably be audible to individuals present in the room.

The ANSI/ASHRAE compatible fresh air ventilation was shown to improve vent effectiveness far more than ceiling shape. This is depicted in figure 10. Figure 10 shows the standard cloud concentration versus ventilation rate. The figure includes model results for the 0° and 63.4° ceilings with hydrogen leakage of 100 liters/min (40 times the experimentally measured rates). This higher hydrogen leakage rate was chosen to produce hydrogen accumulation concentrations in the range of the lean limit of combustion. It can be seen that ceiling shape plays a very small role in the results. For this relatively high leakage rate of hydrogen fresh air ventilation rates of nearly 7.5 liters/sec-m^2 were needed to prevent large volumes of combustible gas from forming. These fresh air ventilation rates would be suggested by ANSI/ASHRAE for transportation vehicles and waiting areas, theater lobbies and auditoriums, bowling alleys, ballrooms,

discos, casinos, hotel assembly rooms, cafeterias, bars, auto repair rooms, and enclosed parking garages (Figures 1 and 2). Figure 11 shows the same results for a hydrogen leakage rate of 10 liters/min and a 63.4° ceiling. The fact that steady state is not reached without fresh air ventilation is shown on the left hand side of the plot.

With zero fresh air ventilation and 10 liters/min leakage flow rate hydrogen concentration does not reach steady state. After one hour has elapsed the hydrogen concentration in the room is well below 4.1% (the upward propagating lean limit for hydrogen) except for locations very near the leak. This is a safe condition. After five hours have elapsed the hydrogen concentration is above 10% (the downward propagating lean limit for hydrogen) and a very dangerous situation exists.

ANSI/ASHRAE compatible fresh air ventilation rates make steady state conditions possible. At a fresh air ventilation rate of 0.3 SCFM/ft^2 (1.5 liter/sec-m^2) and 10 liters/min leakage flow rate steady state occurs with the standard cloud at 1% hydrogen concentration. These are safe conditions. Higher ANSI/ASHRAE compatible fresh air ventilation rates (1.5 SCFM/ft^2 (7.5 liter/sec-m^2)) reduce the steady state standard cloud hydrogen concentration to 0.24%. Again, these are safe conditions.

Effect of Leakage Rate

Leakage rate plays a strong role in determining hydrogen accumulation rate. Figure 12 depicts the steady state standard cloud concentrations for the 0° and 63.4° ceilings. Standard cloud concentrations are shown for 0.3 SCFM/ft^2 (1.5 liter/sec-m^2) and 1.5 SCFM/ft^2 (7.5 liter/sec-m^2) fresh air ventilation rates. It can be seen that hydrogen concentration increases linearly with leakage rate for a given fresh air ventilation rate. For the lower values of ANSI/ASHRAE compatible fresh air ventilation leakage rates of 40 liters/min begin to create a safety problem. For higher values of ANSI/ASHRAE compatible fresh air ventilation a leakage rate of 200 liters/min begins to create problems and 500 liters/min causes a severe safety problem.

Concentration Gradients

Figure 13 depicts a typical room modeled with the "cloud" generated at 3 different concentration levels. Each of the rooms depicted were at the same conditions (100 liters/min leak rate for 1 hour with 0.3 SCFM/ft^2 fresh air ventilation). The room at the top of the figure was generated at a 10.17% level. The cloud in the middle room was generated at a 10.00% concentration level. The cloud in the room at the bottom of the figure was generated at the 4.1% concentration level. As can be seen in the top two rooms a small change on the concentration level generated two very different size clouds. This indicates that the concentration gradients in the room were small.

Higher leakage rates and fresh air ventilation rates produce similar results but with slightly higher concentration gradients.

Conclusions

Lower vent size had a weak effect on combustible gas cloud size unless the lower vent becomes very small. Lower vent position had the least effect on cloud size.

Upper vent size had a stronger effect on cloud size than did lower vent size. The benefit from increasing upper vent size diminishes with large vent sizes.

Upper vent position had the strongest effect on cloud size.

Ceiling slope had little effect on combustible gas cloud size for centrally located upper vents. This held whether or not ANSI/ASHRAE compatible fresh air ventilation was used.

Fresh air ventilation rate and leakage rate both had strong effects on combustible gas cloud size.

Steady state hydrogen concentration decreased linearly with increased fresh air ventilation rate (Figures 10 and 11).

Steady state hydrogen concentration decreased linearly with leakage rate (Figure 12).

For rooms with low values of ANSI/ASHRAE compatible fresh air ventilation (0.3 SCFM/ft^2 (1.5 liters/sec-m^2)) leakage flow rates of 40 liters/min began to produce a severe safety problem.

For rooms with high values of ANSI/ASHRAE compatible fresh air ventilation (1.5 SCFM/ft^2 (7.5 liters/sec-m^2)) leakage flow rates of 500 liters/min began to produce a severe safety problem.

Acknowledgements

The authors would like to thank the Department of Energy and the National Renewable Energy Labs for providing funding for this research effort.

References

Al-Khishali, K.J., Bradley, D., and Hall, S.F., 1983, "Turbulent Combustion of Near-Limit Hydrogen-Air Mixtures", *Combustion and Flame*, 54:61-70

Bebelin, I.N., Belyakov, S.V., Petrenko, V.M., Potekin, G.S, and Shalberov, S.M., 1988, "Some Aspects of Fire and Explosion Safety at the Gaseous Hydrogen Release from Storage and Transport Systems", *Hydrogen Energy Progress VII*, 2:1179-1193

Bell, S.J., and Khati, B., 1983, "Indoor air quality in office buildings.", *Occupational Health in Ontario*, 4:103-118.

Berg-Munch, B., Clausen, B.G., and Fanger, P.O., 1984, "Ventilation requirements for the control of body odor in space occupied by women", *Environment International*, Vol. 12 (1986), pp. 195-199

Edeskuty, F.J., and Stewart, W.F., 1988, "Safety Aspects of Large-Scale Handling of Hydrogen", In *Proc. 7th World Hydrogen Energy Conference*, 1195-1208

Edeskuty, F.J., Haugh, J.J., and Thompson, R.T., 1986, "Safety Aspects of Large Scale Combustion of Hydrogen", *Proc. 6th World Hydrogen Energy Conference*, 147-158

Fischer, M., 1986, "Safety Aspects of Hydrogen Combustion in Hydrogen Energy Systems", *Int. J. Hydrogen Energy*, Vol. 11, 9:593-601

Glassman, I., 1987, *Combustion*, Academic Press Inc., Orlando, Florida

Hicks, J., 1984, "Tight building syndrome: When work makes you sick.", *Occupational Health and Safety*, Jan. pp. 51-56.

Janssen, J.E., and Wolff, A.., 1986, "Subjective response to ventilation", In Managing Indoor Air for Health and Energy Conservation, *Proceedings of the ASHRAE Conference IAQ '86*. Atlanta:American Society of Heating, Refrigerating, and Air-Conditioning Engineers, Inc.

Leaderer, B.P., and Cain, W., 1983, "Air quality in buildings during smoking and non-smoking occupancy", *ASHRAE Transactions*, Vol. 89, Part 2B, pp. 601-613.

Lewis, B., and von Elbe, G., 1987, *Combustion, Flames and Explosions of Gases*, Academic Press Inc., Orlando, Florida

Raijhans, G.S., 1983, "Indoor air quality and CO_2 levels." *Occupational Health in Ontario*, 4:160-167.

Strehlow, R.A., 1968, *Fundamentals of Combustion*, International Textbook Company, Scranton, Pennsylvania

Swain, M.R., and Swain, M.N., 1992, "A Comparison of H_2, CH_4, and C_2H_8 Fuel Leakage in Residential Settings.", *International Journal of Hydrogen Energy*, Vol. 17, No. 10, pp. 807.

Thayer, W.W., 1982, "Tobacco smoke dilution recommendations for comfortable ventilation.", *ASHRAE Transactions*, Vol. 88, Part 2, pp. 291-306.

Figues

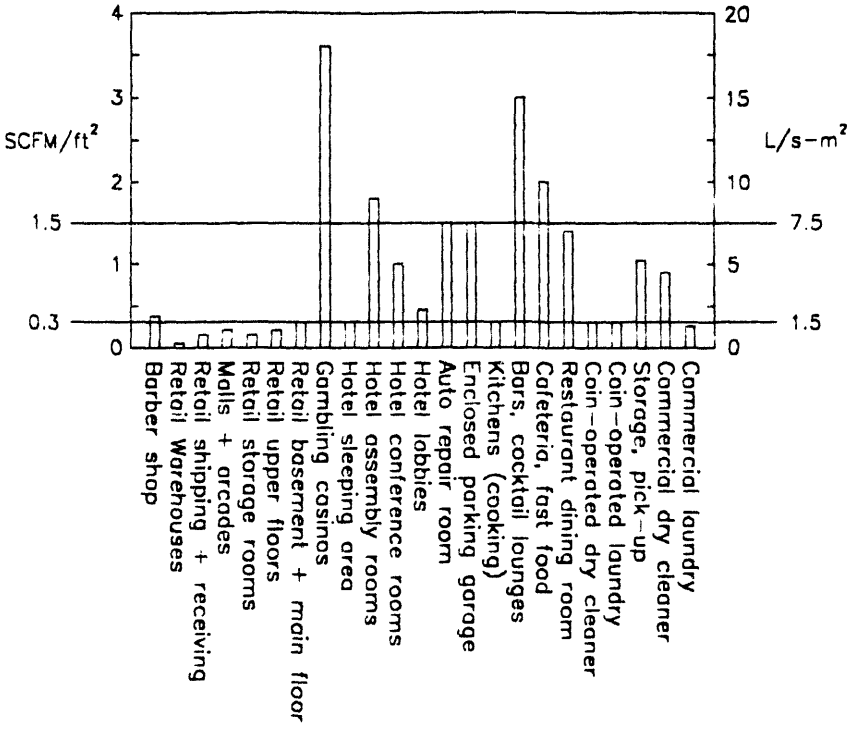

Figure 1 - ANSI/ASHRAE fresh air ventilation rates for various structures

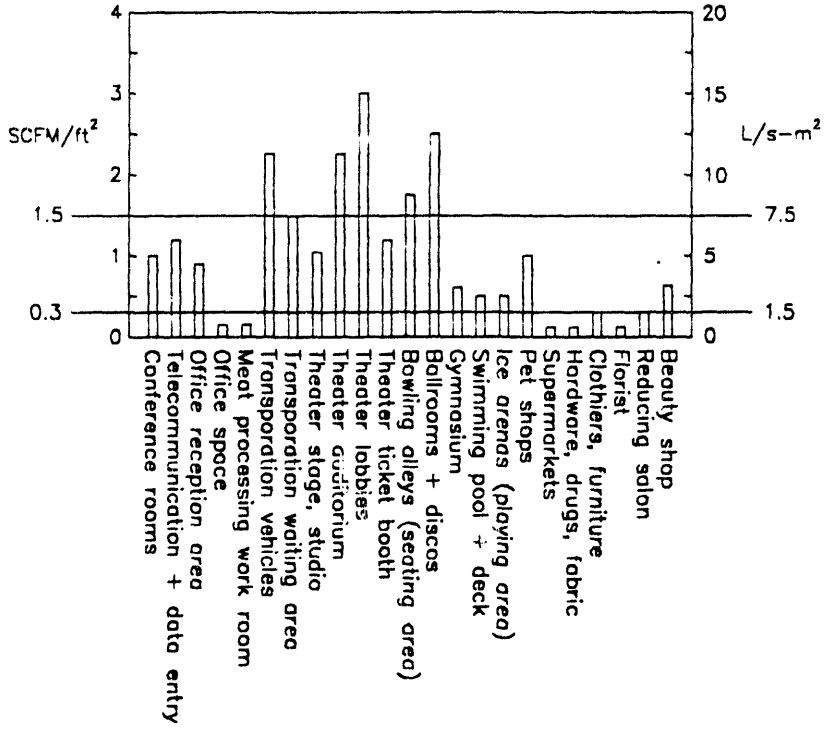

Figure 2 - ANSI/ASHRAE fresh air ventilation rates for various structures

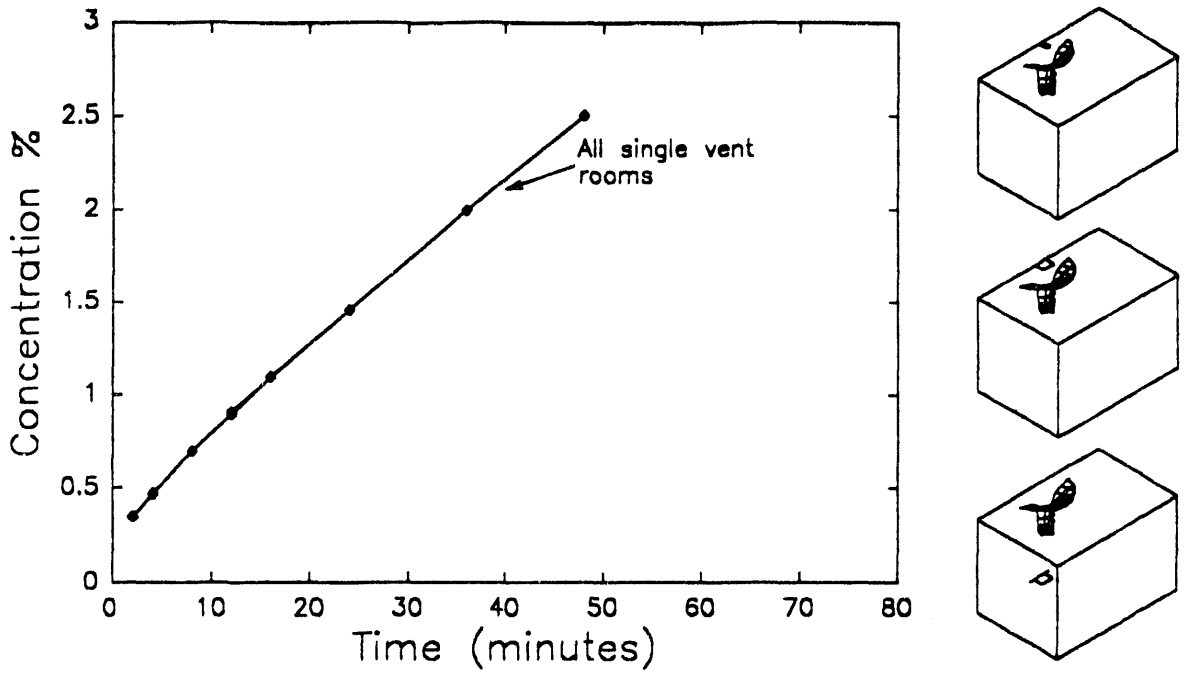

Figure 3 - Hydrogen accumulation in single vent rooms

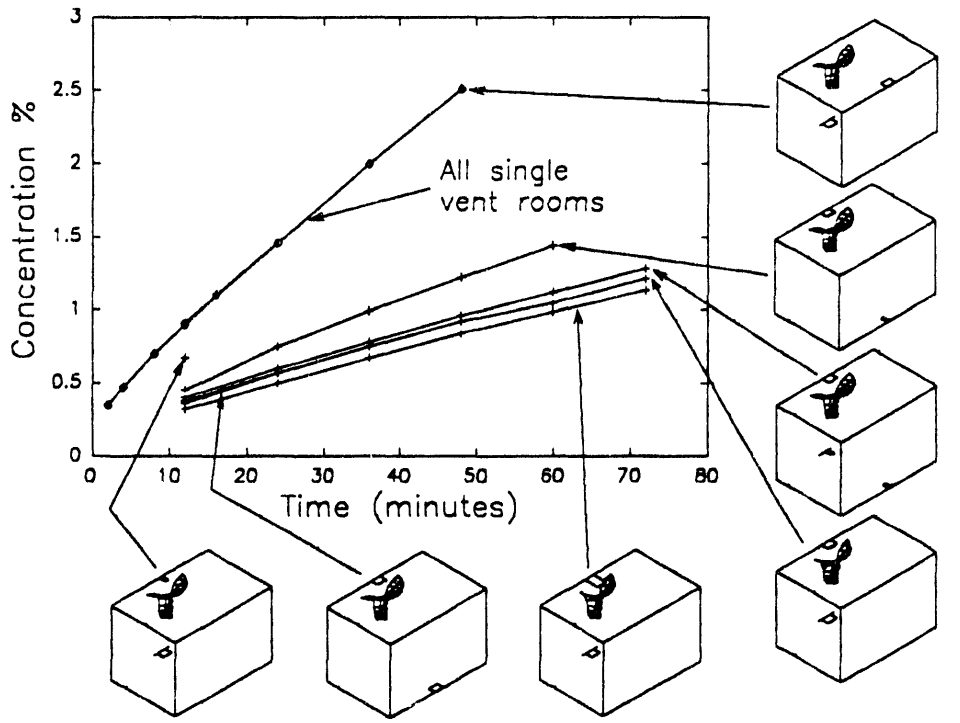

Figure 4 - Hydrogen accumulation in multiple vent rooms

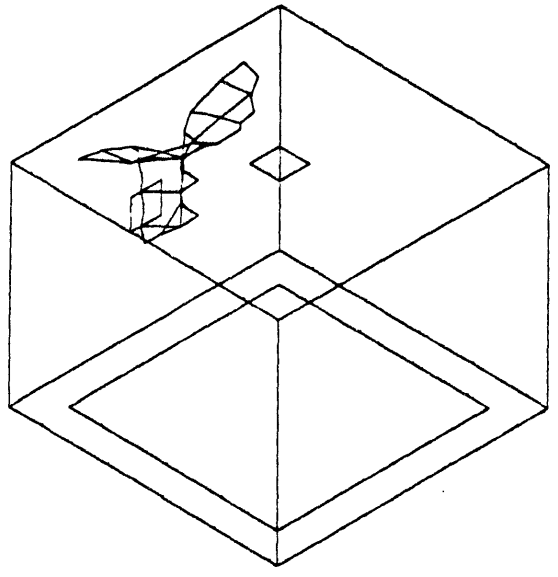

Figure 5- Standard cloud for ceiling shape modeling

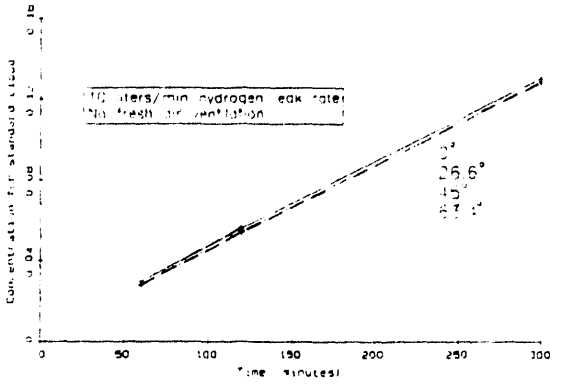

Figure 6 - The effect of ceiling angle on hydrogen accumulation rate

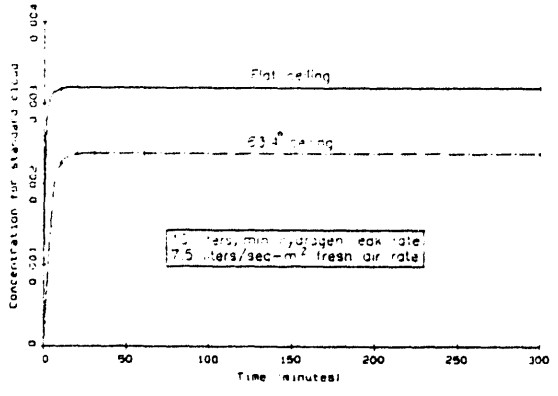

Figure 7 - Hydrogen accumulation rate with ANSI/ASHRAE fresh air ventilation

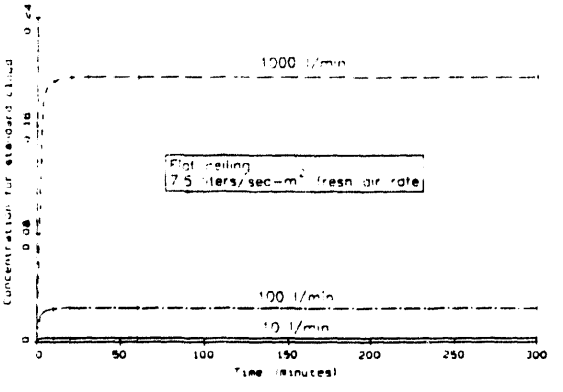

Figure 8 - Effect of leak rate on hydrogen accumulation (with fresh air ventilation)

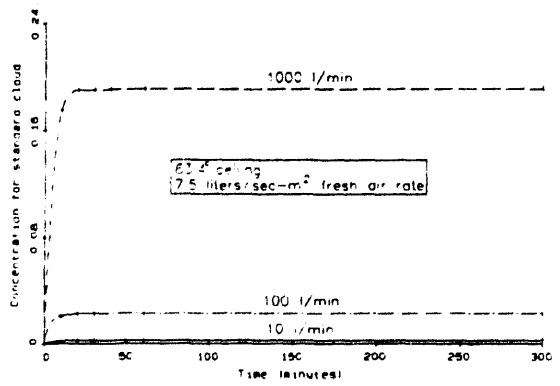

Figure 9 - Effect of leak rate on hydrogen accumulation (with fresh air ventilation)

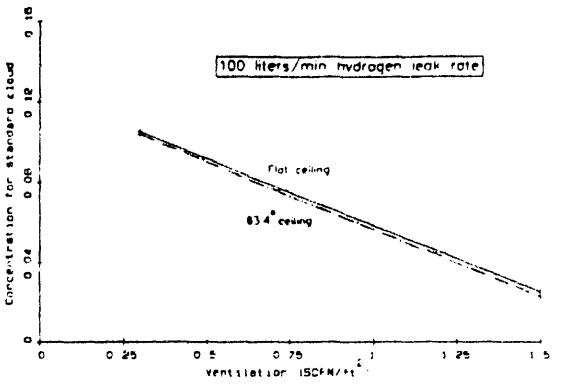

Figure 10 - Effect of fresh air ventilation

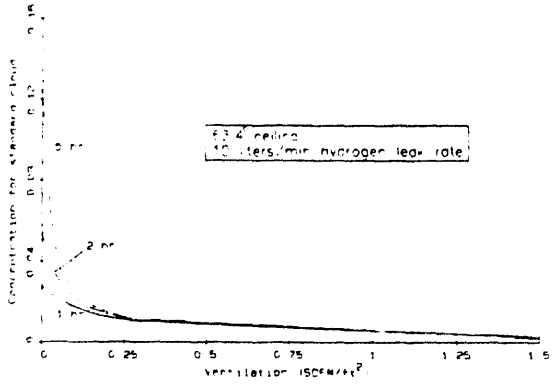

Figure 11 - Effect of fresh air ventilation

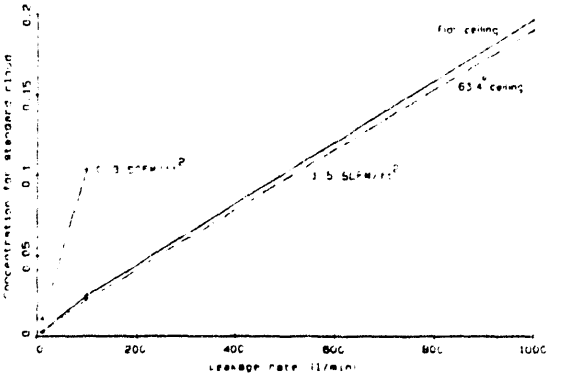

Figure 12 - Effect of hydrogen leakage rate on accumulation with fresh air ventilation

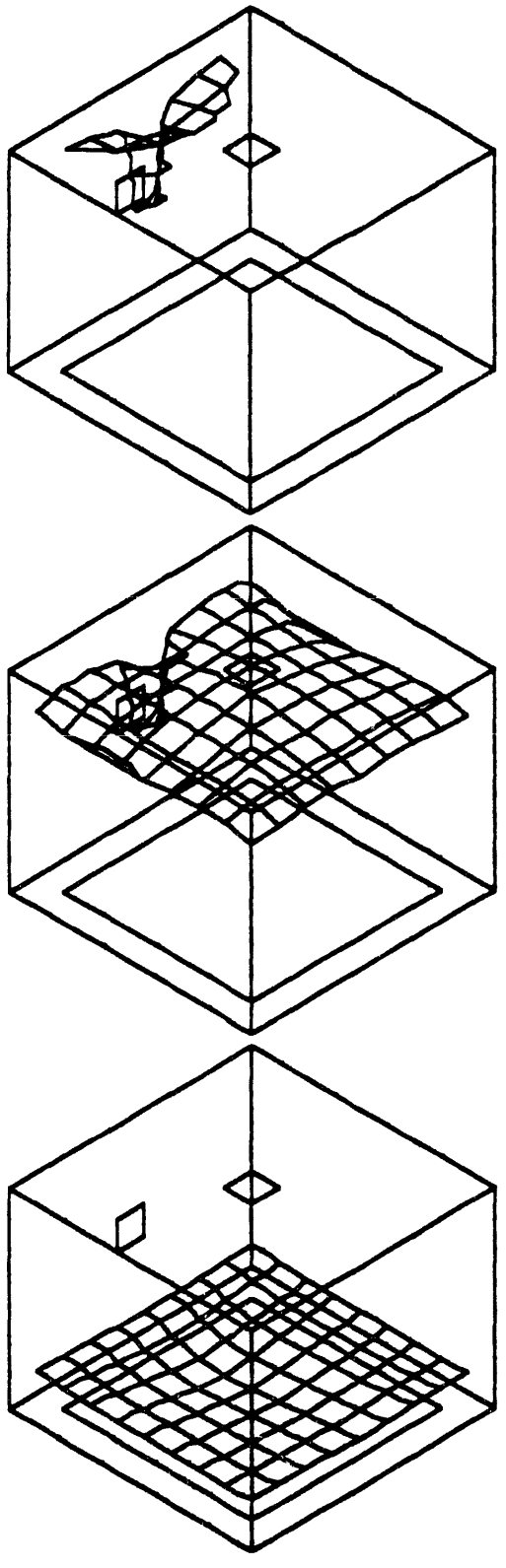

Figure 13 - Concentration Distribution

SYSTEMS STUDY OF METAL HYDRIDE STORAGE REQUIREMENTS

Ali T-Raissi and Arundhati Sadhu
Florida Solar Energy Center
Cape Canaveral, FL 32920

Abstract

Hydrogen can be stored in the form of metal hydrides, polyhydride complexes, compressed gas, liquid, physical adsorption on activated carbons, and chemical carriers (*e.g.* methane, methanol, benzene-cyclohexane, toluene-methylcyclohexane processes, etc.). At this time, none of these storage options are considered to be a solution to the overall problem of cost-effective storage of hydrogen. Metal hydrides can store large amounts of hydrogen, but with very high release temperatures. When the dehydrogenation temperatures are lowered, the amount of hydrogen stored becomes inadequate. Compressed gas may not result in sufficient energy density for the degree of safety and cost required. Liquefaction requires special handling and boil-off losses are problematic. Adsorption on activated carbons require both reduced temperatures (insulated containers, boil off) as well as a pressurized container. Cyclohexane reactions involve toxic chemicals and the recovery of H_2 is complex and equipment intensive.

Considerable work has been carried out in this area since FSEC's 1988 hydrogen storage report to the U.S. DoE. This earlier work focused on technologies most appropriate for the storage of hydrogen on-board internal combustion engine vehicles (ICEVs). Since then, a new scenario that emphasizes the use of fuel cell engines/vehicles (FCV) has gained popularity. Fuel cells are now being developed for the transportation applications due to mounting air pollution and energy security reasons. In the light of these developments, it has become necessary to revisit our earlier vehicular hydrogen storage systems study. More specifically, the hydride storage will be compared to the present and future, competing systems. This study is intended to provide design goals for hydride systems that will allow them to be competitive with other H_2 storage alternatives. In this paper, we provide a brief description of the work performed to date

Introduction

Storage represents a set of technologies that accommodate differences in timing of energy service demands and availability of the energy supply. In the case of on-board storage of hydrogen for vehicular applications, It is desirable to have a light weight, compact, safe and economic containment method. Although, various hydrogen storage technologies are presently available, neither completely satisfies all of these requirements. The main objective of this study is to conduct a comparative analysis of hydrogen storage systems in all three forms (*i.e.* solid, liquid and gaseous). The level of technological maturity, economic viability, infrastructural compatibility and operational safety are the main evaluation criteria. More specifically, the following key criteria are considered:

- Energy density (both volummetric and gravimetric) of the hydrogen carrier
- Normal state (gaseous, liquid or solid) of each chemical component
- Temperature requirement of both hydrogenation and dehydrogenation processes
- Energy requirement of both hydrogenation and dehydrogenation processes
- Type of energy required (shaft work vs. thermal)
- Projected cost of the carrier system
- Improvement potentials over present hydrogen storage options
- Environmental impact

As far as the hydrogen storage is concerned, considerable new developments have occurred since our earlier hydrogen storage assessment report to the U.S. DoE (Block, et al. 1988). Our 1988 report focused, exclusively, on technologies most appropriate for the storage of hydrogen on-board internal combustion engine vehicles (ICEVs). Figure 1 depicts the main conclusions of this earlier work as they relate to H_2 storage on-board ICEVs.

A comprehensive review of the state-of-the-technology for hydrogen energy storage since this report is underway. In recent years, a new scenario that emphasizes the use of fuel cell engines/vehicles (FCV) has become popular. Many argue that the future hydrogen-powered prime movers for transportation will have fuel cell engines. In the light of these recent developments, in the present study, we have revisited our earlier assessment of the prospective vehicular storage, both conventional and emerging technologies. The results of this study is intended to provide design goals for hydride systems that will allow them to be competitive with other H_2 storage alternatives. A brief summary of the findings, to date, is presented below.

On-board Hydrogen Generation and Storage Systems

Under this category, three systems have been considered, namely, (i) Sponge iron/water, (ii) Aluminum and water/alkali and magnesium hydride/steam systems. Of these three techniques, only sponge iron/water system is discussed here. This is so because all developmental activities

on the Al/water/alkali system has been abandoned due to the less than expected performance and poor economics of this system. As far as the magnesium hydride systems are concerned, they are being evaluated in conjunction with our own chemically synthesized compounds (Zidan, et al. 1991; Collier, et al. 1991; Lynch, 1992). Presently, the sponge iron/water concept is in the system level developmental stage (Maceda and Wills, 1992; Maceda, 1994; Werth, 1994). This system is described below:

Sponge Iron/Water System

The basic reaction on which this technology is based:

$$3Fe + 4H_2O \rightleftharpoons Fe_3O_4 + 4H_2$$

Both the forward and backward reactions are known to be high temperature reactions at 700-900°C and 1500°C, respectively.

Recent Developments

Main emphasis has been to develop and optimize Fe/water system for FCVs or ICEVs (Maceda, 1994; Werth, 1994). These efforts have focused on the components identification and a decision has been made that the only reaction carried out on-board the vehicle shall be oxidation of iron. In addition, the reaction temperature has been reduced to 250°C by using catalyst(s) and better reactor engineering. No specific information has been made available to fully assess their optimized system. Apparently, problems with incomplete reactions and hydrogen production rates have been addressed via the use of multiple bed reactor techniques. Obviously, the reverse reaction is one which is used to regenerate the iron. This is carried out outside the vehicle, either in a refuelling station or in commercial plants.

Present Status of the Technology

Sponge iron/water technology has been developed to the point that H-power is ready to build a demonstration prototype/vehicle (Maceda, 1994; Werth, 1994). H-power has already selected a vendor to fabricate the demonstration unit and are looking for a viable partner.

Expected System Performance

1. Energy Density

System volume= 22 ft^3
System weight= 2,480 lbs
Weight% of hydrogen (wt of hydrogen/wt of the storage system) x 100 = 3.6
Installed gravimetric energy density = 2.64 MJ/kg
Installed volummetric density = 4.767 MJ/L

2. Normal State of Chemical Components

Sponge iron -- solid
Water -- liquid
Superheated steam -- gaseous
Hydrogen-- gaseous
Magnetite -- solid

3. Hydrogenation/Dehydrogenation Temperatures and Pressures

The forward reaction is carried out on-board the vehicle. The temperatures normally needed are less than 600-800°C. However, it may be possible to conduct oxidation reaction at temperatures in the range of 200°C or so. The operating pressures are near atmospheric.

4. Ex-Situ Energy Requirements

Performance figures for hydrogen generation via sponge iron/water system are: 0.7 kWh/lb or 51 Wh/in^3 at 4.5 weight percent H_2 equivalent.

5. On-board Energy Requirements

To produce hydrogen on-board, waste heat from the fuel cell engine may be used.

6. Projected Costs

The current cost of sponge iron is in the range of 110-125 $/ton, which is equivalent to 18 cents per kilowatt hour. This is three orders of magnitude less than the prospective lead-acid battery (100-200 $/kWh). As per H-power's cost calculations for a bus application (Maceda and Wills, 1992):

Range:	200 miles
Fuel consumption:	4.125 kWh/mile
Storage energy:	825 kWh
Fuel weight:	90 lbs
Storage system weight:	2,480 lbs
system volume:	22 ft^3
system cost:	$750

7. Improvement Potential

The concept can only be fully verified if the proposed developments and actual vehicular trial runs materialize.

8. Technological Maturity

The technology has been tested at the laboratory scale, though, no published data available. The system components have been identified and tried in the laboratory. However, no trial runs have been conducted at large scale and no practical demonstration of a vehicle (either FCV or ICEV) has been made.

9. Infrastructure Compatibility

For the on-board oxidation, a series of iron beds and a steam generator with associated plumbing and control systems will be required. The reduction will be carried out ex-situ, either at local gas stations using natural gas or larger central stations using urban waste, biomass, electricity or fossil fuels.

The plan for iron supply is from existing supply streams. Current production rate for sponge iron is 400,000 tons per year. According to H-Power, if every new car sold in the US came with a full tank of iron, one million tons of iron would be required. If every vehicle used iron, total of 15 million tons will be needed for on the road vehicles. Considering the global supply of sponge iron, this figure is not expected to affect the price of this commodity, noticeably.

However, considering that each car in the US fills up about 40 times per year, processing capacity of 600 million tons per year will be required. If an average service station fuels 200 cars per day, at least 100,000 iron fueling stations will be required. This figure is about half of the current total in the United States. H-Power's expectation is that "With the enormous profit available from this energy system, there is every likelihood that the retail distribution network will become an oil companies greatest asset."

They have also considered the natural gas availability. In that regard according to H-power's findings "already 75% of the gas stations in the US have pipeline natural gas on their premises. With the use of electrolyzers, off-peak electricity, solar and wind all become viable energy sources. Municipal solid waste and/or biomass gasification/incineration may also be viable options.

Steel and plastic has been suggested as the possible tank materials. However, it is not clear How plastic will manage to withstand long-term, high temperature operation and use under the proposed conditions. In our opinion, Steel may be more appropriate.

10. Safety

According to H-power, the sponge iron/water system will be less hazardous than other techniques such as liquid or gaseous storage since the material to be stored is iron not hydrogen. The only hydrogen on-board the vehicle is expected to be a small amount needed to start and operate the fuel cell as the load demands. This gas, contained within the reactor fuel cell manifold and connecting plumbing, is too little to be of concern.

Another safety related issue concerns a situation in which the output stream containing hydrogen and steam is cut off while the supply of water and heat to the reactor continues. In such a situation, the oxidation reaction may result in pressure built up within the reactor. In any case, the key control parameter appears to be the rate of water injection into the reactor.

11. Refuelling

Refuelling time is expected to be less than five minutes, involving the replacement of magnetite cylinder(s) with new/ fresh sponge iron cylinder(s).

12. Hydrogen Purity

According to H-Power, the purity of hydrogen gas generated on-board is quite high (99.9999%).

13. Poisoning

Effect of other gases and impurities on the performance of the sponge iron/water system is still under investigation and no data are yet available.

Hydrogen Storage by Cryoadsorption

Cryoadsorption of hydrogen refers to storage of hydrogen in cryogenically cooled vessels which contain adsorbing materials. The amount of gas stored depends on:

i) surface area of adsorbent
ii) temperature of the cryogenic vessel
iii) pressure of the vessel

The amount of gas adsorbed is very much dependent on pressure since the percentage of filling space/void is a function of the tank pressure. Therefore, cryoadsorption combines the advantages of low temperature and high pressure storage.

Developmental Status

Different carbons have been tried including: BPL-carbon, CNS-201, NORIT, AX-21, AX-31M and ESC-3 (Schwarz, 1994; Chahine and Bose, 1992; Carpetis and Peschka, 1980). Presently, ESC-3 with surface area of 2,230 m^2/g has demonstrated the feasibility of storing hydrogen up to 9.1% by weight of carbon, 53% by adsorption and 47% by compression in voids, (Schwarz, 1994). According to Schwarz, it is possible to fabricate a storage system that consist of a 100 liter tank holding 32.3 kg of carbon and operating at 8.2 MPa pressure (safety factor 2.25). The total system would weigh 67.9 kg including 2.91 kg of stored hydrogen. This should provide a reasonable driving range, approximately 3.3 kg of hydrogen is needed for a 200 km driving range

in a compact hydrogen ICEV and a greater range may be expected from a FCV. At the present time, 12-13% hydrogen (by weight of carbon) at 77K and 55 atmosphere can be achieved (Young, 1992).

Expected System Performance

1. Energy Density

For ESC-3 carbon, surface area = 2230 m^2/g at 87K, and 6.0 MPa (59 atm) pressure
Installed volummetric density = 2.390 MJ/L
Installed gravimetric density = 5.22 MJ/kg
gravimetric ratio = percent weight of hydrogen/total system weight = 4.2%

2. Normal State of Chemical Components

Highly active carbon -- solid
Hydrogen -- gaseous form

3. Hydrogenation/Dehydrogenation Temperatures and Pressures

In this particular case, it refers to charging and discharging of hydrogen. Two types of charging have been examined. In one approach, pressurization for a short period of time (8.2 MPa for 30 s) was used and equilibrium pressure (4.2 MPa) was arrived at in about 10 minutes. Alternatively, a lower pressure of 6.2 MPa for a duration of 10 minutes has been used, resulting in an equilibrium pressure of 4.9 MPa. No information is available for the exact vehicle refuelling times required. According to DeLuchi, refuelling times are about 5 minutes. No data on the dehydrogenation/discharge times and temperatures available. Discharging, though endothermic, requires minimal energy input.

4. Ex-Situ Energy Requirements

Not needed.

5. On-board Energy Requirements

Discharging is endothermic, but the energy requirements are insignificant. Energy to maintain cryogenic temperatures provided, most probably, from battery or shaft work.

6. Projected Costs

According to 1989 estimates, for Sa-M carbon at 150 K and 54 atm, the cost data are (Amankwah, 1989):
Utility unit -- $.98
Storage unit -- $2.46

Energy consumption -- $2.52
Total Cost per MBTU-- $6.96

No data is available to upgrade these estimates and provide current cost figures for the total carbon-based system. We are told that the cost (per mile travelled) for the carbon storage is approximately 1.3 times higher than that of gasoline per cost/distance, for a small ICE vehicle.

7. Improvement Potential

Research is underway in three directions:

i) Syracuse University (Schwarz, 1994) on new carbon-based materials with organic intercalates-pillar structure.
ii) University du Quebec a Trois-Rivieres (Chahine and Bose, 1992) where higher bulk density has been achieved by squeezing the voids, and improvement in storage capacity as much as 50% over present carbons is expected.
iii) National Renewable Energy Laboratory (Heben, 1994) is engaged in developing carbon nanotubules, having surface area equal to 5000 m^2/g and 1 g/cc density.

8. Technological Maturity

The technology still under development and no on-board storage has been installed and tested. A mid-term to long range technology.

9. Infrastructure Compatibility

Electrolysis has been suggested for producing hydrogen locally in the refuelling stations since it can be scaled up or down as desired. No detailed analysis and/or any station diagrams available.

10. Safety

No data available.

11. Refuelling

Exact refuelling times are not available. According to some reports (DeLuchi, 1993), it is 5 minutes. No detailed information is available regarding discharging times and temperatures. Although, discharging is endothermic, the energy required is insignificant.

12. Hydrogen Purity

No data available.

13. Poisoning

The effect of impurities has been tested in the laboratory scale prototypes and been found that the capacity loss due to nitrogen presence, at 500 ppmv levels, will not exceed 30% (Schwarz, 1991).

Pure Hydrogen Storage Systems

The amount of a gas which can be stored in a vessel depends on three factors:

i) Pressure of the vessel
ii) Temperatures within vessel
iii) Combined effect of pressure and temperature

Therefore, principally three ways of storing hydrogen on-board vehicles may be envisioned. They are: compressed gas storage, liquid hydrogen storage and hybrid cryopressure storage respectively. The compressed gas can also be a cold gas (*e.g.* 150K) which is called thermocooled gas storage. In Table 1, storage pressures and temperatures of pure hydrogen systems are given.

Table 1. Storage Parameters for Pure Hydrogen Systems

Liquid hydrogen	15 psi, 20 K
Hybrid cryopressure	100 psi, 5 kpsi,15 kpsi at 20K
Thermocooled gas-H_2	5-15 kpsi at 150K
Compressed gas	5-15 kpsi at 300K

Compressed Hydrogen Storage

According to DeLuchi (1989), 5.7 kg of gaseous hydrogen with installed volume of 397 L at 300 K and 3000 psi would provide equivalent energy of 7.5 gallons (28.4 L) of gasoline, providing 300-mile range in a 40 mpg ICEV. To make the storage volume practical, a gas pressure of 10,000 psi is required.

The simultaneous requirements of high material strength and lightweight has led to the development of high pressure tanks that use composite materials of very high quality. Table 2 depicts the performance factors for different container technologies.

Table 2. Tank Performance Factors (Kuhn, 1993)

Tank Material	Performance Factor
steel	150,000
Aluminum	240,000
Titanium	420,000
E-Glass/Al	420,000
S-glass/Al	450,000
Aramid/Al liner	650,000
Graphite/Al liner	1,000,000
Graphite/Plastic liner	1,400,000

Performance factor is defined as: (burst pressure x volume)/tank weight. The improvement in performance factors for composite tanks are 6 and 9 times higher than aluminum and steel tanks, respectively.

Compressed hydrogen tanks have been used on-board both ICEVs and FCVs. The first fuel cell powered bus (32 ft long, 22,000 lbs chassis weight) which has operated in streets of Vancouver used on-board compressed hydrogen tanks (Presley, 1994). The hydrogen was compressed and stored in nine fiberglass-wound Aluminum cylinders, beneath the vehicle. The vehicle enjoyed a range of approximately 100 miles. At the present time, the compressed hydrogen gas can be stored at 5,000-15,000 psi pressure using high strength composite vessels. Table 3 depicts the hydrogen storage characteristics of several technologies, all systems are baseline to contain 15 lbs of hydrogen using a safety factor of 3.

With respect to weight requirements, carbon wrapped tank provides a better choice. Table 4 provides a comparison of weight and cost of various tank materials (design pressure of 5,000 psi, burst pressure of 15,000 psi, fuel volume/tank = 5 ft^3 and H_2 fuel weight/tank = 7.15 lbs). Projected cost for mass produced, carbon wrapped hydrogen storage tanks are given in Table 5.

Table 3. Storage Characteristics of 5 kpsi Compressed Hydrogen Tanks, (Kuhn,1993)

Tank	System Wt (lbs)	Wt of H_2 (lbs)	Gravimetric Ratio (%)
carbon	223.9	15	6.7
Kevlar	454.5	15	3.3
S-glass	625.0	15	2.4
E-glass waist	789.5	15	1.9

Storage volume: 7.8 ft^3.
Cost: $1000 (1992), long-term.

Table 4. Comparison of Tank Performance (Kuhn, 1993)

Tank	Weight (lbs)	Cost ($1990)	P.F. (in)
S-glass	288	1,060	450,000
Kevlar 49	207	1,259	625,000
T-1000 carbon	100	3,086	1,300,000

Table 5. Near and Long-Term Costs of C-Wrapped Tanks (Kuhn, 1993)

Tank	Material	Weight (lbs)	Cost ($)	P.F (in)
Near term				
1. C-wrapped storage tank	Al,resin, fiber	130	908	1,000,000
Far term				
2. C-wrapped storage tank	Plastic, Resin, fiber	100	326	1,300,000

Expected System Performance

1. Energy Density

For a 10,000 psi, carbon/Al storage system, we have (Block, et al. 1988):
Volummetric energy density = 5.08 MJ/L
Gravimetric energy density = 141.86 MJ/kg
On-board volummetric energy density = 2.87 MJ/L
On-board gravimetric energy density = 7.7 MJ/kg

These results are for a reference case, 40-mpg, 1000-kg ICE vehicle and a storage tank with outer to inner diameter ratio of 1.075 (also see Figure 1). According to DeLuchi (1992), for a 8,000 psi, Carbon wrapped Aluminum cylinder, the installed fuel-system energy densities are:

Volummetric = 3.4 MJ/L
Gravimetric = 7.0 MJ/kg

2. Normal State of Chemical Components

Hydrogen-- gaseous

3. Hydrogenation/Dehydrogenation Temperatures and Pressures

Temperatures near ambient and pressures are within the range of 5-15 kpsi.

4. Ex-Situ Energy Requirements

Energy required for filling is provided by ex-situ compressors.

5. On-board Energy Requirements

None required.

6. Projected Costs

$1,000 for 5 kpsi unit.

7. Improvement Potential

With continuous improvements occurring within the composite technology/industry, it is expected that cost figures to be lower in near future.

8. Technological Maturity

The technology is sufficiently mature and has already been used on-board a fuel cell driven bus (Presley, 1994).

9. Infrastructure Compatibility

To date, no ultra-high pressure hydrogen storage and refuelling station has been built or demonstrated.

10. Safety

No safety data available.

11. Refuelling

Refuelling station costs has been estimated to be 4-6 $/gJ (DeLuchi, 1992). This figure refers to the full owning and operating cost of the station. The cost of hydrogen is not included in this estimate. Refuelling time has been estimated at 3-5 minutes.

12. Hydrogen Purity

No data available.

13. Poisoning

No data available.

14. Advantages

i) More compact than Cryoadsorption and metal hydride storage.
ii) Faster refuelling time expected. No public use system till 1992.
iii) No thermal or flow management systems and no complicated piping of insulation.

Hydride Systems

Hydride systems can be divided into three categories: (1) Metal hydrides, (2) Nonclassical Polyhydride complexes and (3) Liquid hydrides or hydrogen carrier materials.

Metal Hydrides: often referred to as the rechargeable hydrides store hydrogen in the interatomic spaces of the metal. Hydrogen is discharged (evolved) when the material is heated and charged (absorbed) when the material is cooled. According to their temperature of hydrogenation and

dehydrogenation they can be divided into high temperature and low temperature hydrides (Carter, et al. 1981, Suda, 1987). The most well studied metal hydrides are listed in Table 6. In this Table, compounds are listed by the decreasing order of the percentage hydrogen content. It can be seen that the highest in the list is magnesium hydride, having also the highest high dissociation temperature (290°C).

The most commercially developing hydrides are low temperature hydrides which are listed in Table 7. It can be seen that the hydrogen weight percentage in these materials varies from 1.3-2.1% which is much lower than the high temperature hydrides.

Table 6. Hydrogen Storage Characteristics of Alloys

Hydrogen Storage Alloy	% H_2 by Weight (no containment)	Typical Dissociation Pressure (PSi) & Temperature	Heat of Formation (kcal/mol)
MgH_2	7.6	~15, (290°C)	-17.8
$Fe_{0.8}Ni_{0.2}TiH_6$	5.5	~15, (80°C)	
$Mg_2NiH_{4.0}$	3.6	~15, (250°C)	-15.4
$Ti_{0.9}Zr_{0.1}Mn_{1.4}V_{0.2}Cr_{0.4}H_{3.2}$ $Ti_{0.98}Zr_{0.02}V_{0.45}Fe_{0.10}Cr_{0.05}Mn_{1.5}H_{3.4}$	2.1 2.1	~131, (20°C) ~145, (24°C)	-7.0
$TiFeH_{1.9}$ $TiFe_{0.85}Mn_{0.15}H_{1.9}$ $TiMn_{1.5}H_{2.47}$ $Ti_{0.8}Zr_{0.2}Cr_{0.8}Mn_{1.2}H_{3.0}$	1.8 1.8 1.8 1.8	~145, (50°C) ~73, (40°C) ~101.5, (20°C) ~73, (20°C)	-5.5 -6.8 -6.9
$Ti_{0.8}Zr_{0.2}Mn_{1.8}Mo_{0.2}H_{3.0}$	1.7	~58, (20°C)	-7.0
$MmNi_{4.5}Mn_{0.5}H_{6.6}$	1.5	~58, (50°C)	-4.2
$LaNi_5H_{6.7}$ $MmNi_5H_{6.3}$	1.4 1.4	~58, (50°C) ~493, (50°C)	-7.2 -6.3
$LaNi_{4.6}Al_{0.4}H_{5.5}$ $TiCoH_{1.4}$	1.3 1.3	~29, (80°C) ~15, (130°C)	-9.1 -1.38

Table 7. Present Day Commercially Well Developed Hydrides

Hydrogen Storage Alloy	% H_2 by Weight	Typical Dissociation Temperature & Pressure
$TiFeH_{1.9}$	1.8	50°C (10 atm/150 PSi)
$LaNi_{4.6}Al_{0.4}H_{5.5}$	1.3	80°C (2 atm/30 PSi)
$Ti_{0.98}Zr_{0.02}V_{0.45}Fe_{0.10}Cr_{0.05}Mn_{.6}H_{3.6}$	2.1	24°C (10 atm/150 PSi)

Nonclassical polyhydride complexes (Jensen, 1994): are metal-ligand complexes which have coordination bonding with general formula: IrXH2(H2)(PR3)2.(X=cl, Br, I). Dihydries are just

in the research and development category and it will be a while before they will be in practice. It has been reported that (Jensen, 1994), the solids of this type can also incorporate 2 equivalents of non-bonded hydrogen. This will increase the wt% of available hydrogen from 6.5% to 8.6%.

Liquid Hydrides, also called hydrogen carrier materials: examples include cyclohexane, methyl cyclohexane etc. They are actually organic hydrocarbons and evolve hydrogen upon heating and pressurization.

Technological Maturity

The field of metal hydride is matured with many prototype systems fabricated (see Table 8). The most recent developments are 1994 Mazda-- HR-X: Powered by hydrogen in metal hydride (Hydrogen Today, 1993) and the 1992 Sanyo-Solar/Fuel cell Car with $LaNi_5$ hydride tank, having:

Capacity of storing hydrogen = 300 liters
Tank weight = 30 Kg
Car size = 4.1 m
Car weight = 400 kg including batteries

From materials development side (Suda, 1987): fluorine treatment of metals improves hydride performance appreciably. Development of Ni-coated magnesium powder as a high temperature hydride coupled to a phase change material (project by Arthur D. little). Their approach is to work under the hydrogen agreement of the international energy agency on storage, energy conversion and safety was started in 1983 by Canada, F.R.G., Japan, Sweden, Switzerland and the U.S.A. One major task VII, in the program, involves storage, conversion and safety.

Table 8. Comparison of Vehicular Hydride Storage Systems

Vehicle model	Characteristics of the energy storage system			Amount of H_2 stored		Energy density of the complete system	
	Volume	Alloy	wt (kg)	wt (kg)	Energy (MJ)	MJ/kg	MJ/L
MB 310 Van	170	TiV Mn Ti Fe	568	6.0	848	1.492 1.701	4.988 4.402
Station wagon	135	TiCr Mn Mg	365	5.0	705.7	1.933 2.901	5.227 2.601
Volga-5 Seat	-	$LaNi_5$	180	2.5	353.4	1.962	-
Forklife	130	$LaNi_5$	450	3.4	478.9	1.064	3.683

Vehicle model	Characteristics of the energy storage system			Amount of H_2 stored		Energy density of the complete system	
Minibus	550	Fe Mn Ti	113	1.57	222.6	1.969	0.405
Jeep	250	Fe Mn Ti	90	0.68	97	1.078	0.388
Pick-up	190	Fe Mn Ti	433	5.0	705.7	1.629	3.713
Truck	144	Fe Ti	563	5.44	766.8	1.362	5.321

Generally, literature work on metal hydrides is concentrated on: (i) hydride characterization, (ii) identification of new compounds, and (iii) Purification of hydrogen and dry sorption machines. Desirable characteristics sought are: ease of activation, small volume change on hydriding, high hydrogen absorption capacity, and long term stability on cycling. Basic R&D work has been ongoing in the following areas:

- Li_2PdH_2, Na_2PdH_2 (University of Stockholm)
- Mg and Pd/Mg systems (at 260-360K), 1.33-6666 pa (Chalmers University, Sweden)
- Light weight Mg, Ca, Al (University of Fribourg, Switzerland)
- $LaNi_5$ system, (University of Toronto, Canada)
- Development of reaction bed technology, dynamic pressure composition and cyclic stability (Stuttgart University, F.R.G.)
- Hydrogen uptake rate and durability of microencapsulated alloy compacts, copper coated $LaNi_5$ powder, development of practical reaction bed for $MmNi_{4.8}Al_{0.2}$ (Govt. Industrial Research Institute, Osaka, Japan)
- Metal Hydride Slurries (Brookehaven National Laboratory, U.S.A.)

Important parameters for application-related basic properties are: temperature and pressure of hydrogenation and dehydrogenation, hydrogen storage capacity, cost and stability, activation, volume change and description, heat of reaction, absorption and desorption kinetics, heat transfer (effective thermal conductivity), safety, and cyclic stability and effects of impurities. This parameters are briefly discussed below:

Temperature and pressure of hydrogenation and dehydrogenation: Intermetallic compounds have span of temperature range -20 to 300°C. But the well studied group falls into the category of 20-300°C. The temperature-pressure relationship is well documented in Vant-Hoffs plots (Suda, 1987; Sandrock, 1992).
Hydrogen storage capacity: Table 6 depicts hydrogen storage capacity of most of the well studied metal hydrides. For vehicular application the higher the storage capacity the better. But unfortunately high temperature hydrides(ionic compounds) has higher hydrogen storage capacity than low temperature hydrides(covalently bonded compounds). Best hydrides can be developed by making a compound which has a 50/50 ionic/covalent characters.

Cost and availability: Among the intermetallic hydrides of interest today, (AB, AB_2, AB_5, A_2B) type the hydrides with Ti, Zr, Ca, La turned out to be costly because of the energy required for: (i) extraction from the ore, (ii) purification, and (iii) production.

Activation: For practical applications, activation should be achievable at room temperature and at hydrogen pressures of few times the normal absorption pressure. But, TiFe requires 400°C for proper activation which is too high.

Volume changes: Since most of the metal hydrides are brittle, volume changes during hydriding/ dehydriding leads to cracking and ultimately particle size breakdown. This has advantage and disadvantage. While high surface area is generated, packing becomes difficult.

Heat of reaction: Normally H_2 absorption is exothermic while desorption is endothermic. Enthalpy of reaction is negative. This has to be considered carefully as the required heat of dehydrogenation affects its application in the fuel cell or IC engine vehicles. Figure 2 depicts Van't Hoff plots (dehydrogenation) for various intermetallic and elemental hydrides, upon which the pressure-temperature boundaries of the proton-exchange, phosphoric acid, and solid oxide fuel cell engines are superimposed. Isochores corresponding to the usable range of pressure and temperature for which a given fuel cell technology would be viable are clearly indicated.

Absorption/desorption kinetics: In general, metal hydrides show very high absorption/desorption kinetics.

Heat transfer: Metal hydrides have poor heat transfer properties (1-2 W/m°C). Various techniques including the use of special heat transfer media has been used to augment heat transfer to and from metal hydrides.

Effect of gaseous impurities: Since the vehicular storage will use the new hydrogen therefore it requires to know the effect of impurities. Four kinds of effect are observed. Poisoning, retardation, reaction and innocuous. Poisoning means rapid loss of hydrogen storage capacity with cycling. Mostly H_2S and CH_3SH have very high poisoning effect on AB_5 and AB materials. Retardation means reduction in absorption/desorption kinetics of metal hydrides as affected by NH3 on AB_5 and AB; and by CO and CO_2 on AB_5. Oxygen causes bulk reaction/corrosion of AB_5, leading to irreversible capacity loss. Whereas, N_2 and CH_4 do not seem to have any effect on AB_5 or AB (Innocuous).

Cyclic stability: An important parameter in characterizing the intrinsic effect of impurities causing reduced hydrogen storage capacity.

Safety: Because of the low pressure and near-ambient temperature involved in the use of metal hydrides they are generally viewed to be a safer means of handling and storing hydrogen.

Expected System Performance

1. Energy Density

(a) Conventional Metal hydrides
Installed gravimetric density = 1-2 MJ/kg
Installed volumetric density = 2-4 MJ/L

2. Normal State of Chemical Components

Solid -- for the rechargeable metal hydrides.
liquid -- for the methylcyclohexanes or others in that group.

3. Hydrogenation/Dehydrogenation Temperatures and Pressures

Solid metal hydrides can be divided into high and low temperature hydrides. The high temperature hydrides have smaller cation and are ionically bonded compounds. They have high percentage of hydrogen but it requires higher energy to extract them. Low temperature hydrides are covalently bonded and have low percentage of hydrogen by weight heavy metal component. If a liquid hydride such as methylcyclohexane to be carried carried, on board, a reformer is required. Dehydrogenation reaction must be conducted at 10 atmospheres (150 psi), a temperature of 400°C, a Pt/Rh catalyst, and 28% of hydrogen's higher heating value.

3. Energy Requirement of the Process

The amount of energy required depends on the particular process adopted to extract hydrogen from the material.

Conclusions and Future Activities

- A comprehensive set of criteria for evaluating the feasibility of various on-board hydrogen storage techniques has been devised and used to summarize the performance of several newly proposed and more conventional storage systems. They included: compressed gas, liquid, cryoadsorption, Fe/H_2O, MgH_2/H_2O, liquid hydrides, and metal hydride systems.

- Process of data collection, organization, analysis and verification is still on going for other prospective hydrogen storage systems.

- Both conventional and emerging hydrogen storage methods will be subject to

detailed analysis in accordance with the FC power plant concepts of both near- and long-term application.

Acknowledgments

This work has been funded by the U.S. Department of Energy under subcontract No. XAR-3-13444-01 with the National Renewable Energy Laboratory, Golden, CO. Authors wish to thank following individuals for their support and assistance: Dr. Thomas Cawthor. (NREL), Mr. William Hoagland (NREL), Drs. J. Barclay, M. Heben, C. Jensen, I. Kuhn, F. Lynch, J. Maceda, J. Schwarz, K. Young and FSEC colleagues Drs. D. Block and Kirk Collier.

References

Amankwah, K.A.G., J.S. Noh, and J.A. Schwarz. 1989. *Int. J. Hydrogen Energy*, 14(7), 437-447.

Block D., Dutta S., T-Raissi A. 1988. "Hydrogen for power applications, Task 2: Storage of Hydrogen in solid, liquid and gaseous forms." FSEC-CR-188-87, Subcontract No. XK-7-07158 to SERI.

Carpetis, C., and W. Peschka. 1980. "A Study on Hydrogen Storage by use of Cryoadsorbents." *Int. J. Hydrogen Energy*, 5, 539-534.

Carter, G.C. and F.L. Carter, Metal Hydride for Hydrogen: a review of theoretical and experimental research and critically compiled data in T. Nejat Veziroglu (ed). Metal-Hydrogen Systems. Proceedings Miami Int. Symp. Metal-Hydrogen Systems. 13-15 April, Miami Beach, FL p. 503-529. Pergamon Press, Oxford (1981).

Chahine, R., and T.K. Bose. 1992. "Low Pressure Adsorption Storage of Hydrogen." In *Proceedings of the 9th World Hydrogen Energy Conference*, Vol. 2, 1305-1314. Paris France.

Collier, D.K., C. Linkous, and A. T-Raissi. 1991. "An Overview of Hydrogen Research at the Florida Solar Energy Center." In *Proceedings of the DOE/SERI Hydrogen Program Review*. Washington, DC.

DeLuchi, M.A. 1989. *Int. J. Hydrogen Energy*, 14(2), 81-130.

DeLuchi, M.A. 1992. "Hydrogen fuel cell vehicles." *Institute of Transportation Studies, University of California, Davis.*

DeLuchi, M.A. 1993. "Solar-Hydrogen Fuel Cell Vehicles." Transportation Research, Part A, Policy & Practice, 27A(33), 255-275.

Heben, M.J. 1994. Private communication.

Hydrogen Today, Vol. 4, 1993, No. 1, p. 1-4.

Jensen, C. 1994, private communication.

Kuhn, I.F. 1993. Interim Report, office of propulsion systems conservation and renewable energy.

Lynch, F. 1992. "Hydrolysis of Magnesium Hydrides." In *Proceedings of the Seminar on H_2 Storage Technologies, Status and Challenges,* Montreal, Canada.

Maceda, J.P. and J. Wills. 1992. "Advanced Hydrogen Generation and Storage Systems for Fuel Cell Vehicle Support." *Presented at the Windsor Workshop on Alternative Fuels.*

Maceda, J.P. 1994. Private communication.

Presley, M. 1994. *Hydrogen Today*, 5(1).

Sandrock, G., S. Suda and L. Schlapbach. 1992. "Hydrogen in Intermetallic Compounds II, Surface and Dynamic Properties, Applications, Part 5. Applications." L. Schlapbach (ed), Springer-Verlag, Berlin, p. 197.

Schwarz, J.A. 1994. Private communication.

Schwarz, J.A., J.S. Noh, "Assessment of the Effect of Impurity Gases on the Storage Capacity of Hydrogen on Activated Carbon using the Concept of Effective Adsorbed Phase Molar Volume." 1991. *Int. J. Hydrogen Energy*, 16(5), 339-344.

Suda, S., metal Hydrides. Int. J. Hydrogen Energy 12, 323-331 (1987).
The Hydrogen Letter, April, 1992, Vol. VII, No. 4, p. 1-3.

Werth, J. 1994. Private communication.

Young, K.S. 1992. "Advanced Composites Storage Containment for Hydrogen." *Int. J. Hydrogen Energy*, 17(7), 505-507.

Zidan, R., D.K. Slattery, and J. Burns. 1991. *Int. J. Hydrogen Energy*, 16(12), 821-827.

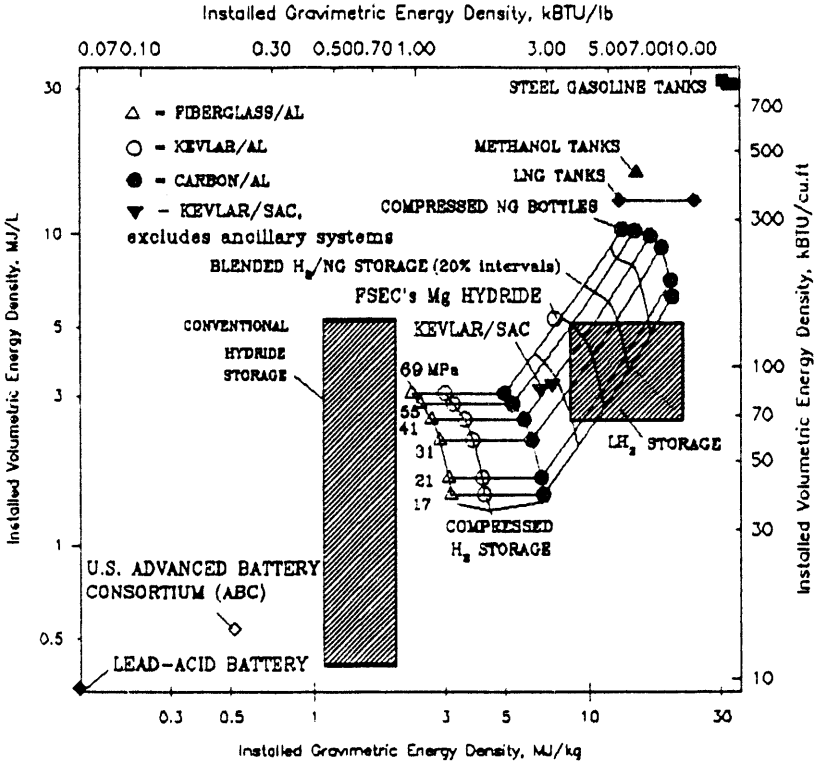

Figure 1. A comparison of various on-board vehicular energy storage options for an ICEV having 1000 kg curb weight, 250-400 mile range and 40 mpg fuel economy.

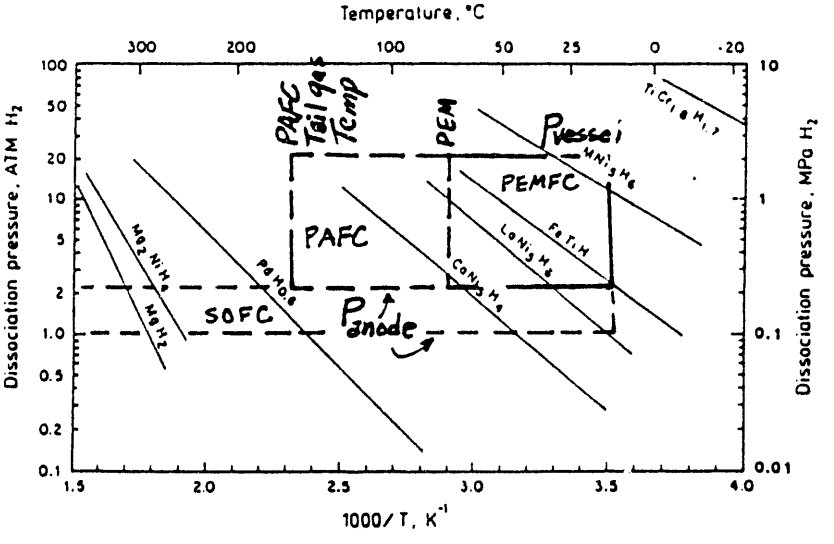

Figure 2. Van't Hoff plots (dissociation) for various intermetallic and elemental hydrides (Sandrock, 1992) and pressure-temperature boundaries for PEMFC, PAFC and SOFC. Note that the higher temperature limit for SOFC extends to 1000/T=0.7855, beyond the graph boundaries.

INTEGRATED TECHNICAL AND ECONOMIC ASSESSMENTS OF TRANSPORT AND STORAGE OF HYDROGEN

G.D. Berry* and J.R. Smith
Lawrence Livermore National Laboratory
Livermore, CA 94550

Abstract

Transportation will be a major market for hydrogen because of its great size and the value of energy at the wheels of a vehicle in comparison to its heating value. Hydrogen also offers important potential efficiency gains over hydrocarbon fuels. However, hydrogen end-use technologies will not develop without a reliable hydrogen supply infrastructure. By the same token, reliable infrastructures will not develop without end-use demand. Our task is to analyze the costs of various infrastructure options for providing hydrogen, as the number of vehicles serviced increased from very small numbers initially, to moderate numbers in the mid-term and to determine if a smooth transition may be possible. We will determine viable market sizes for transport and storage options by examining the technologies and the capital and operating costs of these systems, as well as related issues such as safety, construction time, etc. The product of our work will be data based scenarios of the likely transitions to hydrogen fuel, beginning with small and progressing to larger numbers of vehicles. We are working closely with the suppliers of relevant technologies to 1) determine realistic component costs, and 2) to assure availability of our analyses to business. Preliminary analyses indicate that the cost of transport and storage is as important as production cost in determining the cost of hydrogen fuel to the consumer, and that home electrolysis and centrally processed liquid hydrogen may provide hydrogen in the initial stages.

*Also at University of Illinois
Champaign, Illinois

Rationale

A smooth hydrogen transition will require a good match between technologies, markets, consumers and producers. The pathway from production to end-use must be well-integrated in temporal, economic, and technological terms. To accomplish this, hydrogen infrastructure systems need to be analyzed and evaluated using a consistent, clear methodology. Results of an infrastructure analysis will allow planning of transitional strategies that can achieve rapid energy market penetration. Analysis and minimization of infrastructure losses and costs is especially important for early, successful, hydrogen development because hydrogen production costs are expected to be initially high and hydrogen infrastructure generally has higher costs and lower energy efficiency than conventional energy infrastructure (natural gas, gasoline, electricity).

Background

Before the feasibility of realizing the benefits of hydrogen energy can be determined, at least three questions need to be answered. First, what are the likely costs for various methods of making, storing, and distributing hydrogen for use in automobiles? Second, can hydrogen compete economically as an automotive fuel with gasoline, natural gas, and other fuels? Third, how might a practical transition to hydrogen fuel begin if an infrastructure is not in place to distribute hydrogen to significant numbers of automobiles? In addition, there is doubt about whether a new technology, one that demands significant capital investment, can penetrate the marketplace at a fast enough rate to provide a reasonable return on investment. We address these questions by first assessing the options for hydrogen production, storage, distribution, and use for automobiles and then suggesting scenarios for a possible transition to the use of hydrogen fuel. Ogden and Nitsch (1992) and others have examined various scenarios after hydrogen has penetrated the marketplace. We are concerned in this work about the initial penetration of hydrogen as a fuel into the marketplace.

Hydrogen, like electricity, is an energy carrier and can be produced from a wide variety of energy sources such as natural gas, coal, biomass, solar (thermal, wind and photovoltaic electricity), electricity and water, and wastes such as sewage, municipal solid waste, tires and discarded oil (Texaco, 1994). The logical introduction point for hydrogen energy is in the transportation sector. Consumers currently pay a premium for transportation energy that amounts to about $80/GJ of useful energy delivered to the wheels of a gasoline automobile, compared to $14-30/GJ (5 to 11 ¢/kWh) for electricity and $5-7/GJ for natural gas heating (Hydrogen Program Plan, 1993). The transportation sector also has the greatest potential for fuel efficiency gains, from about 13% in the federal urban driving cycle to the 35-45% possible in fuel cell vehicles (Appleby and Foulkes 1993). In addition to fuel value and the potential for efficiency gains, the transportation market places premiums on efficiency and low emissions, and has a relatively high turnover of vehicles,

thereby aiding market penetration. As an efficient burning fuel, hydrogen can give vehicles performance characteristics (acceleration and range) equal to or better than today's gasoline vehicles.

However, the crucial requirement for hydrogen fuel to be competitive in the transportation sector is an economic vehicle with good performance. Although hydrogen can be used in a standard internal combustion-engine-powered car, the low average efficiency of the engine is such that economical operation on hydrogen fuel does not appear feasible. In addition, the volume of hydrogen necessary for any reasonable range is large and dominates the vehicle design. Our studies (Smith 1994) of series hybrid vehicles (fuel cell or optimized piston-engine-powered) indicate that these vehicles will require about 3.3 kg of hydrogen for a 300 mile range over the combined urban and highway average driving cycles (Figure 1).

Approach

Hydrogen vehicles will not be developed without a reliable hydrogen supply infrastructure, but neither will a hydrogen supply infrastructure develop without hydrogen vehicles to support it. This dilemma could be circumvented if small-scale on-site production of hydrogen at the residential or local station level, is practical and economical. Whether a centralized nydrogen infrastructure will be in place at the point when hydrogen vehicles reach high production levels, or whether a decentralized production system can still compete is an open question that market forces will answer. The technical and economic issues of a hydrogen infrastructure are detailed, complex and interrelated, and have been discussed by several authors (Williams 1989), (Winter and Nitsch 1988), (Peschka 1992) and (Deluchi 1992), but in the early stages of a transition to hydrogen vehicles, only small-scale hydrogen production and delivery options will be economically feasible due to market size. Consequently, we will focus on these options in order to assess the feasibility and the initial cost of operating hydrogen vehicles.

A hydrogen infrastructure pathway typically consists of energy transport from a central production center to a buffer storage and/or distribution center for delivery to a final point of use (Figure 2). Issues of scale, flexibility, vulnerability, safety, energy efficiency, capital and non-energy operating costs, and timelines should be addressed, all within the context of competing with or complementing current energy systems. An infrastructure analysis examining these issues must apply them to energy transmission and transport, hydrogen distribution and storage, and small scale production at or near the point of use.

Various yardsticks apply to each issue. For example, a good measure of the scale of a technology is the number of hydrogen vehicles or homes required to make a viable market. Flexibility and vulnerability are both economic and physical issues and vary widely with infrastructure options. Safety encompasses the parameters of probability and magnitude of accidents. Energy efficiency is the fraction of final delivered energy accounting for that used by the infrastructure to transform, transport, store, and deliver a unit of hydrogen energy. The separation of costs into capital, energy, and operating are important distinctions that make the assumptions of economic projections clear and amenable to critical review. The issue of competition with the current energy system vs. a complementary role for hydrogen will change with time. Obviously a complementary role is desirable in the near term. The timing of phasing in hydrogen over time requires further examination.

Proposed Work

Transmission

Energy can be transmitted as hydrogen in a variety of forms (gas, cryogenic liquid, adsorbed, or chemically bound) and by a number of technologies (pipelines, truck, rail, ship). Alternatively energy can be transmitted as electricity or natural gas using the existing infrastructure and converted to hydrogen at or near the point of use (possibly with cheaper thermal or chemical energy input) thus circumventing some infrastructure issues. Analyses of transmission options will depend critically upon available storage technologies. The energy transmission options we propose to examine are:

- Electricity (for hydrogen production by electrolysis)
- Natural gas pipelines (as a feedstock for hydrogen production)

The hydrogen transmission options we propose to examine are:

- Trucks (cryogenic liquid, microspheres, hydrides, other chemical carriers)
- Trains(cryogenic liquid, microspheres, hydrides, other chemical carriers)
- Hydrogen pipelines

The status and future prospects of these technologies will be looked at in terms of energy efficiency, capital costs, energy and other operating costs, timelines, and scale. This will provide a clear picture of how well each infrastructure option delivers hydrogen, the investment required, and the impact on final delivered hydrogen cost to the consumer. Transmission options which offer reasonable cost, presently or in the near term, for hydrogen in small quantities will be done first. Analyses of larger scale infrastructure will be done if time and resources permit. Each of these distribution systems has its own storage requirements.

Storage

Hydrogen can be stored in a number of forms (compressed gas, cryogenic liquid, in glass microspheres, chemically absorbed (e.g., hydrides), or physically adsorbed (e.g., carbon aerogels). These various technologies need to be examined in terms of capital costs of storage, energy cycle costs, cycle life, mobility, safety and compatibility with other infrastructure elements. Storage for transport by truck or rail is particularly important in providing a small to medium scale hydrogen infrastructure with access to low production cost hydrogen. An infrastructure storage analysis will focus on the impact of storage parameters (e.g., hydrogen weight fraction stored, storage density, storage energy cycle requirements, capital and operating costs, etc.) upon final hydrogen distribution and delivery cost. Because of the wide range of attributes, different storage technologies should be optimum for different infrastructure missions. Factors such as cycling frequency, energy prices, transport distance, and dormancy will influence the optimum choice of a storage technology. A hydrogen storage technology assessment is required to estimate the final delivered hydrogen cost to the consumer, and the importance of market size and structure to achieving lower costs.

We propose to examine the current status of and future prospects for the following bulk storage

technologies in terms of storage cycle energy costs, capital and operating costs, suitability as a transport technology, and compatibility with other portions of a hydrogen infrastructure:

- Compressed Gas
- Liquid Hydrogen
- Microspheres
- Metal hydrides

Distribution

Hydrogen distribution will be examined at the fleet, local outlet, and individual residence scale. Some parameters of interest are total distribution costs, storage costs, and space and power requirements for a typical size distribution station. The choice of a storage technology will probably depend upon the number of vehicles served. The focus of the distribution infrastructure analysis is to identify any major stumbling blocks at the distributor level to hydrogen development, and estimate the investment required and the distribution costs on a total and per car basis. The market penetration required for viable distribution stations at the varying scales can also be estimated. The distribution analysis will be integrated with the hydrogen transport and decentralized production analyses.

Small Scale Production

The choice of early hydrogen production technologies has profound infrastructure implications. This is particularly true of small scale decentralized production. Hydrogen could circumvent early problems due to lack of low cost infrastructure modes through on-site production at either the local station or residential level. The production processes which have potential for using existing large scale infrastructures (electricity or natural gas) for viable small scale production will be examined in terms of capital, operating, and energy costs. Some technologies are relatively mature while others are in research and development stages. We propose to include the following small scale production technologies:

- Electrolysis (conventional alkaline).
- Steam electrolysis (high temperature and pressure to increase efficiencies and lower costs).
- Small scale natural gas reforming (from the work of Joan Ogden).
- Small scale natural gas decomposition.
- Mediated electrochemical oxidation (partially substituting chemical for electrical energy in electrolysis).

Small scale production of hydrogen is crucial to the beginning stages of a hydrogen transition, and will eventually create markets for larger scale, lower cost, production. For example off-peak electrolysis using 10% of U.S. electricity consumption could supply roughly 40 million hydrogen powered vehicles.

Preliminary Results

Based on a cursory examination of the estimated costs of components in each scenario, we compile the costs shown in Figure 3. We emphasize that these costs are preliminary and their detailed components will be thoroughly examined and documented during the course of this work. For these results we have used off-peak electrolysis at a cost of 5¢/kWh, together with 88 hours of off-peak electrolysis per week (8 hrs per weekday and 24 hrs per day on weekends) for residential customers, and 16 hours per day for stations. Technical details of this electrolyser storage system have not yet been completed. Hydrogen production on the single user scale was assumed to require a $4000 capital investment. Residential users are assumed to borrow money at 10%. Capital cost of hydrogen gas storage at stations was estimated at $300,000 ($1000/GJ capital cost) using high pressure storage. The hydrogen volume required for 2500 kg at 80 MPa is 58 m^3 (15,500 gallons). Natural gas for station steam reforming was assumed to cost $2.40/GJ and for liquid hydrogen from central plants we assumed two costs; $25 and $45/GJ, delivered with rental on the tank trailer. The discount rate used for stations is 20%. As shown in Figure 3, the final operational cost of hydrogen to the consumer is projected to cost 2.6 - 9¢/mile for the hydrogen hybrid-electric vehicle described previously. For reference, today's 30 mpg car at a U.S. gasoline price of 33 ¢/litre ($1.25/gallon) requires 4.2¢/mile for fuel. Europeans often pay as much as $1.40/litre ($5.30/gallon), or 17.6¢/mile for their automobile fuel.

Proposed Future Work

In the coming months, we have set the following milestones:

September 1994:

- Identify technologies and estimated costs for home electrolysis.
- Liquid hydrogen delivery costs for small fleets.
- Establish delivery conditions (quantities, temperature and pressure) for on-board vehicle storage options.

March 1995:

- Preliminary analysis of technologies and costs for small station electrolysis and steam reforming (interface with Joan Ogden and ORNL).

March 1996:

- Final report.

Our work will be integrated with the analyses of Joan Ogden, particularly with respect to natural gas reforming at local gas stations and with ORNL regarding the technologies and economies of local service stations. We will work with Energetics Inc. to ensure that our results are compatible for input to their pathway analyses.

With publication of our report, our work will be available to industry.

During this summer, we will employ four graduate students who are interested in working on hydrogen technology.

Acknowledgment

This work was performed under the auspices of the U.S. Department of Energy by the Lawrence Livermore National Laboratory under contract No. W-7405-Eng-48.

References

Appleby, A.J., F.R. Foulkes. 1993. *The Fuel Cell Handbook.* Malabar, Florida: Krieger Publishing.

Deluchi, Mark. 1992. *Hydrogen Fuel Cell Vehicles.* University of California, Davis: Institute of Transportation Studies.

Hydrogen Program Plan. 1993. Washington, DC: U.S. Department of Energy.

Ogden, Joan and Joachim Nitsch. 1992. *Renewable Energy: Sources for Fuels and Electricity* (Chapter 22). Island Press.

Peschka, Walter. 1992. *Liquid Hydrogen: Fuel of the Future.* Springer-Verlag.

Smith, J.Ray. 1993. *The Hydrogen Hybrid Option*, Report UCRL-JC-115425. Livermore, CA: Lawrence Livermore National Laboratory.

"Texaco Tire Liquefaction/Gasification Project." 1994. *The Green Car Journal*, Vol.3, p.8, January 1994.

Winter, Carl-Jochen and Joachim Nitsch eds. 1988. *Hydrogen as an Energy Carrier.* Springer-Verlag.

Figure Captions

Figure 1: Conceptual Hydrogen Power Vehicle

Figure 2: Hydrogen Distribution Needs to be Examined

Figure 3: Component Cost for Fueling Options

Conceptual hydrogen powered vehicle

Electric drive motor - 40 kW (average power)
Body and frame - C_d = 0.19; 1323 kg
Cross sectional area - 1.9 m^2
Regenerative braking
95 mpg energy equivalent

PRIMARY ENERGY CONVERSION:

30 kW Optimized ICE
ICE or PEM fuel cell

or

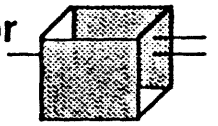

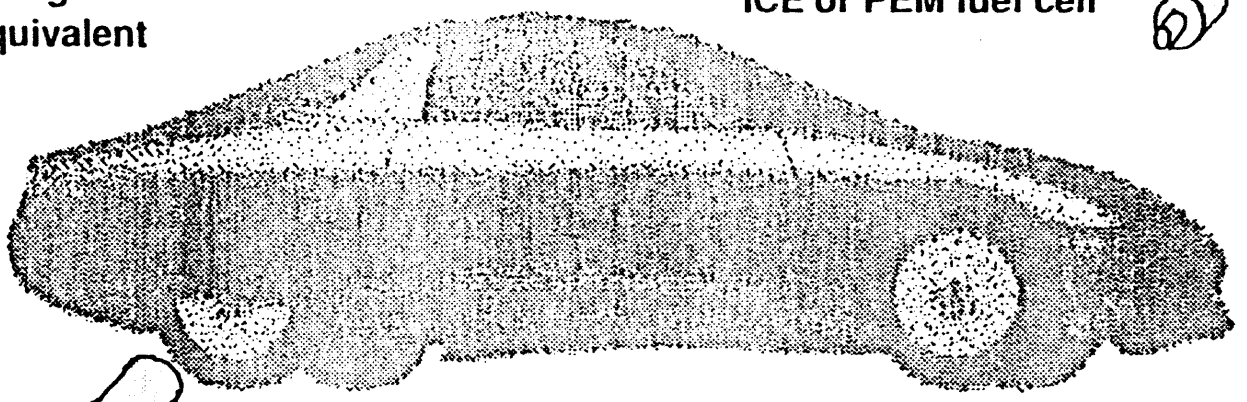

FUEL STORAGE:
3.3 kg/300 mile range

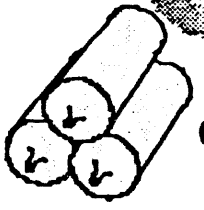

Compressed hydrogen
or

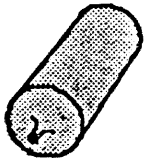

Cryo-compressed hydrogen
or activated cryo-carbon
hydrogen storage
or

Liquid hydrogen
or

Light-weight hydride

SECONDARY ENERGY STORAGE (2 kWh, 100 kW peak)

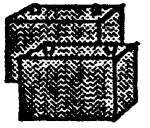

Advanced Batteries
or

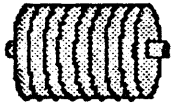

Ultracapacitors
or

Advanced Flywheel

Figure 1

Hydrogen distribution needs to be examined

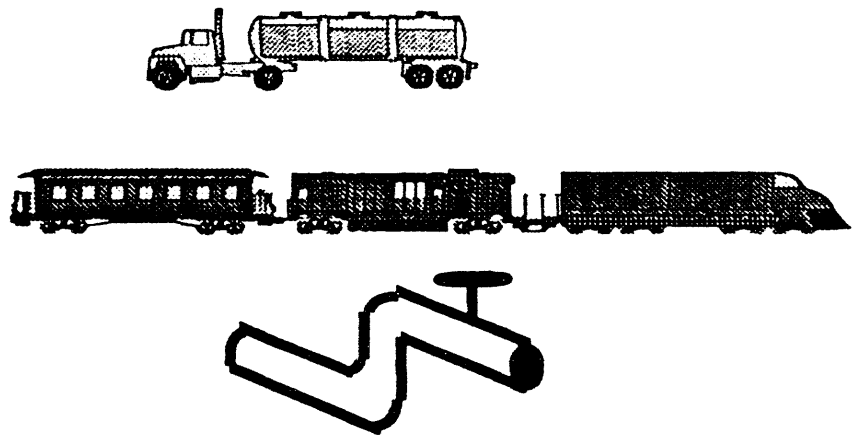

	Transport	Storage
Mass Market Options		
	Truck	Cryogenic liquid
	Rail	Metal hydride
	Dedicated pipeline	Compressed gas
Small Market Options		
	High voltage transmission	Electricity for on-site electrolysis
or	Natural gas pipeline	Natural gas for on-site reforming

Figure 2

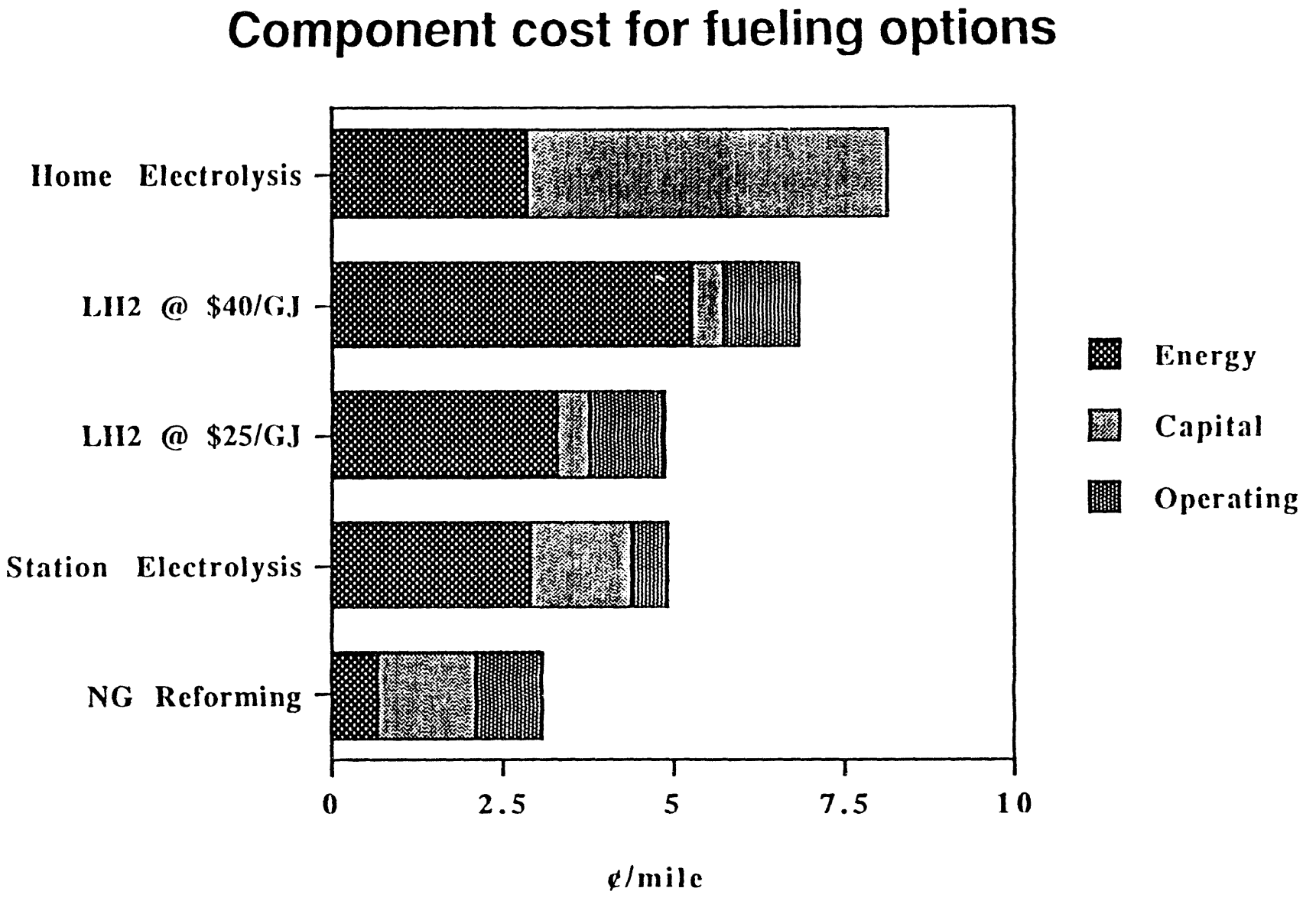
Component cost for fueling options
Home Electrolysis
LH2 @ $40/GJ
LH2 @ $25/GJ
Station Electrolysis
NG Reforming
0
2.5
5
7.5
10
¢/mile
Energy
Capital
Operating

Figure 3

ENGINEERING AND REGULATORY REQUIREMENTS FOR HYDROGEN REFUELING FACILITY

Suman P. N. Singh
Chemical Technology Division
Oak Ridge National Laboratory
Oak Ridge, Tennessee 37831-6495

ABSTRACT

The project consists of conducting an engineering assessment (including infrastructure analysis) for a small scale (~ 1 MMSCFD) stand-alone natural gas reforming facility to produce fuel hydrogen for a fleet (e.g., intra-city buses) fueling facility. This project is being undertaken as part of the U. S. Department of Energy (DOE) Hydrogen Fuels Infrastructure Development Program. The goal of the program is to demonstrate the viability of using hydrogen as an environmentally desirable replacement for currently-used fossil-derived transportation fuels and to serve as a test-bed for future hydrogen fueling stations.

The study is envisaged to require a one person-year level of effort and is expected to commence in April/May 1994. The study will result in a draft assessment report on the infrastructure analysis for a small-scale stand-alone hydrogen fueling facility and a draft systems requirements document for the stand-alone hydrogen fueling station demonstration facility.

The project plan consists of the following steps:

- Assimilate data on conventional and innovative natural gas-to-hydrogen conversion processes such as steam reforming, partial oxidation, and direct conversion.
- Develop the near-term end use fuel requirements for a typical fleet operations facility such as daily fuel requirements, buffer storage facilities, and environmental considerations.
- Engineer a stand-alone hydrogen production facility to meet the above requirements including developing process designs, cost estimates, and treatment and disposal of the secondary wastes from the production of hydrogen using the alternate natural gas conversion processes.

- Perform systems studies of the alternate hydrogen fueling station designs including conducting cost/benefit analyses of differing environmental and permitting requirements likely to be imposed on the fueling facility.
- Identify impediments to market penetration of hydrogen as a fuel or energy vector.
- Propose solutions to resolve the impediments including identifying research, development, and demonstration opportunities for DOE to spearhead and complete.
- Develop systems requirements for the demonstration of a prototype small-scale stand-alone natural gas-to-hydrogen conversion operation producing merchantable hydrogen.

The following activities could be conducted as follow-on activities to the assessment in later years, at DOE's request:

- Coordinate the conduct of the stand-alone small-scale prototype hydrogen fueling station demonstration.
- Perform engineering assessments and infrastructure analyses of for example, other hydrogen production processes (e.g., from biomass and other renewable resources) and other hydrogen fuel applications such as fueling stations for personal automobiles (similar to present-day "gas stations"), space heating, and power generation.
- If requested, coordinate prototype demonstrations for the other hydrogen fuel applications to establish the viability of these applications and conversion processes.

The project is part of the DOE Hydrogen Fuels Infrastructure Development Program and will interact closely with industry, other research organizations, and universities to encourage and result in optimum technology transfer.

FY 1994 Funding: $ 200 K.

HYDROGEN UTILIZATION IN INTERNAL COMBUSTION ENGINES

J.D. Naber, R.M. Green, and D.L. Siebers
Sandia National Laboratories
Combustion in Engines & Furnaces Department
MS 9053, Org. 8362
Livermore, CA 94550-0696

Abstract

Using hydrogen as a fuel in an internal combustion engine offers a number of important advantages to the engine designer along with significant challenges. The wide flammability limits, high flame speed, and high octane-rating of hydrogen/oxygen mixtures allow significant flexibility in the design and optimization of the combustion system. By employing engine design features such as lean and/or dilute fuel mixtures and high compression ratios, hydrogen-fueled engines offer the potential of very low NO_x emissions (with no CO_2 in the exhaust) combined with high thermal efficiency.

Introduction

The development and optimization of internal combustion (IC) engines utilizing hydrogen must focus on the issues of fuel preparation and engine operating conditions that are integrally connected. Selection of a fuel preparation technique such as carburetion versus direct-injection dictates many aspects of the combustion control mechanisms. For example, a carburetor allows the use of premixed lean mixtures to control emissions (Das 1987) which is not possible with a late direct-injection, compression-ignition system. Whereas direct-injection compression-ignition systems eliminate concerns such as preignition and flashback that have been problematic with hydrogen engines in the past (Das 1991).

Hydrogen Utilization in IC Engines

The IC engine hydrogen utilization projects at Sandia are focused on advancing the technology base for developing and optimizing hydrogen engines for a wide array of uses including transportation and heavy-duty applications. An example in the transportation class is a reciprocating IC engine operating at a single speed and load that has been optimized for efficiency and emissions for use in a hydrogen/electric hybrid vehicle (Smith 1993). Examples for use in heavy-duty applications include engines for locomotives, trucks, buses, and stationary power sources. With this wide range of applications in mind, two tracks of combustion research are being conducted simultaneously. In the first project, premixed spark-ignition combustion systems are being evaluated, investigating the effects compression ratio, engine speed, and equivalence ratio have on thermal efficiency and NO_X emissions. A goal in this project is to quantify the effects of these parameters in order to define optimal engine conditions for the design of a single speed-load engine. In the heavy-duty applications project, the direct-injection of hydrogen and hydrogen/methane fuel mixtures is being explored. Goals in this project are to quantify the fuel/air mixing, autoignition, and NO_X formation processes in DI hydrogen engines.

Spark-Ignition Engine

In support of the objective of defining a spark-ignition engine design optimized for hydrogen fuel applications, we will direct our initial experimental effort at verifying the currently accepted relationship between NO_X emissions and equivalence ratio. The principal data are those of Das 1987 (see Figure 1). These data represent engine operating conditions of 2000 rpm and compression ratios varying from 6:1 to 11:1. Figure 1 shows the effect of equivalence ratio on brake thermal efficiency and NO_X emissions for compression ratios of 6:1, 8:1, and 11:1. The essential feature of the data is the precipitous drop in NO_X emissions at equivalence ratios between 0.4 - 0.7. The other important area that we will address in our initial effort concerns the thermal efficiency of the spark-ignition engine running on hydrogen fuel. Figure 2 illustrates this aspect of engine performance using the data of Das 1987, King 1958, and Oehmichen 1942, showing the relationship of thermal efficiency with compression ratio.

In our experimental work, we intend to verify the existing equivalence ratio/NO_X emission data

and extend them to higher engine speeds and compression ratios. In addition, we will investigate the trade-off between lean and dilute operation as regards to its affects on the NO_x emissions. Further, we intend to validate the thermal efficiency data described above and attempt to extend the results to illustrate the effects of engine speed, equivalence ratio and dilute operation. We will carry out our experimental work using a single cylinder CLR (Cooperative Lubrication Research) engine modified to allow the compression ratio to be varied and EGR (exhaust gas recirculation) to be added. We intend to operate the engine premixed and normally aspirated. The primary instrumentation will be in-cylinder pressure measurements for combustion performance indication and CLA (chemiluminescence analyzer) for the measurement of NO_x in the exhaust.

We expect that the data we obtain in this work, along with the results that already exist in the literature, will assist in the design of an optimized, premixed spark-ignition engine for operation on hydrogen fuel so that it can be carried out in an efficient and timely manner.

Direct-Injection Compression-Ignition Engine

In support of the design and optimization of a hydrogen engine for heavy-duty applications we will be examining a direct-injection combustion system with possible compression-ignition. In this combustion system the fuel injection process is a major design parameter that controls combustion and is used to optimize engine efficiency and emissions. We will initially focus on the fuel injection system and fuel/air mixing processes. For this work we will be using various optical diagnostic techniques to visualize and quantify the fuel/air mixing process under typical engine operating conditions. Also as part of this work, we will be investigating the conditions under which hydrogen and hydrogen/methane fuel mixtures may be used in compression-ignition (CI) engine applications. Only a limited number of studies on the use of hydrogen in a CI engine are available (see the review by Das 1991) and even less is known about the use of hydrogen/methane fuel mixtures under CI conditions. Previous studies on the use of hydrogen in CI engines show conflicting results. In studies done by Homan 1978, in a high compression ratio engine, a glow plug was required to assist the ignition process. However, Ikegami *et al.* 1980, 1982 found that pure compression-ignition of a hydrogen fueled engine was possible.

Another important engine design parameter to reduce NO_x emissions that has not been fully explored in a direct-injection, mixing-controlled combustion engine is the use of dilution of the intake air charge by either EGR or scavenging. These dilution techniques work by reducing the flame temperature and oxygen availability of the hydrogen/oxidizer mixture thereby reducing the NO_x formation which is highly sensitive to temperature (Heywood 1988).

The diesel engine simulation facility at the Combustion Research Facility at Sandia will be used for the initial experiments. This facility (Siebers 1985, Naber *et al.* 1994) offers significant flexibility. First, the simulation facility is capable of producing an extended range of thermodynamic conditions including typical diesel engine top-dead-center conditions. The thermodynamic conditions (temperature, pressure, and dilution) at the time of injection can be varied simply, quickly, and independently in the facility without hardware changes that may be required in an engine. Second, the facility's combustion chamber has full optical access for visualization and quantification of the fuel/air mixing processes at operating engine thermodynamic conditions. The combustion facility has been previously used to investigate the

ignition properties of gaseous fuels such as methane, methane/ethane mixtures, and natural gas (Naber *et al.* 1994, Fraser *et al.* 1991), and liquid fuels such as methanol, ethanol, and diesel fuel (Siebers et al. 1985).

In the experimental work we intend to investigate the fuel/air mixing processes that dominate the control of combustion. A high pressure (350 atm) electronic fuel injection system has been incorporated into the facility that allows independent control of injection timing, injection pressure, and ambient gas thermodynamic state. In addition, the fuel injector can be fitted with a number of different sized orifices (0.25 - 1.0 mm in diameter). The mixing process will be examined using high speed schlieren photography along with planar laser diagnostic techniques. These studies will provide a data base on the mixing and air utilization fundamentals of a gaseous direct-injection fuel system for optimization of the fuel injector and engine combustion chamber design. This data base will also be provided to Los Alamos National Laboratory for validation of the fluid mechanics models being developed for engine design tools.

In addition to the fuel/air mixing studies, autoignition studies of hydrogen will be investigated using the diesel engine simulation facility coupled with the kinetics models developed at Lawrence Livermore National Laboratory. Using the flexibility built into the facility, the ignition process will be studied over a range of ambient thermodynamic states, including dilution affects simulating EGR. This will lead to the identification of conditions most appropriate for hydrogen compression-ignition in an engine. The ignition data base provided through these studies will define the engine's compression ratio and intake systems. In addition the hydrogen ignition experimental data along with comparisons to chemical kinetic predictions from Lawrence Livermore National Laboratory's chemical kinetic models will determine the controlling factors of hydrogen ignition. These data are useful in both improving the compression ignitability in CI engines and eliminating the preignition and knocking problems in SI engines.

References

Das, L. M. 1987, Ph.D. Thesis, IIT Delhi, India, *Studies on Timed Manifold Injection in Hydrogen Operated Spark Ignition Engine: Performance, Combustion and Exhaust Emission Characteristics.*

Das, L. M. 1990, "Hydrogen Engines: A View of the Past and a Look into the Future." *Int. J. Hydrogen Energy*, 15: 425-443.

Das, L. M. 1991, "Exhaust Emission Characterization of Hydrogen-Operated Engine System: Nature of Pollutants and Their Control Techniques." *Int. J. Hydrogen Energy*, 16: 765-775.

Fraser, R.A., Siebers, D.L., and Edwards, C.F. (1991), "Autoignition of Methane and Natural Gas in a Simulated Diesel Environment," *Trans. of the SAE*, 100: 33-45 (SAE paper 910227).

King, R. O., Hayes, S. V., Allan, A. B., Anderson, W. P. and Walker, E. J. 1958, "The Hydrogen Engine: Combustion Knock and the Related Flame Velocity." *Trans of the E.I.C.*, 2: 143-148.

Heywood, J.B. 1988, *Internal Combustion Engine Fundamentals*, McGraw-Hill.

Homan, H.S. 1987, *An Experimental Study of Reciprocating Internal Engines operated on Hydrogen*, Ph.D. Thesis Cornell University.

Ikegami, M., Miwa, K., Shioji, M. 1980, "A Study of Hydrogen-Fuelled Diesel Combustion." *Bull. JSME*, 23.

Ikegmai, M. 1982, "A Study of Hydrogen-Fuelled Compression Ignition Engines." *Int. J. Hydrogen Energy*, 7.

Naber, J.D., Siebers, D.L., Di Julio, and Westbrook, C.K. 1993, "Natural Gas Fuel Variability Effects of Ignition Delay Under Diesel Conditions." Western States Section of the Combustion Institute, paper WSS/CI F 93-097.

Oehmichen, M. 1942, "Hydrogen as an Engine Fuel," Engine Laboratory of the Technische Hochschule, Dresden, Germany, *V.D.I.* Paper No. 68, (English translation).

Siebers, D.L. 1985, "Ignition Delay Characteristic of Alternative Diesel Fuels: Implications on Cetane Number." *Trans. of the SAE*, 94: 673-686, (SAE paper 852102).

Smith, J.R. 1993, "The Hydrogen Hybrid Option." Workshop on Advance Components for Electric and Hybrid Electric Vehicles, Gaithersurg, MD.

Figure Captions

1. Brake thermal efficiency and NO_X emission in a SI hydrogen-fueled engine (Das 1987).

2. Brake thermal efficiency as a function of compression ratio in SI hydrogen-fueled engines.

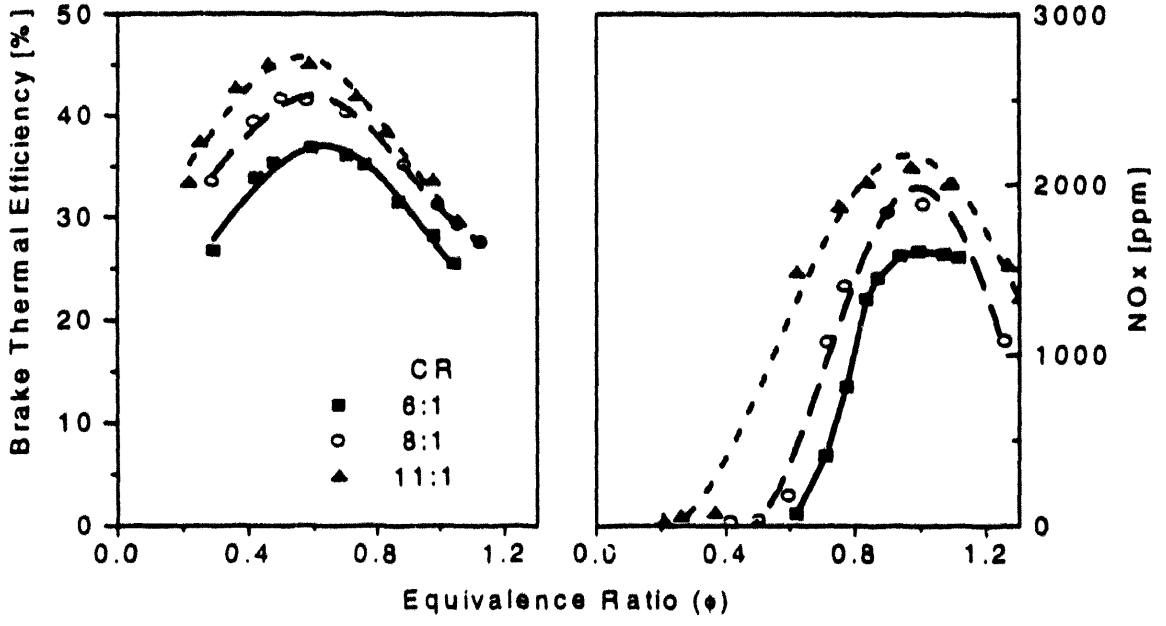

FIGURE 1

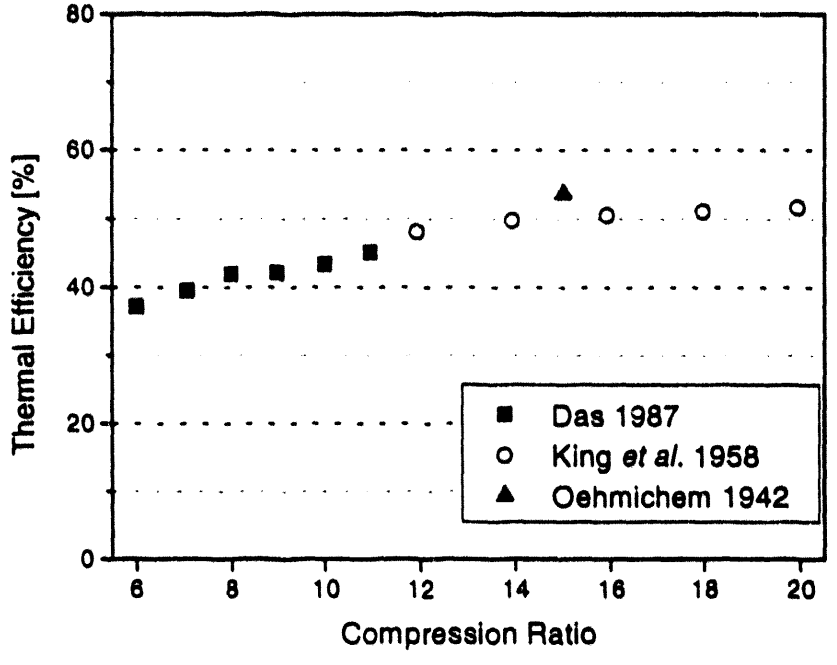

FIGURE 2

HYDROGEN PROGRAM COMBUSTION RESEARCH: THREE DIMENSIONAL COMPUTATIONAL MODELING

Anthony A. Amsden, T. Daniel Butler, and Norman L. Johnson
Los Alamos National Laboratory
Los Alamos, NM 87545

Abstract

The hydrodynamics of hydrogen gas injection into a fixed-volume combustion chamber is analyzed and simulated using KIVA-3, a three-dimensional, reactive flow computer code. Comparisons of the simulation results are made to the preliminary data by Sandia National Laboratory. The gas injection problem is found to be of comparable difficulty as the liquid fuel injection of diesel engines. The primary challenge in the hydrodynamics is to describe the large change of length scale from the flow of gas in the orifice to the penetration in the combustion chamber. For the current experiments, the change of length scale is on the order of 4000. A reduction of the full problem is proposed that reduces the change in length scale to about 400, with a comparable improvement in computational times. Comparisons of the simulation to the experimental data shows good agreement at early times in the penetration history. At late times the comparison is sensitive to the method of determination of the penetration in the simulations. Because the preliminary experiments include combustion and the KIVA simulations do not, further analysis and experimental data are required for a final comparison.

Introduction

Los Alamos has developed a family of computer models that have gained wide acceptance in the automotive industry, as well as the gas turbine, stationary combustion and aerospace industries, primarily for hydrocarbon fuels. These models are being applied to hydrogen injection and combustion to support industrial collaboration in the DOE Hydrogen Program. The work contributes to two areas by developing the knowledge (1) to enable industry to build a stationary hydrogen-fueled internal combustion engine to power an electric generator system, and (2) to

build an advanced, high-power-density internal combustion engine fueled by hydrogen to meet zero emission requirements. The thrust of this effort is to understand the operation of internal combustion engines using such fuels in order to design new, efficient engines, thereby accelerating hydrogen utilization in the private sector. The approach that is taken to fulfill these goals is to modify appropriately the latest of the publicly released codes, KIVA-3, and one soon to be released, KIVA-F90, to facilitate the analysis of hydrogen combustion with both pure hydrogen as a fuel and mixtures of hydrogen and natural gas.

This report focuses on the first stage of the development of the models for hydrogen combustion: the comparison and analysis of the experimental data of natural gas and hydrogen injection in a constant-volume combustion vessel as performed by Sandia National Laboratory at Livermore (apparatus and natural gas injection is described in Naber et al., 1993). In particular, the hydrodynamics of the injection process is examined in detail. Modeling strategies developed for the SNL experiments will be applicable to later modeling of full engines. Because only preliminary data is currently available from SNL, the present analysis should also be considered preliminary.

Description of SNL Experiments

The combustion vessel in the SNL experiments is a pancake combustion chamber with a 114.3-mm diameter and a 28.6-mm axial width. The two circular walls of the chamber are sapphire windows that permit full field-of-sight optical access to the chamber. Characteristics and operating conditions of the chamber and injector are summarized in Table 1. The gas is introduced through a single orifice. The injection profile is a square pulse with a 100-μs rise time to 0.9 of its steady state value.

Table 1 Details Of SNL Gas Combustion Experiments

Chamber volume (cm^3)	**293.2**
Chamber wall temperature (°K)	**450**
Orifice diameter (μm)	**250.0**
Orifice length (μm)	**1000**
Injection pressure (MPa)	**20.7**
Injection duration (s)	**0.011**
Mass of H_2 injected (gm)	**0.00490**

The initial conditions of the air mixture in the chamber before injection are achieved by the premixed combustion of a small amount of combustible gas (H_2 and C_2H_4), such that the resulting composition is similar to air (Table 2). After combustion, the heated mixture is allowed to cool until the desired chamber pressure and gas density are achieved, and the gas fuel injection is initiated. The experimental results reported here are for hydrogen gas injection, although methane injection experiments have also been performed and analyzed. Because of the transparency of hydrogen in the air mixture, the penetration of the gas jet cannot be visually observed until the hydrogen autocombusts.

Table 2 Initial Species Gas Density in g-cm^{-3} Before Injection

Oxygen	0.00398
Nitrogen	0.01312
Carbon dioxide	0.00115
Water	0.00067
Average molecular weight:	29.47

Computational Modeling

Description of the KIVA Reactive Flow Code

The KIVA family of codes, developed at Los Alamos National Laboratory (LANL), is a mature, three-dimensional, computational fluid dynamics software for chemically reactive, transient flows with fuel sprays (Amsden et al., 1989). The code features sophisticated sub-models, which simulate the complex flow, thermodynamic and chemical processes accompanying combustion. These models include for applications to combustion engines: turbulence, spray atomization, fuel penetration and vaporization, auto-ignition and combustion. The chemical combustion model can describe complex equilibrium and kinetic reactions, giving it the capability of modeling soot in the presence of carbon and NOx production. The KIVA-3 version (Amsden, 1993) enables complex geometries to be modeled, typical of combustion engines with moving pistons and inlet and exhaust ports. KIVA-3 runs on generic workstations and on supercomputers. A new version of KIVA, KIVA-F90, is written in FORTRAN-90 and will execute on massively parallel machines. For the current application, KIVA-3 is used to model the SNL experiments.

Computational Approach

The physical processes that are important in the SNL experiments are the flow of the injected gas in the injector nozzle, the transitional flow from the tip of the injector into the chamber, the interaction of the gas jet with the gas in the chamber and the consequent generation of turbulence and the heat exchange, mixing and eventual combustion of the hydrogen and air. The production of NOx and timing of the autocombustion are sensitive to the extent of turbulence mixing. For the purposes of the present study, the focus is on the flow dynamics of the injection, penetration, and mixing; the combustion processes will be considered in a later report.

Computational modeling of the SNL hydrogen combustion experiments requires specification of the initial conditions of the combustion chamber and an approach to the modeling of the gas injection process. Despite the apparent simplicity of the injection of a combusting gas into air, the disparate length scales in the flow present a formidable challenge to the computational modeling. The ratio of the largest length scale, the penetration of the gas jet, to the smallest length scale, the flow variations within the orifice (taken to be 1/10th the orifice diameter), is about 4000. This large ratio precludes the straightforward approach of treating the entire process in a single computational mesh that resolves all length scales, which would lead to impractical computational times.

Because the final goal of the computational modeling is to provide tools for designers of hydrogen fueled engines, a computational approach is ultimately required that will give accurate results on the comparatively coarse meshes that are necessary for full or partial engine simulations. Throughout the modeling of the SNL experiments, the modeling choices were made with this goal in mind and are outlined in the following sections. The approach is to divide the flow problem into tractable problems that can be analyzed separately and then sequentially coupled. These are (1) the flow in the nozzle, which determines the nozzle exit conditions, (2) the expansion and cooling of the flow from the nozzle in the region just next to the nozzle, and (3) all processes that follow. The advantage of this approach is that the smallest length scales, a fraction of the orifice diameter, can be eliminated from the simulation of the jet penetration and combustion, thereby, significantly improving the simulation times.

As a point of reference, special modeling is also required for the more traditional injection of liquid hydrocarbon fuels for diesel engines. Comparable challenges in the disparity of length scales also occur. The technique that has been employed is to treat the liquid fuel jet as Lagrangian droplets that flow through a stationary mesh (Amsden et al., 1989). In this manner the orifice of the injector does not need to be resolved and the computation can proceed significantly more efficiently than if the injection of the liquid fuel were resolved. This approach has proven to be accurate and is well accepted by the modeling community. The challenge for the modeling of the injection of a gas is that no comparable approach has been developed.

Choked Flow Nozzle Dynamics

The known experimental conditions for the gas injector are the pressure and temperature of the hydrogen reservoir behind the orifice and measurement of the mass injection rate. The exit conditions from the nozzle can be estimated by assuming, and later verifying, that the flow is limited by the sound speed of the gas, i.e., the flow is choked. If we further assume that under these flow conditions the hydrogen is nearly a perfect gas and flows isentropically through the short nozzle, the pressure, density, sound speed and temperature at the exit are given by:

$$P^* = P_0\left(\frac{2}{\gamma+1}\right)^{\frac{\gamma}{\gamma-1}} = 10.9 \text{ MPa}$$

$$\rho^* = \rho_0\left(\frac{2}{\gamma+1}\right)^{\frac{1}{\gamma-1}} = 0.00707 \text{ g cm}^{-3}$$

$$c = \left(\frac{\gamma p}{\rho}\right)^{\frac{1}{2}} = 147{,}000 \text{ cm s}^{-1}$$

$$T^* = 375 \text{ K}$$

where γ is calculated to be 1.39, the pressure and temperature have values as in Table 1, and the density and temperature are found from the equation of state for hydrogen. Because of viscous losses on entry to the nozzle, the flow rate is typically lower than as determined from the soundspeed by some factor, taken to be 0.85 for a short nozzle with sharp corners. This gives an actual value for the exit velocity to be:

$$v_{act} = 0.85\ c = 127{,}000\ cm\ s^{-1}.$$

and the mass flow rate, assuming a uniform velocity profile for fully developed turbulent flow, of 0.444 g s^{-1}. This value is in agreement with the experimentally-observed mass flow rate of 0.445 g/s, resulting in a discharge coefficient of 0.87, which is close to the assumed value of 0.85.

Highly Resolved Modeling of Near-Nozzle Dynamics

Upon exiting the orifice, the hydrogen undergoes expansion and cooling and rearrangement of the velocity field across the jet. To better understand this process and to provide inflow conditions for the less resolved simulations discussed in the following section, a detailed simulation of the fluid dynamics in the neighborhood of the nozzle was performed. The flow in the region of the nozzle is assumed to be axi-symmetric, because the curvature of the walls is small and other bounding surfaces are far removed. Therefore, a highly resolved two-dimensional mesh was used. Five cells of uniform spacing were used across the radius of the nozzle outlet. Away from the nozzle, radially and axially, the mesh size was expanded to reduce the total number of cells in the simulation. The inflow conditions for hydrogen gas are the values determined in the previous section, assuming the velocity profile at exit from the nozzle is flat. The turbulence is described by a k-ϵ model. The turbulence intensity of the inflowing gas jet is taken to be 1/100th of the kinetic energy of the jet. A solid wall boundary of constant temperature as in Table 1 is used on the side of the mesh where the jet exits. The other two sides of the mesh are specified to be outflow boundaries of constant pressure, taken to be the initial pressure of the gas in the chamber. The initial conditions and composition of the gas mixture are initialized with the values specified in Tables 1 and 2.

After about 60 μs, the mass of hydrogen within the mesh is constant and the system has reached a steady-state flow. The velocity vector field, Mach number and H_2 mass fraction at steady state are found in Figures 1 through 3. The angle of expansion of the jet is observed to be about 7 degrees. In Figure 4, the normalized velocity, pressure, density and temperature along the axis are plotted. Significant expansion, subsequent cooling and acceleration occurs shortly after the hydrogen leaves the nozzle at about 0.04 cm from the exit and then quickly stabilizes and remains constant. This is typical behavior for an choked nozzle flow at these conditions. Also shown in Figure 4 are the spatially averaged values over the diameter of the nozzle just after the exit gas has stabilized. The averaged values differ from the centerline values because of the drag, heat transfer, and mixing of the gas in the chamber with the hydrogen. Comparisons of the averaged values with the axial values show that the major effect of the surrounding gas is to diffuse momentum away from the axis, as can be observed in the velocity field in Figure 1. The averaged values plotted in Figure 4 are given in Table 3.

Table 3. Steady State And Spatially Averaged Values Of The Expanded Jet At An Axial Position Of 0.037 Cm

Axial velocity (cm s^{-1})	**141,000**
Temperature (K)	**329**
Pressure (MPa)	**6.26**
Density (g cm^{-3})	**0.0050**

The results of this simulation shows that the effect of the expansion of the jet is significant and must be taken into consideration. The decrease in hydrogen temperature by 12 percent, or 45° K, will likely lead to a delay in ignition. Furthermore the expansion occurs at a length scale that cannot be resolved on the typical mesh size required for practical engine simulations. Hence, if the exit conditions had been used on a coarse mesh, the expansion of the jet would not be simulated correctly and the simulation would be suspect.

Three-Dimensional Modeling of SNL Combustion Bomb

The averaged values determined from the fine-scale simulation in the last section were used in a simulation of the injection into the full SNL combustion chamber. In Figure 5, the 3D mesh that was used is shown. The mesh dimensions are 36 by 12 by 10. Also drawn on Figure 5 is the size of the 2D mesh used in the previous section in a blowup of the corner of the 3D mesh. This illustrates the drastic change of length scales that occur in this flow problem. For the 3D injection problem, the size of the orifice is the smallest dimension of the cell in the corner of the mesh within the proscribed 2D box. To minimize the computational times, only one fourth of the full system is modeled by taking advantage of the two planes of symmetry in the experiment. The orifice was resolved with a single cell with one fourth the area of the orifice, with correspondingly 1/4 the mass flow into the mesh. The boundary conditions are chosen appropriately: the chamber walls are modeled as solid walls of constant temperature, the internal fluid boundaries are reflective symmetry planes. The initial conditions of the gas in the mesh are specified as in the last section.

Many three-dimensional simulations were made to determine the sensitivity to the meshing and the numerical and physical models in KIVA. It was found that the penetration was most sensitive to the mesh size near the orifice and the turbulence model. With either a poorly resolved mesh or the standard turbulence treatment, the simulations severely underpenetrated, even at early times. We concluded that to obtain the penetration necessary to describe the experimental data, a standard modeling approach would require a much finer mesh than would be practical for repetitive 3D simulations. Hence we examined modifications to the turbulence model that would allow an accurate computation on a coarser mesh.

Because of difficulties that arise with the turbulence model on a coarse mesh, primarily the generation of unrealistic turbulent length scales, modifications were made to the KIVA runs to limit the largest length scales in the region of the hydrogen jet. The approach used is to limit the length scale in the KIVA simulation to a length equal to the distance away from the orifice within a 7 degree cone along the axis.

In Figure 6 the preliminary experimental data are plotted for a gas temperature of 1150 K, along with the most promising simulation results to date. A question arises as to how best to determine the penetration

of the jet for comparison to the experiments. Plotted in Figure 6 are the penetration as determined by the 1 and 3 percent contours of hydrogen gas density. Although either of these penetration determinations by KIVA match the experimental penetration at early times quite well, at later times, the two specifications of the penetration bracket the experimental data. This trend will continue as the hydrogen front becomes more diffuse. Because the hydrogen jet cannot be observed in these preliminary experiments until combustion has begun, data is not shown for early times. The KIVA results in Figure 6 do not include combustion at present. Consequently, there is an unanswered question as to the effect of combustion on penetration, and it is possible that the comparison of the simulation and the experimental data will differ when combustion is included into the simulation or when noncombusting experimental data is available. Because of these uncertainties, the simulation was not extended to later times.

Future Work

To resolve the sensitivity to the method of determination of the penetration history at late times of the KIVA simulations, we plan to examine the penetration history with finer meshes. Concurrently, SNL is planning experiments that examine the penetration in the absence of combustion and replacing the preliminary data in Figure 6 with final data. Together, these should resolve the accuracy of the present modeling approach. Ultimately an approach will be developed for the description of a gas injection that will be usable by industry on their in-house computing systems.

When the noncombusting penetration is well described, the effects of combustion will be examined. Initially a 22-reaction hydrogen combustion model (NASP, 1990) will be used until the LLNL developed kinetics model is available and implemented into KIVA.

Later work will include comparison of KIVA-3 code predictions with the optically based experimental data gathered in-cylinder during engine operation, the use of massively parallel computer architectures for such analyses by modifying and extending KIVA-F90 to apply to hydrogen fuels, and the transfer of the validated codes to appropriate industrial engine developers for their use in analyses of engine designs.

Conclusions

The current state of numerical modeling of gas injection is comparable to the early state of modeling of liquid fuel injection for diesel engines in the late 1970's. Given the increased understanding of the liquid injection problems over time, special techniques were developed to model accurately the problem on meshes of practical interest. This report describes the comparable challenge of resolving the large disparity of length scales for gas injection and an approach to numerically modeling the problem.

From a simulation and analysis of the dynamics of the exit of the gas from the orifice, significant modifications of the exit conditions of the gas occur at a length scale about 1/200 the size of the combustion chamber and must be included in a realistic simulation of the injection process.

Many fully three-dimensional simulations were made of the SNL experiments with methane and hydrogen injection, with and without combustion. From simulations performed to date, the penetration history if found to be highly sensitive to the mesh refinement and the treatment of turbulence. Overall, the

outstanding challenge of the modeling will be the description of the penetration history of the gas jet on poorly resolved meshes. The approach taken in this report is to remove the details of the jet dynamics upon exit from the orifice and model the expanded jet on a coarser mesh. This approach reduces run times by a factor of 10 and is shown to be accurate for early to moderate times in the SNL experiments.

References

Amsden, A. A. 1993. "KIVA-3: A KIVA Program with Block Structured Mesh for Complex Geometries," Los Alamos National Laboratory report LA-12503-MS.

Amsden, A. A., Butler, T. D., and O'Rourke, P. J. 1989 "KIVA-II: A Computer Program for Chemically Reactive Flows with Sprays," Los Alamos National Laboratory report LA-11560-MS.

Naber, J. D., Siebers, D. L., Di Julio, S. S., and Westbrook, C. K. 1993. "Natural Gas Fuel Variability Effects on Ignition Delay Under Diesel Conditions," Sandia National Laboratories report WSS/CI F 93-097.

NASP Technical Memorandum 1107, "Hypersonic Combustion Kinetics," May 1990.

Figure Captions

Figure 1. Velocity vector field for the 2D injection simulation near the orifice.

Figure 2. Mach number contour plot for the 2D injection simulation near the orifice. The contour range is from 0.12 (marked L) to 1.1 (marked H) with intervals of 0.123.

Figure 3. Hydrogen mass fraction contour plot for the 2D injection simulation near the orifice. The contour range is from 0.10 (marked L) to 0.90 (marked H) with intervals of 0.01.

Figure 4. Plot of the axial profiles at steady state for the 2D injection simulation near the orifice.

Figure 5. The three-dimensional mesh of one quarter of the SNL combustion chamber. A blow up of the corner where the injection occurs is show in the lower figure. The box in the corner of this figure is the size of the mesh used in the simulations shown in Fig. 1-4.

Figure 6. Comparison of the penetration history of the hydrogen jet of the KIVA simulation and the preliminary SNL experiments. The penetration in the KIVA simulations are presented for two methods for determining the penetration history: the maximum axial extent of the one and three percent hydrogen density contours.

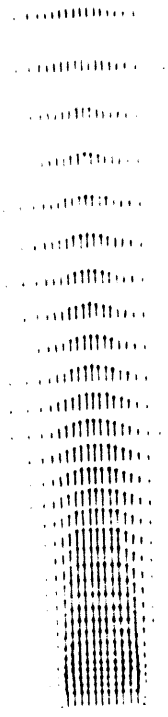

Figure 1. Velocity vector field for the 2D injection simulation near the orifice.

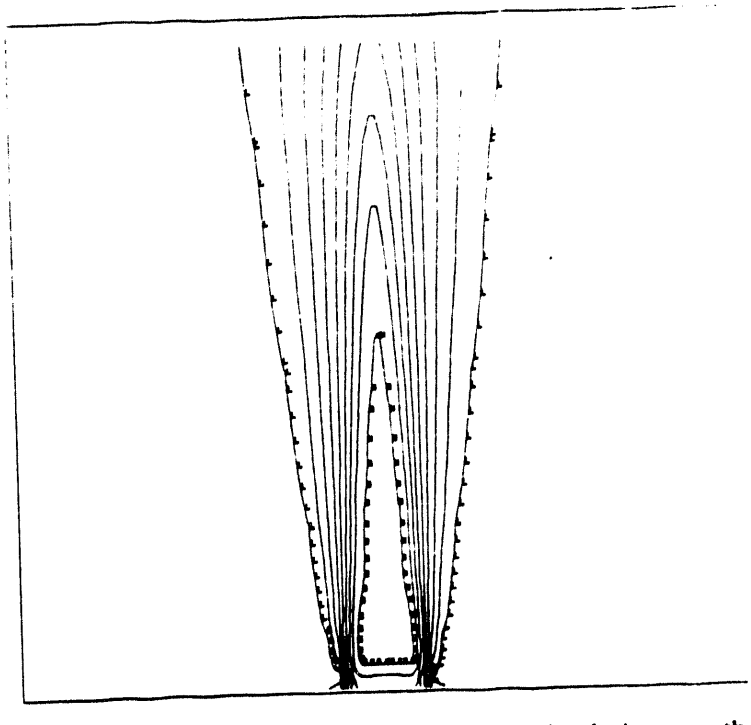

Figure 2. Mach number contour plot for the 2D injection simulation near the orifice. The contour range is from 0.12 (marked L) to 1.1 (marked H) with intervals of 0.123.

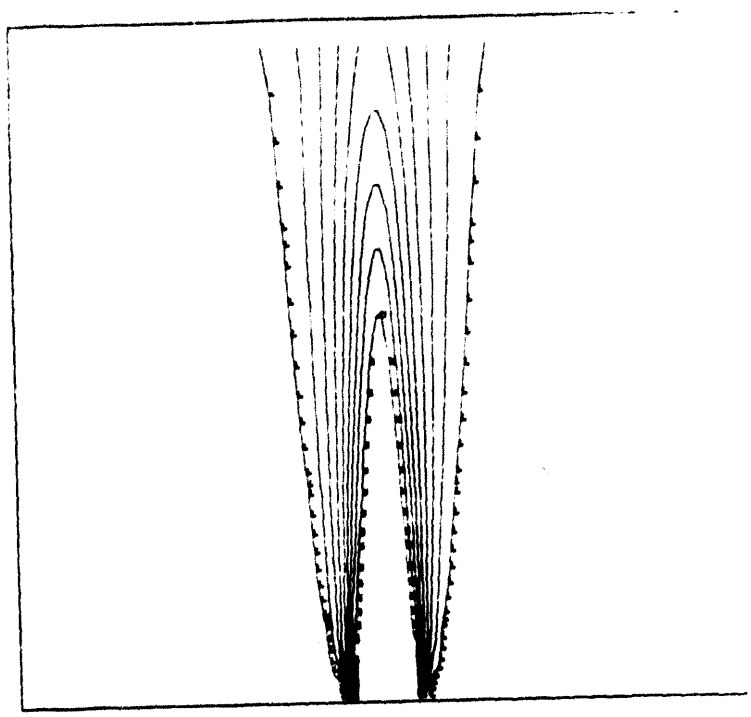

Figure 3. Hydrogen mass fraction contour plot for the 2D injection simulation near the orifice. The contour range is from 0.10 (marked L) to 0.90 (marked H) with intervals of 0.01.

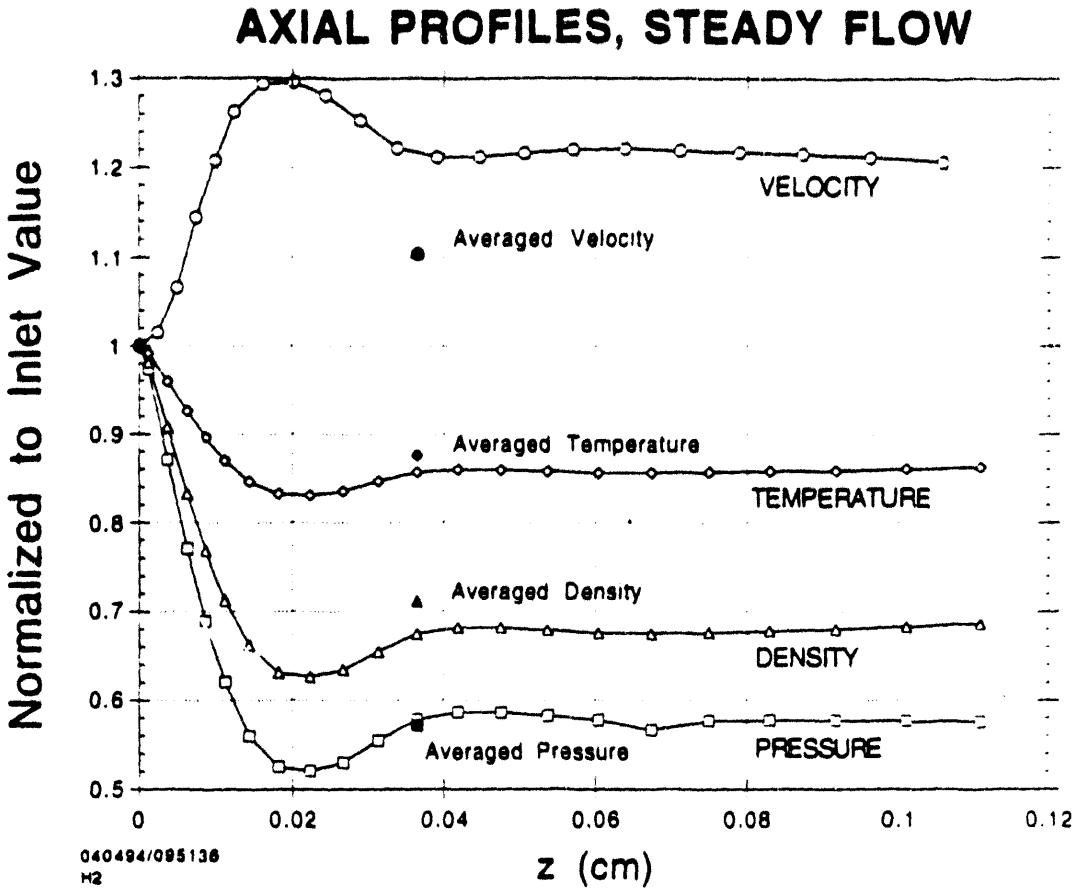

Figure 4. Plot of the axial profiles at steady state for the 2D injection simulation near the orifice.

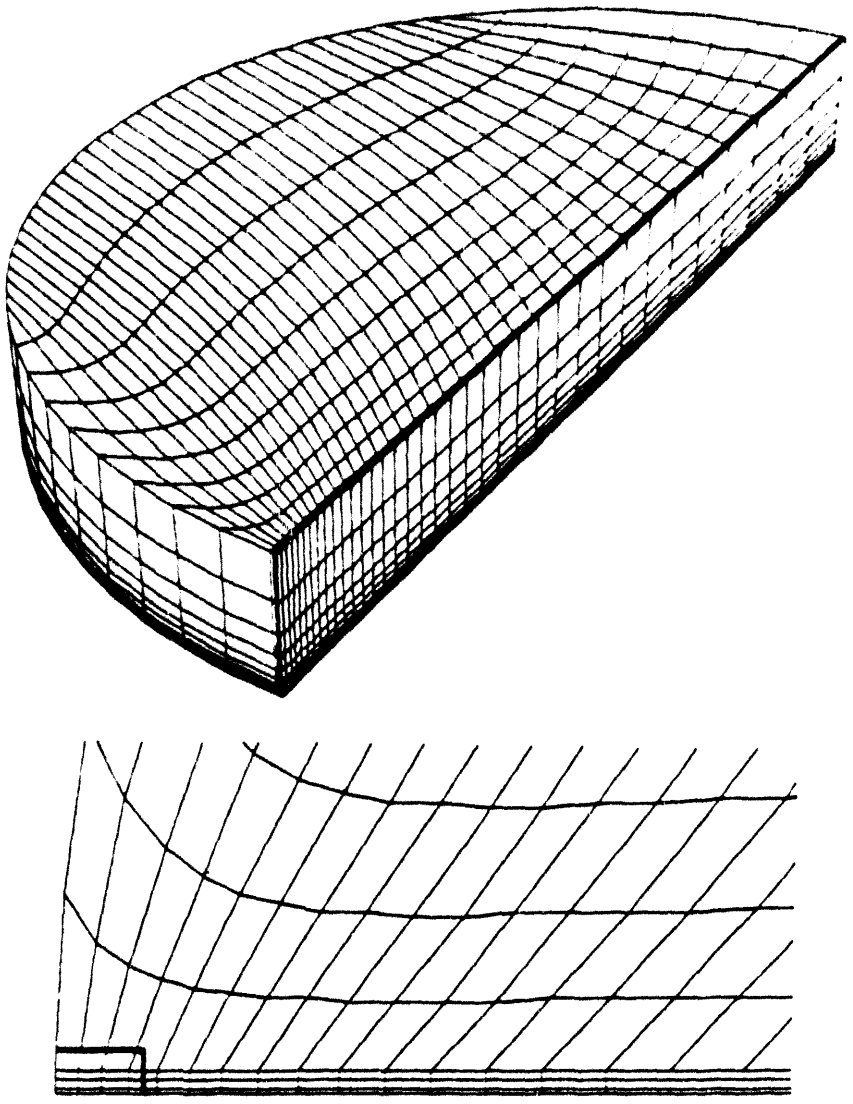

Figure 5. The three-dimensional mesh of one quarter of the SNL combustion chamber. A blow up of the corner where the injection occurs is show in the lower figure. The box in the corner of this figure is the size of the mesh used in the simulations shown in Fig. 1-4.

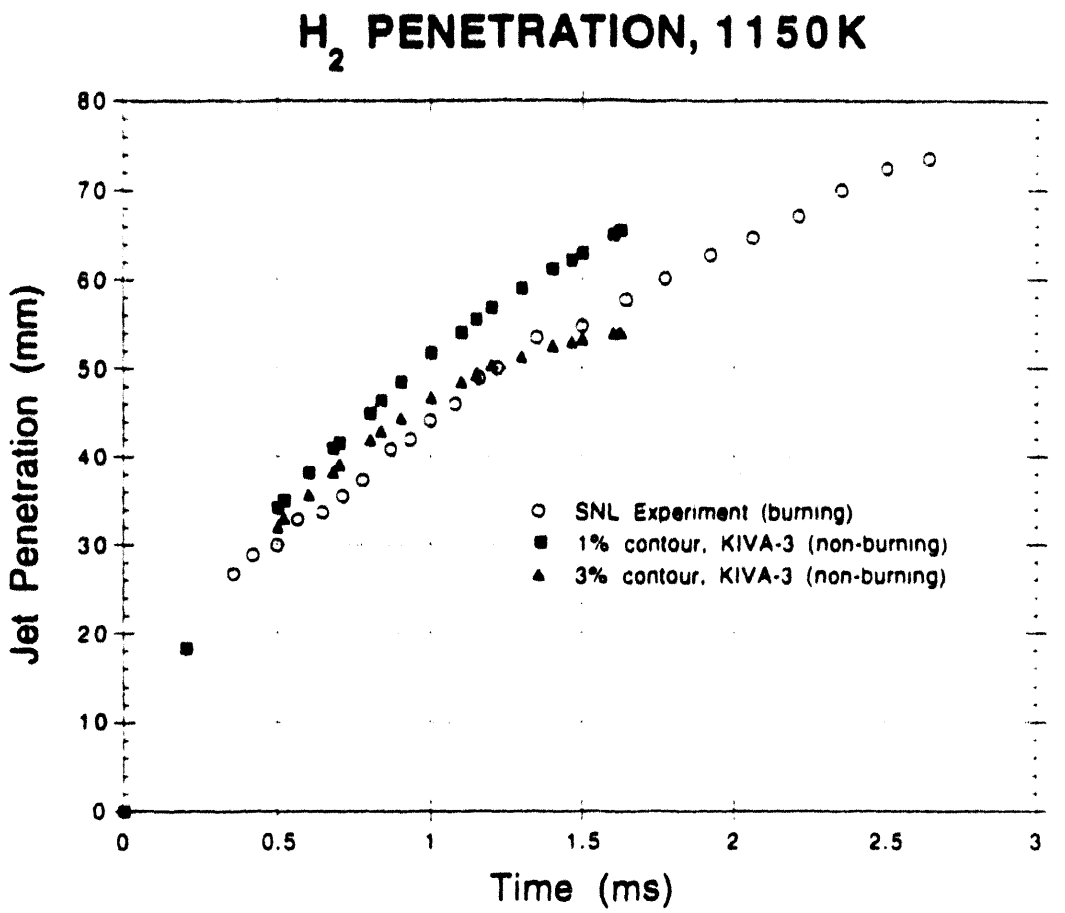

Figure 6. Comparison of the penetration history of the hydrogen jet of the KIVA simulation and the preliminary SNL experiments. The penetration in the KIVA simulations are presented for two methods for determining the penetration history: the maximum axial extent of the one and three percent hydrogen density contours.

CHEMICAL KINETIC MODELING OF H_2 APPLICATIONS

Charles K. Westbrook, William J. Pitz,
Lawrence D. Cloutman, and Nick Marinov
Lawrence Livermore National Laboratory
Livermore, CA 94550

Abstract

This project is intended to develop detailed and simplified kinetic reaction mechanisms for the combustion of practical systems fueled by hydrogen, and then to use those mechanisms to examine the performance, efficiency, pollutant emissions, and other characteristics of those systems. In the first year of this program, LLNL is funded at a level of 1 FTE. To date, we have done a variety of flame model calculations, comparing flame propagation with detailed kinetic models with simplified models in which the fuel consists both of hydrogen as well as hydrogen mixed with natural gas. We are currently developing the simplified analog reaction mechanisms that are computationally simple, yet still reproduce many of the macroscopic features of flame propagation. These flame models have also been used to examine the feasibility of using hydrogen addition to natural gas as a practical means of reducing the lean flammability limit of natural gas systems, which could lead to stable system operation with significantly reduced pollutant emissions. In addition to classical flame propagation models, internal combustion engine and industrial burner models in two and three space dimensions have been developed and studies including parametric variations of operating variables are being carried out. In addition to fluid dynamics models, hydrogen combustion is being linked to submodels of pollutant species production and destruction, particularly using detailed kinetic models of the chemical kinetics of oxides of nitrogen (NOx).

Introduction

Kinetic modeling of combustion of hydrogen has been pursued at Lawrence Livermore National Laboratory for many years, with numerous publications describing laminar flames, detonations, and other systems in which hydrogen is the fuel (e.g., Westbrook, 1982; Westbrook and Urtiew, 1982). Hydrogen is produced and subsequently consumed during the oxidation of all larger fuel molecules, and the reaction mechanism for H_2 oxidation is an essential subset of the reaction mechanisms for virtually all hydrocarbon fuels. The kinetic modeling program at LLNL has been prominent in developing capabilities to describe oxidation of hydrogen and other fuels and in using kinetic models to study practical and other combustion systems in a wide range of environments. Reviews of hydrocarbon oxidation (Westbrook and Dryer, 1981, 1984) have emphasized the fact that reactions involving H_2 and other species in the H_2 oxidation mechanism have a dominant influence on the rate of hydrocarbon combustion. As a result of these and other efforts, LLNL has the capability to simulate the oxidation of H_2 over a wide range of conditions and in internal combustion engines in particular.

Program Goals

There are two major approaches to combustion modeling in practical systems. In the first approach, the physical geometry of the combustion system is simplified to deal with a zero or one-dimensional formulation. This makes it possible then to deal in great detail with selected subprocesses, including the detailed chemical kinetics of fuel oxidation, NO_x production and pollutant emission. On the other hand, it is also possible to simplify the detailed chemical and physical process submodels and deal in detail with the multidimensional fluid mechanics. Both approaches have been used extensively in the past to study combustion in practical systems, including particularly internal combustion engines. In the present program, both approaches are being pursued, using current models for complex chemical kinetics and multidimensional fluid mechanics. As the program develops in time, it will eventually become feasible to combine both features together and carry out model analyses on a scale that was not possible previously.

With both of these approaches in mind, the work to be done at LLNL will provide kinetic and fluid mechanical models that will both advance our current capabilities and will also address specific applications problems. In the area of simplified fluid mechanics modeling, we will examine a number of problems associated with hydrogen oxidation. We will also develop and apply simplified kinetic submodels for use within complex fluid mechanics models.

Kinetics Studies

Hydrogen flames burn much more rapidly than hydrocarbon fuels such as methane or propane, with a stoichiometric laminar burning velocity close to 300 cm/sec compared with hydrocarbon values close to 40 cm/sec. This difference offers the possibility that hydrogen could be used to displace some of the hydrocarbon in hydrocarbon/air systems and increase the overall burning rate and flame velocity. In particular, this difference in burning rate might be used to use hydrogen addition to lower the overall fuel/air equivalence ratio normally required in the hydrocarbon/air system and reduce the product temperature and the rate of production of NO_x from practical systems, all while retaining the overall rate of flame propagation and heat release. To examine this possibility, we are carrying out a variety of flame

propagation studies. In particular, we are focusing on methane/air and natural gas/air flames, with hydrogen being used to displace the hydrocarbon in varying amounts. In these modeling studies, we are especially concerned with the adiabatic (product species) flame temperature for very lean mixtures. If these temperatures can be reduced and normal flame propagation can still take place, then there are important advantages to be obtained with hydrogen addition to hydrocarbon/air mixtures. These studies are well under way.

We are combining the kinetics of hydrogen oxidation with the kinetics of detailed NO_x production to study processes that may reduce NO_x emissions from practical combustion devices. The thermal (Zeldovich) NO_x mechanism is still active in hydrogen combustion, and the low-temperature path through N_2O formation is also still operational. However, prompt NO that is a result of CH radical reactions with N_2 will clearly not contribute when hydrogen is the fuel. We are working to examine the implications of the use of hydrogen on NO_x production.

The detailed kinetic models are also being used to develop simplified kinetic models for hydrogen and hydrocarbon/hydrogen mixtures that can be used in multidimensional fluid mechanics models for real system analysis. This process has been used in the past (Westbrook and Dryer, 1981) to develop flame models with simplified kinetics, and it is recognized that such simplified submechanisms are needed to deal with real chemistry and real fluid mechanics.

Fluid Mechanics Models

We are studying a variety of applications in which the chemical kinetics must be simplified in order to consider the computational needs of the fluid mechanics model. Simulations of hydrogen combustion in automotive engines, industrial burners, and other practical systems often require full three-dimensional modeling treatments, although some types of devices may possess enough symmetry to permit two-dimensional treatment. In either case, the computational needs of the fluid dynamics portion of the model alone are considerable, and it is not yet possible in most cases to also include a full chemical kinetic submodel, even for hydrogen oxidation. In such models, it is possible to develop and use a single or global reaction submodel that provides a reasonably accurate description of the overall rate of heat release. We have developed such submodels in the past for a range of hydrocarbon fuels (Westbrook and Dryer, 1981), which have then been incorporated into large-scale combustion models (Amsden, 1993), and we are repeating that process for hydrogen. The global reaction rate parameters must be properly evaluated in order to reproduce the stoichiometric laminar burning velocity as well as its variation with equivalence ratio, pressure, and unburned fuel/air temperature. Since we are also interested in simulating the combustion of various hydrogen/hydrocarbon mixtures in practical devices, we are including fuel mixture effects in the global reaction rate formulations being developed. The results of this project will then be available to other hydrogen program participants for use in their own modeling studies.

Several types of practical combustion systems will be analyzed with the multidimensional model with simplified hydrogen kinetics. For internal combustion engine simulations, the model will be used to examine the possibilities of hydrogen addition to hydrocarbon fuels to reduce NO_x emissions. For engines fueled entirely by hydrogen, the model will examine such features as optimal hydrogen/air equivalence ratio, NO_x production, potential for autoignition or knock (Westbrook et al., 1991), and ignition requirements. In addition, the potential of engine modifications such as prechamber ignition for further NO_x reduction will be examined. If time and resources permit, the model will be extended to study

hydrogen combustion in industrial burners. Current studies at LLNL are examining natural gas combustion in these burners, and modifications to describe hydrogen would not be difficult.

Finally, since the detailed chemical kinetic reaction mechanism for hydrogen is quite simple, consisting of only eight chemical species (H, H_2, O, O_2, OH, H_2O, HO_2 and H_2O_2), there are some applications for which a full CFD and detailed chemical kinetic treatment may be feasible. For example, if an axisymmetric burner model requiring only two spatial dimensions were combined with a kinetic model that perhaps omitted the minor species HO_2 and H_2O_2, selected model calculations could be carried out in order to determine quantities of interest. As models are converted to use massively parallel computers or clusters of workstations, this type of calculation will gradually become more realistic.

Acknowledgments

This work is supported by the U. S. Department of Energy, Office of Utility Technology, and was carried out under the auspices of the U. S. Department of Energy by the Lawrence Livermore National Laboratory under contract No. W-7405-ENG-48.

References

Amsden, A. A. 1993. "KIVA-3: A KIVA Program with Block-Structured Mesh for Complex Geometries." Los Alamos National Laboratory report LA-12503-MS.

Westbrook, C. K., and F. L. Dryer. 1981. "Simplified Reaction Mechanisms for the Oxidation of Hydrocarbon Fuels in Flames." Combustion Science and Technology, 27:31-43.

Westbrook, C. K., and F. L. Dryer. 1981. "Chemical Kinetics and Modeling of Combustion Processes." Eighteenth Symposium (International) on Combustion, 749-767. Pittsburgh: The Combustion Institute.

Westbrook, C. K. 1982. "Hydrogen Oxidation Kinetics in Gaseous Detonations." Combustion Science and Technology, 29:67-81.

Westbrook, C. K., and P. A. Urtiew. 1982. "Chemical Kinetic Prediction of Critical Parameters in Gaseous Detonations." Nineteenth Symposium (International) on Combustion, 615-623. Pittsburgh: The Combustion Institute.

Westbrook, C. K., and F. L. Dryer. 1984. "Chemical Kinetic Modeling of Hydrocarbon Combustion." Progress in Energy and Combustion Science. 10:1-57.

Westbrook, C. K., W. J. Pitz, and W. R. Leppard. 1991. "The Autoignition Chemistry of Paraffinic Fuels and Pro-Knock and Anti-Knock Additives: A Detailed Chemical Kinetic Study." SAE-912314. Warrendale, PA: Society of Automotive Engineers.

ADVANCED MATERIALS FOR HYDROGEN STORAGE: CARBON NANOTUBULES

T.A Bekkedahl and M.J. Heben
National Renewable Energy Laboratory
Golden, CO 80401-3393

Abstract

The lack of convenient and cost-effective hydrogen storage is a major impediment to wide scale use of hydrogen in the United States energy economy. Improvements in the energy densities of hydrogen storage systems, reductions in cost, and increased compatibility with available and forecasted systems are required before viable hydrogen energy use pathways can be established. Possible approaches to hydrogen storage include: (i) physical storage via compression or liquefaction; (ii) chemical storage in hydrogen carriers (e.g. methanol, ammonia, and diborane); (iii) metal hydrides, and (iv) gas-on-solid adsorption. Although each storage method possesses desirable attributes, no approach satisfies all of the efficiency, size, weight, cost and safety requirements for transportation or utility use. Carbon-based hydrogen adsorption materials, in particular, hold promise for meeting and exceeding the U.S. Department of Energy hydrogen storage energy density targets for transportation if concurrent increases in hydrogen storage capacity and carbon density can be achieved. Although these two goals are in conflict for conventional porous materials such as activated carbons, the desired results may be obtained if the void spaces in high surface area materials can be organized into optimal configurations. Recent demonstrations of the synthesis of carbon nanotubules by the process of spark-gap evaporation indicate that such organization is possible. In addition to surface adsorption storage, pores within assemblies of carbon nanotubules might be of the proper size to allow nanocapillary filling mechanisms to become operative. This paper describes our investigations of the hydrogen storage properties of carbon nanotubules. Preliminary results indicate that nanotubule-containing samples can store 8.4 wt% H_2 at 82K and 10.6 psi H_2. Recent results from our in-house synthesis of carbon nanotubes are also presented.

Statement of the Problem / Relevance of the Work

Background

Implementation of a domestic renewable hydrogen energy economy would reduce all forms of pollution associated with the use of fossil and nuclear fuels, and decouple the United States from volatile and unmanageable foreign energy markets. Additionally, the development of an international hydrogen energy economy would undoubtedly open new opportunities for the sale of U.S. hydrogen-related technologies.

Hydrogen *storage* is a key enabling technology that must be significantly advanced in terms of performance and cost effectiveness if the U.S. hydrogen energy economy is to be established. As described in the U.S. DOE Hydrogen Program Plan for FY 1993 - FY 1997, compact and lightweight hydrogen storage systems for transportation do not presently exist, and low-cost, low-loss bulk storage systems for utility use are not available. Possible approaches to hydrogen storage include: (i) physical storage via compression or liquefaction; (ii) chemical storage in hydrogen carriers (e.g. methanol, ammonia); (iii) metal hydrides, and (iv) gas-on-solid adsorption. Although each storage method possesses desirable attributes, no approach satisfies all of the efficiency, size, weight, cost and safety requirements for transportation or utility use. Table 1 displays a compilation of the advantages and disadvantages associated with the various H_2 storage technologies.

Table 1: Advantages and Disadvantages of Storage Technologies.

Compressed Gas	Ad:	Well-developed technology base, good gravimetric performance, good dormancy characteristics.
	Dis:	Bulky, compression costs, safety.
Cryogenic Liquid	Ad:	Excellent volumetric and gravimetric energy density for large containers.
	Dis:	Liquefaction costs, boil-off losses, poor performance in small systems.
Gas-on-Solid	Ad:	Fair volumetric and gravimetric energy densities, potentially inexpensive.
	Dis:	Requires compression and cooling. Complexity.
Metal Hydrides	Ad:	High volumetric energy density. Safe.
	Dis:	Poor gravimetric performance. Trade-off high of wt% and high dissociation temperature.
Chemical Storage	Ad:	High gravimetric storage density.
	Dis:	Toxicity, impure hydrogen stream, rehydrogenation reaction.

Current Status

Gas-on-solid adsorption and metal hydride storage are inherently safer methods of storing hydrogen than either (i) or (ii) above. In addition, these two methods of hydrogen storage avoid the use of toxic chemicals (a concern normally associated with (ii)), and both have the potential to be more energy efficient than physical storage methods. Figure 1 compares the performance of systems based on (i), (iii), and (iv) in terms of volumetric and gravimetric energy densities. The Figure also displays the energy density values for gasoline and diesel fuel, and the DOE target for hydrogen storage systems for vehicular use. Clearly, the DOE storage density goals can only be met with significant advances in hydrogen storage technologies.

The hydrogen storage properties of high-surface-area "activated" carbons have been extensively studied (Carpetis and Peshka, 1980; Schwarz, 1; Agarwal et al., 1987; Schwarz, 1993). These carbons are normally prepared from a variety of biological or mineralogical carbonaceous materials by processing that includes; i) chemical activation to produce dehydration or decomposition of organic constituents during subsequent heat treatments, ii) low-temperature carbonization (400-500 °C) to remove volatile organics, and iii) high-temperature oxidation (800-1000 °C) to develop porosity and surface area (Kirk et al., 1978). These methods produce microcrystalline, non-graphitic carbon materials with specific surface areas of 300-2500 m^2/gm. One of the best currently available activated carbon adsorbs ~4.8 wt% H_2 at a temperature of 87K and a pressure of 59 atm. Under these same conditions a carbon fiber-wrapped pressure vessel containing this activated carbon would store H_2 at 4.2 wt% and 16.8 kg/m^3 (Schwarz, 1993). In this system, a portion of the hydrogen is stored as a compressed gas in the macro-voids of the activated carbon. The performance of the system falls short of both the DOE Hydrogen Program Plan storage goals (6.5 wt % H_2 and 62 kg H_2/m^3). Researchers at A.D. Little (Hynek et al., 1992) have predicted that both Hydrogen Program Plan storage goals could be met if the gravimetric energy density could be maintained at 8 wt% while carbon density was increased from ~0.4 to 0.8 gm/cc. This is a technically challenging task since the surface area and density of porous materials are generally inversely related.

To date, most research on solid-state hydrogen storage materials has been empirical in nature. Most studies of gas-on-solid adsorption have simply reported the hydrogen adsorption/desorption properties of commercially available carbons and zeolites. The materials parameters which are critical for hydrogen adsorption system performance (surface area, pore size distribution, micropore volume, heat of adsorption, thermal conductivity, material integrity, kinetics, etc.) are typically *measured* but not *controlled.* A complete understanding and optimization of hydrogen adsorption mechanisms will only be achieved when critical material parameters can be controllably varied to establish relationships between properties and performance. Proper design and materials engineering in the nanometer size regime may allow high performance adsorbents to be synthesized in order to meet and exceed the DOE energy density targets for vehicular hydrogen storage.

Technical Approach

Ideal and Real Hydrogen Adsorbents

The gas adsorption performance of a porous solid is maximized when the pores are not larger than a few molecular diameters (Gregg & Sing, 1982). Under these conditions the potential fields from the walls of the so-called micropore can overlap to produce a stronger interaction than would be possible for adsorption

on a semi-infinite plane. At sufficiently low temperatures, where the escaping tendency of the gas is much less than the adsorption potential, the entire micropore may be filled with a condensed adsorbate phase. For the case of hydrogen, with a van der Waals diameter of ~4.4 Å (CRC, 1975), pores would be required to be smaller than ~40 Å to access this so-called nanocapillary filling regime. Ideally, the entire porous volume of an adsorbent would be of the microporous variety, and the volume and mass of the adsorbent skeleton would be the minimum necessary to develop the adsorption potential and provide thermal conductivity for management of heat fluxes associated with adsorption and desorption. Such a material would meet the technical challenge outlined above by providing increased material density while maintaining, and perhaps increasing, gravimetric storage density.

The heat of adsorption in a micropore will be a function of the ratio of the pore diameter to the adsorbate diameter. The heat of adsorption for methane in model pores consisting of two infinite parallel graphite sheets at various separation distances has recently been calculated (Cracknell et al., 1993). When the graphite planes were separated by a methane diameter, the heat of adsorption was peaked at a value ~2 times that for adsorption on the isolated planes. Such a substantial increase in the strength of interaction should allow storage systems to be operated at relatively lower pressures and higher temperatures. Operation of storage systems under conditions closer to ambient would offer savings in costs associated with compression, cooling, and container design.

The model materials used in these calculation are distinctly different from most real materials in that all sites for adsorption are equivalent. Thus, adsorption continues with a constant driving force until all sites are occupied. The adsorption of H_2 on Graphon (exfoliated graphite) proceeds in this manner with a heat of adsorption of 3.8 kJ/mol until a monolayer is formed (Pace and Seibert, 1959). In contrast, activated carbons show a higher initial heat of adsorption (~6.5 kJ/mol in one case: Schwarz, 1992) that can be reduced by more than a factor of 5 across the adsorption isotherm (Schwarz, 1). In the former case, the hydrogen adsorption is driven by pure van der Waals forces at structurally similar sites while, in the latter case, a variety of structural and chemical environments are evidently active (Agarwal, 1987). Storage system designed to be used with activated carbons must operate under conditions were some weakly adsorbing sites can be populated. Systems utilizing materials with uniform pore sizes need only operate under condition were the representative pore is active.

Calculations by Pedersen and Broughten have shown HF molecules will be strongly stabilized (by 29 kJ/mol) within carbon nanotubules (Pedersen and Broughten, 1992). The same type of "molecular straw" phenomena is expected to occur for non-polar species like H_2, and ensembles of tubes are expected to promote condensation more effectively than individual tubes (J.Q. Broughten, personal communication). The recent demonstration of the incorporation of Pb and other metals into carbon nanotubules by capillary forces (Ajayan and Iijima, 1993) is in agreement with this concept. Broughten and Pedersen's simulation of the interaction between a single nanotube and a neon reservoir indicates that capillary forces will also promote adsorption on the external surfaces of the tube as well (Broughten and Pederson, 1992).

It is difficult to obtain adsorbent materials with specific pore sizes and narrow pore size distributions. A semi-empirical model which describes pore growth during pyrolysis and/or gasification of coal shows that pore number densities vary with $1/r^3$, where r is the pore radius (Simons & Finson, 1979). Thus, although the number of micropores is relatively large, the small number of larger pores comprise a large fraction of the total pore volume. Porous carbons synthesized by conventional thermal processing generally exhibit more than 50% of total pore volume as macroporosity (Quinn & MacDonald, 1992) with pore dimensions greater than c.a. 40 Å. Macro pores only participate in monolayer adsorption, and are therefore relatively ineffective in adsorption storage. Consequently, high volumetric energy densities are expected for

adsorbent materials with large microporous and minimal macroporous volumes.

Carbon Nanotubes as Nearly Ideal Adsorbents

As the preceding discussion indicates, the ideal hydrogen adsorbent should have several features; (i) high surface area, (ii) minimal macroporosity, (iii) uniform and tailored microporosity, and (iv) high thermal conductivity. In FY 93 we initiated a research program to identify and investigate new solid-state hydrogen storage options which possess the potential for quantum jump improvements over currently available technologies. Our preliminary conceptual model indicated that carbon nanotubule assemblies could be fabricated to have all of the features that are found in the ideal adsorbent. Figure 2 displays an model assembly of 20 Å diameter graphitic tubules. Although the figure is idealized, such nanotube bundles are ubiquitous in deposits formed under certain growth conditions (Ebbesen et al., 1993). A simple calculation demonstrates that a close-packed assembly of 20Å diameter tubules would have a surface area close to the theoretical maximum for graphite (~5000 m^2/gm), and a density of ~1 gm/cc. Further calculation indicates that a single 20 Å tube could meet both DOE energy density targets by storing H_2 at densities of 7.8 wt% and 65 kg/m^3. This latter calculation considers a close-packed arrangement of H_2 as a first internal monolayer, with subsequent volume filling by liquid H_2. Even though contributions from adsorption in volume between tubes in an assembly (Fig. 2) are neglected, the calculated storage capacities exceed the DOE target energy densities. Furthermore, if nanocapillary forces are active in ensembles of carbon nanotubes, these H_2 storage capacities could be obtained at higher temperatures and lower pressures than are normally employed with activated carbons (e g. 87K, 740 psi - Schwarz, 1993).

Results and Discussion

Our approach to assessing the viability of employing engineered carbon nanotubules in hydrogen storage applications has involved two closely coupled Tasks. In the first Task, we utilize a customized microbalance to investigate the hydrogen adsorption properties of nanotubule-containing samples under a variety of temperature and pressure conditions. The second Task is focused on the synthesis of carbon nanotubes and nanotubule assemblies. Our goals in this activity are to produce research quantities for analysis in Task #1, and to develop an understanding of the nucleation and growth of carbon nanotubules so that mass production of optimal materials may be achieved.

Hydrogen Adsorption on Nanotubules

Initial investigations of the H_2 adsorption properties of carbon nanotubes have been performed on samples obtained through a collaboration with D.S. Bethune and his research group at IBM. The samples were produced via the spark gap evaporation process using carbon rods that had been doped with cobalt metal (Bethune et al., 1993). Transmission electron microscopy (TEM) performed at IBM and in our laboratory by Kim Jones revealed that the produced soot consists of three components; (i) single-walled, ~1.2 nm diameter carbon tubes, (ii) cobalt particles ranging in size from ~2-20 nm, and (iii) amorphous carbon. Electron probe microanalysis of the soot obtained from IBM (performed by A. Mason, NREL) reveals an average cobalt content of ~ 5 wt%. The as-produced tubes are expected to be closed at the ends (Ajayan et al., 1993), but can be opened with mild heating in oxygen (Pang et al., 1993).

The microbalance system we employ for H_2 adsorption measurements is consists of a modified Perkin-Elmer TGS-2 thermogravimetric analyzer, a vacuum station, a gas dosing manifold, and a computer for data acquisition. The sample temperature is altered by placing either heating tape or a vessel containing liquid nitrogen (LN_2) around the tubes which enclose the sample and tare pans of the microbalance. The samples were treated with various steps during an adsorption measurement;

i) Degassing (several hours) at room temperature and high vacuum ($< 5 \times 10^{-5}$ torr).
ii) Degassing at 270°C under high vacuum.
iii) Exposure to partial atmospheres of oxygen at 470 - 490°C.
iv) Cooling to LN_2 temperature while under high vacuum.
v) Dosing with H_2 to 550 Torr.

Samples were weighed (~1 to 4 mg), placed in either an aluminum or platinum pan, and covered with a crimped-on aluminum lid before being loaded in the microbalance. Samples were first run without step (iii) in order to assess the H_2 uptake of as-received samples. Figure 3 shows data acquired during step (v) for a typical sample which was not subjected to step (iii). The weight signal deflected sharply in the negative direction with the first admission of H_2. The microbalance had been evacuated to $< 5 \times 10^{-5}$ prior to the first H_2 dose, and thermal equilibrium had not yet been established between the sample and tare pans and the LN_2 reservoir. The weight signal returned to the baseline after ~300 s indicating the sample had reached LN_2 temperatures (82K at P_{atm} = 620 torr). Subsequent increases in the H_2 pressure led to small increases in the measured weight of the sample with a total weight gain of 0.98 wt% at 600 torr. As with most samples investigated so far, a second processing of the sample as listed above with the inclusion of step (iii) produced similar H_2 adsorption results in step (v). During step (iii) the sample was heated for 85 s in 0.5 torr O_2 at 488 °C and lost 253 μgm, or 11.4% of its initial weight (2.211 mg).

One sample to date has demonstrated substantially different behavior. The data from the first run on this particular sample without step (iii) was quite similar to the behavior described above. During step (iii) of a second run, the sample lost 124 μgm (2.9% of initial weight, 4.235 mg) after being heated for 85 s in 0.6 torr O_2 at 470°C. The adsorption data subsequently obtained in step (v) is displayed in Figure 4. As described above, the initial H_2 dose results in a negative deflection in the weight signal which recovers to the baseline as thermal equilibrium is achieved. Additional doses produce large increases in weight until, at 550 torr of H_2, 8.4 wt % H_2 is stored. Qualitatively, the time constant for relaxation to a new weight value decreases with increasing pressure as would be expected for a heat transfer limited adsorption process. Importantly, this result suggests that nanotubule-containing sample can compete with the best known activated carbons while operating at much lower pressures. The stored hydrogen was liberated when the temperature was allowed to rise to room temperature at 1100 seconds (Fig. 4).

Macroscopically, the soot received from IBM consisted of sponge-like and crumbly, granular components. Ajayan et al. have recently shown that the sponge component formed during co-evaporation of Co and C contains a higher tubule content than is found in the crumbly component (Ajayan et al., 1993). The sample used to obtain the data of Figure 4 was predominantly spongy in character. In contrast, most other samples we have investigated can be described as "mostly granular". Another indication of a high tubule content in the sample that stored 8.4 wt % is found by considering the weight lost during the high temperature exposure to oxygen. Nanotubes, except for their capped ends, are more resistant to oxidation than graphite, C_{60}, soot, and even diamond (Pang et al., 1993). The low loss of weight (2.9% as compared to 11.4% for the sample of Figure 3) which accompanied exposure to oxidation at 470°C is consistent with a high tubule content.

Although preliminary, our results suggest that carbon nanotubes may prove to be important hydrogen storage materials. Clearly, more work is required before the roles of the various components in these heterogeneous samples can be ascertained and optimized. Our future research plans are discussed in a following section.

Nanotubule Synthesis

If nanotubes and nanotubule assemblies prove to be useful for hydrogen adsorption, the production of mass quantities of material in a cost effective manner will be an important research goal. The nucleation and growth mechanisms responsible for producing these material in spark-gap evaporation and other synthetic approaches is poorly understood (Rodriguez, 1993). In order to investigate the physics and chemistry of tubule synthesis, we have constructed a modular and flexible synthesis apparatus. Initial runs with the apparatus were trouble-free and generated large quantities of multi-walled nanotubules. Figure 5 is a TEM image (taken by K. Jones, NREL) of soot generated by striking a 150 amp (AC) arc between two co-axial carbon rods (6 and 9 mm) with 20 volts in 500 torr of helium. Hollow nanotubes with diameters ranging from 5 -50 nm are readily seen. The large fiber bundle which crosses the image from top to bottom demonstrates that the van der Waals forces between tubes encourage self-assembly to form arrangements like the one depicted in Figure 2.

Future Work

Much work needs to be done in order to determine and perhaps achieve the full promise of carbon nanotubes in hydrogen storage applications. Of principal importance will be a determination of the different material parameters that give rise to the contrasting hydrogen adsorption behaviors displayed in Figures 3 an 4. We will attempt to separate and purify the various volume fractions in soots formed by the co-evaporation of Co and C so that adsorption data may be obtained from the individual components. Several possible purification routes exist such as chromatography, ultracentrifugation, train sublimation, and chemical etching schemes. We will rely heavily on transmission electron microscopy in order to correlate adsorption behaviors with structural features. Measurements of H_2 adsorption will be performed at temperatures above 82 K and at pressure above 600 torr to map-out the available operating parameter space. Programmed linear temperature sweeps at a constant pressure will be used to measure heat of adsorption and activation energy data. Adsorption measurements on compacted materials and plugs produced by spark-gap evaporation will determine achievable volumetric energy densities.

Our in -house tubule synthesis capabilities will be directed towards synthesis of small, single-walled nanotubules via the co-evaporation of carbon and metals to provide sufficient quantities of material for adsorption analysis. Attempts to control the geometry of the deposit will involve choices in electrode spacing, starting materials, deposition conditions (i.e. pulsed or AC currents), and ambient gas composition (e.g. other inert gases, or perhaps a carbon containing gas to provide a carbon source (CH_4)). Wedge-shaped electrodes will also be employed to investigate if large-area arrays of tubules can be formed from a plasma which is swept along the surface of a planar substrate. We will attempt to control the packing density and the size distribution of the tubules by establishing nucleation sites for tubule growth. In one approach we will utilize a self-assembled monolayer of C_{60} as an electrode in the spark-gap evaporation system. Tubule growth may proceed by addition of carbon atoms to the C_{60} monolayer to produce a hexagonally close-packed tubule arrangement. Tubule diameters would be identical in this configuration, and the interstitial sites would be available for nanopore condensation. We will also continue our

collaboration (not discussed in this document) with Clark Fields at NREL's High Flux Solar Furnace Facility to determine if intense solar radiation may be useful in the cost effective synthesis of bulk quantities of nanotubules. We also plan to utilize the patterned alumina membranes developed by Prof. C. Martin of Colorado State University to determine if nanotubule growth can be templated.

Acknowledgments

The authors would like to thank D.S. Bethune for providing single-layer carbon nanotube samples, A. Cahill and D. Burrows for technical assistance, J.Q. Broughten for useful discussions, K.M. Jones for transmission electron microscopy, and A. Mason for electron probe microanalysis.

References

Agarwal, R.K., .J.S. Noh, J.A. Schwarz, and P. Davini. 1987. "Effect of Surface Acidity of Activated Carbon on Hydrogen Storage." *Carbon*, 25:219-226.

Ajayan, P.M., and S. Iijima. 1993. "Capillarity-induced Filling of Carbon Nanotubules." *Nature*, 361:333-334.

Ajayan, P.M., J.M. Lambert, P. Bernier, L. Barbedette, C. Colliex, and J.M. Planeix. 1993. "Growth Morphologies During Cobalt-catalyzed Single-shell Carbon Nanotube Synthesis.", *Chem. Phys. Lett.* , 215: 509-517.

Bethune, D.S., C.H. Kiang, M.S. de Vries, G. Gorman, R. Savoy, J. Vazquez and R. Beyers. 1993. "Cobalt-catalyzed Growth of carbon Nanotubes with Single-layer Walls." *Nature*, 363: 605-607.

Broughten, J.Q., and M.R. Pederson. 1992. "Simulated Fullerene Tubules Act as Straws", *Science News*, Nov. 14.

Carpetis, C., and W. Peshka. 1980. "A Study on Hydrogen Storage by Use of Cryoadsorbents." *Int. J. Hydrogen Energy*, 5:539-554.

Cracknell, R.F., P. Gordon, and K.E. Gubbins. 1993. "Influence of Pore Geometry on the Design of Microporous Materials for Methane Storage." *J. Phys. Chem.* 97:494-499.

CRC, 1975. Handbook of Chemistry and Physics.

Ebbesen, T.W., H. Hiura, J. Fujita, Y. Ochiai, S. Matsui, and K. Tanigaki. 1993. "Patterns in the Bulk Growth of Nanotubes." *Chem. Phys. Lett.*, 209 (1,2): 83-90.

Gregg, S.J., and K.S.W. Sing. 1982. *Adsorption, Surface Area and Porosity*, New York: Academic Press.

Hynek, S., J. Bentley, B. Barnett, E. Shanley, and G. Melhem. 1992. Hydrogen Storage Technologies:

Press.

Hynek, S., J. Bentley, B. Barnett, E. Shanley, and G. Melhem. 1992. Hydrogen Storage Technologies: Present and Future.", presentation to the Hydrogen Energy Council, December 9, Montreal, Quebec.

Kirk, R.E., D.F. Othmer, M. Grayson, and D. Eckroth. 1978. *Kirk-Othmer Encyclopedia of Chemical Technology*. New York: John Wiley & Sons.

Pace, E.L., and A.R. Siebert. 1959. "Heat of Adsorption of Parahydrogen and Orthodeuterium on Graphon." *J. Chem. Phys.* 53:1398-1400.

Pang, L.S.K., J.D. Saxby, and S.P. Chatfield. 1993. "Thermogravimetric Analysis of Carbon Nanotubes and Nanoparticles." *J. Phys. Chem.*, 93: 6941-6942.

Pedersen, M.R., and J.Q. Broughten. 1992. "Nanocapillarity in Fullerene Tubules." *Phys. Rev. Lett.* 69:2689-2692.

Quinn, D.F., and J.A. MacDonald. 1992. "Natural Gas Storage." *Carbon*, 30: 1097-1103.

Rodriguez, N.M. 1993. "A Review of Catalytically Grown Carbon Nanofibers." *J. Mater. Res.*, 8: 3233-3250.

Schwarz, J.A., 1. "Modification Assisted Cold Storage (MACS).", contract report to Brookhaven National Laboratories, contract # 186193-S.

Schwarz, J.A., 1992. "Activated Carbon Based Storage System." in *Proceedings of the 1992 DOE/NREL Hydrogen Program Review*, 271-278. Honolulu, HI.

Schwarz, J.A., 1993. "Activated Carbon Based Storage System." in *Proceedings of the 1993 DOE/NREL Hydrogen Program Review*, 89-102. Cocoa Beach, FL.

Simons, G.A., and M.L. Finson. 1992. "The Structure of Coal Char: Part I. Pore Branching." *Comb. Sci. Techn.*, 19: 217-225.

Figure Captions

1) Comparison of existing hydrogen storage technologies.

2) Idealized nanotubule assembly.

3) Hydrogen adsorption data for granular nanotube-containing sample.

4) Hydrogen adsorption data for spongy nanotube-containing sample.

5) Transmission electron micrograph of carbon nanotubes.

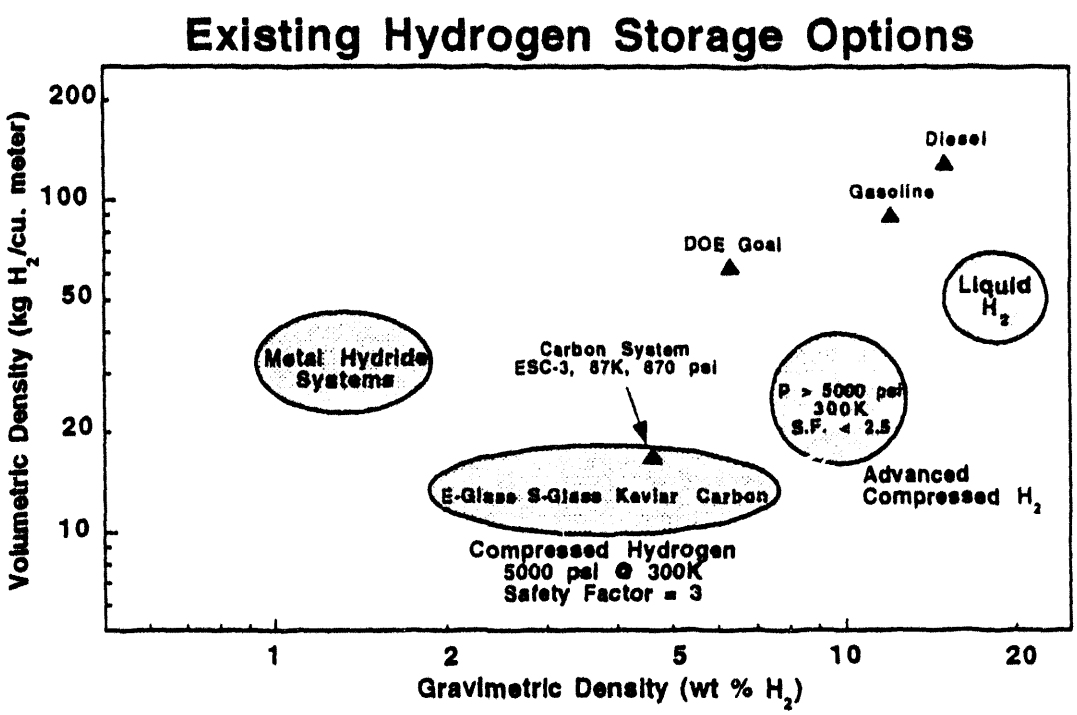

After S. Hynek et al.,'Hydrogen Storage Technologies:Present and Future' with data from I. Kuhn presented at Workshop on Hydrogen Storage Technogies, Nov. 11, 1993, Golden , CO and from J.A. Schwarz, 1993 DOE/NREL Hydrogen Program Review.

Figure 1

Assemblies of Carbon Nanotubules

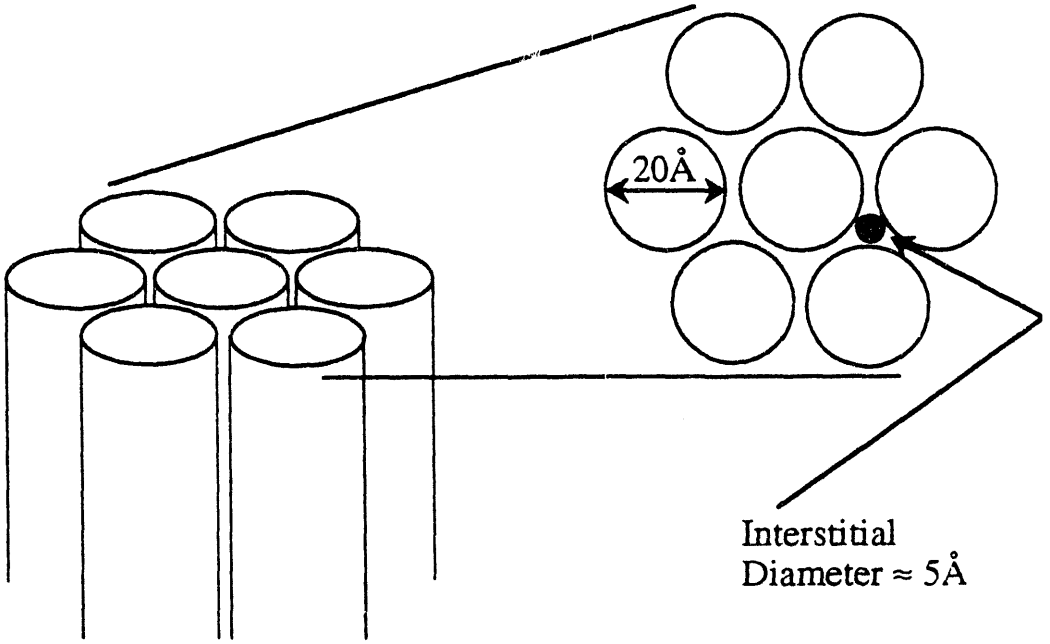

Synthetic Control:

Pressure and Composition of Background Gas
Electrode and Plasma Geometry
Starting Materials

Expected Properties:

Density:	≈ 1 gm/cc
Surface Area:	≈ 5000 m^2/gm
Heat of H_2 Adsorption:	> 4 kJ/mole

Storage Densities: Single Tube

7.8 wt% H_2

65 kg/m^3

Figure 2

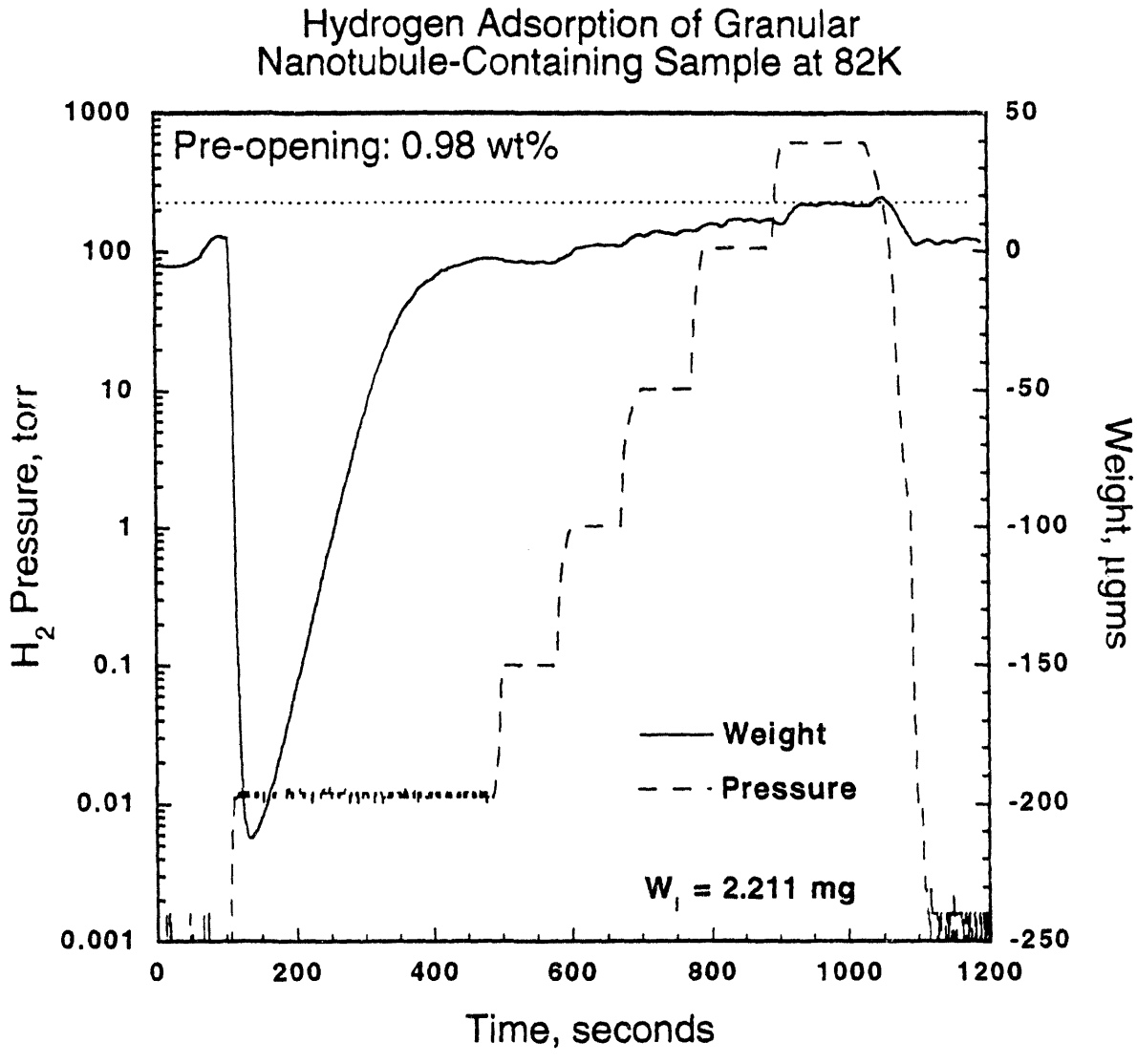
Hydrogen Adsorption of Granular
Nanotubule-Containing Sample at 82K
Pre-opening: 0.98 wt%
1000
100
10
1
0.1
0.01
0.001
H2 Pressure, torr
50
0
-50
-100
-150
-200
-250
Weight, µgms
Weight
Pressure
Wi = 2.211 mg
0
200
400
600
800
1000
1200
Time, seconds

Figure 3

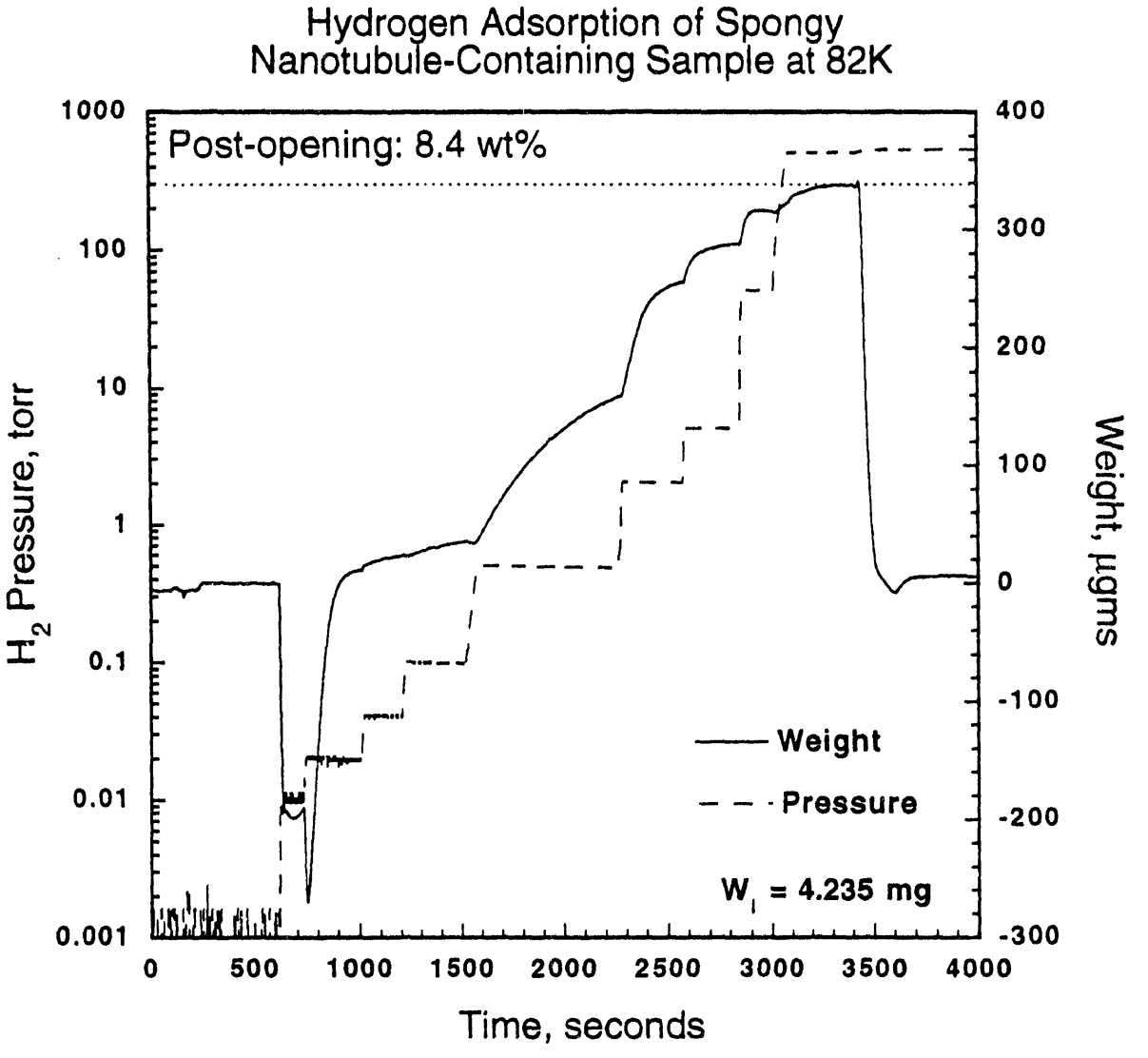
Hydrogen Adsorption of Spongy
Nanotubule-Containing Sample at 82K
Post-opening: 8.4 wt%
H2 Pressure, torr
Weight, μgms
Weight
Pressure
W, = 4.235 mg
Time, seconds
1000
100
10
1
0.1
0.01
0.001
400
300
200
100
0
-100
-200
-300
0
500
1000
1500
2000
2500
3000
3500
4000

Figure 4

KMJ/NREL

Figure 5

NONCLASSICAL POLYHYDRIDE METAL COMPLEXES AS HYDROGEN STORAGE MATERIALS

Craig Jensen
Department of Chemistry
University of Hawaii
Honolulu, HI 96822

Abstract

An alternate class of metal hydrides, nonclassical polyhydride metal complexes, are being developed as hydrogen storage materials. The reversible release of H_2 from the complexes, $IrXH_2(H_2)(PPr^i)_2$ (X = Cl, Br, I) has been studied by variable temperature ^{31}P NMR spectroscopy. Rate constants for this process were obtained from line shape analysis of the spectra. Eyring plots of the rate constants gave activation parameters from which the kinetic barriers to the release of H_2 from the chloro, bromo, and iodo derivatives were calculated to be 10.1 ± 0.6, 10.9 ± 0.8, and 11.4 ± 0.6 kcal/mole respectively. This trend matches the thermodynamic stabilities of the complexes and is apparently the result of the increasing σ-donating strength of the halide ligands. This conclusion is supported by inelastic neutron scattering experiments from which the barrier to rotation of the dihydrogen in the chloro, bromo, and iodo complexes were determined to be 0.51(2), 0.53 and 0.90 kcal/mole respectively. The reversible binding of H_2 by the unsaturated complexes, $IrXH_2(PPr^i_3)_2$ (X = Br, I), has been studied in the solid state through infrared spectroscopy. Under 1 atm of H_2, these complexes are completely converted to the corresponding dihydrogen complexes. Reversible binding of H_2 by the indenyl complex, $[IrH_3(\eta^5\text{-}C_9H_7)(PPr^i_3)]^+$, has been demonstrated by ^1H NMR spectroscopy.

Introduction

A major concern in the development of hydrogen as a fuel is the problem of hydrogen storage. Solid hydrogen storage systems based on metal hydrides are safer and require far less volume than either high pressure or cryogenic storage systems. Unfortunately, the metals and alloys which reversibly bind hydrogen at adequate rates, generally form hydrides which contain less than 1.0 weight per cent hydrogen. As a result, the weight of hydrogen storage systems based on traditional metal hydrides severely restricts their practical application [1]. Although alloys such as iron-titanium have shown acceptable kinetic behavior and can attain up to 2.0 weight per cent hydrogen, their utilization for hydrogen storage is extremely limited due to other problems such as high sensitivity to impurities [2]. Metals and alloys may eventually find limited commercial hydrogen storage applications, but it would appear that a new class of materials must be developed to allow utilization of hydrogen as an energy carrier.

We are developing an alternate class of metal hydrides, nonclassical polyhydride metal complexes, as hydrogen storage materials. Polyhydride metal complexes with relatively high hydride weight percentages have been known for many years. However, classical polyhydride complexes generally undergo irreversible dihydrogen elimination. Recently, a new class of metal hydride complexes in which hydrogen bonds to the metal center while retaining a significant amount of H-H bonding have been recognized [3]. Many of these nonclassical hydride or dihydrogen complexes have been found to undergo complete and reversible loss of H_2 under mild conditions. The ability of these complexes to undergo complete loss of H_2 without application of a high vacuum system is quite remarkable and demonstrates the high potential of metal complexes of this type as hydrogen storage materials. An understanding of how the energetics of hydrogen binding can be fine-tuned by small changes in the ligand environment is emerging through our continuing studies of the reversible loss of H_2 from these complexes [4,5,6]. These studies have elucidated how nonclassical polyhydride complexes can be tailored to reversibly release hydrogen at virtually any rate and temperature.

In order to produce materials which contain high weight percentages of available hydrogen, we have explored the synthesis of iron and cobalt nonclassical polyhydride complexes that are stabilized by cyclopentadienyl. We are also investigating the possibility that indenyl hydride complexes will undergo reversible hydrogenation at both the metal center **and** the indenyl ligand thus greatly elevating the hydrogen storage capacity of these complexes.

The funding level for this work by the DOE/NREL hydrogen program for FY94 was $94,714, making a cumulative total of $359,777 of funding for this project since its beginning in 1988.

Results

Iridium Nonclassical Polyhydride Complexes

In our laboratory we have synthesized and characterized the nonclassical polyhydride complexes: $IrClH_2(H_2)(PR_3)_2$ (R = Pr^i, **1**; Cy, **2**, Bu^t, **3**) and $IrXH_2(H_2)(PPr^i_3)_2$ (X = Br, **4**; I, **5**) [4,5,6]. These complexes reversible release hydrogen as seen in equation 1. We have studied this rapid equilibrium

Equation 1

in solution by variable temperature ^1H and ^{31}P NMR spectroscopy and in the solid state by infrared spectroscopy [4,5,6]. The rapid kinetics of the reversible loss of H_2 from these complexes is exceptional among metal hydrides in general. We have demonstrated that the kinetics and thermodynamics of the reversible loss of H_2 by these complexes can be very sensitive to the steric constraints introduced by the phosphine alkyl groups [5]. We have also studied the influence of halide ligands on H_2 binding by the **1**, **4**, and **5** by variable temperature solution ^1H NMR spectroscopy. These studies demonstrated that the thermodynamic stability of our dihydrogen complexes follows the trend $I^->Br^->Cl^-$ [6]. Additionally, the ^1H NMR spectroscopic data also allowed us to estimate activation energies of 10.5, 10.9, and 11.9 kcal/mol for the interconversion of the dihydrogen and unsaturated chloro, bromo, and iodo complexes respectively.

During the past year we have more accurately determined the kinetic barriers to the elimination of H_2 from the dihydrogen complexes through variable temperature $^{31}P\{^1H\}$ NMR spectroscopic studies. These studies show similar temperature dependent dynamic effects as were observed in the earlier ^1H NMR studies. Spectra (202.46 MHz) of a sample of iodo dihydrogen complex, **5**, which was dissolved in toluene-d_8 under 0.5 atm of H_2 are displayed as Figure 1. Below -10° C, separate resonances are observed for **5** at 58.2 ppm and $IrIH_2(PPr^i_3)_2$, **6**, at 32.4 ppm. Similar spectra were observed for a sample of the bromo dihydrogen complex, **4**, which was dissolved under 0.5 atm of H_2 in toluene-d_8 and seen to establish an equilibrium with $IrBrH_2(PPr^i_3)_2$, **7**. Rate constants for the complex inter-conversions were approximated from line shape analysis of variable temperature spectra of the equilibrating solutions of **5/6** and **4/7** which were obtained at 10° C increments over the temperature range -60 to -10° C. The simulated and experimental variable-temperature $^{31}P\{^1H\}$ NMR spectra over this temperature range of an equilibrium mixture of **5** and **6** are displayed in Figure 2. Additionally, rate constants were also determined from parallel experiments with equilibrating solutions of $IrClH_2(H_2)(PPr^i_3)_2$/$IrClH_2(PPr^i_3)_2$ which were based on spectra obtained at 10° C increments over the temperature range -70 to -20° C. From the activation parameters obtained from Eyring plots

of the estimated rate constants, kinetic barriers to the elimination of H_2 from the chloro, bromo, and iodo dihydrogen complexes at 0° C were calculated to be 10.1 ± 0.6, 10.9 ± 0.8, and 11.4± 0.6 kcal/mol respectively.

Both the thermodynamic stability of the dihydrogen complexes and the kinetic barriers to the elimination of H_2 follow the $I^->Br^->Cl^-$ trend in σ-donor strengths. Increasing halide σ-donation results in increased electron density at the metal center and thus enhancement of the d-σ* metal-dihydrogen interaction. We conclude that the σ-donor abilities of ancillary ligands contribute to the kinetic and thermodynamic stabilities of dihydrogen complexes.

In order to test our hypothesis that increasing σ-donation from ancillary ligands stabilizes coordinated dihydrogen, inelastic neutron scattering (INS) experiments have been conducted in collaboration with Dr. Juergen Eckert of Los Alamos National Laboratory and Dr. Jacqueline Nicol of NIST. The barrier to rotation of dihydrogen ligands can be directly determined through inelastic neutron scattering (INS) techniques [7]. The barrier to rotation of dihydrogen ligand in these complexes is directly related to the strength of the d-σ*, metal-dihydrogen π interaction which must be disrupted for this rotation to occur and reflects the stabilization of the dihydrogen ligand at the metal center.

Experiments were carried on 1 g samples of **1**, **4**, and **5** which were sealed under an atmosphere of hydrogen. Data for **1** were collected at 1.7, 5, and 15 K using the cold neutron time-of-flight spectrometers MIBEMOL at the Orphee Reactor of the Laboratoire Leon Brillouin and the Institut Laue-Langevin, Grenolble, France. The rotational tunneling spectrum obtained from MIBEMOL at 1.7 K is shown in Figure 3. The data for **4** and **5** were collected on a spectrometer at the reactor at NIST. Additional experiments were also conducted on the FDS instrument at the Manuel Lujan Jr. Neutron Scattering Center at Los Alamos National Laboratory. These experiments involved a spectral difference technique which using samples of $IrClH_2(H_2)(PPr^i_3)_2$ and $IrClD_2(D_2)(PPr^i_3)_2$ which were sealed under atmospheres of hydrogen and deuterium gas respectively. The measurements at Los Alamos provided vibrational data including the transition to the excited librational state ("torsion") of the dihydrogen ligand.

Analysis of this data yielded a barrier to rotation of the dihydrogen in the chloro complex, **1**, of 0.51(2) kcal/mol [8]. This barrier is the **lowest** value for a barrier to dihydrogen ligand rotation observed to date. This result supports our conclusion of the presence of a very weak d-σ*, metal-dihydrogen π interaction in this complex. The barrier to rotation of the dihydrogen ligand in the bromo and iodo complexes were determined to be 0.53 and 0.90 kcal/mole respectively. Thus, the barrier to rotation of the dihydrogen ligands which have been determined through the INS studies verify our hypothesis that the thermodynamic stability of it can be explained simply by the $I^->Br^->Cl^-$ trend in σ-donor strengths in the halide ligands.

We have studied the reversible binding of H_2 by the unsaturated iodo and bromo complexes, **6** and **7** in the solid state by infrared spectroscopy. Under 1 atm of H_2, these complexes are converted to the corresponding dihydrogen complexes, **4** and **5**. As seen in Figure 4, the M-H stretches at 2260 and 2248 cm^{-1} for a sample of the bromo complex, **7**, under 1 atm of N_2 completely disappear and are replaced by M-H stretches of the dihydrogen complex, **4**, at 2210, 2186, and 2153 cm^{-1}. These studies show that, unlike the chloro complex, $IrClH_2(PPr^i_3)_2$, which establishes a ca. 20:80 equilibrium with the dihydrogen complex, **1**, [6] the bromo and iodo complexes are completely converted to the dihydrogen complexes under 1 atm of hydrogen.

Nonclassical Polyhydride Complexes Containing Cyclopentadienyl Ligands

We have initiated several efforts to prepare iron and cobalt complexes stabilized by η^5-cyclopentadienyl ligands. The low cost and relatively low molecular weight of these metals as well as the cyclopentadienyl ligand make these complexes especially attractive candidates as hydrogen storage materials. Early efforts to produce the iron complexes were complicated by complex instability and characterization problems which arose due to the rapid intermolecular exchange of the metal bound hydrogen in these complexes. Attempts to generate an analogous nonclassical polyhydride ruthenium complex were also unsucessful. Protonation of the diruthenium complex $[\{\eta^5\text{-}C_5(CH_3)_5\}Ru(\mu\text{-}H)_2]_2$, **8**, [17] with $HOSO_2CF_3$ followed by neutralization with a hydride source, $LiBH(C_2H_5)_3$ under an atmosphere of hydrogen in arene and chlorinated solvents resulted in the formation of η^6-arene complexes and μ-chloro substituted dimeric products respectively. When the protonation of **8** was carried out in the nonchlorinated solvent, tetrahydrofuran solution, the diruthenium cation $[\{\eta^5\text{-}C_5(CH_3)_5\}Ru(\mu\text{-}H)_3Ru\{\eta^5\text{-}C_5(CH_3)_5\}]^+$ was obtained. T_1 measurements [10] on the signals observed by ^1H NMR spectroscopy for the metal bound hydrogens in this complex indicate that they are nighly stabilized, classical hydride ligands. Treatment of the diruthenium pentahydrido cation with $LiBH(C_2H_5)_3$ under an atmosphere of hydrogen simply leads to the regeneration of the starting material **8**. We have more recently explored the reaction of $\{\eta^5\text{-}C_5(CH_3)_5\}Co(\mu\text{-}H)_3Co\{\eta^5\text{-}C_5(CH_3)_5\}$ [11] with $HOSO_2CF_3$ in pentane under an atmosphere of hydrogen gives rise to a mixture of diamagnetic hydrides which we have identified on the basis of ^1H NMR as $\{\eta^5\text{-}C_5(CH_3)_5\}CoH_2(H_2)$ and $[\{\eta^5\text{-}C_5(CH_3)_5\}CoH(H_2)]^{1+}$. However, these products have proven to be too unstable to isolate.

Future Directions

While we have had modest success at generating iron and cobalt complexes of the type $\{\eta^5\text{-}C_5(CH_3)_5\}MH_x(H_2)_y$, they have routinely been too unstable to isolate. Greater complex stability can be achieved by introduction of ancillary ligand such as CO or PMe_3. For example, $\{\eta^5\text{-}C_5(CH_3)_5\}FeH(H_2)(PMe_3)$ has been previously prepared [12]. However, even if this complex is found to reversible release the dihydrogen ligand, it represents only a 0.76 weight percentage.

Closely related to cyclopentadienyl ligand, $C_5H_5^-$, is the indenyl ligand, $C_9H_7^-$, which contains an unsaturated 6-membered ring, can be hydrogenated under mild conditions while the 5-membered ring remains coordinated to the metal center [13]. Also the coordinated 5-membered ring of the indenyl ligand is known to undergo "ring slippage" from an η^5 to an η^3 coordination mode thus creating an additional coordination sight at the metal center [14]. An indenyl complex would take up 4 equivalents of H_2 when fully hydrogenation of to an η^3-indanyl complex containing an additional dihydrogen coordinated to the metal center. This increased hydrogen storage potential of indenyl ligands would allow us to incorparate stabilizing ancillary ligands into complexes while maintaining high available hydrogen weight percentages.

Recently, we began investigating the possibility of reversible hydrogenation of indenyl complexes. We found that the indenyl complex, $[Ir(\eta^5\text{-}C_9H_7)(C_2H_4)_2]^+$, under 1 atm of H_2 is readily hydrogenated at room temperature to the tetrahydroindenyl complex, $[Ir(\eta^5\text{-}C_9H_{11})(C_2H_4)_2]^+$. However, this complex

does not dehydrogenate even at elevated temperatures and in the presence of the hydrogen acceptor, t-butylethylene. However, the η^6-indanyl complex, $[Ir(\eta^6\text{-}C_9H_{10})\{P(C_6H_5)_3\}]^+$, will dehydrogenate at 80 °C to the η^5-indenyl complex, $[IrH(\eta^5\text{-}C_9H_7)\{P(C_6H_5)_3\}]^+$ [15]. Our interpretation of these results is that the presence of a hydride ligand in the η^5-indenyl complex is required for reversible hydrogenation. To test this hypothesis, we have investigated the reactivity of $[IrH_3(\eta^5\text{-}C_9H_7)(PPr^i_3)]^+$, 9, with H_2 by ^1H NMR spectroscopy. The signals for both the hydride and indenyl protons are seen to shift and broaden upon introduction of 1 atm of hydrogen to a toluene-d_8 solution of 9. These spectral effects can be reversed upon freeze-pump-thaw degassing of the solution to remove all traces of H_2. This result firmly establishes that 9 reversibly binds hydrogen. However, it is not clear at this time whether the reaction of 9 with H_2 entails simply an equilibrium with a dihydrogen, η^3-indenyl complex as seen in the first step of Scheme 1 or also involves the reversible hydrogenation of the indenyl ligand to a tetrahydroindanyl ligand as seen in the second step of Scheme 1. It should be possible to distinguish between these possibilities through varible temperture ^1H NMR spectroscopic studies similar to those which we have carried out for the $IrXH_2(H_2)(PR_3)_2$ complexes. The exchange between 9 and its hydrogenated equilibrium partner should be slow enough at low temperature to allow observation of seperate signals for both species thus allowing the characterization of the hydrogenated complex.

We plan to extend our studies to iron indenyl hydride complexes. Although the synthesis of the iron will be somewhat more exploratory than our synthesis of the iridium indenyl hydride complexes, it should not be as arduous as our efforts to synthesize the $\{\eta^5\text{-}C_5(CH_3)_5\}MH_x(H_2)_y$ complexes. As mentioned above, $\{\eta^5\text{-}C_5(CH_3)_5\}FeH(H_2)(PMe_3)$ has previously been synthesized. Substitution of sodium indenide in the place of lithium pentamethylcyclopentadienide will most likely yield $\{\eta^5\text{-}C_9H_7\}FeH(H_2)(PMe_3)$. Furthermore, substition of CO for PMe_3 should lead to the preparation of $(\eta^5\text{-}C_9H_7)FeH(H_2)(CO)$. We will then investigate the reversible hydrogenation of this complex through variable temperature NMR spectroscopy. As seen in Scheme 2, the occurrence of ring slippage in conjunction with hydrogenation of the indenyl ligand would result in the uptake of 3 equivalents of H_2 by the indenyl ligand and 1 equivalent of H_2 at the metal center. Thus the η^3-tetrahydroindanyl complex in Scheme 2 would contain 3.9 weight percent available hydrogen despite baring the weight penalty of a stabilizing CO ligand.

References

1. (a) Selvan P., B. Viswanathan, and C.S. Srinivassan. 1986. *Int. J. Hydrogen Energy* 11:169 and references therein.
   (b) Suda S. 1987. *Int. J. Hydrogen Energy* 12:2323.

2. (a) Wallace W.E., R.S. Craig, and O.V.S. Rao. 1980. *Adv. Chem.Ser.* 186:207.
   (b) Pick M.A., and M. Wenzel. 1977. *Int. J. Hydrogen Energy* 1:413.

3. (a) Kubas G.L. 1988. *Acc. Chem Res.* 21:120 and references therein.
   (b) Crabtree, R.H. 1990 *Acc. Chem. Res.* 23:95 and references therein.

4. Mediati, M., G.N. Tachibana, and C.M. Jensen 1990. *Inorg. Chem.* 29:3.

5. Mediati, M., G.N. Tachibana, and C.M. Jensen 1992. *Inorg. Chem.* 31:1827.

6. Le-Husebo, T., and C.M. Jensen 1993. *Inorg. Chem.* 32:1827.

7. (a) Eckert, J., and G.J. Kubas 1993. *J. Phys. Chem.* 97:2378.
   (b) Eckert, J., H. Blank, M.T. Bautista, and R.H. Morris 1990. *Inorg Chem.* 29:747.

8. Eckert, J., C.M. Jensen, G. Jones, E. Clot, and O. Eisenstein 1993. *J. Am. Chem. Soc.* 115:11057

9. Suzuki, H., H. Omori, D.H. Lee, Y. Yoshida, Y. Moro-oka. 1988 *Organometallics* 7:2243.

10. (a) Crabtree, R.H. and D.G. Hamilton 1988. *Adv. Organomet. Chem.* 28:299.
    (b) Luo, X., and R.H. Crabtree 1990. *Inorg. Chem.* 29:2788.

11. Kersten J.L., A.L. Rheingold, K.H. Theopold, C.P. Casey, R.A. Widenhoefer, C.E.C.A. Hop 1992. *Angew. Chem. Int. Ed. Engl.* 31:1341.

12. Paciello, R.A., J.M. Manriques, J.E. Bercaw 1990. *Organometallics* 9:260.

13. Osiechi, J.H., C.J. Hoffman, and D.P. Hollis 1965. *J. Organomet. Chem.* 3:107.

14. Crabtree, R.H. 1988. *The Organometallic Chemistry of the Transition Metals.* New York: John Wiley & Sons p 79-80.

15. Crabtree, R.H. and C.P. Parnell 1984. *Organometallics* 3:1727.

Scheme 1.

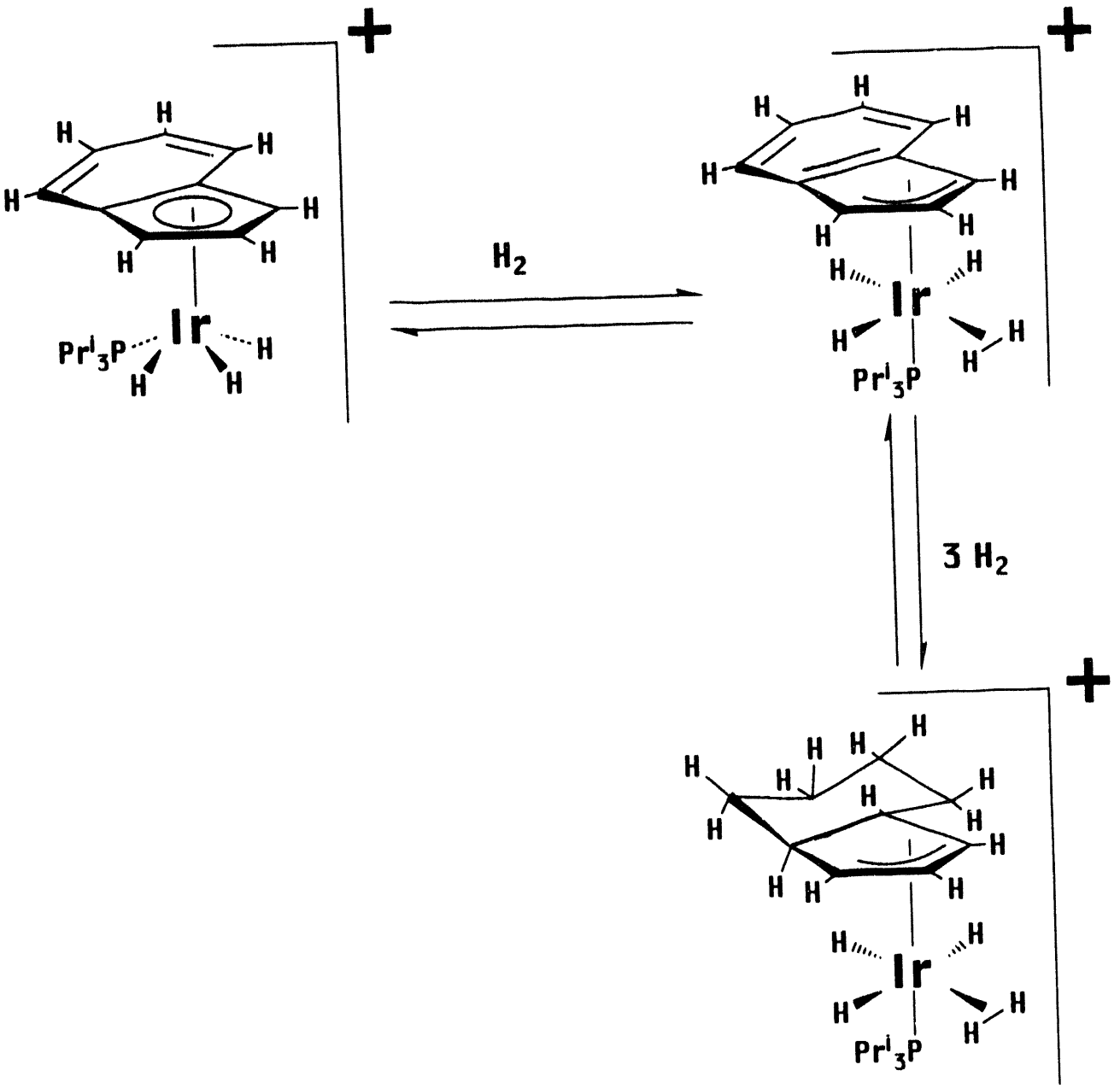

Scheme 2

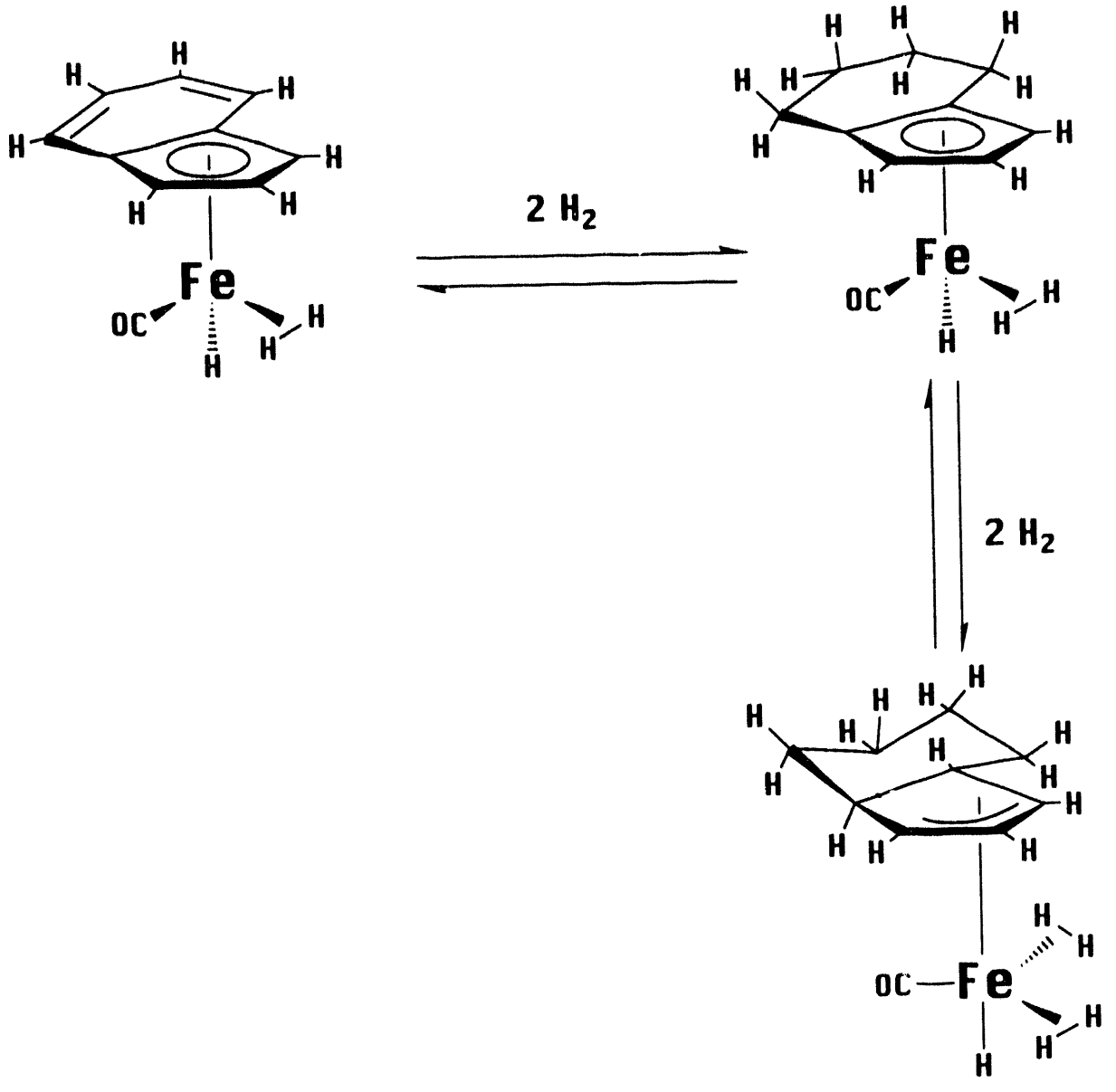

Figure Captions

Figure 1. Variable-temperature $^{31}P\{^1H\}$ NMR spectra (202.46 MHz) of $IrIH_2(H_2)(PPr^i3)_2$, 4, dissolved in toluene-d_8 under 0.5 atm of H_2 (total pressure).

Figure 2. Simulated and experimental variable-temperature $^{31}P\{^1H\}$ NMR spectra of equilibrium mixture of $IrIH_2(PPr^i_3)_2$ and $IrIH_2(H_2)(PPr^i3)_2$.

Figure 3. Inelastic neutron scttering spectrum of $IrClH_2(H_2)(PPr^i_3)_2$ obtained at T = 1.7 K on MIBEMOL using an incident neutron wavelength of 4.5 Å. Rotational tunneling peaks appear at approximately 20 cm^{-1}.

Figure 4. Infrared spectra: (a) $IrBrH_2(PPr^i_3)_2$ under 1 atm of nitrogen; (b) Initial spectrum of $IrBrH_2(PPr^i_3)_2$ under 1 atm of H_2; (c) $IrBrH_2(H_2)(PPr^i_3)_2$ under 1 atm of H_2.

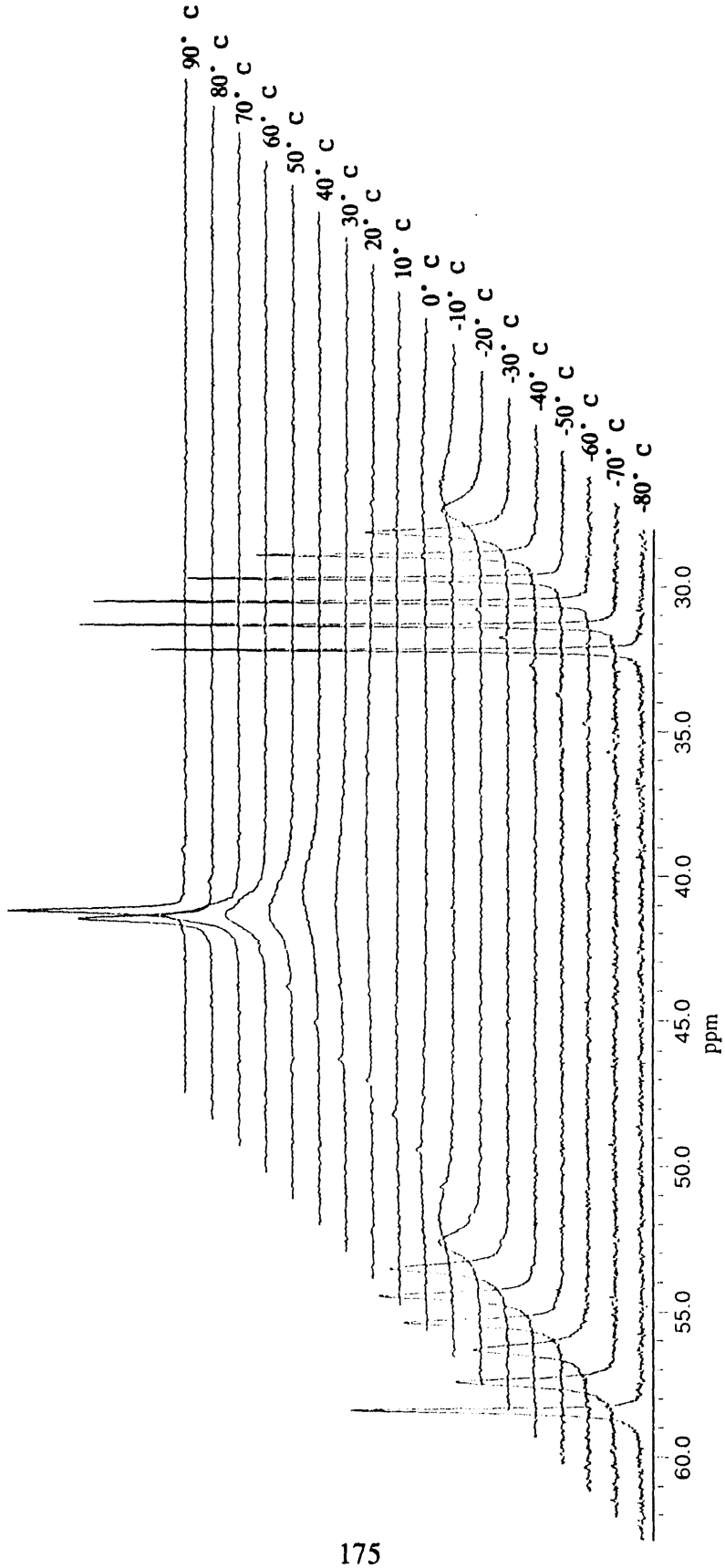
90° C
80° C
70° C
60° C
50° C
40° C
30° C
20° C
10° C
0° C
-10° C
-20° C
-30° C
-40° C
-50° C
-60° C
-70° C
-80° C
30.0
35.0
40.0
45.0
50.0
55.0
60.0
ppm

FIGURE 1

FIGURE 2

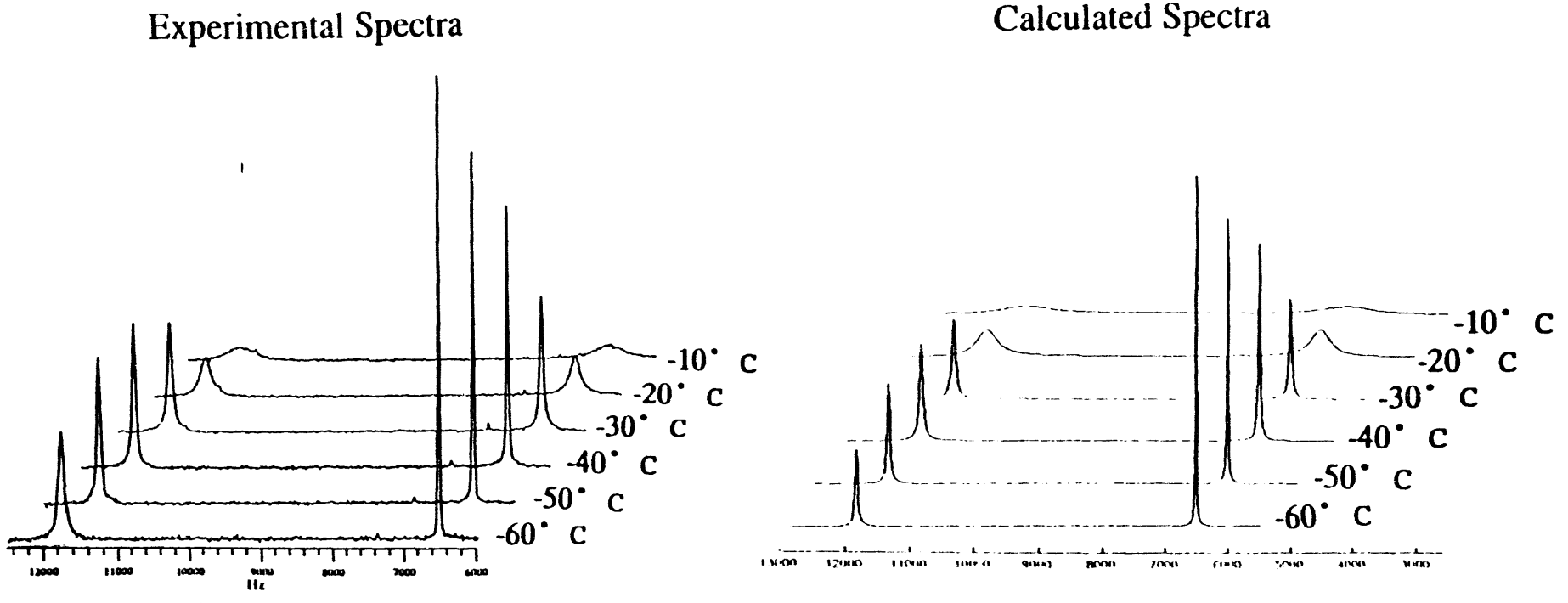
Experimental Spectra
-10° C
-20° C
-30° C
-40° C
-50° C
-60° C
Hz
Calculated Spectra
-10° C
-20° C
-30° C
-40° C
-50° C
-60° C

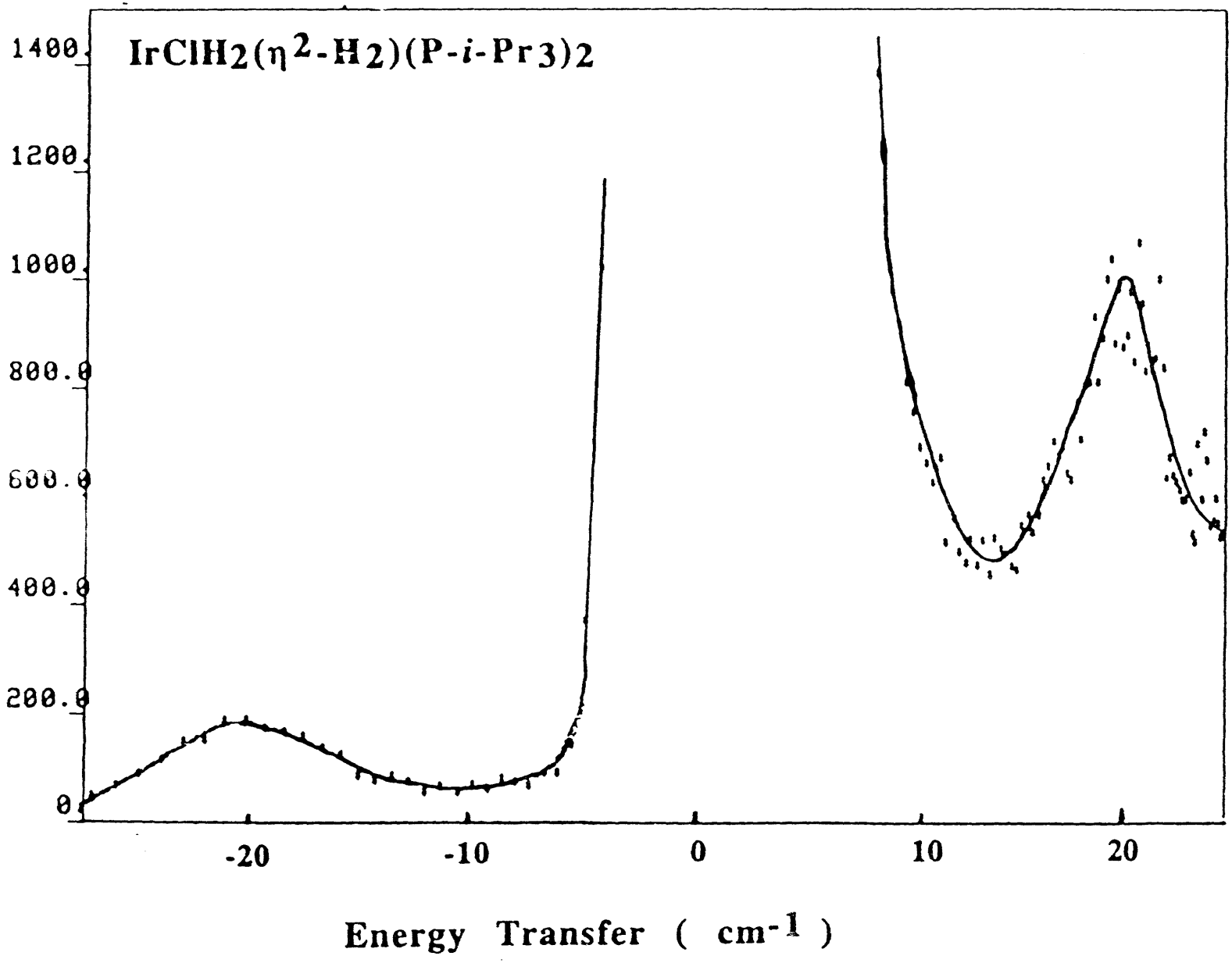
IrClH2(η2-H2)(P-i-Pr3)2
1400
1200
1000
800.0
600.0
400.0
200.0
0
-20
-10
0
10
20
Energy Transfer (cm-1)

FIGURE 3

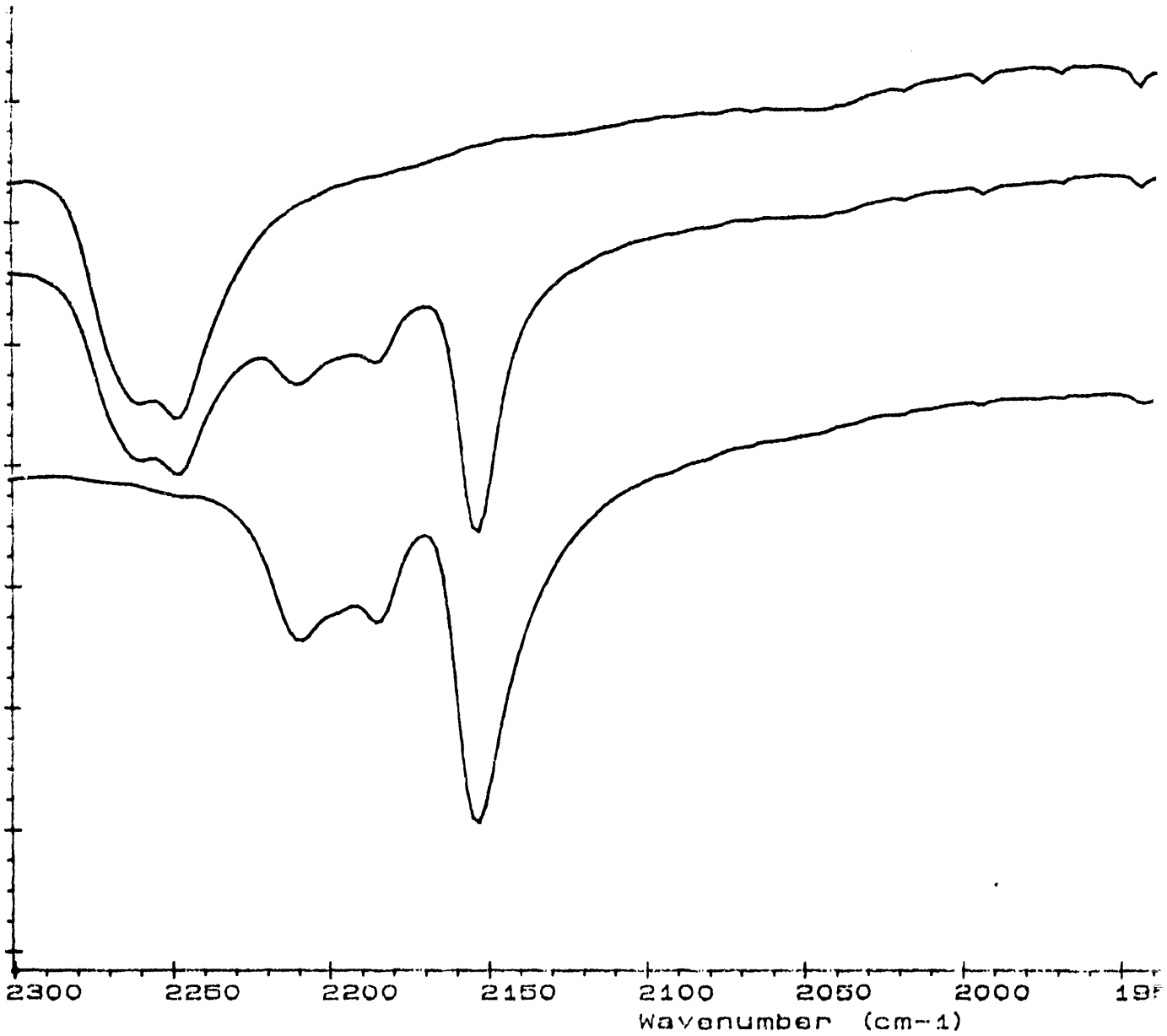

FIGURE 4

CHEMICALLY SYNTHESIZED HYDROGEN STORAGE COMPOUNDS

Darlene K. Slattery
Florida Solar Energy Center
300 State Road 401
Cape Canaveral, FL 32920

Abstract

Research during this contract year has thus far focused on the hydriding of alloys that are known to exist but which require extreme conditions to affect the hydrogenation. The major goal has been to synthesize several of these materials to confirm that the necessary conditions are milder than those required with the traditional approach. In this paper, comparative results are presented that confirm the advantages to the chemical approach. Several hydrides have been prepared under conditions which are much milder than any previously reported. Conditions and results are presented, as well as plans for the remainder of the contract year.

Introduction

In order for hydrogen to be used as a fuel, there must be a method for storage that results in a high volumetric and gravimetric density while being safe and economical. Currently, no ideal storage system exists. The most frequently mentioned methods of storage are cylinders of compressed gas, liquid hydrogen, cryogenic adsorption on activated carbon and metal hydrides. Each of these methods has its advantages and disadvantages. Metal hydrides have long been considered to be excellent for hydrogen storage. Some of the advantages are the high volumetric density possible (frequently higher than that of liquid hydrogen), the inherent safety of hydrides, and the ability to deliver high purity hydrogen at a constant pressure.

Just as there is no perfect storage method, there is no metal hydride that meets all of the requirements. A practical metal hydride must be reversible, have a high H_2 pressure at a reasonable temperature, a high hydrogen density per unit volume and per unit weight, rapid kinetics and a reasonable cost.

Currently there are more than 80 known metals. Virtually all of these metals are capable of interacting with hydrogen, forming either solid solutions or hydrides. Only two, magnesium and vanadium, form binary hydrides that could be useful for energy storage (Reilly, 1979). It is possible, however, to hydride many alloys and intermetallic compounds and these frequently have very different properties than those of the binary hydrides. Some metals, which themselves do not form hydrides, can be hydrided if alloyed with one or more other metals.

One such example is iron. Iron has no stable hydride but alloying with titanium allows the formation of both FeTiH and $FeTiH_2$. These alloys dissociate at approximately 0 °C but contain less than 2 wt% hydrogen. Magnesium, on the other hand, is one metal that can contain a large amount of hydrogen, a theoretical 7.6 wt%. Unfortunately, it is also a relatively stable hydride, requiring 280 °C for a dissociation pressure of 1 atmosphere.

Although thermodynamically stable, magnesium hydride has long been a leading candidate for hydrogen storage because it is light weight, inexpensive and plentiful. In both volumetric and gravimetric density, it comes very close to meeting the DOE goals as set forth in the Hydrogen Program Implementation Plan released in October of 1993 (see Fig. 1).

Technical Approach

While many researchers, over a number of years, have studied magnesium hydride, most of these investigations have involved metallurgical preparations. In the metallurgical approach, the metal is exposed to hydrogen at an elevated temperature and pressure, i.e., 200 atmospheres at 570 °C (Faust, et. al, 1960). The resulting hydride has extremely poor kinetics and contains far less than the theoretical amount of hydrogen. An approach that has proven to be superior is the chemical synthesis of the hydride, developed at the Max Planck Institute in Germany in the 1980's (Bogdanovic, 1984). In this method, finely powdered magnesium is suspended in an organic solvent, such as tetrahydrofuran and several activators, the most important of which is anthracene, are added. After an initial formation of magnesium anthracene, the suspension is hydrogenated at 60 °C under a hydrogen pressure of 50 - 100 atm. Following the initial hydrogenation, the product is removed from solution via filtration and can then be cycled as the dry powder. This hydride has greatly improved kinetics when compared to the metallurgical hydride (see Fig. 2) and more closely approaches the theoretical hydrogen content of 7.6 wt%. Unlike

the traditionally prepared hydride, the kinetics and hydrogen capacity do not significantly decrease, even after repeated cycling.

Most important to our current research is that the chemical approach allows the hydrogenation to occur under much milder conditions than does the metallurgical method. This becomes extremely important when one looks at metals and alloys that should, theoretically, contain a high percentage of hydrogen but that are not known to absorb hydrogen. Applying the chemical synthesis approach may well allow the hydriding of these materials.

Objectives

The primary goal for the year, is the chemical formation of hydrides of alloys. As a first step, the current goal has been to establish that the conditions necessary to hydride alloys will be milder using this approach than is required when using the metallurgical method. These initial alloys are materials known to form hydrides. After establishing some base line conditions, work will move on to the attempted synthesis of the hydrides of alloys not currently known to uptake hydrogen.

Results and Discussion

Because nickel doped magnesium hydride has been our standard material, it was only natural that Mg_2Ni would be the first alloy that we would attempt to hydride using the chemical synthesis method. The alloy, HY-STOR® 301 magnesium-nickel alloy, was purchased from Aldrich Chemical Company. HY-STOR® requires activation before use. To activate the magnesium-nickel alloy, Aldrich recommends heating to 300 - 350 °C, under vacuum, followed by exposure to hydrogen at 20-30 atmospheres for 2-3 days, with occasional cycling. After activation, Mg_2Ni will react rapidly with hydrogen at 14 atmospheres at 200 °C to form Mg_2NiH_4.

Using the same procedure as for our standard material, a sample of the HY-STOR® alloy was heated to 375 °C under argon to remove the hydroxide/oxide layer. With no additional activation, the alloy was put through the chemical process and hydrogenated at 70 °C and 100 atm of hydrogen for 15 hours. The apparent uptake of hydrogen was only slightly slower than that observed for the standard magnesium hydride, although preliminary chemical steps were somewhat slower.

Subsequent characterization of the magnesium nickel alloy established the hydrogenation had been successful (see Fig. 3). Figure 4 shows the thermogram for a Mg_2NiH_4 / MgH_2 sample. The two peaks, one for the alloy and one for the magnesium hydride are evident. Rehydrogenation was then possible at 8 atm at 222 °C.

Magnesium nickel is, of course, not an ideal storage medium. While the temperature required for hydrogen release is lower (240 °C versus 286 °C for MgH_2), and the kinetics are excellent, the hydrogen content has been reduced by over one-half, by weight.

Another well studied hydrogen absorbing alloy is magnesium-copper, Mg_2Cu. This alloy is available from Aldrich as HY-STOR® 302. It is much more difficult to activate, requiring 10-15 days at 300 °C and 24 atm. The same process was repeated as was used for the magnesium-nickel. The reaction was noticeably slower. The color changes, during the chemical process, were less intense in spite of allowing the reaction

to proceed for an extended period of time. The hydrogenation was carried out at 100 °C and 120 atm of hydrogen.

While hydrogenation of the Mg_2Cu was accomplished (see Fig.5), the reaction was very slow and the yield lower than for the corresponding nickel alloy. It is possible that the results would be better if a different organic is substituted for the anthracene or the $CrCl_3$ is replaced with a different catalyst. For example, Liao and his co-workers (Liao, et. al, 1985) used the chemical approach to prepare lithium hydride. They found that the use of naphthalene and titanium tetrachloride resulted in almost quantitative lithium conversion in four hours while the anthracene/$CrCl_3$ combination gave no reaction.

These two alloys are just two of many that researchers have investigated. Our results indicate that milder conditions are required for the chemical process than the metallurgical process (see Fig. 7 and 8). However, achieving optimum conditions would require the variation of solvent, activators and temperature. This will not be done with these alloys since they are not of interest for our ultimate goals.

Conclusions and Future Direction

The magnesium nickel alloy was found to hydride very well using the mild conditions of the chemical approach. The product cycles well and has excellent kinetics. The magnesium copper alloy absorbed hydrogen under the conditions employed. However, it is believed that use of a different set of catalysts will give improved yields.

Much work still lies ahead for the remainder of the contract year. Alloys that have already been ordered and are expected to arrive soon include magnesium iron, aluminum iron, and magnesium aluminum iron. Each of these will be tested to ascertain the optimum catalyst combinations to accomplish the chemical synthesis. Should any of these show promise as a hydrogen storage compound, it will be fully characterized to determine hydrogen content, kinetics and p-c-t curves will be obtained.

Acknowledgments

The author wishes to thank DOE and NREL for continued support of this project under subcontract no. XAR-3-13444-01 and Dr. Michael D. Hampton for the DSC analyses, as well as many helpful discussions.

References

Bogdanovic, B; 1984. "Magnesium Hydride: A Homogeneous-Catalyzed Synthesis and Its Use in Hydrogen Storage." *Int. J. Hydrogen Energy*, 9(11): 937-941.

Faust, J.P., E.D. Whitney, H.D. Batha, T.L. Heying, and C.E. Fogle. 1960. "Catalytic Preparation of Magnesium Hydride." *J. Appl. Chem*, 187-188.

Liao, S., W. Kong, H. Liu, and Y. Xu. 1985. "Catalytic Synthesis of Lithium Hydride Under Mild Conditions." In *Proceeding of the International Symposium on Hydrogen Systems*, 475-486. Beijing, China.

Reilly, J.J. 1979. "Metal Hydride Technology." *Z. Phys. Chem.*, 117: 155-184.

Figure Titles

Figure 1

Hydrogen storage system comparison

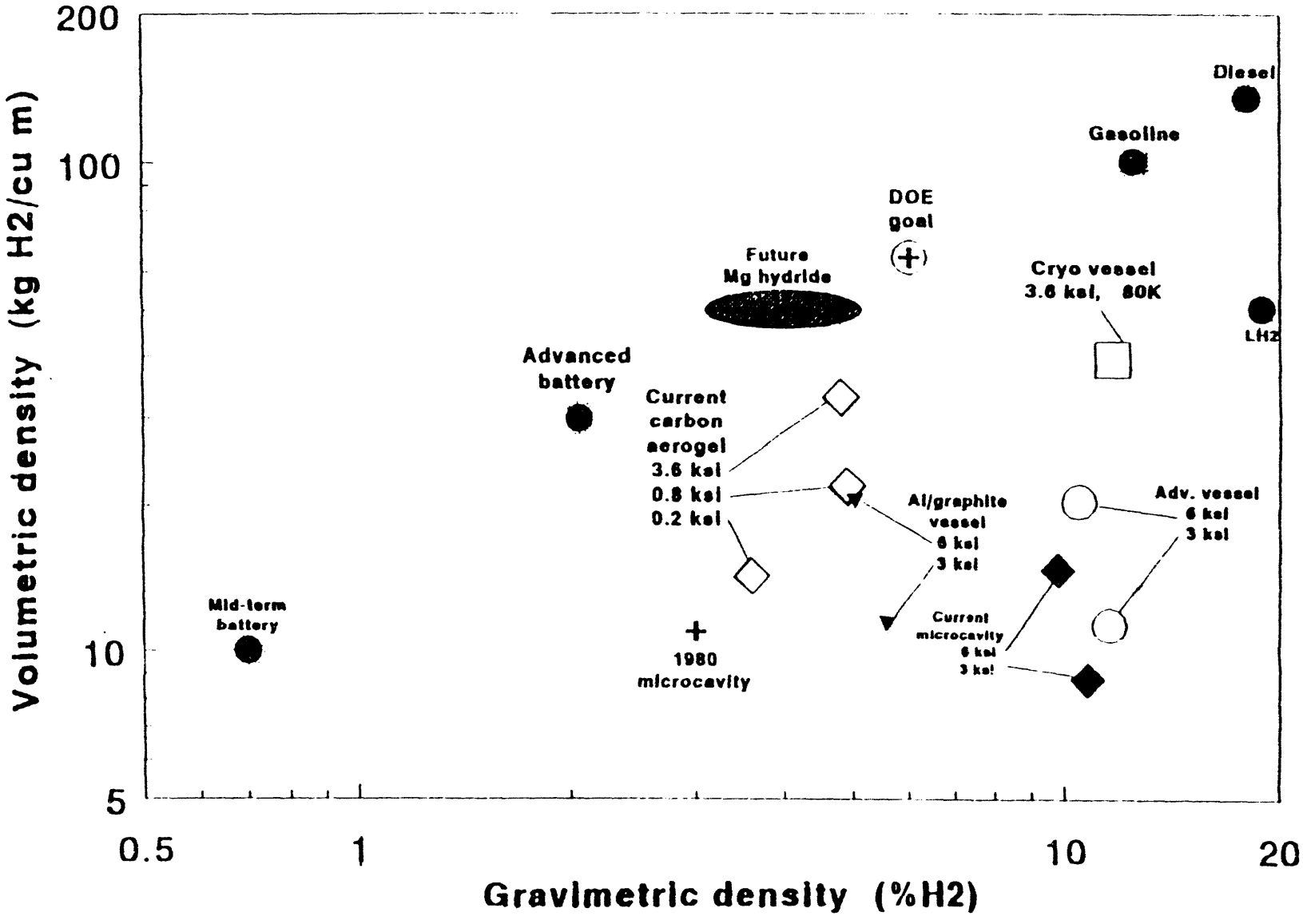

Source: Hydrogen Program Implementation Plan

Figure 2

Hydrogen desorption plots

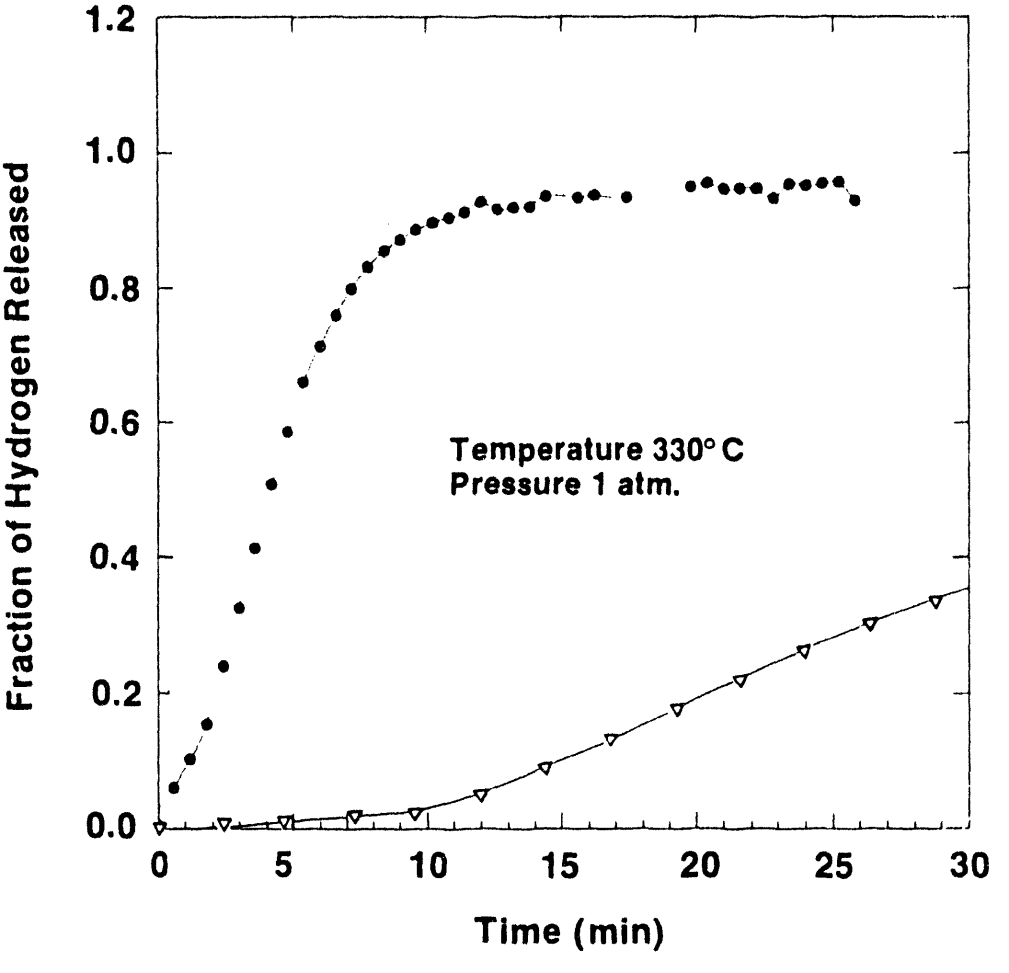

Figure 3: Dehydrogenation of MgNiH4

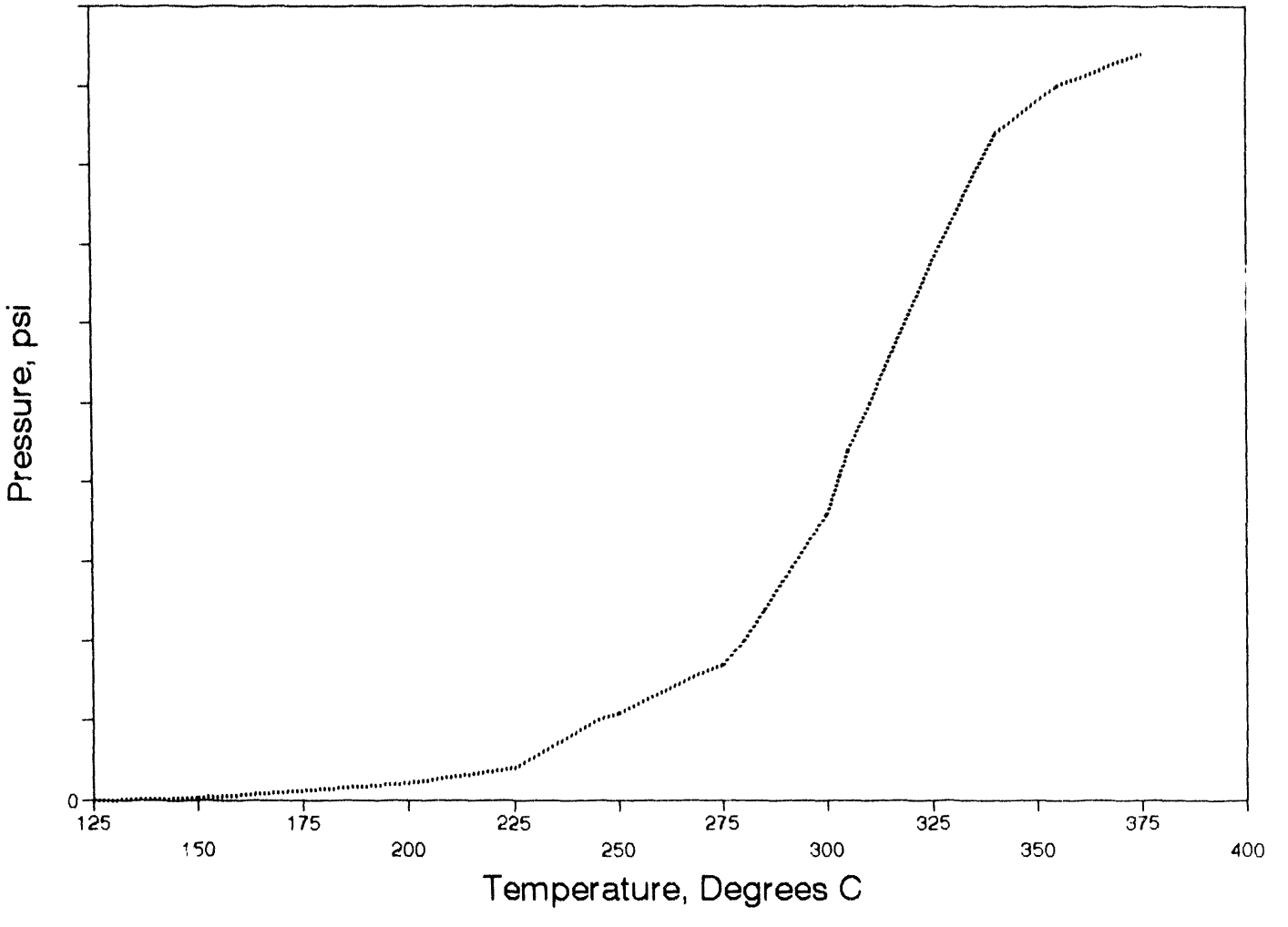

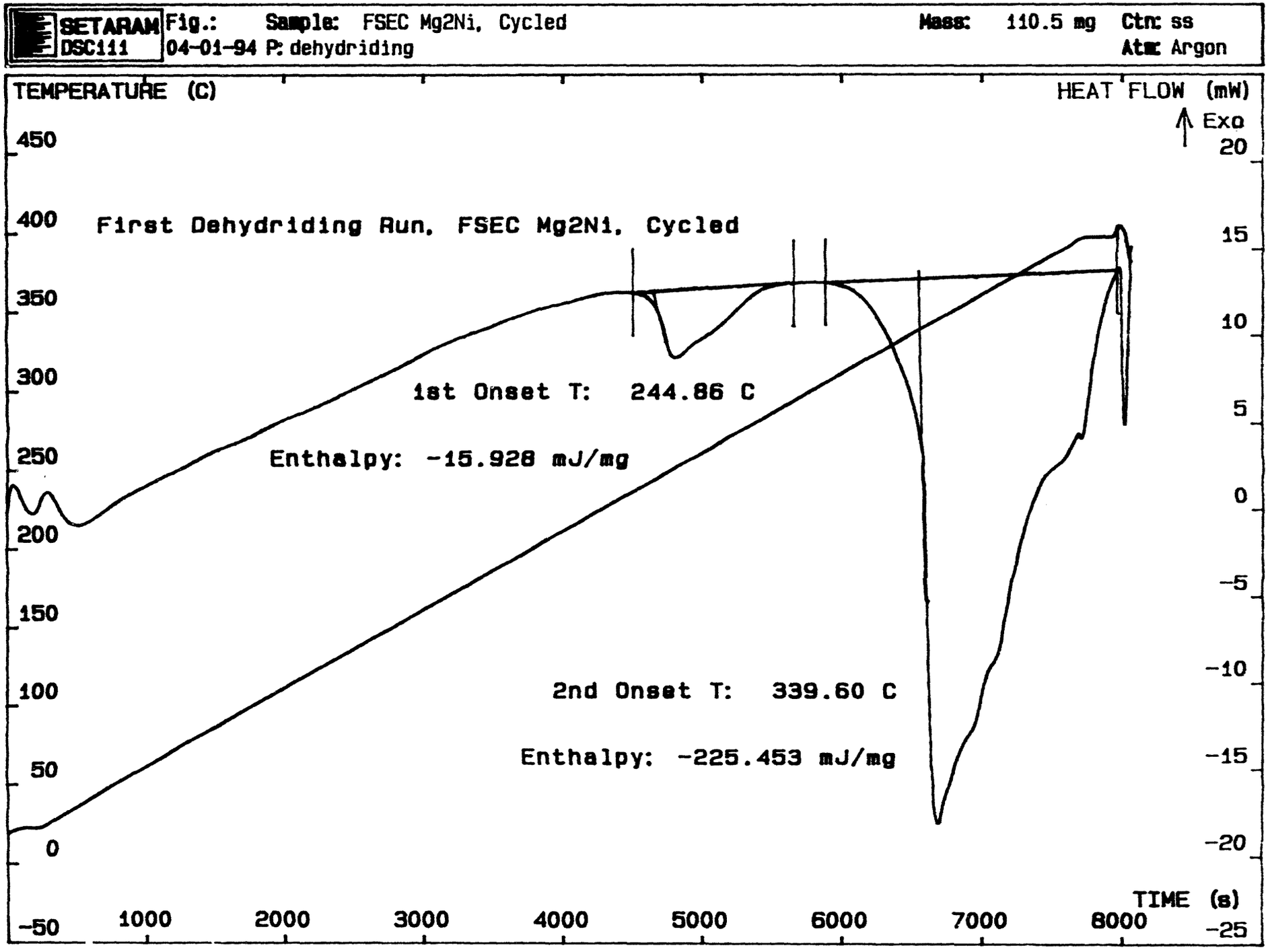
SETARAM
DSC111
Fig.:
04-01-94 P: dehydriding
Sample: FSEC Mg2Ni, Cycled
Mass: 110.5 mg
Ctrl: ss
Atm: Argon
TEMPERATURE (C)
HEAT FLOW (mW)
Exo
First Dehydriding Run, FSEC Mg2Ni, Cycled
1st Onset T: 244.86 C
Enthalpy: -15.928 mJ/mg
2nd Onset T: 339.60 C
Enthalpy: -225.453 mJ/mg
TIME (s)
450
400
350
300
250
200
150
100
50
0
-50
20
15
10
5
0
-5
-10
-15
-20
-25
1000
2000
3000
4000
5000
6000
7000
8000

Figure 5: Dehydrogenation of MgCuH4

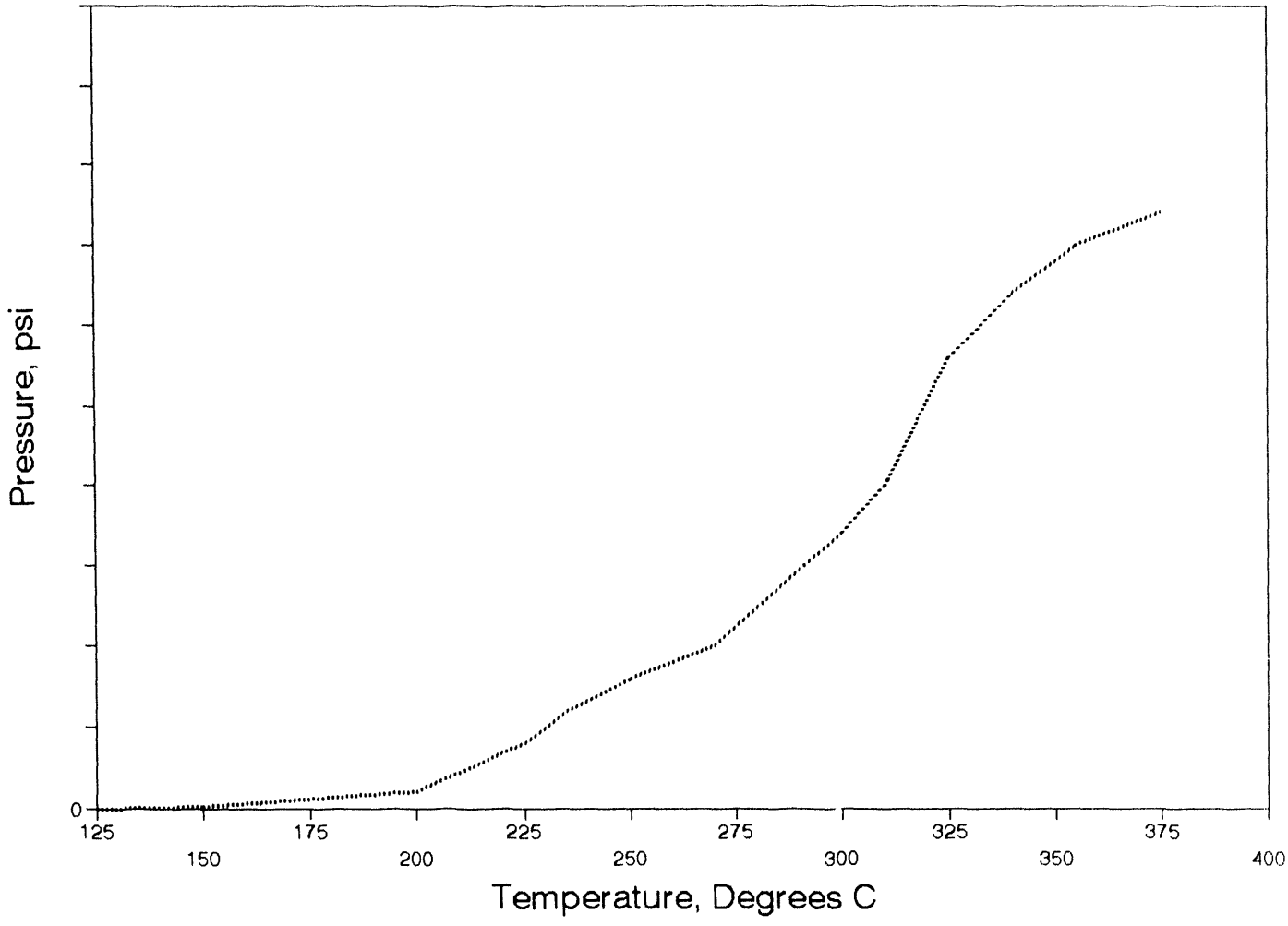

Figure 6:Comparison of Activation Temps
for Metallurgical vs Chemical

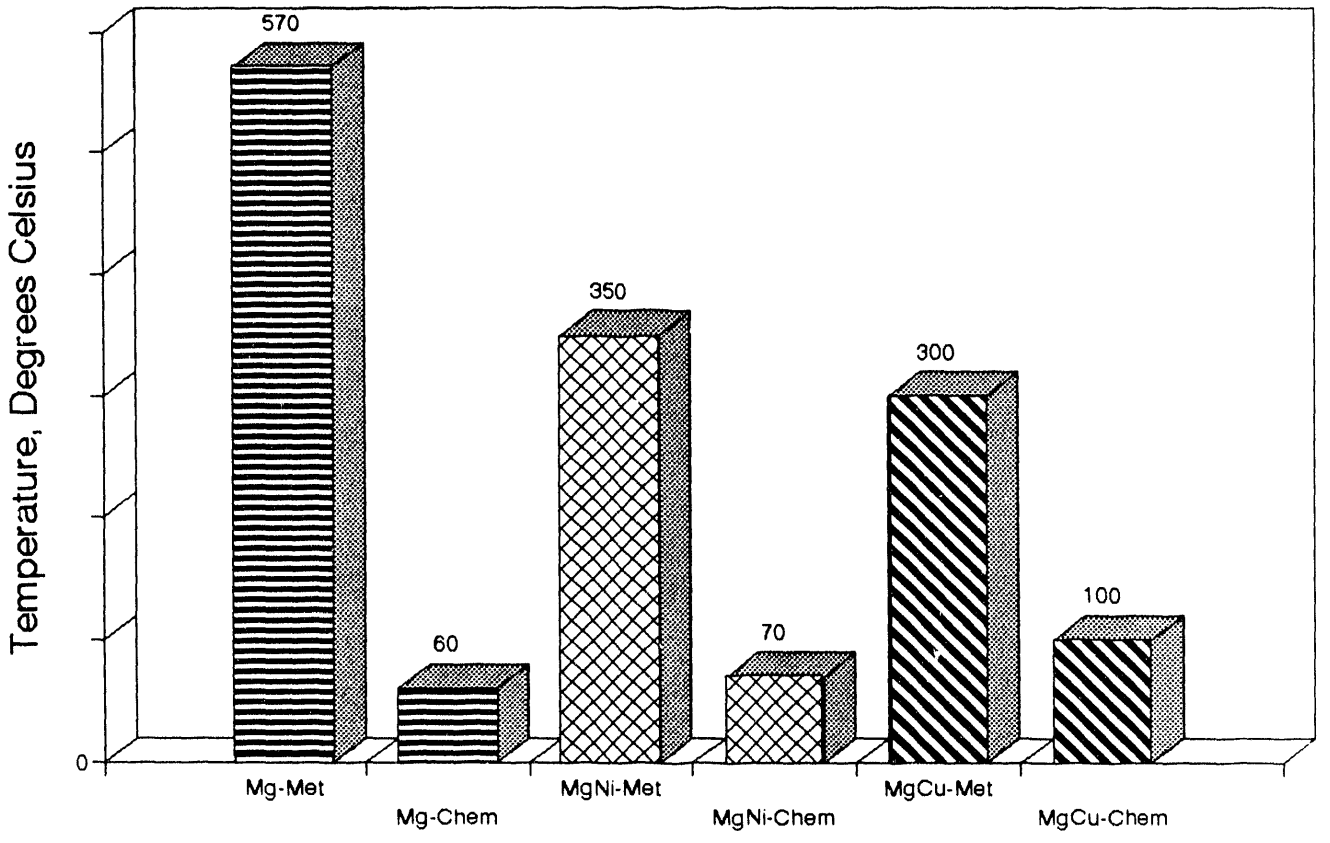

Figure 7:Comparison of Activation Times for Metallurgical vs Chemical

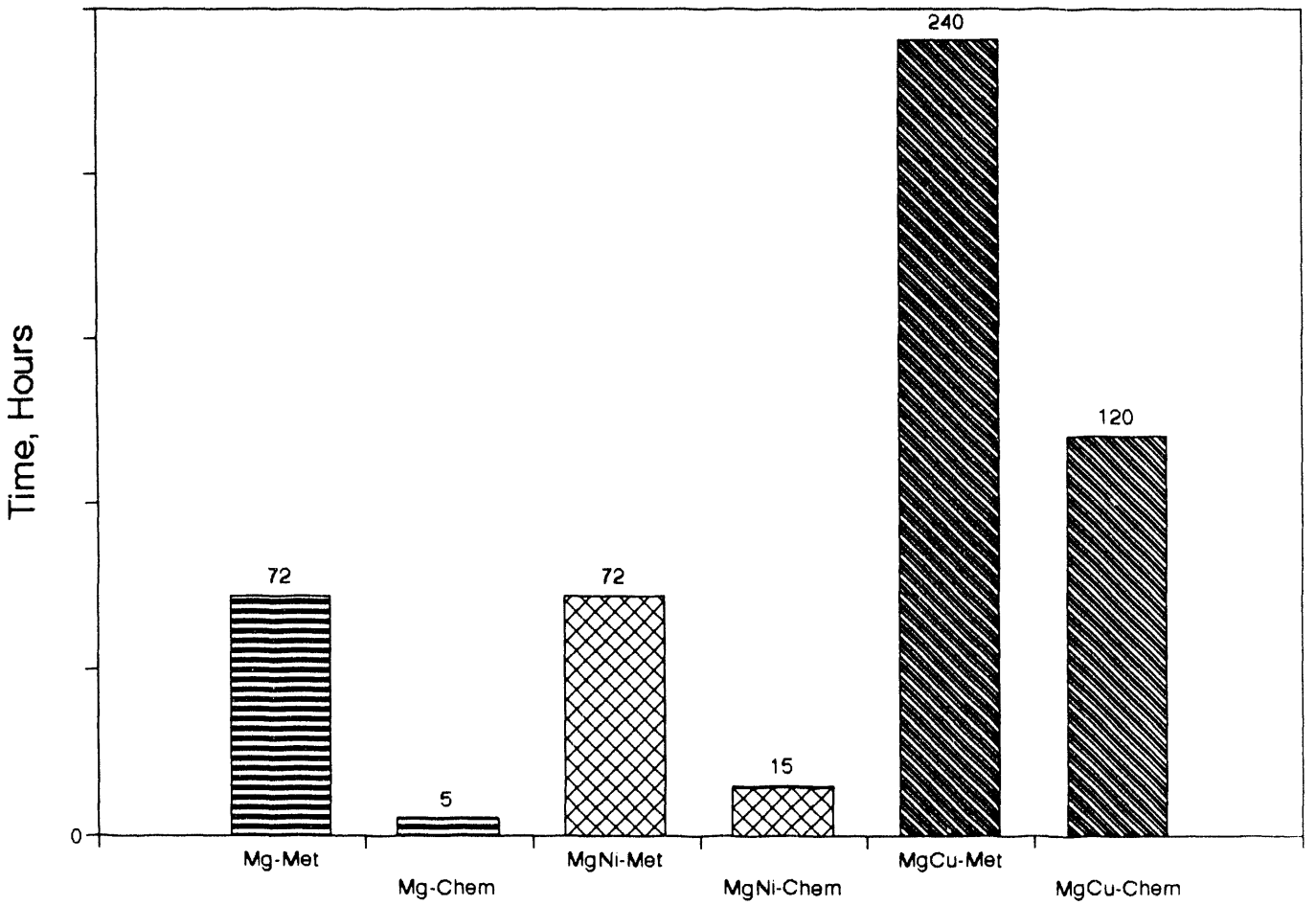

ACTIVATED CARBON-BASED HYDROGEN STORAGE SYSTEMS

James A. Schwarz
Syracuse University
Syracuse, NY 13244

Abstract

Engineering parameters necessary to provide rapid charge of hydrogen for use in fuel cell powered vehicles is presented. Our strategy is to recirculate pre-cooled hydrogen through an adsorbent bed of activated carbon contained in a light-weight-composites wound vessel isolated from the surroundings with passive insulation. Stored amounts of greater than 4% by system weight have been demonstrated with fill times that are less than twenty minutes. The major factor controlling the system's operating conditions is limited by currently available adsorbents. New procedures to molecularly engineer carbons that will relax these constraints provide the incentive to further refine hydrogen storage on activated carbon based technologies.

Introduction

For more than a decade Syracuse University has had an active program centered on the general task of developing practical storage systems for hydrogen based on its adsorption on activated carbons. During this time we have licensed the technology described in our US Patents 4,716,736 and 4,960,456, collaborated with Mazda North America in their program to develop hydrogen powered vehicles, constructed a hydrogen/fuel cell powered display vehicle with on-board storage of hydrogen using activated carbon technology, and established contracts with Niagara Mohawk Power Corporation which are directed towards residential use of hydrogen. The objective of this report is to describe the research and development tasks that we, as a result of our relationships with the commercial sector, have deemed essential for the realization of hydrogen, as a renewable energy source, to be successfully implemented into our energy infrastructure.

The potential number of end use applications for hydrogen is enormous. However, a common factor that pervades any end use is the loading properties of the hydrogen storage medium. Each end use places certain demands on the hardware and software required for this sub-system's design. In this report we will examine critically one end use application, i.e., vehicles, and will consider one type of propulsion system, i.e., fuel cell/electric motor. Our rationale for these choices is that success in this area will provide the elements for comprehensive systems' design which could then be readily adapted to other load use applications. Thus, the loading characteristics of an on-board hydrogen storage system is the focus of discussion.

Experimental

Apparatus

Our data base for assessing the dynamic storage properties of activated carbons is determined by a volumetric method conducted in our Process Development Unit (PDU).

In order to determine the optimum conditions for a practical hydrogen storage system, a number of experiments were performed in order to answer the following question: for a chosen carbon sample, how does the charging procedure affect the adsorption characteristics and amount of hydrogen stored. Charging procedures consist of rate of charging, maximum pressure reached during charging and amount of time it takes for charging. Charging characteristics refer to the rate at which the system pressure falls off until an approximate steady value is reached. The structural heterogeneity and chemical functionality of the chosen carbon plays a significant role during the whole process of adsorption.

The vessel used in our experiments has an internal volume of 1 liter and is made from a composite of carbon fiber/epoxy filament windings. This vessel is charged with 306 g of carbon sample. The carbon sample is first conditioned by evacuation, followed by a purge of warm helium gas, and further evacuation to 1.3×10^{-5} atmospheres. The vessel is surrounded with passive insulation. Two thermocouple probes are inserted into the vessel, one in touch with the carbon sample while the other measures the temperature of the gas in the void space. The pressure within the vessel is measured by means of a pressure transducer (model EA) and a pressure indicator (model PL-1), both of which were obtained from Data Instruments in Acton, MA. Figure 1 shows a schematic of the apparatus.

Adsorption is carried out by passing hydrogen gas through a 50-ft coiled copper tube that sits in a heat exchanger; cold gas enters the carbon-containing vessel. Using this experimental procedure, a number of charging variables can be studied.

A Brooks mass flow controller is installed on the downstream side of the system. This controller is connected to a totalizer which measures the amount of hydrogen stored in the vessel. Discharged amounts from the vessel can be measured when pressure swing is applied.

Materials

In all experiments, hydrogen gas, of ultra-high purity grade (99.9999%), was supplied by Linde Specialty Gas Division of Union Carbide. The hydrogen is further purified by means of a de-oxo unit and a molecular sieve-unit immersed in a liquid nitrogen trap.

We have tested a number of commercial carbon samples. The results reported herein were obtained for ESC-1. This is a granular carbon with a BET surface area of 2000 m^2/g and a bulk density of 0.31 g/cc.

Procedures

We have adopted three procedures for charging a carbon containing pressure vessel with pre-cooled hydrogen gas. The first approach is to charge the system with a "spike" of high pressure cooled gas (duration ~30 s), closing the inlet valve and monitoring the system's response as it adsorbs gas. We designate this period as the fill time and terminate the experiment when the pressure and temperature became essentially constant (< 5% variation.)

The second approach is to maintain the bed at a constant temperature by active cooling provided by a surrounding dewar. The storage system is pressurized by a "spike" (duration ~30 s) and the pressure is monitored as a function of time. Data from these experiments, in conjunction with earlier microbalance results at the same temperature allows us to evaluate the amount of hydrogen actually stored in the vessel.

The third approach is to charge the vessel at a constant pressure. In this case the fill time is the time required for the temperature of the system to become essentially constant (< 5% variation.) The flow rate of hydrogen into the vessel goes to zero at this point.

In all cases the system's dynamic storage properties are recorded as a function of time. From such data one can then assess the performance characteristics of the storage system once an end use application is chosen.

Results

Approach I

Figure 2 shows typical response curves for different initial pressure steps. The maximum pressure applied in one case (72 atmospheres) was lower than that of the other (75 atmospheres.) However, the final pressure (39 atmospheres) attained for the first case was higher than that in the case of the latter (34 atmospheres.) Fill times are about 10 minutes for both tests. The reason for this reversal is due to

different initial conditions of the carbon before charging took place. In the first test, cold hydrogen gas was flushed through the system at very low pressures for a longer period than for the second test. This longer period also accounts for the time it takes the gas molecules to penetrate the micropores of the carbon bed. Consequently, most of the higher energy sites for adsorption had been occupied before the final charging was started. That explains why, even at a lower charging pressure, the equilibrium pressure was higher than the second test. This aspect of initial conditioning of the bed thus becomes very important in determining the maximum allowable temperature the carbon should reach during the discharge process as in, for example, an automobile. The amount of hydrogen stored at 39 atmospheres was 7.63% by weight of carbon while that stored at 34 atmospheres was 6.24%.

Approach II

The pressure vessel maintained at constant temperature was charged with pre-cooled hydrogen to an initial pressure of 81.22 atmospheres. After 10:34 minutes, the system had come to a pressure of 41.16 atmospheres. The temperature of the system was maintained at 90 K for all subsequent trials. The stored amount (adsorbed plus void) at a pressure of 41.16 atmospheres was 8% hydrogen by weight of the ESC-1 carbon. Every initial pressure will correspond to a particular final pressure. There will also be an effective fill time after which there is essentially no significant drop in pressure as a function of time.

Figure 3 depicts the impact of different initial pressures on the final pressures as a function of effective fill times. We see that the higher the initial pressure, the higher the final pressure, a trend to be expected. The higher the initial pressures the shorter the fill times. From Figure 3, one can determine directly what final pressure to expect if the system is charged at a given initial pressure; the fill time can also be assessed. For example, for a final pressure of about 37 atmospheres a fill time of 11.5 min can be expected.

Based on isotherm data from our gravimetric experiments on this carbon and assuming equilibrium is reached in the PDU, we determine the amount of hydrogen stored at each final pressure. Since the temperature in the PDU is constant, the amount stored is "pinned" to a specific value once the final pressure is known. We then can analyze the data from the dynamic experiments to provide a "user friendly" design plot as shown in Figure 4. Summarizing the analysis method, for this particular carbon, an initial pressure of 81 atmospheres will load a storage vessel in ~ 11 min with hydrogen such that the amount stored is ~ 8% by weight of carbon.

Approach III

Figure 5 shows typical temperature relaxation data as a function of fill time for ESC-1 carbon for a charging pressure of 76 atmospheres. Table 1 compiles data for a range of charging pressures; we report the final temperatures, fill times and the amounts of hydrogen stored per gram of carbon. It is important to note that from this dynamic data we cannot assess the amount of hydrogen stored at any time during the "filling" process because the temperature is changing.

Discussion

Our dynamic storage data are analyzed on the basis of the following rhetorical questions: In conjunction with our objective, what fill times are necessary to achieve a desired range? For a light weight composites

wound pressure vessel commercially available (Structural Composites Inc., Pamona CA) that is passively insulated, what are the size and weight factors for on-board storage of hydrogen in a fuel cell/electric motor powered vehicle that is to be designed to have a range of 300 miles?

Table 1. Characteristics of Activated Carbon Storage System

	Charging Pressure (atm)	Final Temperature (K)	Fill Time (mins)	Stored Amount Wt % Basis: Carbon
A	88.4	143	26.3	6.95
B	88.9	130	20.8	7.70
C	82.2	129	20.4	7.36
D	82.2	144	26.7	6.54
E	74.5	129	20.4	6.85
F	76.3	149	28.8	5.90
G	69.0	131	21.3	6.24
H	70.0	155	31.3	5.20

We will use our laboratory data from Approach II to establish reasonable answers for the first question. Recognizing that Approach II requires active cooling of the storage media, which might be a disadvantage for vehicle applications, we use our laboratory data from Approach III to provide answers for the second question.

A filament wound carbon/epoxy composites pressure vessel is available for on-board hydrogen storage application. It is structured as a conventional dome-ended cylinder with an aluminum liner and one end-port. With passive (vacuum jacket shell made of carbon/epoxy) insulation it has the following characteristics: operating pressure 1300 psig; burst pressure 3000 psig; specific volume 150 in^3/lb.

In order to achieve a range of 300 miles, 2.65 kg of hydrogen is required provided the efficiency of conversion of its energy content in a proton exchange membrane (PEM) fuel cell/electric motor arrangement is 100%. However, such an efficiency is unrealistic. Based on research report UCD-ITS-RR-92-14 by DeLuchi (1) we use the following estimates: once-through efficiency of electric motor = 0.89; once-through efficiency of motor-controller and invertor = 0.94; once-through efficiency of motor to wheel transmission = 0.95. These factors lead to an over-all efficiency of 0.69 which means that to achieve the desired range of 300 miles, 3.84 kg of hydrogen would be actually required.

With this additional information we proceed as follows. The results presented in Figure 4 give the amount of hydrogen stored at a fixed temperature (active cooling of vessel) and final systems pressure as a function of fill time. We assume a standard size for the composites vessel of 163 liter which will hold 49.9 kg of carbon. The total hydrogen contained in the vessel is the sum of the hydrogen adsorbed on

the carbon and that in the gas phase in the void space at the prevailing pressure and temperature. From this amount and the overall efficiency of the vehicle propulsion system we can calculate a vehicle range as a function of fill time; the results are shown in Figure 6. The trade-off between pressure, range, and fill-time is apparent. Higher final pressures (which require higher initial pressures) lead to shorter fill times and a longer vehicle range. However, active cooling is required. We used our laboratory data at 90K because we have extensive gravimetric data that was collected during our earlier studies when we were evaluating the storage performance of various commercial carbons.

If we eliminate active cooling and utilize the pre-cooled hydrogen to lower the temperature of the adsorbent bed we can analyze the data from Approach III. Based on the pressure vessel specifications we can convert the storage data presented in Table 1 to a system weight basis. The results are presented in Table 2 for each of the cases. For comparison purposes we also present equivalent results for a compressed gas storage system at the prevailing pressure, room temperature, and assuming the same pressure vessel is used as in the activated carbon case. We chose room temperature because compressed gas technology does not require temperatures lower than ambient.

Table 2. Comparison of Activated Carbon Based and Compressed Gas System. Wt % Basis

	Wt % Basis: Carbon	Wt % Basis: Total System	Compressed Gas Basis: Total System
A	6.95	4.15	3.63
B	7.70	4.57	3.65
C	7.36	4.39	3.38
D	6.54	3.92	3.38
E	6.85	4.10	3.07
F	5.90	3.54	3.14
G	6.24	3.74	2.85
H	5.20	3.14	2.89

Table 3 re-examines the laboratory data (Table 1) on the basis of storage system size. The volume of a pressure vessel containing activated carbon and hydrogen at the pressure and temperature of the experiment is determined by scaling the experimental amount of storage by the required 3.84 kg of hydrogen necessary to achieve the 300 mile range. We also provide for comparison the size of an equivalent compressed gas storage tank at the same pressure, room temperature, and weight of hydrogen. In the last column we present the size for the compressed gas tank assuming the systems at room temperature.

Finally, we present a comparison of the size and weight demands for a activated carbon based hydrogen storage system for the conditions examined using Approach III with that of a conventional gasoline

Table 3. Comparison of Activated Carbon Based and Compressed Gas Systems. Volume Based

	Activated Carbon (liters)	Compressed Gas Room Temperature, Same Pressure (liters)
A	180.7	551.9
B	163.1	548.6
C	170.6	593.6
D	192.0	594.5
E	183.3	655.3
F	212.9	639.5
G	201.3	708.3
H	241.5	697.3

powered vehicle. We assume a performance of 15 miles/gallon. The weight of a 20 gallon steel gasoline tank (19.79 kg) filled with fuel (52.99 kg), results in a combined weight of 72.78 kg; this corresponds to a volume of 75.7 liters. Table 4 presents our data. Again for comparison purposes we also consider the size and weight demands for compressed gas storage. The results are apparent, the activated carbon

Table 4. Comparison of Activated Carbon Based and Compressed Gas Total Volume and Weight Basis

	Activated Carbon System		Compressed Gas System	
	Vol (liters)	Total Wt. (Kg)	Vol (liters)	Total Wt. (Kg)
A	180.7	92.5	551.9	105.9
B	163.1	83.8	548.6	105.2
C	170.6	87.5	593.6	113.6
D	192.0	98.0	594.5	113.7
E	183.3	93.7	655.3	124.9
F	212.9	108.3	639.5	122.0
G	201.3	102.6	708.3	134.8
H	241.5	122.3	697.3	132.7

based storage system places less of a demand on vehicle modifications to accommodate the additional weight and size of the "gas" tank compared to compressed gas storage.

Conclusions

Activated carbon based hydrogen storage systems with passive insulation are compatible with vehicle propulsion systems using fuel cell/electric motor technology. We find that refueling times are certainly reasonable for fleet vehicle applications and that desired vehicle range is not burdened by excessive size and weight requirements of the storage system.

Commercially available activated carbons are most suitable for use at temperatures in the range of 78-90K. The technology to achieve these temperatures is well-established and can be centrally located at "gas" stations to pre-cool hydrogen during vehicle refueling without placing any additional demands for on-board maintenance of low temperatures.

The future of this technology is promising considering the development of new carbon adsorbents which could relax the temperature requirements. In that regard, we have found that ion-exchange resins are a class of "cheap" and readily available starting materials for one step activated carbon synthesis to form adsorbents with developed microporosity. The tuning of microporosity to the molecular dimensions of hydrogen, which will result in adsorbents with a higher storage capacity at higher temperatures compared to existing carbons, is part of our present and future research goals.

Acknowledgment

This work was supported by the DOE/NREL under Contracts XC-1-11081-1 and XAE-3-13346-01.

References

Deluchi, M. 1992, *Hydrogen Fuel-Cell Vehicles*, Research Report UCD-ITS-RR-92-14. Institute of Transportation Studies, University of California, Davis, California.

List of Figures

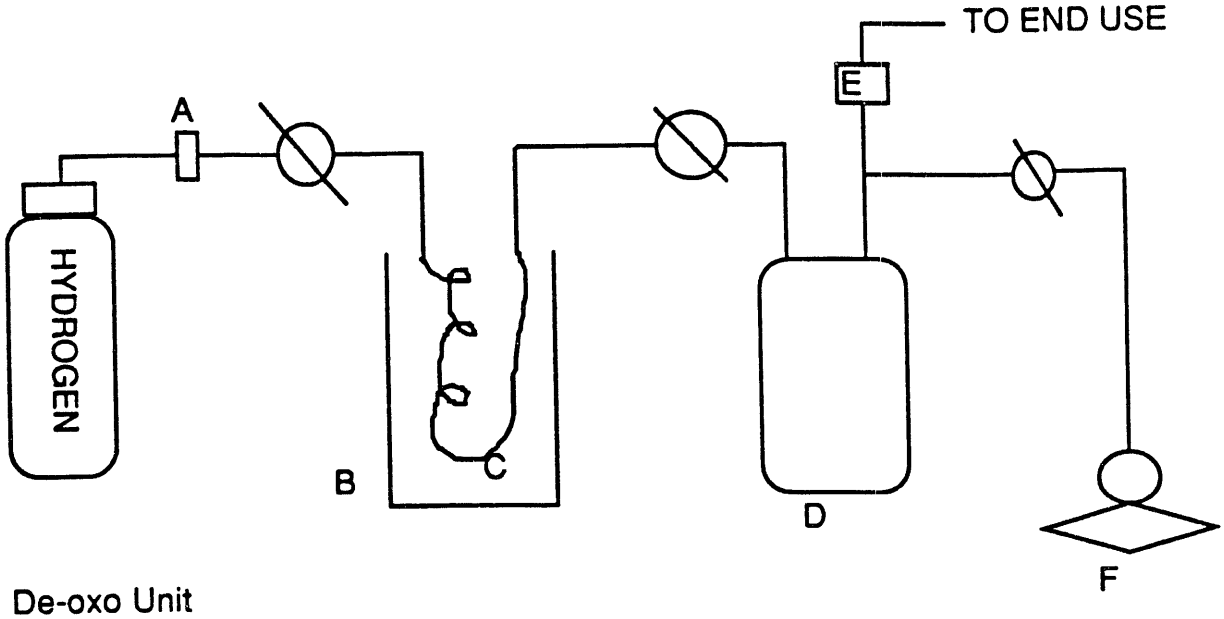

A. De-oxo Unit
B. Heat Exchanger
C. Cooling Coil
D. Storage Vessel
E. Flow Controller
F. Vacuum Pump

Figure 1

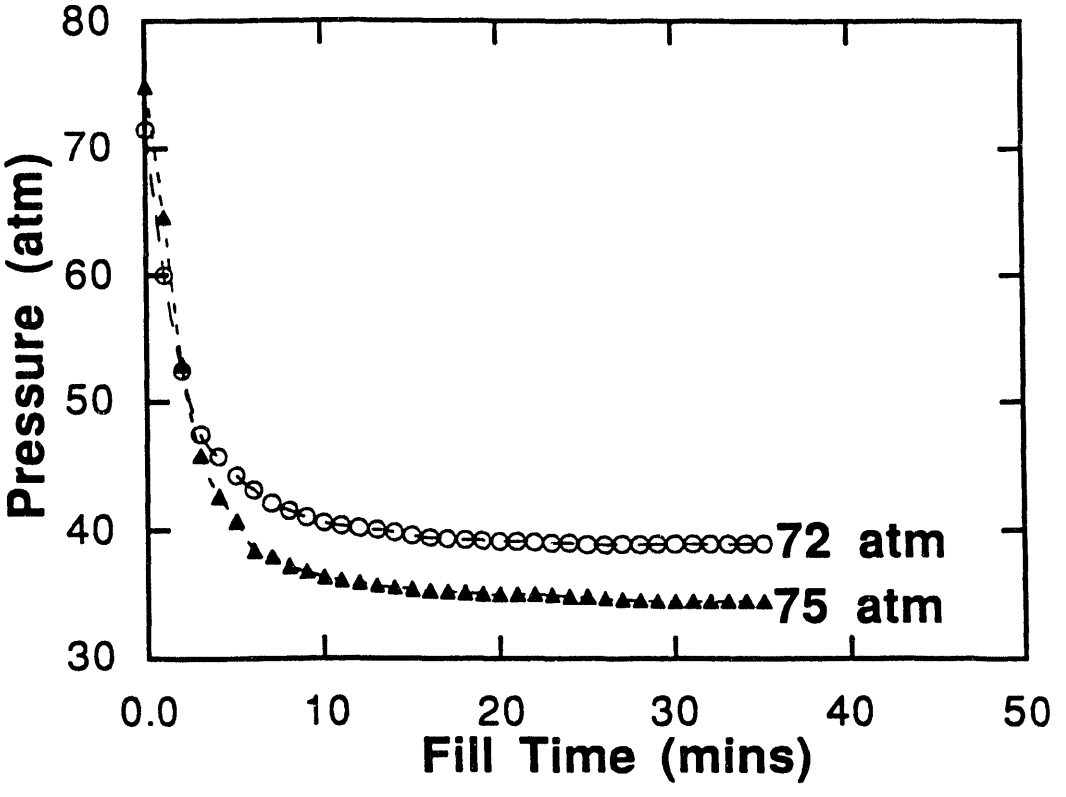
80
70
60
50
40
30
Pressure (atm)
0.0
10
20
30
40
50
Fill Time (mins)
72 atm
75 atm

Figure 2

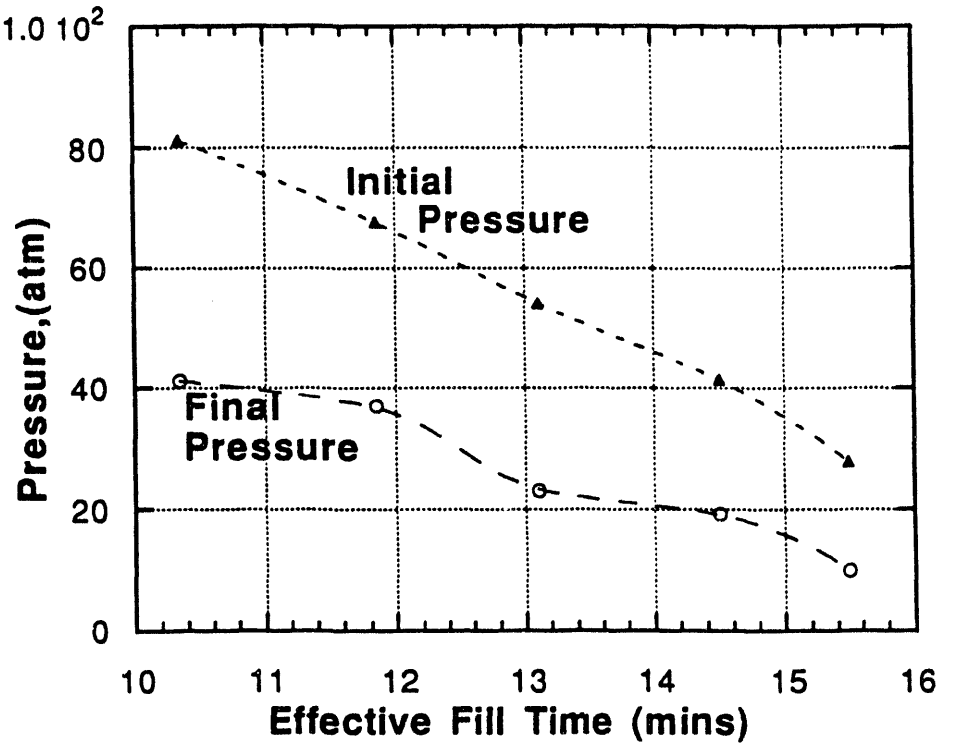
1.0 10²
80
60
40
20
0
Pressure,(atm)
Initial
Pressure
Final
Pressure
10
11
12
13
14
15
16
Effective Fill Time (mins)

Figure 3

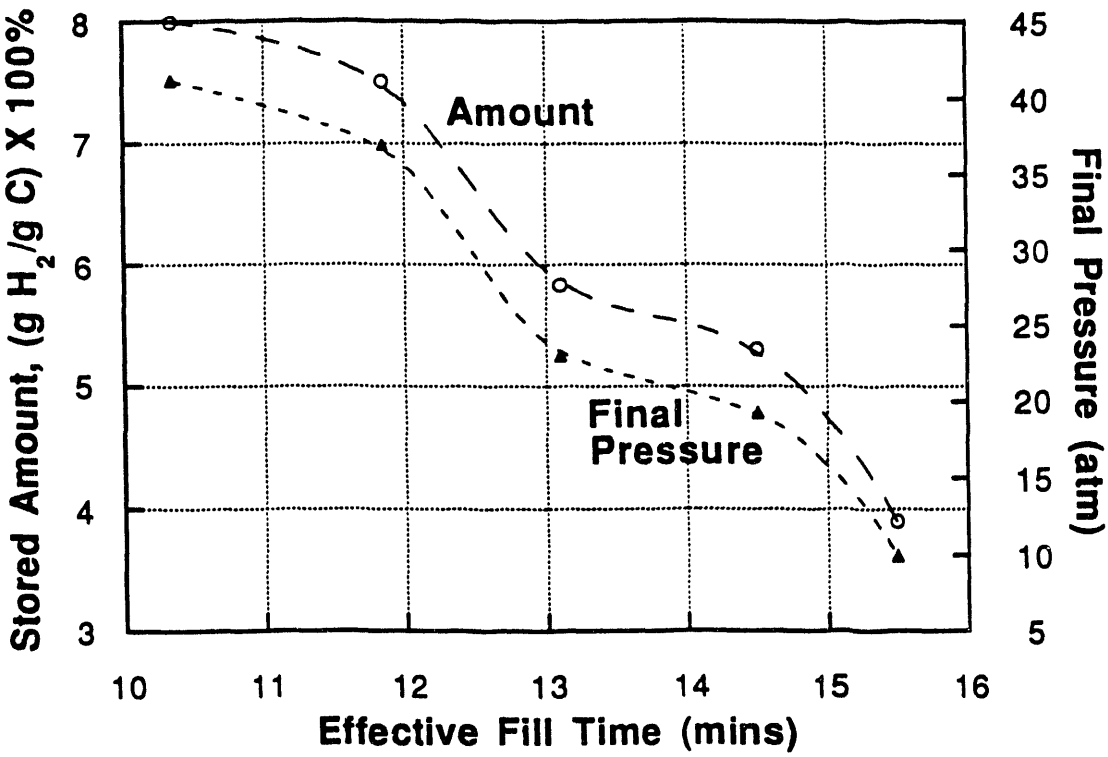
Stored Amount, (g H_2/g C) X 100%
8
7
6
5
4
3
Amount
Final
Pressure
45
40
35
30
25
20
15
10
5
Final Pressure (atm)
10
11
12
13
14
15
16
Effective Fill Time (mins)

Figure 4

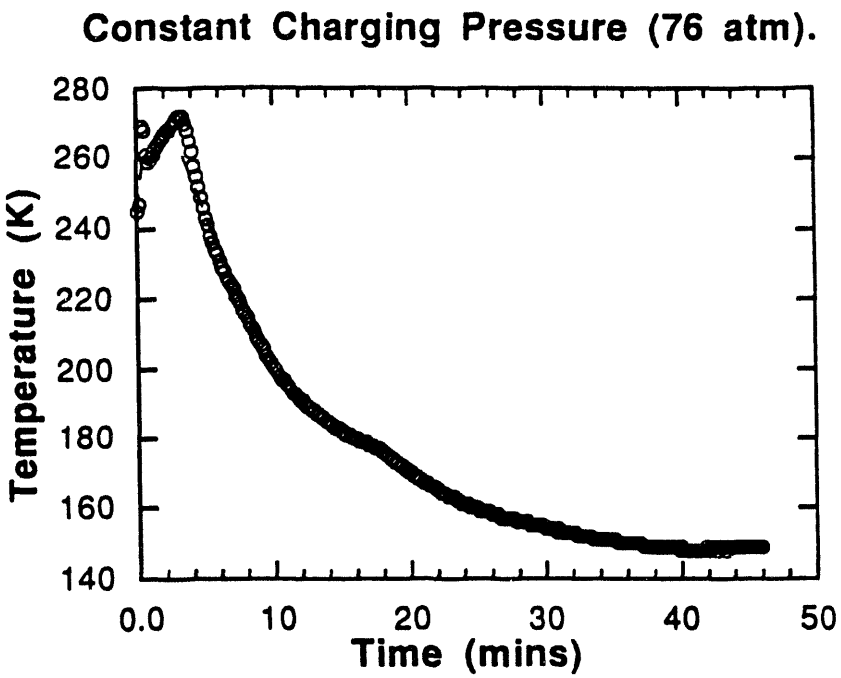
Constant Charging Pressure (76 atm).
Temperature (K)
280
260
240
220
200
180
160
140
0.0
10
20
30
40
50
Time (mins)

Figure 5

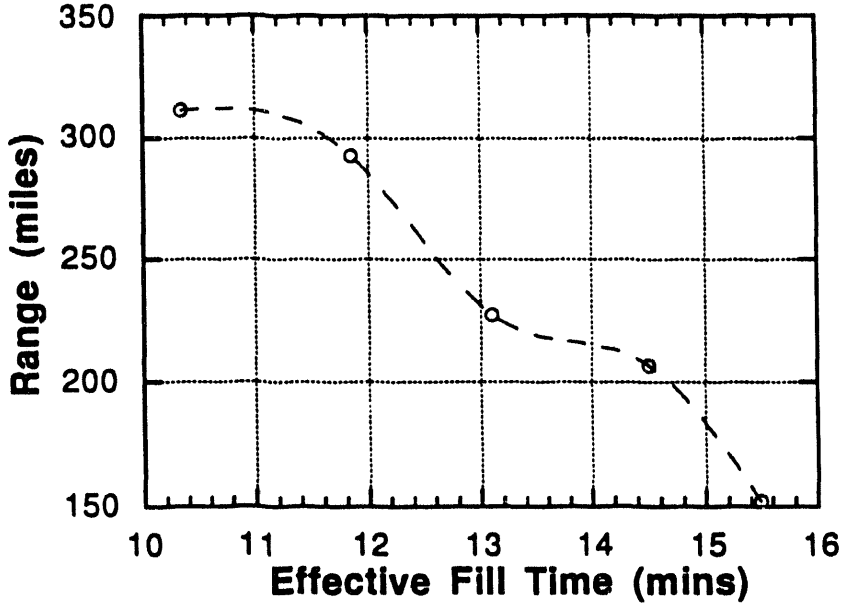
350
300
250
200
150
Range (miles)
10
11
12
13
14
15
16
Effective Fill Time (mins)

Figure 6

HIGH EFFICIENCY STATIONARY HYDROGEN STORAGE

Scott Hynek, Ware Fuller, and David Friedman
Arthur D. Little, Inc.
Acorn Park, Cambridge MA 02140

Abstract

This 12-month effort will require $317,972, of which 20% will be cost-shared by ADL and its lower-tier subcontractor. The eventual hydrogen infrastructure will require stationary storage, to facilitate intermittent sources and to permit methane reformers to run base-loaded. Both energy efficiency and added cost are more important to this application than are either gravimetric or volumetric efficiency. ADL's approach is to maintain a high-temperature metal hydride in intimate thermal contact with a phase change material (PCM), so that the PCM retains hydriding energy as heat of fusion, returning that heat as heat of dehydriding. ADL's approach is to put the hydridable alloy (nickel-coated magnesium powder) on the tube side, and the PCM (perhaps a eutectic mixture of salts) on the shell side, of a shell-and-tube heat exchanger. We will consider this approach successful if the nickel-coated magnesium powder operates with acceptable kinetics and without poisoning, and if the PCM can be fused and solidified without excessive temperature differences. The key result to be presented eventually will be the pressure swing required to effect hydrogen storage in, and discharge from, the laboratory prototype stationary hydrogen storage device.

Introduction

Stationary storage of hydrogen has two applications, both near-term, as depicted in Figure 1:

1. It can accommodate the intermittent nature of most renewable sources of electrical energy, such as wind turbines and photovoltaic (PV) arrays, when used with an electrolyzer.

2. During the transition to a hydrogen economy, it can also store hydrogen produced by natural gas fuel processors (reformers plus shift reactors), whether centrally or terminally located, thus

permitting these fuel processors to be sized for the average hydrogen demand (e.g., fueling demand for hydrogen vehicles) rather than the peak load.

Figure 1 - Stationary hydrogen storage is essential to the hydrogen infrastructure.

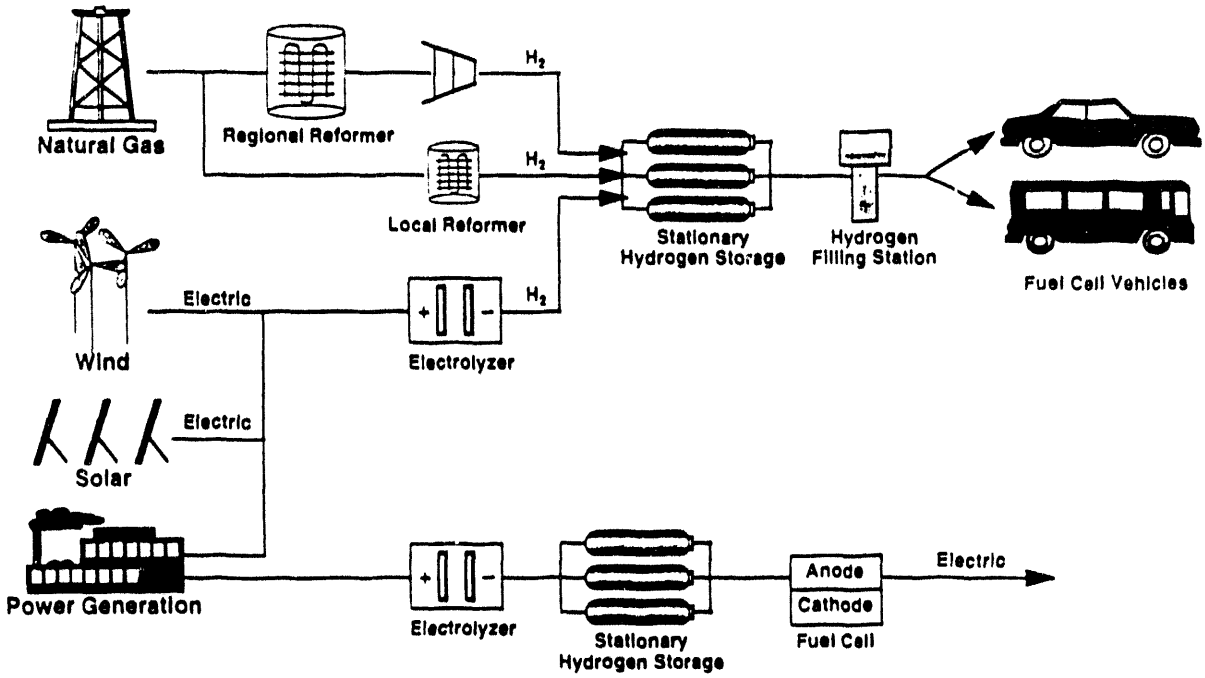

The DOE Hydrogen Program Plan's long-range stationary hydrogen storage goals relate to storage efficiency and added cost ratio, defined as follows:

- Storage Efficiency = HHV / (HHV + PTPE)

  where: HHV = higher heating value of delivered hydrogen
  PTPE = process total primary energy associated with storage and retrieval

- Added Cost Fraction = Added Cost of Storage Retrieval / Cost of Delivered Hydrogen

We have calculated that our approach to stationary storage more than meets both of these goals, per Table 1:

Table 1 - Efficiency and Cost, Our Projections vs. DOE's Goals

	ADL's Projected Value	DOE HPP Goal
Storage Efficiency	94%	75%
Added Cost Ratio	24%	50%

Approach

Five hydrogen storage technologies are available for use today; none is without drawbacks, and each has its niche, per Table 2:

Table 2 - Hydrogen Storage Technologies Available Today

Storage Technology	Comments
Liquefied hydrogen	Has the highest system volumetric density, but also the highest energy penalty; it is used by NASA for on-board and stationary storage.
Compressed hydrogen gas	Comprises the simplest system, but has low volumetric density; it is used on the Ballard fuel cell bus and by Electrolyser in conjunction with PV arrays.
Carbon-adsorbed hydrogen	Can improve volumetric density of compressed hydrogen gas system, at the expense of the gravimetric density.
Low-temperature metal hydrides	Create the most crash-worthy on-board storage system, but one which is quite heavy; it is used by Mazda on its hydrogen-powered Miata. More expensive than high-temperature metal hydrides.
High-temperature metal hydrides	Are inappropriate on board vehicles, because they require dehydriding energy at higher temperature than is available for free on board vehicles.

Figure 2 presents a Van't Hoff plot that serves to

1. describe the equilibrium pressure-temperature characteristics of various metal hydrides,

2. distinguish between high-temperature metal hydrides (those grouped on the left-hand side) and low-temperature metal hydrides (those grouped on the right-hand side), and

3. show why only low-temperature metal hydrides are suited for use on-board fuel cell vehicles (discharging high-temperature metal hydrides requires higher-temperature heat than vehicular fuel cells generate).

However, if one can store the heat given off during the charging (hydriding) of a high-temperature metal hydride, and re-use that energy during discharging (dehydriding), then one can take advantage of the relatively higher gravimetric and volumetric efficiencies of high-temperature metal hydrides (which do matter insofar as they affect system cost) and the relatively low cost of the metals from which high-temperature metal hydrides are made. Figure 3 suggests how this heat can be stored, using a bed of phase change material (PCM).

Figure 2 - High-temperature metal hydrides are inappropriate for on-board storage.

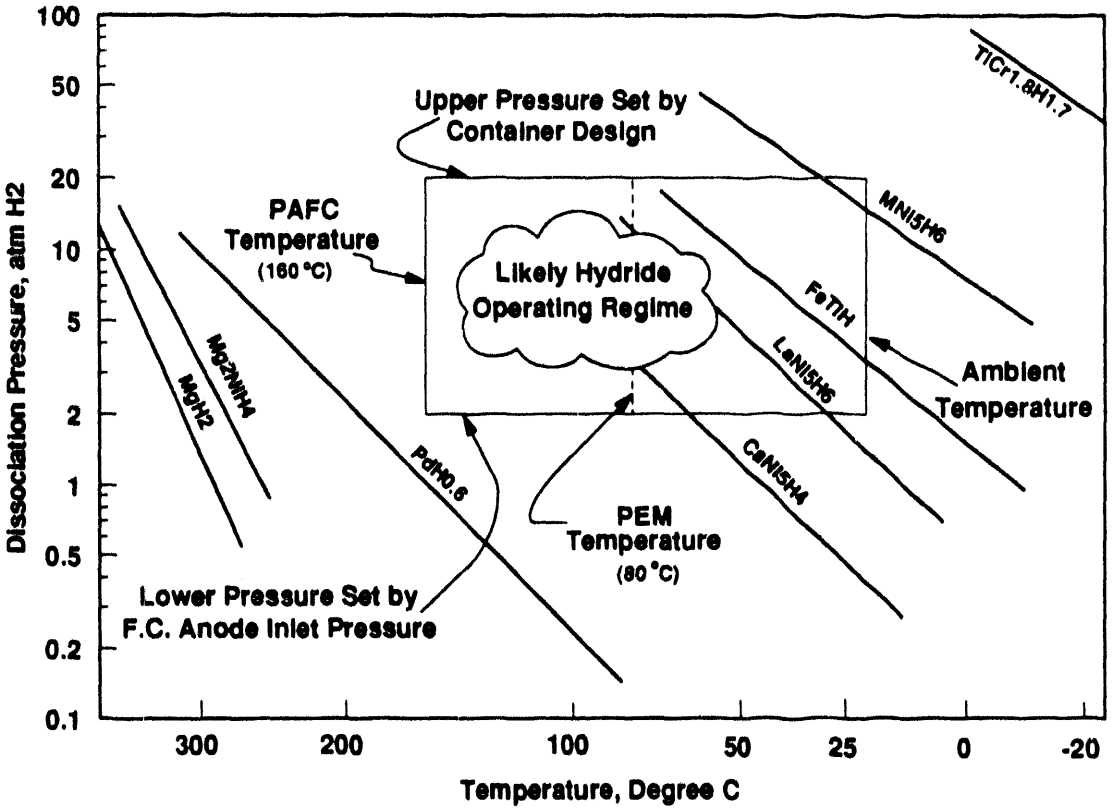

Figure 3 - Thermal Schematics for Storing and Retrieving Hydriding Energy

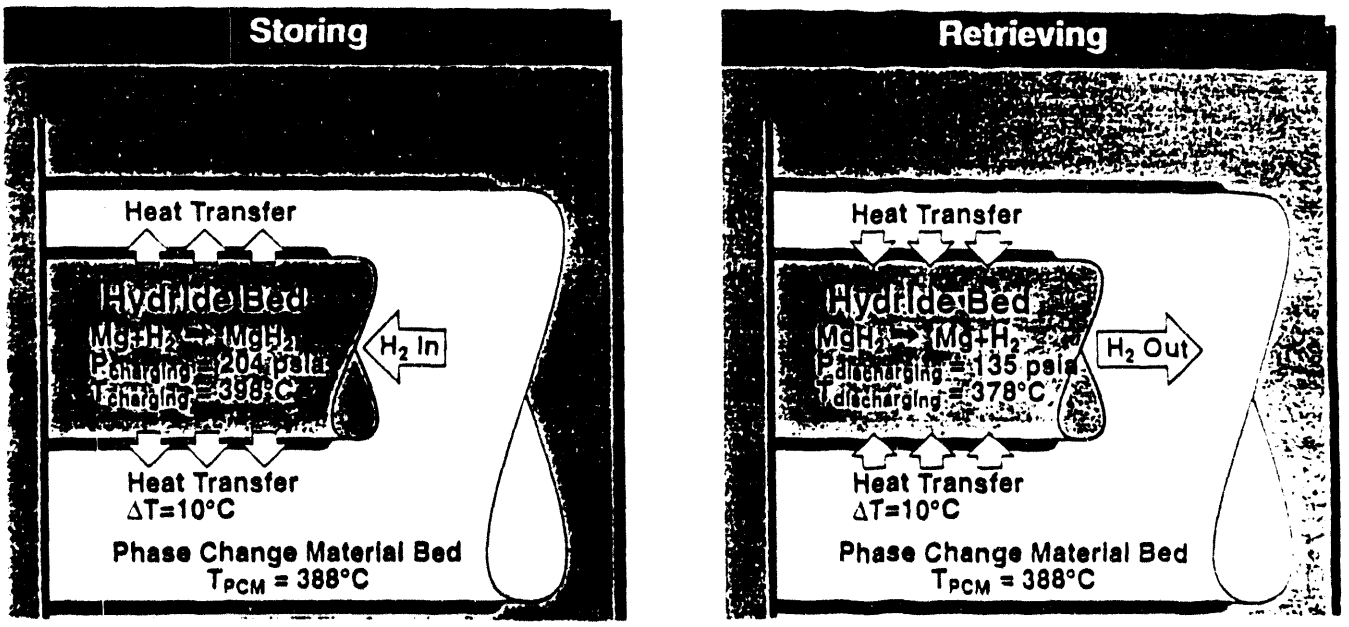

The phase change material (PCM) could be any of a number of salts which melt at the right temperature. Better yet, the PCM could be a eutectic mixture of salts, for these appear to offer higher heats of fusion than do pure salts of comparable phase change temperature.

Figure 4 presents the MgH_2 isochor (that is, the MgH_2 line from Figure 2, the Van't Hoff plot), plotted as pressure vs. temperature rather than log(p) vs. $1/T_{ABSOLUTE}$. The pressures corresponding to temperatures 10°C above and 10°C below the phase change temperature would correspond to the charging and discharging pressures, respectively, if the temperature differences between the hydride bed and the PCM can indeed be held to 10°C (an arbitrarily selected, but fairly representative, value). The difference between charging and discharging pressures, called the 'pressure swing,' represents the major energy loss associated with this system for stationary storage of hydrogen. The only other loss is heat lost from the vessel, which can be minimized as required with thermal insulation.

Figure 4 - Magnified MgH_2 Isochor Showing Magnitude of Pressure Swing

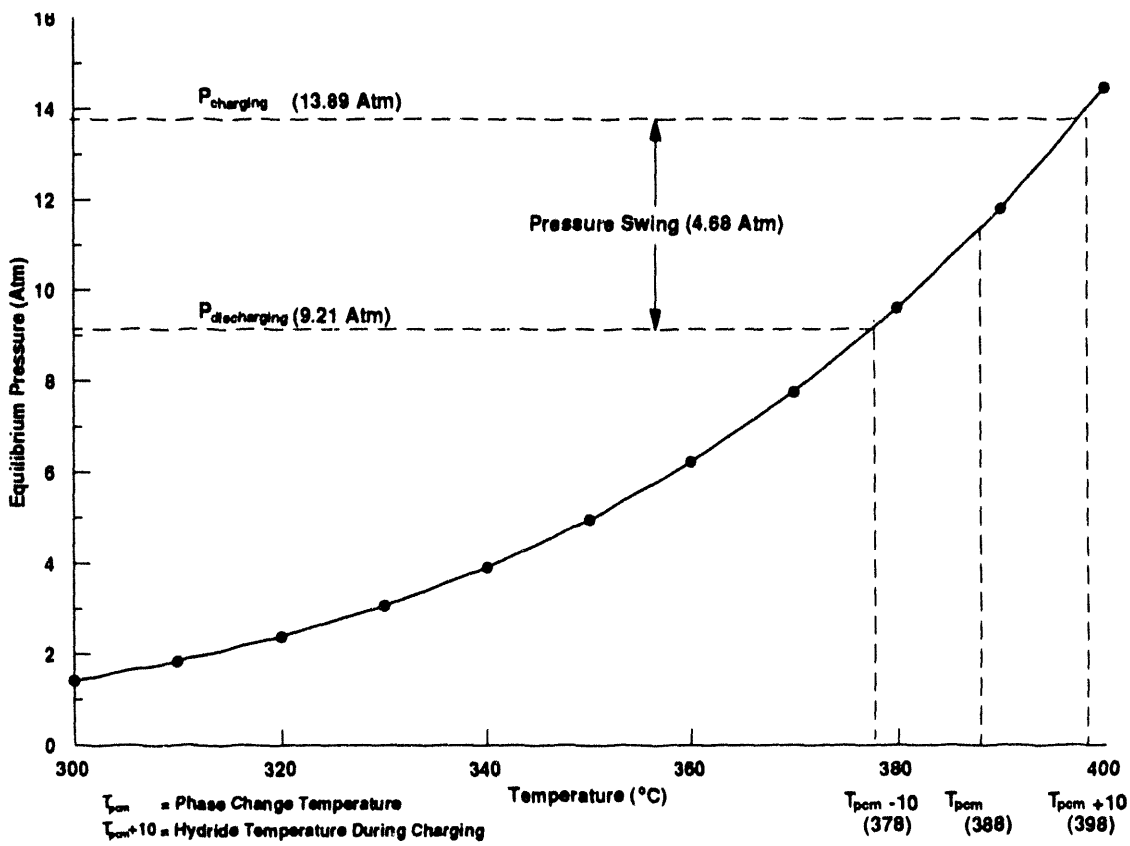

Figure 5 shows a simple, yet effective, means by which the hydride bed and the PCM bed can be kept chemically distinct yet thermally intimate: a shell-and-tube heat exchanger. Only the tube side need withstand high pressure, but both shell and tube sides must be made of stainless steel to withstand the corrosive attack of the PCM.

Figure 5 - Thermally and Physically Integrated Metal Hydride and Phase Change Material

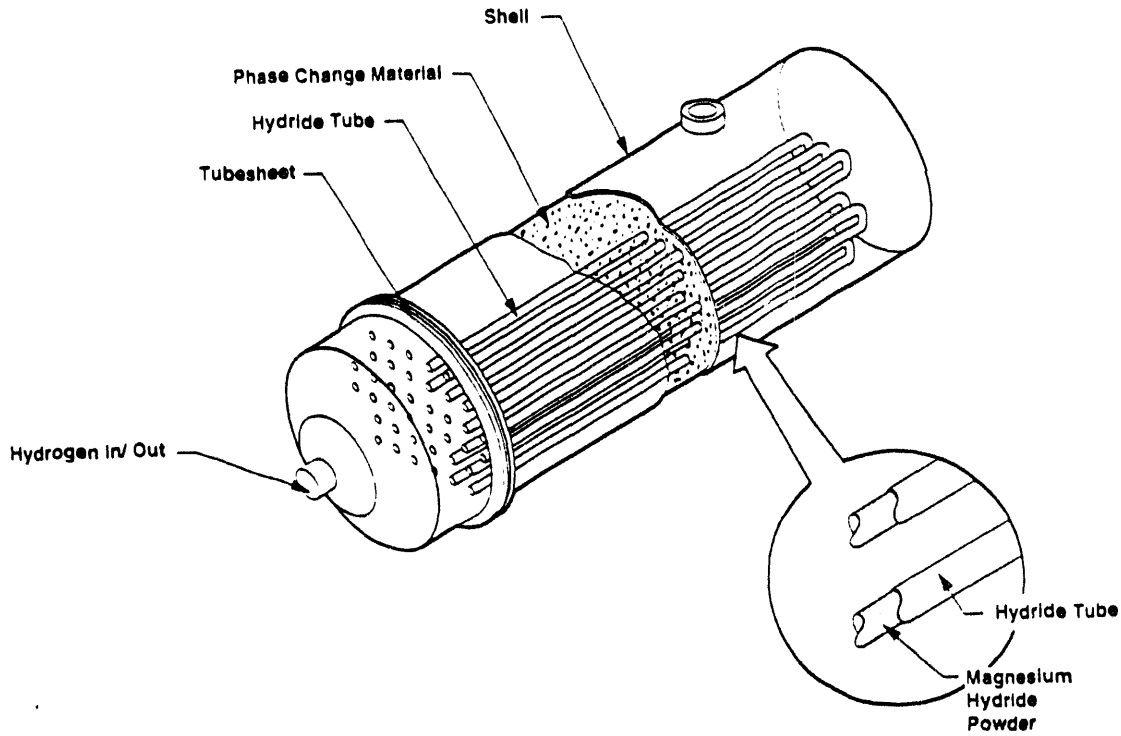

Results

To date we have specified the nickel-coated magnesium powder to be provided us by our lower-tier subcontractor, selected the phase change material and arranged for its manufacture, and designed the shell-and-tube heat exchanger sufficiently to secure quotations from prospective fabricators.

Specifications of the Nickel-Coated Magnesium Powder

We have subcontracted with Dr. Robert Tuffias of Ultramet, of Pacoima, CA to make the nickel-coated magnesium powder to serve as the hydridable alloy, because Ultramet has made exactly that before. We have engaged, as a consultant, Dr. Borislav Bogdanovic of the Max-Planck-Institut für Kohlenforschung in Mülheim-an-der-Ruhr, Germany, who has impressive experience, publications, and patents regarding the magnesium-nickel system in the context of high-temperature metal hydrides.

As a result of discussions between Drs. Tuffias and Bogdanovic and Arthur D. Little personnel, we have decided that the magnesium particles, before coating, should be 270 mesh (<50Xμ in diameter), and that the magnesium coating should correspond to roughly 2% nickel by weight.

In determining the particle diameter, we considered the following factors:

1. *Difficulty of Handling* - Particles must not only be coated, but they must be captured once coated.

2. *Ratio of Nickel to Magnesium* - This ratio is to be minimized, and the existence of a minimum practical thickness of magnesium suggests that this ratio will increase as the diameter of the particle is decreased.

3. *Entrainment* - Smaller particles are more easily dislodged and entrained by the velocity head of the hydrogen discharge.

4. *Diffusion* - Too large a particle would result in too great a time for the center of the particles to be affected by the hydriding and de-hydriding reactions taking place at the particles' surface.

5. *Fluidization* - Too large a particle would require excessive fluidizing velocity, resulting is wastage of reactants and thus excessive cost to manufacture.

6. *Decrepitation* - Large metal hydride particles tend to decrepitate, or shatter, upon repeated cycles of hydriding/de-hydriding. A coated particle that shatters becomes several particles with only partial coating.

Selection of the Phase Change Material

Table 3 presents pertinent information regarding five different phase change materials (PCMs) that operate in the temperature range of interest.

Table 3 - Candidate Phase Change Materials

Phase Change Material (PCM)	Phase Change Temperature, (°C)	Equilibrium Pressure, MgH_2 (atm)	Equilibrium Pressure, Mg_2NiH_4 (atm)	Mass of PCM to Store 76 lbm of H_2	Cost of PCM to Store 76 lbm of H_2 (1992$)
5NaCl·95$NaNO_3$ *	297	1.3	2.9	15,000	4,600
$NaNO_3$ *	307	1.8	3.7	14,000	4,400
NaOH+8%$NaNO_3$ *	313	2.3	4.8	6,250	2,900
10KBr·10KCl·80KNO_3 *	342	4.3	8.0	18,000	6,400
27NaCl·73NaOH **	370	8.0***	14	7,000	2,000
24NaCl·20KCl·55$MgCl_2$ **	388	13***	20	6,250	1,000

Source: "Evaluation of Industrial Advanced Heat Recovery/Thermal Energy Storage Systems," Volume 2, EPRI EM-2573, December 1982. Source cost figures in 1981$ were multiplied by 1.538 to convert to 1992$.

* can be contained in carbon steel

" must be contained in stainless steel
"" based on extrapolating published data

One criterion to be used in selecting a PCM is its phase change temperature, and the implications of that temperature to irreversible pressure losses. We envision this system being used, for example, to store the hydrogen created by a baseloaded fuel processor (methane reformer and shift reactors) located at a dispensing station for filling hydrogen-fueled vehicles. A situation to be avoided is

1. charging the metal hydride bed at a pressure less than that of the final shift reactor discharge pressure, followed by

2. discharging the metal hydride bed at a pressure less than that of the vehicular hydrogen storage system.

This consideration favors storage at higher temperatures/pressures. Of the two highest-temperature eutectics in Table 3, we are inclined to favor $24NaCl{\cdot}20KCl{\cdot}55MgCl_2$ over $27NaCl{\cdot}73NaOH$ because of its lower cost and its (probably) lower corrosivity.

Most of these PCMs were manufactured in bulk at one time, and the cost figures in Table 3 reflect their bulk cost. We can find bulk manufacturers for none of the eutectic PCMs now, and are faced with making or having made experimental quantities of these.

Figure 6 presents the phase diagram of the $(KCl)_2$-$(NaCl)_2$-$MgCl_2$ system. Note that whereas the melting temperatures of NaCl, KCl, and $MgCl_2$ are 801°C, 778°C, and 712°C, respectively, there is a tertiary eutectic with a melting temperature of 385°C (presented in Table 3 as 388°C, from a different source).

Figure 6 - Phase Diagram for the $(KCl)_2$-$(NaCl)_2$-$MgCl_2$ System

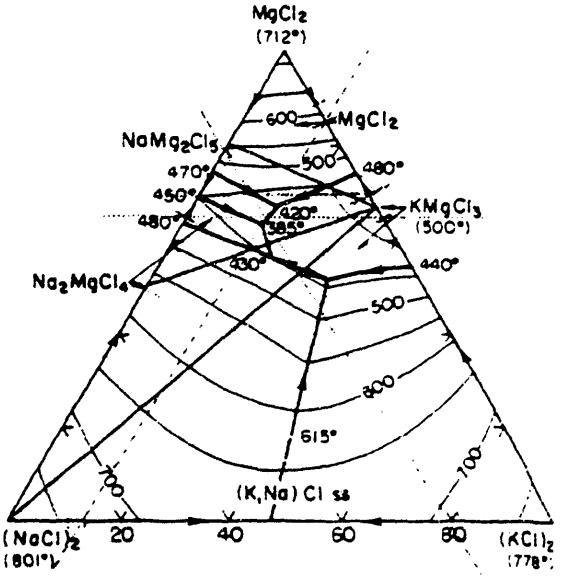

Source: Ernst Jänecke, *Z. Anord. Allgem. Chem.*, **261,** 218 (1950).

One way of making this eutectic is to mix 24% NaCl, 20% KCl, and 55% $MgCl_2$ (all three are weight percentages, not mole fractions) and heat this mixture to 801°C so that all three components melt. Another method, suggested to us recently and currently in the process of verification, is to ball-mill all three components into a fine, well mixed powder, and then heat it to just greater than the eutectic temperature, on the theory that fine, well mixed powder has plenty of inter-component interfaces promoting the forming and melting of binary and tertiary eutectics.

This method probably does not apply to the NaCl-NaOH system, for NaOH is too soft to ball-mill.

Shell-and-Tube Heat Exchanger Design

The shell-and-tube heat exchanger design parameters depend, to a great extent, on the PCM that is selected. For example, the tube spacing is determined by the relative volumes of PCM and metal hydride. Assuming that $24NaCl{\cdot}20KCl{\cdot}55MgCl_2$ is indeed our PCM of choice, the shell-and-tube heat exchanger to contain two kilograms of nickel-coated magnesium powder and the appropriate mass of PCM would have the dimensions given by Table 4.

Table 4 - Dimensions of Shell-and-Tube Heat Exchanger

Dimension	Value
Tube Diameter	0.5"
Tube Spacing	1.0"
U-tube Length	41"
Number of U-tubes	15
Shell Diameter	6" (nominal)
Shell Length	42"
Material	Stainless steel 316

Definition of Success

We will consider this concept to be successful if

1. we can operate the laboratory prototype device repeatedly on commercial-grade hydrogen without the metal hydride becoming poisoned,

2. we can operate the laboratory prototype device within an equilibrium temperature swing of 20°C, and

3. the materials of construction successfully repel the corrosive attack of the molten phase change material.

Publications

To date this concept has been described in two publications:

1. Hynek, S. J., Fuller, W. D., & Bentley, J. M., "Hydrogen Storage to Support Fuel Cell Vehicles," presented at the 5th Annual U.S. Hydrogen Meeting, March 24, 1994.

2. Hynek, S. J. & Fuller, W. D., "Hydrogen Storage Within the Infrastructure," to be presented at the 10th World Hydrogen Energy Conference, June 23, 1994.

Proposed Future Work

Once the laboratory prototype High Efficiency Stationary Hydrogen Storage (HESHS) device has proven the concept, we would propose to scale up this device to a useful size. Two promising applications have presented themselves:

1. *Short-range transport* - In the absence of a pipeline connecting the point of hydrogen manufacture and the point of use, hydrogen is generally transported in the liquefied state, by truck or by barge. For short distances, however, the superior gravimetric and volumetric density afforded by liquefaction cannot justify the energy loss associated with liquefaction. The HESHS device, once scaled up, could be mounted on trucks or barges and could become the preferred short-range means of transporting hydrogen.

2. *Remote utility energy storage* - Parts of Alaska and northern Canada are sufficiently remote that no outside electric grid reaches them. It is in such places that renewable energy sources can first displace petroleum-based electrical generation on the basis of economics. Intermittent renewable energy sources such as wind turbines and photovoltaic arrays (close to the Arctic Circle, the former makes more sense) can be made to fit the energy demand profile by electrolyzing water when wind is available, storing that hydrogen in a scaled-up HESHS device, then using that hydrogen to heat homes, fuel vehicles, or generate electricity with a fuel cell. The author is currently actively involved in promoting this concept.

Scale-up of the shell-and-tube heat exchanger should present little problem; large shell-and-tube heat exchangers are in common industrial use. Scaled-up manufacture of the eutectic mixture of salts should also present no problem to a manufacturer, other than to convince that manufacturer that a market of sufficient size will materialize. Scaled-up manufacture of the nickel-coated magnesium powder involves making a continuous process of what is now a batch process, and will probably involve technology transfer from our lower-tier subcontractor to an investor.

HYDROGEN STORAGE: ADVANCED MATERIALS DEVELOPMENT AND INTEGRATED SYSTEM DESIGN

G. J. Thomas, B. A. Meyer, S. E. Guthrie, and D. F. Cowgill
Sandia National Laboratories
Livermore, CA 94550

Abstract

Hydrogen storage remains an important factor in effective hydrogen utilization for energy applications and is a major element of the FY 1994-1998 Hydrogen Program Implementation Plan. The objective of this new project is to develop storage/delivery systems for use with energy conversion devices. Specifically, a near-term goal will be the demonstration of an internal combustion engine/storage/delivery subsystem. The longer term goal will be the optimization of storage technologies for use in vehicles and in industrial stationary uses.

Storage development will be focused on solid storage materials – lightweight hydrides or adsorbent materials. Our hydride development will use a systematic approach to enhance the kinetic, equilibrium and cycling behavior of light weight hydrides, especially magnesium alloys. Our adsorption material development will focus on enhancing the hydrogen binding energy in these materials through doping with metals, metalloporphyrins and nanophase materials.

The bed design and construction will be integrated with hydride material properties in order to realize the volumetric benefits of a hydride system and to minimize weight. Hydride properties, such as thermal conductivity and hydrogen kinetics, will be incorporated into modeling of the heat and mass transport in bed designs to optimize their performance. Light weight containment materials will also be investigated. Low and high temperature hydride storage beds will be built and tested for fuel delivery performance and input requirements.

This work is integrated into the new Field Work Proposal entitled Hydrogen Utilization in Internal Combustion Engines.

Project Rationale

A key to the introduction of hydrogen into the U.S. energy supply is the development of efficient utilization systems. In the long term, fuel cells will play an important role in the use of hydrogen as an effective energy carrier. However, internal combustion engines, optimized for hydrogen burning and with efficient hydrogen storage systems, can achieve much more rapid market penetration and immediate pollution reductions. Furthermore, this approach can lead to near-term demonstration projects which can benefit the hydrogen program by highlighting progress as well as proving feasibility. The FY 1994-1998 Hydrogen Program Implementation Plan identifies utilization and storage technologies as two major development areas and includes near-term demonstration projects.

The objective of this new project is to develop storage/delivery systems for use with energy conversion devices. It is integrated with a parallel effort on optimizing internal combustion engines for hydrogen use. Specifically, a near-term goal will be the demonstration of an internal combustion engine/storage/delivery subsystem with performance exceeding current capabilities. The longer term goal will be the optimization of storage technologies for use in vehicles and in industrial stationary uses. Storage development will be focused on solid storage materials – light weight hydrides or adsorbent materials.

This work is integrated into the new Field Work Proposal entitled Hydrogen Utilization in Internal Combustion Engines. See the related paper for further information.

Approach

The project will have two major elements – advanced materials development and storage/delivery system development. These material R&D and engineering studies will be done in parallel, with coordinated milestones and decision points aimed at achieving an integrated system demonstration.

Our hydride development will use a systematic approach to enhance the kinetic, equilibrium and cycling behavior of light weight hydrides, especially magnesium alloys. The focus will be on the development of hydride materials for use in practical hydrogen storage systems, and will consider surface coatings, composite systems and particle size control, as well as alloy content. We will be working in collaboration with a material supplier (MEI-Reade) and the Univ. of CA - Irvine, Mech. Eng. Department (Materials Section), in the synthesis of alloy materials.

Our adsorption material development will focus on two aspects, (1) carbon-based materials with high macroscopic density (e.g., >50% of theoretical density) as well as high microporosity and, (2) enhancing the hydrogen binding energy in these materials through doping with metals, metalloporphyrins and nanophase materials. We will also be collaborating with Lawrence Livermore National Laboratory by measuring hydrogen properties of their aerogel carbons and other storage materials.

Another important area will be the integration of bed design and construction with hydride material properties in order to realize the volumetric benefits of a hydride system and to minimize weight. Hydride properties, such as thermal conductivity and hydrogen kinetics, will be

incorporated into modeling of the heat and mass transport in bed designs to optimize their performance. Light weight containment materials will also be investigated. Low and high temperature hydride storage beds will be built and tested for fuel delivery performance and input requirements.

Each of these areas will be discussed in the following sections.

Adsorption Material Development

A major limitation with the use of adsorption materials for hydrogen storage is the need for cryogenic temperatures. Hydrogen is weakly physisorbed onto materials by electronic polarization (Van der Waals) forces. The polarizability of the H_2 molecule is very small, resulting in binding energies varying from .04eV on metals to .08eV on ionic solids. Also, enhanced adsorption in microporous materials, such as due to capillary condensation, is unlikely to occur at temperatures much above the critical temperature of H_2, 33K. Our analysis of published experimental data on high surface carbon materials (Amankwah 1989) shows that at temperatures of 150 K or more, hydrogen adsorption exhibits Langmuir type behavior with coverages of about a monolayer or less. The binding of H_2 by physisorption on strongly polarized surfaces is not known.

Much stronger chemisorption of hydrogen occurs on materials by the exchange or sharing of electrons. Dissociated H binds to carbon with an energy of 1.3eV, and appreciable dissociation only occurs at temperatures above 300°C. On Ni, H_2 dissociation does not require additional activation energy and H is bound with 1.3eV, decreasing to 0.2eV at high coverage. Beeck, et.al., (1945) have reported that about one-third of the hydrogen adsorbed onto Ni at room temperature and high pressure is reversible and easily removed by pumping. It is not known whether this fraction is the final 1/3 monolayer, perhaps weakly chemisorbed, or additional H_2 strongly physisorbed onto the highly polarized chemisorbed-H surface. If the latter, there is potential for a reversible capacity of a full second monolayer. High surface area Ni and Fe nano-cluster materials (1-10 nm particles) have been synthesized in micro-heterogeneous inverse micelle solutions to explore this possibility.

High temperatures (>300°C) are required to desorb chemisorbed H from carbon. Since both chemisorption and desorption from Ni is somewhat easier, we are examining the possibility of using metal-catalyzed high surface area carbon materials. Binding energetics will transfer H from Ni to C, by hydrogen spillover, much like that observed from Pt to C, by Robell, et.al (1964). As the H-coverage on Ni nanoclusters rises, H atoms are attracted to the lower energy states on adjacent C. Reversible desorption should occur from the Ni sites without the additional recombination barrier occurring with C. The kinetics for both the adsorption and desorption processes are expected to be limited by the surface diffusion of H on C. Using the model of Robell, we estimate an adsorption time of one minute can be achieved at 100°C using ~1% Ni coverage; and at 20°C using 5% Ni. Although desorption will be slower since diffusion is from a distributed source to point sinks, the same time restriction is not critical for automotive use.

There is a possibility of non-activated, weak chemisorption occurring on oxide materials. Reports in the literature (Beebe 1938) indicate binding energies of 0.22eV for H on Cr_2O_3. This possibility is also supported by the observation that Al_2O_3 serves as a good promoter for Pd and Pt supported catalysts, increasing their catalytic performance.

Weak chemisorption may also occur on supported catalysts. Sokolskii and Gil'debrand (1971) report hydrogen loading for Pd on Al_2O_3 to reach 5 H/Pd; and for Pt, 10 H/Pt. This may result from spillover to adjacent sites on the Al_2O_3, as described above, or may be due to a decreasing chemisorption energy on the metal with increasing H-coverage. There is some indication that similar effects occur for Ni supported on Al_2O_3 (Selwood 1967). Accordingly, we are examining hydrogen storage using a high density of supported metals on high surface area oxides.

Hydride Development

The metal alloy systems that we will study initially are based on magnesium or titanium. Both of these metals form highly exothermic binary hydrides in their unalloyed form. The strong binding of hydrogen to these metals presents two distinct but interrelated problems. One is the requirement for an external energy source to dissociate the hydride and recover the gas fuel at pressures which are practically useful. The source of this heat must come either parasitically from waste heat or directly from the fuel itself. The second facet of the problem is the kinetic limitation of the hydride dissociation process. Metal hydride kinetics may be rate limited by either the chemical activity of the surface (molecular dissociation and recombination for absorption and desorption, respectively) or the intrinsic diffusion parameters of the bulk material. Material forms with a high surface to volume ratio (e.g., powders) are therefor favored on both counts. Summarizing these issues, an improved storage material based on Mg or Ti requires the development of a less stable hydride which has good transport properties.

Our initial results in the Mg-Ni system shown in Figure 1 indicate that Mg_2Ni is an acceptable baseline material from a kinetics standpoint. However, this alloy is significantly heavier (3.6 wt.% H capacity) than pure Mg and still requires a relatively high temperature. Nevertheless, it does serve as a useful benchmark and also gives us a material to use for high temperature hydride bed development. We have also found that the Ni fraction can be significantly decreased from the stoichiometric Mg_2Ni phase without a loss in kinetics, in agreement with existing literature data (Song 1987). This will result in a much lighter alloy. Other independent data (Rohy 1982, Selvam 1986) suggests the feasibility for improving the alloy dissociation temperature by the addition of other metals. There is also ample evidence for improvements in titanium based alloys by the use of more complicated AB_2 intermetallics.

We are investigating hydrogen transport enhancement from a materials standpoint by investigating different material forms and morphologies. These parameters also play an important role in the structural integrity of the hydride system from the standpoint of swelling, cycling and breakup. One aspect of this approach is the exploration of rapid solidification techniques to form small diameter powders that reduce diffusion effects (Pedersen 1987) and increase the surface to volume ratio. This technique also permits the possibility for additional phase and microstructure controls that are more difficult to access in ingot and mechanical manufacturing techniques (Lavernia 1991). Surface enrichment of active species may also be possible with this method, although our preliminary work has demonstrated that this can be economically accomplished simply by mechanical means. The inclusion of both university and commercial interests in this phase of our alloy development is desirable both for using existing expertise as well as insuring a practical and easily transferred technology.

The properties of the hydrides are determined from two measurement techniques. The first is a pressure-composition isotherm (PCT) measurement which provides the fundamental

thermodynamic data for modeling and thermal balance. The second measurement will be aimed towards providing kinetic parameters which are intrinsic to the material. We are measuring the dissociation kinetics of very small amounts of materials in a constant pressure, isothermal environment. Unlike the desorption curve in the PCT measurement, the constancy of the pressure insures that the chemical driving force remains constant and the measurement becomes a steady state rather than an equilibrium measurement. This approach more closely approximates a probable system operation and allows the determination of the rate and optimum material limits as the hydride deviates from equilibrium. Monitoring of the electronic feedback control variables for both temperature and pressure will provide data for modeling the thermal and mass transfer functions of the material, and this information will be used in the bed model described below.

Storage System Design

The hydride alloys developed in this program will be incorporated initially into prototype storage system designs. Low and high temperature hydride storage beds will be built and tested for fuel delivery performance and input requirements. These will then lead to an integrated storage system and internal combustion engine. As stated earlier, hydride material fabrication will be a consideration in the bed design in order to realize the volumetric benefits of a hydride system and to minimize weight. A model will also be developed which incorporates hydride properties, such as thermal conductivity and hydrogen kinetics, to simulate heat and mass transport in bed designs and optimize their performance. Light weight containment materials will also be investigated.

The model development will include experimental measurements as well as a mathematical investigation. A transient two dimensional model will be developed which will include hydrogen mass flow, vessel geometry, bed conductivity, dissociation energy, reaction rates and temperatures. In the model each of the properties can be a function of position, time, and hydrogen loading. These prediction will be compared against the experimental data obtained in this study on FeTi and MgNi beds.

The experimental work will evaluate material and bed properties (permeability, conductivity, heat of formation, reaction rates and pressure composition temperature relationships) at various conditions for Fe-Ti and Mg-Ni alloys. For example, temperatures measured during steady radial heat flow are used to determine the bed thermal conductivity. Typical radial temperatures are shown in Figure 2. The effective bed thermal conductivity determined from this data is 0.13 W/m K.

References

Amankwah, K.A.G., J.S. Noh, and J.A. Schwarz, Int. J. Hydrogen Energy 14, 437 (1989).

Beebe, R.A., and D.A. Dowden, J. Amer. Chem Soc. 60, 2912 (1938).

Beeck, O., Rev. Mod. Phys. 17, 61 (1945).

Lavernia, E. J. et al , Material Science and Engineering, A132 (1991) 119

Pedersen, A. S. et al , J. Less-Common Met., 131 (1987) 31

Robell, A.J., E.V. Ballou, and M. Boudart, J. Phys. Chem. 68, 2748 (1964).

Rohy, D. A. et al , D.O.E Report on *Development of Lightweight Hydrides*, DOE/CS 52059 (1982)

Selvam, P. et al , Int. J. Hydrogen Energy, vol 11, no.3 (1986) 169

Selwood, P:.W., in *The Solid-Gas Interface*, edited by E.A. Flood (Marcel Dekker Inc., N.Y., 1967) Vol. 2, p 550.

Sokolskii, D.V., and E.I. Gil'debrand, in N.M. Popova and D.V. Solol'skii, Tr. Inst. Org. Katal. Electro. Akad. Nauk. Kaz. SSR 1, 3 (1971); see P.A. Sermon and G.C. Bond, Catalysis Rev. 8, 211 (1973).

Song, M. Y. et al , J. Less-Common Met., 131 (1987) 71

Figure Captions

Figure 1

Hydrogen desorption rate data for Mg_2Ni at two temperatures. The rate for an ICE was calculated using a 4000 BTU/mile requirement at 40 mph (from the USDOE Hydrogen Program Plan FY1993-FY1997).

Figure 2

Thermal conductivity data for La-Ni powder

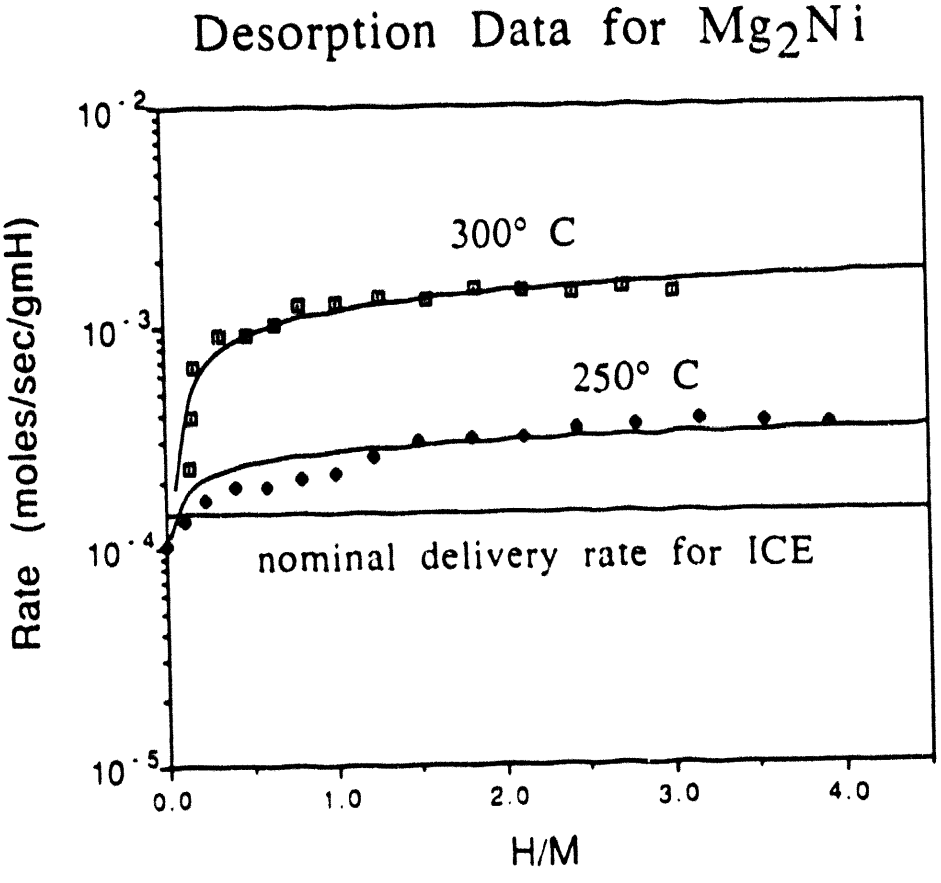
Desorption Data for Mg_2Ni
Rate (moles/sec/gmH)
10^{-2}
10^{-3}
10^{-4}
10^{-5}
300° C
250° C
nominal delivery rate for ICE
0.0
1.0
2.0
3.0
4.0
H/M

FIGURE 1

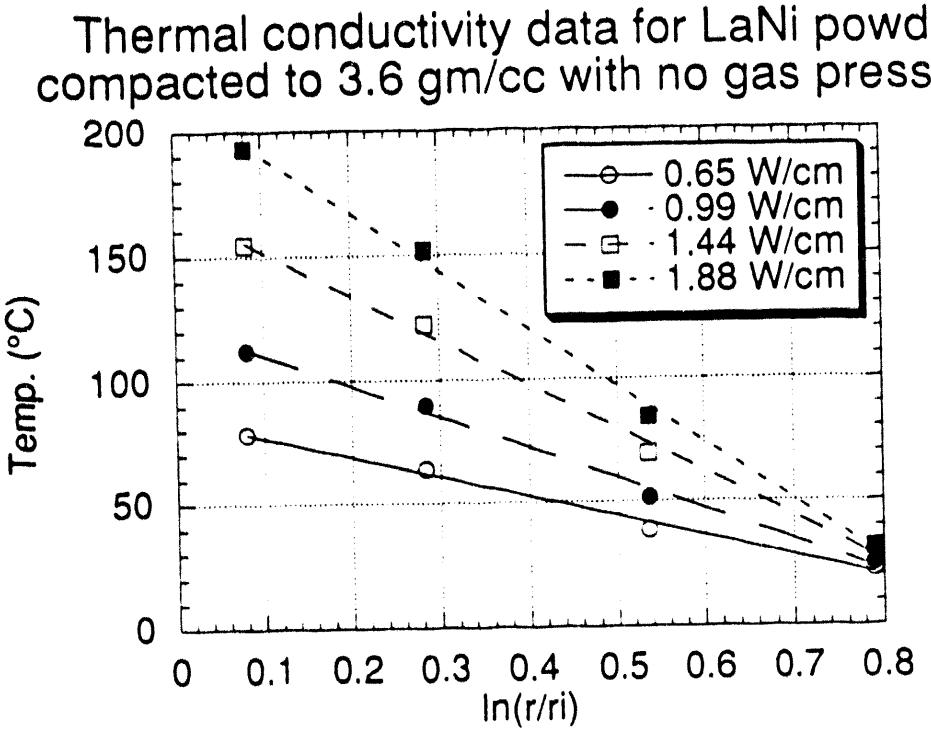
Thermal conductivity data for LaNi powder compacted to 3.6 gm/cc with no gas pressure.
Temp. (°C)
200
150
100
50
0
0
0.1
0.2
0.3
0.4
0.5
0.6
0.7
0.8
ln(r/ri)
0.65 W/cm
0.99 W/cm
1.44 W/cm
1.88 W/cm

FIGURE 2

CARBON AEROGELS FOR HYDROGEN STORAGE

R.W. Pekala, P.R. Coronado, and D.F. Calef
Chemistry & Materials Science Department
Lawrence Livermore National Laboratory
Livermore, CA 94550

Abstract

Carbon aerogels are a special class of open-cell foams with an ultrafine cell/pore size (<50 nm), high surface area (600-800 m^2/g), and a solid matrix composed of interconnected colloidal-like particles or fibers with characteristic diameters of 10 nm. These materials are usually synthesized from the aqueous polycondensation of resorcinol (1,3 dihydroxybenzene) with formaldehyde, followed by supercritical extraction of the solvent and pyrolysis in an inert atmosphere. The resultant aerogel has a nanocrystalline structure with micropores (<2 nm diameter) located within the interconnected carbon particles. Carbon aerogel monoliths can be prepared at densities ranging from 0.05-1.0 g/cm^3, leading to volumetric surface areas (> 500 m^2/cm^3) that are much larger than commercially available materials. We have also developed an inverse emulsion process for the preparation of carbon aerogel microspheres (i.e., powders) in a semi-continuous fashion. This research program is directed at optimization of the aerogel structure for maximum hydrogen adsorption over a wide range of temperatures and pressures. Computer modeling of hydrogen adsorption at carbon surfaces as a function of micropore diameter, edge vs. basal planes, and surface functional groups has also been initiated.

Introduction

The chemistry and physics of small clusters of atoms (1-100 nm) has received considerable attention in recent years because these assemblies often have properties between the molecular and bulk solid-state limits. The different properties can be explained in terms of the large fraction of atoms that are at the surface of a cluster as compared to the interior. Although the synthesis and properties of metal and semiconductor clusters, metallocarbohedrenes, fullerenes, and nanotubes are the subject of extensive investigations, little attention has been paid to cluster-assembled porous materials. This oversight is of particular interest to us since we believe that aerogels are one of the few monolithic materials presently available where the benefits of cluster assembly can be demonstrated. In particular, the unique optical, thermal, acoustic, mechanical, and electrical properties of aerogels are directly related to their nanostructure.

Traditional sol-gel polymerizations involve the hydrolysis and condensation of metal alkoxides (e.g. tetramethoxysilane) to form inorganic aerogels [Fricke 1986; Teichner *et al.* 1976]. Several organic reactions that proceed through a sol-gel transition have been identified at LLNL [Pekala 1989; Pekala *et al.* 1992]. The most-studied reaction involves the aqueous polycondensation of resorcinol (1,3-dihydroxybenzene) with formaldehyde. The resultant crosslinked gels are supercritically dried from carbon dioxide (T_c= 31°C, P_c = 7.4 MPa) to give resorcinol-formaldehyde (RF) aerogels. Because resorcinol-formaldehyde aerogels are composed of a highly crosslinked aromatic polymer, they can be pyrolyzed in an inert atmosphere to form carbon monoliths. The resultant aerogels are black in color and no longer transparent but they retain the high porosity (40-98 %), ultrafine cell/pore size (< 50 nm), high surface area (400-800 m^2/g), and interconnected particle (~10 nm) morphology of their organic precursors. In addition to monoliths, carbon aerogels can be produced as microspheres (spherical powder) using an inverse emulsion process. This chemistry-structure-property relationships of carbon aerogels and their potential use for hydrogen storage are discussed in this paper.

Technical Approach

Synthesis

The preparation of resorcinol-formaldehyde (RF) gels involves mixing the reactants in a 1:2 molar ratio, respectively. Deionized and distilled water is added as the diluent and sodium carbonate as the base catalyst. After stirring to form a homogeneous solution, the mixture is poured into glass vials, sealed, and cured at elevated temperature. Upon completion of the cure cycle, the crosslinked gels are removed from their glass vials, and the pore fluid (i.e., water) is exchanged with acetone. The acetone-filled gels are then placed in a jacketed pressure vessel, exchanged with liquid carbon dioxide, and supercritically dried (T_c= 31 °C; P_c= 7.4 MPa). This procedure has resulted in the production of monolithic RF aerogels in cylindrical form (25 mm diameter x 60-85 mm long). These materials are subsequently pyrolyzed in an inert atmosphere to form carbon aerogels.

RF and carbon aerogels can also be produced in the form of spherical particles. An inverse emulsion polymerization is used to produce aerogel particles that we refer to as microspheres. In a glass reaction kettle, 1 liter of cyclohexane or mineral oil is heated to 50-70 °C. In a separate

beaker, an RF solution is partially polymerized until it approaches the gel point. Approximately 150 ml of the RF solution is added slowly to the cyclohexane with agitation. The RF solution is dispersed into spherical droplets throughout the cyclohexane --- their size depending upon the agitation rate and the presence or absence of surfactant. After the inverse emulsion has been heated for 2-8 hours, the agitation is stopped and the spherical gel particles are allowed to settle. The cyclohexane is decanted from the reaction kettle and replaced with acetone. The solution is agitated to assist in the solvent exchange of acetone for water inside the gel particles. After sufficient solvent exchanges, the gel particles are supercritically dried from carbon dioxide or air-dried under certain conditions. The resultant microspheres can range in size from microns to millimeters depending upon the emulsification procedure. Carbon aerogel microspheres result from the pryolysis of RF aerogel microspheres.

Adsorption Measurements

Hydrogen adsorption measurements were performed in an apparatus similar to that shown in Figure 1. Carbon aerogels/microspheres were heated at ~ 250 °C under vacuum in sample holder "A" to remove surface contaminants (e.g., water). The sample holder was then submerged in liquid nitrogen (77 K), and hydrogen (99.999 %) was bled slowly through a set of control valves from reservoir "B" into "A". The pressure in "A" was monitored as a function of the hydrogen delivered. The total volume of the carbon aerogel was calculated from the skeletal density (~ 2 g/cc). Next, a stainless steel "plug" of the proper volume was inserted into "A" and the run was repeated. The difference in the adsorption curves allowed us to calculate the amount of hydrogen adsorbed at the carbon surface as a function of pressure.

Modeling

Molecular dynamic and semi-empirical quantum chemical calculations are being performed on hydrogen interacting with carbon clusters. Initial calculations on the separation of two coronene ($C_{24}H_{12}$) molecules show that the preferred separation distance is increased by ~0.5 Å when hydrogen is inserted. These calculations will assist us in tailoring the structure of carbon aerogels for enhanced hydrogen adsorption.

Results and Discussion

While monolithic aerogels are ideal candidates for many applications, they would be difficult to fabricate in the size and shape of a pressure vessel. As such, we are emphasizing the formation of aerogel microspheres for hydrogen storage. The aerogel microspheres can be produced in a semi-continuous process, and the supercritical extraction step can be eliminated if the gel precursors are made at sufficiently high monomer concentrations to withstand the capillary forces associated with drying. These recent advances will make carbon aerogel microspheres much cheaper than their monolithic counterparts.

Figure 2 shows an optical micrograph of RF and carbon microspheres. A relatively broad size distribution is observed in each case, with the RF spheres averaging 40-50 μ in diameter. The carbon microspheres are smaller than their RF precursors as a result of shrinkage during pyrolysis. Scanning electron micrographs reveal that the carbon microspheres have smooth surfaces with

high sphericity.

The structure and properties of carbon aerogels are largely controlled by three factors: (1) the [Resorcinol]/[Catalyst] (R/C) ratio of the starting solution, (2) the pyrolysis temperature, and (3) chemical activation procedures. The R/C ratio affects the number of RF clusters generated in solution and the size to which they grow. The particle size, surface area, and interconnectivity of both RF and carbon aerogels strongly depend on this parameter. Interestingly, the specific surface area of carbon aerogels is practically independent of the bulk density for samples prepared *at the same R/C ratio.* These data are corroborated by transmission electron micrographs that show interconnected particles of approximately the same size. Thus, carbon aerogels with a higher bulk density simply have more interconnected particles per unit volume than their low density counterparts, leading to very *high volumetric surface areas* that may enable us to meet the DOE volumetric energy density requirement for hydrogen storage (62 kg H_2/m^3).

The pyrolysis temperature impacts both the composition and nanostructure of carbon aerogels. Resorcinol-formaldehyde aerogels pyrolyzed at 1050 °C in an inert atmosphere are converted into a nanocrystalline carbon structure. Helium pycnometry reveals a skeletal density of 2.06 g/cm^3 which is much higher than most conventional glassy carbons (~1.5 g/cm^3). These data imply that carbon aerogels have very few closed pores within the solid skeleton. Raman data reveal an in-plane microcrystallite size (L_a) of ~2.5 nm for carbon aerogels (R/C=200; 1050 °C) independent of the bulk density. Even samples pyrolyzed at 2100 °C reveal a large disorder-induced Raman line, with the microcrystallite size only growing to ~ 4.0 nm. Thus, the picture that emerges for carbon aerogels is one in which 2.5-4.0 nm wide graphene sheets intertwine to make up the individual ~12 nm diameter particles [Fung *et al.*, 1993].

The final method for modifying the carbon aerogel structure involves chemical activation. In the carbon industry, activation is commonly achieved by exposing carbon particles or fibers to an oxidizing atmosphere such as steam, air, or carbon dioxide at 750-1000 °C. This procedure usually results in high surface areas (> 1000 m^2/g). A different type of chemical activation can be achieved when carbon is heated in concentrated acids. We are modifying carbon aerogel microspheres using each of these procedures to evaluate their effect upon hydrogen storage.

Figure 3 shows our first adsorption isotherm for carbon aerogel microspheres. These materials were synthesized using the inverse emulsion process (60 %w/v RF; R/C=200), followed by air-drying from acetone, and pyrolysis at 1050°C. The carbon microspheres had a BET surface area of ~600 m^2/g and a bulk powder density of ~0.6 g/cm^3. Hydrogen adsorption of 3.7 wt.% was achieved at 1200 psia. While this value is lower than other carbon materials that have been examined in the DOE program, one should keep in mind that these materials have not been optimized through control of surface area, pore size distribution, or surface chemical groups.

Future Work

Future research will be conducted in the following areas:

- Continue development of the inverse emulsion process for the production of organic aerogel microspheres and their carbonized derivatives. Demonstrate that >50 g batches of material can

be synthesized using this process.

- Examine particle size distribution and study hydrogen adsorption properties of carbon aerogel microspheres.

- Compare the hydrogen adsorption properties of carbon aerogels that have been supercritcally dried vs. air dried.

- Evaluate the effects of chemical doping (e.g., P) on carbon structure and subsequent hydrogen storage

- Develop method for the chemical activation of carbon aerogel microspheres, leading to increased surface area and improved hydrogen storage.

- Evaluate hydrogen adsorption properties of resorcinol-formaldehyde and melamine-formaldehyde microspheres

- Continue computer modeling of hydrogen adsorption at carbon surfaces as a function of micropore diameter and surface group distribution.

Acknowledgments

This work was performed under the auspices of the U.S. Department of Energy by Lawrence Livermore National Laboratory under contract #W-7405-ENG-48.

References

Fricke, J. 1986, *Aerogels*, New York: Springer-Verlag.

Fung, A.W. P., Z.H. Wang, K. Lu, M.S. Dresselhaus, and R.W. Pekala, 1993. "Characterization of Carbon Aerogels by Transport Measurements," *J. Mat. Res.*, **8**:1875-1885.

Pekala, R.W. 1989. "Organic Aerogel from the Polycondensation of Resorcinol with Formaldehyde," *J. Mat. Sci.*, **24**:3221-3227.

Pekala, R.W., C.T. Alviso, F.M. Kong, and S.S. Hulsey, 1992. "Aerogels Derived from Multifunctional Organic Monomers," *J. Non-Cryst. Solids*, **145**:90-98.

Teichner, S.J., G.A. Nicolaon, M.A. Vicarini, G.E.E. Gardes, 1976. "Inorganic Oxide Aerogels, " *Adv. Coll. Interf. Sci.*, **5**:245-273.

Figure Captions

Figure 1. Schematic diagram of hydrogen adsorption apparatus.

Figure 2. Optical micrographs of (a) resorcinol-formaldehyde and (b) carbon aerogel microspheres synthesized from an inverse emulsion. The wire in each photo is 35 μm in diameter.

Figure 3. Adsorption isotherm for carbon aerogel microspheres (60 % monomer; R/C=200; air-dried; 1050 ^{0}C).

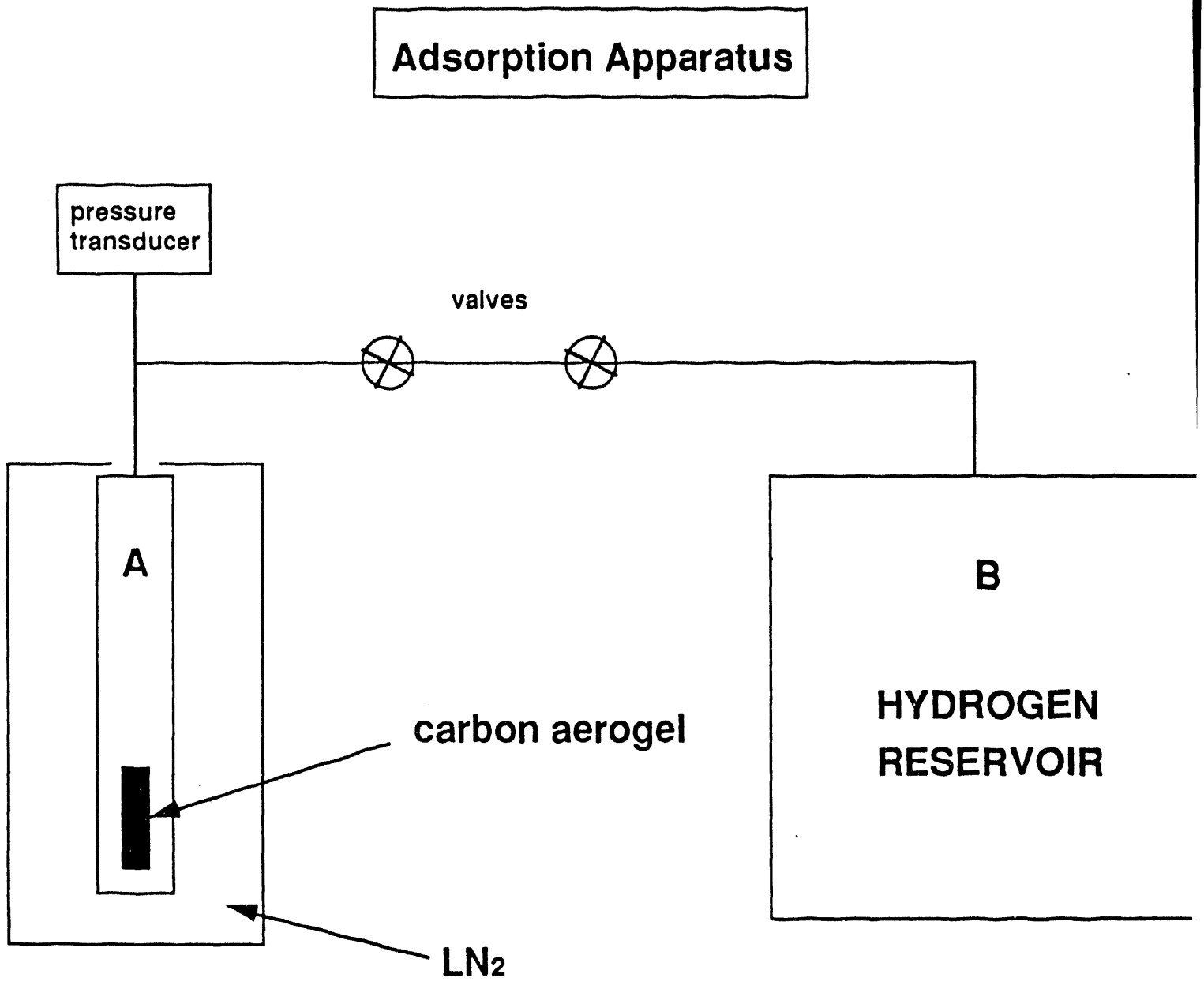
Adsorption Apparatus
pressure transducer
valves
A
B
HYDROGEN RESERVOIR
carbon aerogel
LN2

Figure 1

(a)

Resorcinol-formaldehyde

(b)

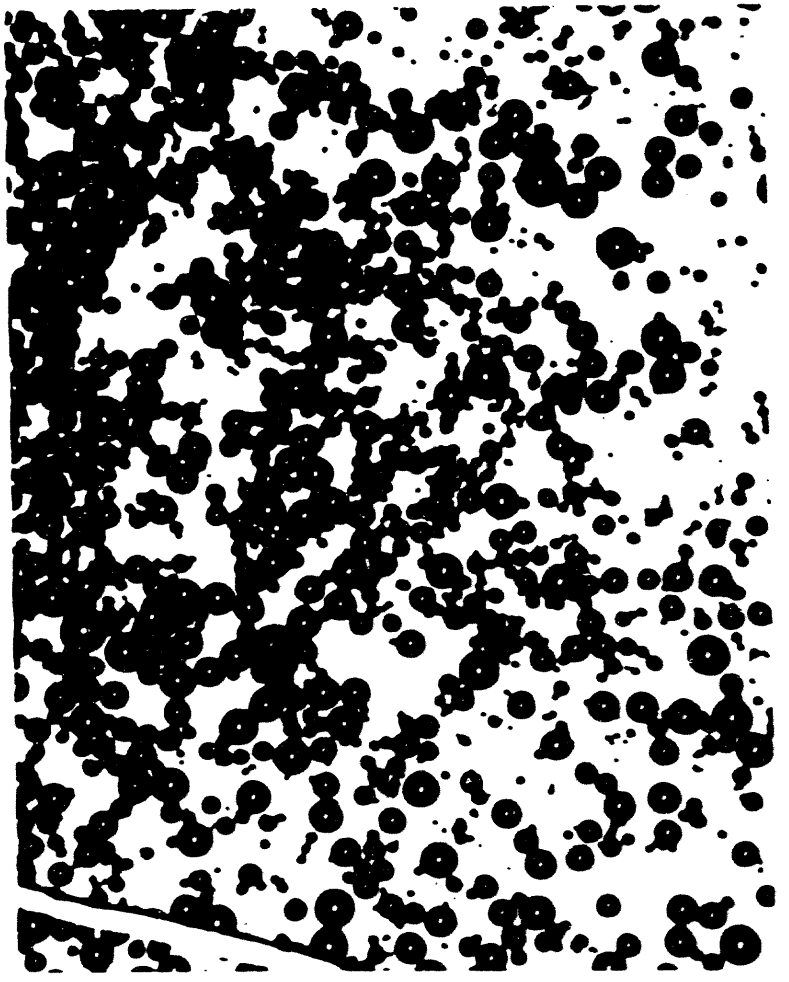

Carbon

Figure 2

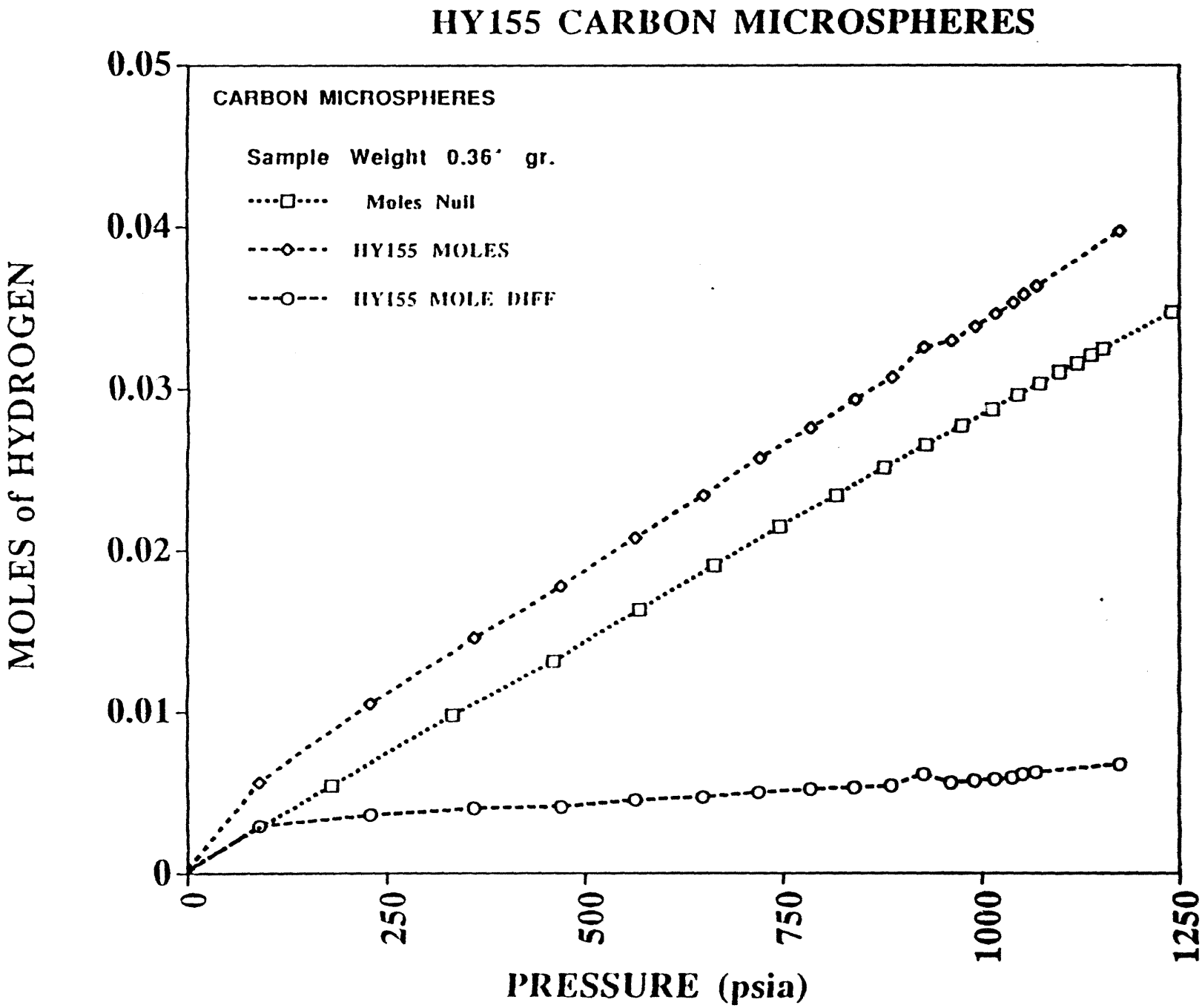
HY155 CARBON MICROSPHERES
CARBON MICROSPHERES
Sample Weight 0.36' gr.
Moles Null
HY155 MOLES
HY155 MOLE DIFF
MOLES of HYDROGEN
0.05
0.04
0.03
0.02
0.01
0
0
250
500
750
1000
1250
PRESSURE (psia)

HYDROGEN TRANSPORT AND STORAGE IN ENGINEERED GLASS MICROSPHERES

G. D. Rambach
Lawrence Livermore National Laboratory
Livermore, CA 94550

Abstract

New, high-strength, hollow, glass microspheres filled with pressurized hydrogen exhibit storage densities which make them attractive for bulk hydrogen storage and transport. The hoop stress at failure of our engineered glass microspheres is about 150,000 psi, permitting a three-fold increase in pressure limit and storage capacity above commercial microspheres, which fail at wall stresses of 50,000 psi. For this project, microsphere material and structure will be optimized for storage capacity and charge/discharge kinetics to improve their commercial practicality. Microsphere production scale up will be performed, directed towards large-scale commercial use.

Our analysis relating glass microspheres for hydrogen transport with infrastructure and economics, indicate that pressurized microspheres can be economically competitive with other forms of bulk rail and truck transport such as hydride beds, cryocarbons and pressurized tube transports. For microspheres made from advanced materials and processes, analysis will also be performed to identify the appropriate applications of the microspheres considering property variables, and different hydrogen infrastructure, end use, production and market scenarios.

This report presents some of the recent modeling results for large beds of glass microspheres in hydrogen storage applications. It includes plans for experiments to identify the properties relevant to large-bed hydrogen transport and storage applications, of the best, currently producible, glass microspheres. This work began in March, 1994. Project successes will be manifest in the matching of current glass microspheres with a useful application in hydrogen bulk transport and storage, and in developing microsphere materials and processes that increase on the storage density and reduce the storage energy requirement.

This task is being carried out with W.J. Schafer Associates. A potential industrial partner has interest in

becoming involved, through the CRADA process, in the development of microspheres for the above applications.

Introduction

Commercially produced glass microspheres were studied in the late 1970s for their application to storage of hydrogen (Teitel, 1981). These spheres, shown in Figure 1, have diameters of 25 to 500 μm and membrane thicknesses of approximately 1 μm. At elevated temperatures of 150 - 400C the increased permeability of the glass permits the microspheres to be pressurized by immersion in high pressure hydrogen for a period of time. Fill rates are a function of glass properties, permeating gas, temperature and pressure differential. The commercial spheres were usually made by spraying glass frits or gels into a furnace. Because the manufacturing process resulted in defects in the sphere membrane, the membrane hoop stress at failure for the commercial microspheres was limited to about 50,000 psi. Because LLNL's Laser Fusion Program had need for glass microspheres made under much more controlled conditions, a method of microsphere production was developed which resulted in defect-free microspheres. All microspheres produced from this method have diameters that fall within a few micron band and can be treated as a monodispersion. One result of this new process is that the absence of defects in the membrane raises the hoop stress at failure of the engineered microspheres to about 150,000 psi, permitting a three-fold increase in pressure limit for microspheres of the same dimensions and materials as the commercial ones. Further improvements in the microsphere process should significantly increase the strength in hoop of glass microspheres above 150,000 psi, enabling an increase in mass fraction and bed density while decreasing fill times.

A bed of 50-μm-diameter engineered microspheres with 1.1-μm-thick membranes and 150,000 psi hoop stress at burst, containing hydrogen at 9000 psi at a 1.5 safety factor, could exhibit a hydrogen mass fraction of 10% and a hydrogen bed density of 20 kg_{H2}/m^3.

Background

The key intrinsic properties that are relevant to hydrogen storage in glass microspheres fall into two categories. First are those related to the gravimetric and volumetric hydrogen capacities, and second are those related to the energy required to fill and release hydrogen. Our current understanding of all these parameters for high-strength glass microspheres is based on semi-empirical expressions developed early in the 1970s for laser fusion targets (Woerner, Weinstein, Moen, and Rittman, 1979). A microsphere would be individually fabricated into a target after being filled with the hydrogen isotopes of deuterium and tritium. Since the fill process for laser fusion applications was done on single microspheres, the heat supplied to raise the glass temperature and the time used to fill the spheres were both much greater than the minimum necessary to do the job. For large beds of microspheres to be used in economic transport and storage of hydrogen, it will be necessary to use as little fill energy and time as possible.

Storage Capacity

As in any pressure vessel, the storage capacity of a microsphere is limited by the burst pressure of the container and an applied safety factor. The burst pressure of the sphere (P_b) is given by

$$P_b = 4s_{max}Dr/D \quad (1)$$

where s_{max} is the biaxial tensile (hoop) stress in the sphere membrane at failure, Dr is the membrane thickness and D is the sphere outer diameter. Figures 2 and 3 show the mass fraction and of hydrogen and the volumetric density of hydrogen that can be stored in a bed of 50 μm diameter microspheres with a safety factor of 1.5. These only consider the mass and volume of the hydrogen and sphere bed. The safety factor of 1.5 is reasonable because a bed of 50-μm diameter microspheres would have a sphere number density of $10^7/cm^3$. A failure of the primary container holding the microspheres or a failure of any microspheres themselves will not result in the propagation of a failure through the rest of the bed.

In Figure 2, it can be seen that high-strength, glass microsphere beds can offer hydrogen mass fractions of hydrogen greater than 12% at internal pressures of 3600 psi and greater than 10% at 9000 psi. The packing fraction considered here is 63%, which is reasonable for beds of monodisperse spheres. As shown in Figure 3, the parameter that limits glass microsphere applications for on-board vehicle storage is the volumetric density. Even at internal pressures of 9000 psi, the density is about 20 kg_{H2}/m^3bed. A very efficient vehicle may require 3 - 5 kg of hydrogen on board, which, at 9000 psi, would require a bed volume of 150 - 250 liters (39 - 66 gallons). In addition, on-board microsphere storage would need added weight and volume for heat exchangers and other processing equipment. However, when considering bulk transport of hydrogen, such as by rail car or truck, the heat exchangers and other processing equipment can be located at the end points of the transport lines.

Energy and Time Required for Loading and Unloading

The energy needed to fill a bed of microspheres is the sum of the energy used to pressurize the hydrogen to the overpressure for filling and the heat used to raise the bed temperature for a suitable increase in permeability. For glasses, the permeability (K) can be expressed as (Souers, 1986, Woerner, Weinstein, Moen, and Rittman, 1979)

$$K = K_oTexp(-\theta/T) \quad (2)$$

where T is the temperature of the glass and K_o and θ are constants that are functions of the mole percent of network modifiers (M) in the glass. For silicate glasses

$$K_o \approx 3.4 + \{(8x10^{-4})M^3\} \times 10^{-17} \quad (3)$$

and

$$\theta \approx 3600 + 165M \quad (4)$$

For a given pressure differential (ΔP) across the glass microsphere membrane, the internal pressure (Pi) at any time during fill or release of hydrogen is

$$P_i = P_{io} \pm \Delta P\{1-exp(-t/\tau)\} \quad (5)$$

where P_{io} is the original internal pressure and t is time. The + sign applies to filling and the - sign applies to releasing. The term τ is the fill or release time constant, which can be expressed as

$$\tau = r_i^2 \Delta r / 3RTKr_o \quad (6)$$

where r_i and r_o are the inside and outside radii, respectively of the microspheres, and R is the gas constant. For a step function in temperature, 63% of the hydrogen would transfer in one time constant, and 86% would transfer in two time constants.

Figures 4 through 7 are related to the energy needed to fill and release the microspheres with hydrogen. Figure 4 shows the heat required, as a fraction of the lower heating value of the hydrogen stored, to raise the temperature of the combined masses of microspheres and hydrogen. The increase in heat required for increases in pressure are primarily due to the increased mass of glass needed to maintain the same safety factor. For pressurization, the energy required is a function of, among other parameters, the compressor efficiency and the number of stages. In Figure 5 the compression energy for a 75% efficient, three-stage compressor is added to twice the value for heat from Figure 4, to give a total energy required for a fill and release cycle of hydrogen. The figure shows that the "round trip" energy for reasonable pressures and temperatures ranges from 10% and 20% of the lower heating value of the hydrogen stored.

Figures 6 shows the variation with temperature, in permeability to hydrogen of silicate glass. The resulting fill and release time constant is given in Figure 7 for 30-mm-diameter microspheres with a 0.675-mm-thick membrane made with a glass containing 15% network modifiers. An increase of 200C in temperature results in a decrease of the time constant by four orders of magnitude. However, the fill, release time constant is still about one hour, which means it would take three hours at 220C to fill or release the microsphere by 95%. An increase in temperature to 370C would give the same result in fifteen minutes.

Microspheres developed in this project, and produced in quantities sufficient for batch transport of hydrogen, will be much less costly to produce and be significantly safer than conventional pressurized gas or cryogenic liquid containers. Their storage mass fraction will be several times greater than for hydrides or pressurized tube transports, resulting in significant cost reductions in hydrogen transportation cost. When considering a possible transition to a hydrogen energy economy, one of the major limiters to such a transition is the availability of cost effective and safe bulk hydrogen storage and transport technology. High capacity microspheres can be a major contributor to enabling an early transition to a hydrogen energy economy.

When exposed to high temperature product gases in a hydrogen production facility, such as steam reformed natural gas, gasified coal or municipal solid waste, the microspheres' hydrogen-specific permeability will preferentially separate hydrogen from the stream. Similarly, the materials developed for the microspheres may be configured in geometries other than spheres to serve as superior gas separation membranes for hydrogen or other permeability-specific gases.

Approach

In the first year an extended literature survey will be performed to identify known values of hydrogen permeability and related properties of known glasses and other potential materials. The literature survey

will seek to identify known values of material properties such as material strength, morphology, formability, fabrication process, cost and the effect of fields on permeability. We will also begin to setup a facility to fabricate the best, current glass microspheres. This facility will include the glass-forming, chemistry mixing equipment, a droplet generator for the uniform production of microsphere precursor droplets and a drying and forming, drop tower furnace.

When this facility is operational, microsphere batches on the order of a few cm^3 will be produced to compare the pressure crush statistics with the model and with microsphere physical and material properties. With these microspheres we will also evaluate the durability of spheres in a bed configuration, looking at surface-surface and point loading effects, as well as the packing fraction behavior for monodispersions.

In the second year, a batch heating, pressurizing system will be fabricated. This will permit the measurement of fill and release rates as a function of temperature and material. We will also measure burst and crush statistics to understand the relationship between strength and surface quality. The glass microsphere forming process will be modified to increase the ultimate strength of the glass walls, permitting a higher mass fraction of hydrogen storage. It is expected that this can be done by adding an annealing stage to microsphere fabrication column. This should further improve the microsphere surface quality and, since the ultimate tensile stress of glass in the 10^6 psi range, raise the failure hoop stress above 150,000 psi.

In the third year, we will perform analysis of results to identify the best production methods and materials and the appropriate applications of optimized microspheres considering microsphere production, cost, property variables, and different hydrogen infrastructure, end use, production and market scenarios.

Conclusions

The performance of glass microspheres appears to be sufficient for applications to bulk storage and transport of hydrogen based on the analysis using semi-empirical modeling. To date there is still some uncertainty in the behavior of hydrogen-permeable glasses with regard to the effect of network modifiers, and to strengths. Also, the behavior of large beds of high-strength microspheres has not been studied. This project will identify the properties relevant to large-bed hydrogen transport and storage applications, of the best, currently producible, glass microspheres. These measurements will be used to validate and enhance the density and kinetic models recently developed for microsphere hydrogen storage beds. We will then identify and implement the best possible material and process modifications to improve charge/discharge kinetics and minimize cycle energy requirements. Once the best material and process is identified, the methodology for scale up of the microsphere fabrication process for industrial and commercial use will be developed.

Acknowledgments

The author wishes to thank Charles Hendricks of W. J. Schafer Associates, Incorporated for his help in developing the plans for this project. This work performed under the auspices of the U. S. Department of Energy by the Lawrence Livermore National Laboratory under contract No. W-7405-ENG-48.

References

Shelby, J. E. 1973. *A Comprehensive Review of Gas Permeation, Diffusion, and Solubility in Inorganic Glasses*, Technical Report SLL-73-0259, Sandia National Laboratory, Livermore.

Souers, P. C., Moen, I., Lindahl, R. O., and Tsugawa, R. T. 1978. "Permeation Eccentricities of He, Ne, and D-T from Soda-Lime Glass Microbubbles." *J. American Ceramic Soc.*, 61#1-2:42-46.

Teitel, Robert J. 1981. *Microcavity Hydrogen Storage - Final Progress Report*, Technical Report BNL 51439, Brookhaven National Laboratory, New York.

Woerner, R. L., Weinstein, B. W., Moen, I. M., and Rittman, J. G. 1979. *Working Strengths and D-T Fill Procedures for Glass Microsphere Laser Fusion Targets*, Technical Report UCRL-82728, Lawrence National Laboratory, Livermore.

Souers, P. Clark 1986, *Hydrogen Properties for Fusion Energy*, Berkeley: University of California Press

Figure Captions

Figure 1. Geometry and dimensions of glass microspheres for hydrogen storage.

Figure 2. Mass fraction of hydrogen stored in a bed of high-strength glass microspheres.

Figure 3. Volumetric density of hydrogen stored in a bed of high-strength, glass microspheres.

Figure 4. Fraction of hydrogen lower heating value needed for one heating cycle to raise the temperature of a microsphere bed and hydrogen.

Figure 5. Fraction of hydrogen lower heating value needed for one pressure cycle and two heating cycles to load and unload a bed of microspheres with hydrogen.

Figure 6. Permeability constant vs. temperature increase above 20C, for hydrogen in glass microspheres with 15% of network modifiers.

Figure 7. Time constant vs. temperature increase above 20C, for exponential fill or release of hydrogen using above glass microspheres with diameters of 30 μm and 0.675 μm-thick walls. These microspheres could contain hydrogen at 9000 psi with a safety factor of 1.5.

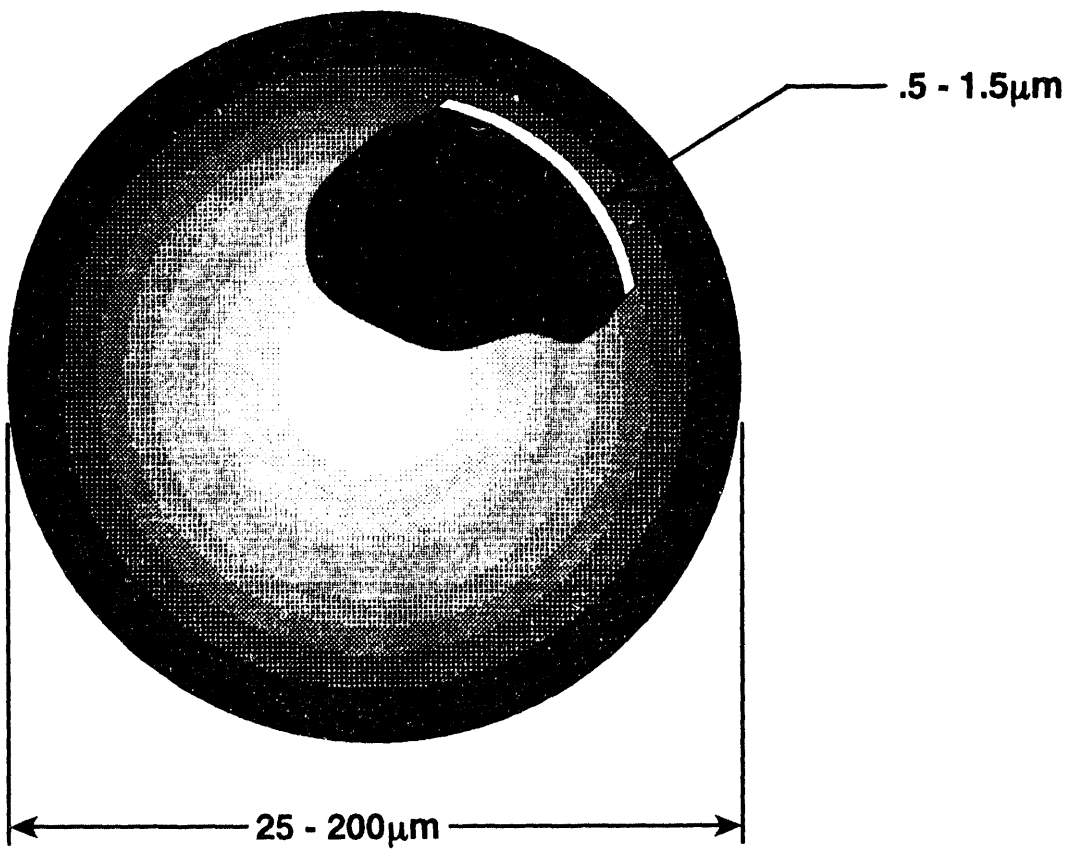

Figure 1. Geometry and dimensions of glass microspheres to be used for hydrogen storage.

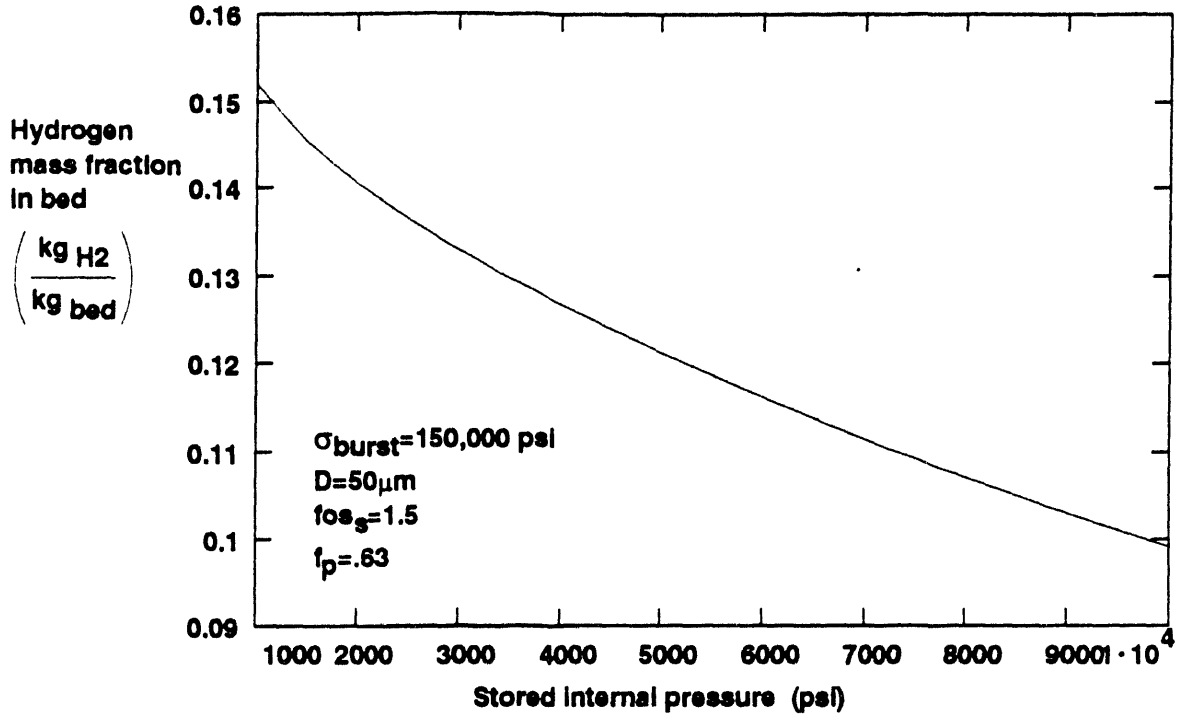

Figure 2. Mass fraction of hydrogen stored in a bed of high-st ength, glass microspheres.

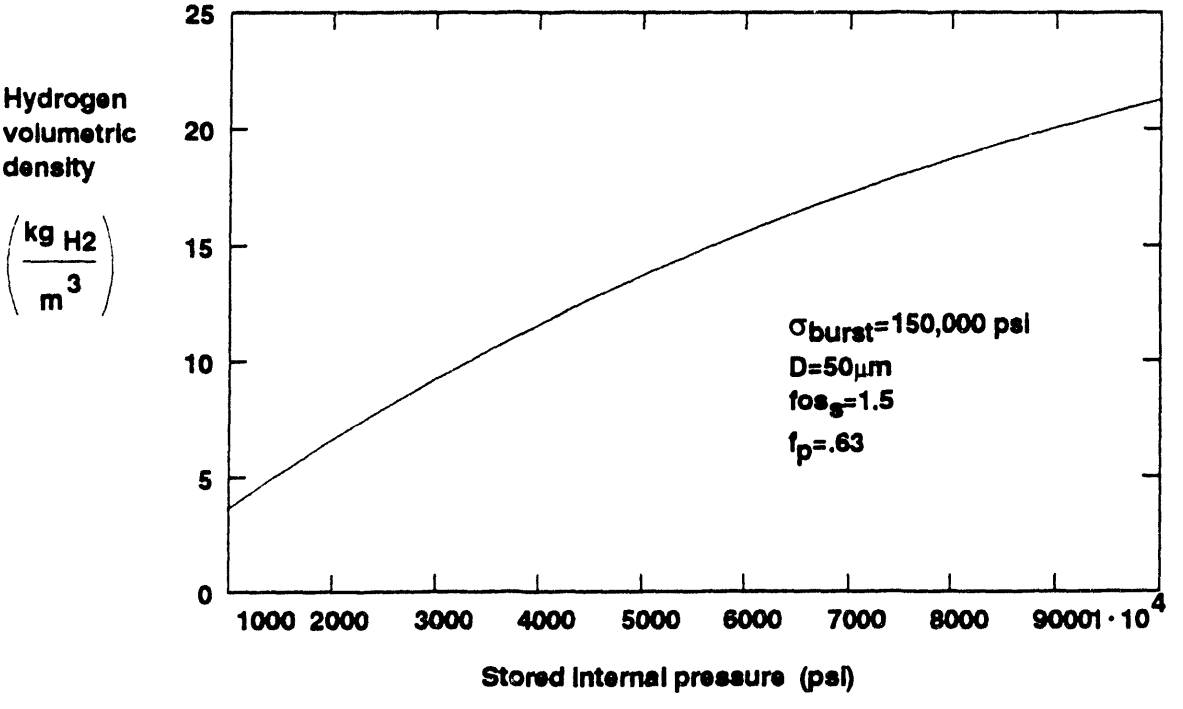

Figure 3. Volumetric density of hydrogen stored in a bed of high-strength, glass microspheres.

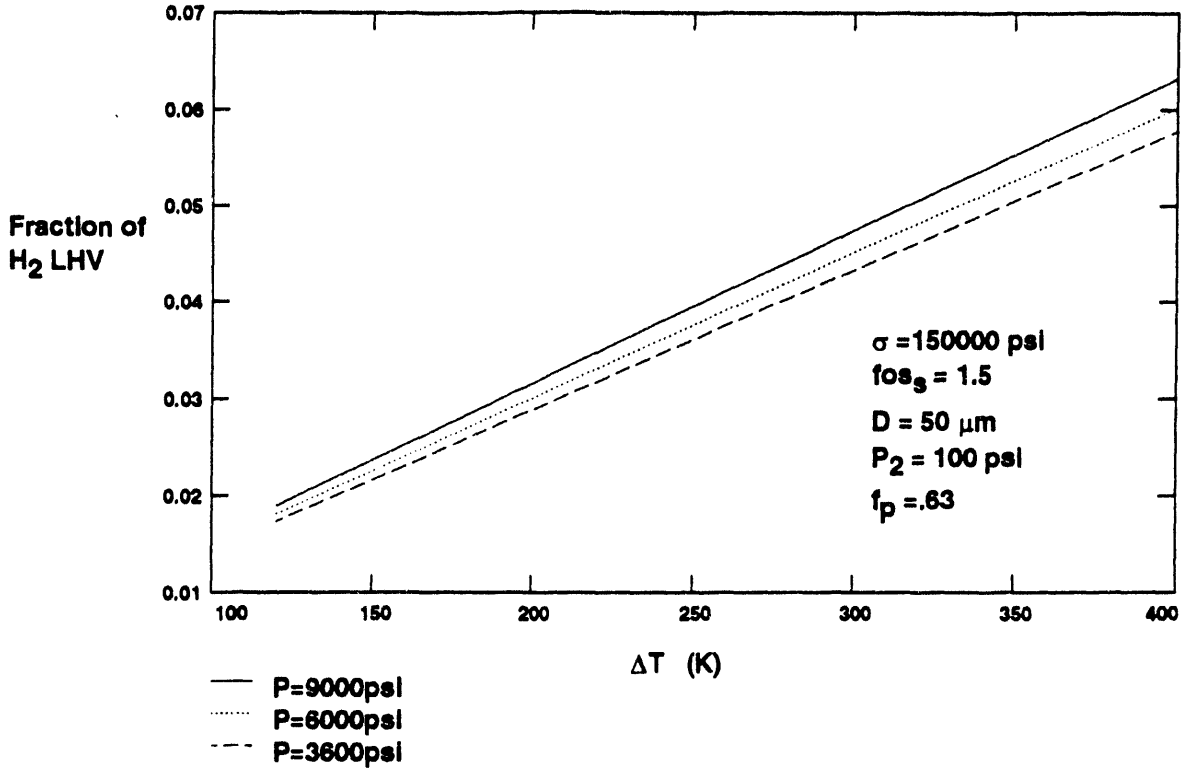

Figure 4. Fraction of hydrogen lower heating value needed for one heating cycle to raise the temperature of a microsphere bed and hydrogen.

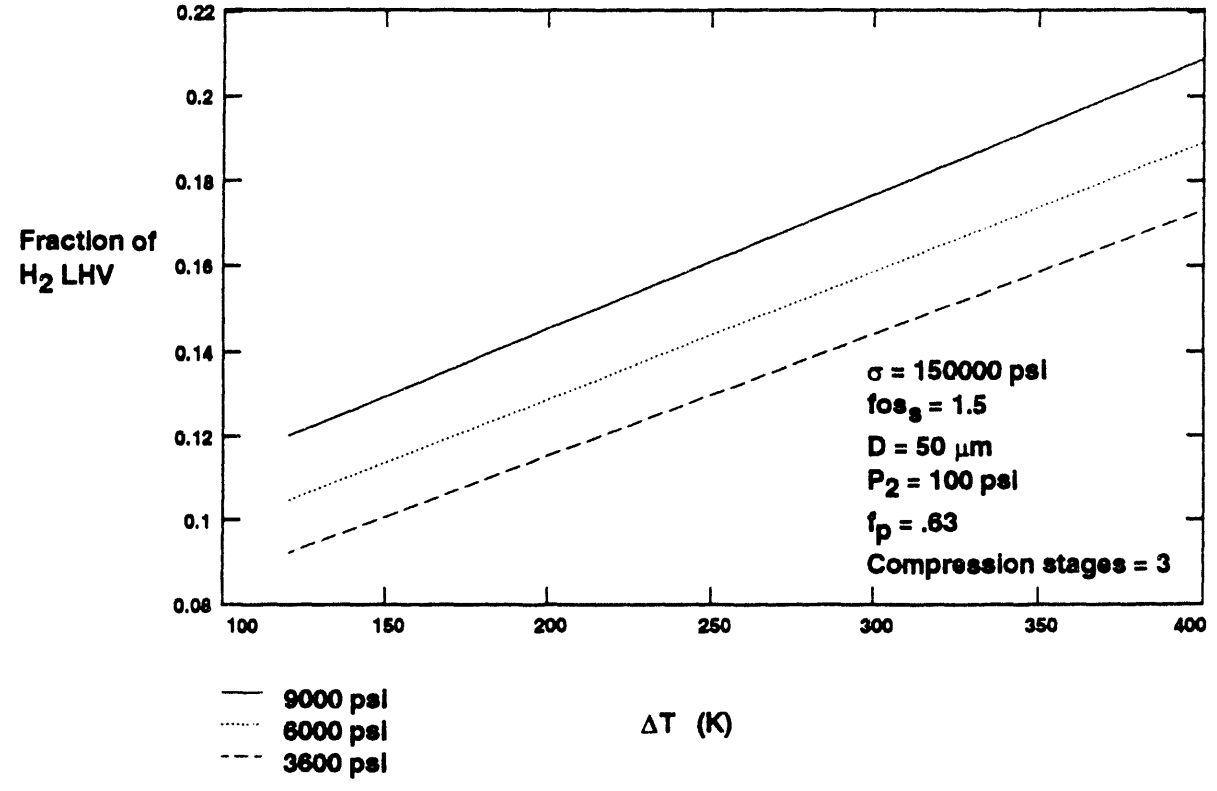

Figure 5. Fraction of hydrogen lower heating value needed for one pressure cycle and two heating cycles to load and unload a bed of microspheres with hydrogen.

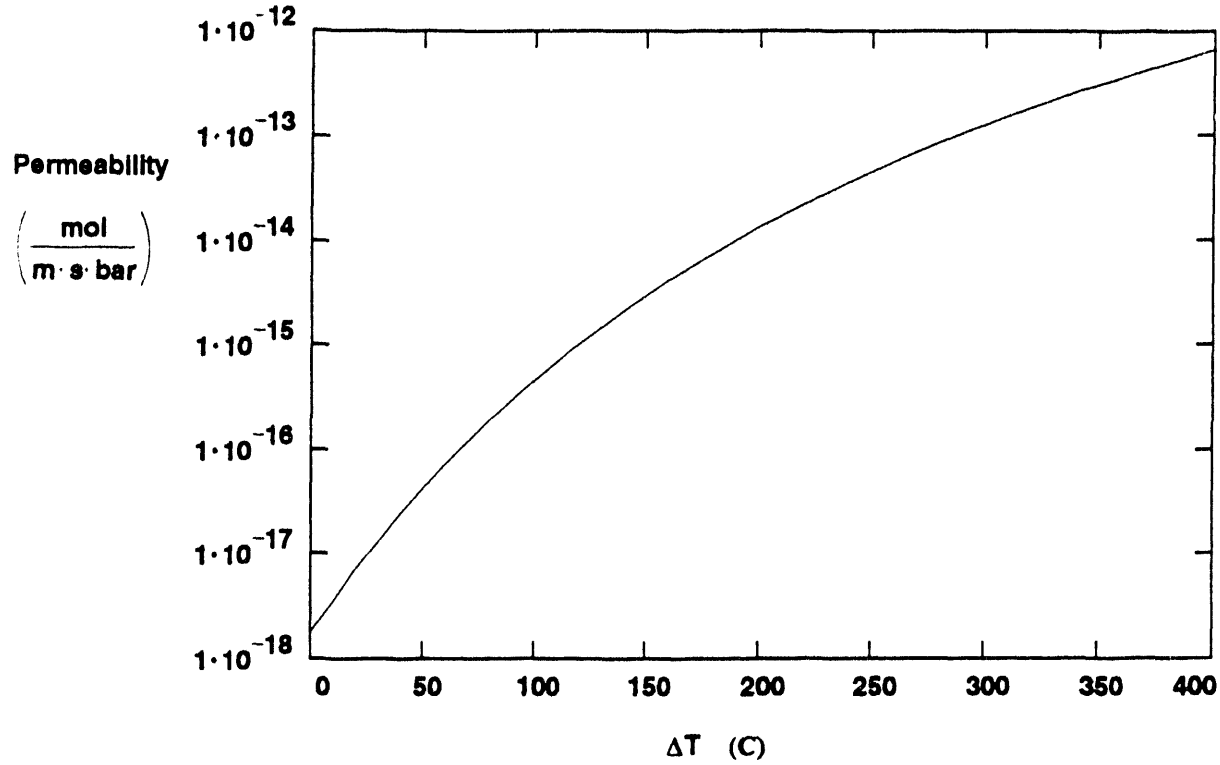

Figure 6. Permeability constant for temperature increase, starting from 20C, for hydrogen in glass microspheres with 15% of network modifiers.

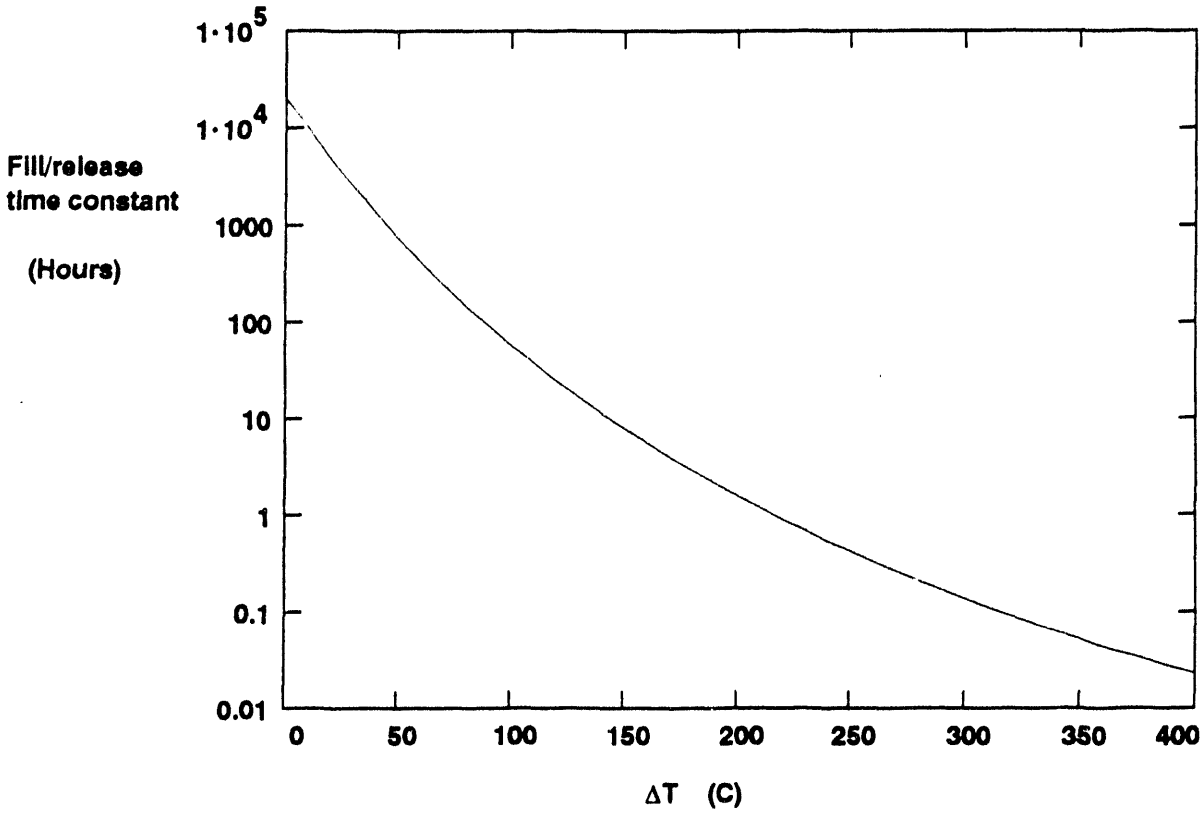

Figure 7. Time constant vs. temperature increase, starting from 20C, for exponential fill or release of hydrogen in above glass microspheres having diameters of 30μm and 0.675-μm thick walls. These microspheres could contain hydrogen at 9000 psi with a safety factor of 1.5.

STORAGE OF HYDROGEN MADE FROM BIOSYNGAS, USING IRON REDUCTION AND OXIDATION

John Werth and John Straus
H-Power Corporation
Belleville, NJ

Abstract

The reduction of iron oxide with biosyngas to sponge iron and the later oxidation of the sponge iron with steam offers the potential of shifting and purifying biosyngas and storing and transporting its energy in the form of cheap, compact, safe, stable, and relatively lightweight sponge iron. Later the iron is steamed to produce clean (moist or dry) hydrogen on demand.

This study focuses on upgrading a thermodynamic computer model of the iron oxide reduction process to make it usable with any biosyngas composition; choosing one or more promising compositions with the help of recognized authorities on the economic and gasification of biomass; using the model to estimate yields and efficiencies; and estimating the resulting cost effectiveness relative to a no-storage option.

The composition and reaction thermodynamics of one promising biosyngas are presented in this report, along with the basic features of the computer model.

Project Rationale

This work addresses a quadruple need that could potentially be met by a single device. The need is for the shift of usable CO contained in biosyngas into H_2 and CO_2, the removal of unconverted CO residues, the inexpensive storage of the biomass-derived chemical energy over many months, and the safe and inexpensive transportability of the stored energy over long distances (Figure 2). The device that potentially meets those four needs is a redox bed of porous iron or "sponge iron."

CO is generally incompatible with fuel cells, especially proton exchange membrane (PEM) fuel cells where even small CO residues are unacceptable. Such residues are also undesirable in engines and turbines because of the difficulty of removing all CO emissions without producing NO_x.

Storage of the chemical energy in the form of raw or dried biomass, or biogas, or biosyngas, or hydrogen, tends to be unwieldy or expensive or both. Transporting any of these materials tends to be expensive as well, and in some cases dangerous.

A scheme that could simultaneously shift, purify, store, and transport what starts out as biosyngas and ultimately ends up as clean hydrogen could well enhance the prospects of generating electricity from biomass via fuel cells or via clean hydrogen heat engines.

Figure 3 shows how a shift reactor can, by reacting with steam, convert most but not all of the CO in biosyngas to hydrogen and CO_2. The shifted gas mixture is deficient in two respects, however. The small residue of CO tends to degrade the performance of an otherwise desirable PEM fuel cell. If used to fuel an engine or turbine in a fuel-rich mixture, that mixture can shift back to CO and steam from hydrogen and CO_2, thus unduly burdening the exhaust catalyst system. If the mixture is fuel- lean, NO_x becomes a problem. Therefore gas purification or separation beyond the shift reaction might well be needed to achieve a clean exhaust.

Figure 4 lists some of the potential drawbacks of one scheme or another for storing and transporting hydrogen in various forms.

Approach

Our objective is to study the conversion of suitable types of biomass into sponge iron by directly reducing iron oxide with the usable fractions of hydrogen and CO in biosyngas (Figure 5). The resulting sponge iron could then be transported safely and compactly over long distances and the energy it contains could be stored cheaply for long periods with little or no degradation or shelf loss (Figure 6). On demand, moist or dry hydrogen, free of CO and CO_2, can be generated by steam oxidation for fuel cells or super-clean engines or gas turbines.

Figure 7 shows the estimated composition of a biosyngas made from dried biomass in a modified Shell gasifier (Larson and Katofsky, 1994). The high concentration of CO relative to CO_2 means that a considerable amount of chemical energy can be transferred from CO to Fe before the $CO = CO_2$ equilibrium is reached in the presence of $Fe = Fe_3O_4$. Also, the utilization of H_2 for Fe_3O_4 reduction can be enhanced by condensing H_2O upstream of the reducing reactor and again, in a multi-stage reduction scheme, upstream of each reducing reactor (Figure 8).

Figure 9 is a block diagram showing how sponge iron can generate moist (or dry, if desirable) hydrogen which is free of CO, CO_2 and nitrogen. The dry version is obtained by inserting a steam condenser directly downstream of the oxidizing reactor to remove the water in equilibrium with H_2 at the reactor exit.

Thermodynamic computer models for both Fe_3O_4 reduction and Fe oxidation had been previously developed at H Power based on both steam-reformed and partially oxidized natural gas (Figures 10a and 10b). These models are being expanded and made more versatile so as to accommodate a variety of biosyngas compositions. We have received and hope to continue to receive valuable inputs and guidance in the selection of economically attractive biosyngas compositions from Princeton University's Center for Energy and Environmental Studies and from relevant research activities at NREL (Figure 11).

Key Results

Biosyngas data have been collected for industrial wastes, such as wood chips and paper scraps; food processing wastes, such as hulls and shells; and crops grown specifically for gasification, such as Alamo switchgrass. Product gas composition data for several species falling into the above categories have been obtained (Figure 12).

A scheme for using biomass (predried to a 5% moisture content) from eucalyptus trees (currently grown commercially on a large scale in Southeast Brazil (Hall, et al., 1993)) after passing it through a modified Shell gasifier (Larson and Katofsky, 1992 and 1994) has been identified as being particularly attractive for use with the iron redox system. The biomass from the eucalyptus trees, if grown in Northeast rather than Southeast Brazil, is estimated to be cheaper ($1.40 per GJ) than any other suitable biomass, even cheaper than the $2 per GJ of U.S. natural gas (Katofsky, 1993, Carpentieri, et al., 1993, and Hall, et al., 1993). Large-scale eucalyptus plantations in Southeast Brazil currently supply pulp, steel and cement producers (Carpentieri, et al., 1993). Iron is a uniquely economical way to transport energy from Brazil and to store it for long periods before, during, and after shipment. The reasons (Figure 13) are its extremely low capital cost of storage, its small shipping volume, and its safe handling compared to hydrogen in various forms. An additional reason is that Brazil already exports large amounts of iron ore: the end product of the iron redox system is Fe_3O_4, which can be used to make steel and thus can replace some of the iron ore normally shipped for that use.

Although methanol is slightly more compact than iron for the same energy content, it appears to be more expensive to produce from biomass and more difficult to convert into a low-CO or CO-free hydrogen of the kind needed by PEM fuel cells or ultra clean engines and turbines.

A preliminary analysis of a biosyngas (average composition similar to eucalyptus as processed by the modified Shell gasifier of Figure 7) as used in the reduction of Fe_3O_4 is given in Figure 14. A high input composition ratio of CO to H_2 would suggest that two reactors operating at different temperatures would prove to be more effective than the design as shown. This change in design needs to be considered. As the model is currently in a spreadsheet format, it is adequate for initial studies of this kind, but its inflexibility in accommodating significant changes to the system layout hinders the design process.

Programming the model in QuickBasic offers a versatile analytical tool for determining the viability of a number of systems for processing biosyngas. Particular biosyngas specimens could require different treatments as preparation for Fe_3O_4 reduction. As a number of biosyngas samples will be investigated,

it is probable that a number of system configurations will also be considered. This type of analysis will best be handled by a program written in a modular type format. Each thermodynamic system, such as a heat exchanger, reformer, or iron-oxide reactor, will be programmed separately as a module or subroutine. Changes made to the system such as an additional condenser-reactor pair can be made relatively painlessly. Changes made to process variables such as operating temperature or mass flow rate will also be simplified.

To date, the mass and energy conservation equations for each module as presented in Figures 10a and 10b have been verified. A generic module format has been identified. A standard array will be used to describe state and process variables at the inlet(s) and exit(s) of each module. As the analysis becomes more advanced, losses in "pipes" connecting the modules will have their own modules.

Goals Of Study

The success criteria for this work are listed in Figure 15.

Proposed Future Work

Figure 16 summarizes the future work being proposed for the hydrogen iron project.

Acknowledgments

We gratefully acknowledge the financial support of NREL through subcontract ZAR-4-13294-02, covering the potential use of the iron-redox system in the storage of hydrogen made from biomass.

H Power has worked closely with and obtained critical biosyngas information from Princeton University's Center for Energy and Environmental Studies. Our principal source of guidance and information at the Center have been Eric Larson, Ryan Katofsky, Joan Ogden, and Robert Williams.

We have also obtained valuable information on biomass in Northeast Brazil from papers published in part by A.E. Carpentieri of the Division of Alternative Energy Sources, Hydroelectric Company of Sao Francisco, Brazil, and in part by Eric Larson of NREL and J.Woods of King's College, London.

We also acknowledge helpful inputs from the monthly progress reports of NREL's internal "Biomass-to - Hydrogen" project, as reported by Chornet, Czernik, Gregoire, Mann and Wang.

We also acknowledge the useful information compiled by Susan Leach of NREL in the "Fiscal Year 1993 Hydrogen Program Summary."

References

Carpentieri, A.E., Eric Larson, and J. Woods, 1993, "Future Biomass-Based Electricity Supply in Northeast Brazil", *Biomass and Bioenergy*, Vol. 4, No. 3, pp. 149-173.

Hall, David O., Frank Rosillo-Calle, Robert H. Williams, and Jeremy Woods, 1993, "Biomass for Energy: Supply Prospects", Renewable Energy/Sources for Fuels and Electricity, Island Press, Washington D.C. & Covelo, CA.

Katofsky, R. June, 1993, *The Production of Fluid Fuels from Biomass*, PU/CEES Report No. 279. Princeton, NJ.

Larson, Eric D., and Ryan Katofsky. 1994, "Production of Hydrogen and Methanol via Biomass Gasification," Advances in Thermochemical Biomass Conversion, edited by A.V. Bridgewater, London: Blackie Academic & Professional.

Larson, Eric D. and Ryan Katofsky; July 1992, "Production Of Methanol And Hydrogen from Biomass", Center for Energy and Environmental Studies, Princeton University, Report No. 271.

Leach, Susan, Hydrogen Program Summary, Fiscal Year 1993, NREL/MP-470-6229.

Ogden, Joan. 1993, "Renewable Hydrogen Energy Studies", Center for Energy & Environmental Studies, Princeton University, Final Report submitted 1/20/93, DOE Contract XR-2-11265-1.

Figure Captions

Figure 1. Level of Effort

- Level of Effort for the Year: $23,529
- Cumulative Level of Effort: $23,529

Figure 2. Biosyngas to Clean Hydrogen: A Wish List

- SHIFT CO TO H_2
- PURIFY THE SHIFTED MIXTURE
- STORE THE PURIFIED H_2
  - Cheaply
  - Safely
  - Compactly
  - Stably
- TRANSPORT THE STORED H_2
  - Cheaply
  - Safely
  - Compactly
- RECOVER THE H_2 FROM STORAGE
  - Efficiently
  - Cleanly

Figure 3. CO Shift Reaction

$$CO + H_2O \longrightarrow CO_2 + H_2$$

Figure 4. Some Hydrogen Storage and Transportation Problems

SAFETY:	HIGH PRESSURE EXPOSURE OF H_2 TO ATMOSPHERE VULNERABILITY TO AMBIENT TEMPERATURE RISE VULNERABILITY TO WATER
COST:	CONTAINERS ALLOYS ADSORBENTS
EFFICIENCY:	LIQUEFACTION COMPRESSION DESORPTION
WEIGHT & VOLUME:	CONTAINERS ALLOYS ADSORBENTS
STABILITY:	EVAPORATION DESORPTION AT RAISED TEMPERATURES OXIDATION FROM LEAKS

Figure 5. Biosyngas to Sponge Iron

$$4H_2 + Fe_3O_4 \rightleftharpoons 3Fe + 4H_2O$$

$$4CO + Fe_3O_4 \rightleftharpoons 3Fe + 4CO_2$$

Figure 6. Potential Benefits of Sponge Iron

- UTILIZES BOTH CO AND H_2 FROM BIOSYNGAS
- SUPPLIES CLEAN H_2 FREE OF ALL C-COMPOUNDS
- STORES THE ENERGY OF H_2 CHEAPLY:
  - 7 cents per pound; 12 cents per kW-hr of LHV
- STORES THE ENERGY OF H_2:
  - Safely
  - Stably
  - Compactly (2,400 LHV W-hr/l)
  - Lightly (1,300 LHV W-hr/kg)
- ALLOWS THE ENERGY OF H_2 TO BE TRANSPORTED OVER LONG DISTANCES:
  - Cheaply
  - Safely
  - Stably
  - Compactly
  - Lightly

Figure 7. Biosyngas from Modified Shell Gasifier (Per Katofsky, 1993)

COMPONENT	CALC. MOLE %*
H_2O	16.3
H_2	30.2
CO	43.3
CO_2	10.1
CH_4	0.0

*** Based on a biomass feed moisture content of 5%.**

Figure 8. Steam Condensation at Reactor Inputs

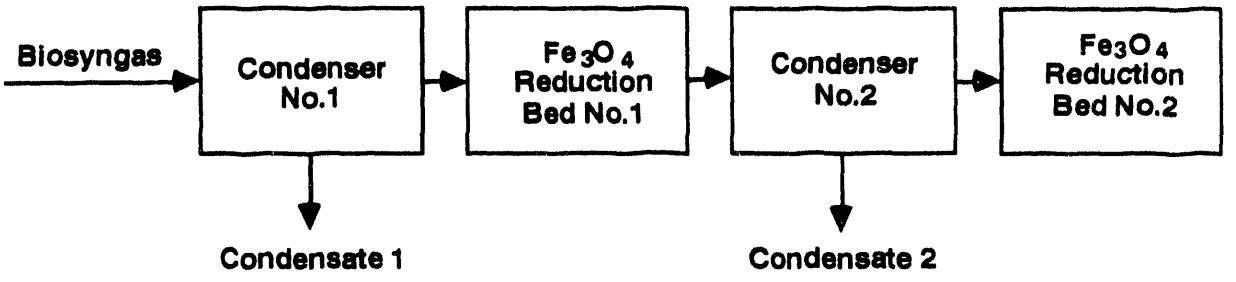

Figure 9. Sponge Iron Oxidation Block Diagram

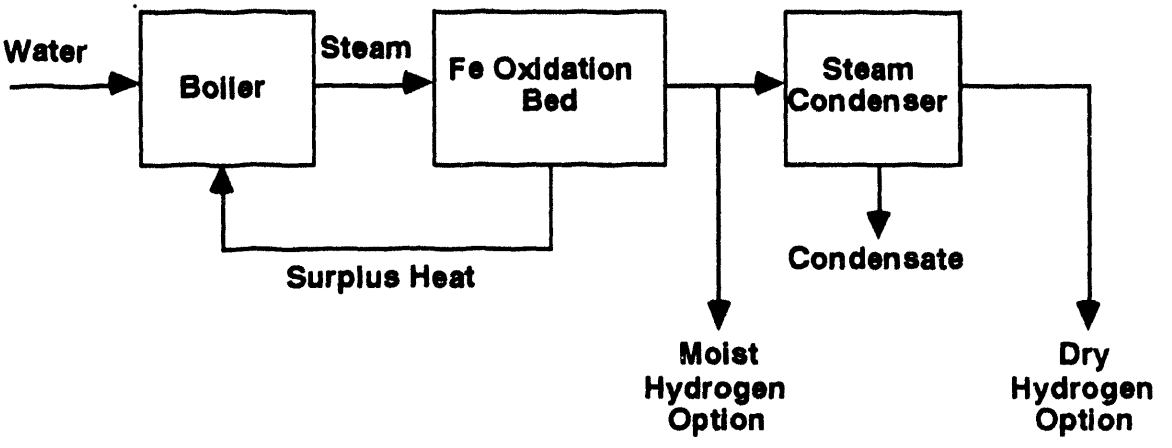

Figure 10a. Thermodynamic Diagram for Fe Oxidation

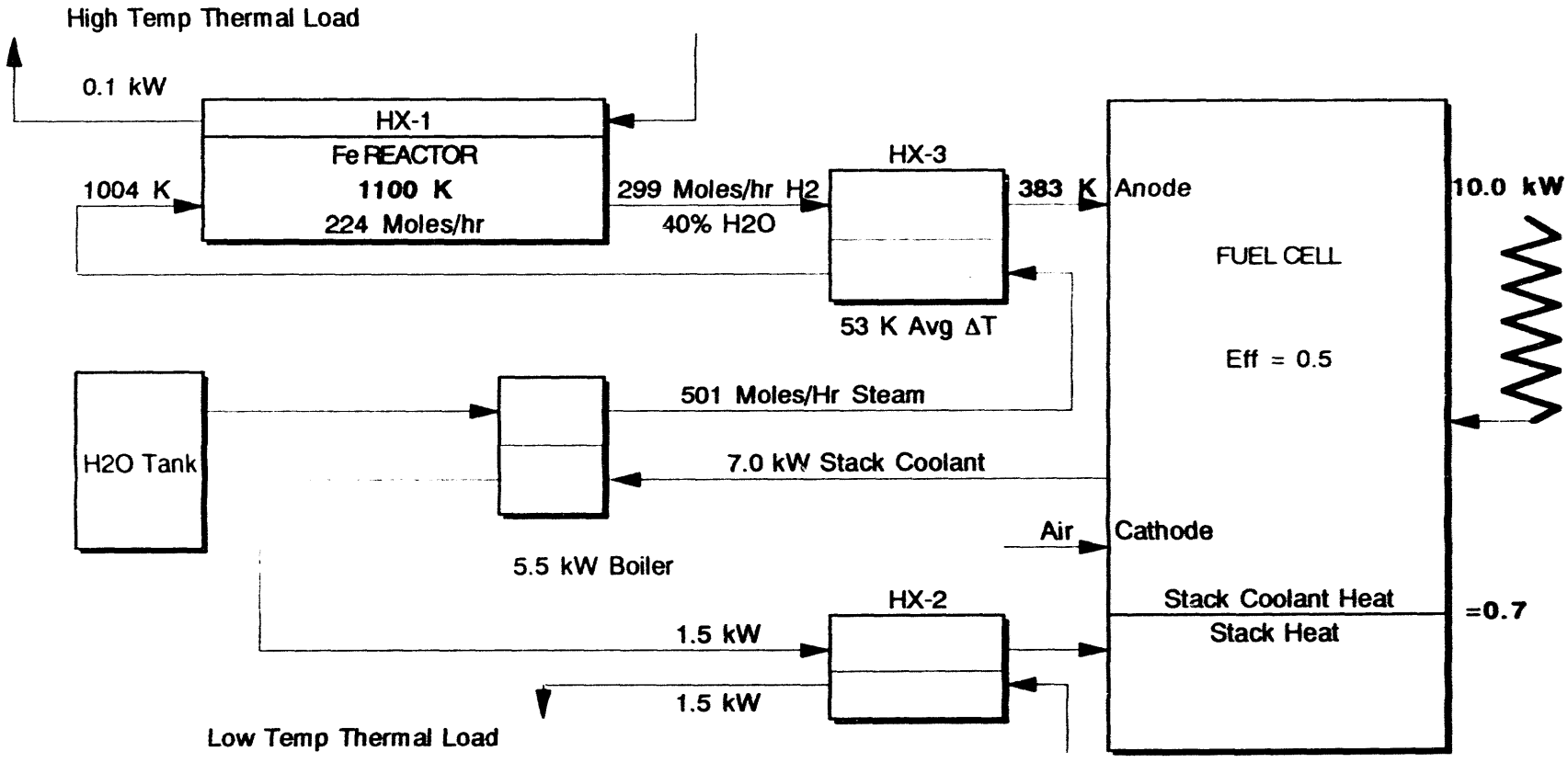

Figure 10b. Thermodynamic Diagram for Fe_3O_4 Reduction from Methane

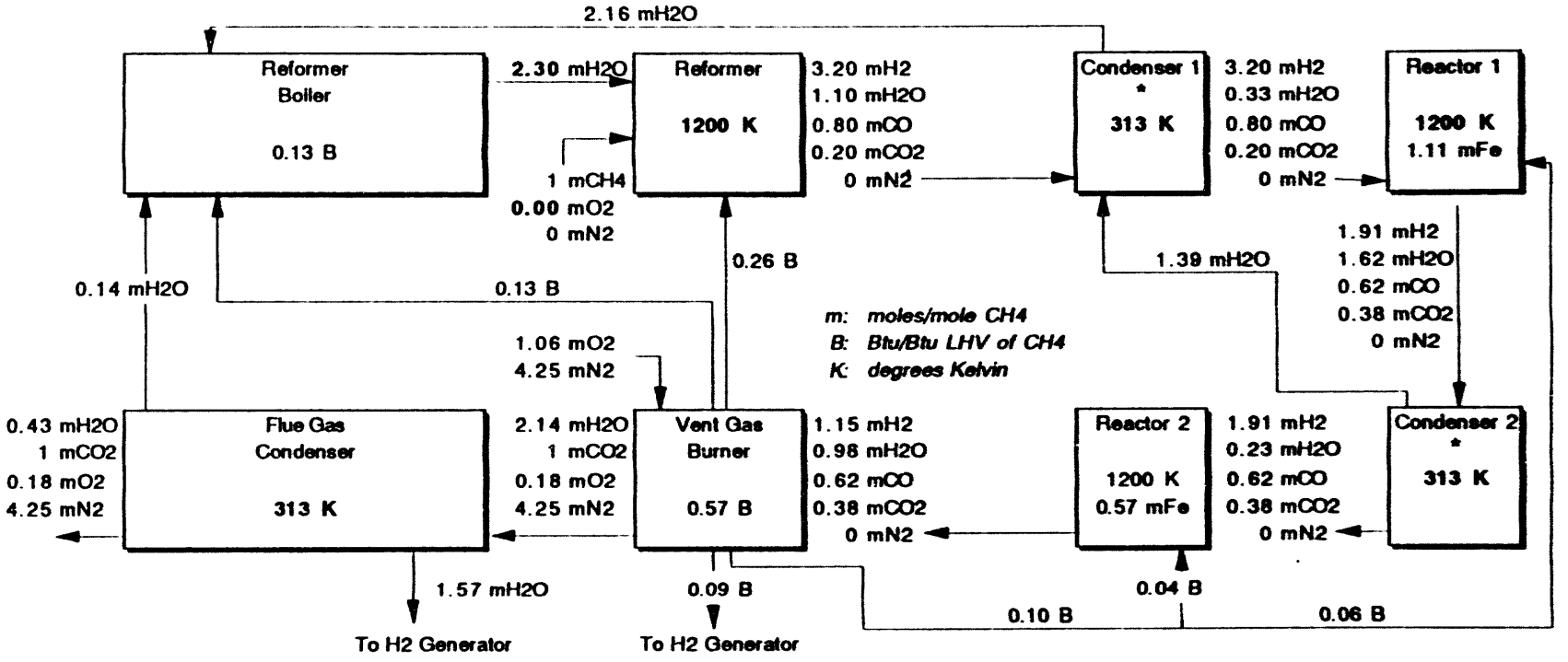

* With no shift catalyst, chemical equilibrium is not reached at the condensing stages

Figure 11. Biosyngas Compositions for Various Gasifier Types (Per Larson and Katofsky, 1994)

Components	Indirect Gasifiers		Directly-Heated Gasifiers	
	Wright-Malta	Batelle-Columbus	Inst. of Gas Technology	Modified Shell*
H_2O	42.0	30.8	31.9	15.4
H_2	12.0	14.6	20.9	28.7
CO	4.0	32.4	15.1	42.9
CO_2	22.0	7.8	24.0	12.6
CH_4	20.0	10.3	8.0	0.2
C_2 + Compounds	-	4.2	0.3	-

* Results based on a biomass feed moisture content of 11%.

Figure 12. Biosyngas Compositions for Various Biomass Sources

Municipal Waste		Industrial Waste		Food Processing				Energy Crops			
Recycled Paper/Plastic[1]		Wood Chips[1]		Rice Hulls[1]		Kraft Mill Sludge[1]		Miscanthus Crop[2]		Cellulosic Biomass[3]	
H_2:	50.5%	H_2:	50.5%	H_2:	48.1%	H_2:	42.8%	H_2:	61.6%	H_2:	30.2%
CO:	19.3%	CO:	19.3%	CO:	22.9%	CO:	19.7%	CO:	17.7%	CO:	43.3%
CO_2:	20.1%	CO_2:	20.1%	CO_2:	20.2%	CO_2:	24.4%	CO_2:	20.1%	CO_2:	10.1%
CH_4:	8.42%	CH_4:	8.42%	CH_4:	8.32%	CH_4:	11.6%	CH_4:	0.29%	H_2O:	16.3%
C_2:	1.72%	C_2:	1.72%	C_2:	0.48%	C_2:	1.5%	H_2S:	0.05%		
								N_2:	0.21%		

1- MTCI Pulse-Enhanced Indirect Steam Reformer
2- DMT Steam Reformer, Simulated Output
3- Shell Gasifier, Simulated Output

Figure 13. Potential Benefits of Biosyngas-Derived Sponge Iron in Brazil

- CHEAP FEEDSTOCK: EUCALYPTUS PLANTATIONS
- LARGE IRON ORE DEPOSITS
- CHEAP STORAGE = SUPPLY SMOOTHLY MATCHED TO DEMAND
- SAFE AND CHEAP TRANSPORTABILITY
- SHIPPING SPONGE IRON AND THEN OXIDIZING IT IS LOGISTICALLY EQUIVALENT TO SHIPPING IRON ORE AND BIOMASS

Figure 14. Thermodynamic Diagram for Fe made from Shell-Gasified Biomass

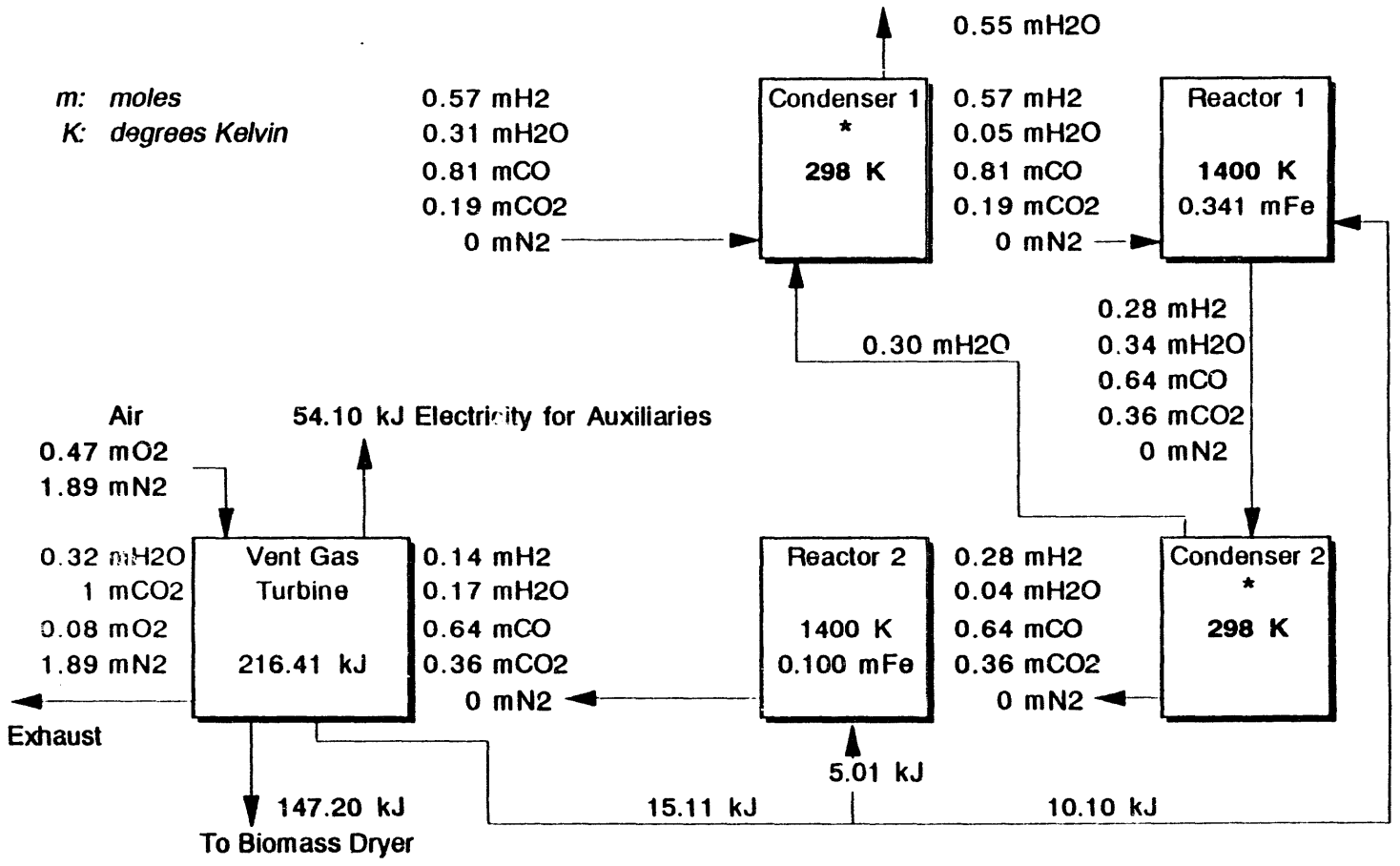

* With no shift catalyst, chemical equilibrium is not reached at the condensing stages

Figure 15. Project Success Criteria

1. UPGRADE THERMODYNAMIC MODEL OF IRON OXIDE REDUCTION FROM METHANE ONLY TO ANY BIOSYNGAS.

2. USE THE UPGRADED MODEL TO MAXIMIZE EFFICIENCY AND ESTIMATED COST EFFECTIVENESS.

3. PERFORM TRADE-OFF ANALYSES AMONG DIFFERENT CONFIGURATIONS OF THE IRON REDUCTION SYSTEM AND COMPARE THEIR COST EFFECTIVENESS TO THAT OF THE NO-STORAGE OPTION.

Figure 16. Proposed Future Work

1. VERIFY EXPERIMENTALLY THE PERFORMANCE OF IRON OXIDE REDUCTION SYSTEMS WITH BIOSYNGAS INPUTS.

2. IF JUSTIFIED, CONSTRUCT AND TEST A SCALED-UP REACTOR OR PILOT PLANT.

3. COMPARE THE ABOVE TO OTHER STORAGE SCHEMES.

4. DETERMINE EXPERIMENTALLY THE KINETICS OF GENERATING HYDROGEN FROM IRON AND STEAM AT TEMPERATURES SUITABLE FOR VEHICLE APPLICATIONS, ON A SMALL SCALE.

5. DESIGN A FULL-SCALE ON-BOARD HYDROGEN DISCHARGE SYSTEM.

6. COMPARE THE FULL-SCALE DESIGN WITH OTHER ON-BOARD HYDROGEN SOURCES.

PREPARATION AND CHARACTERIZATION OF Mg (Fe, Al, Ni, Ti) ALLOYS FOR USE AS HYDROGEN STORAGE MATERIALS

K. Sapru, L. Ming, B.S. Cho, and J. Gavulic
Energy Conversion Devices, Inc.
1675 West Maple Road
Troy, MI 48084

Abstract

Our previous work on sputtered thin film alloys (Mg-Fe-Al-Ni-Ti) has shown these alloys to have excellent properties as hydrogen storage materials. We report here our preliminary efforts on the scale up of these alloys using bulk production techniques such as resistive heating, induction melting, and mechanical alloying. The alloys are characterized by scanning electron microscopy (SEM), energy dispersive x-ray spectrometry (EDS), x-ray diffraction, and for their hydrogen storage capacities.

All the alloys show the presence of multiple phases. The mechanically alloyed sample shows the presence of structural disorder. The desorption kinetics of Mg-Al was significantly improved by the addition of Fe-Al and sintering the mixture for five days at 400°C.

Hydrogen storage capacities of the alloys varied between 2.5 wt.% and 6.2 wt.% depending on the composition.

Through our collaboration with the University of Michigan, we have developed an analytical model which will be used to further advance our understanding of the complex relationships between alloy properties and their incorporation into the design of the alloy bed and eventually into prototype systems design and engineering. The detailed model is attached as Appendix I.

Introduction

Introduction of hydrogen on a large scale needs cost-effective and environmentally sound means of hydrogen production, and efficient means of storing the hydrogen for use in mobile and stationary applications. While hydrogen storage can be accomplished by various methods such as physical storage (gas and liquid), gas/solid absorption, and in metal hydrides, our work is confined to metal hydrides which have potential for being the most promising, safe and economically viable method for hydrogen storage. However, to make metal hydride storage practical will require the development of new improved alloys that have gravimetric energy density of about 2.5 kWh/kg, and a volumetric energy density of 2500 kWh/M^3 (U.S. D.O.E 1992).

Most metal hydride work by others has focussed on the hydrides of FeTi, Mg_2Ni, and $LaNi_5$, and their modifications produced by partial substitution of one or both elements of the alloys. Hydrogen storage in these stoichiometric crystalline alloys depends on the availability of certain well-defined sites such as the tetrahedral or octahedral sites where the H atom can bond to the elements of the alloy (Reilly and Sandrock 1980). This introduces limitations in the design of improved H-storage capacity, H-sorption kinetics and other properties because of the restricted ability to modify such stoichiometric alloys. FeTi-based and $LaNi_5$-based alloys store between 1%-2% by weight hydrogen, resulting in low gravimetric energy density. Conventional Mg-based alloys (MgNi) have larger H-storage capacity (3 wt.%-4 wt.%), but their major drawback is that they are difficult to hydride and require very high temperatures to release the hydrogen.

Over the last fifteen years Energy Conversion Devices (ECD) has made major efforts towards the development of cost-effective hydrides having superior properties, for its Ni/metal hydride battery, which has two times the energy density of a Ni-Cd battery for equal weight and volume. The challenge in the present program is to use ECD's extensive experience in metal hydride technology to develop improved hydriding alloys that are low cost and have all of the following properties:

- High hydrogen storage capacity
- Good reversibility/long cycle life
- Good hydrogen absorption/desorption kinetics
- Desired PCT relationships
- Desired enthalpy of reaction
- Good thermal conductivity

Many of the ECD hydrides were originally developed and tested in the form of thin films prepared by vacuum sputtering. However, several of these, including the battery alloys and some alloys for metal hydride heat pump applications, have now been made in our laboratories using bulk processing technologies such as RF induction melting and melt-spinning and/or rapid solidification.

Table 1 shows some examples of hydriding alloys developed by ECD (Ovshinsky et. al 1984; Hong & Sapru 1985). Two families of alloys are shown, the TiV-based low temperature alloys having H-storage capacities ranging between 1.6 wt %-2.9 wt %, and the Mg based higher temperature alloys with H-storage capacities ranging between 3.6 wt %-7.3 wt. %. As shown in Figures 1A and 1B, the sorption kinetics of ECD's Mg-based thin-film alloys are much better than that of pure Mg or Mg-based alloys reported in literature (Douglass, 1975).

Table 1: Some Examples of Metal Hydrides Developed at ECD

Material Composition (atomic %)	H-Storage Capacity wt. %	Typical Desorption Temp. (°C)
$Ti_{23}Mn_{13}V_{40}Fe_{24}$	1.6	> 0°
$Ti_{33}Mn_{10}V_{47}Fe_{20}$	1.8	> 0°
$Ti_{33}Mn_{10}V_{47}Fe_{10}$	2.8	> 0°
$Ti_{33}Mn_{10}V_{47}Fe_{7}$	2.9	> 0°
$Mg_{55}Al_{43}Ni_{2}$	3.6	> 200°
$Mg_{66}Al_{19}Fe_{30}$	5.0	200°
$Mg_{82}Al_{16}Ni_{2}$	5.5	> 200°
$Mg_{90}Ti_{4}Fe_{6}$	7.3	> 220°

Table 2 shows some results of experiments performed to test the poison resistance (and hydrogen gas separation) properties of some of the MgFeAl thin films tested under various conditions. As can be seen, these alloys have excellent resistance to poisoning.

Table 2: Gas Separation and Poisoning Study

Sample No.	Gas Mixture	Test T°C	Condition Time	H Wt. %
OV-3A*	40% H_2 + 60% N_2	180	16 Hrs	3.05
	50% H_2 = 50% N_2	180	13 Hrs	2.90
	90% H_2 + 10% CO_2	200	13 Hrs	2.51
OV-38**	90% H_2 + 10% CO_2	180	15 Hrs	3.50
	80% H_2 + 20% CO_2	170	14 Hrs	3.90
	50% H_2 + 50% CO_2	115	15 Hrs	3.25
OV-1A	50% H_2 + 50% CH_4	250	24 Hrs	4.56
	28% H_2 + 72% CH_4	250	24 Hrs	4.42
	5% H_2 + 95% CH_4	250	5 Hrs	1.52
	99.5% H_2 + 0.5% H_2S	300	24 Hrs	4.77
	99% H_2 + 1% H_2A	300	3 Hrs	3.67
	95% H_2 + 5% H_2A	300	5 Hrs	2.62
	98.4% H_2 + 1.6% SO_2	250	24 Hrs	2.22
OV-4A	0.02% CO + 99.98% H_2	200	15 Hrs	2.99
	0.1% CO + 99.9% H_2	200	15 Hrs	3.01
	1.0% CO + 99.0% H_2	200	15 Hrs	2.89
	5.0% CO + 95.0% H_2	200	15 Hrs	2.75
	0.1% H_2S + 99.9% H_2	200	15 Hrs	2.53
	1.0% H_2S + 99.0% H_2	200	15 Hrs	2.47
	0.1% SO_2 + 99.9% H_2	200	15 Hrs	2.47
	1.0% SO_2 + 99.0% H_2	200	15 Hrs	2.41
	5.0% SO_2 + 95.0% H_2	200	15 Hrs	1.61

Development Approach

The basic hydriding reaction ($2M + H_2 = 2MH + Heat$) is a two-step process. First, molecular hydrogen (H_2) must dissociate into atomic hydrogen (H) which is reactive and which must then be able to readily form M-H bonds with the atoms of the alloy matrix. So in the design of hydride formers there are two basic requirements: (i) the presence of many catalytically active sites where the H_2 molecule can split into atomic H and (ii) the availability of a large number of H-storage sites.

It is well known that catalysts act by chemisorption, and in general maximum catalytic activity occurs at some intermediate strength of chemisorption. Also, since the chemical reactivity of the transition metals decreases as one moves from the left to the right across each period (for example from Ti to Cu) because of the filling of the d-orbitals, the best catalysts are found in the middle of the TM series. Hence, catalytic activity can be enhanced by the addition of elements from the middle part of the transition metal (TM) series of the periodic table.

Good kinetics is related to the M-H bond strengths and the rate of H-diffusion in the alloy. Therefore, kinetics can be improved by the addition of elements that form very weak M-H bonds, or only form such bonds at very high hydrogen pressures. It is well known that H-diffusion along the grain boundaries of a disordered material (having a large number of grain boundaries) can be orders of magnitude higher than in a perfect crystalline material. Thus, special attention must be paid to the alloy processing techniques so that the alloys have small grain sizes (about 100A°). In addition, alloy particle size should also be small so as to provide large surface area for enhanced catalytic activity.

Program Objectives

The current program has four main objectives:

1) Scale-up of promising alloys previously developed as thin films

One of the important challenges is to prepare the Mg-based high H-storage capacity alloys of Table 1 using bulk production techniques, and reproduce the results previously obtained in thin films. Problems can be encountered when making bulk alloys which require simultaneous melting of metals of widely differing melting temperatures and no known mutual solubility. This is because the vapor pressures of Mg at 500 and 1000°C are 10-2 and 103 torr, respectively, while the vapor pressure of Fe is less than 10-12 torr at 500°C and less than 10-6 at 1000°C, which is several orders of magnitude lower. Vapor pressure of Al at 500°C is less than 10-11 torr and increases to 10-4 torr at 1000°C.

2) Optimization of alloy properties

Simultaneously with developing alloy preparation techniques, the Mg-based alloys will be optimized to lower the desorption temperatures, increase the equilibrium pressure, and improve the kinetics of hydrogen absorption and desorption at lower temperatures. All this needs to be done without substantially reducing the hydrogen storage capacity.

3) Alloy characterization

This consists of (i) studying the H-absorption and desorption properties of the alloys, and (ii) studying the relationship between structure/morphology, composition, alloy preparation conditions, and the alloy

properties.

4) Analytical modelling

Examining the hydride bed/system from an engineering and design perspective will lead to a better understanding of the system and allow us to design an optimum system incorporating the improved alloy properties. This effort will be aided by a computer model which will be used to analyze the system performance. A realistic model of the system includes the dynamics of the processes such as finite heat transfer and hydrogen flow through the system.

Experimental Details

Preparation of Mg-Fe-Al-Ni alloys

All materials and gases used were of high purity. One or more of the following bulk alloy preparation techniques will be used to arrive at the most desirable method of making the desired Mg-based hydriding alloys.

* Resistive heating
* Induction melting
* Arc melting
* Melt spinning
* Mechanical alloying

Except for one sample of MgFeNi (sample MA-1) which was prepared by mechanical alloying, during the initial phase of this work we have used resistive heating and induction melting to prepare the alloys. Melting was carried out in argon atmosphere. The starting materials were weighed to an accuracy of 0.001g and pressed into half inch pellets at a pressure of 5-10 tons. The pellets were loaded into BN-coated graphite crucibles or alumina crucibles either directly or after being tightly wrapped in Fe, Ni, or steel foil to form a capsule. In most cases the pellet was melted once for about two hours. In some cases the melt was crushed or filed into powder, re-pressed and re-melted 2-3 times.

After some initial experiments with using elements as the starting materials which resulted in substantial loss of Mg, we decided to use binary alloys as starting materials. The binaries used were Mg-Al, Fe-Al, Mg-Ni, and Fe-Ni. All of these except Fe-Al were prepared in-house. In general, it seems possible to reduce Mg loss by (1) encapsulation, (2) using binaries as starting materials, and by (3) control of melting parameters such as temperature/time.

Alloy Characterization

Prior to measurement of the hydrogen absorption/desorption properties the alloys were subjected to an activation procedure which typically consisted of heating the sample at 350°C under 700 psi hydrogen atmosphere for 24-48 hours. This length of time was chosen only for convenience, to keep the samples in the reactor over the week-end. Three absorption/desorption cycles were done on each sample before recording the kinetics.

Scanning electron microscopy (SEM), energy dispersive x-ray spectrometry (EDS) and x-ray diffraction are routinely used to characterize all the alloys. A portion of the alloy is embedded in epoxy, followed by mechanical polishing to ascertain a smooth surface before SEM/EDS examinations.

Results and Discussions

Mg-Fe-Al

Figure 2 shows the dehydriding kinetics of two samples of MgFeAl (I-10 and I-21). Both samples were made by induction melting. The starting compositions were approximately $Mg_{75}Fe_{15}Al_{10}$. The major difference was that I-10 was made using individual elements as starting materials and I-21 was made from a mixture of Mg and $FeAl_2$. During melting there was substantial loss of Mg in both cases. While both samples show poor desorption kinetics below 350°C, I-21 shows slight improvement over I-10. The SEM photographs of the two samples (Figure 3A and Figure 3B) show interesting differences in the morphological features. The H- storage capacity is greater than 3 wt.%.

Figure 4 shows the desorption kinetics of a sample having the nominal composition $Mg_{85}Al_{15}$ made by resistive heating (Sample I-01). This figure also shows hydrogen desorption of a sample consisting of a mechanical mixture of $Mg_{85}Al_{15}$ (0.22g) and $Fe_{80}Al20$ (2 g) (Sample I-02). The desorption kinetics of the mixture is better than for MgAl, and further improvement occurred when the mixture was sintered at 400°C for five days under vacuum. This suggests some interdiffusion between the two binary alloys. This sample desorbed about 6 wt.% hydrogen at 350°C.

Mg-Ni-Fe-Al

This alloy was made by two methods, both using Mg_2Ni and Fe-Al as starting materials. Low temperature resistive heating at 400°C for 36 hours and induction heating at 800°C for 2 hours. However, it must be noted that during resistive heating there was no loss of Mg by vaporization. Figure 5A and Figure 5B show the SEM photographs of the two samples. The induction melted sample (I-11) had four major phases which were $Mg_{35}Ni_{51}Al_5Fe_9$ (light area), $Fe_{83}Ni_8Al_9$ (light area), $Mg_{66}Ni_{30}Al_2Fe_1$ (grey area), and $Al_{98}Ni_2$ (dark area). The resistively heated sample had three major phases, $Fe_{80}Al_{20}$ (bright round areas), $Mg_{69}Ni_{39}$ (bright irregular shapes), and Mg (dark areas). Both samples showed similar hydrogen desorption kinetics and storage capacities. The hydriding and dehydriding kinetics at 250°C and 300°C are shown in Figure 6A and Figure 6B respectively. About 2.5 wt.% hydrogen is released in 10 minutes at 300°C.

Mg-Ni-Fe

One sample of MgNiFe was attempted by mechanical alloying of Mg_2Ni (11g) and Fe (5g) in an attritor, for three hours. Figure 7 is the corresponding XRD trace which shows very interesting features. All diffraction peaks can be identified to alpha-Fe and Mg_2Ni phases. The broad linewidth of the peaks is related to the small particle size, the surface roughness of the particles, and variations in composition.

Conclusions

1. We have shown that it is possible to make bulk alloys of Mg-(Fe-Ni-Al,...).

2. The challenge is to retain maximum amount of Mg in the final alloy since this is the major hydrogen storing component. This goal can be achieved by utilizing a combination of alloy preparation techniques.

3. Mechanical alloying technique has the potential to be used either by itself or as a precursor to resistive and induction heating.

4. Materials made so far have multiple phases. Some of these phases may be important to H-storage while others may be acting primarily as catalysts. The boundary/interface between the various phases may be playing an important role. This will be determined only on further detailed analysis.

5. Preliminary and completely unoptimized alloys have shown up to 6 wt.% H-storage capacity. The temperature at which the hydrogen is released is still too high. This will be addressed in the follow-up work.

Plan for Future Work

We are not terribly concerned with preparing homogeneous, single-phase alloys since this is not crucial to obtaining good hydriding alloys. During the next few months we will focus on developing alloy preparation techniques that will prevent the loss of Mg. Approaches used will include the following:

1. Pursue various low temperature methods of alloy preparation
2. Use of various encapsulation methods
3. Modification of the induction melting method
4. Addition of small quantities of other transition metals to improve kinetics to lower the dehydriding temperature
5. Pursue mechanical alloying method.

References

Douglass D.L., *Metal. trans.* 6A, 1975, p. 2179

Hong K. C. and Sapru K., "Hydrogen Absorption in Mg-based Thin Film Alloys", The *Int. Symp. on Hydrogen Systems*, May 1985, p. 403-414.

Ovshinsky S.R., Sapru K., Dec K. and Hong K., "Hydrogen Storage Materials and Methods of Making the Same", *US patent no. 4,431,561*, Feb. 1984.

Reilly J.J., and Sandrock G.D., Scientific American, Feb. 1980.

U.S. Department of Energy, "Hydrogen Program Plan", FY 1993-FY 1997, document no. DE92010556, published by the *National Renewable Energy Laboratory*, June 1992.

Figure Captions

Figure 1A & 1B Hydriding and dehydriding kinetics of thin-film alloys

Figure 2 Dehydriding kinetics of MgFeAl

Figure 3A & 3B SEM photographs of MgFeAl (Sample 1-10 and Sample 1r-21

Figure 4 Dehydriding kinetics of MgAl and mixture of MgAl and FeAl, and effect of sintering

Figure 5A & 5B SEM photographs of MgNiFeAl prepared by induction melting (Sample 1-11) and by resistive heating (T8)

Figure 6A & 6B Hydriding and dehydriding kinetics of MgNiFeAl

Figure 7 XRD trace of mechanically alloyed sample

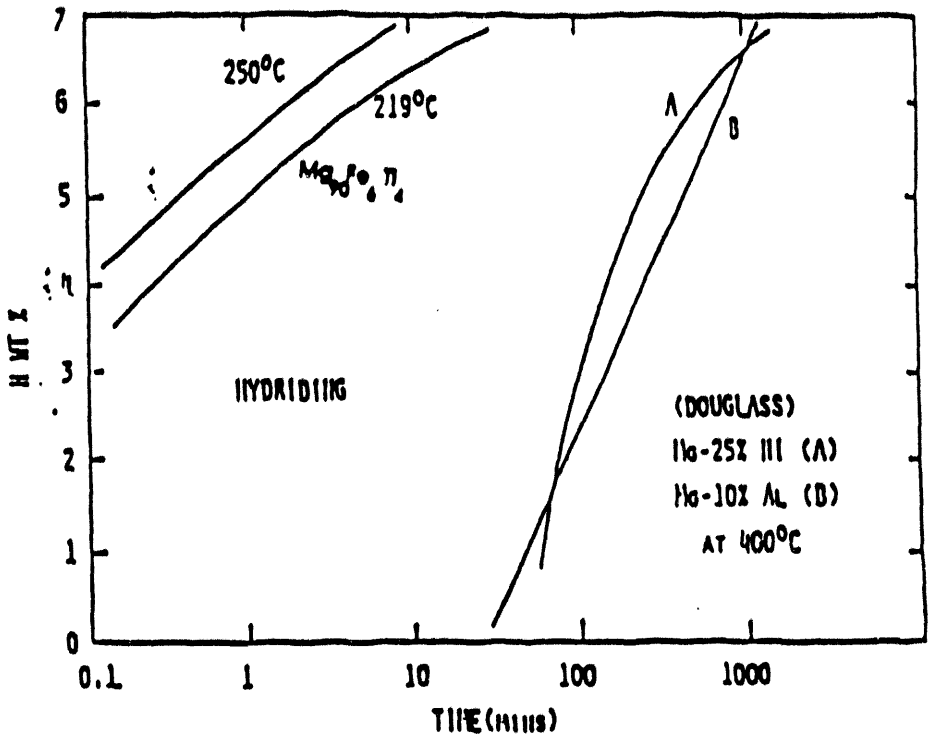

Figure 1 A: Hydriding kinetics of thin-film alloys

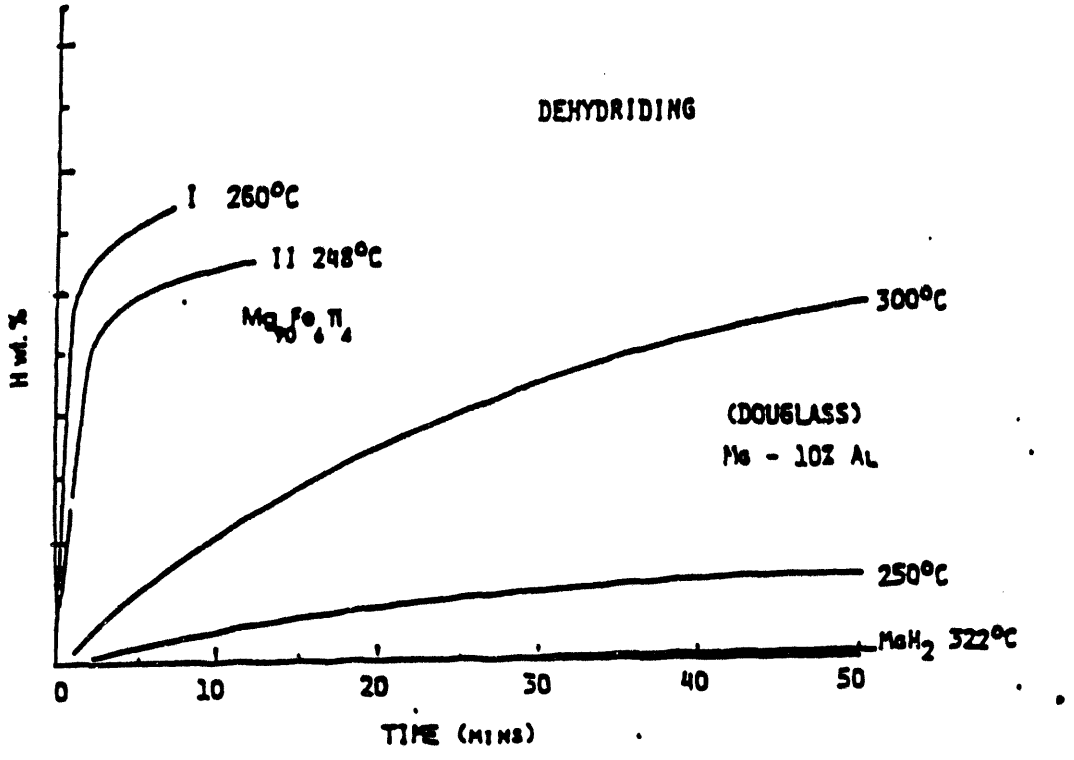

Figure 1B: Dehydriding kinetics of thin-film alloys

Figure 2: Dehydriding kinetics of Mg-Fe-Al

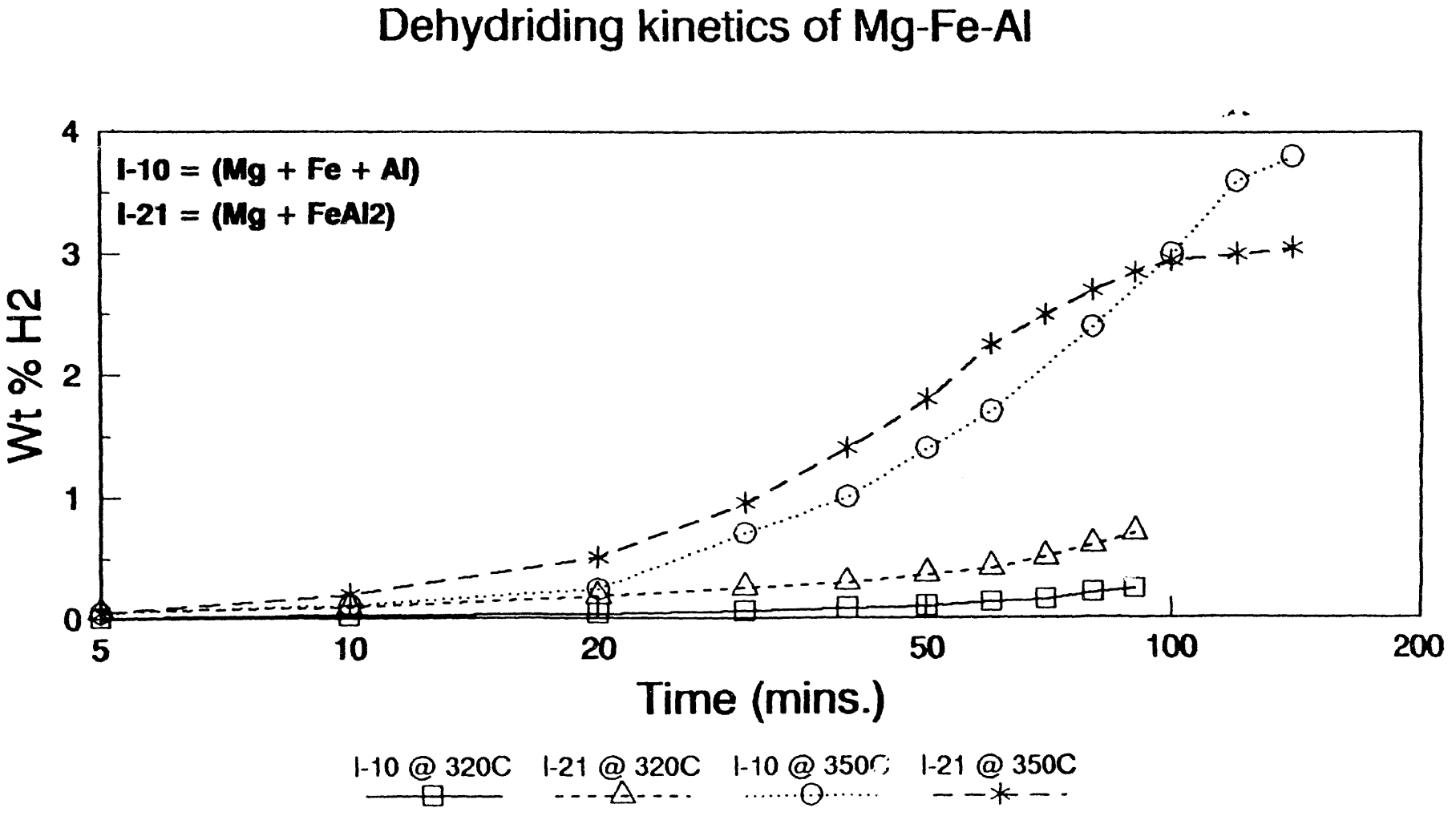

Figure 3A: SEM photographs of Mg-Fe-Al (Sample I-10)

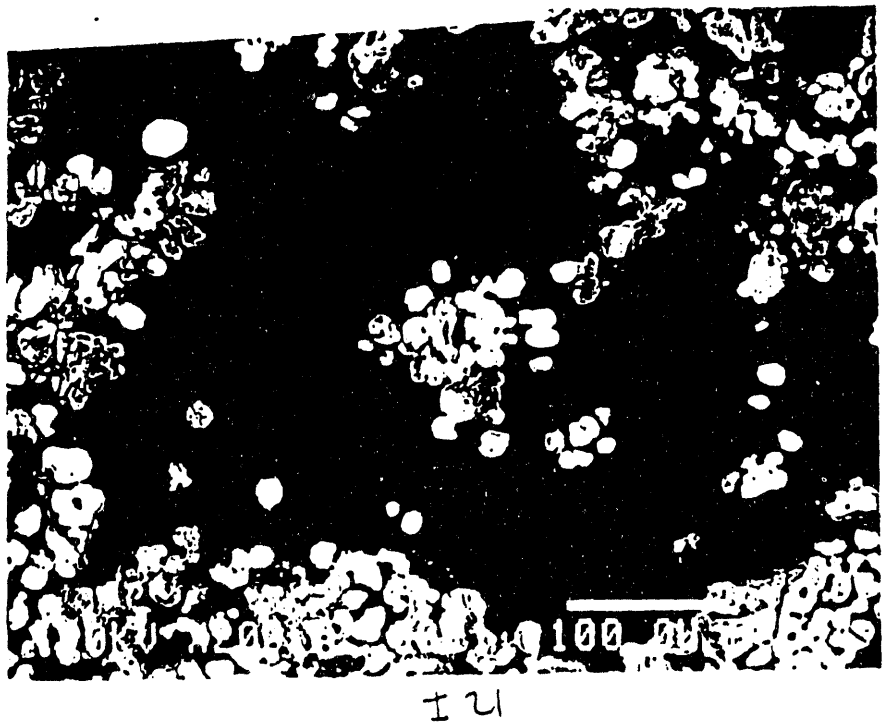

Figure 3B: SEM photographs of Mg-Fe-Al (Sample I-21)

Figure 4: Dehydriding kinetics of Mg-Al and mixture of Mg-Al and Fe-Al, and effect of sintering

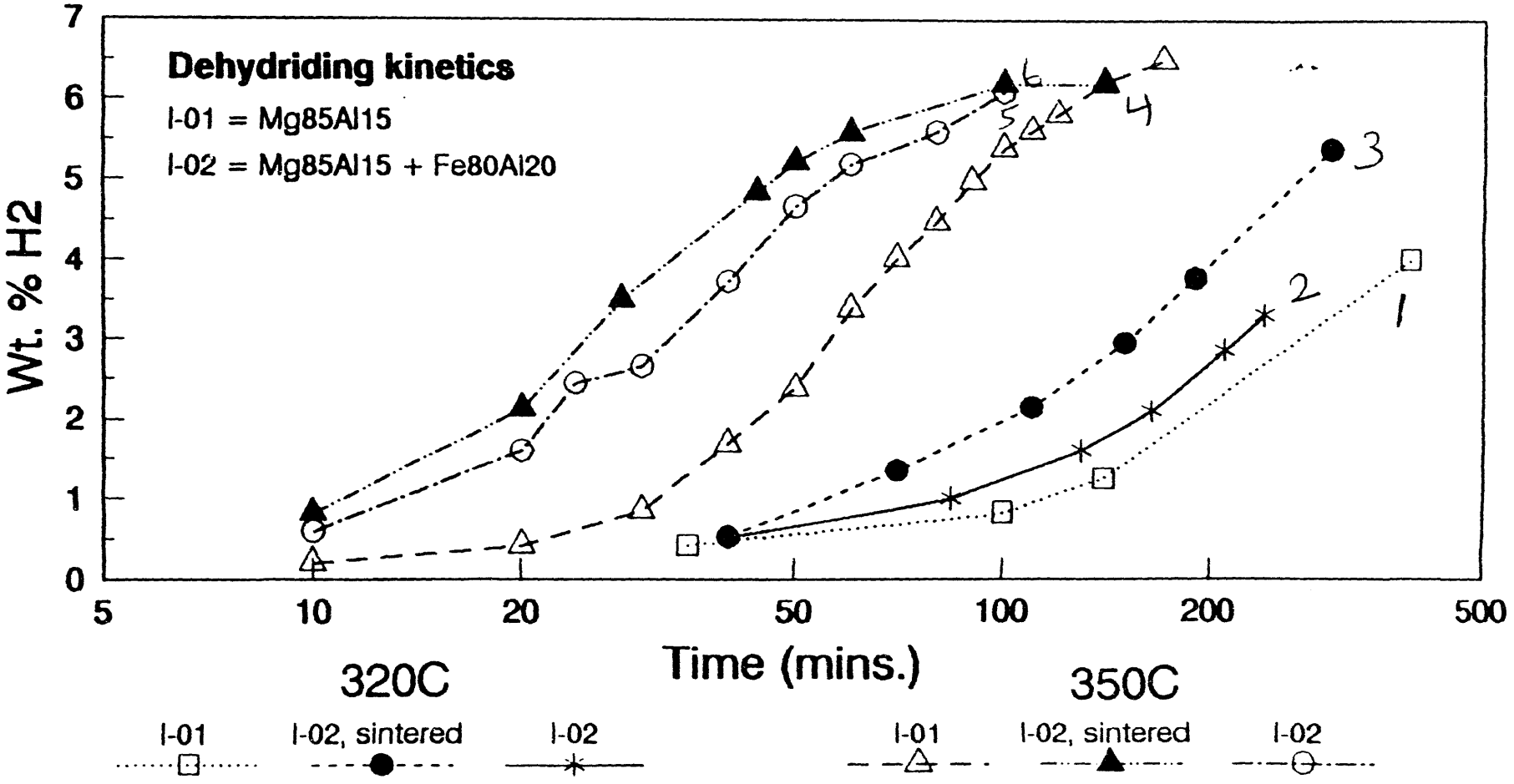

Figure 5A: SEM photographs of Mg-Ni-Fe-Al prepared by induction melting (Sample I-11)

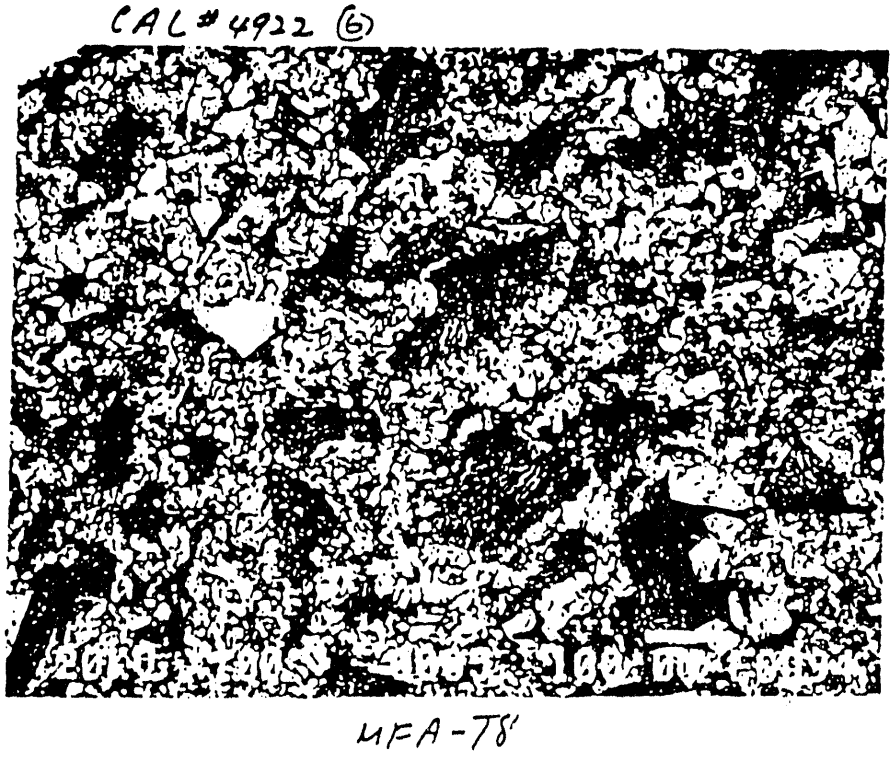

Figure 5B: SEM photographs of Mg-Ni- Fe-Al prepared by resistive heating (T8)

Figure 6A: Hydriding kinetics of Mg-Ni-Fe-Al

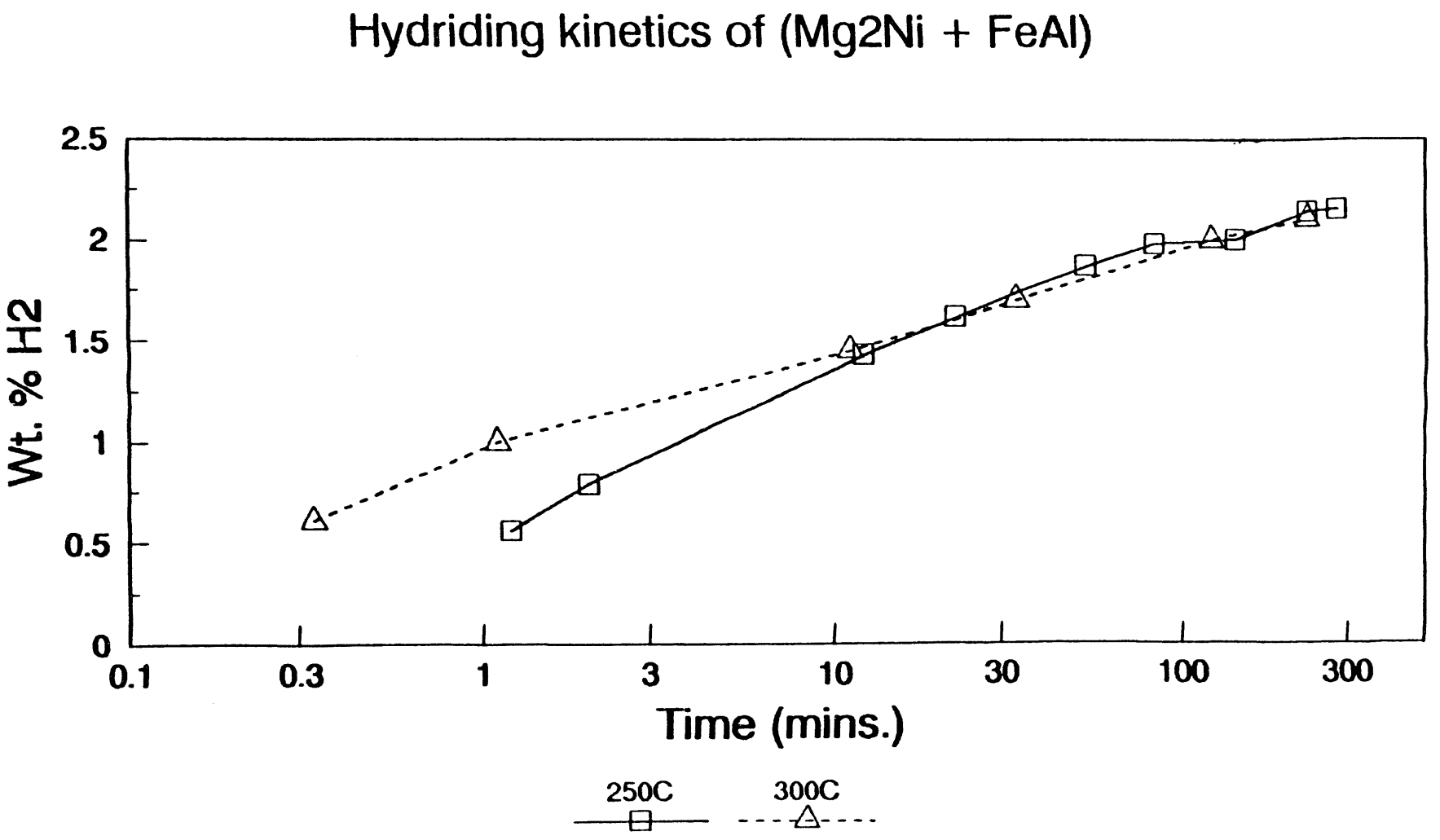

Figure 6B: Dehydriding kinetics of Mg-Ni-Fe-Al

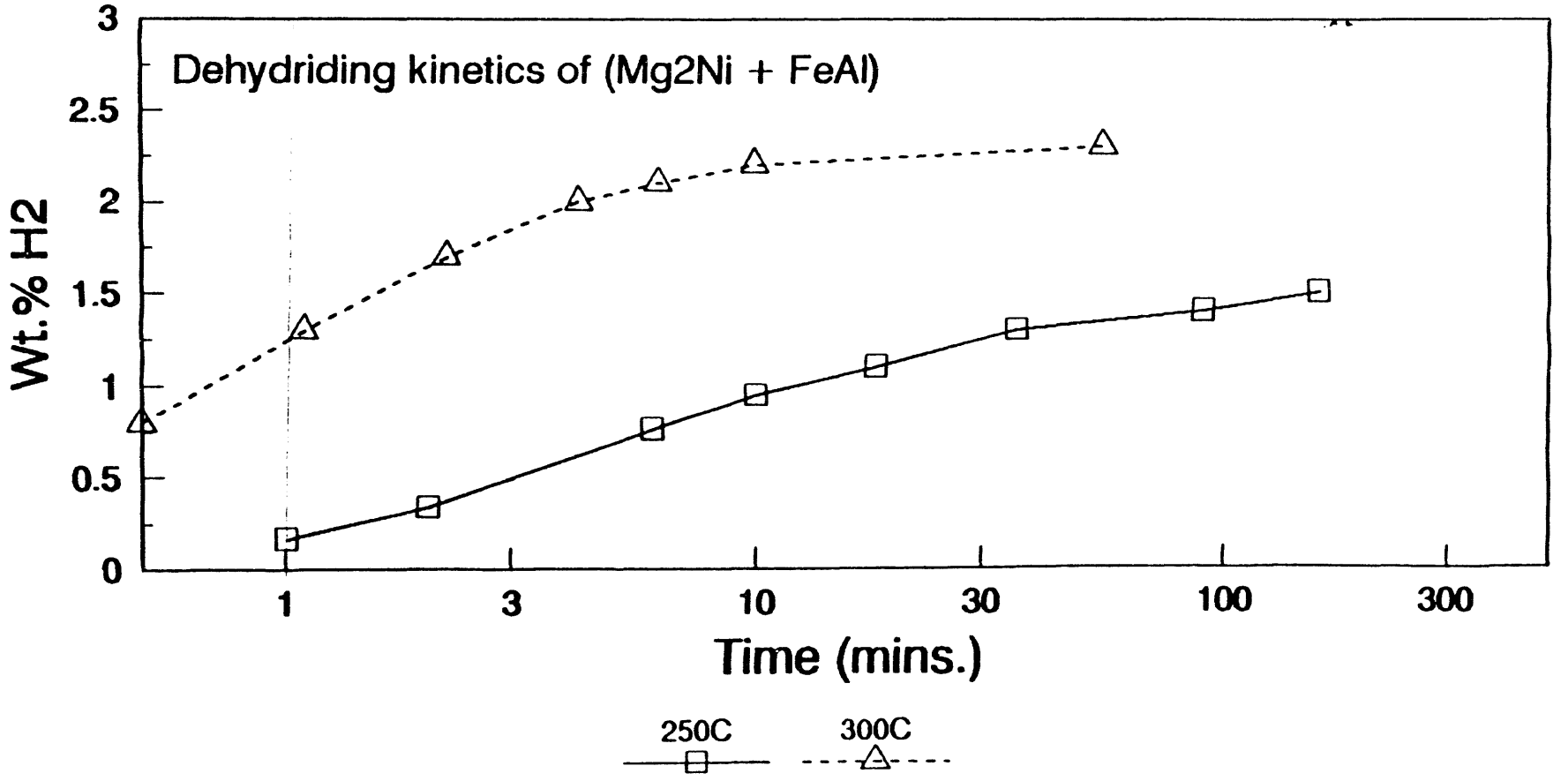

Figure 7: XRD trace of mechanically alloyed sample

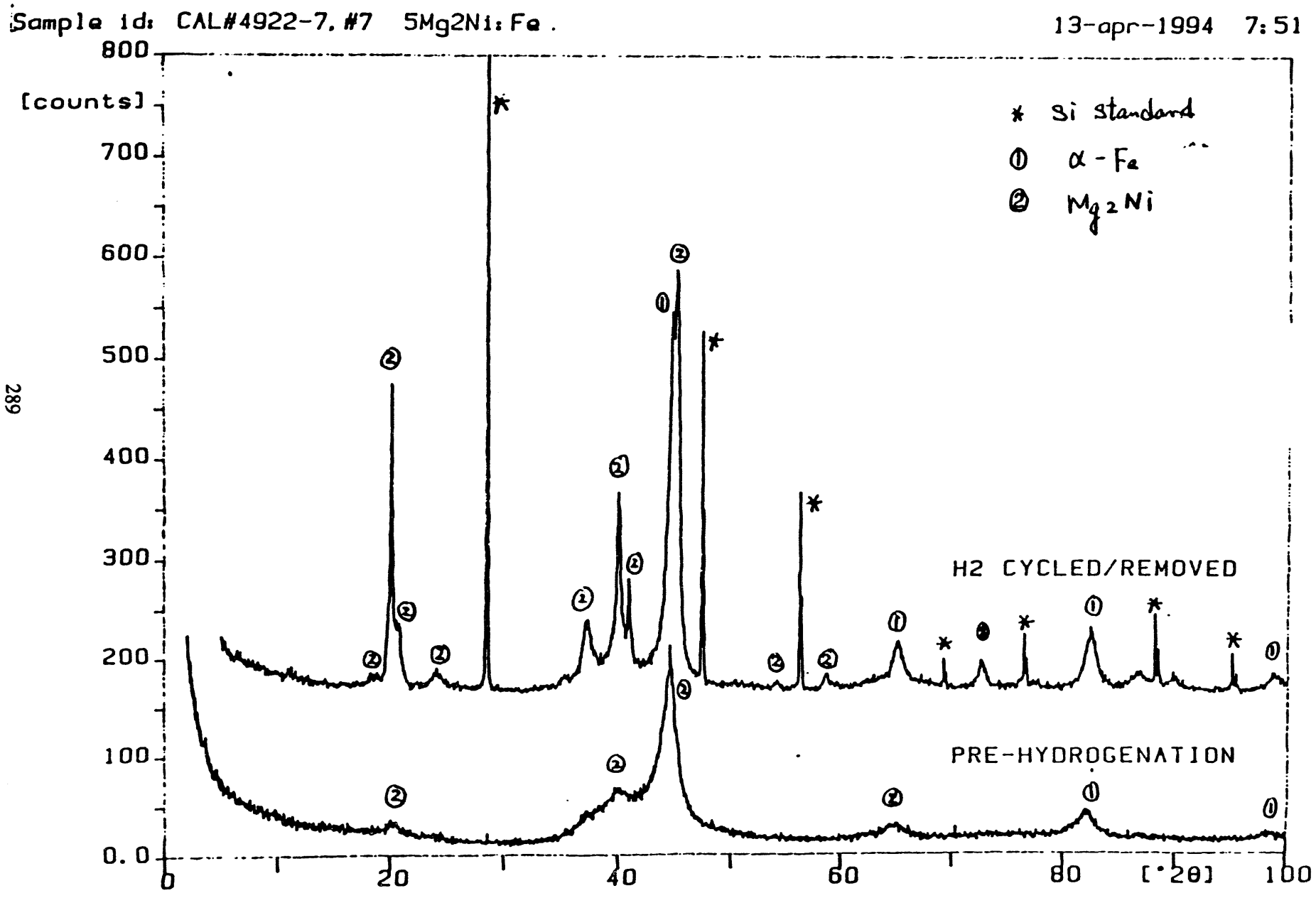

SOLAR THERMAL HYDROGEN

Kent Scholl and Clark Fields
National Renewable Energy Laboratory
Golden, CO 80401

Abstract

As the capital costs of high-temperature solar concentrators decrease, several processes utilizing this high-temperature heat become appropriate research areas. One of these is the production of hydrogen from direct thermal dissociation of water vapor. Water will thermally decompose into a mixture of H_2O, H_2, H, OH, O and O_2 when heated to sufficiently high temperatures; the extent of dissociation increases with increasing temperatures and decreasing pressures. Currently, the only practical energy source for the temperature range of interest (2000 -3000K) is concentrated solar thermal energy. The hydrogen formed at these temperatures must be separated from the other water decomposition products before recombination can occur. High thermal efficiencies are theoretically possible for an idealized process. The selection and development of a viable separation technique and the development of the requisite construction and separation materials are the most critical issues to be resolved in any water thermolysis process. The design of the thermal energy receiver will follow from the separation method selected. Capital costs of the required solar concentrator determine, to a large extent, the cost of the hydrogen produced. Once a viable separation technique is determined and a suitable solar energy plant designed, rigorous engineering and economic studies of the overall process will be needed in order to determine if a water thermolysis process is, in fact, a viable one. Since the end products are hydrogen and oxygen (or, hydrogen and oxygenated water), no hazardous chemicals or wastes are used or produced, and high system efficiencies appear feasible, direct thermal water splitting may represent an attractive path to renewable hydrogen energy. Other avenues of investigation are expected to emerge as the direct thermal dissociation process is examined. These include very-high-temperature steam electrolysis utilizing and extending technology being developed for high-temperature fuel cells and electrolyzers. Reactor systems that produce hydrogen and carbon from organic substances such as methane could be developed to capture and store the solar resource.

Introduction

The direct thermal dissociation process for the production of hydrogen from water (water thermolysis) has been promoted in the past as a potential method for the production of hydrogen from water (Bilgen and Bilgen, 1981; Fletcher and Moen, 1977; Ford, 1975; Ihara, 1980; Nakamura, 1977). All the heat and work flows necessary in the process can, in principle, be generated from the sun. No toxic chemicals are used; no CO_2 or hazardous wastes are produced. Process efficiencies can, theoretically, be quite high. The process has received little experimental attention primarily due to three issues:

1) cost of the solar thermal plants necessary to produce the high temperatures,

2) requisite materials to withstand the high temperatures,

3) an efficient, practical method to separate the products of water dissociation.

In the past few years, experimental advances have provided a new impetus to re-examine the direct thermal process. For example, the relatively new science of non-imaging optics and their application to solar concentrators has the potential to greatly reduce the cost of the highly-concentrating solar-thermal plants necessary to produce the high temperatures required (O'Gallagher, et al., 1993). Also, high-temperature materials that may have applications in the process have been developed and refined in other research areas, primarily the development of thin-film solid electrolytes for high-temperature fuel-cells and electrolyzers (van Dieten and Schoonman, 1992).

Separation Techniques

Several methods of preventing the recombination of the water dissociation products have been proposed and some have been tested. In general terms, the procedures fall into two separate categories. The first is those in which the dissociated water vapor is rapidly quenched to freeze in the high temperature chemistry; the hydrogen is then separated from the mixture at relatively low temperatures. Examples of these types of processes are found in the work of Lede, et al (1983) and Jellinek and Kachi (1984). The second category is those where oxygen and/or hydrogen are separated from the mixture at high temperatures. Fletcher and Moen (1977), Noring, et al (1981) and Cales and Baumard (1982), among others, have investigated these types of devices. These types of separation processes include jet separators, and porous and non-porous membranes.

Advanced solid electrolytes are being developed for high-temperature batteries, fuel cells and electrolyzers (Iwahara, 1992). Some of these may be applicable to the high-temperature separation of oxygen and hydrogen from dissociated water vapor.

Water-Splitting Thermodynamics

Figure 1 shows the equilibrium products of water decomposition at 1 atm total system pressure for the temperature range of 1000 to 4000K; these numbers were calculated using the NASA program CET-85 (Gordon and McBride, 1971). The extent of dissociation increases with decreasing pressure and increasing temperature. Although very little free hydrogen is evident at 1 atm until about 2000K, this does not necessary mean that little hydrogen can be produced at temperatures lower than this. Systems that continuously remove the evolved hydrogen and oxygen from the system can produce large amounts of

product gases (Ihara, 1979).

Following the work of Bilgen and Bilgen (1981), the efficiency, η_p, of a process that separates the dissociated water products and compresses them to atmospheric pressure can be defined as

$$\eta_p = \frac{\Delta H_f^\circ}{Q_{input} + W_s + W_c}.$$

Here, ΔH°_f is the standard enthalpy of formation of liquid water, Q_{input} is the total amount of thermal energy input, W_s is the work of separation, and W_c is the work required to pump the products isothermally to atmospheric pressure. Figure 2 shows Bilgen's results for system pressures of 0.1 and 1 bar. In this graph, the separation and compression work efficiencies are assumed equal to 1; the actual case will, therefore, display lower efficiencies at every temperature. Low efficiencies at the lower end of the temperature range shown in Figure 2 are primarily due to the large work inputs necessary to pump the low-pressure products up to atmospheric pressure.

Solar Collection Efficiency

The only practical source of energy available to produce the high temperatures necessary for efficient water thermolysis is concentrated solar energy. We can define solar collection efficiency as

$$\eta_{collection} = \frac{Q_{solar}}{IA} = \frac{\alpha \eta_{op} IC - \varepsilon \sigma T^4}{IC},$$

where Q_{solar} is the amount of solar energy collected, I is the normal solar intensity, A is the collection area normal to the sun, α is the target absorptivity, C is the concentration ratio (defined as A/a, where a is the area of the reradiating aperture), η_{op} is the optical efficiency of the concentrator, ε is the target emissivity, σ is the Stefan-Boltzman constant, and T is the temperature. Figure 3 is a plot of solar collection efficiency versus temperature at various concentration ratios. Note that in order to efficiently capture solar energy at high temperatures, concentration ratios >10,000 are necessary. As mentioned previously, the development of non-imaging, secondary concentrating devices may help lower the costs of solar plants that can achieve these types of concentrations.

Overall System Efficiency

The overall system efficiency is the product of the process efficiency and the solar collection efficiency. The result is plotted in Figure 4 for a system pressure of 1 bar as shown in Figure 2. These figures indicate that the process temperatures based on system efficiency should be around 2500K.

Approach

The research plan has been divided into three phases:

1) Phase I is Proof-of-Concept,

2) Phase II is the Resolution of Critical Issues and Detailed Design and Analysis,

3) Phase III is the Design and Construction of a Pilot Plant.

We anticipate completing Phase I at the end of FY94. We have initiated a literature review to document past analytical and experimental efforts and to determine current efforts into direct thermal water-splitting world-wide. We have also initiated a review of new materials that relate to the effort. Issues relating to the costs of solar thermal energy and the development of high-temperature materials are being addressed within other DOE programs. In Phase I of this research plan we are primarily interested in addressing the means of separating the products of water dissociation.

Results to Date

A preliminary economic analysis indicates that with the on-going advances in solar-thermal concentrators, high-temperature solar heat may cost on the order of $7/MBtu. Until an efficient separation scheme is identified, the actual cost of hydrogen produced in a direct thermal water-splitting system cannot be determined. However, a rudimentary analysis indicates that, with an efficiency of 25%, the process would produce hydrogen for around $30/MBtu.

Processes that do not recirculate water are, in theory, more efficient than those that remove the entire volume of water and dissociation products away from the hot zone; i.e., based on equilibrium water dissociation conditions, high-temperature membrane systems should be more efficient than quenching systems (Noring, et al, 1981). For this reason, the NREL staff is currently focusing on the development of a two-membrane water splitter. In this setup, the reactor contains two outlets, one for hydrogen and one for oxygen. We envision the use of solid-electrolytes for both outlet membranes. Literature reviews indicate that high-temperature hydrogen membrane materials are being developed, but none currently under investigation can withstand the very high temperatures required for water dissociation at or near 1 atmosphere (Iwahara, 1992). The hydrogen membrane will, therefore, need to be placed at some distance from the high-temperature zone. Oxygen removal will take place at the high temperature site.

A two-membrane reactor utilizing solid electrolytes, as described above, may be operated in several modes. Membranes based on ZrO_2 or other oxide ceramics will allow oxide ions to continuously flow through the material in response to an oxygen activity gradient (oxygen partial-pressure gradient). Thus the use of electrodes at the very high temperatures of the reactor may not be needed. It is also possible to electrically pump the oxygen and hydrogen through their respective membranes. Electrically pumping the product gases through the membrane should increase the separation efficiencies as compared to membranes with large pressure drops. Finally, by increasing the electrical potentials across the membranes, it becomes possible to electrolyze the water vapor to produce hydrogen and oxygen; these can then be pumped through the membranes. This may be the most straightforward way to decrease the temperatures and reduce the materials problems involved in the process.

During the course of our literature review, we located a small research organization in Richmond, CA which is involved primarily in the research and construction of renewable hydrogen energy systems. H-Ion Solar Co. is currently building and testing a novel water-splitting device that employs a nozzle and

skimmer (jet separation) to separate hydrogen from the other dissociation products. A zirconia-coated quartz nozzle is placed at the focal point of a parabolic reflector. A feed ring admits water vapor into the volume ahead of the nozzle and behind a quartz window. The water vapor is heated to high temperatures and accelerated to sonic velocities at the throat of the nozzle. At the outlet of the nozzle, a supersonic jet forms, with the lighter dissociation products - primarily H and H_2 - diffusing rapidly outward away from the central axis of the jet. The heavier dissociation products - H_2O, OH, O, and O_2 - remain along the central stream and are collected in a skimmer located very near the outlet of the nozzle. H-Ion uses a non-isothermal, low-pressure plasma (glow discharge) located between the feed ring and the zirconia nozzle to excite the water molecules and increase the amount of water dissociation beyond what an equilibrium calculation would predict. The amount of electrical energy needed to maintain this glow discharge is less than 1% of the solar input to the process. By operating their system under non-equilibrium conditions, it is very possible that they can produce hydrogen at lower temperatures and at greater overall efficiencies than an equilibrium analysis would indicate. We have arranged for H-Ion to produce a document that explains their process and experimental results in detail.

Future Work

Our immediate need is a thermodynamic model of a two-membrane system that effectively captures all the various parameters of the process. This effort is currently underway. A parallel effort will be the design, construction and testing of a small-scale water-splitting device at NREL's High-Flux Solar Furnace. The experimental results will be used to validate the model. The model will then be used to determine the performance of an optimized system designed on state-of-the-art and future developments.

A close analysis of H-Ion Solar Corp.'s process will be made following the completion of their report to NREL. By operating under non-equilibrium conditions, their process may prove to be feasible at temperatures several hundreds of degrees lower than those temperatures at which a two-membrane system might operate efficiently.

Direct thermal water splitting is the first application of high-temperature solar heat that we have chosen to analyze. Very-high-temperature water electrolysis is another process that is a direct extension of the current work. Another process that may be worthy of consideration is the thermal dissociation of methane to produce hydrogen and carbon as solar energy storage mediums.

References

Bilgen, C., and Bilgen, E. 1981. "Solar Synthetic Fuel Production." *Int. J. Hydrogen Energy*, 6:349-362.

Cales, C. and Baumard, J.F. 1982. "Production of Hydrogen by Direct Thermal Decomposition of Water with the Aid of a Semipermeable Membrane." *High-Temperatures - High Pressures*, 14:681-686.

Fletcher, E.A., and Moen, R.L. 1977. "Hydrogen and Oxygen from Water." *Science*, 197:1050-1056.

Ford, N.C. 1975. "Analysis of a System to Thermally Dissociate Water Using a Semi-Permeable Membrane." ANL-75-65.

Gordon, S. and McBride, B.J. 1971. "Computer Program for Calculation of Complex Chemical Equilibrium Compositions, Rocket Performance, Incident and Reflected Shocks, and Chapman-Jouguet Detonations." NASA SP-273, NASA, Washington D.C.

Ihara, S. 1979. *Solar Hydrogen Energy Systems.* T. Ohta, ed. Oxford: Pergamon Press. 59-79.

Ihara, S. 1980. "On the Study of Hydrogen Production from Water Using Solar Thermal Energy." *Int. J. Hydrogen Energy*, 5:527-534.

Iwahara, H. 1992. *Chemistry of Solid State Materials 2: Proton Conductors.* P. Colomban, ed. Cambridge University Press. 511-522.

Nakamura, T. 1977. "Hydrogen Production from Water Utilizing Solar Heat at High Temperatures." *Solar Energy*, 19:467-475.

Noring, J.E., Diver, R.B. and Fletcher, E.A. 1981. "Hydrogen and Oxygen from Water - V. The ROC System." *Energy*, 6:109-121.

O'Gallagher, J.J., Winston, R. and Lewandowski, A. 1993. "The Development of Two-Stage Nonimaging Concentrators for Solar Thermal Applications." In *Proceedings of the ASES Solar 93 Conference*, Washington, D.C.

van Dieten, V.E.J., and Schoonman, J. 1992. "Thin Film Techniques for Solid Oxide Fuels Cells." *Solid State Ionics*, 57:141-145.

Figure Captions

Figure 1: Equilibrium water and dissociation products at 1 atm total pressure.

Figure 2: Process efficiency of an idealized water-splitter, (Bilgen and Bilgen, 1981).

Figure 3: Solar collection efficiency at various levels of solar concentration.

Figure 4: Overall system efficiency of the idealized water splitting device at various levels of solar concentration.

Figure 1

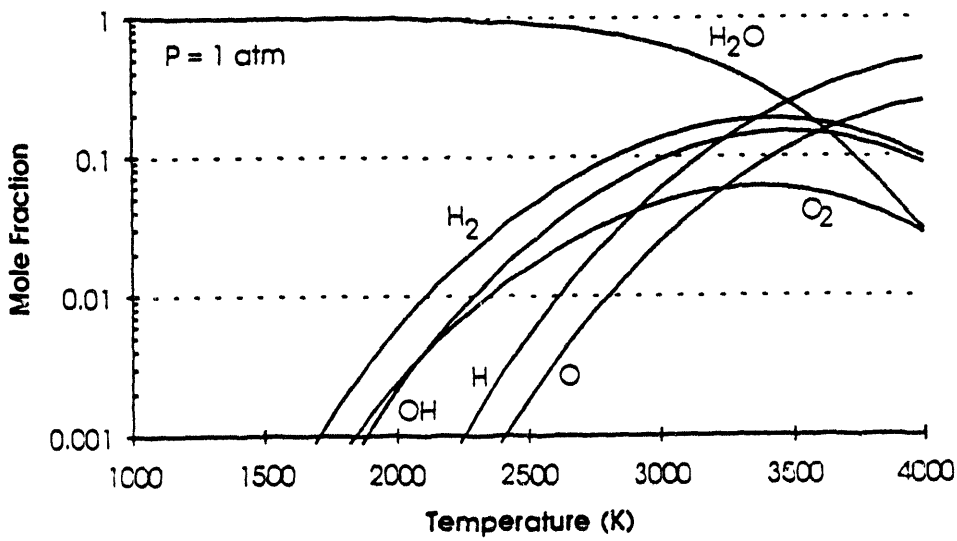

Figure 2

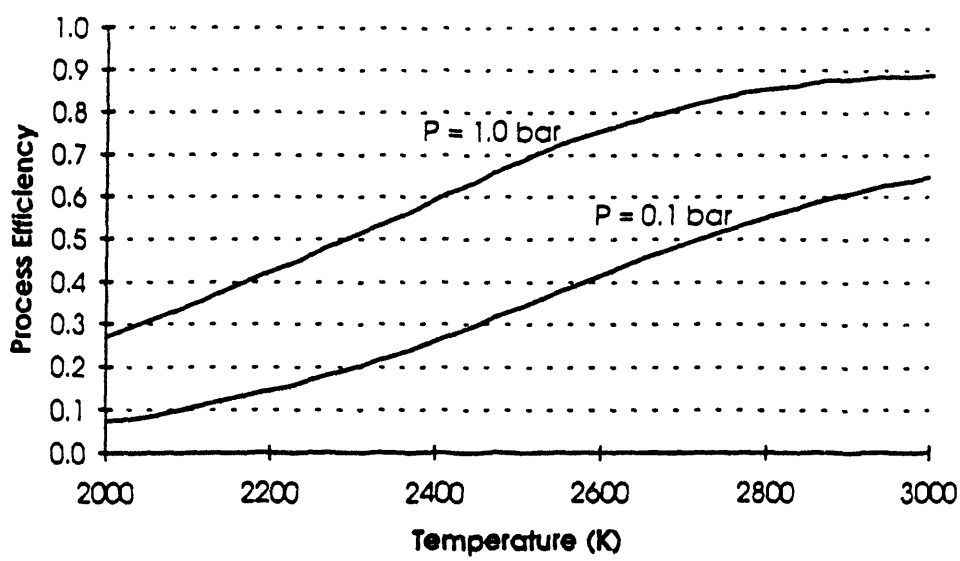

Figure 3

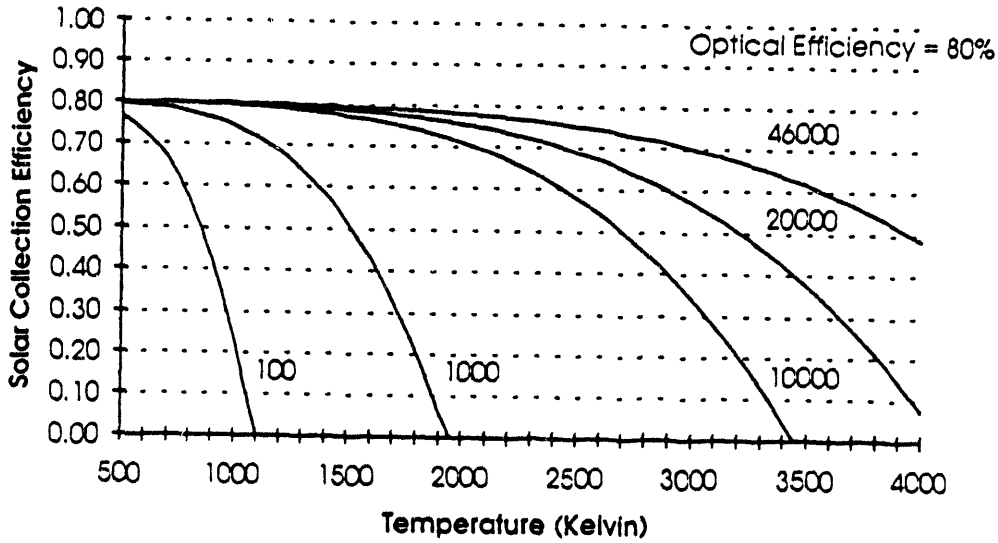

Figure 4

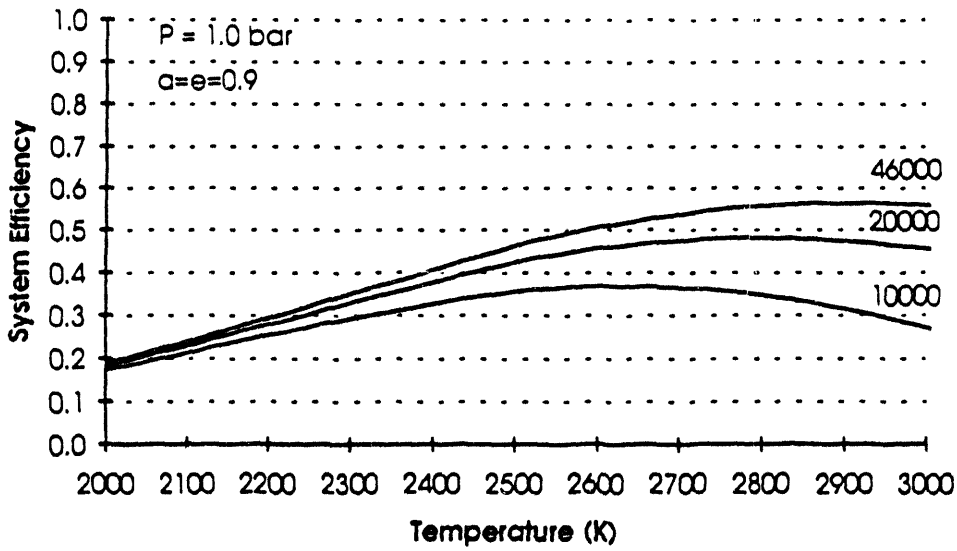

PHOTOELECTROCHEMICAL BASED DIRECT CONVERSION SYSTEMS

Shyam Kocha, Mark Peterson, Hikmat Hilal, Doug Arent, and John A. Turner
National Renewable Energy Laboratory
Golden, CO 80401-3393

Abstract

The goal of this research is to develop a stable, cost effective, photoelectrochemical based system that will split water directly upon illumination producing hydrogen and oxygen. This type of direct conversion system combines a photovoltaic material and an electrolyzer into a single monolithic device. We report on the ternary semiconductor $Ga_{0.5}In_{0.5}P$ (hereafter, $GaInP_2$), studied in two configurations: (i) as a single crystal electrode in contact with various aqueous electrolyte solutions and (ii) as one component of a multijunction multiphoton tandem photoelectrochemical device. We also report on our work in developing synthetic techniques for the attachment of transition metal complexes to semiconductor electrodes directed at forming highly catalytic and stable surfaces.

Introduction

Photoelectrolysis is the process whereby sunlight, illuminating a semiconductor, is used to split water into hydrogen and oxygen. The incident light, absorbed in a semiconductor electrode, splits water directly. A one-step monolithic system such as this eliminates the need to generate electricity externally and subsequently feed it to an electrolyzer. This configuration requires only the piping necessary for the transport of hydrogen to an external storage system or gas pipeline.

For a one-step process to be viable, the light harvesting system must generate sufficient voltage to effect the decomposition of water, and the system must be stable in an aqueous environment. Splitting water into hydrogen and oxygen requires a thermodynamic potential of 1.23 eV at 25 °C. Typical values of the overvoltage for the cathode (hydrogen evolving) and anode (oxygen evolving) reactions are 100 mV and 250 mV respectively. A potential then, of at least 1.6 eV, is required for a water splitting system.

For a single gap semiconductor based direct conversion water splitting system, the fundamental requirement of at least 1.6 eV implies a minimum bandgap of 1.6 electron volts. Surface catalysts would also be required in order to bring the overvoltage for the oxygen and hydrogen evolution reactions down to acceptable levels. An additional requirement is that the semiconductor band edges span both redox potentials of the hydrogen and oxygen evolution reactions.

Tandem cell technology connects photovoltaic layers (pn junctions) with different semiconductor bandgaps in series, one behind the other, in a single monolithic cascade device. This configuration offers a greater utilization of the solar spectra, resulting in higher solar conversion efficiencies. The monolithic structure also minimizes the amount of active area needed for specific power applications. The National Renewable Energy Laboratory currently is developing in house, a tandem cell consisting of a GaAs back cell and a $GaInP_2$ front cell. This system has shown solar to electrical conversion efficiencies of up to 29.5% and open circuit voltages of up to 2.3 volts(1). If the band edge potentials at the semiconductor-electrolyte interphase are favorable and a sufficient photovoltage generated then a configuration using the tandem device immersed in an aqueous electrolyte (photoelectrochemical mode) should not require any external electrical bias to electrolyze water.

Technology Description

Figure 1 gives the energetic picture for a semiconductor electrode. Hydrogen is produced at the surface of an illuminated p-type semiconductor; oxygen is produced at the surface of an illuminated n-type semiconductor. This occurs due to injection of electrons into the solution (for p-type) or because holes (e.g., electron vacancies) appear at the semiconductor/electrolyte interface (for n-type). Photo-generated holes can be considered strong oxidizing agents and may oxidize the semiconductor itself, causing decomposition. Stability then depends on the competition between semiconductor decomposition and possible redox reactions in the electrolyte. The most stable situation is the p-type semiconductor where electron flow is directed towards the illuminated side effecting the evolution of hydrogen. Oxygen evolution, therefore, is a less desirable situation. Catalysts speed up the redox reactions and improve the stability of the semiconductor.

The nature and coverage of the catalyst are critical for an optimized direct water-splitting system. Catalyst coverage must be sufficient to both protect the semiconductor from undesirable side reactions (corrosion) and provide sufficient catalytic activity to handle the current flux. Transparency of the catalyst is also essential so as to minimize light losses. The type of catalyst needed depends on whether oxygen or hydrogen is being generated at the illuminated surface of the electrode. The best catalyst for oxygen

evolution is ruthenium dioxide, for hydrogen evolution it is platinum.

Discussion

Gallium Indium Phosphide Studies

Our investigations have shown that while the bandgap of $GaInP_2$ (1.8–1.9 eV) is optimum for water electrolysis, the bandedges are 300–400 mV too negative and therefore do not straddle the hydrogen and oxygen redox levels. Part of our work is directed at modifying the surface of $GaInP_2$ in order to produce a energetically more favorable band edges. We have shown that some surface treatments are beneficial in improving the energetics. For example, the treatment of the surface with 8-hydroxyquinoline shifts the band edges positive, although not sufficient to effect water splitting. Understanding and controlling the nature and type of the surface species of $GaInP_2$ is important in order to be able to apply a good surface coat of colloid or to be able to do surface modification. We have investigated various wet chemical etching processes to see their effect on luminescence intensity, luminescence lifetime and capacitance (Mott-Schottky) data. The magnitude of the photoluminescence (PL) peak intensity and the photoluminescence lifetime can be used as an indicator of the non-radiative surface recombination rate. A low surface recombination rate indicates a good surface and typically results in higher efficiencies and faster charge transfer rates. Capacitance data is used to measure the energetic position of the band edges. Any displacement of the flat-band potential produced by etching or caused by a change in the surface composition or surface alloy ratio is determined by capacitance measurements.

The etching solutions used are presented in Table 1. Before and after etching, the samples were rinsed in acetone, ethyl alcohol, and deionized water and dried in a stream of nitrogen gas.

Table 1: Composition of etching solutions

Etch #	Composition
1	conc. H_2SO_4 (SUL)
2	1:20:1 HCl :CH_3COOH: H_2O_2 (EA)
3	1:20:1 HCl :H_3PO_4: H_2O_2 (EP)
4	conc HNO_3 (HN)
5	1:3:1 HNO_3:HCl:H_2O (Aqua)
6	1M KOH + 1.0M $K_3[Fe(CN)_6]$ (EF)

The samples obtained from the MOCVD reactor had a grayish mirror finish prior to surface treatment. The surface as observed under a Nomarsky microscope showed no deterioration with most etching treatments, which concurs with the results of Flemish et al. (2). Etching with nitric acid, which is a very strong oxidizing agent, resulted in mild bubbling, although the resulting surface remained relatively smooth and pit free. Copious bubble evolution from the surface was observed for a 5–10 s aqua regia etch resulting in uneven removal of material and the formation of striations on the resulting sample surface.

The etch (EF) 1M KOH + 1.0 M $K_3[Fe(CN)_6]$ was used only as a representative of a basic etch and did not produce significant results in any of the studies and hence is not reported on in detail. It should be noted that sulfates, chlorides and nitrates of both gallium and indium [e.g., $Ga(NO_3)_3.xH_2O$, $In(NO_3)_3.3H_2O$, $GaCl_3$, $InCl_3$, $Ga_2(SO_4)_3$, $In_2(SO_4)_3$] are soluble in cold water (3) and are expected to be removed from the surface leaving little, if any, residue. On the other hand, oxides of gallium and indium, $Ga(OH)_3$, amorphous GaOOH, Ga_2O_3, $Ga_2O_3.H_2O$, $In(OH)_3$, In_2O_3, InO are insoluble (3,4). Also, the ferrocyanides of gallium and indium are soluble in alkaline solutions but precipitate in acidic solutions. The etch rate for most of the etches was about 0.1 mm/min. as reported in literature (2,5).

The samples were etched in each of the above-mentioned etchants for different periods of time and the PL intensity monitored. A higher PL intensity is indicative of a superior surface (lower number of surface states). The minimum etching time required to increase (or decrease) the PL to its highest (lowest) possible value was determined. Figure 2 shows the gradual increase of PL intensity for a sample etched in concentrated sulfuric acid with time. After 2 min. of etching, no further increase in PL was detected. Similar experiments carried out with the other etchants resulted in the determination of optimum times of 20–25 s for etch EA and EP and 5–10 s for etches HN, Aqua, and EF. Using these optimum etch times, the PL spectra before and after different etches were obtained. Figure 3 shows an increase in PL for etches EP and EA as a result of etching. We observed that the maximum PL after etching was obtained for the sulfuric acid etch and the lowest for conc. HNO_3. The HNO_3 etch did not raise or lower the PL intensity considerably compared to an as grown sample. The sample was therefore first etched with the EA etch and subsequently etched with HNO_3. A clear decrease in the PL intensity was observed (Figure 4) indicating the possible formation of a surface oxide layer; which was confirmed later with XPS analysis. Based on the enhancement of steady state PL intensity, concentrated sulfuric acid provides the best surface, with other etches following in the order 1>2>3>4>5>6 for all samples. This trend in PL intensities was observed for samples of all the misorientations.

TRPL decays carried out in air are plotted in Figure 5 for various etched surfaces. We observe an increase in the carrier lifetime as manifested in the decay profiles. The concentrated sulfuric acid etch showed an increase in magnitude of the average decay time by a factor of four. This increase in lifetime correlates with the increase in steady state PL intensity again indicating that the SUL etchant effectively removes non-radiative recombination oxide sites.

A study was also conducted to inquire into the period of time for which the enhanced PL intensity was maintained. Figure 6 shows steady state PL measurements before and after a conc. sulfuric acid etch followed by exposure to ambient air. The PL intensity was found to stay at its enhanced value after etch for two days air exposure following which the PL fell to the value shown in Figure 6 after 10 days exposure. Beyond that 10 days of air exposure, the PL did not drop any further towards its initial value before the etch. We speculate that this is possibly due to the formation of a somewhat more uniform and defect-free surface oxide film on exposure of the etched surface to air. In addition, it should also be noted that the decay times decrease much less rapidly with exposure to air than the PL peak intensity. Although the surface is cleaned and oxide films removed, the surface is not passivated by the etches as indicated by a drop in the PL with time on exposure to air. Subsequent treatment with 8-hydroxyquinoline was found to stabilize of the PL intensity, effectively protecting the surface. This etching study shows the importance of cleaning the surface and removing recombination centers prior to any passivating surface treatment for either solid-state purposes or photoelectrochemistry.

The energetic position of semiconductor band edges are very sensitive to the charge of the ions at the electrode/electrolyte interphase. We have proposed that it is possible to shift the energetic position of the band edges by covalently attaching charged species to the surface. A positively charged ion would shift the band edges positive, likewise a negatively charged species would shift the band edges negative. We

now have evidence to show that covalent attachment of positive charged species will shift the band edges to positive potentials. Because of the scarcity of $GaInP_2$ samples, this initial work was done using n-GaAs. The surface of the GaAs was modified with tetra(-4-pyridyl)prophyrinatomaganese(III) using 3-chloropropyltrimethoxysilane as a coupling agent. The onset of photocurrent for the derivatized electrode was shifted positively by up to 180 mV with respect to the unmodified electrode. Capacity measurements confirm a positive voltage shift of 190 mV (Figure 7), in good agreement with the photocurrent data. Since the GaAs surfaces are similar to the $GaInP_2$, we expect that this work will directly transfer to $GaInP_2$.

Tandem Cell Studies

Our studies of the tandem cell systems have focused on increasing the efficiency for water splitting, improving the lifetime, and studying the phenomena of the co-evolution of hydrogen and oxygen at the illuminated electrode surface. In our initial work on the tandem cells, it was assumed that hydrogen would be evolved from the illuminated solution side and oxygen would be evolved from the backside of the electrode. Correspondingly, we modified the front surface with platinum catalysts, as platinum is the best catalyst for hydrogen evolution. However, with the discovery that oxygen and hydrogen are simultaneously evolved, we have determined that ruthenium dioxide provides the best stability for these systems.

Following the work of McMurray (6) we have prepared RuO_2 colloids starting with RuO_4. The resulting RuO_2 colloids readily adsorb to the surface of the tandem cells. The time required for appearance of a visible coat depends on the concentration of the colloid solution. This time ranges from overnight for a concentrated sol to one week for a dilute sol. The coating appear to be very stable in concentrated sulfuric acid, phosphoric acid and 1M sodium hydroxide. Further, the RuO_2 treated tandem cells will split water in 1M NaOH, something the platinum coated electrodes could not do. This is significant in that the overvoltage for the oxygen evolution reaction is much lower in concentrated base.

The lifetime of the platinum colloid treated tandem cells for oxygen production is typically less than 10 hours. After that the oxygen evolution decreases and the surface begins to show significant corrosion. On the other hand, some ruthenium dioxide treated electrodes have run for two weeks with no obvious degradation of the oxygen response. This is a major advance in the stability of these systems. The RuO_2 treated electrodes also show increased efficiency; two different tandem cell samples have shown a water splitting efficiency of greater than 10%.

We have continued to study the process whereby the tandem cells evolve oxygen and hydrogen simultaneously from the same surface. Tandem cells were mounted as photoelectrochemical cells (a wire connected to the back of the sample, insulated and sealed with epoxy). The samples were then connected to a platinum counter electrode externally through a digital oscilloscope and illuminated using a shutter. If the tandem cell worked as expected, then one would anticipate electrons flowing from the platinum counter electrode to the tandem cell, effecting oxygen evolution at the platinum electrode and hydrogen evolution at the surface of the tandem cell. However, transient photocurrents were observed with the current initially flowing in the correct direction and then decaying away within a few milliseconds (Figure 8). This indicates that an electric field is somehow built up within the tandem cell device itself. This electric field then act as a barrier for the holes and they subsequently end up at the electrode's surface. We will continue to study different tandem cell configurations to try and determine the cause of this effect.

One of the interesting possibilities for using the tandem cell phenomena of producing hydrogen and oxygen on the same surface is the splitting of water in the vapor phase at relatively low temperatures (<200 °C.) This is of interest because it typically requires very high temperatures (>>1000 °C) to split water thermally or complicated thermal cycles at lower temperatures. Low temperature gas phase water

splitting would also reduce or eliminate many of the corrosion problems found in solution reactions.

NREL has a molecular beam mass spectroscopy system connected to a gas phase photoreactor. This photoreactor is used to study photodegradation processes for pollution abatement schemes. We have completed some initial experiments to determine if their system can detect the low levels of hydrogen and oxygen produced. Our attempts to use room temperature water saturated helium as the source of water failed, likely due to the amount of evolved gases falling below the detection limit of their system. However, the mass spectrometer was able to detect significant hydrogen flow from an illuminated tandem cell submerged to a depth of 1 mm in 1M sodium hydroxide. An estimate of the conversion efficiency based on this flow was found to be 10.4%, further confirming the high efficiency of these devices. The mass spectrometer was not calibrated for oxygen but its profile followed that of hydrogen. We hope to repeat this experiment using steam as the source of water.

Conclusions

One of the goals of this research is to improve the stability and efficiency of the tandem cell water splitting system. This has been accomplished. Another goal is to show that covalent attachment of positively charged species would shift the band edges to positive potentials. This also has been accomplished.

Future Work

We plan to investigate new tandem cell structures and catalytic coatings for increased efficiency and proper operation (separated oxygen and hydrogen evolution reactions). We intend to explore new semiconducting materials and design semiconductor systems specifically for water splitting. We will also continue to work on the surface modification of $GaInP_2$ focusing on its application as a single bandgap water splitting system.

Acknowledgments

The XPS work was performed by Art Nelson. We thank Art Frank for helpful discussions and guidance on surface modification techniques. Part of H.S.H. funding is from a merit scholarship from the Islamic Development Bank.

References

(1) Olson, J.M.; Kurtz, S. R.; Kibbler, A. E.; and Faine, P. *Appl. Phys. Lett.*,**1990,** *56*, 623
(2) Flemish, J. R.; Jones, K. A. *J. Electrochem. Soc.*, **1993**, *140*, 844.
(3) *CRC Handbook of Chemistry and Physics*, 74th edition, **1993-1994,** CRC Press, David R Lide, Editor in Chief.
(4) Kolthoff, I. M.; Sandell, E. B.; Meehan, E. J.; Bruckenstein, S. *Quantitative Chemical Analysis*; 4th ed, **1969,** The Macmillan Company: London, Chapter 12.
(5) Lothian, J. R.; Kuo, J. M.; Hobson, W. S.; Lane, E.; Ren, F.; Pearton, S. J. *J. Vac. Sci. Technol. B* **1992**, *10 (3)*, 1061.
(6) McMurray ;J. Phys. Chem., **1993,** *97*, 8039.

Figure Captions

Figure 1 The energetics of liquid junctions formed by p- and n-type semiconductors immersed in aqueous electrolytes.

Figure 2 Photoluminescence spectra of $GaInP_2$ before and after etching in concentrated H_2SO_4 for 30, 60, 90, and 120 seconds.

Figure 3 Photoluminescence spectra of $GaInP_2$ before and after etch (EA) 1:20:1 HCl :CH_3COOH: H_2O_2 and etch (EP) 1:20:1 HCl :H_3PO_4: H_2O_2 for 20 seconds.

Figure 4 Photoluminescence spectra of $GaInP_2$ before and after etch (EA) 1:20:1 HCl :CH_3COOH: H_2O_2 prior to an etch in HNO_3.

Figure 5 Time resolved photoluminescence spectrum of $GaInP_2$ samples before and after etchents EA, EP and SUL.

Figure 6 Photoluminescence spectra of $GaInP_2$ before and after etch in concentrated H_2SO_4 and after 10 days exposure to air.

Figure 7 Mott-Schottky data for n-GaAs, **G** -- as etched, **J** -- after the coupling agent, and **C** -- after modification with Mn (TPyP).

Figure 8 Transient photoresponse of tandem cell.

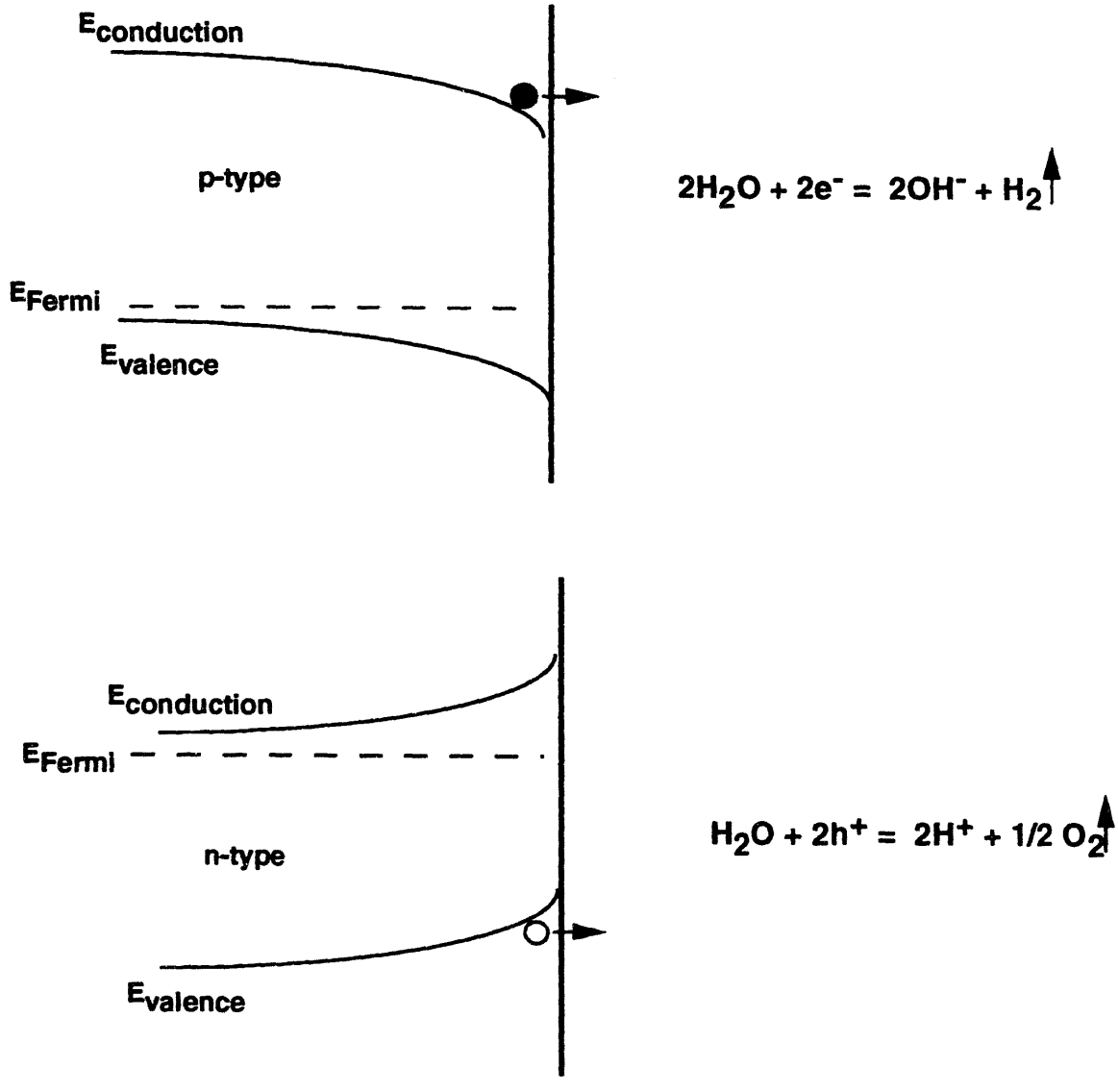
E conduction
p-type
E Fermi
E valence
2H2O + 2e- = 2OH- + H2
E conduction
E Fermi
n-type
E valence
H2O + 2h+ = 2H+ + 1/2 O2

FIGURE 1

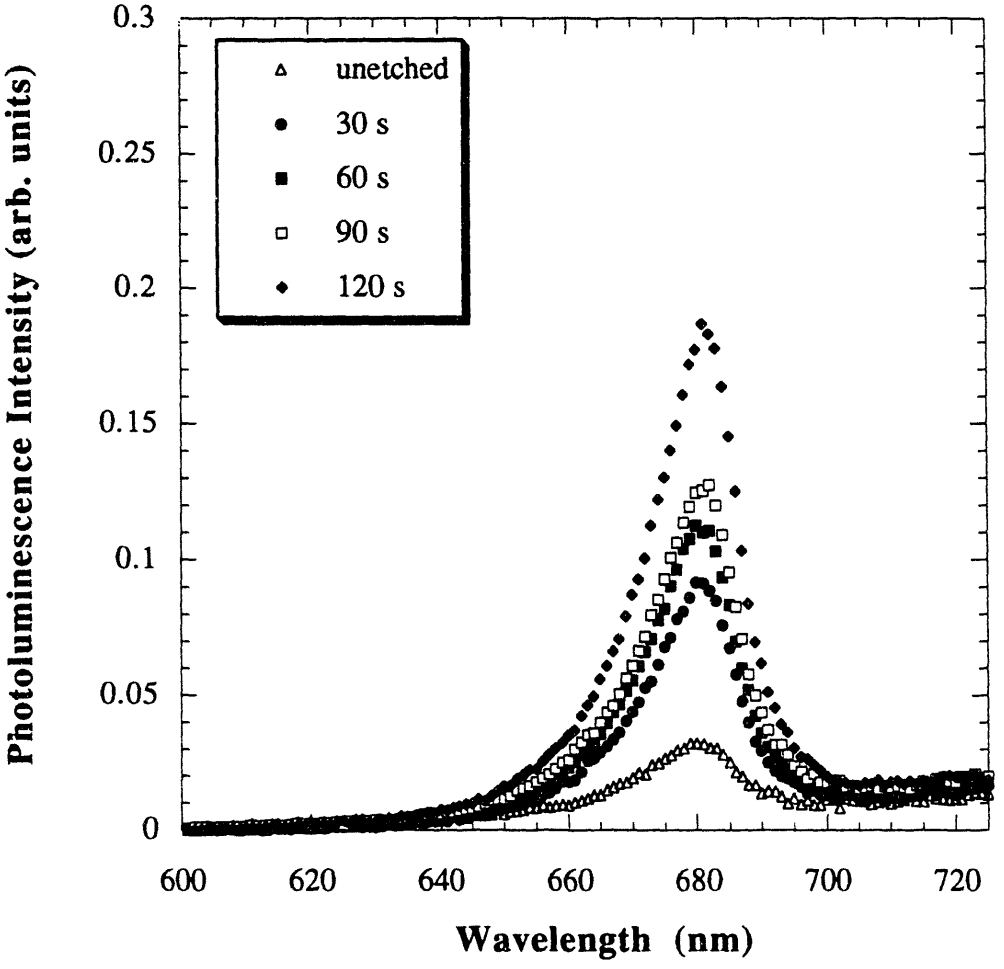
Photoluminescence Intensity (arb. units)
0.3
0.25
0.2
0.15
0.1
0.05
0
600
620
640
660
680
700
720
Wavelength (nm)
unetched
30 s
60 s
90 s
120 s

FIGURE 2

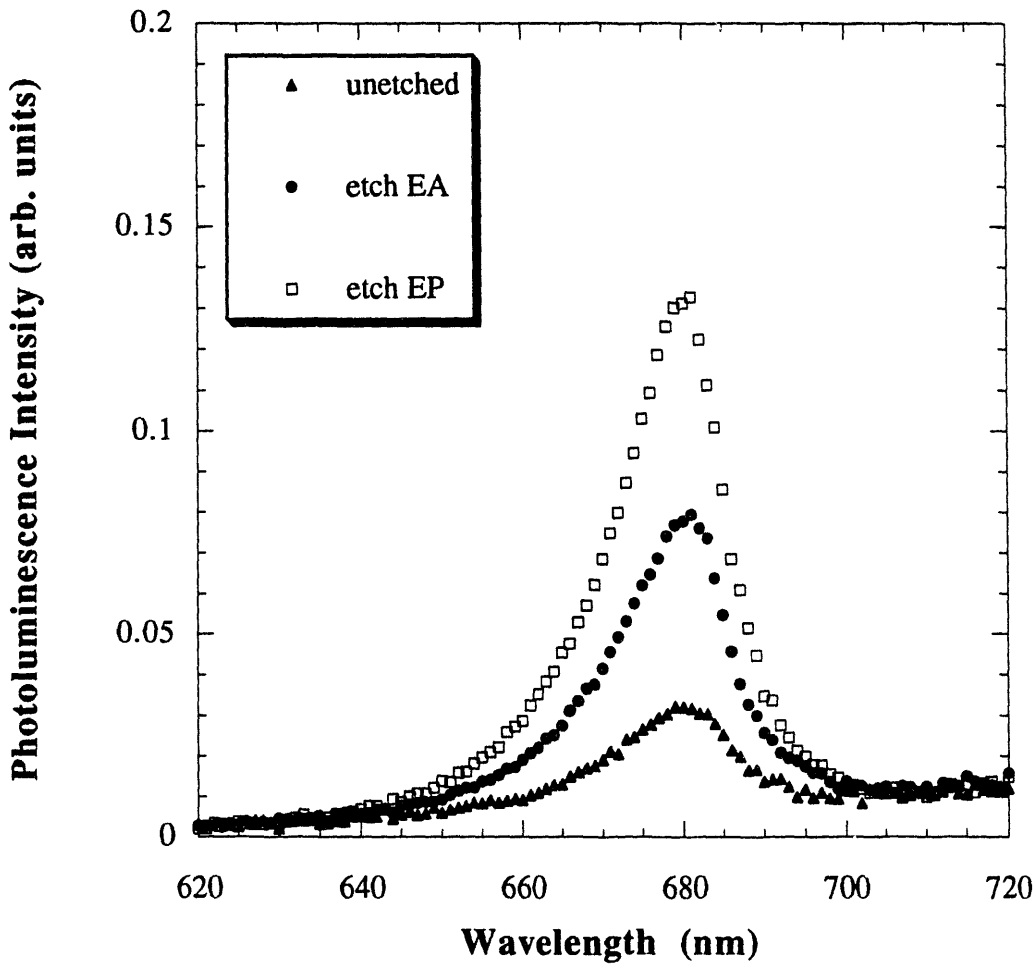
0.2
0.15
0.1
0.05
0
620
640
660
680
700
720
unetched
etch EA
etch EP
Photoluminescence Intensity (arb. units)
Wavelength (nm)

FIGURE 3

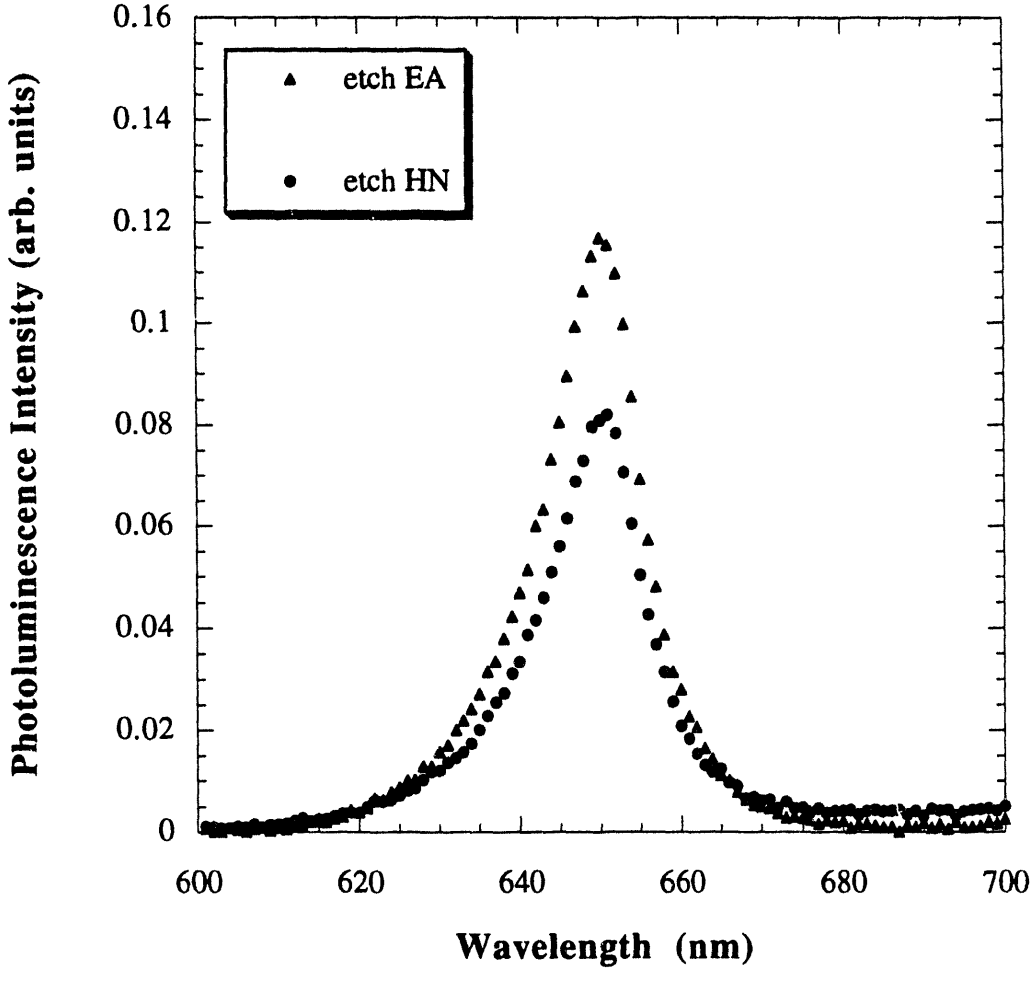
0.16
0.14
0.12
0.1
0.08
0.06
0.04
0.02
0
600
620
640
660
680
700
etch EA
etch HN
Photoluminescence Intensity (arb. units)
Wavelength (nm)

FIGURE 4

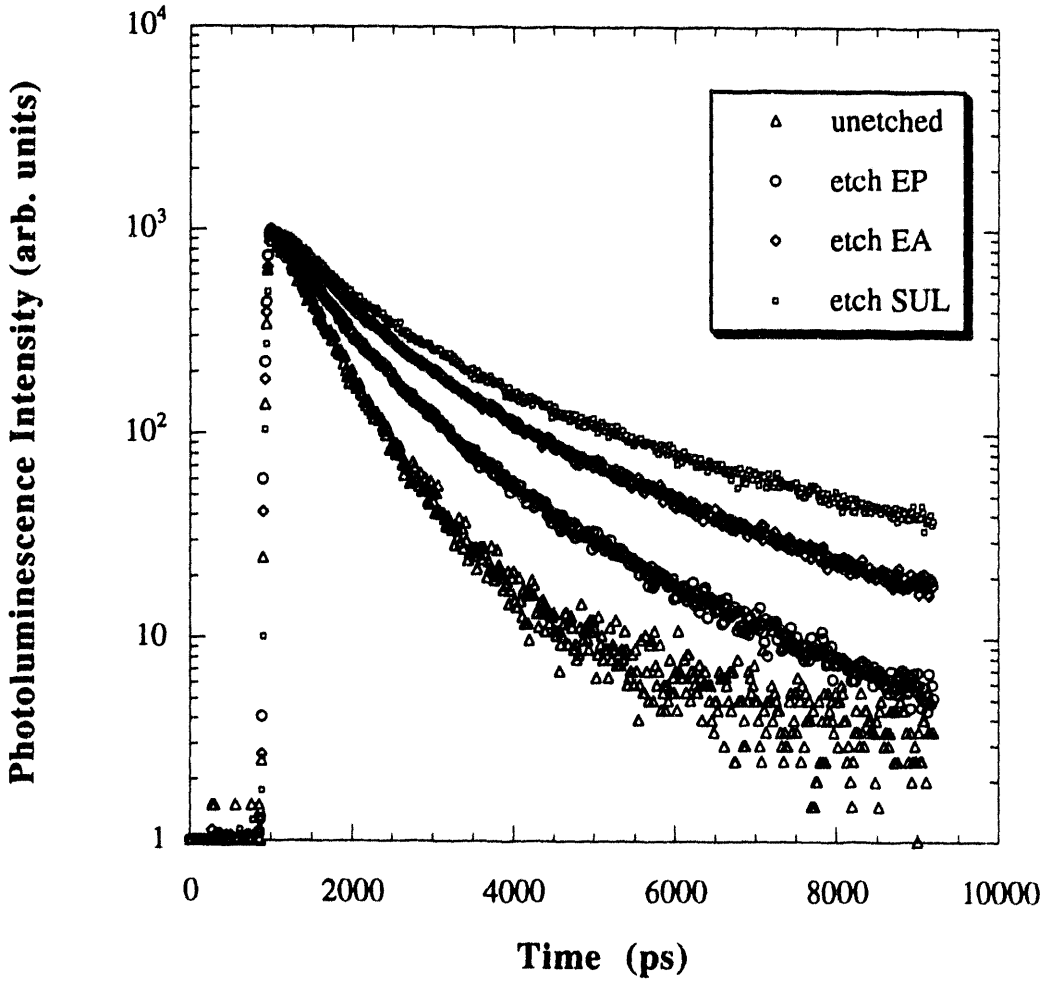
Photoluminescence Intensity (arb. units)
10^4
10^3
10^2
10
1
0
2000
4000
6000
8000
10000
Time (ps)
unetched
etch EP
etch EA
etch SUL

FIGURE 5

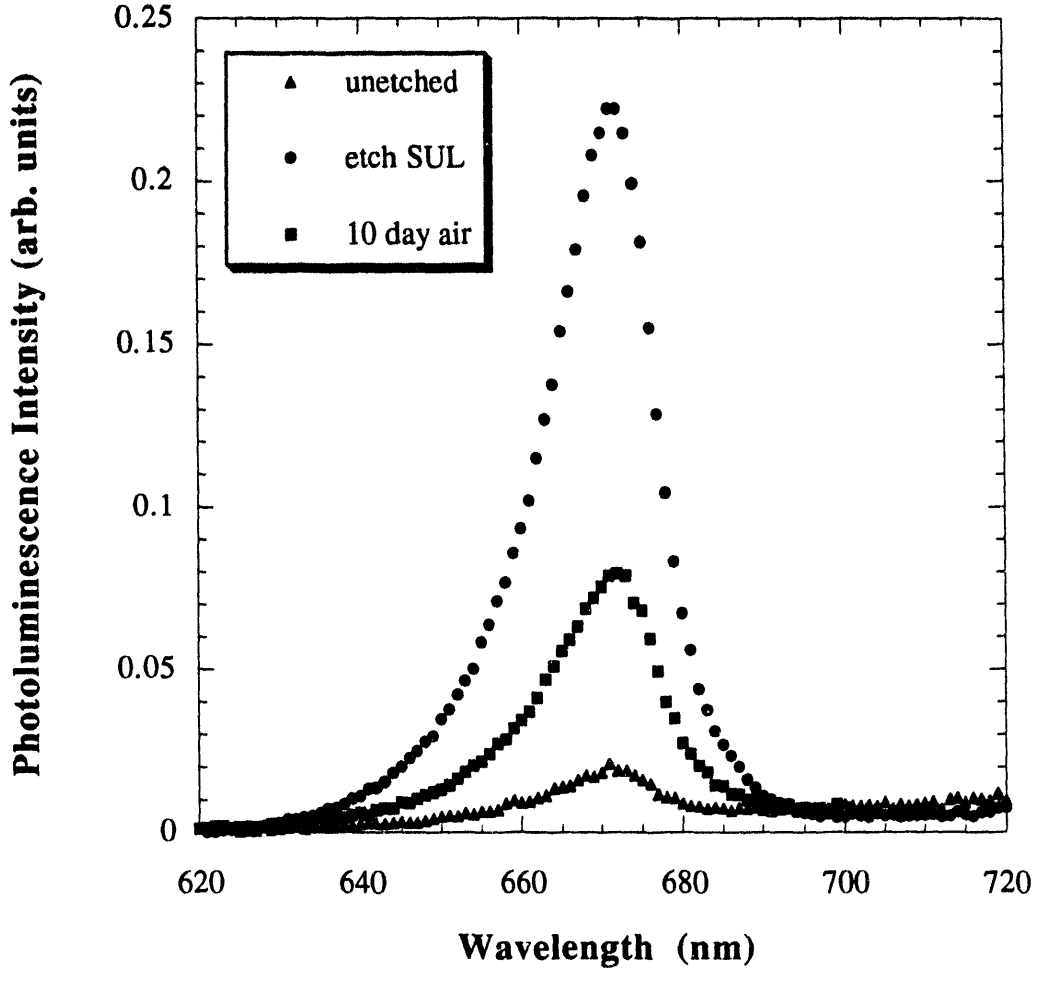
0.25
0.2
0.15
0.1
0.05
0
620
640
660
680
700
720
unetched
etch SUL
10 day air
Photoluminescence Intensity (arb. units)
Wavelength (nm)

FIGURE 6

FIGURE 7

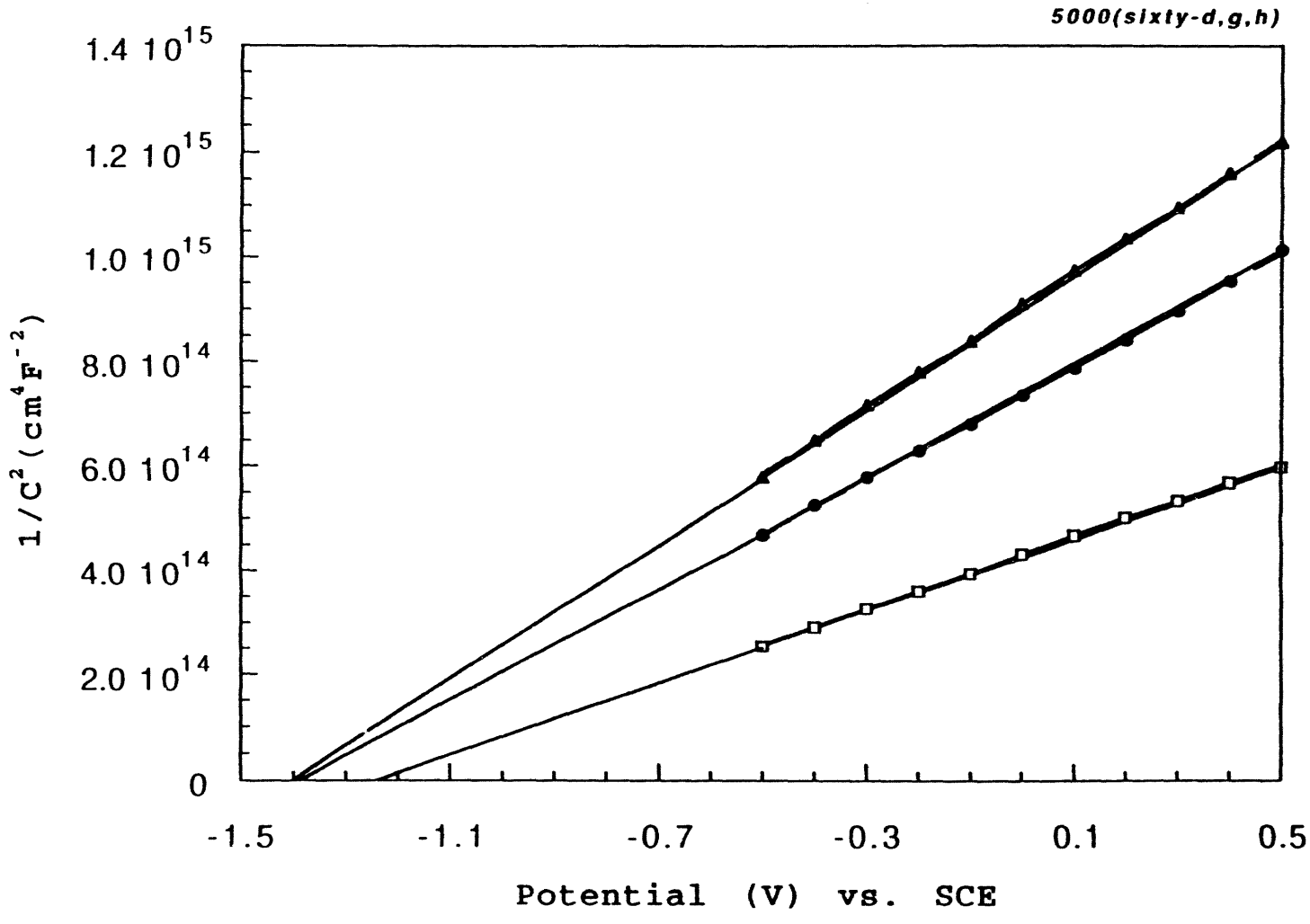
5000(sixty-d,g,h)
1.4 10^15
1.2 10^15
1.0 10^15
8.0 10^14
6.0 10^14
4.0 10^14
2.0 10^14
0
1/C^2 (cm^4F^-2)
-1.5
-1.1
-0.7
-0.3
0.1
0.5
Potential (V) vs. SCE

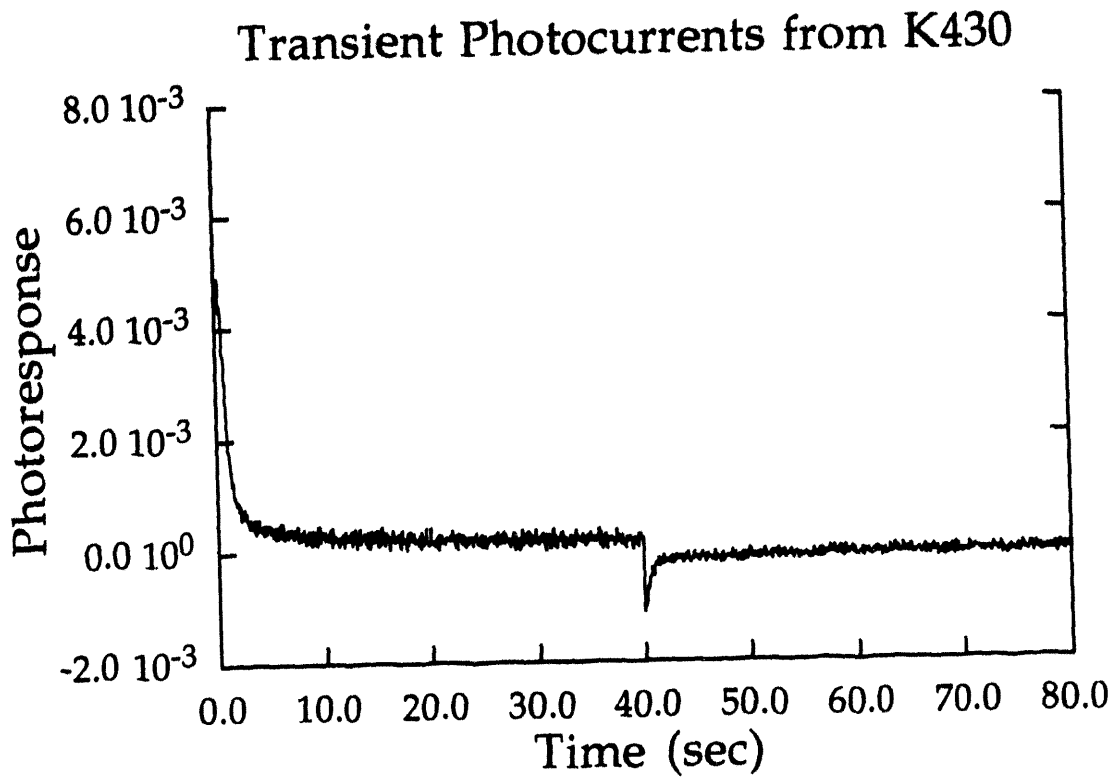
Transient Photocurrents from K430
Photoresponse
8.0 10-3
6.0 10-3
4.0 10-3
2.0 10-3
0.0 100
-2.0 10-3
0.0
10.0
20.0
30.0
40.0
50.0
60.0
70.0
80.0
Time (sec)

FIGURE 8

HYDROGEN PRODUCTION BY PHOTOSYNTHETIC WATER SPLITTING

Elias Greenbaum
Chemical Technology Division
Oak Ridge National Laboratory
Oak Ridge, TN 37831-6194

Abstract

The objective of this mission-oriented research program is the production of renewable hydrogen. This program will build upon promising results that have been obtained in the Chemical Technology Division of Oak Ridge National Laboratory on the utilization of intact microalgae for photosynthetic water splitting. In this process, specially adapted algae are used to perform the light-activated cleavage of water into its elemental constituents, molecular hydrogen and oxygen.

The great potential of hydrogen production by microalgal water splitting is predicated on quantitative measurement of their hydrogen-producing capability. These are: (1) the photosynthetic unit size of hydrogen production; (2) the turnover time of photosynthetic hydrogen production; (3) thermodynamic efficiencies of conversion of light energy into the Gibbs free energy of molecular hydrogen; (4) photosynthetic hydrogen production from sea water using marine algae; (5) the original development of an evacuated photobiological reactor for real-world engineering applications; (6) the potential for using modern methods of molecular biology and genetic engineering to maximize hydrogen production. The significance of each of these points in the context of a practical system for hydrogen production is discussed.

This program will be enhanced by collaborative research between Oak Ridge National Laboratory and senior faculty members at Duke University, the University of Chicago, and Iowa State University. The special contribution that these organizations and faculty members will make is access to strains and mutants of unicellular algae that will potentially have useful properties for hydrogen production by microalgal water splitting.

Purpose

The purpose of this project is applied research and development for the design and construction of a real-world engineering system that is capable of producing renewable hydrogen from water. The basis for further development work in this field is based on quantitative measurement of a number of important parameters and figures of merit that characterize the ability of microalgae to split water into molecular hydrogen and oxygen.

The Photosynthetic Unit Size of Hydrogen Production

Using the technique of saturating flash and individual hydrogen burst resolution, it was demonstrated (Greenbaum 1977) that the photosynthetic unit size of hydrogen evolution was comparable to and stoichiometrically related to the photosynthetic unit size of oxygen evolution. This work unambiguously demonstrated that hydrogen evolution was not a trivial side reaction of photosynthesis but, in fact, derived its reducing equivalents from the main stream of the electron transport chain of photosynthesis.

The experimental data upon which these statements are made are illustrated in Fig. 1. Figure 1 represents two experiments plotted on the same absolute axes. The hydrogen data are the absolute yield of hydrogen per saturating flash of light from the green alga *Chlamydomonas reinhardtii*. Four simultaneously triggered xenon flash lamps of 1-2 μsec duration were used as the light source. The oxygen data are derived from the same algae except that an electron acceptor, parabenzoquinone, was used. The main points of the data of Fig. 1 are (1) the stoichiometric ratio of hydrogen to oxygen is approximately two; and (2) the absolute values of the respective oxygen and hydrogen photosynthetic sizes are what would be expected if the source of reductant for hydrogen production was derived from the main stream of the electron transport chain of photosynthesis.

The Turnover Time of Photosynthetic Hydrogen Production

Using the technique of double-flash illumination, a direct measurement of the turnover time of photosynthetic hydrogen production was determined to be in the millisecond time range (Greenbaum 1979). This is comparable to the turnover time of oxygen evolution. The key significance of this result is that kinetics of hydrogen evolution is not rate limiting in the overall steps associated with photosynthetic hydrogen production.

The experimental data upon which these statements are made are illustrated in Fig. 2. Figure 2 contains four different experiments in which the turnover times of molecular hydrogen production are determined for *Chlamydomonas*, *Chlorella*, *Scenedesmus*, and *Chlamydomonas* grown on a Tris-acetate-phosphate medium. In these experiments, the algae were subjected to a pair of saturating light flashes of variable spacing between them. Note that on the microsecond time scale the flash pair is unresolvable by the overall photobiochemistry of the algae. The flashes are resolved on the millisecond time scale, which is also the normal turnover time of photosynthesis. The key point of these experimental data is that the kinetic steps associated with hydrogen formation in green algae are not the limiting aspects of hydrogen production by microalgal water splitting.

Energetic Efficiency of Hydrogen Photoevolution by Algal Water Splitting

It was demonstrated that under light-limiting conditions (i.e., in the linear low-intensity region of the light saturation curve) equivalent solar energy conversion efficiencies of 5-10% could be achieved with the green alga *Chlamydomonas moewusii* (Greenbaum 1988). These are the highest efficiencies for hydrogen production ever recorded and were achieved with an original experimental apparatus designed and constructed at Oak Ridge National Laboratory. Figure 3 is a schematic illustration of the experimental apparatus used for the measurements. The heart of the detection system is comprised of the oxygen and hydrogen sensors that are located downstream from the photosynthetic reaction chamber. An example of the experimental data obtained with this system for the alga *Scenedesmus* is illustrated in Fig. 4. Table 1 summarizes the energy conversion efficiencies obtained with the algae investigated thus far. Please note that equivalent solar energy conversion efficiencies of 10% have been obtained with the alga *Chlamydomonas moewusii*.

Table 1. Energy Conversion Efficiencies of Green Algae for Hydrogen and Oxygen Production

Alga	Light on	Efficiency (PAR)
	*no.**	%**
Scenedesmus D_3	1	16
	2	23
C. reinhardtii (sup)	1	13
	2	16
	3	18
	4	19
	5	21
	6	21
	7	18
C. reinhardtii (UTEX 90)	1	6
	2	8
	3	8
C. moewusii	1	24
	2	22
	3	18

*The entries in this column correspond to the ordinal number of successive periods of illumination. The light was on for either a 3- or 4-hour period, after an equal period of darkness.

**Conversion efficiency based on absorbed photosynthetically active radiation. PAR = photosynthetically active radiation. Based on repeated measurements and calibrations, it is estimated that the experimental error in these measurements is, at most, ±15%. The efficiencies were computed for the rates of hydrogen evolution at the end of the period of illumination when the algae were in a steady (or nearly steady) state.

These values of energy conversion efficiencies, obtained under strictly light-limiting conditions, are consistent with the measurements described above on the absolute photosynthetic unit sizes and turnover times.

Control of Photosynthetic Reductant

By controlling the concentration of atmospheric carbon dioxide, it is possible to improve the rates of photosynthetic hydrogen production (Cinco et al. 1993). The strategy here is to maintain sufficient CO_2 such that the CO_2/HCO_3 binding site of Photosystem II is competent, while at the same time depriving the Calvin cycle pathway of its utilization of CO_2. These results demonstrate that CO_2 control is a rational approach to improving the rates of photosynthetic hydrogen production.

Three different light intensity/CO_2 concentrations (58 ppm, 30 ppm, and 0.8 ppm) are presented as rates of hydrogen and oxygen evolution versus time (Fig. 5). The onset of light-activated hydrogen and oxygen photoproduction is evident as is their decline when the light was turned off. Dark hydrogen evolution was subsequently observed (a phenomenon described by Gaffron and Rubin 1942 and amplified by Klein and Betz 1978). Using these data, one can obtain gas yields during light periods by integrating the peaks. For hydrogen profiles, the first half-life measures the time of decay from the maximum rate to half maximum. All yields were normalized to 1 mg of chlorophyll (Chl) by dividing by the amount of Chl present for each trial (usually 0.1 mg).

Lower CO_2 Concentrations Increase H_2 Yields

The results of 11 experiments at varying carbon dioxide levels and 130 W/m^{-2} irradiance were demonstrated (Fig. 6). This light level was chosen because it generated the highest oxygen yields at most of the CO_2 concentrations used without causing photoinhibition. Oxygen yields indicated the activity of water splitting, which supplied the bulk of reductant for hydrogen synthesis. The six other light intensities exhibited patterns similar to 130 W/m^{-2}. Fifty-eight ppm was the highest CO_2 concentration tested because 350 ppm CO_2, which is close to normal atmospheric levels, produced similar gas yields. As the CO_2 levels for algae decreased, hydrogen yields climbed slowly, reaching a maximum at 0.8 ppm (11,360 nmol), where the Calvin cycle was impaired presumably because of insufficient CO_2 supply. At the other extreme, CO_2 levels greater than 30 ppm allowed the Calvin cycle to dominate so that only quick bursts of hydrogen formed. The noteworthy result is the highest yield of hydrogen at 0.8 ppm CO_2, not at 0 ppm, where the Calvin cycle would be totally deprived of external inorganic carbon.

Lower CO_2 Concentrations Inhibit H_2 Decay

Hydrogen rates peaked and declined in most of the 1.5-h light periods. (The low light intensities are a notable exception.) First half-lives ($t_{1/2}$) indicated the duration of hydrogenase activity at various CO_2 concentrations. These are not implied to be the half-lives of exponential decay. They reflect the real-time loss of light-activated hydrogenase activity, due to competition with the Calvin cycle and/or depletion of alternate donor reductant pools. No permanent damage to hydrogen-forming capacity resulted from this decline, as indicated by resurgent rates of hydrogen evolution during subsequent light periods. The decay is slowest at the 0.8 ppm CO_2 level, indicating that hydrogen photoproduction had its slowest decay at this level. The general trend showed first half-lives rising with decreasing CO_2 and roughly following the behavior of hydrogen yields.

O_2 Yields Decrease with CO_2 Deprivation

The decline in O_2 yields can be seen with decreasing CO_2 levels. The trend is downward with less carbon dioxide. The algae require CO_2 (*in vivo*) at some level to maintain high rates of electron-transport, as indicated by oxygen production. At 0 ppm (pure helium) oxygen activity was 12% that at 58 ppm. However, an addition of only 0.8 ppm CO_2, the value where H_2 was maximized, more than doubled the oxygen rate. As expected, oxygen rates did not decline appreciably during the 1.5-h light periods. The significance of this result is discussed below in the Discussion section.

Hydrogen to Oxygen Ratios

Only below 10 ppm CO_2 did hydrogen/oxygen-yield ratios approach two, in contrast to levels greater than 30 ppm, where the ratio remained less than two. These numbers approximately indicate activity of the hydrogen pathway versus the Calvin cycle. For levels >30 ppm, carbon dioxide assimilation receives the bulk of photoproduced reductant. A yield ratio of two or more does not necessarily mean that reductant from PS I and II goes exclusively to the hydrogen pathway because of the presence of transient alternate reductant pools (Klein and Betz 1978).

Discussion

These experiments indicate that atmospheric control of CO_2 concentration is a method of controlling the fate of photosynthetic reductant. In the present case, the amount of carbon dioxide in the algal environment was titrated such that the decreasing CO_2 concentration led to increasing hydrogen yields and greatest sustained rate at the 0.8 ppm level. This observation can be explained by a slowing of Calvin cycle activity. With this usual sink for light-generated reductant impaired, the hydrogen pathway (through hydrogenase) can take up an increasing share of electrons. Below 10 ppm CO_2 is where the hydrogen pathway begins to overtake the Calvin cycle, where the yield ratios (H_2/O_2) are ≈2. Conversely, low hydrogen yields (compared to oxygen) combined with short first half-lives above 30 ppm CO_2 indicate that the Calvin cycle is the predominant pathway for photogenerated reductant in that region.

On the other hand, we can clearly see the importance of carbon dioxide for high rates of electron transport. Carbon dioxide, or its dissolved form, bicarbonate (HCO_3^-), acts on the acceptor side of PS II as various investigators have confirmed (Eaton-Rye and Govindjee 1984; Xu *et al.* 1991; Jursinic and Stemler 1992; reviewed by Vermaas and Govindjee 1982). In addition to being the well known substrate for and

activator of the Calvin cycle, carbon dioxide (or HCO_3^-) helps to assure normal, rapid rates of electron flow through PS II's primary (Q_A) and secondary quinone (Q_B) acceptors, and the plastoquinone (PQ) pool. When the concentration of CO_2 was decreased, reduced efficiency of electron flow occurred, prompting the oxygen-evolving complex to slow its activity accordingly. This "bicarbonate effect" on oxygen-evolving capability by depletion of CO_2 (or HCO_3^-) has been discussed by Jursinic and Stemler (1992).

In considering the extent to which photosynthetic reductant can be used to produce molecular hydrogen, it is useful to ask the following question: what is the rate-limiting aspect of this process? The limiting step is definitely not the kinetics associated with the chemistry of hydrogen formation which occur on a millisecond time scale (Greenbaum 1979). This can partially be seen in the rapid initial bursts of hydrogen observed. The limiting step is the generally sluggish movement of electrons generated via photosynthetic water splitting and movement through the electron transport chain.

As discussed above, in a pure helium atmosphere the rate of electron transport is 12% that at 58 ppm CO_2, whereas only 0.8 ppm CO_2 more than doubles it to 28%. Although hydrogenase is an oxygen sensitive enzyme, the oxygen evolved in this system is not inhibiting it. Prior experiments have demonstrated this by titrating in oxygen upstream from the algal cell and observing its effect on hydrogenase activity. The photosynthetically produced oxygen is below this threshold.

It is concluded from these experiments that the differential affinity of CO_2 to the Calvin cycle and the Photosystem II binding site is the key parameter in determining the extent to which CO_2 assimilation can be bypassed while simultaneously maintaining a fully functional electron transport chain as expressed by photosynthetic oxygen evolution.

Future accomplishments will be based on advances that have been achieved in this program to date. These include the observation that it is possible to control the fate of photosynthetic reductant and improve hydrogen production by microalgal water splitting by controlling the partial pressure of atmospheric carbon dioxide. Also, development of photobiological reactors using subambient atmospheric pressure technology will continue to be studied.

Evacuated Photobiological Reactors

These results are based on U.S. Patent #4,476,105 (Inventor: E. Greenbaum, assigned to U.S. Department of Energy). Hydrogen production in an evacuated photobiological reactor has been achieved. The significance of this result is that it greatly simplifies and improves upon previous methods that have been used for hydrogen production by microalgal water splitting. Figure 7 is a schematic illustration of the prototype evacuated photobiological reactor constructed for proof-of-principle experiments performed thus far. In Fig. 7 a three-way ball valve is used to connect the algal reactor chamber or calibration electrolysis cell to the hydrogen sensor. The use of an evacuated chamber eliminates the need for a sweep gas to create anaerobiosis and hydrogenase activation. The electrolysis cell is used for absolute calibration of the hydrogen sensor via Faraday's Law of Electrochemical Equivalence. Figure 8 contains the time profile of hydrogen evolution from the green alga *Chlamydomonas reinhardtii* along with calibration data in an evacuated atmosphere created by a conventional mechanical roughing pump.

In this task, hydrogen production will be measured using a tin-oxide gas sensitive semiconductor as the sensing element. The sensor will be located between the reactor and a mechanical vacuum pump. Hydrogen production by microalgal water splitting as a function of light intensity, temperature and other selected experimental variables will be performed. In addition, an improved version of this apparatus using a six-port sampling valve is planned. With this apparatus, both the hydrogen and oxygen evolved in the water splitting reaction will be detectable. The measurement of both gases simultaneously will provide important insight into the variability of the stoichiometric ratios of hydrogen and oxygen and information on the immediate source of reductant that provides reducing equivalents for hydrogen evolution. The bulk of these reducing equivalents are, of course, derived from water. There are, however, others that make important contributions to the overall hydrogen yields.

References

Cinco, R., J. M. MacInnis, and E. Greenbaum. 1993. "The Role of Carbon Dioxide in Light-Activated Hydrogen Production by *Chlamydomonas reinhardtii*." *Photosyn. Res.*, 38:27-33.

Eaton-Rye, J. J., and Govindjee. 1984. "A Study of the Specific Effect of Bicarbonate on Photosynthetic Electron Transport in the Presence of Methyl Viologen." *Photobiochem. Photobiophys.*, 8:279-288.

Gaffron, H., and J. Rubin. 1942. "Fermentative and Photochemical Production of Hydrogen in Algae." *J. Gen. Physiol.*, 26:219-240.

Greenbaum, E. 1977. "Measurement of the Photosynthetic Unit Size of Hydrogen Evolution." *Science*, 196:878-879.

Greenbaum, E. 1979. "The Turnover Times and Pool Sizes of Photosynthetic Hydrogen Production by Green Algae." *Sol. Energ.*, 23:315-320.

Greenbaum, E. 1988. "Energetic Efficiency of Hydrogen Photoevolution by Algal Water Splitting." *Biophys. J.*, 54:365-368.

Jursinic, P. A., and A. Stemler. 1992. "High Rates of Photosystem II Electron Flow Occur in Maize Thylakoids When the High-Affinity Binding Site for Bicarbonate is Empty of All Monovalent Anions or has Bicarbonate Bond." *Biochem. Biophys. Acta*, 1098:359-367.

Klein, U., and A. Betz. 1978. "Fermentative Metabolism of Hydrogen Evolving *Chlamydomonas moewussi*." *Plant Physiol.*, 61:953-956.

Vermaas, W. F. J., and Govindjee. 1982. "Bicarbonate or Carbon Dioxide as a Requirement for Efficient Electron Transport on the Acceptor Side of Photosystem II." In *Photosynthesis Vol. II* (Govindjee, Ed.), 543-556. New York: Academic Press.

Xu, C., S. Taoka, A. R. Crofts, and Govindjee. 1991. "Kinetic Characteristics of Formate/Formic Acid Binding at the Plastoquinone Reductase Site in Spinach Thylakoids." *Biochem. Biophys. Acta*, 1098:32-40.

Figure Legends

Fig. 1. Absolute yields of hydrogen and oxygen per saturating flash from the green alga *Chlamydomonas reinhardtii*. The oscillations in the oxygen yield with periodicity four correspond to the normal Joliot-Kok pattern.

Fig. 2. The turnover times of light-driven photosynthetic hydrogen production in several species of green algae. The abscissa, Δt, is the spacing between two flashes of light, each of which is of saturating intensity. The ordinate is the absolute yield of hydrogen per mole of chlorophyll per saturating flash pair. The turnover time is defined, operationally, as the point in time at which there is a 50% increase between the initial and final steady state yields. For all experiments, the algae were anaerobically adapted in the dark prior to illumination for about 2 hours.

Fig. 3. Schematic illustration of experimental apparatus used to measure absolute light absorption and hydrogen and oxygen production by filter-paper entrapped microalgae. The chamber is an integral part of a helium-carrier flow system with connecting ports as indicated. Hydrogen and oxygen sensors are located downstream from the chamber. Absolute calibration of these sensors is achieved using Faraday's law of electrochemical equivalence with an electrolysis cell that is located in tandem with the chamber.

Fig. 4. Simultaneous photoevolution of hydrogen and oxygen from the anaerobically adapted green alga *Scenedesmus* D_3. The algae are irradiated with a projector lamp at normal incidence to the plane defined by the filter-paper entrapped algae. Two 4-hour intervals of illumination are indicated. The values of hydrogen evolution used in the energy efficiency calculation were those at the end of each 4-hour interval.

Fig. 5. Representative results of hydrogen (solid line) and oxygen (dashed line) evolution by *C. reinhardtii* at 58, 30, and 0.8 ppm carbon dioxide. A 2-hour calibration period preceded the actual light reactions, which started at the third hour. Seven cycles of 1.5 h light and 1 h dark were performed for each of the seven irradiances (in order, from left): 227, 130, 64, 25, 6.3, 2.4, and 0.1 $W \cdot m^{-2}$ ($\uparrow$ = light on, $\downarrow$ = light off). The peak areas, after background subtraction, represent yields of H_2 or O_2 and first half-lives (the decay time from maximum rate to half-maximum) were compiled for hydrogen. Other experimental conditions are described in the text.

Fig. 6. (a) Algal photoproduction of hydrogen (■, dashed line) and oxygen (•, solid line) at various carbon dioxide levels. Shown are the trends of the gas yields (integration of peaks as in Fig. 2) for 1.5-h light periods (130 $W \cdot m^{-2}$ irradiance). All yields are normalized to 1 mg Chl. Of the 11 CO_2 levels tested, hydrogen production is greatest near 1 ppm, but oxygen yield at this point has dropped to 30% of the value at 58 ppm CO_2. (b) First half-lives of decay for hydrogen rates. These measure the time it takes for the maximum H_2 rate to decay to half-maximum. Shown here are the first half-lives (•) for the 130 $W \cdot m^{-2}$ light level, taken from the data for (a), with a solid line as the "smooth fit" through the data. Since all the hydrogen rates experienced a notable decay from an initial burst, this half-life describes how sustained the hydrogenase activity of the algae was during the 1.5 h of light. The peak near 1 ppm CO_2 indicates that the most sustained hydrogen evolution occurred here. (c) Hydrogen:oxygen yield ratios. These ratios (•) are derived

from the yields shown in (a) (1.5 h of 130 W · m^{-2} light). The trend (solid line) is toward ratios of ≥2 below 10 ppm CO_2.

Fig. 7. Schematic illustration of the prototype evacuated photobiological reactor for hydrogen and oxygen production by microalgal water splitting. The three-way ball valve can connect the hydrogen sensor with either the algal reaction chamber (left) or the electrolysis calibration cell (right).

Fig. 8. Time profile of hydrogen evolution from the alga *Chlamydomonas reinhardtii* in an evacuated photobiological reactor. Calibration data are generated by electrolysis of water using Faraday's Law of Electrochemical Equivalence to convert electrolytic current to rates of hydrogen and oxygen production.

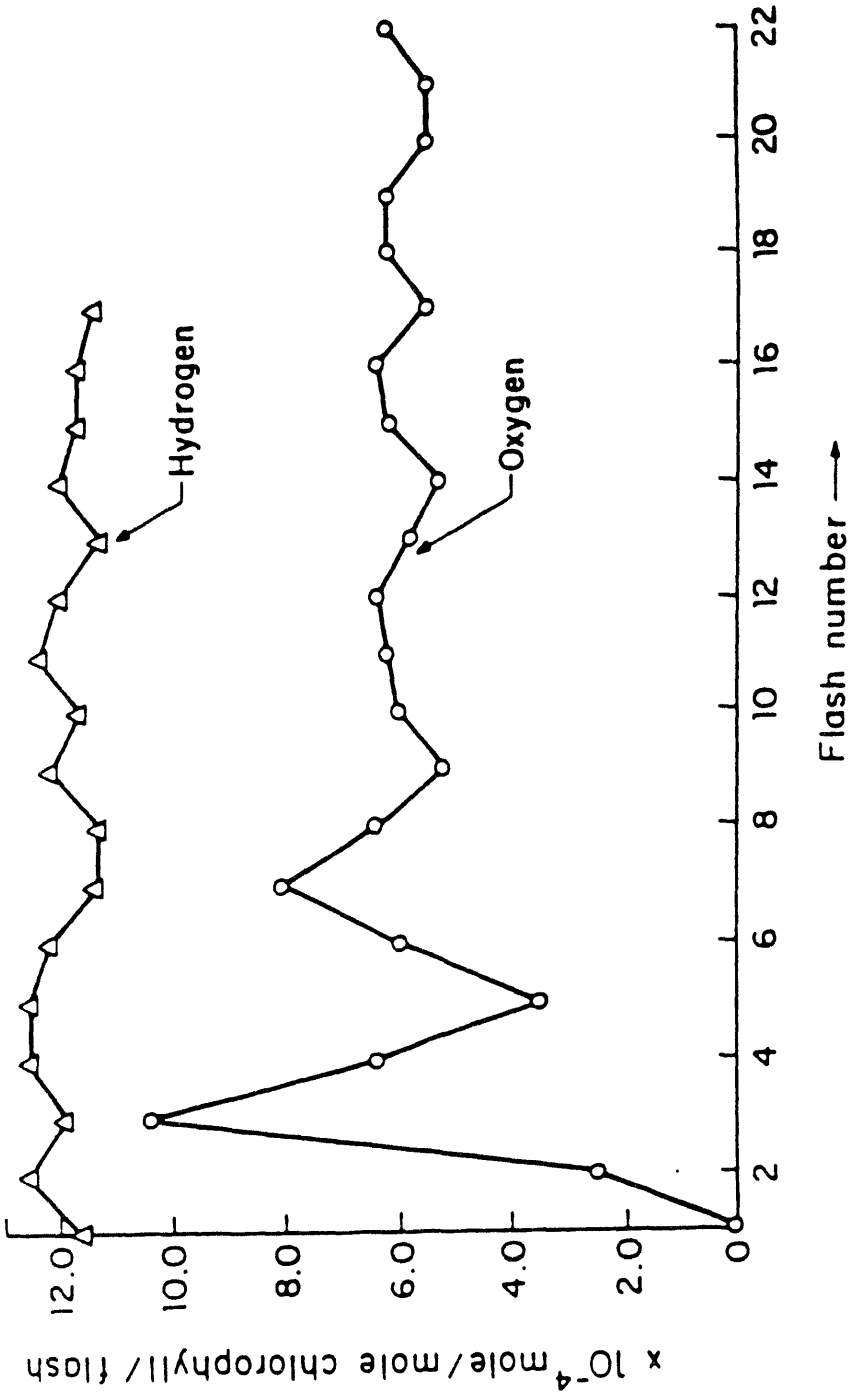
Hydrogen
Oxygen
12.0
10.0
8.0
6.0
4.0
2.0
0
2
4
6
8
10
12
14
16
18
20
22
Flash number ⟶
x 10^{-4} mole/mole chlorophyll/ flash

FIGURE 1

FIGURE 2

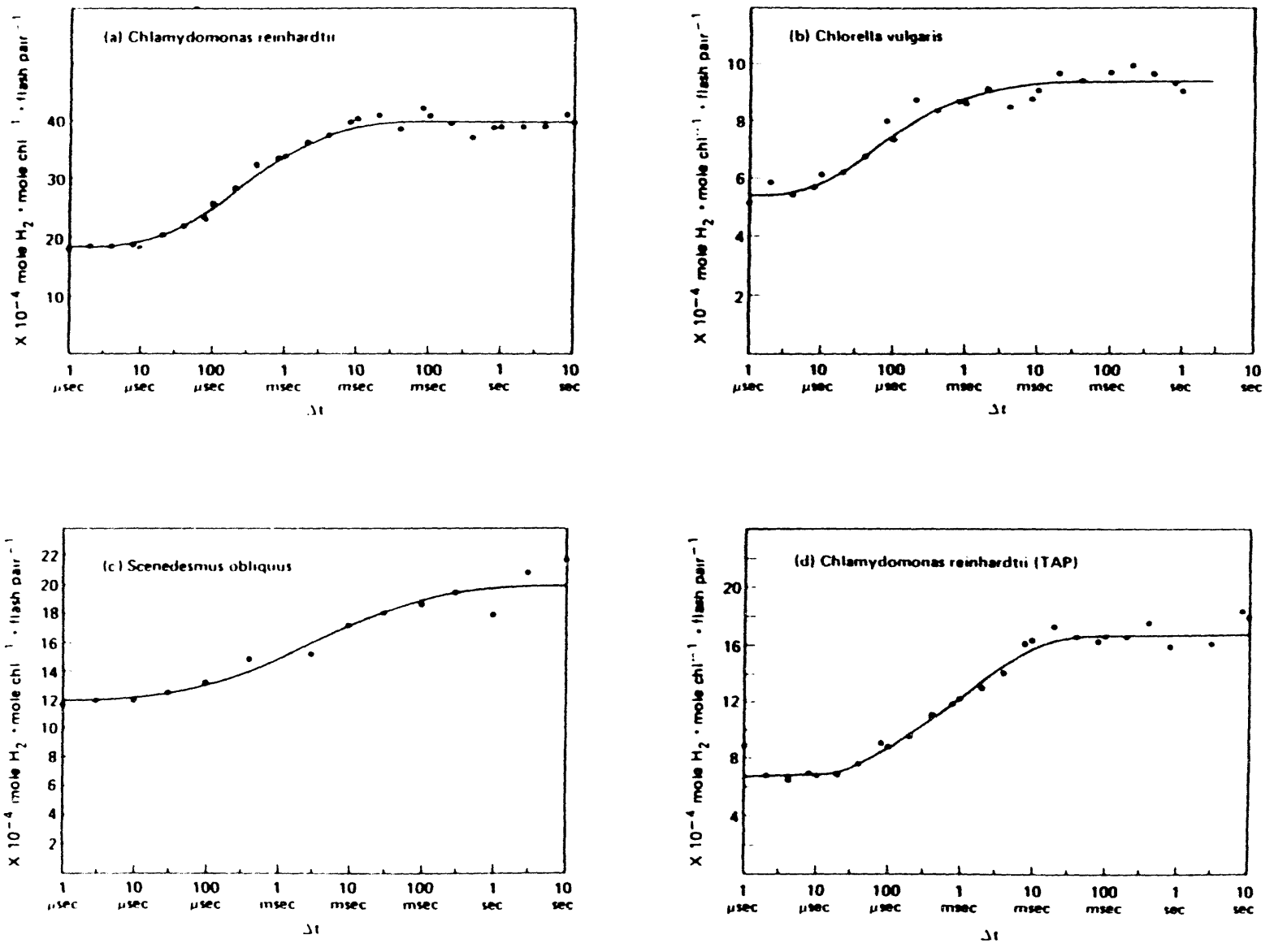
(a) Chlamydomonas reinhardtii
(b) Chlorella vulgaris
(c) Scenedesmus obliquus
(d) Chlamydomonas reinhardtii (TAP)
X 10⁻⁴ mole H₂ · mole chl⁻¹ · flash pair⁻¹
1 μsec 10 μsec 100 μsec 1 msec 10 msec 100 msec 1 sec 10 sec
Δt

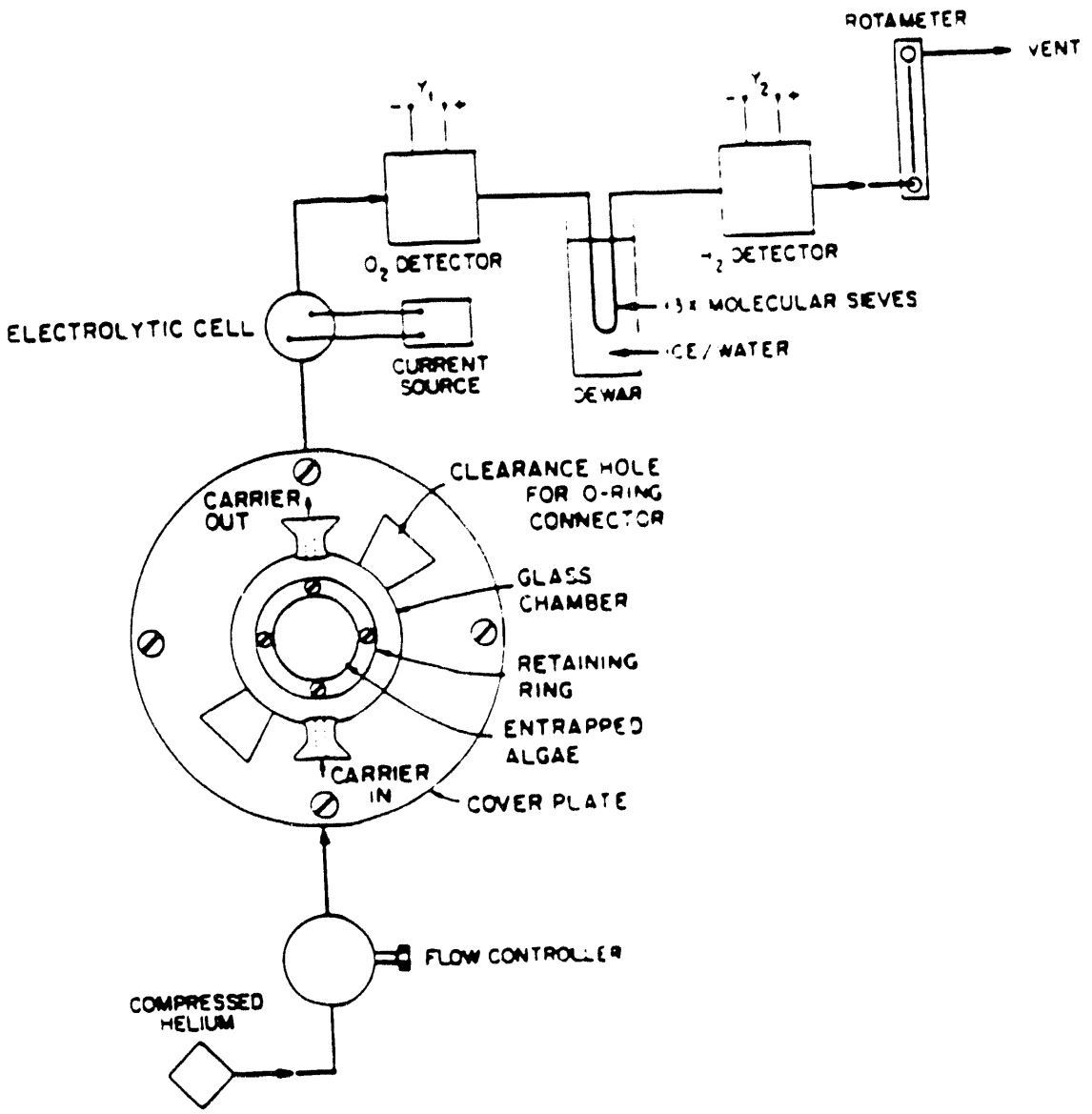
ROTAMETER
VENT
Y_1
Y_2
O_2 DETECTOR
H_2 DETECTOR
ELECTROLYTIC CELL
CURRENT SOURCE
5 Å MOLECULAR SIEVES
ICE / WATER
DEWAR
CARRIER OUT
CLEARANCE HOLE FOR O-RING CONNECTOR
GLASS CHAMBER
RETAINING RING
ENTRAPPED ALGAE
CARRIER IN
COVER PLATE
FLOW CONTROLLER
COMPRESSED HELIUM

FIGURE 3

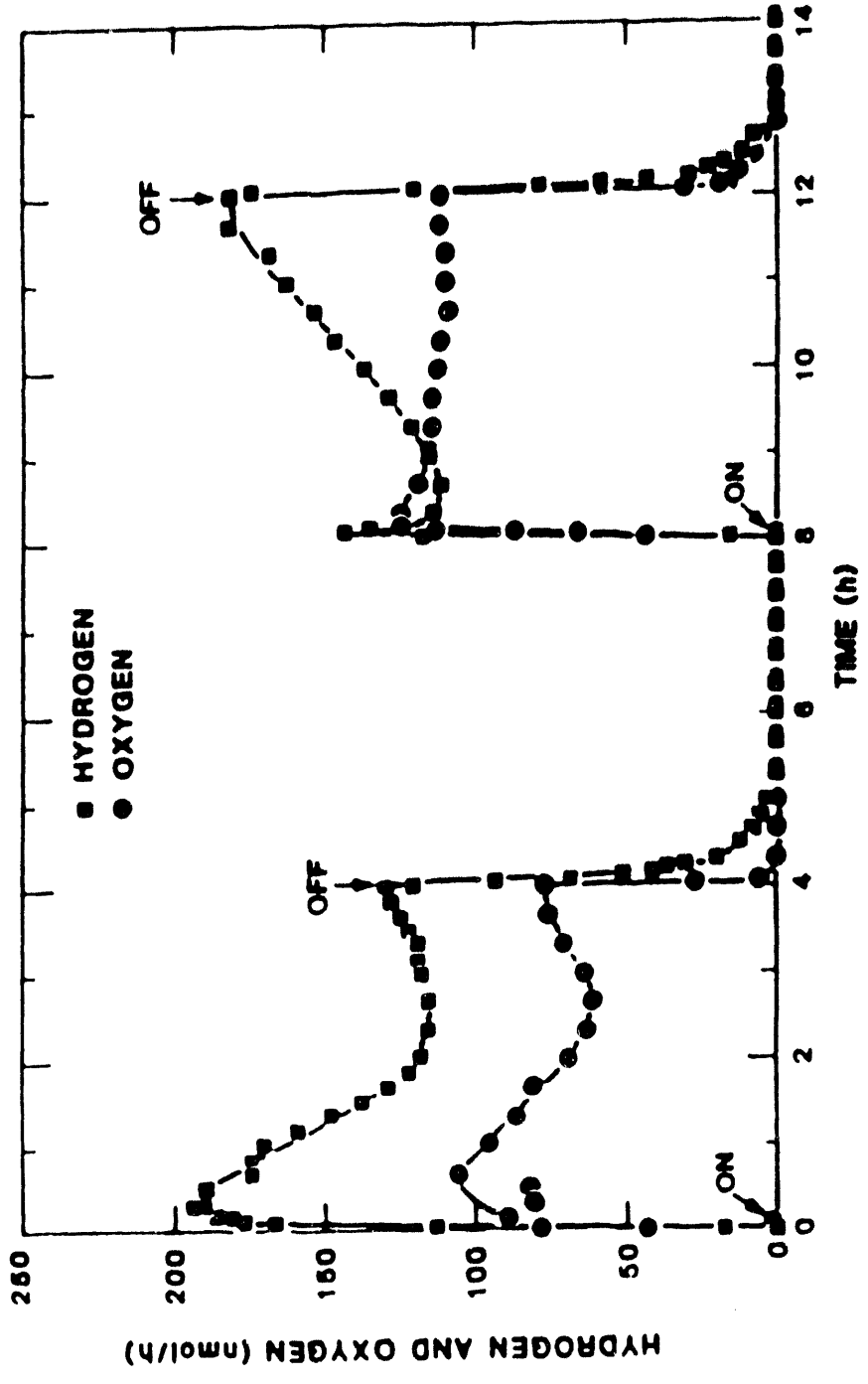
HYDROGEN AND OXYGEN (nmol/h)
250
200
150
100
50
0
0
2
4
6
8
10
12
14
TIME (h)
HYDROGEN
OXYGEN
OFF
ON
OFF
ON

FIGURE 4

SIMULTANEOUS PHOTOEVOLUTION OF MOLECULAR HYDROGEN AND OXYGEN AS A FUNCTION OF ATMOSPHERIC CARBON DIOXIDE CONCENTRATION

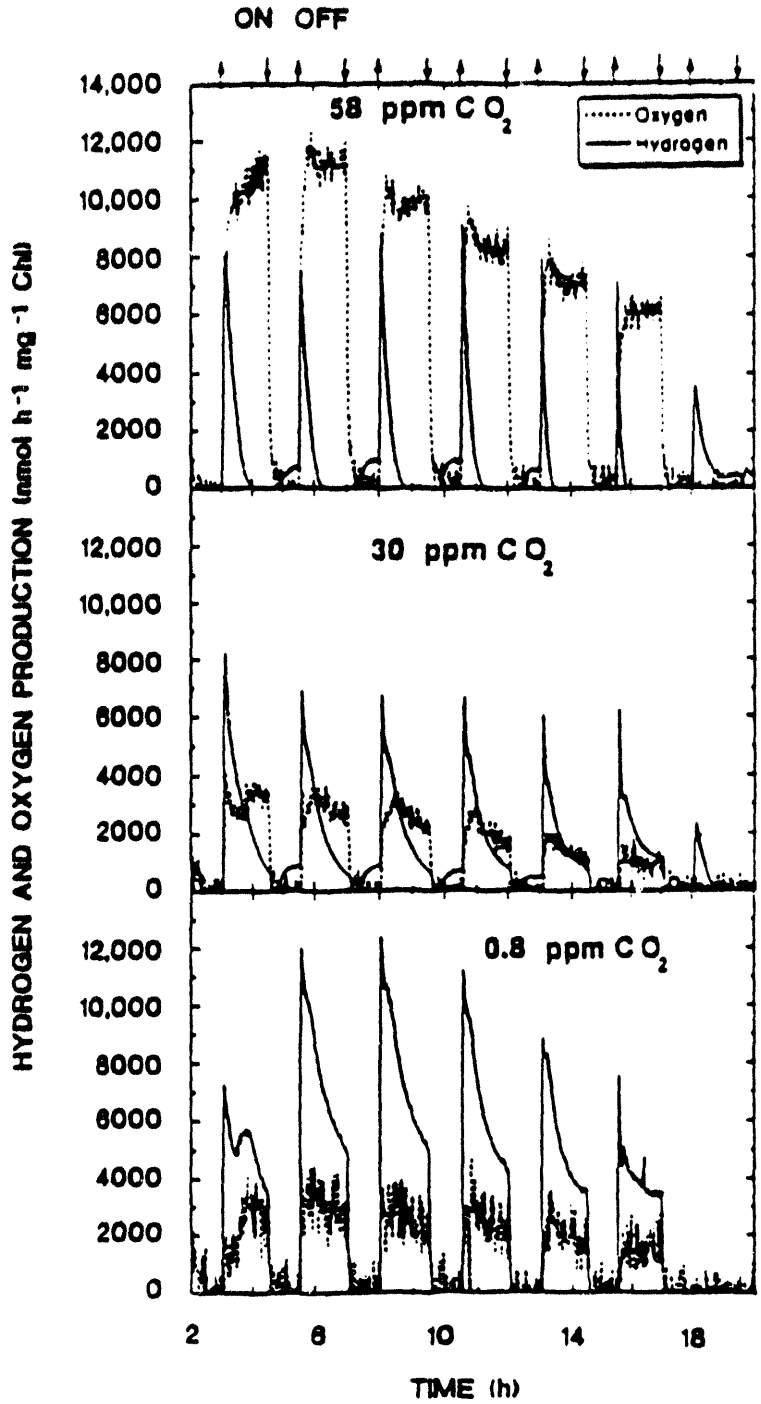

FIGURE 5

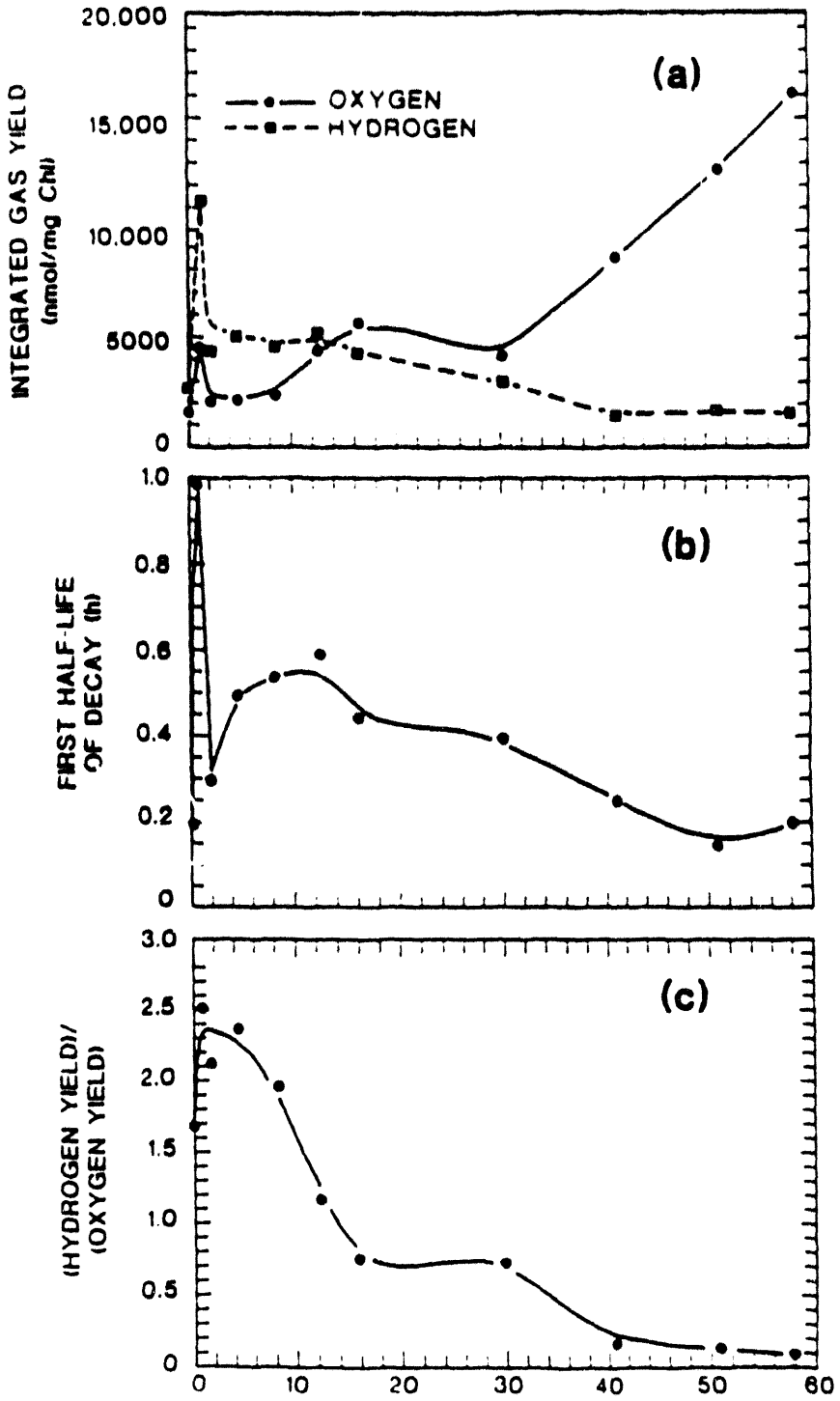
20,000
15,000
10,000
5000
0
INTEGRATED GAS YIELD
(nmol/mg Chl)
OXYGEN
HYDROGEN
(a)
1.0
0.8
0.6
0.4
0.2
0
FIRST HALF-LIFE
OF DECAY (h)
(b)
3.0
2.5
2.0
1.5
1.0
0.5
0
(HYDROGEN YIELD)/
(OXYGEN YIELD)
(c)
0
10
20
30
40
50
60

FIGURE 6

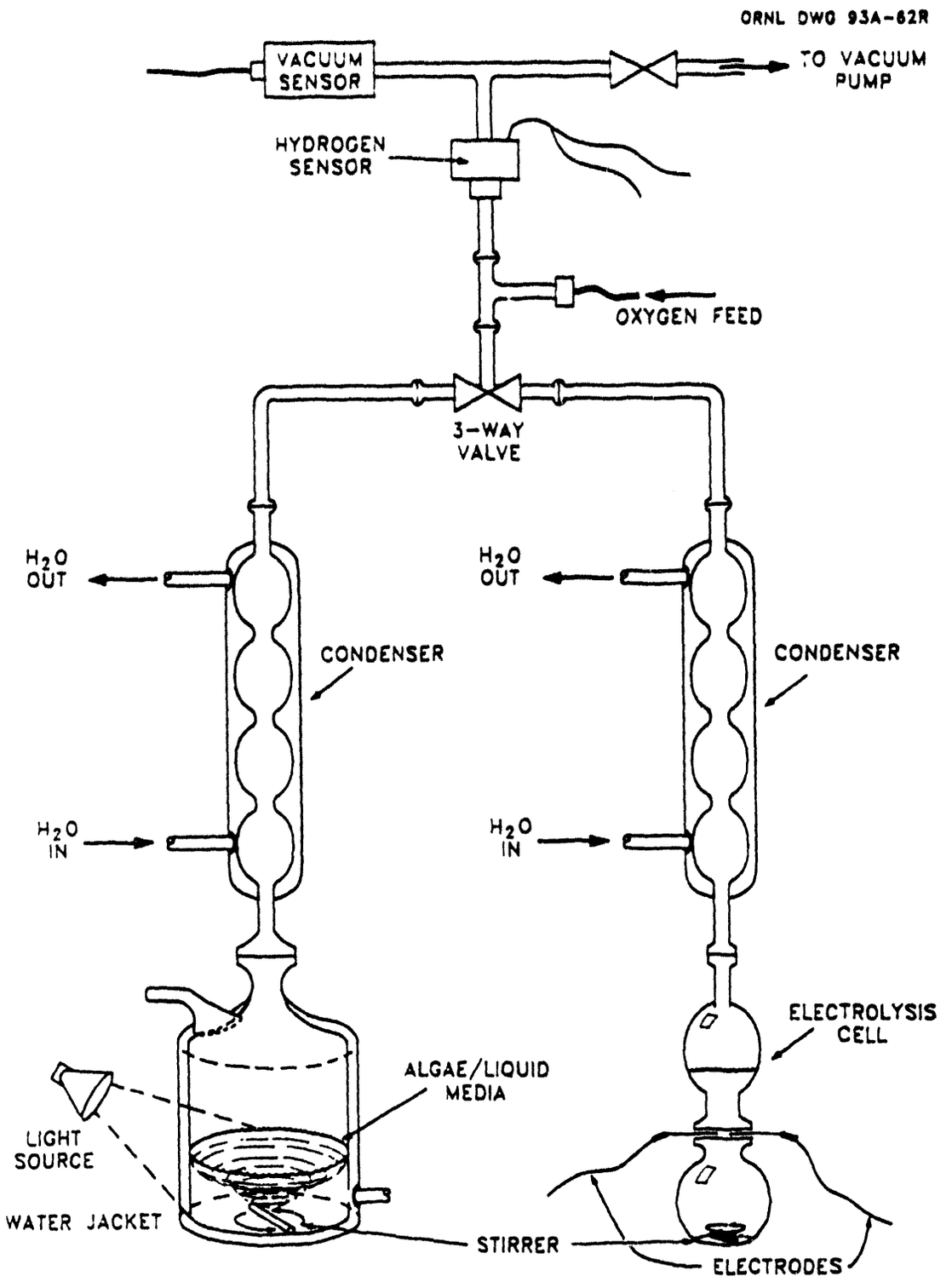
ORNL DWG 93A-62R
VACUUM SENSOR
TO VACUUM PUMP
HYDROGEN SENSOR
OXYGEN FEED
3-WAY VALVE
H_2O OUT
H_2O OUT
CONDENSER
CONDENSER
H_2O IN
H_2O IN
ELECTROLYSIS CELL
ALGAE/LIQUID MEDIA
LIGHT SOURCE
WATER JACKET
STIRRER
ELECTRODES

FIGURE 7

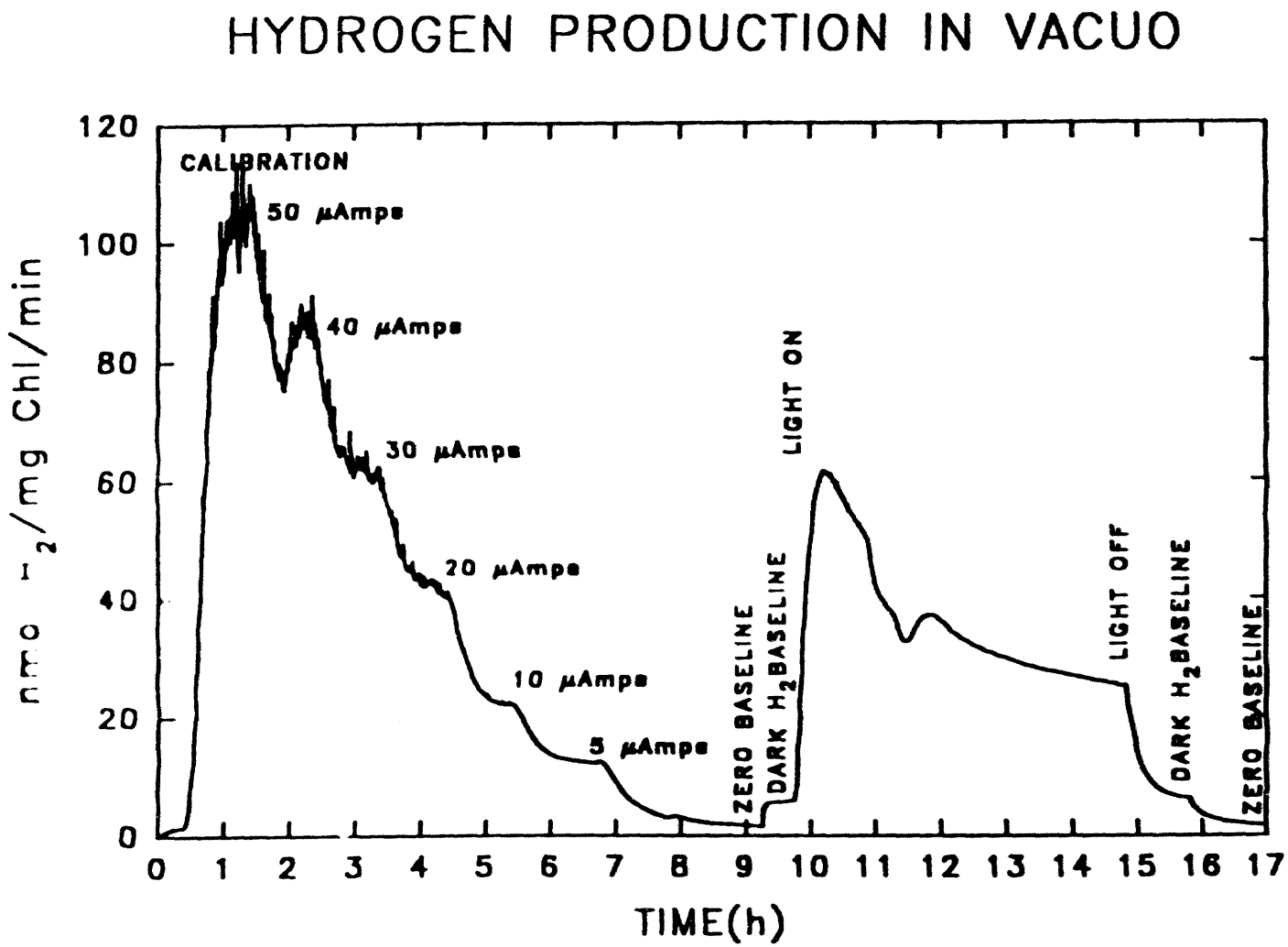
HYDROGEN PRODUCTION IN VACUO
nmo H_2/mg Chl/min
120
100
80
60
40
20
0
CALIBRATION
50 µAmps
40 µAmps
30 µAmps
20 µAmps
10 µAmps
5 µAmps
ZERO BASELINE
DARK H_2BASELINE
LIGHT ON
LIGHT OFF
DARK H_2BASELINE
ZERO BASELINE
0 1 2 3 4 5 6 7 8 9 10 11 12 13 14 15 16 17
TIME(h)

FIGURE 8

PHOTOELECTROCHEMICAL HYDROGEN PRODUCTION

Richard E. Rocheleau, Zhe Zhang, Eric Miller, and Qing-hua Gao
Hawaii Natural Energy Institute
School of Ocean Earth Science and Technology
University of Hawaii at Manoa
Honolulu, HI 96822

Abstract

Semiconductor-based photoelectrochemical cells remain promising as an option to meet the Department of Energy's goals for the production of hydrogen from a renewable resource. In this report, we describe progress in an integrated program involving electrode fabrication, characterization, and engineering modeling with the objective to develop a high efficiency, low-cost photoelectrochemical system for the direct production of hydrogen. Loss analysis indicates significant advantages of multi-photon processes multijunction amorphous and hybrid crystalline-amorphous silicon photoelectrodes compared to single photon processes. Optimal bandgaps for high efficiency hydrogen production have been identified. Photoelectrodes have been fabricated using triple junction amorphous silicon solar cells with (Sm-Fe-Mn-Ni)O_x as the oxygen catalyst and Co-Mo as the hydrogen catalyst. Hydrogen and oxygen were produced without external bias in 1 molar KOH at a rate equivalent to a current density of 6.5 mA/cm^2, corresponding to a solar to hydrogen conversion efficiency greater than 7.5% (LHV of H_2/power of incident light) . The photoelectrode performance remained stable for over two hours, the duration of the stability test.

Introduction

The Department of Energy goal for the production of hydrogen using renewable resources can be met with photoelectrochemical hydrogen production systems using water as the feedstock and sunlight as the energy source. The feasibility of producing hydrogen in such systems, based on a light absorbing semiconductor or photovoltaic devices coated with water splitting catalysts, has been demonstrated in several laboratories including ours. However, additional advancements and lower materials costs are needed to achieve the DOE efficiency goals (10%), long-term stability, and economical operation.

The objective of this work is to develop high efficiency, stable, potentially low-cost electrodes for the direct photoelectrolysis of water using only sunlight as the energy source. Specific objectives to meet these goals include: (1) characterization of the electrode/electrolyte interface, (2) identification of efficiency limitations imposed by the reactor and photoelectrode design, and (3) development of high efficiency photoelectrodes. Our results indicate that a demonstration scale project is likely to be feasible within the next two years.

Background

The search for high efficiency processes for the photoelectrochemical (PEC) production of hydrogen from water accelerated following reports that n-TiO_2 photoanodes could provide a significant fraction of the energy needed to split water (Fujishima and Honda 1972). Significant advances were made in semiconductor photoelectrochemistry (Nozik 1978 and Gerischer 1979) and high solar conversion efficiencies were demonstrated with reversible redox couples (e.g. Heller et.al 1981, Rosenbluth and Lewis 1986). However, progress in the development of an efficient system for direct hydrogen production from an aqueous electrolyte has been limited by the high voltage required to dissociate water and the corrosiveness of the aqueous electrolytes. Practical difficulties such as increased optical losses and lowered barrier heights can also result from deposition of catalysts at the electrode/electrolyte interfaces as required to improve charge transfer kinetics. These difficulties have been so great that the only single photon processes capable of splitting water without external bias have used very wide bandgap materials such as $SrTiO_3$ and $KTaO_3$ (Wrighton et. al. 1977, Kraeutler and Bard 1978). Unfortunately, these materials utilize only the UV part of the spectrum resulting in low solar efficiencies.

The lack of progress in solving these problems and, as shown in this work, efficiency limitations of even the best theoretical single photon systems, pointed to a different approach. Multiphoton processes using classic solid state homo- or hetero-junctions which can use a larger fraction of the solar spectrum are more promising. The use of solid state multijunction devices provides greater flexibility in the photoelectrode design and wider choice of materials to be used for protection and catalyzation of the interface. These systems allow direct photoelectrolysis at high efficiency with a greater choice of semiconductors and coatings (Weber and Dignam 1986). Direct hydrogen production, albeit at less than optimal efficiency, has been demonstrated with monolithic multijunction solar cells immersed in electrolyte using amorphous (Lin et. al. 1989, Matsumura et. al. 1986) and hybrid crystalline-amorphous silicon (Sakai et.al.), and crystalline III-V materials (Turner 1992). Based on reasonable expectations for catalyst performance, we have concluded that the amorphous silicon and hybrid crystalline-amorphous silicon based

devices have the greatest potential of meeting DOE efficiency goals at a reasonable cost. As detailed in this report, we have recently demonstrated stable solar to hydrogen conversion efficiencies (LHV of H_2 produced/incident sunlight) greater than 7.5%, using photoelectrodes fabricated in our laboratory. These stable high efficiency photoelectrodes were fabricated using multijunction amorphous silicon solar cells (provided by Solarex Thin Film Division) coated with thin-film catalysts developed under this task. The hydrogen production rate without external bias remained constant for more than 2 hours, the length of the stability test.

In this report, we describe the loss analysis model that has been used to identify optimal semiconductor bandgaps. We also describe the development of high activity thin-film catalysts for use as both oxygen and hydrogen electrodes and report progress in the development of high efficiency amorphous silicon photoelectrodes. Finally, research needs and plans for the future are discussed.

Scope/Technical Approach

Quantitative loss analysis based on widely accepted models for photocell operation has been combined with models of the electrolysis reactions to determine the hydrogen production potential (efficiency) of single and multiphoton semiconductor systems. Low-cost multijunction amorphous silicon solar cells and novel structures using affordable multijunction amorphous silicon on crystalline silicon devices have the potential for hydrogen production efficiencies above 10%. Under this task, photoelectrodes are fabricated using commercially available multijunction solar cells and thin-film catalysts developed in our laboratory.

The development of improved catalytic films, especially transparent anodic catalysts has been identified as being critical to the successful development of stable high efficiency photoelectrodes. We are fabricating a-SiC:H/catalysts test structures to characterize the semiconductor/catalyst interface and catalyst stability. Test structures and completed photoelectrodes are characterized and tested in both acidic and alkaline electrolytes. Potentiodynamic measurements are used for performance testing. Surface analysis techniques are used to examine chemical bonding and morphology of the materials. Engineering and equivalent circuit models, a, integral part of our program, are under continual development for analysis of our results.

Results

Loss Analysis

The results summarized in this section are based on a paper accepted for presentation at the next World Hydrogen Energy Conference (Cocoa Beach Florida, June 1994). Only those elements of the analysis necessary to justify our focus on the multijunction amorphous silicon structures are presented here.

The current response for a photocell, whether solid-state or photoelectrochemical, behaving according to the widely accepted equivalent circuit shown in Figure 1 is described by:

$$J = J_o \left(\exp \frac{V-JR_s}{nV_t} - 1\right) + \frac{V-JR_s}{R_{sh}} - J_L \qquad (1)$$

where J and V are the cell current and voltage, JL is the photogenerated current, Jo the dark forward or saturation current, n the diode parameter, Rs the internal series resistance, Rsh the shunt resistance, and Vt the thermal voltage (kT/q). Equation 1, which assumes superposition of the photogenerated and back injection current through the forward biased diode (Jo), is an accurate representation for well-behaved crystalline materials such as Si and the III-V compounds and adequately represents the behavior of amorphous photocells if the circuit parameters are carefully specified.

The hydrogen production rate for unbiased photoelectrochemical cells can be determined from the intersection of the diode (Eq 1) and load response where the latter is defined by the kinetics of the chemical reaction (e.g. HER and OER) and system resistances. Determination of this operating point for different circuit elements (e.g. for different bandgaps and solar spectrum) and catalyst properties allows comparison of the potential hydrogen production rates for different photoelectrode designs.

In our analysis all losses at the anodic and cathodic catalyst surfaces and in the electrolyte are included in the load response. Using the Butler-Volmer relation for overpotential at the oxygen and hydrogen producing interfaces, and including additional terms for the potential drop across the Helmholtz layer, mass transfer in the electrolyte and membrane resistances, the electrochemical load can be approximated as :

$$V = V_{eq} + JR_{ec} + 2V_t \ln(J/i_o) \qquad (2)$$

where V_{eq}, the decomposition potential for water, is taken as 1.23V; R_{ec}, the combined resistance of the Helmholtz layer, electrolyte and membrane, is estimated as 1.9 W based on typical resistance for commercial electrolyzers (Ismail ed 1989, Scribner and Taylor eds. 1990), the transfer coefficient in the Butler-Volmer equation is 0.5, and the exchange current densities (i_o) for the OER and HER are equal.

Values for J_L are calculated directly from standard AM1.5 global spectral data at 1000W/m^2 assuming that all incident photons with energies greater than the bandgap generate electron-hole pairs while photons with energies lower than the bandgap pass through unadsorbed. The light generated current for any absorber layer is then given by :

$$J_L = q \int_{Eg}^{Eg1} \frac{E(\lambda)}{hc} \lambda \, dE \qquad (3)$$

where Eg is the bandgap of the layer of interest and Eg1 is the lowest bandgap of the previous absorber layers.

The saturation current, Jo, is estimated from equations describing the behavior of various

types of barriers. For ideal p-n junction diodes, the reverse saturation current can be approximated as:

$$J_o = C \exp\left(\frac{-E_g}{nkT}\right)$$

$$1 \leq n \leq 2 \qquad (4)$$

where the values of C and n are characteristic of the semiconductor used.

Models of semiconductor-electrolyte junctions (Gerischer 1979, Kuhne and Schefold 1990, and Sze 1980) yield expressions for the saturation current densities similar to those derived for standard solid-state Schottky barriers:

$$J_o = A^* T^2 \exp\left(\frac{-\Phi_B}{nkT}\right) \qquad (5)$$

where Φ_B is the barrier height. Since the barrier height may approach but will not exceed the bandgap use of equation 4 instead of equation 5 to calculate Jo for electrolyte junctions will tend to overestimate the photopotential for higher bandgaps. In our analysis we use this somewhat optimistic analysis of the performance of wide bandgap semiconductor-electrolyte junctions.

The diode parameter, n, is assumed equal to 1 for photoelectrodes fabricated from crystalline materials and equal to 2 for amorphous silicon alloys. Values for C are determined using values of open circuit voltage and light generated currents reported for high quality devices. Based on open circuit voltages for Si (.694V, Green 1984) and GaAs(1.04V, Gale 1984) C values of 8.4×10^8 mA/cm^2 and 8.7×10^7 mA/cm^2 were calculated.

Values of C were also determined for amorphous silicon alloys using data from three high quality solar cells with bandgaps from 1.47 to 1.75 eV (Pawlikiewicz et. al. 1990). A C value of 2.6×10^7 mA/cm^2 was used to represent all amorphous Si alloys independent of bandgap. While no internal resistances were included in the analysis of the crystalline silicon and III-V materials, an internal series resistance of 8 ohm-cm^2 for each pin junction and an additional resistance of 2 ohm-cm^2 at each tunnel junction was included in determining the diode characteristics and hydrogen production potential of amorphous silicon alloy photocells.

Figure 2 shows hydrogen production rates, plotted as the equivalent current density, as a function of bandgap and catalyst exchange current for single junction photoelectrodes characterized using the most optimistic value for C, 8.7×10^7 mA/cm^2. For each i_o, there is an optimal bandgap for maximum production of hydrogen. Our analysis considers a range of i_o between 10^{-6} and 10^{-4} A/cm^2. These values are based on published data for commercial and experimental catalysts (Lsia 1993, Ho et. al. 1988). As the exchange current density

increases, the optimal bandgap decreases and the maximum hydrogen production rate increases. We consider exchange current densities around 10^{-5} A/cm^2 to be a reasonable near-term goal for catalysts with the smooth morphology and optical properties required for photoelectrode applications. With i_o equal to 10^{-5} A/cm^2, a current density of 11.1 mA/cm^2 under one sun illumination can be achieved with the optimal semiconductor with a bandgap of 2.1 eV assuming no optical losses in the system. A reduction in the photoelectrode bandgap from 2.1 to 2.0 eV reduces the current density to 7mA/cm^2. Such as large drop in hydrogen production rate is due to a shift of the operating point (intersection of diode and load curve) closer to Voc. A higher than optimal bandgap results in a more gradual reduction in current densities due to reduced photon absorption.

Figure 3, shows the hydrogen production rate for catalyzed triple junction a-Si cells as a function of the bandgap of the top and middle cells, assuming a bottom cell bandgap of 1.3 eV and an exchange current densities of 10-5 A/cm^2. Cathodic current densities greater the 10.5 mA/cm^2. As is evident in the Figure, near- maximum current densities can be achieved over a relatively wide range of bandgaps, making this device insensitive to changes in catalyst activity. Hydrogen production rates comparable to the best single junction photoelectrodes occurs in spite of a lower solid state efficiency for the amorphous silicon. This performance is found to be due to an improved match of the output voltage and electrochemical load. Although current densities as high as 11 mA/cm^2 can also be obtained with an a-Si tandem configuration (with bandgaps of 2.1 nd 1.55 eV), these devices are sensitive to small changes in the exchange current density similar to the single junction photoelectrodes.

The results presented in Figure 3 were based on a bandgap for the bottom a-SiGe cell of 1.3 eV consistent with near-term expectations for a-SiGe materials. The analysis indicates that further reductions in the bandgap of the lower cell would result in even higher hydrogen production rates. There have been several reports recently of crystalline Si/amorphous silicon heterojunction and tandem hybrid cells showing high conversion efficiencies for electricity production (Tanaka et. al 1992). Figure 4 shows the cathodic current density, for i_o = 10^{-5} A/cm^2, as a function of the bandgap of the two a-Si cells The performance of the 1.12 eV crystalline silicon cell was calculated using C equal to 8.4 x 10^8 A/cm^2. The performance of the a-Si cells was calculated using the same parameters as used for Figure 3. Although the maximum conversion efficiency of the Si/a-Si hybrid is only 24%, several percent below that of the best single junction solar cell on the same basis (~30%), the voltage characteristics of the hybrid are well matched for hydrogen production. As shown in Figure 4, current densities over 14 mA/cm^2 are possible for a broad range of bandgaps of the two upper cells. It is very important to note that this high current can be achieved with a-Si bandgaps between 1.55 and 1.85 eV, the range for which optimum material is available today.

High efficiency multijunction solar cells can also be synthesized using the III-V materials. The higher voltage of these materials compared to a-Si makes hydrogen production with catalyzed tandem devices feasible. With junctions characterized by C equal to 8.7 x 10^7 mA/cm^2, cathodic current densities around 20 mA/cm^2 are predicted over a reasonable range of bandgaps around 1.0 eV and 1.65 eV for the lower and upper cell respectively.

Even with the optimistic assumptions used to calculate photopotential, single junction photoelectrodes, whether based on solid-state or electrochemical junctions, require

semiconductor bandgaps greater than 2.0 eV and have hydrogen production rates only about half that of the best multiphoton devices. These estimates are in agreement with previous studies of this type (Weber and Dignam 1986). The multijunction electrodes based on the III-V compounds perform best, but up to 75% of their best hydrogen production rate can be achieved using the potentially less costly crystalline/a-Si hybrid cells. Triple junction a-Si photoelectrodes are predicted to achieve hydrogen production rates equal to the best single junction devices using III-V quality semiconductors but with greater robustness to changes in catalyst activity. The development of high activity stable catalysts for both oxygen and hydrogen producing reaction is required to meet these projections.

Catalyst Development

Conventional electrochemical catalysts derive a significant activity enhancement by having high effective surface area in a porous structure, often synthesized through a high temperature sintering process. Unfortunately, these catalysts and processes may not be applicable to semiconductor photoelectrodes due to additional requirements for optical transparency, restrictions on processing temperature imposed by the semiconductor devices, and compatibility of the process itself with the semiconductor materials. Due to these restrictions and the critical need for improved coatings to serve as both catalysts and protective coatings, a large fraction of our recent efforts have been focused on developing stable high-activity catalysts with properties optimized specifically for application to photoelectrodes. To address DOE's cost goals, high cost materials such as Pt and Ir are not being considered for use. A variety of lower cost catalysts are currently being synthesized and tested. The thin film catalysts are synthesized using three gun magnetron sputtering and electrodeposition techniques. These facilities and procedures have been described in detail in earlier reports.

Of particular interest for the a-Si structures used in our work is the development of transparent oxygen producing catalysts which also protects the semiconductor. Efforts are focused on mixed metal oxide catalysts for this application because of the potential for high catalyst activity and transparency. Doped NiO_x, TiO_x-NiO_x, or ZnO_x-NiO_x combinations have been synthesized and characterized for use as transparent anodes in alkaline solution. High activity, stability, and high transparency have been demonstrated but further optimization of all three properties simultaneously is required. The J-V characteristics for several mixed metal oxide catalysts are shown in Figure 5. The (Fe-Mn-Sm-Ni)O_x shows the lowest overpotential, is stable, and is reasonably transparent for thicknesses below 0.2 micron. This catalyst is currently synthesized by electrochemical deposition. Targets to reactively sputter this catalyst have been synthesized and will be tested in the near future.

For both a-Si cell configurations available to us (glass/TCO/pinpinpin from Solarex and SS/nipnipnip from ECD), the requirement for transparency is relaxed for the cathodic (hydrogen) catalyst. However, stability, activity, and compatibility with the a-Si devices still requires materials development in this area. Lower cost group VIII and VI-VIII metal mixtures are being evaluated as cathodes in alkaline solution. Co-Mo looks particularly promising. Figure 6 shows the voltammetry behavior of this hydrogen catalyst in alkaline solution while Figure 7 shows its stability in alkaline solution. The stability test was conducted for two hours at a constant current density of 10mA/cm^2. The Co-Mo exhibits

overpotentials for hydrogen production even lower than that of our Pt catalyst for current densities below 10 mA/cm^2.

Thin film catalysts are also being developed for use in acid electrolytes. Heteropolyacid modified nickel alloys have been synthesized and tested. Although thin films of this catalyst deposited by electrodeposition exhibit overpotentials comparable to Pt, procedures compatible with the amorphous silicon have not yet been developed. Some metal-oxides such as RuO_x are reported to be stable in acid electrolytes. Initial testing has been conducted but stability and transparency issues remain to be solved. Based on the stability and low overpotentials achieved in alkaline electrolytes, current high efficiency photoelectrodes are being developed for testing in 1N KOH. Further improvements in catalysts for both acidic and basic electrolytes are expected.

Amorphous silicon photoelectrodes

Photoelectrodes have been fabricated from high efficiency triple junction amorphous silicon solar cells provided by Solarex Thin Film Division. These cells were approximately 10.3% efficient in the solid-state under one sun conditions with an open-circuit voltage of 2.4V, shot-circuit current of 6.1 mA/cm2, and fill factor of 70.3. The test samples were provided as an array of 16 square devices each $0.27cm^2$ in area. Individual cells were cut from the glass with a border of several mm allowing access to the underlying CTO. Photoelectrodes were fabricated from individual cells cut from the array. The cathodic (exposed) surface was protected with a thin Ni foil catalyzed with approximately one micron of electrodeposited Co-Mo. To allow access to the CTO fort testing as a three terminal device (which is necessary to characterize the full J-V), an electrical lead was attached to the CTO and connected to a counterelectrode. The counterelectrode consisted of a thin Ni foil with electrodeposited (Sm-Fe-Mn-Ni)O_x catalyst. The edges and exposed CTO of the photoelectrode were encapsulated in epoxy to prevent shorts to the electrolyte. The photoelectrode structure and test apparatus are shown in Figure 8.

The photoelectrode was characterized using a standard three terminal configuration with a saturated calomel reference electrode. The three terminal configuration was used to allow anodic and cathodic half cell performance to be measured. The polarization curves were measured using the apparatus previously described (HNEI 1991 and 1992). This set-up includes a Keithley Model 236 source-measurement unit interfaced to a Macintosh LC computer running labview software. Data were acquired every 20 to 50 mV at a rate of 2 seconds per step.

Figure 9 shows the solid-state J-V curve of the triple junction solar cell measured in our ELH simulator. Also shown on Figure 9 is the load response from modeling presented last year and the actual operating point of the a-Si photoelectrode under unbiased conditions. The current obtained from the photoelectrode is slightly higher than the solid-state solar cell. The difference is attributed to the electrolyte acting as an anti-reflection coating for the cell and up to $0.3mA/cm^2$ may be due to noise in our light source and calibration errors. The shift in our operating point off the projection is due to the very low overpotential of the Co-Mo catalyst under these low current conditions. The current-voltage curve of the photodiode in the three-terminal configuration was entirely consistent with the solid state device. No loss in either voltage or current was found. Some decrease in fill factor was noted due to the

higher resistance of the interfaces compared to solid state measurements but this did not effect the hydrogen production rate since the operating point is near the flat part of the curve.

Figure 10 shows the current measured between the oxygen and hydrogen producing surfaces as a function of time under one sun conditions with no external bias added to the cell. The current has been converted to a current density using the area of the solar cell and cathodic surface. Using the lower heating value for hydrogen (1.23V) the hydrogen production rate inferred from the greater than 6.5 mA/cm2 corresponds to a solar to hydrogen conversion efficiency of greater than 7.5%. Throughout this test, hydrogen bubbles were observed on the surface of the cathodic Co-Mo, while O2 evolution was apparent on the (Sm-Fe-Mn-Ni)O_x counterelectrode.

To our knowledge this is the highest conversion efficiency ever reported for an unbiased photoelectrode using such low cost materials. The high efficiency is due to the high quality of the initial solar cell, the low overpotentials achieved with the thin film catalysts developed under this program, and the ability of the structure to withstand alkaline electrolytes which contributed to the low overpotentials. The photoelectrode was removed from electrolyte and retested as a solid state device with no reduction in efficiency. It is also the first time that a-Si devices with high efficiencies have been reported in alkaline electrolytes.

Summary and Plans

Demonstration of direct hydrogen production with a solar to chemical conversion efficiency greater than 7.5% is a very positive result. Further optimization of the catalytic coatings with improved transparency and affording greater protection to the underlying semiconductor will be necessary for additional efficiency gains and alternate photoelectrode configurations such as those reported last year using the SS/a-Si structure produced by ECD. More detailed characterization of the catalyst/p-Si interface will be conducted to improve the protective properties of our catalyst coatings.

We plan to measure the hydrogen production rates directly for the current high efficiency photoelectrodes and to confirm gas composition using gas chromatography. With the demonstration of stable high efficiency reported here, studies should be initiated to determine optimal photoelectrode designs and system configurations for larger prototype systems. It is our intent to continue our collaborations and with the success to date, obtain greater participation from industrial partners.

The hydrogen production rates reported for the triple junction photoelectrode developed in this work are consistent with the results of the loss analysis. Improved catalyst activity will not result in significantly higher hydrogen production rates unless the bandgaps of the devices are altered to better match the voltage requirements for hydrogen production. In the future, we hope to garner sufficient interest from industry to make these special samples for our use. In the longer term, a research effort to develop the hybrid crystalline/amorphous triple junction device will be required to reach full hydrogen production potential for low cost materials. Our laboratory is well equipped for such an effort with personnel

experienced in the synthesis of high efficiency photovoltaic devices and the highest efficiency low cost photoelectrodes reported to date.

Acknowledgments

I wish to thank the National Renewable Energy Laboratory for support of this project under subcontract No. XD-0-10089-1 and XAR-3-13514-01. I also wish to thank Dr. Liu Yang and Dr. Robert Oswald of Solarex Thin Film Division and Dr. Rosa Young of Energy Conversion Devices for the amorphous silicon samples used in this work.

References

Fujishima, A. and K. Honda. Nature (London) 238, 37(1972).

Gerischer, H. "Solar Photoelectrolysis with Semiconductor Electrodes" in Topics in Applied Physics, Ed. B.O. Seraphin. 31, 115(1979).

Gale R. P., in Proc. SERI Photovoltaic Advanced Research and Development Project 6th Annual Review Meeting, Golden CO, 1984) SERI/CP-211-2507 pp105.

Green M., et. al. in Conf Rec. 17th IEEE Phtotvoltaic Specialists Conf. 386(1984).

Ho, S., et al., J. Electrochem. Soc. 135(6), 1452(1988).Heller, A., B. Miller, and F. Thiel, Appl. Phys. Lett. 38, 232(1981).

Ismail M. I. (ed.), "Electrochemical Reactors: Their Science and Technology", Elesevier Science Publishers B. V., Amsterdam, 248-274(1989).

Kuhne H. M. and J Schefold, J. Electrochem. Soc. 137(2), 568(1990).

Kraeutler, B. and A. J. Bard, J. Am. Chem. Soc. 100, 4317 (1978).

Lasia, A., Int. J. Hydrogen Energy 18(7), 557(1993).

Lin, G. H., M. Kapur, R. C. Kainthla, and J. O'M.Bockris, Appl Phys. Lett. 55(4), 386(1989).

Matsumura, A. J., Y. Sakai, S. Sugahara, Y. Nakato, and H. Tsubomura. Solar Energy Materials, 12, 57(1986).

Nozik, A. J. Ann. Rev. Phys. Chem., 29, 189(1978).

Pawlikiewicz A., et. al., IEEE Trans. on Electron. Devices, 37(2), 403(1990).

Rosenbluth, M. and N. S. Lewis, J. Am. Chem. Soc. 108,4689(1986).

Sakai, Y., S. Sugahara, M. Matsumura, Y. Nakato, and H. Tsubomura, Can J. Chem. 66, 1853(1988).

Scribner L. L. and S. R. Taylor (eds.), "The Measurement and Correction of Electrolyte Resistance in Electrochemical Tests", ASTM STP 1056, 1-60(1990).

Sze, S. M., "Physics of Semiconductor Devices", 2nd ed., Wiley Interscience, New York, 790-838(1980).

Tanaka M., et. al., Jpn. J. Appl. Phys. 31, 3518(1992).

Turner, J. , Presented at the 1992 DOE NREL Hydrogen Program Review, Honolulu HI May 1992.

Weber, M. F. and M. J. Dignam, Int. J. Hydrogen Energy, 11(4), 225(1986).

Wrighton, M. S., P. T. Wolczanski, and A.B. Ellis, J. Solid State Chem. 22, 17(1977).

Figure Captions

Fig 1. Equivalent circuit for photodiode.

Fig 2. Cathodic current density for single junction photoelectrodes for different exchange current densities.

Fig 3. Hydrogen production rates (as cathodic current density) for a-Si triple junction photoelectrodes (1.3 eV bottonm cell and io = 10-5A/cm2.)

Fig 4. Hydrogen production rates (as cathodic current density) for hybrid crystal/amorphous photoelectrode (io = 10-5A/cm2).

Fig 5. Behavior of doped-NiOx anodic catalysts in 1 M KOH.

Fig 6. Behavior of electrodeposited Co-Mo cathodic catalyst in 1 M KOH.

Fig 7. Stability of electrodeposited Co-Mo cathodic catalysts in 1 M KOH.

Fig 8. Schematic of triple junction a-Si photoelectrode and test apparatus.

Fig 9. Solid state diode response, predicted load curve, and measured operating point for triple junction a-Si photoelectrode.

Fig 10. Current density of triple junction a-Si photoelectrode in 1 N KOH with no external bias.

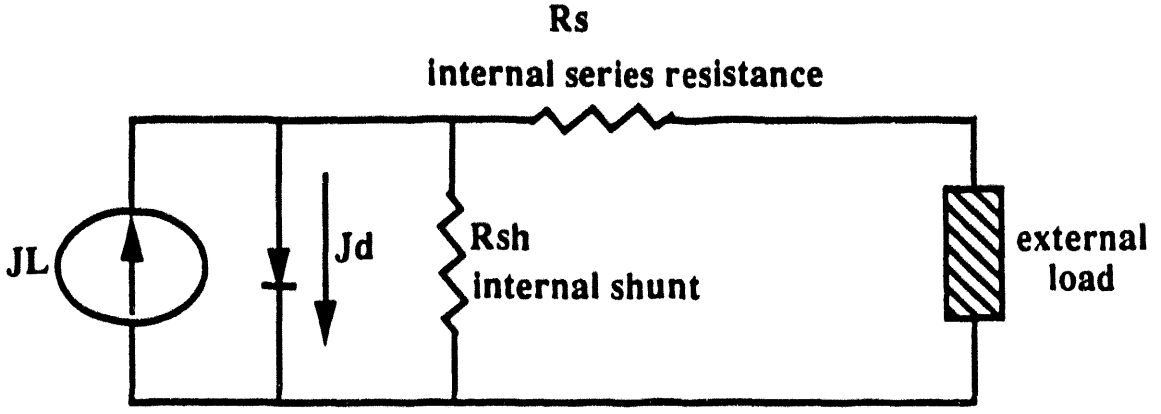

Fig. 1: Equivalent circuit for photodiode with internal resistance and shunt elements shown.

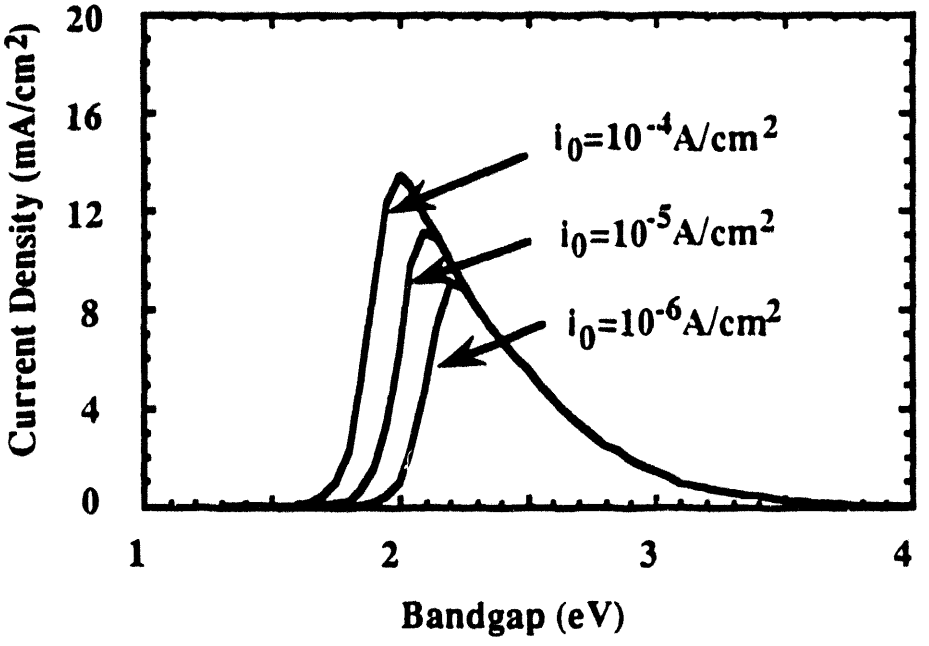

Fig. 2: Cathodic current density as a function of semiconductor bandgap for different exchange current densities.

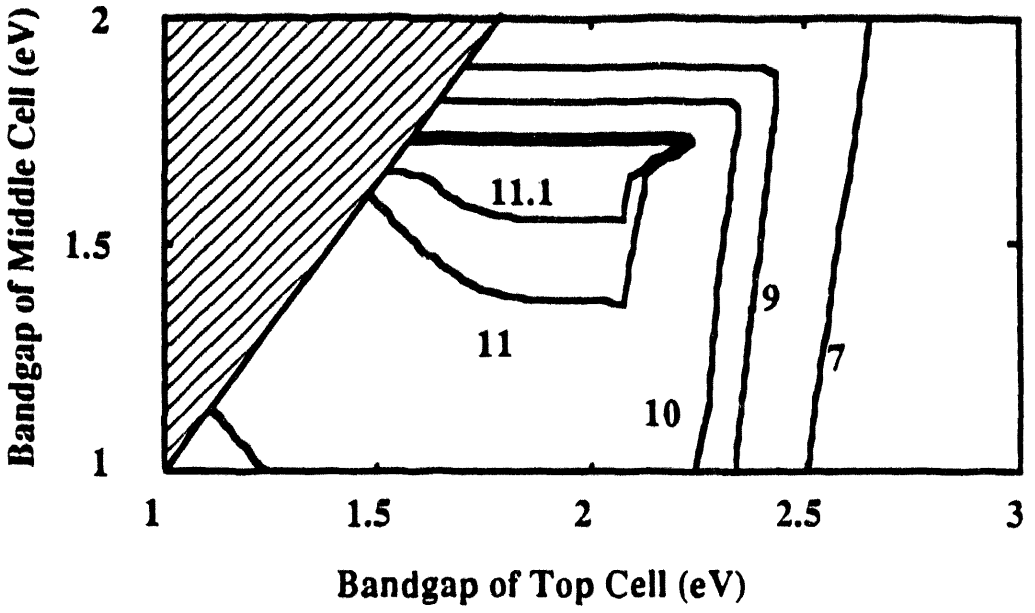

Fig. 3: Cathodic current density for a-Si triple junction in series with electrochemical load ($i_0=10^{-5}A/cm^2$) with 1.3 eV bottom cell and no optical losses.

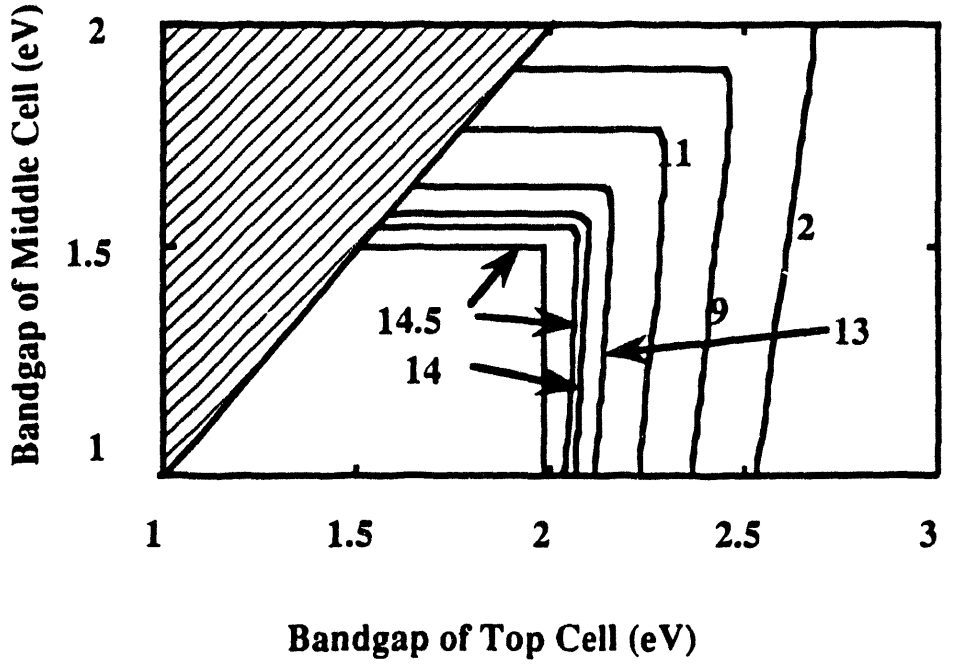

Fig. 4: Cathodic current density for crystal Si/nip-aSi/nip-aSi hybrid cell in series with electrochemical load ($i_0=10^{-5}A/cm^2$), no optical losses.

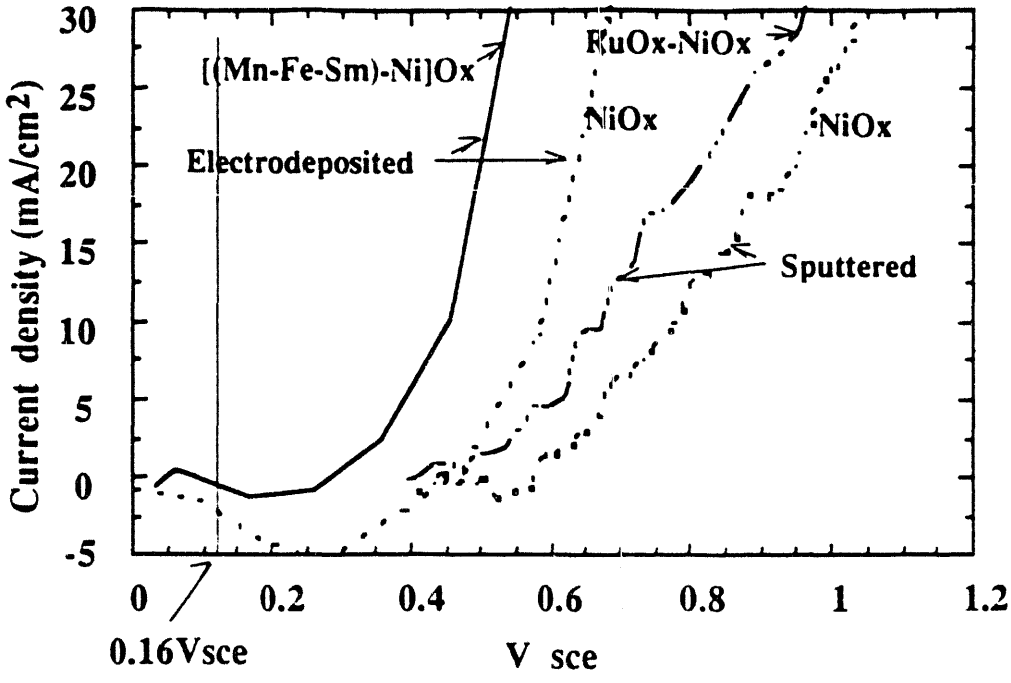

Fig. 5: Current voltage curves for doped NiOx anodes in 1 M KOH (deposited on Ni substrates).

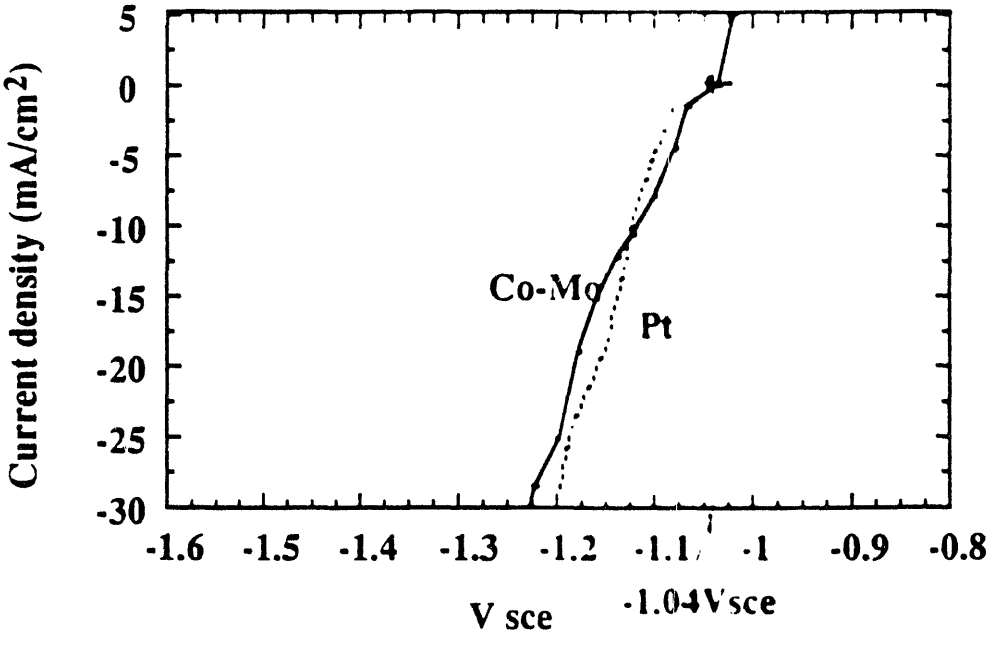

Fig. 6: Current voltage curves for electrodeposited Co-Mo and Pt.

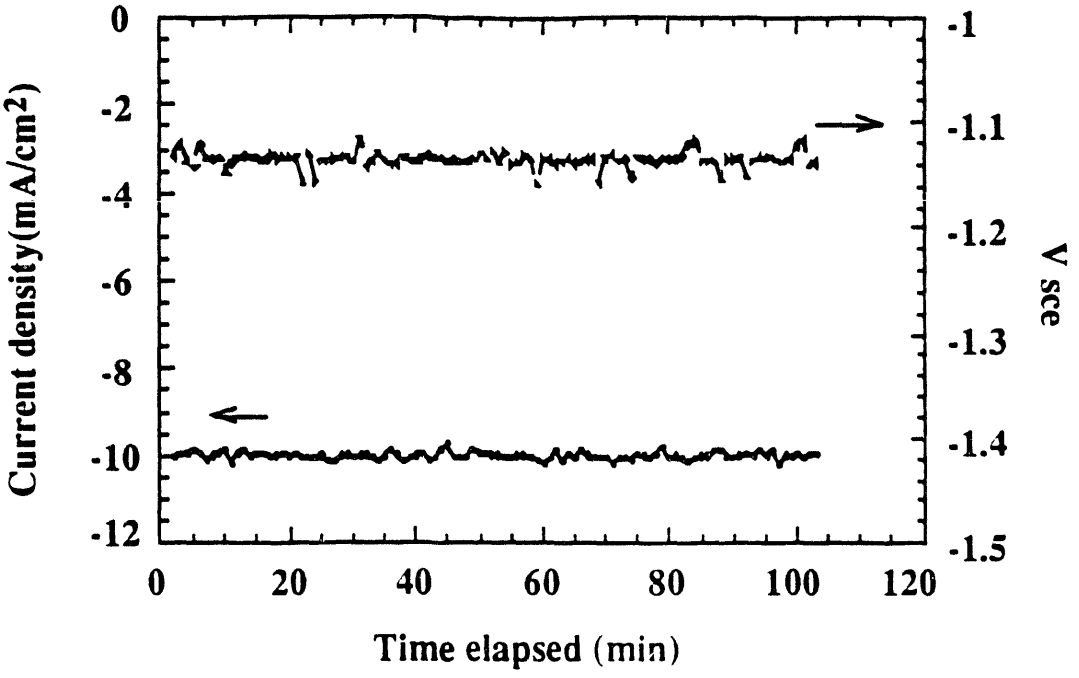

Fig. 7: Cathode potential (Vsce) required to maintain current density of 10 mA/cm^2 with Co-Mo catalyst in 1M KOH.

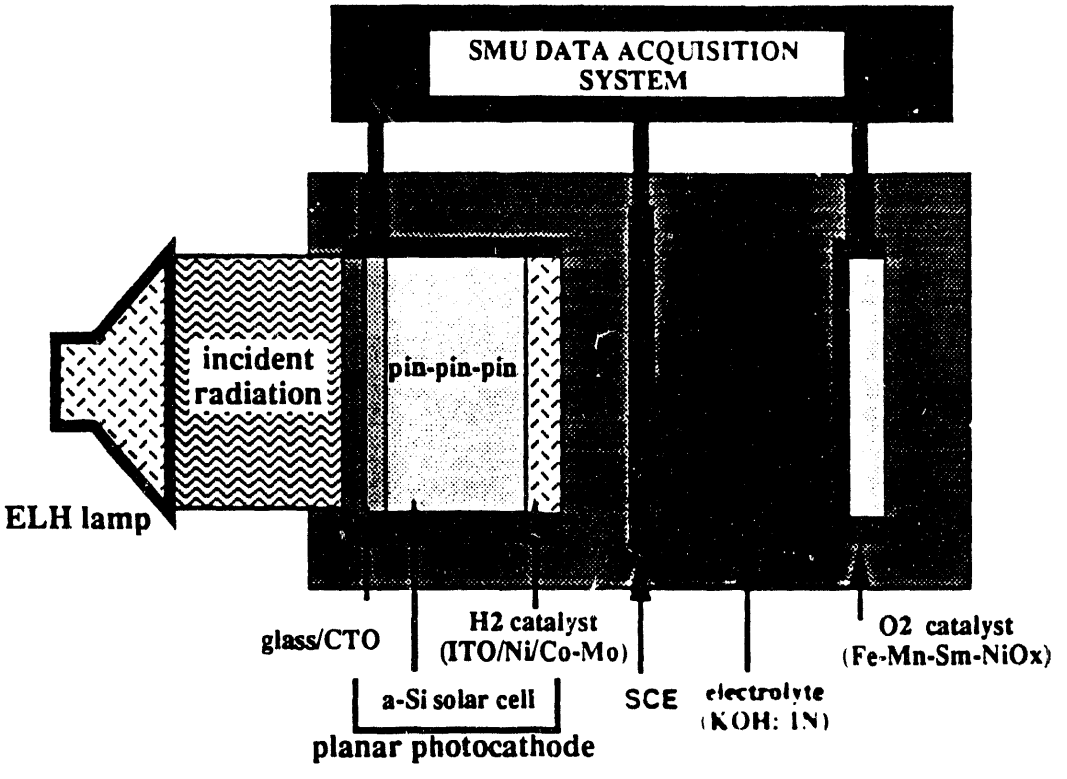

Fig. 8: Schematic of photoelectrode and test apparatus for glass/cto/a-si/catalyst design.

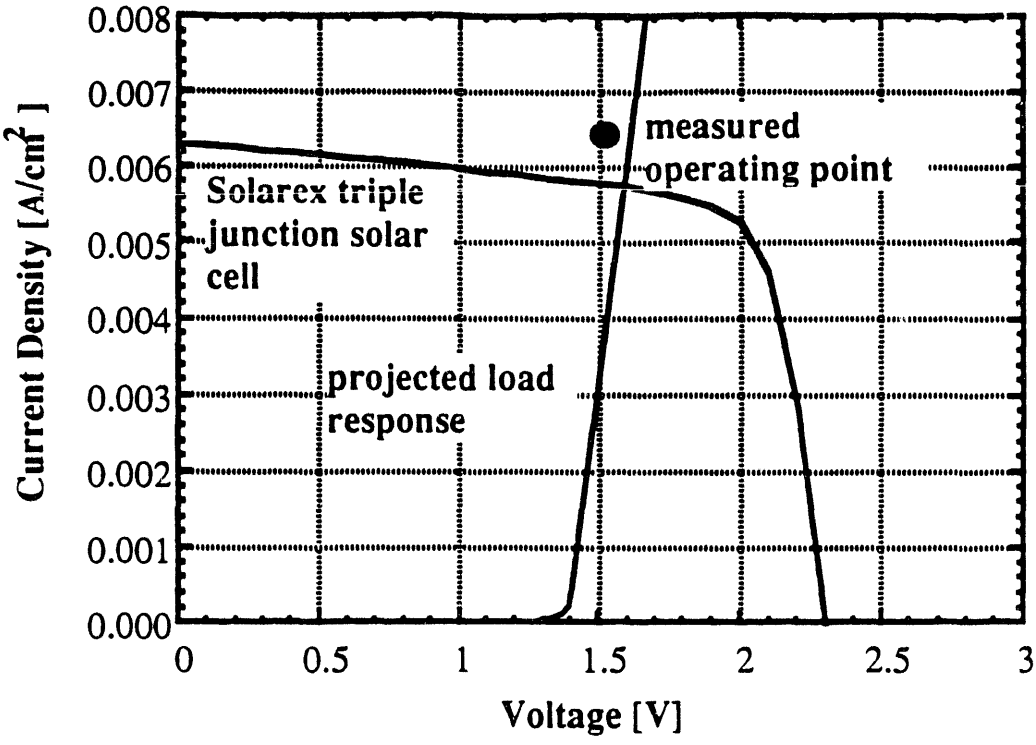

Fig. 9: Diode response and measured operating point for triple-junction a-Si solar cell operating as a photodiode.

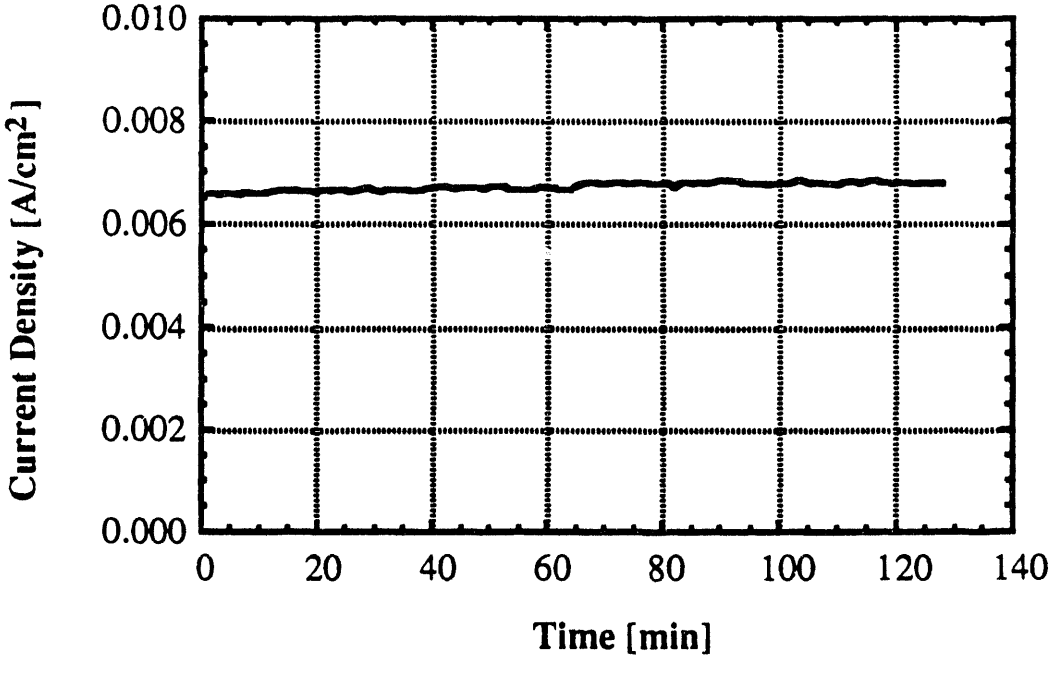

Fig. 10 : Current density vs time for triple-junction a-Si based photoelectrode with no external bias in 1N KOH under 1 sun illumination.

BIOLOGICAL HYDROGEN PHOTOPRODUCTION

Dr. Akira Mitsui
Professor, Division of Marine Biology and Fisheries and
Director, International Research Center for Biological Hydrogen Photoproduction,
Rosenstiel School of Marine and Atmospheric Sciences,
University of Miami
4600 Rickenbacker Causeway, Miami, FL 33149

Abstract

Following are the major accomplishments of the 5th year's study of biological hydrogen photoproduction which were supported by DOE/NREL.

1) Using synchronously growing unicellular aerobic nitrogen fixing cyanobacterium, *Synechococcus* sp. Miami BG 043511, light energy conversion efficiency to H_2 was estimated to be as high as 2.6%, if both H_2 production period and photosynthetic period were considered (i.e., one cell cycle). If only H_2 production period is considered, the efficiency is calculated as 5.5%.

2) Accumulation and degradation of cellular glycogen granules were directly observed by light and electron microscopy during the synchronous culture of this strain, and the intimate relationship between the accumulation of glycogen and the appearance of nitrogenase activity was reconfirmed. Some characteristic structure was also found only at the phase of high nitrogenase activity.

3) Externally added organic substances, such as glucose, pyruvate, sucrose, maltose, fructose and glycerol, enhanced H_2 production significantly in old batch cultures. This suggests that these externally added substances could be used by cells as electron donors for H_2 production only when the cellular glycogen was used up.

4) Expression of one of the structural genes of nitrogenase (*nifH*) was examined using the synchronized cells of *Synechococcus* sp. Miami BG 043511, and mRNA for this gene was found to be present only at the phase of high nitrogenase activity. This indicates that the

activity of nitrogenase is regulated at the transcriptional level in this strain. Since H_2 production in this strain is catalyzed by nitrogenase, it is very important to elucidate the gene structure of nitrogenase and its regulatory mechanisms, in order to establish a highly efficient hydrogen photoproduction system using this highly H_2-producing strain and genetic engineering techniques in future.

5) Polypeptides of nitrogenase were suggested to be synthesized only at the phase of high nitrogenase activity. This result is consistent with the result of transcription analysis above.

6) An attempt was made to purify nitrogenase protein from this strain using agarose gel electrophoresis.

Introduction

Biological hydrogen production has many advantages over other non-biological hydrogen production technologies, some of which are listed below.

1) Hydrogen can be produced by solar energy, water (including seawater) and photosynthetic microorganisms under ambient temperature and atmospheric pressure.

2) In contrast to non-living hydrogen production systems, biological hydrogen production does not need new materials. Living cells multiply by themselves, and are a renewable source of hydrogen.

3) The production method is simple, pollution-free and environmentally friendly.

4) By coupling with the utilization of byproducts, hydrogen production can be made more economical.

However, living organisms have very complex systems in their physiology, biochemistry and genetics, and controlling the complex metabolism to enhance hydrogen photoproduction is generally difficult. Therefore, projects dealing with living organisms need more time and more laborious efforts than those of non-living systems.

In previous intensive efforts and long years of research for photosynthetic microorganisms which have high hydrogen producing capabilities from marine environments, we found a very unique, aerobic, nitrogen-fixing, unicellular cyanobacterial strain *Synechococcus* sp. strain Miami BG 043511, which has an exceptionally high hydrogen production capability. Since this strain is a single celled organism, it is amenable to synchronous culture under nitrogen-fixing conditions. The studies of synchronous culture of this strain revealed that hydrogen production from water consists of two processes; (1) photosynthetic process which involves water photolysis and CO_2 fixation, produces O_2, and finally accumulates carbohydrate (glycogen), and (2) hydrogen production process that utilizes glycogen synthesized during the former process and produces H_2 and CO_2 using light and nitrogenase. CO_2 can be recycled between

the two processes. Therefore, the overall reaction of both processes is as follows:

$$H2O + light \rightarrow H2 + \frac{1}{2}O2$$

It is well known that nitrogenase and hydrogenase, which catalyze hydrogen photoproduction, are extremely oxygen sensitive enzymes. A small amount of oxygen inhibits hydrogen photoproduction. Therefore, it was previously believed that these two seemingly incompatible reactions, oxygen producing photosynthesis and anoxygenic hydrogen photoproduction, could not coexist within the same cell. However, we found that these two reactions are temporally separated within the cell cycle in the unicellular cyanobacterium, *Synechococcus* sp. strain Miami BG 043511. We also found this same phenomenon during the incubation of non-growing cells which were harvested from well synchronized cultures of this strain.

Significant enhancement of hydrogen photoproduction was successfully made during the past several years in this project, using the techniques and basic knowledge of synchronously growing cells of this strain. Objectives in this year's research project were:

1) To measure the actual light energy conversion efficiency to H_2 production in synchronously grown cells of the unicellular cyanobacterium, *Synechococcus* sp. strain Miami BG 043511.

2) To increase the light energy conversion efficiency further, and to investigate factors regulating H_2 photoproduction, particularly;

i) glycogen synthesis and degradation during a cell cycle

ii) relationship between cellular glycogen metabolism and the activity of nitrogenase which catalyzes the H_2 photoproduction of this strain

iii) effects of externally added glucose and other organic substances for the maintenance of nitrogenase activity and the elongation of the hydrogen photoproduction period

iv) changes of mRNA and protein of the nitrogenase during synchronous growth in this strain.

v) isolation and characterization of the nitrogenase from this strain

3) To develop a method of elongating the high rates of H_2 photoproduction by efficient recycling of CO_2 and cellular glycogen.

I. Light Energy Conversion Efficiency to Hydrogen Production as Measured by the Hydrogen Accumulation Method in a Closed Vessel

Hydrogen photoproduction by photosynthetic microorganisms has been studied as one of the ways to produce clean renewable energy source (Mitsui and Kumazawa 1977, Mitsui 1992, 1993). Among photosynthetic microorganisms, N_2-fixing cyanobacteria, which carry out both oxygenic photosynthesis and anoxygenic nitrogenase-catalyzed H_2 production (Jones and Bishop 1976), seem to be suitable for the study on H_2 production. However, concurrent H_2 oxidation was shown to substantially reduce the net amount of H_2 produced (Bothe et al. 1978, Tel-Or et al. 1978). A marine aerobic N_2-fixing unicellular cyanobacterium *Synechococcus* sp. strain Miami BG 043511 is one of strains with little H_2 oxidation activity, hence sustained H_2 photoproduction in closed vessels at high rates was observed (Mitsui et al. 1983, 1985, Reddy and Mitsui 1984). When the H_2 production capability in synchronously grown cells of this strain was examined, cells at the phase of maximum carbohydrate content exhibited highest H_2 production capability (Suda et al. 1992). So far, H_2 production rate of 250 μmol (mg chl)$^{-1}$ h^{-1} was reported (Mitsui et al. 1985). From the applied point of view, however, efficiency of H_2 production in terms of amount of H_2 produced per vessel or per light energy irradiated is one of the important factors. In this study, therefore, optimum H_2 yield per reaction vessel was examined using synchronously grown cells with high H_2 production capability. Based on the strategy of H_2 and O_2 production in strain Miami BG 043511, energy conversion efficiency was estimated.

Materials and Methods

Synechococcus sp. strain Miami BG 043511 was grown in a combined nitrogen-free artificial seawater medium A-N enriched with $NaHCO_3$ (Mitsui and Cao 1988). Synchronously grown cells were obtained as described previously (Suda et al. 1992). Light intensity (photosynthetically active radiation, PAR) and temperature for growth were 25 W/m^2 and 30°C, respectively.

Cells were harvested 10 h after the onset of synchronous growth by centrifugation, washed once and resuspended with HEPES (20 mM) enriched A-N medium without $NaHCO_3$ (pH 7.5). Aliquots of 3 ml were put into 25 ml micro-Fernbach flasks, and sealed with argon gas by repeated evacuation and gassing. Then the flasks were incubated in an illuminated shaker water bath at 30°C. The flasks were illuminated by a bank of fluorescent tubes from underneath. To ensure that light is received only from the bottom of flasks, the side surface of flasks was covered with a black vinyl tape. Light intensity at the bottom surface of the flasks was measured by the energy (400-700 nm, PAR) sensor (SKP 410, Skye Instruments Ltd., UK). For the estimation of energy conversion efficiency, free energy contents of H_2 produced (237 kJ/mol) was divided by irradiated light energy at the bottom surface of the reaction vessels. No correction for reflection or transmission of light was made.

Amounts of H_2 and O_2 were determined by gas chromatography as described previously (Kumazawa and Mitsui 1981). Using a gas-tight syringe, 0.2 ml of gas was withdrawn and injected into gas chromatograph. In order to maintain the pressure in the flask positive, 0.2 ml of argon gas was injected into the flask and mixed well before withdrawing gas for the assay. Since the gas-tight syringe was not equipped with stopcock (i.e., positive pressure in the flask was not maintained in the syringe when transferred from the vessel into gas chromatograph), the amounts of H_2 and O_2 detected by gas chromatograph were corrected for pressure in this study. The correction factor for the pressure increase was calculated as follows:

$$\text{correction factor} = 0.2/(0.2 - a - b)$$

where a and b were amounts (ml) of H_2 and O_2, respectively, detected in 0.2 ml (ambient pressure) of gas sample. For the assay of CO_2, 0.5 ml of 4 M sulfuric acid was added by a syringe into flasks immediately after the H_2 and O_2 assay. Then, 0.5 ml gas was withdrawn by a gas-tight syringe and injected into the gas chromatograph equipped with Chromosorb 102 column and thermal conductivity detector. To obtain the amounts of CO_2 produced by cells, amounts of CO_2 detected in flasks without cells (i.e., dissolved CO_2 in suspending medium) were subtracted from those with cells. Volumes of gas (H_2, O_2 and CO_2) expressed in Results section were those under standard conditions (0°C and 1 atmosphere).

Chlorophyll *a* was extracted with methanol and determined spectrophotometrically by the method described previously (Holm-Hansen and Riemann 1978).

Results

To obtain conditions for maximum H_2 production per vessel, vessels with different cell densities were incubated under H_2 production conditions. Amounts of H_2 and O_2 produced after 12 h (A) and 24 h (B) incubation under the light intensities of 17 and 25 W/m^2 are shown in Figs 1 and 2, respectively. Within the cell densities examined, vessels containing about 0.2 to 0.3 mg chl exhibited optimum H_2 yield per vessel under both light conditions. Under 17 W/m^2, 4.6 ml and 6.4 ml of H_2 accumulated after 12 h and 24 h incubation, respectively, in vessels containing 0.27 mg chl (Fig 1). Under 25 W/m^2, 5.0 ml and 6.5 ml of H_2 accumulated after 12 h and 24 h incubation, respectively, in vessels containing 0.30 mg chl (Fig 2). Thus, maximum amount of H_2 produced was similar under the both light intensities. In contrast, net production of O_2 differed between those two light intensities. During the initial 12 h incubation period, minimum or no net O_2 production was observed under both light intensities. However, compared with those under 17 W/m^2, substantial O_2 production was observed under 25 W/m^2. Thus, under 17 W/m^2, ratios of H_2/O_2 accumulated after 24 h were 11 in vessels containing 0.27 mg chl per vessel, while 2.3 in vessels containing 0.30 mg chl per vessel under 25 W/m^2.

Fig 3 shows the patterns of H_2 and O_2 production in vessels containing 0.045 mg chl (A) and 0.27 mg chl (B) under 17 W/m^2. As expected from the results shown in Figs 1 and 2, there was a phase of active H_2 production at the initial period of the incubation. In vessels with lower cell density (Fig 3A), notable production of O_2 was observed during 19 h to 24 h and 36 h to 48 h periods. During these O_2 production periods, H_2 production was minimal. A similar pattern of H_2 and O_2 production was also observed under higher cell density (Fig 3B), though the ratios of accumulated H_2/O_2 at 24 h and 48 h were somewhat higher than those observed under lower cell density conditions. The ratios of accumulated H_2/O_2 under lower cell density conditions (Fig 3A) were 4.7 and 2.2 at 24 h and 48 h, respectively, while 11 and 3.1 under higher cell density conditions (Fig 3B).

Under 25 W/m^2, O_2 production was observed during 12 h to 24 h and 36 h to 48 h period in vessels with lower cell density (Fig 4A). During 24 h to 36 h period, there was a net consumption of O_2. The pattern of H_2 production was similar to that observed under lower light intensity (Fig 3). Under higher cell density (Fig 4B), however, O_2 production started from 12 h and continued at much reduced rate after 24 h. The rate of H_2 production started to decrease from 12 h, and the increase was quite small after 24 h. The ratios of accumulated H_2/O_2 under lower cell density conditions (Fig 4A) were 2.4 and 2.3 at 24 h and 48 h, respectively, while 2.3 and 1.8 under higher cell density conditions (Fig 4B).

Fig 5 shows the change in the amounts of H_2, O_2 and CO_2 during 24 h incubation period. As shown, active H_2 and CO_2 production was observed during the initial 12 h period, and then CO_2 uptake and O_2 production occurred during the subsequent 12 h period. At 24 h period, the ratio of H_2/O_2 produced was

2. It has to be mentioned, however, that H_2/O_2 ratios fluctuated from 2 to 3 in repeated experiments. Although the data was not shown, $H_2/(O_2 + CO_2)$ was about 2 at 24 h period, while H_2/O_2 ratios were 2.6 and 3.0.

Since it was suspected that the increased pressure in flasks may interfere the sustained H_2 production, H_2 production was examined under conditions with (Fig 6A) and without (Fig 6B) periodical gas replacement. Gas replacement was done immediately after the assay of H_2 and O_2, by repeated evacuation and flushing with argon gas at every 24 h measurement interval. H_2 and O_2 accumulated during each intervals were shown cumulatively. In vessels with gas replacement, H_2 production continued, though the rate gradually decreased during the period (8 days) examined (Fig 6A). Cumulative amounts of H_2 and O_2 after 8 days were about 21 ml and 8.2 ml, respectively. On the other hand, increase in H_2 and O_2 after 1 day incubation was quite small in vessels without gas replacement (Fig 6B). After 8 days, accumulated amounts of H_2 and O_2 were 11 ml and 6.2 ml, respectively.

Discussion

Previously, we observed that the capability of H_2 production in synchronously grown cells of *Synechococcus* sp. Miami BG 043511 changes within a cell cycle and that cells with maximum carbohydrate contents (10 h after the onset of synchronous growth) exhibit highest capability of H_2 production (Suda et al. 1992). To examine optimum H_2 yield per reaction vessel, therefore, capabilities for H_2 production under high cell densities were examined in this study using cells 10 h after the onset of synchronous growth.

As shown in Figs 1 and 2, vessels containing about 0.2 to 0.3 mg chl exhibited optimum H_2 production per vessel. As expected from previous observation (Suda et al. 1992), H_2 and O_2 production by synchronously grown cells was not simultaneous (Figs 3 and 4). H_2 production preceded O_2 production. As seen in Figs 3 and 4A, O_2 production occurred at certain periods during incubation. In addition, such periodic appearance of O_2 production occurred as if there were alternate periods of active H_2 photoproduction and photosynthesis within a 24 h interval. As shown in Fig 5, H_2 and CO_2 production occurred during the initial 12 h period. This is in agreement with a previous observation that strain Miami BG 043511 consumes endogenous carbohydrate (glycogen) during the phase of nitrogen fixation under synchronous diazotrophic growth (Mitsui et al. 1986, 1987). Since H_2 production observed in this study is nitrogenase-dependent, the simultaneous production of H_2 and CO_2 indicates that cellular carbohydrate (glycogen) was used as a source of electron donor for the H_2 production. During the following 12 h to 24 h period, uptake of CO_2 and production of O_2 by photosynthesis occurred concurrently (Fig 5). During this period, H_2 production occurred at a reduced rate. Thus, H_2 production by strain Miami BG 043511 seems to occur in two steps: initial H_2 production using endogenous carbohydrate and subsequent supply of carbohydrate by photosynthesis. However, whether such two processes can proceed compatibly seems to be dependent on the experimental conditions. As shown in Fig 4A, periodic production of O_2 was observed under low cell density, and the H_2/O_2 ratios at 24 h and 48 h were 2.4 and 2.3, respectively. In contrast, periodic pattern of O_2 production was not observed after 24 h in vessels with higher cell density (Fig 4B). This could be a pressure effect as discussed later.

Maximum slope of H_2 production per vessel was 0.44 ml H_2/h (Fig 3B, 4 h to 8 h period). Since light intensity was 17 W/m^2, light energy received at the bottom of flask (13.8 cm^2) was 84.5 J/h (= 17 W/m^2 x 13.8 x 10^{-4} m^2 x 60 sec/min x 60 min/hour). As 237 kJ of free energy is released by the oxidation of one mole of H_2 to H_2O, 0.44 ml (19.6 µmol) of H_2 can release 4.65 J upon oxidation. Thus, 4.65 J was conserved as H_2 when 84.5 J of light energy was irradiated. If one simply calculates the conversion

efficiency based on (H_2 produced)/(light irradiated), conversion efficiency of 5.5% (4.65 / 84.5 x 100) is obtained. However, this value of 5.5% does not reflect the real energy conversion efficiency. As described already, H_2 production occurred using carbohydrate as a source of electron donor. On the other hand, during a cycle of 24 h, most of CO_2 released was refixed by photosynthesis (Fig 5). If one assumes that H_2 production and photosynthesis operates compatibly, overall product would be H_2 and O_2. As shown in Fig 4, H_2/O_2 ratios at 24 h and 48 h were relatively close to 2. In addition, duration of H_2 and O_2 production could be prolonged by gas replacement at each 24 h interval. During initial 24 h incubation, 7.4 ml H_2 (78.7 J) was produced using 2,980 J (= 25 W/m^2 x 13.8 x 10^{-4} m^2 x 60 sec/min x 60 min/hour x 24 hour) of light energy (Fig 5). Thus, the conversion efficiency in this period would be 2.6% (78.7 / 2,980 x 100). The conversion efficiency of 2.6% (PAR) estimated here is, however, an upper estimate, since H_2/O_2 ratios varied from 2 to 3 from one experiment to the others (mentioned already) and since the rate of production gradually decreased with time.

It has to be mentioned here that, in green algae, conversion efficiencies of 6% to 24% of PAR were observed under low light intensities (about 2 to 9 $\mu W/cm^2$) using a continuous inert gas flushing apparatus (Greenbaum 1988). In green algae, however, O_2 produced by biophotolysis of water could be a major obstacle to sustain H_2 and O_2 production at higher light intensities in closed reaction vessels. Apparently, green algae do not possess a mechanism to protect H_2 production from O_2 inhibition (Rosenkrans et al. 1983) as in cyanobacteria.

N_2-fixing cyanobacteria, known to carry out oxygenic photosynthesis and anoxygenic N_2 fixation (Fay 1992, Gallon 1992), exhibit nitrogenase-catalyzed H_2 formation in which the enzyme system is protected from O_2 inactivation. There is, however, another constraint for the sustained H_2 production. In N_2-fixing cyanobacteria, concurrent H_2 oxidation activity was shown to substantially reduce the net amount of H_2 produced (Bothe et al. 1978). Using a continuous inert gas flushing apparatus, which reduced the buildup in partial pressure of H_2 and O_2, sustained H_2 production by nitrogen-limited cells was observed and their energy conversion efficiencies were estimated (Miyamoto et al. 1979a, 1979b). However, as mentioned in one of the reports (Miyamoto et al. 1979a), contribution of endogenous carbohydrate accumulated during nitrogen-limited growth conditions to H_2 production as a source of electron donor was not taken into account. Glycogen was also shown in heterocystous cyanobacteria to serve as a source of electrons for the nitrogenase catalysis (Ernst and Böger 1985). Since strain Miami BG 043511 exhibits little H_2 oxidation in closed vessels, the use of a gas flow apparatus was not necessary. In addition, production of H_2 and O_2 at periodic intervals was close to stoichiometric (Fig 5). In this study, therefore, energy conversion efficiency was estimated based on overall reductant (H_2) and oxidant (O_2) accumulated in vessels.

Interestingly, compared with the vessels without gas replacement, H_2 production was sustained for longer periods in vessels with gas replacement (Fig 6). The cumulative amount of H_2 produced was significantly higher in vessels with gas replacement. It seems relevant to mention here that cyclic production of H_2 and O_2 was prolonged in a vessel equipped with a syringe to maintain the pressure in the flask at ambient level (unpublished data observed by A. Mitsui, S. Suda, W. Lee and H. Takeyama, Univ. of Miami). Thus, the pressure buildup somehow inhibited both H_2 and O_2 production. If one considers the amounts of H_2 and O_2 produced, pressure in the flasks must be increased to about 1.4 (Fig 4B) or 1.5 (Fig 6B) atmosphere after 24 h incubation. It is not clear how the increase in pressure affected H_2 and O_2 production. H_2 oxidation was shown to substantially reduce the net amount of H_2 production in other cyanobacteria (Bothe et al. 1978, Tel-Or et al. 1978). In this study, although conditions favorable for H_2 oxidation were created by the increase in partial pressure of H_2 and O_2, no uptake of H_2 was observed even when O_2 was consumed (Fig 4A). Therefore, it is not likely that H_2 oxidation was the major cause of curtailed H_2

production observed in Figs 4B and 6B. Further study is needed to clarify the cause of the pressure effect and to enhance H_2 and O_2 production when the pressure builds up in vessels.

References

Bothe, H., E. Distler and G. Eisbrenner. 1978. "Hydrogen Metabolism in Blue-green Algae." *Biochimie*, 60:277-289.

Ernst, A. and P. Böger. 1985. "Glycogen Accumulation and the Induction of Nitrogenase Activity in the Heterocyst-Forming Cyanobacterium, *Anabaena variabilis*." *J. Gen. Microbiol*, 131:3147-3153.

Fay, P. 1992. "Oxygen Relations of Nitrogen Fixation in Cyanobacteria." *Microbiol. Rev*, 56:340-373.

Gallon, J.R. 1992. "Reconciling the Incompatible: N_2 Fixation and O_2." *New Phytol*, 122:571-609.

Greenbaum, E. 1988. "Energetic Efficiency of Hydrogen Photoevolution by Algal Water Splitting." *Biophys. J*, 54:365-368.

Holm-Hansen, O. and B. Riemann. 1978. "Chlorophyll *a* Determination: Improvements in Methodology." *OIKOS*, 30: 438-447.

Jones, L.W. and N.I. Bishop. 1976. "Simultaneous Measurement of Oxygen and Hydrogen Exchange from the Blue-Green Alga *Anabaena*." *Plant Physiol*, 57:659-665.

Kumazawa, S. and A. Mitsui. 1981. "Characterization and Optimization of Hydrogen Photoproduction by a Saltwater Blue-Green Alga, *Oscillatoria* sp. Miami BG 7. I. Enhancement through Limiting the Supply of Nitrogen Nutrients." *Int J. Hydrogen Energy*, 6: 339-348.

Mitsui, A. 1992. "Hydrogen Photoproduction by Marine Cyanobacteria for Alternating the Carbon Energy Sources." In J.C. Hunter-Cevera (ed.) *Short communications of the 1991 International Marine Biotechnology Conference*, Volume II, 710-723. Wm C. Brown Publishers, Dubuque, Iowa.

Mitsui, A. 1993. "Recent Research Development on Biological Hydrogen Photoproduction." In T.Ohta and T.Homma (ed.) *Energy System and Conversion*, S11-S24. Universal Academy Inc., Tokyo.

Mitsui, A. and S. Cao. 1988. "Isolation and Culture of Marine Nitrogen-Fixing Unicellular Cyanobacteria, *Synechococcus*." *Methods Enzymol*, 167 105-113.

Mitsui, A., S. Cao, A. Takahashi and T. Arai. 1987. "Growth Synchrony and Cellular Parameters of the Unicellular Nitrogen-Fixing Marine Cyanobacterium, *Synechococcus* sp. strain Miami BG 043511 under Continuous Illumination." *Physiol. Plant*, 69 1-8.

Mitsui, A and S. Kumazawa. 1977. "Hydrogen Production by Marine Photosynthetic Organisms as a Potential Energy Source." In: A. Mitsui, S. Miyachi, A San Pietro and S. Tamura (ed.) *Biological solar energy conversion*, 23-51. Academic Press, New York.

Mitsui, A., S. Kumazawa, E.J. Phlips, K.J. Reddy, K. Gill, T Matsunaga, B.R. Renuka, T. Kusuni, G. Reyes-Vasquez, K. Miyazawa, L. Haynes, H. Ikemoto, E Duerr, C.L. Leon, D. Rosner, R. Sesco and E. Moffat. 1985. "Mass Cultivation of Algae and Photosynthetic Bacteria: Concepts and Application." In T.K. Ghose (ed.) *Biotechnology and Bioprocess Engineering*, 119-155. International Union of Pure and Applied Chemistry and Indian National Science Academy. United India Press, New Delhi.

Mitsui, A., S. Kumazawa, A. Takahashi, H. Ikemoto, S Cao and T Arai. 1986 "Strategy by which Nitrogen-Fixing Unicellular Cyanobacteria Grow Photoautotrophically." *Nature*, 323:720-722.

Mitsui, A., E.J. Phlips, S. Kumazawa, K.J. Reddy, S. Ramachandran, T. Matsunaga, L. Haynes and H. Ikemoto. 1983. "Progress in Research toward Outdoor Biological Hydrogen Production using Solar Energy, Sea Water, and Marine Photosynthetic Microorganisms." *Ann. NY Acad. Sci*, 413:514-530.

Miyamoto, K., P.C. Hallenbeck and J.R. Benemann. 1979a. "Nitrogen Fixation by Thermophilic Blue-Green Algae (Cyanobacteria): Temperature Characteristics and Potential Use in Biophotolysis." *Appl. Environ. Microbiol*, 37:454-458.

Miyamoto, K., P.C. Hallenbeck and J.R. Benemann. 1979b. "Solar Energy Conversion by Nitrogen-Limited Cultures of *Anabaena cylindrica*." *J. Ferment. Technol*, 57:287-293.

Reddy, K.J. and A. Mitsui. 1984. "Simultaneous Production of Hydrogen and Oxygen as Affected by Light Intensity in Unicellular Nitrogen Fixing Blue-Green Alga *Synechococcus* sp. Miami BG 043511." In C. Sybesma (ed.) *Advances in Photosynthesis Research*, Vol II, 785-788. Martinus Nijhoff/Dr. Junk Publishers, Hague.

Rosenkrans, A.M., M.M. Rosen and A.I. Krasna. 1983. "Effect of Oxygen Removal on Hydrogen Photoproduction in Algae." *Biotechnol. Bioeng*, 25:1897-1904.

Suda, S., S. Kumazawa and A. Mitsui. 1992. "Change in the H_2 Photoproduction Capability in a Synchronously Grown Aerobic Nitrogen-Fixing Cyanobacterium, *Synechococcus* sp. Miami BG 043511." *Arch Microbiol*, 158:1-4.

Tel-Or,E., L.W. Luijk and L. Packer. 1978. "Hydrogenase in N_2-Fixing Cyanobacteria." *Arch. Biochem. Biophys*, 185:185-194.

II. To Investigate Factors Regulating the H_2 Photoproduction in Order to Increase Light Conversion Efficiency Further

(I) Glycogen Synthesis and Degradation during a Cell Cycle

Several strains of unicellular cyanobacteria can grow diazotrophically under aerobic photoautotrophic conditions (Fay 1992). Among these cyanobacteria, *Synechococcus* sp. strain Miami BG 043511 has unique characteristics in that it is able to grow rapidly under high light intensities with vigorous aeration, and it is amenable to synchronous growth (León et al. 1986, Mitsui et al. 1986, 1987, 1993). During synchronous growth, there is a cyclicity of cellular activities such as photosynthetic oxygen evolution, nitrogen fixation, and hydrogen evolution (León et al. 1986, Mitsui et al. 1986, 1987, 1993, Mitsui 1993, Suda et al. 1992). Cyclic cellular glycogen synthesis and degradation have also been observed (Mitsui et al. 1987, Mitsui 1993). These phenomena have been interpreted as cell cycle events (Mitsui et al. 1986, 1987, 1993).

In this study, ultrastructural changes observed during synchronous growth by phase contrast and electron microscopy are described. In addition, possible correlations between ultrastructural changes and previously studied cellular activities and events are discussed.

Material and Methods

Strain and Culture Conditions

A marine unicellular cyanobacterium, *Synechococcus* sp. strain Miami BG 043511, was grown under batch culture conditions for 5 to 7 days in a combined nitrogen-free medium (A-N medium) as described by Mitsui and Cao (1988). Fifty ml of batch culture was inoculated into a water jacketed glass cylinder (8.5 cm in diameter) containing 3.3 l of A-N medium with sodium bicarbonate, and cultured at 30°C, under a light intensity of 150 $\mu E\ m^{-2}\ s^{-1}$ (Mitsui and Cao 1988). Air containing ca. 4% CO_2 was bubbled in through the bottom of the culture cylinders at a rate of 200-500 ml/min. The pH of the medium was maintained at 7.6±0.1 by slight adjustment of the CO_2 concentration. After 72-hr culture in the light, 16-hr dark, 16 hr-light and 16-hr dark pretreatment periods were introduced (Mitsui and Cao 1988). Cells were then grown synchronously under subsequent continuous illumination.

Nitrogenase Assay

Nitrogenase activity was determined as described by León et al. (1986). Five ml aliquots were taken from the culture cylinder and transferred into 25-ml Fernback flasks fitted with a rubber stopper. After the inner atmosphere was replaced with argon gas, 2 ml of acetylene gas (Matheson) was injected into the flask with a syringe through the rubber stopper. Incubation was carried out in a shaker bath at 150 $\mu E\ m^{-2}\ s^{-1}$ at 30°C for 30 min. The reaction was terminated by injecting 1 ml of 20% trichloroacetic acid through the rubber stopper. A 0.5 ml gas sample was taken from the flask, and the amount of ethylene that was formed was determined using a gas chromatograph (Hewlett Packard, model 5710A) fitted with a flame ionization detector and dual columns (Porapak R).

Determination of Cell Number and Dry Weight

Cell number was determined using a Thoma hemocytometer, after fixing a 1 ml sample with 50 µl of 10% Lugol solution. Cell dry weight was measured after cells were collected on pre-weighed glass microfiber filters (Whatman, 934AH), washed twice with distilled water and dried at 90°C for 24 hr.

Light Microscopy

Cell suspensions were taken from the culture cylinder at 4 hr intervals and fixed by adding an equal volume of A-N medium containing 2% glutaraldehyde. Cells were observed with a phase contrast microscope (Olympus, BH-2).

Electron Microscopy

Cells fixed with glutaraldehyde as described above were stored at 4°C overnight. These cells were washed sequentially for 30 min each with a 4:1, 3:2, 2:3 and 1:4 (v/v) mixture of A-N medium and 100 mM cacodylate buffer (pH 7.0). Cells were then suspended in cacodylate buffer and embedded in the cacodylate buffer containing 1% agarose. Small blocks (ca. 0.5 mm) were further fixed in the cacodylate buffer containing 1% osmium tetroxide for 3 hr at room temperature, dehydrated in a graded series of ethanol and embedded in Spurr resin. Ultrathin sections were cut in a Sorvall MT-2 microtome, double-stained with uranyl acetate and lead citrate, and observed in a Philips EM 300 electron microscope.

Results

Cyclicity of Cell Division and Nitrogenase Activity during Synchronous Growth

Fig 7 shows changes in cell number, the ratio of doubling cells (dividing cells per total cell number) and nitrogenase activity during synchronous growth under continuous illumination. As has been previously reported (Mitsui et al. 1987, Mitsui and Cao 1988), the first cell division occurred 4 hours after the onset of synchronous growth in the light. Within 2 hours, all of the cells have divided, and the total cell number increases by approximately two-fold.

Nitrogenase activity appeared at approximately the 8^{th} hour, reached peak activity at approximately the 12^{th} to 14^{th} hour, and disappeared during the following several hours. The second nitrogenase activity appeared at the 28^{th} hour, and sharply increased during the next 4 hour period. The timing of nitrogenase activity was similar to that in previous studies (León et al. 1986, Mitsui et al. 1986).

Samples were taken at 4 hr intervals during synchronous growth and ultrastructural changes examined by phase contrast and electron microscopy.

Light Microscopy

Fig 8 shows the intracellular structural changes observed by phase contrast microscopy. At the onset (0^{th} hour) of synchronous growth under continuous illumination, fine membrane-like structures were observed in the peripheral regions of each cell. These appeared to project from the inner region of the cell to the cell surface. At the 4^{th} hour, when most cells were in the dividing stage, these structures were not apparent. During hours 8-12, the peripheral region became clear with no visible structures observed, and the central region appeared more densely packed than before. At the 16^{th} hour, the membrane-like structures which appeared at the 0^{th} hour reappeared. The overall intracellular structure at the 16^{th} hour was similar to that at the 0^{th} hour, although the structures were more clearly observed at the 0^{th} hr. At the 20^{th}

hour, when second cell division occurred, the intracellular structures were similar to those observed during the first cell division.

Intracellular structural changes from the 24th hour to the 32nd hour appeared to recur between the 8th and 12th hours, although the degree of growth synchrony decreased to some extent.

Electron Microscopy

The ultrastructural changes in these cells as seen by electron microscopy are shown in Fig 9. The majority of cells at a particular time during synchronous growth exhibited ultrastructure similar to that shown in Fig 9. At the 0th hour, thylakoid membranes are clearly seen in the peripheral region of the cells. Therefore, the membrane-like structures observed by light microscopy at the 0th hour (Fig 8) correspond to thylakoid membranes.

In the peripheral region, relatively large granules (diameter 0.4-0.5 μm) which are slightly darkened in the micrograph, were observed at the 0th hour. At the 4th hour (cell division phase) these granules were also observed in the peripheral region. In addition, another smaller type of granule was also observed in this region (diameter 0.1-0.2 μm). These granules were almost transparent in appearance. From the 8th hour to the 12th hour (the phase of cell elongation), these small granules grew in size (0.2-0.3 μm). These cells were filled with the granules except for the central region of the cells which contained the DNA, and from 3 to 10 of these small granules formed chains along the cell wall. Several of these chains were observed in each cell. Each chain of granules was surrounded by a membrane-like structure resembling green peas lining a pea shell. During the 8th hour and 12th hour, the larger granules observed at the 0th and 4th hour disappeared. At the 16th hour, the size and number of the smaller granules decreased, and the larger granules and thylakoid membranes appeared again. Intracellular structural changes from the 16th hour to the 32nd hour essentially repeated those seen from the 0th to the 12th hour, although the degree of synchrony in the culture decreased somewhat.

Discussion

Significant temporal changes in both the number and size of the cells' smaller granules (0.1 to 0.3 μm) were found during synchronous growth under continuous illumination (Fig 9). Changes in these smaller granules were closely related to cellular content of glycogen (Mitsui et al. 1987). Cellular glycogen synthesis began after the onset of synchronous growth, and maximum glycogen accumulation in the cells occurred approximately at the 12th hour. The glycogen content decreased during the following several hours. This process was repeated at approximately 20-24 hour intervals at least three times during synchronous growth under continuous illumination (Mitsui et al. 1987). The minimum and maximum glycogen content was 10-20% and 50-60% per dry weight basis, respectively (Ikemoto and Mitsui, unpublished). Observation by both electron and phase contrast microscopy in this study indicated that the smaller granules increased gradually from the 4th to 8th hour and packed the cells at the 12th hour. The number and size of these granules decreased during the next four hour period, and then increased again. Therefore, we can conclude that the smaller granules observed in this study were glycogen. Previous studies (Mitsui et al. 1986, 1987, Suda et al. 1992, Mitsui 1993, Ikemoto and Mitsui 1994) indicated that cellular glycogen was the energy source for nitrogenase activity. In this study, it was observed that nitrogenase activity was maximum when the smaller granules accumulated within the cells during synchronous growth and decreased when these granules decreased in size and number (Figs 7 and 9). These data further support the hypothesis that these granules are glycogen.

The nature of the larger sized granules (0.4-0.5 μm) which appeared at the 0th hour and the 16th hour are unknown at present. These will be the subject of future studies.

It is well known that nitrogenase is very sensitive to small amounts of oxygen (Fay 1992). The mechanisms of nitrogenase protection from internally photosynthetically produced oxygen are understood in this unicellular cyanobacterium; A temporal separation of photosynthetic oxygen production and nitrogen fixation occurs within a cell cycle (Mitsui et al. 1986, 1987, 1993). However, nitrogen protection mechanisms from external oxygen that penetrates the cells of this unicellular cyanobacterium have not been studied. In heterocystous filamentous cyanobacteria, the cell wall prevents oxygen from penetrating into the heterocysts, and protect the nitrogenase from oxygen (Fay 1992). The unicellular cyanobacterium, however, lacks this protective cell wall. During synchronous growth in this study, specific cell wall structures did not appear during the nitrogen fixation phase.

It was reported that the nitrogenase protein in some cyanobacteria is distributed throughout the cell (Fay 1992, Rai et al. 1992). If the nitrogenase proteins in this unicellular cyanobacterium are arranged in this manner, the nitrogenase should not be functional, because there is no protection from external oxygen. Therefore, it is quite interesting to investigate whether the unit of glycogen granules surrounded by a membrane contains nitrogenase proteins and the unit itself has a mechanism of nitrogenase protection from externally derived oxygen. Future immunological studies which investigate the location of the nitrogenase and/or biochemical study of the structures after isolation should be conducted.

References

Fay, P. 1992. "Oxygen Relations of Nitrogen Fixation in Cyanobacteria." *Microbiol. Rev*, 56:340-373.

Ikemoto, H. and A. Mitsui. 1994. "Diazotrophic Synchronous Growth of a Marine Unicellular Cyanobacterium, *Synechococcus* sp. Miami BG 043511, under Aerobic and Anaerobic Conditions." (in press)

León, C., S. Kumazawa and A. Mitsui. 1986. "Cyclic Appearance of Aerobic Nitrogenase Activity during Synchronous Growth of Unicellular Cyanobacteria." *Current Microbiol*, 13:149-153.

Mitsui, A. 1993. "Recent Research Development on Biological Hydrogen Photoproduction." In T.Ohta and T.Homma (ed.) *Energy System and Conversion*, S11-S24. Universal Academy Inc., Tokyo.

Mitsui, A. and S. Cao. 1988. "Isolation and Culture of Marine Nitrogen-Fixing Unicellular Cyanobacteria, *Synechococcus*." *Methods Enzymol*, 167:105-113.

Mitsui, A., S. Cao, A. Takahashi and T. Arai. 1987. "Growth Synchrony and Cellular Parameters of the Unicellular Nitrogen-Fixing Marine Cyanobacterium, *Synechococcus* sp. strain Miami BG 043511 under Continuous Illumination." *Physiol. Plant*, 69:1-8.

Mitsui, A., S. Kumazawa, A. Takahashi, H. Ikemoto, S. Cao and T. Arai. 1986 "Strategy by which Nitrogen-Fixing Unicellular Cyanobacteria Grow Photoautotrophically." *Nature*, 323:720-722.

Mitsui, A., S. Suda and N. Hanagata. 1993. "Cell Cycle Events at Different Temperatures in Aerobic Nitrogen-Fixing Marine Unicellular Cyanobacterium *Synechococcus* sp. Miami BG 043511." *J. Mar Biotechnol*, 1:89-91.

Rai, A.N., M. Borthakur and B. Bergman. 1992. "Nitrogenase Derepression, its Regulation and Metabolic Changes Associated with Diazotrophy in the Non-Heterocystous Cyanobacterium *Plectonema boryanum* PCC 73110." *J Gen Microbiol*, 138:481-491.

Suda, S., S. Kumazawa and A. Mitsui. 1992. "Change in the H_2 Photoproduction Capability in a Synchronously Grown Aerobic Nitrogen-Fixing Cyanobacterium, *Synechococcus* sp. Miami BG 043511." *Arch Microbiol*, 158:1-4.

(ii) Cellular Glycogen Metabolism and H_2 Photoproduction

The relationship between cellular glycogen metabolism and H_2 photoproduction was investigated using synchronous growth techniques. It was found that cell cycle events occurred in the following sequence:

Photosynthetic O_2 Evolution
↓
Accumulation of Cellular Glycogen
↓
Degradation of Cellular Glycogen Coupled to the Appearance of Nitrogenase Activity
↓
Nitrogenase Catalyzed H_2 Photoproduction.

When cellular glycogen was used up, nitrogenase activity and H_2 production ceased simultaneously.

(iii) Effect of Externally Added Glucose and Other Organic Substances on the Nitrogenase Activity and H_2 Production

The aerobic nitrogen fixing unicellular cyanobacterium, *Synechococcus* sp. strain Miami BG 043511, which was isolated from subtropical marine environment (Mitsui 1978, Mitsui et al. 1985), has unique characteristics for both basic and applied studies (MItsui 1993, Mitsui et al. 1985). This strain is amenable for synchronous growth under nitrogen fixing conditions (León et al. 1986, Mitsui and Cao 1988, Mitsui et al 1986, 1987), and cells at a specific stage of their synchronous growth show a very high H_2 photoproduction capability (Mitsui 1993, Mitsui et al 1993, Suda et al. 1992).

A series of synchronous growth studies (Mitsui 1993, Suda et al. 1992) revealed that endogenous H_2 photoproduction from water in this strain involves two processes; the photosynthetic process which synthesizes glycogen from CO_2 and exhibits oxygen production from H_2O, and the H_2 and CO_2 producing process with the degradation of cellular glycogen. Hydrogen production ceases when cellular glycogen is used up (Suda et al. 1992). Therefore, it is assumed that the efficient recycling of CO_2 which is released during the H_2 photoproduction process or the external addition of organic carbon sources could be a basic principle for prolonging H_2 production.

In this study, in order to elucidate the above mentioned hypothesis, the effect of externally added glucose and other organic substrates on H_2 photoproduction in batch cultures was studied. The effects of organic substrates on nitrogenase activity were also examined, since nitrogenase is known to be the major enzyme for H_2 photoproduction in this strain (Mitsui 1992).

Materials and Methods

Organism and Culture Conditions

Synechococcus sp. strain Miami BG 043511 was cultured as described previously (Mitsui and Cao 1988) in a 2.5 l culture flasks containing a combined nitrogen-free artificial seawater medium A-N at 27±1 °C under continuous illumination of 150 μE m^{-2} s^{-1}. Cultures were constantly aerated by bubbling air from the bottom.

Preparation of Organic Substances

Organic compounds which are listed in Table 1 were dissolved in A-N medium containing 10 mM HEPES buffer (pH 7.6). When the pH of the organic compound solution deviated more than ±0.1, it was adjusted to 7.6 with 4N NaOH or HCl solution. 2 M stock solutions were prepared from each of the organic compounds.

Measurements of Cellular Glycogen (Glucose)

Cells after different culturing periods were harvested by centrifugation, washed twice with A-N medium and suspended in distilled water. Cellular glycogen (glucose) was then determined by the method of Dubois et al. (1956).

Assay for the Determination of H_2 and O_2 Production

Cells of the batch culture were harvested by centrifugation, washed twice with A-N medium and then suspended in A-N medium. Defined amounts of the organic stock solutions were added to the cell suspension. Aliquots of 5 ml of these cell suspensions containing the final substrate concentration were placed into 25 ml micro-Fernbach flasks and sealed with butyl rubber stoppers. The air was replaced by argon gas by repeated evacuation and gassing. The amounts of H_2 and O_2 evolved were determined by gas chromatography (GC-8A, Shimadzu) using the method described previously (Kumazawa and Mitsui 1981).

Assay of Nitrogenase Activity

Nitrogenase activity was determined by the acetylene reduction method as described previously (León et al. 1986) using a gas chromatograph Hewlett Packard GC 5710A attached to an integrator chromatopac (Shimadzu C-R5A).

Dry Weight and Chlorophyll Measurement

Dry weight of the cell suspension was determined as described previously (Mitsui 1992). In some cases, the dry weight of the cell suspension was estimated from its chlorophyll concentrations using a standard curve correlating dry weight and chlorophyll concentrations. Chlorophyll was determined by the method of Holm-Hansen and Riemann (1978).

Results

Cellular Glucose Content and H_2 Photoproduction Activity

Fig 10 shows the relationship between cellular glucose content and H_2 photoproduction in a random batch culture of *Synechococcus* sp. strain Miami BG 043511. High rates of H_2 photoproduction activity were observed in younger batch cultures (2-4 days). These rates decreased drastically when the cultures grew older (older than 4 days), suggesting that decreasing carbohydrate content coincides with the decrease of H_2 evolution.

Effects of Glucose Addition on H_2 Photoproduction

Earlier growth stages (3-day old batch culture) of this strain exhibited high H_2 photoproduction capability without any addition of glucose, and added glucose showed little effect (Fig 11A). However, when cultures grew older the situation changed significantly. Although hydrogen photoproduction capability decreased sharply in the 7-day old culture without addition of glucose, H_2 photoproduction capability could be restored significantly when glucose was added (Fig 11B). In the 15-day old culture, the situation was

similar to that of a 7-day old culture (Fig 11C). However, the restoration effect of glucose on H_2 photoproduction was lower to some extent.

H_2 Photoproduction from Various Organic Substrates

To study the effects of the addition of not only glucose, but also various other organic compounds such as other carbohydrates, organic acids and alcohols (Table 1), 6-day old cultures were employed. Among the carbohydrates tested, glucose, fructose, maltose and sucrose enhanced the H_2 production remarkably. The addition of carbohydrates, such as arabinose, cellobiose, lactose, xylose, and dextrin had, in contrast, little effect on H_2 production. Among the tested organic acids, pyruvate enhanced H_2 production remarkably whereas other organic acids showed little effect. Among the tested alcohols, glycerol was the best electron donor. Ethanol showed only little enhancement on hydrogen production.

Table 1 Hydrogen Photoproduction from Batch Culture (6-day old) of *Synechococcus* sp. strain Miami BG 043511 with or without Substrate

	H_2 production (ml/mg dry wt./100hr)	With substrate/ without substrate
Control (without substrate)	0.07	1.0
Treatments (with substrate) (25 mM)		
I. Organic acids		
Acetate	0.03	0.4
Citrate	0.00	0.0
Formate	0.06	0.9
Fumarate	0.01	0.1
Lactate	0.08	1.1
Malate	0.01	0.1
Oxalate	0.12	1.7
Pyruvate	0.83	11.9
Succinate	0.15	2.1
II. Alcohol		
Butanol	0.00	0.0
Ethanol	0.17	2.4
Glycerol	0.45	6.4
Methanol	0.11	1.6
Phenol	0.00	0.0
III. Carbohydrates		
Arabinose	0.11	1.6
Cellobiose	0.21	3.0
Dextrin	0.14	2.0
Fructose	0.27	3.9
Glucose	0.77	11.0
Lactose	0.11	1.6
Maltose	0.75	10.7
Mannitol	0.05	0.7
Mannose	0.00	0.0
Sorbitol	0.08	1.1
Starch	0.08	1.1
Sucrose	0.74	10.6
IV. Other organic compounds		
DL-Arginine	0.05	0.7
DL-Aspartate	0.02	0.3
Benzoate	0.00	0.0

Caprylate	0.00	0.0
Glutamate	0.06	0.9
Glycerophosphate	0.09	1.3
Malonate	0.08	1.1
Phthalate	0.01	0.1
Propionate	0.01	0.0
Tartarate	0.00	0.0

Effects of Pyruvate Concentrations on H_2 Photoproduction

Fig 12 shows the effects of different concentrations of pyruvate on H_2 production. A small enhancement of H_2 production was observed with 5 mM pyruvate in the 3-day old culture, which showed high endogenous H_2 photoproduction without addition of substrates. H_2 photoproduction was even inhibited at a higher pyruvate concentration (105 mM). However, in the 7- and 15-day old cultures which exhibited low endogenous H_2 photoproduction capability, a significant enhancement of H_2 production by the addition of pyruvate was observed (Figs 12B and 12C). The optimum concentrations of pyruvate were observed to be 15 mM and 35 mM in the 7- and 15-day old cultures, respectively.

Rates of H_2 Photoproduction from Organic Substances

In Fig 13, the rates of H_2 photoproduction from 6 selected organic substrates (pyruvate, glucose, maltose, sucrose, fructose and glycerol) in 6-day old culture were compared. In these cultures, without the addition of organic substrates, H_2 was produced only during the first 20 hrs incubation period in considerable amounts. No H_2 was produced after 20 hrs of incubation. During the first 20 hrs when endogenous H_2 production was observed, H_2 production was inhibited by the addition of organic substrates. High rates of H_2 production from organic substrates occurred during the 20-40 hrs incubation period when no more endogenous H_2 production could be observed. The maximum rates of H_2 production from pyruvate, glucose, maltose, sucrose, fructose and glycerol in 6-day old batch culture during this period were 1.11, 0.62, 0.50, 0.47, 0.30 and 0.39 µmole per mg cell dry weight per hour, respectively.

Effects of the Addition of Organic Substrate on Nitrogenase Activity

As previously reported, H_2 photoproduction is catalyzed by nitrogenase in *Synechococcus* sp. strain (Mitsui 1978, 1992). Therefore, the effects of the addition of organic substrates on nitrogenase activity were examined. As organic substrates, glucose and pyruvate were chosen for these experiments. Without the addition of the compounds, nitrogenase activity in the 6-day old batch cultures appeared shortly after incubation started and had a maximum activity at approximately 10 hrs of incubation (Fig 14). However, nitrogenase activity ceased completely after this maximum activity was reached. Hydrogen production stopped at the time when nitrogenase activity disappeared. When glucose or pyruvate was added to the culture, a higher maximum nitrogenase activity appeared at the 10th hr of incubation. Nitrogenase activity then decreased, but a certain constant level of its activity remained during the subsequent incubation period. Hydrogen photoproduction also continued while nitrogenase activity remained constant.

Discussion

In addition to H_2 production from cellular glycogen, it was shown here that *Synechococcus* sp. Miami BG 043511 has a high H_2 photoproduction capability after external addition of various organic substrates, such as pyruvate, glucose, maltose, sucrose, fructose and glycerol. The maximum rates of H_2 production in 6-day old batch culture were as high as 1.11, 0.62, 0.50, 0.47, 0.30 and 0.39 µmoles per mg dry weight per hour, respectively. It is well known that photosynthetic bacteria with anoxygenic photosynthesis lack the

capability of water photolysis, but only produce H_2 from various organic compounds (Mitsui et al. 1985). Although substrate specificity varies from species to species, the most preferred substrates for H_2 production in photosynthetic bacteria are organic acids. Carbohydrates are less preferred by these organisms.

In our cyanobacterial strain, only pyruvate among the organic acids is found to be an effective substrate for hydrogen photoproduction. It was reported previously for other cyanobacteria that glucose (Mitsui et al. 1985), fructose (Tel-Or and Sandovsky 1982, Troshina et al. 1992) and sucrose (Troshina et al. 1992) are good hydrogen donors. Thus, it can be concluded that the substrate specificity of cyanobacteria is different from that observed for photosynthetic bacteria.

The strain Miami BG 043511 has a high H_2 production capability from mono- and di-saccharides. Therefore, it is speculated that this cyanobacterium may have an advantage for H_2 photoproduction from carbohydrate rich waste water. *Synechococcus* sp. has approximately 1/3 of the capability in hydrogen photoproduction from pyruvate compared to photosynthetic bacteria (Table 1 and Mitsui et al. 1985).

It is also shown for this strain of *Synechococcus* sp. that the capability of H_2 production in batch culture cannot be activated by the substrates of the TCA cycle, such as acetate, citrate, succinate, malate and fumarate (Table 1). This indicates an important difference of this strain of cyanobacteria from the non-sulphur photosynthetic bacteria reported by Mitsui et al. (1985). In the latter, all organic acids of the TCA cycle are primary substrates for H_2 production. The second difference is that glycerol cannot be utilized by non-sulphur photosynthetic bacteria (Mitsui et al. 1985), but it is one of the primary substrates for H_2 production in cyanobacteria.

Pyruvate has been found to be the major organic source of electrons for ferredoxin reduction in cyanobacteria (Cox and Fay 1969). In *C. pasteurianum*, pyruvate undergoes a phosphoroclastic type of cleavage which results in the synthesis of ATP so that pyruvate itself can supply both basic requirements of electrons and ATP for nitrogen fixation.

Pyruvate in cyanobacteria is metabolized by pyruvate:ferredoxin oxidoreductase. Although reports about the occurrence of this enzyme in cyanobacteria are controversial, evidence is given from the recent identification of the *nifJ* gene coding for pyruvate:ferredoxin oxidoreductase in nitrogen-fixing cyanobacteria (Shmitz et al. 1993). This firmly supports its presence in cyanobacteria. Therefore, it may be assumed that the organic substrates applied as H_2 donors in this study were metabolized to pyruvate, and that pyruvate then could be directly the source of electrons and ATP for hydrogen production. This is, however, highly speculative at present.

As previously described, H_2 production is catalyzed by nitrogenase in our cyanobacterial strain. As shown in Fig 14, organic substrates maintained nitrogenase activity when cellular glycogen (glucose) is used up in the cells. Added organic substrates had little effect, or were inhibitory in some case, on H_2 photoproduction, when glycogen was still present in the cells. Only when the cellular glycogen (glucose) is exhausted, externally added organic substrates became effective electron donors. It is therefore concluded that this cyanobacterial strain has a higher affinity for its cellular glycogen (glucose) for H_2 photoproduction than for externally added organic substrates (Figs 10, 11 and 12).

References

Cox, R.M and P. Fay. 1969. "Special Aspects of Nitrogen Fixation by Blue-Green Algae." *Proc. Roy. Soc. B*, 172: 357-366.

Dubois, M., K.A. Gilles, J.K. Hamilton, P.A. Rebers and F. Smith. 1956. "Colorimetric Method for Determination of Sugars and Related Substances." *Anal. Chem*, 28: 350-356.

Holm-Hansen, O. and B. Riemann. 1978. "Chlorophyll *a* Determination: Improvements in Methodology." *OIKOS*, 30: 438-447.

Kumazawa, S. and A. Mitsui. 1981. "Characterization and Optimization of Hydrogen Photoproduction by a Saltwater Blue-Green Alga, *Oscillatoria* sp. Miami BG 7. I. Enhancement through Limiting the Supply of Nitrogen Nutrients." *Int J. Hydrogen Energy*, 6: 339-348.

León, C., S. Kumazawa and A. Mitsui. 1986. "Cyclic Appearance of Aerobic Nitrogenase Activity during Synchronous Growth of Unicellular Cyanobacteria." *Current Microbiol*, 13:149-153.

Mitsui, A. 1978. "Marine Photosynthetic Organisms as Potential Energy Resources: Research on Nitrogen Fixation and Hydrogen Production." In *Proceedings of the 5th International Ocean Development Conference*, Volume 1, B1 29-52. IODC Organizing Committee, Tokyo.

Mitsui, A. 1992. "Hydrogen Photoproduction by Marine Cyanobacteria for Alternating the Carbon Energy Sources." In J.C. Hunter-Cevera (ed.) *Short communications of the 1991 International Marine Biotechnology Conference*, Volume II, 710-723. Wm C. Brown Publishers, Dubuque, Iowa.

Mitsui, A. 1993. "Recent Research Development on Biological Hydrogen Photoproduction." In T.Ohta and T.Homma (ed.) *Energy System and Conversion*, S11-S24. Universal Academy Inc., Tokyo.

Mitsui, A. and S. Cao. 1988. "Isolation and Culture of Marine Nitrogen-Fixing Unicellular Cyanobacteria, *Synechococcus*." *Methods Enzymol*, 167:105-113.

Mitsui, A., S. Cao, A. Takahashi and T. Arai. 1987. "Growth Synchrony and Cellular Parameters of the Unicellular Nitrogen-Fixing Marine Cyanobacterium, *Synechococcus* sp. strain Miami BG 043511 under Continuous Illumination." *Physiol. Plant*, 69:1-8.

Mitsui, A., S. Kumazawa, E.J. Phlips, K.J. Reddy, K. Gill, T. Matsunaga, B.R. Renuka, T. Kusuni, G. Reyes-Vasquez, K. Miyazawa, L. Haynes, H. Ikemoto, E. Duerr, C.L. Leon, D. Rosner, R. Sesco and E. Moffat. 1985. "Mass Cultivation of Algae and Photosynthetic Bacteria: Concepts and Application." In T.K. Ghose (ed.) *Biotechnology and Bioprocess Engineering*, 119-155. International Union of Pure and Applied Chemistry and Indian National Science Academy. United India Press, New Delhi.

Mitsui, A., S. Kumazawa, A. Takahashi, H. Ikemoto, S. Cao and T. Arai. 1986 "Strategy by which Nitrogen-Fixing Unicellular Cyanobacteria Grow Photoautotrophically." *Nature*, 323:720-722.

Mitsui, A., S. Suda and N. Hanagata. 1993. "Cell Cycle Events at Different Temperatures in Aerobic Nitrogen-Fixing Marine Unicellular Cyanobacterium *Synechococcus* sp. Miami BG 043511." *J. Mar Biotechnol*, 1:89-91.

Schmitz, O., T. Kentemich, W. Zimmer, B. Hundeshagen and H. Bothe. 1993. "Identification of the *nifJ* Gene Coding for Pyruvate:Ferredoxin Oxidoreductase in Dinitrogen-Fixing Cyanobacteria." *Arch Microbiol*, 160: 62-67.

Suda, S., S. Kumazawa and A. Mitsui. 1992. "Change in the H_2 Photoproduction Capability in a Synchronously Grown Aerobic Nitrogen-Fixing Cyanobacterium, *Synechococcus* sp. Miami BG 043511." *Arch Microbiol*, 158:1-4.

Tel-Or, E and T. Sandovsky. 1982. "The Response of the Nitrogen-Fixing Cyanobacterium *Anabaena azollae* to Combined Nitrogen Compounds and Sugar." *Isr. J. Bot*, 31: 329-336.

Troshina, O. Yu and I.N. Gogotove. 1992. "Effect of Physiologically Active Compounds on the growth and Nitrogenase Activity of the Cyanobacterium *Anabaena variabilis*." *Prikl. Biokhim. Mikrobiol*, 28: 380-386.

(iv) Changes in mRNA and Protein of Nitrogenase during the Synchronous Growth

The genus *Synechococcus* is a ubiquitous unicellular cyanobacterium. Members of this genus are found in the open ocean, neritic water and fresh water. Most species of *Synechococcus* which have been studied so far did not, however, exhibit aerobic nitrogen-fixing capabilities. *Synechococcus* sp. strain Miami BG 043511 is a unique, marine unicellular, aerobic nitrogen-fixing cyanobacteria. This strain was isolated near the Bahamas (Mitsui et al. 1985), and found to fix nitrogen under high oxygen concentrations. This strain was also found to produce large quantities of hydrogen gas from sunlight and seawater, and has the potential to be used to harvest hydrogen gas for energy (Mitsui et al. 1985, Mitsui 1992).

Synechococcus sp. strain Miami BG 043511 must be able to carry out both oxygen sensitive nitrogen fixation and oxygen evolving photosynthesis within the same cell. Mechanisms used by cyanobacteria to separate these two incompatible processes may be divided into spatial, temporal, and nutritional separation, and are accomplished at either the transcriptional or translational level, or at both. It was shown previously that this strain of *Synechococcus* exhibits a temporal separation of many of its metabolic functions with a cyclicity of approximately 20 hours (Mitsui et al. 1986, 1987). In order to study the diurnal cycle of strain Miami BG 043511, it was necessary to induce the cells to divide synchronously. In this strain it was found that a treatment of 16 hr dark, 16 hr light and 16 hr dark periods was the best to induce the cells to divide synchronously (Mitsui et al. 1987). During the study of synchronous growth in this strain, it was found that oxygenic photosynthesis and nitrogen fixation were temporally separated within a cell division cycle (Mitsui et al. 1986, 1987).

On the other hand, *Anabaena* sp. PCC 7120 has been used as a model for the genetic characterization of nitrogenase. It has been assumed that the structural genes of *Synechococcus* have a similar arrangement to those in *Anabaena* heterocystous cells. Since the genes in *Anabaena* have been fairly well characterized, the structural genes have been sequenced, and the nitrogenase protein seems to be highly conserved structurally, this strain was chosen as a comparison strain. Since *Synechococcus* is such a diverse genus genetically, however, it is possible that the structural and regulatory genes for nitrogenase differ in this genus. It is therefore necessary to elucidate these structural and regulatory genes in the strain *Synechococcus* sp. Miami BG 043511. The nitrogenase genes and their transcription have been studied in a genetically similar strain, *Synechococcus* sp. RF-1, a slow growing, fresh water strain isolated from rice fields in China (Huang et al. 1988, 1991, Huang and Chow 1990). In strain RF-1, mRNA of *nifK*, one of the structural genes of nitrogenase, was studied, and found to exhibit a diurnal cycle. It was demonstrated in this strain that new synthesis of mRNA for nitrogenase was necessary each time nitrogenase activity appeared.

This experiment tested for the cyclic synthesis of nitrogenase through the characterization of mRNA for *nifH* gene, as it compared to the temporal appearance of nitrogenase activity in synchronously grown cells of *Synechococcus* sp. strain Miami BG 043511. Once the cells were induced to divide synchronously, RNA was isolated from the cells throughout the cell cycle. The *nifH* gene was chosen for this study because the structural genes of nitrogenase have been found to be highly conserved among those species in which they have been sequenced (Mevarech et al. 1980).

The temporal separation of nitrogen fixation and oxygen evolving photosynthesis could be caused by two different mechanisms; the nitrogenase protein is newly synthesized when photoevolution of oxygen stops,

or the nitrogenase protein is synthesized constitutively and the protein is modified to become inactive when photosynthesis occurs. In this study it was shown that the former case is true.

Methods and Materials

Culture Growth Conditions

Batch cultures of *Synechococcus* sp. strain Miami BG 043511 were grown in combined nitrogen-free media, A-N, with 18 g/l NaCl at pH 8.5 (Mitsui and Cao 1988). Batch cultures of *Anabaena* PCC 7120 were grown in A-N medium without the addition of NaCl. Cultures were grown under continuous illumination of 150 $\mu E\ m^{-2}\ s^{-1}$ at room temperature for approximately 92 hours and bubbled with air.

Synchronously dividing cells were obtained by growing *Synechococcus* sp. strain Miami BG 043511 in A-N media with 2.5 g/l NaHCO3, following the method of Mitsui et al. (1986) and Mitsui and Cao (1988). Cells were subjected to a pretreatment of 16 h dark, 16 h light and 16 h dark periods, and cultured synchronously under continuous illumination. Synchronously grown cells were harvested at 4 h intervals for 48 h. During synchronous growth, pH and temperature were measured at each time point that the cells were harvested. Cell were counted after a 1 ml sample was fixed with 50 µl of 10% Lugol's solution. Nitrogenase activity was measured by the acetylene reduction method as was described in Mitsui and Kumazawa (1988).

DNA Extraction

Chromosomal DNA was extracted from 10 day old batch cultures of both *Anabaena* PCC 7120 and *Synechococcus* sp. strain Miami BG 043511. The method for DNA extraction was modified from the CsCl-ultracentrifugation method of Sambrook et al. (1989). A 500 ml sample of batch culture was harvested by centrifugation at 3200 x g for 10 min at 4°C. The cell pellet was suspended in 15 ml of 25% sucrose, 50 mM Tris (pH 8.0) and 100 mM EDTA, and again centrifuged at 3200 x g for 10 min at 4°C. The pellet was resuspended in TE buffer (10 mM Tris, pH 8.0, 1 mM EDTA) and cells were disrupted by Beadbeater (Biospec Products) using 0.1 mm acid-washed, baked glass beads (Golden et al. 1987). Cell debris was removed by centrifugation at 8200 x g for 10 min. Protein was removed by proteinase K treatment (0.1 mg/ml) with SDS (1%) at 50°C for 2 hours (Kentemich et al. 1991). DNA was extracted with phenol:chloroform:isoamyl alcohol (25:24:1), precipitated with cold ethanol and resuspended in TE buffer. DNA was further purified by ultracentrifugation with CsCl (1g/ml) at 200,000 x g for 48 h, and resuspended in 75 µl TE buffer.

RNA Extraction

Total RNA was extracted from synchronously grown cells of *Synechococcus* sp. strain Miami BG 043511 using a modification of the method of Golden et al. (1987). Culture samples were taken at 4 hour intervals. A 1-liter sample of synchronous culture was harvested and centrifuged at 3200 x g for 10 min at 4°C. The cells were resuspended in 15 ml of washing buffer (10 mM Tris, 50 mM NaCl, 50 mM EDTA), and centrifuged again. The pellet volume was adjusted to 0.5 ml and resuspended in 5 ml of GTC solution (5.7 M guanidium thiocyanate, 250 mM lauroylsarcosyl, 400 mM sodium citrate, 0.67 % β-mercaptoethanol). The cells were transferred into 2 ml screw cap tubes with 0.5 ml acid-washed, baked 0.1 mm glass beads, and disrupted by Beadbeater 5 times each for 1 min. The supernatant was extracted three times with phenol:chloroform. Nucleic acids were precipitated with cold ethanol for 2 hours at -20°C, and redissolved in 6 ml of 50/100 TE (50 mM Tris, 100 mM EDTA) with 3 g of CsCl added. The suspension was layered onto 2.5 ml of 5.7 M CsCl solution, and centrifuged overnight at 105,000 x g at

20°C. The pellet containing RNA was dissolved in TE buffer, precipitated with cold ethanol and redissolved in TE buffer. The concentration of the RNA was measured using a spectrophotometer.

Polymerase Chain Reaction (PCR)

The primer sequences for PCR were designed from the sequence of the *nifH* gene from *Anabaena* PCC 7120 (Mevarech et al. 1980); Primer 1 sequence is GCT TTC TAC GGT AAA GGC GGT ATC GGT AAA and Primer 2 sequence GGT GAA ATG ATG GCG ATG.

Using the synthetic primers, a probe for the nitrogenase structural gene, *nifH*, was synthesized using the polymerase chain reaction. This probe is an internal fragment of the *nifH* gene. The probe was synthesized using GeneAmp^R PCR Reagent Kit (Perkin Elmer Cetus). PCR probes for the *nifH* gene were synthesized using chromosomal DNAs from *Anabaena* PCC 7120 and *Synechococcus* sp. strain Miami BG 043511. DNA was diluted to a concentration of 0.1 µg/µl, and boiled for 10 min to facilitate hybridization of the primers. The primers were diluted to a final concentration of 1 µM. Temperature cycling for amplification of the DNA was performed using Thermal Cycler (Perkin Elmer Cetus, Model 480). The initial melting was performed at 92°C for 5 min. Amplification occurred during 30 cycles of 2 min at 92°C, 3 min at 65°C and 3 min at 72°C. The PCR probes were purified on 1% low melting temperature agarose (Seaplaque GTG). A PCR product of 456 bases was cut from the agar, and purified by extraction with phenol:chloroform and precipitation with cold ethanol.

Southern Hybridization

The PCR probes for *nifH* from *Synechococcus* or *Anabaena* were labeled using Genius System DNA Non-Radioactive Labeling and Detection Kit (Boehringer Mannheim).

The restriction enzymes *Hae* III, *Hinc* II, *Hind* III, *Nco* I, *Pst* I, *Pvu* I, *Pvu* II, *Sca* I, *Sma* I and *Xho* I were used to digest chromosomal DNA from *Synechococcus*.

Digested DNA was run on gel electrophoresis in 1% agarose in TBE. The DNA in the gel was denatured in 0.5N NaOH and 1.5M NaCl, and neutralized in 1.0 M Tris and 1.5 M NaCl. The DNA was transferred to a nylon membrane (Hybond-N+, Amersham) by capillary transfer overnight (Sambrook et al. 1989).

The DNA was cross-linked to the nylon membrane by UV illumination for 3 min. The membrane was then baked for 1 hr at 80°C. The digested DNA attached to the nylon membrane was hybridized to labeled *Synechococcus* PCR probe by incubating the membrane at 65°C overnight in 1.5 ml hybridization solution [5 x sodium citrate salt (SSC), 1% blocking reagent, 0.1% N-lauroylsarcosine, 0.02% SDS] with 10 ng of labeled PCR probe. After hybridization, the membrane was washed in diluted SSC and SDS, and incubated with diluted DIG-dUTP antibody (diluted 1:5000 in 2% blocking reagent in 150 mM NaCl and 100 mM Tris). Excess antibody was washed off with 150 mM NaCl and 100 mM Tris. The membrane was then covered with 500 µl of Lumiphos 530 (Boehringer Mannheim) for chemiluminescent detection. After a 1 hr incubation, the membrane was exposed to X-ray film for 1 hr at room temperature.

Northern Hybridization

Total RNA was run on agarose/formaldehyde gel electrophoresis. The amounts of RNA were 5 µg/lane. Gel was then soaked in 20 x SSC for 45 min. The RNA was transferred to a nylon membrane. The nylon membrane was then baked for 1 hr at 80°C and hybridized to labeled *Synechococcus* or *Anabaena* probe. The hybridization solution contained DEPC treated water, 50% formamide, 5 x SSC, 2% blocking reagent in 15 mM maleic acid, 0.02% SDS and 0.1% N-lauroylsarcosine The membrane was hybridized at 42°C overnight. After hybridization, the membrane was washed,

and incubated with diluted DIG-dUTP antibody (diluted 1:5000 in 2% blocking reagent in 150 mM NaCl and 100 mM maleic acid in DEPC treated water). Excess antibody was washed off with 150 mM NaCl and 100 mM maleic acid in DEPC treated water. Hybridization was detected as described above.

Cell Fractionation and Analysis of Protein Components

One liter and 500 ml samples of culture were harvested at 0 and 12 hours, respectively, by centrifugation at 4,000 x g for 10 min. They were washed with 0.75 M potassium phosphate buffer, pH 7.0, containing 10 mM EDTA (P buffer) and resuspended in 2 ml of the same buffer according to Tandeau de Marsac and Houmard (1988). After 1 g of glass beads (diameter 0.1 mm) were added, cells were disrupted three times each for 1 min using a mini-beadbeater cell disrupter (Biospec Products, model 3110BX). Between treatments, cells were cooled on ice for 1 min. The broken cells were centrifuged at 1,700 x g for 10 min, and the pellet containing glass beads and unbroken cells was discarded. The supernatant was layered onto a discontinuous sucrose density gradient (3 ml each of P buffer containing 0.5 M, 1.0 M and 1.5 M sucrose), and centrifuged at 180,000 x g for 3 hr at 20°C. Fractions of 1 ml each were taken from the top, and proteins in each fraction were analyzed by SDS-polyacrylamide gel electrophoresis according to Laemmli (1970). Gels were stained with Coomassie Brilliant Blue R-250. Bio-Rad protein standards for the low molecular weight range were used as molecular weight markers.

Results

Amplification of nifH by PCR

The PCR probe generated for this experiment was based on the known sequence of *nifH* in *Anabaena* PCC7120 (Mevarech et al. 1980). Synthetic 27-mer primers were used in conjunction with purified chromosome from both *Anabaena* and *Synechococcus* in PCR. The resulting fragment from the *Synechococcus* chromosome was measured against a 1 kb DNA ladder, and estimated to be approximately 456 bases in length, which also agreed with the known length of the fragment in *Anabaena*, calculated from the sequence data of Mevarech et al. (1980). The PCR probe generated from the *Anabaena* chromosome was also seen to be the same length as the *Synechococcus* probe. The PCR probe was thought to be an internal fragment of the *nifH* gene.

Southern Hybridization between Synechococcus Chromosome and nifH Probe

Synechococcus chromosome was digested with 6 restriction enzymes. It appeared that only one enzyme, *Hinc* II, fully digested the chromosome. λ-phage DNA was digested simultaneously by the same restriction enzymes in order to test for enzyme activity. The enzymes were all found to fully digest the λ-DNA.

After the digestion with *Hinc* II, the *nifH* probe was found to hybridize to only one fragment of *Synechococcus* chromosome. The size of this fragment was approximately 1.1 kb.

Northern Hybridization during the Synchronous Culture using nifH Probe

In order to determine the temporal patterning of the mRNA from nitrogenase after extraction from synchronously grown cells of *Synechococcus*, Northern hybridization was performed. *Synechococcus* PCR probe was used to ensure the best binding to mRNA since both of these are from the same strain.

Samples were taken from synchronous cultures of *Synechococcus* over two complete cell cycles (48 hr) at 4 hr intervals beginning 2 hr after the onset of continuous illumination. Enzyme activity of nitrogenase measured at the same time showed cyclic appearance and disappearance, as is shown in the upper part of Fig 15. One cycle was approximately 20 hr in length.

The mRNA appeared cyclically at approximately 20 hr intervals (Fig 15). This indicates that *nifH* mRNA is newly synthesized each time nitrogenase activity appears. The mechanism is still unclear, but as O_2-evolving photosynthesis begins each day, the nitrogenase operon ceases to be transcribed into mRNA. After photosynthetic activity decreased, the nitrogenase operon was actively transcribed again, and nitrogenase activity was seen to increase (Fig 15).

Analysis of Proteins by SDS-gel Electrophoresis

Cells of the 0 and 12 hr were dirupted, and their respective cellular components were fractionated on a sucrose density gradient. Protein components in each fraction were then analyzed by SDS-polyacrylamide gel electrophoresis.

As shown in Fig 16A (0 hr cells) and Fig 16B (12 hr cells), the general protein components were similar in the 0 hour and the 12 hour cells. However, significant differences were found in the proteins from sucrose gradient fraction 2 and 3. Two polypeptides of 54 kDa and 57 kDa were clearly observed from the 12 hr cells, and no such polypeptides were seen in the fractions from the 0 hr cells.

Discussion

From the data shown in Fig 15, it is suggested that the structural proteins of nitrogenase are regulated, at least in part, at the transcriptional level. The multiple banding pattern seen in Fig 15 might be contributed to incomplete transcripts of the *nif* operon. Due to the size of the largest band (5.4 kb), this fragment was most likely a transcript containing not only *nifH* but *nifK* and *nifD* as well. This data concurs with previous studies of the *nif* operon in single cell cyanobacteria (Rogers and Gallon 1988). The temporal separation of nitrogen fixation and oxygen evolving photosynthesis could be caused by two different mechanisms; the nitrogenase protein is newly synthesized when photoevolution of oxygen stops, or the nitrogenase protein may be synthesized constitutively and the protein modified to become inactive under non nitrogen-fixing conditions (Rai et al. 1989, Stal and Bergman 1990). In this study it was shown that the former case is true. Transcriptional regulation of nitrogenase is most likely the dominant regulatory mechanism for nitrogenase activity. There may, however, be other regulatory mechanisms to protect this extremely sensitive protein from oxygen. These other mechanisms may include physical protection (as in compartmentalization), or regulation of cofactors, or even post translational modification. Other studies have shown that the nitrogen fixation cycles are not related to either cell cycles or to circadian rhythms (Rai et al. 1989, Stal and Bergman 1990). This does not apply to this strain of *Synechococcus*. Further studies on the structural genes of nitrogenase and their regulation are needed, however, to elucidate the specific factors which allow the nitrogenase to function in this unique unicellular cyanobacteria.

SDS-polyacrylamide gel electrophoresis analysis of the protein component indicated that two polypeptides (molecular weight, 54 kDa and 57 kDa) are abundantly found in the cells at 12 hr (Fig 16), when the nitrogenase activity is maximum (Fig 15). The molecular weights of these polypeptides are quite close to those of α and β subunits of Mo-Fe protein (Eady 1986), although further study is needed to prove this.

References

Eady, R.R. 1986. "Enzymology in Free-Living Diazotrophs." In W.J. Broughton and A. Pühler (ed.) *Nitrogen Fixation, Vol 4 Molecular Biology*, 1-49. Clarendon Press, Oxford.

Golden, S.S., J. Brusslan and R. Haselkorn. 1987. "Genetic Engineering of the Cyanobacterial Chromosome." In P. Wu and L. Grossman (ed.) *Methods Enzymol*, 153:

Huang, T.C. and T.J. Chow. 1990. "Characterization of the Rhythmic Nitrogen-Fixing Activity of *Synechococcus* sp. RF-1 at the Transcription Level." *Current Microbiol.* 20:23-26.

Huang, T.C., T.J. Chow and I.S. Hwang. 1988. "The Cyclic Synthesis of the Nitrogenase of *Synechococcus* RF-1 and its Control at the Transcription Level." *FEMS Microbiol. Lett*, 50:127-130.

Huang, T.C., K.C. Lay and S.R. Tong. 1991. "Resetting the Endogenous Circadian N_2-Fixing Rhythm of the Prokaryote *Synechococcus* RF-1." *Bot. Bull. Academia Sinica*, 32:129-133.

Kentemich, T., G. Haverkamp, and H. Bothe. 1991. "The Expression of a Third Nitrogenase in the Cyanobacterium *Anabaena variabilis*." *Z. Naturforsch*, 46c:217-222.

Laemmli, U.K. 1970. "Cleavage of Structural Proteins during the Assembly of the Head of Bacteriophage T4." *Nature*, 227:680-685.

Mevarech, M., D. Rice and R. Haselkorn. 1980. "Nucleotide Sequence of a Cyanobacterial *nifH* Gene Coding for Nitrogenase Reductase." *Proc. Natl. Acad. Sci*, 77:6476-6480.

Mitsui, A. 1992. "Hydrogen Photoproduction by Marine Cyanobacteria for Alternating the Carbon Energy Sources." In J.C. Hunter-Cevera (ed.) *Short communications of the 1991 International Marine Biotechnology Conference*, Volume II, 710-723. Wm C. Brown Publishers, Dubuque, Iowa.

Mitsui, A. and S. Cao. 1988. "Isolation and Culture of Marine Nitrogen-Fixing Unicellular Cyanobacteria, *Synechococcus*." *Methods Enzymol*, 167:105-113.

Mitsui, A., S. Cao, A. Takahashi and T. Arai. 1987. "Growth Synchrony and Cellular Parameters of the Unicellular Nitrogen-Fixing Marine Cyanobacterium, *Synechococcus* sp. strain Miami BG 043511 under Continuous Illumination." *Physiol. Plant*, 69:1-8.

Mitsui, A and S. Kumazawa. 1988. "Nitrogen Fixation by Synchronously Growing Unicellular Aerobic Nitrogen-Fixing Cyanobacteria." *Methods Enzymol*, 167: 484-490.

Mitsui, A., S. Kumazawa, A. Takahashi, H. Ikemoto, S. Cao and T. Arai. 1986 "Strategy by which Nitrogen-Fixing Unicellular Cyanobacteria Grow Photoautotrophically." *Nature*, 323:720-722.

Mitsui, A., S. Kumazawa, E.J. Phlips, K.J. Reddy, K. Gill, T. Matsunaga, B.R. Renuka, T. Kusuni, G. Reyes-Vasquez, K. Miyazawa, L. Haynes, H. Ikemoto, E. Duerr, C.L. Leon, D. Rosner, R. Sesco and E. Moffat. 1985. "Mass Cultivation of Algae and Photosynthetic Bacteria: Concepts and Application." In T.K. Ghose (ed.) *Biotechnology and Bioprocess Engineering*, 119-155. International Union of Pure and Applied Chemistry and Indian National Science Academy. United India Press, New Delhi.

Rai, A., M. Borthakur, S. Singh. and B. Bergman. 1989. "*Anthoceros-Nostoc* Symbiosis: Immunoelectromicroscopic Localization of Nitrogenase, Glutamine Synthetase, Phycoerythrin and Ribulose-1,5-Biphosphate Carboxylase/Oxygenase in the Cyanobiont and the Cultured Free-Living Isolate *Nostoc* 7801." *J. Gen. Microbiol*, 135:385-395.

Rogers, L.J., and J.R. Gallon. 1988. *Biochemistry of the Algae and Cyanobacteria*. Calrendon Press, Oxford.

Sambrook, J., E.F. Fritsch, and T. Maniatis. 1989. *Molecular Cloning: A Laboratory Manual*,Vol 1-3. Cold Spring Harbor Laboratory Press, New York.

Stal, L.J. and B. Bergman. 1990. "Immunological Characterization of Nitrogenase in the Filamentous Non-Heterocystous Cyanobacterium *Oscillatoria limosa*." *Planta*,182:287-291.

Tandeau de Marsac, N and J. Houmard. 1988. "Complementary chromatic adaptation: physiological conditions and action spectra." *Methods Enzymol.*.167:318-328.

(v) Isolation and Characterization of Nitrogenase which Catalyzes H_2 Photoproduction

Since nitrogenase is the major enzyme to catalyze H_2 photoproduction in this cyanobacterial strain, and characterization of this nitrogenase may lead to an increase in the light energy conversion efficiency, an attempt was made to isolate and characterize the nitrogenase from this strain. Using the cells which exhibited high nitrogenase activity during the synchronous growth of this strain, nitrogenase was isolated by the agarose column electrophoresis technique, and also by the sucrose gradient technique. Thus far we have isolated two brown colored proteins, one seems to be the Mo-Fe protein, and the other the Fe protein. These proteins are partially purified. We are now in the process of further purification and characterization of these proteins. Preliminary studies indicated that the nitrogenase of this strain has unique characteristics. After purification, we intend to study the effect of environmental stress, such as O_2, pH, temperature, and salinity, in order to obtain information regarding the stability of enzyme activity.

III. To Develop a Method of Elongating the High Rates of H_2 Photoproduction with High Light Energy Conversion Efficiency

As described already, a very high rate of H_2 photoconversion efficiency was observed in a closed vessel system when synchronously grown cells were used. However, it was found that the high rates of H_2 photoproduction from water in a 24 hour cycle decreased in the 2nd and 3rd 24 hour cycles. The main reason for this decrease in H_2 photoproduction was attributed to the decrease in the available amounts of cellular glycogen (glucose). Therefore, the key to prolonging H_2 photoproduction periods should be to find a method to efficiently recycle the H_2 photoproduction system by the cyclic synthesis of large amounts of glycogen. This was experimentally demonstrated during this year's study. When CO_2 was added to an incubation vessel every 24 hours at the point when cellular glycogen was used up, significant enhancement of H_2 photoproduction and prolonged H_2 production from water continued for at least 10 days (10 cycles). When immobilized synchronously grown cells were used, the enhancement and prolongation of H_2 production were extended for more than one month.

Conclusion

As was described above, studies of this year on the biological H_2 photoproduction in the unique unicellular cyanobacterium, *Synechococcus* sp. strain Miami BG 043511 advanced several steps further in both basic and applied areas. The efforts will continue, and other new efforts will begin for the improvement of the H_2 photoproduction rates and high rates of light energy conversion efficiency in future study.

Future Work

(I) Light Energy Conversion Efficiency to Hydrogen Production in Various Light Intensities and Cell Densities using Synchronously Growing *Synechococcus* sp. Miami BG 043511

Two temporally separated phases are involved in the hydrogen production from water in this strain; an oxygenic, photosynthetic phase and an anoxygenic hydrogen production phase. Each phase is approximately 12 hr long.

The maximum light energy conversion efficiency to H_2 was approximately 5.5% during the 12 hour H_2 production period. As was mentioned above, O_2 was produced, but no H_2 was produced in the 12 hour photosynthetic period. Therefore, the light energy conversion efficiency for a 24 hour incubation period (one cycle) was 2.6%. These values are the highest obtained among green algal and cyanobacterial strains in which H_2 accumulation has been measured thus far in a closed vessel. The maximum light energy conversion efficiency obtained in the cyanobacterium was equivalent to a maximum value reported in the photosynthetic bacteria, which lack the ability of water photolysis and carried out H_2 production using externally added organic substances. The high solar energy conversion efficiency obtained by H_2 production (accumulation) in a closed vessel is important when compared to values obtained under special dim light conditions or in inert gas flow sparging systems which remove O_2 and simultaneously dilute the H_2 that is produced. The re-concentration of diluted H_2 involves the input of energy and expensive procedures. In the H_2 production system in a closed vessel, H_2 can be simply harvested.

Since the light energy conversion efficiency at one or two light intensities was studied in the previous years, those of different light intensities with different cell densities will be examined in this year. Particularly, light energy conversion efficiency in high light intensities equivalent to outdoor sunlight conditions will be examined in the laboratory. Then, those will be tested under outdoor sunlight conditions. The optimum solar energy conversion efficiency will be found by changing cell density and various environmental factors.

(ii) Measuring of Synthesis and Degradation of mRNA and Protein of Nitrogenase during Synchronous Growth

There are two alternating possibilities; (1) the nitrogenase proteins always exist in the cells, and nitrogenase activity changes during synchronous growth by activation and inactivation of the protein, or (2) nitrogenase proteins are temporally synthesized during synchronous growth. This information is one key to the development of technology for a high rate of H_2 photoproduction with a high light energy conversion efficiency.

As described above, we found that mRNA for the nitrogenase protein temporally appeared and disappeared during synchronous growth within a cell cycle and that the nitrogenase protein also seemed to appear temporally during synchronous growth. Thus, the latter assumption of the above hypothesis is true thus far.

In this year, using both agarose gel column electrophoresis method and sucrose density gradient method, nitrogenase proteins will be isolated and measured quantitatively during synchronous growth in every 4-5 hours intervals and confirm the preliminary results.

(iii) Further Purification and Characterization of the Nitrogenase Proteins from *Synechococcus* sp. Miami BG 043511

In this year, nitrogenase proteins will be completely purified and components of nitrogenase protein will be characterized.

(iv) To Design, Construct and Operate the Small Scale Bioreactor for H_2 Production from Water by *Synechococcus* sp. Miami BG 043511

A small scale bioreactor will be designed, constructed and operated at first in the laboratory for high rate and stable H_2 photoproduction with high light energy conversion efficiency, and then operated under outdoor sunlight conditions.

(v) Finally Using the Data Obtained Above, Sea Floating Bioreactor in a Larger Scale Will Be Designed for Future Development.

Acknowledgments

The principal investigator, A. Mitsui, expresses many thanks to Dr. Kumazawa, Dr. Dörnemann, Dr. Luo, Dr. Nemoto, Dr. Tsuzuki and Ms. Campbell for their excellent participation in this project and very hard work, including many overnight experiments, and to Dr. Nemoto for the assistance in manuscript preparation.

Legends to Figures

Fig 1 Effects of cell densities on H_2 and O_2 production in *Synechococcus* sp. strain Miami BG 043511. Light intensity was 17 W/m^2. A and B indicate 0-12 h and 0-24 h incubation periods, respectively. Kumazawa and Mitsui (1994) in press.

Fig 2 Effects of cell densities on H_2 and O_2 production in *Synechococcus* sp. strain Miami BG 043511. Light intensity was 25 W/m^2. A and B indicate 0-12 h and 0-24 h incubation periods, respectively. Kumazawa and Mitsui (1994) in press.

Fig 3 Changes in H_2 and O_2 during incubation under the light intensity of 17 W/m^2 in *Synechococcus* sp. strain Miami BG 043511. Cell densities in A and B were 0.045 and 0.27 mg chl/vessel, respectively. Kumazawa and Mitsui (1994) in press.

Fig 4 Changes in H_2 and O_2 during incubation under the light intensity of 25 W/m^2 in *Synechococcus* sp. strain Miami BG 043511. Cell densities in A and B were 0.03 and 0.3 mg chl/vessel, respectively. Kumazawa and Mitsui (1994) in press.

Fig 5 H_2, O_2 and CO_2 exchange during incubation under H_2 production conditions in *Synechococcus* sp. strain Miami BG 043511. Light intensity was 25 W/m^2. Kumazawa and Mitsui (1994) in press.

Fig 6 Effects of gas replacement on the H_2 and O_2 production in *Synechococcus* sp. strain Miami BG 043511. Amounts of H_2 and O_2 were assayed at 24 h intervals with (A) and without (B) the gas replacement by argon gas. Light intensity was 25 W/m^2. Kumazawa and Mitsui (1994) in press.

Fig 7 Synchronized cell growth and nitrogenase activity of *Synechococcus* sp. Miami BG 043511 under continuous illumination. Nemoto, Blackwelder and Mitsui (1994) in press.

Fig 8 Phase contrast photomicrographs of the synchronously growing cells of *Synechococcus* sp. Miami BG 043511. Numbers shown in photographs indicate the hours after the onset of synchronous growth. Bar represents 5 μm. Nemoto, Blackwelder and Mitsui (1994) in press.

Fig 9 Electron micrographs of the synchronously growing cells of *Synechococcus* sp. Miami BG 043511. Numbers shown in photographs indicate the hours after the onset of synchronous growth. Bar represents 1 μm. Nemoto, Blackwelder and Mitsui (1994) in press.

Fig 9 *(continued)*

Fig 10 Changes of cellular glucose content, H_2 photoproduction activity and nitrogenase activity in the batch culture of *Synechococcus* sp. strain Miami BG 043511. Luo and Mitsui (1994) submitted.

Fig 11 Stimulating effects of glucose (5 mM) on H_2 production in different ages of batch cultures of *Synechococcus* sp. Miami BG 043511. A, 3-day old culture; B, 7-day old culture; C, 15-day old culture. Luo and Mitsui (1994) submitted.

Fig 12 Effects of various concentrations of pyruvate on H_2 production. A, 3-day old culture; B, 7-day old culture; C, 15-day old culture. Luo and Mitsui (1994) submitted.

Fig 13 Hydrogen photoproduction with 25 mM of pyruvate, glucose, sucrose, maltose, fructose, glycerol and control (without substrate) using a 6-day old batch culture of *Synechococcus* sp. strain Miami BG 043511. Luo and Mitsui (1994) submitted.

Fig 14 Effects of exogenous glucose (25 mM) and pyruvate (25 mM) on nitrogenase activity and H_2 production in the batch culture of *Synechococcus* sp. Miami BG 043511. Luo and Mitsui (1994) submitted.

Fig 15 Relationship between the nitrogenase activity and the amount of *nifH* mRNA during the synchronous culture of *Synechococcus* sp. strain Miami BG 043511. Upper part shows the nitrogenase activity and lower part shows Northern analysis of total RNA using PCR product of *nifH* as a probe. Campbell, Takeyama and Mitsui (1994) submitted.

Fig 16 Composition of polypeptide components of sucrose density gradient fractions analyzed by SDS-polyacrylamide gel electrophoresis. (A) Cells of the 0th hour (no nitrogenase activity), and (B) cells of the 12th hour (highest nitrogenase activity) after the onset of synchronous growth. Two polypeptides were found to be specific to the 12th hour cells, one is 57 kDa (*) and the other is 54 kDa (**). Nemoto, Blackwelder and Mitsui (1994) in press.

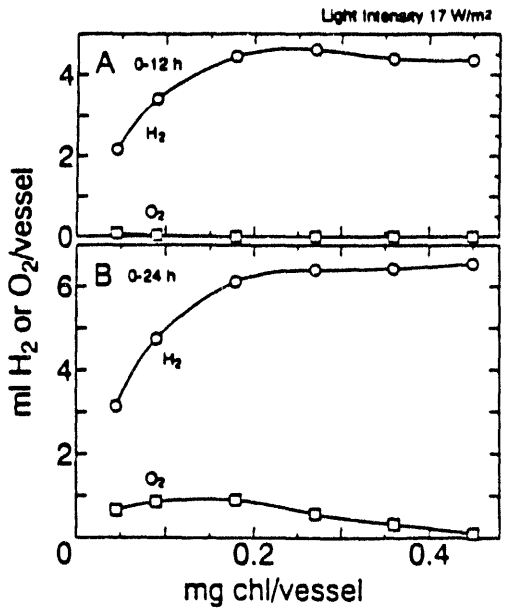

Fig 1 Effects of cell densities on H_2 and O_2 production in *Synechococcus* sp. strain Miami BG 043511. Light intensity was 17 W/m². A and B indicate 0-12 h and 0-24 h incubation periods, respectively. Kumazawa and Mitsui (1994) in press.

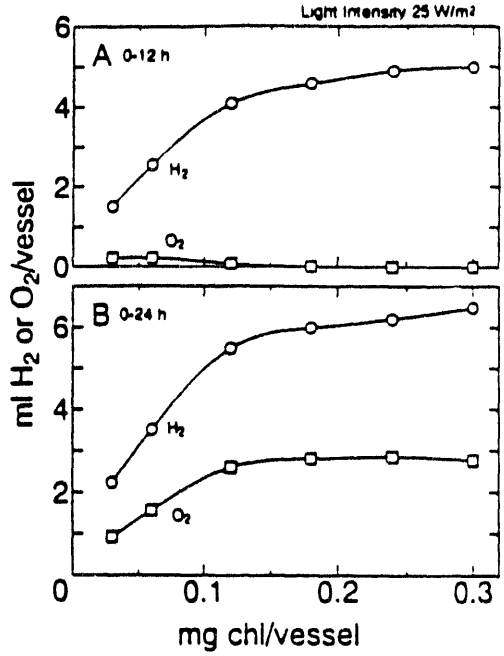

Fig 2 Effects of cell densities on H_2 and O_2 production in *Synechococcus* sp. strain Miami BG 043511. Light intensity was 25 W/m². A and B indicate 0-12 h and 0-24 h incubation periods, respectively. Kumazawa and Mitsui (1994) in press.

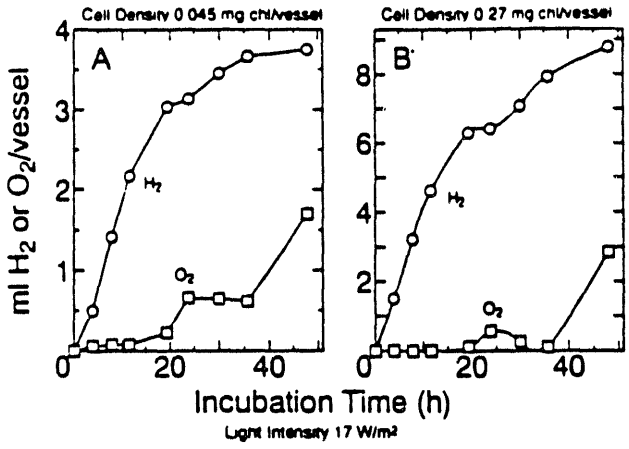

Fig 3 Changes in H_2 and O_2 during incubation under the light intensity of 17 W/m² in *Synechococcus* sp. strain Miami BG 043511. Cell densities in A and B were 0.045 and 0.27 mg chl/vessel, respectively. Kumazawa and Mitsui (1994) in press.

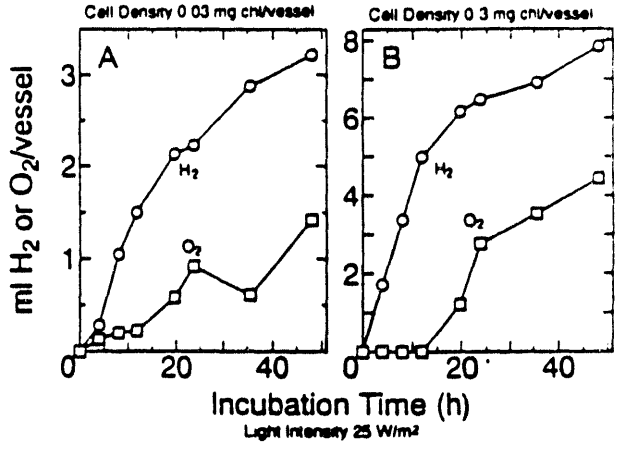

Fig 4 Changes in H_2 and O_2 during incubation under the light intensity of 25 W/m² in *Synechococcus* sp. strain Miami BG 043511. Cell densities in A and B were 0.03 and 0.3 mg chl/vessel, respectively. Kumazawa and Mitsui (1994) in press.

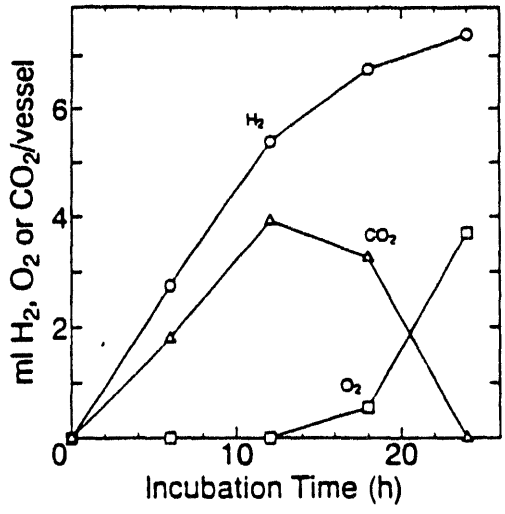

Fig 5 H_2, O_2 and CO_2 exchange during incubation under H_2 production conditions in *Synechococcus* sp. strain Miami BG 043511. Light intensity was 25 W/m². Kumazawa and Mitsui (1994) in press.

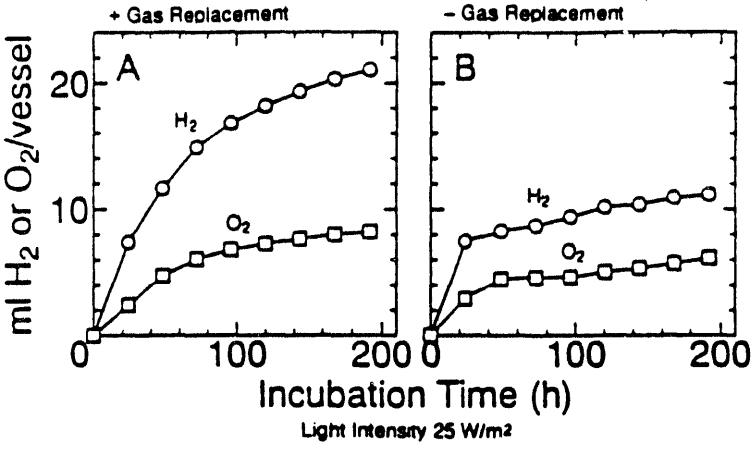

Fig 6 Effects of gas replacement on the H_2 and O_2 production in *Synechococcus* sp. strain Miami BG 043511. Amounts of H_2 and O_2 were assayed at 24 h intervals with (A) and without (B) the gas replacement by argon gas. Light intensity was 25 W/m². Kumazawa and Mitsui (1994) in press.

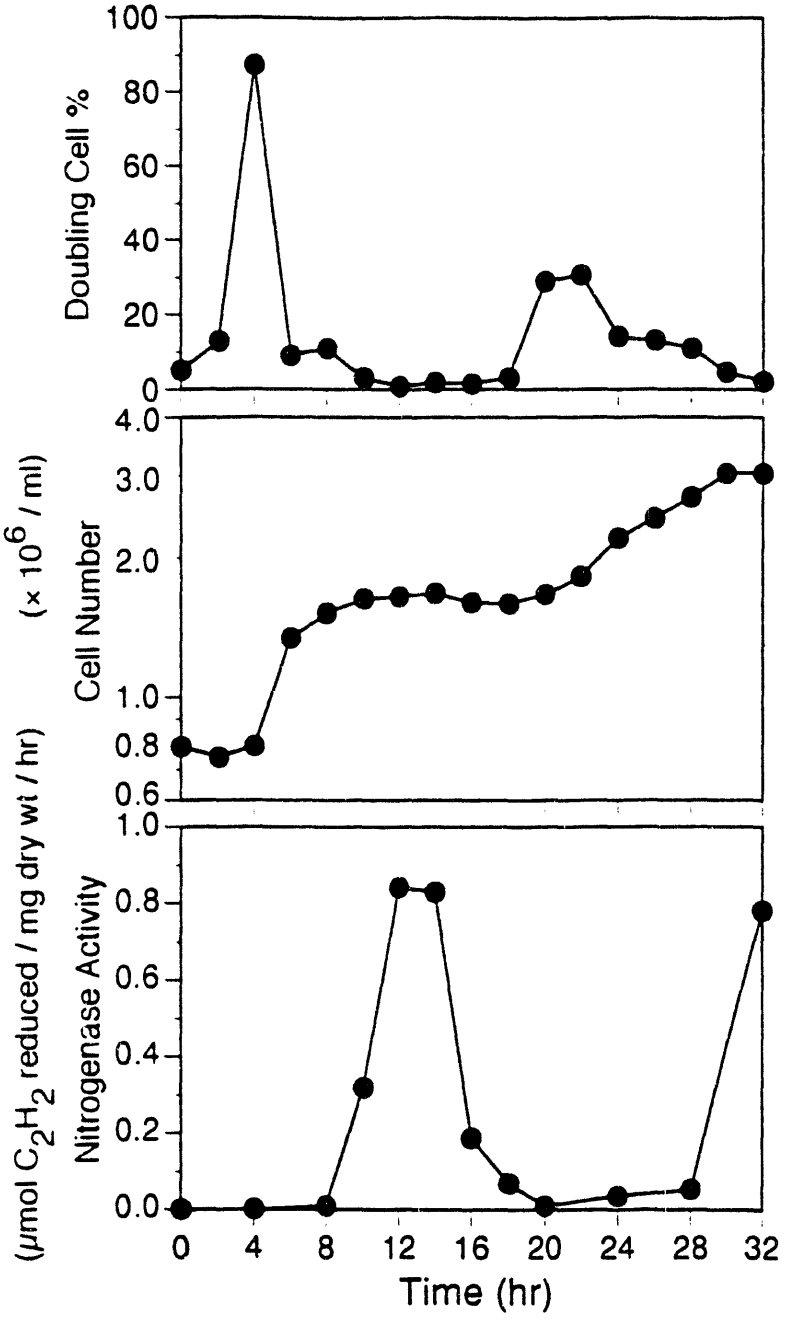

Fig 7 Synchronized cell growth and nitrogenase activity of *Synechococcus* sp. Miami BG 043511 under continuous illumination. Nemoto, Blackwelder and Mitsui (1994) in press.

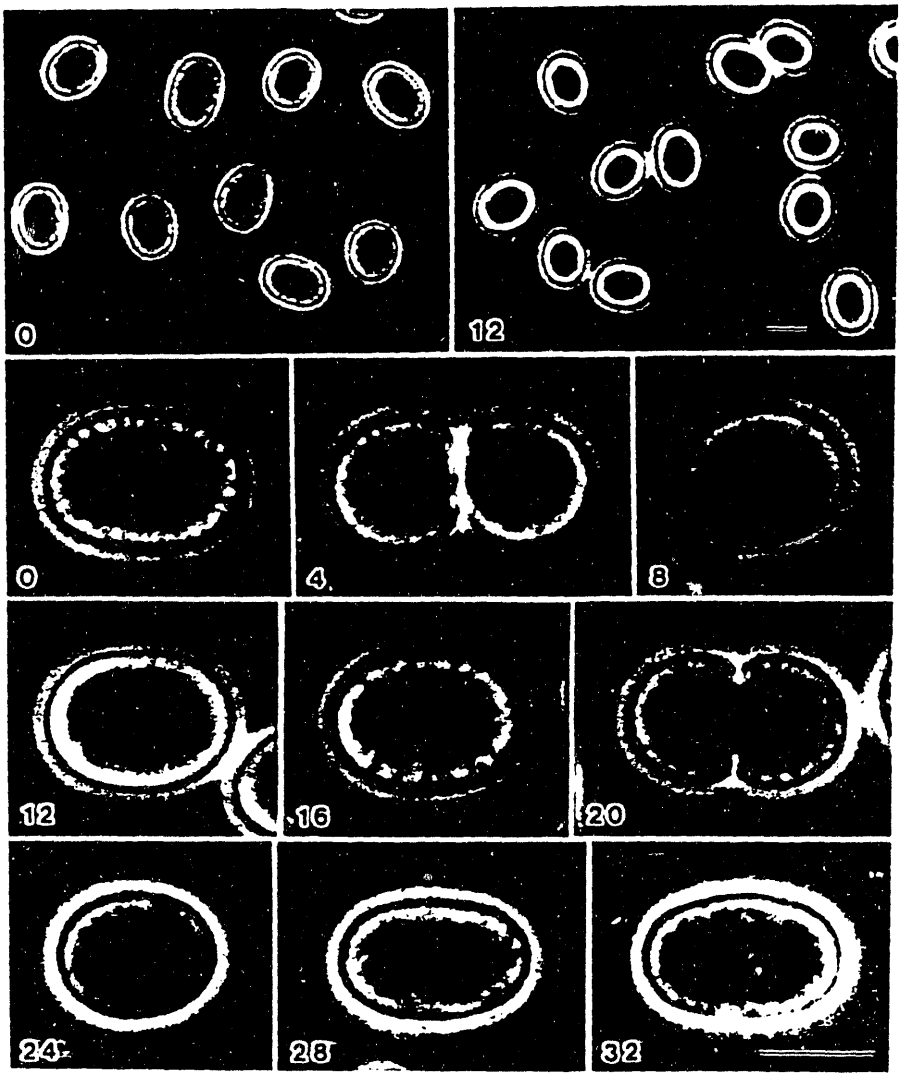

Fig 8 Phase contrast photomicrographs of the synchronously growing cells of *Synechococcus* sp. Miami BG 043511. Numbers shown in photographs indicate the hours after the onset of synchronous growth. Bar represents 5 μm. Nemoto, Blackwelder and Mitsui (1994) in press.

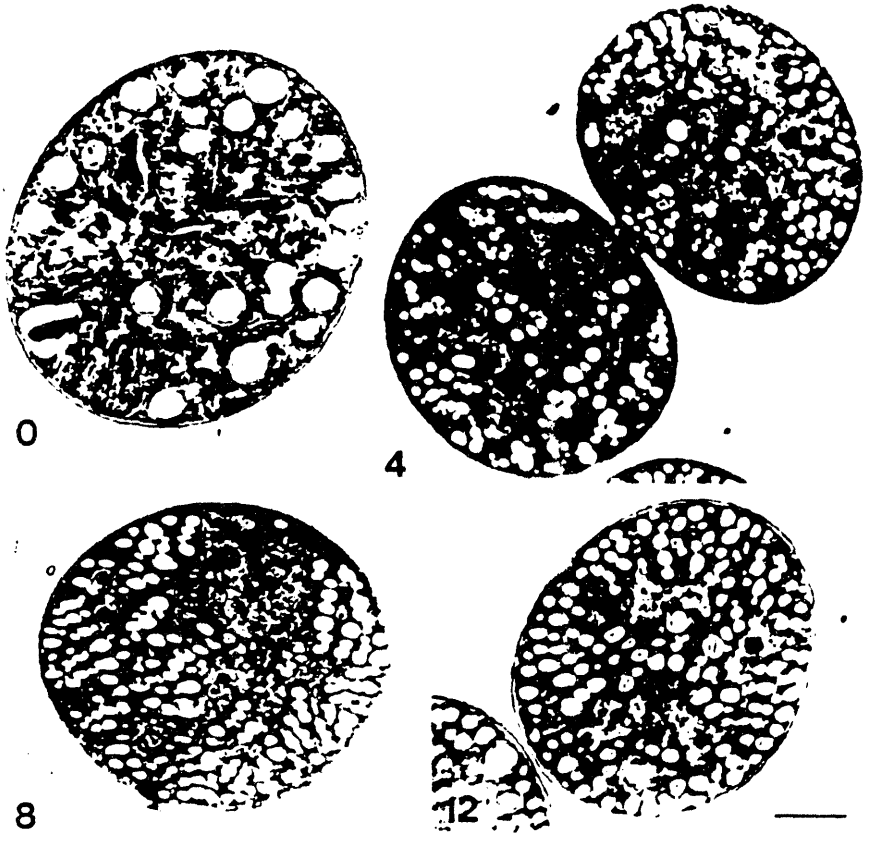

Fig 9 Electron micrographs of the synchronously growing cells of *Synechococcus* sp. Miami EG 043511. Numbers shown in photographs indicate the hours after the onset of synchronous growth. Bar represents 1 μm. Nemoto, Blackwelder and Mitsui (1994) in press.

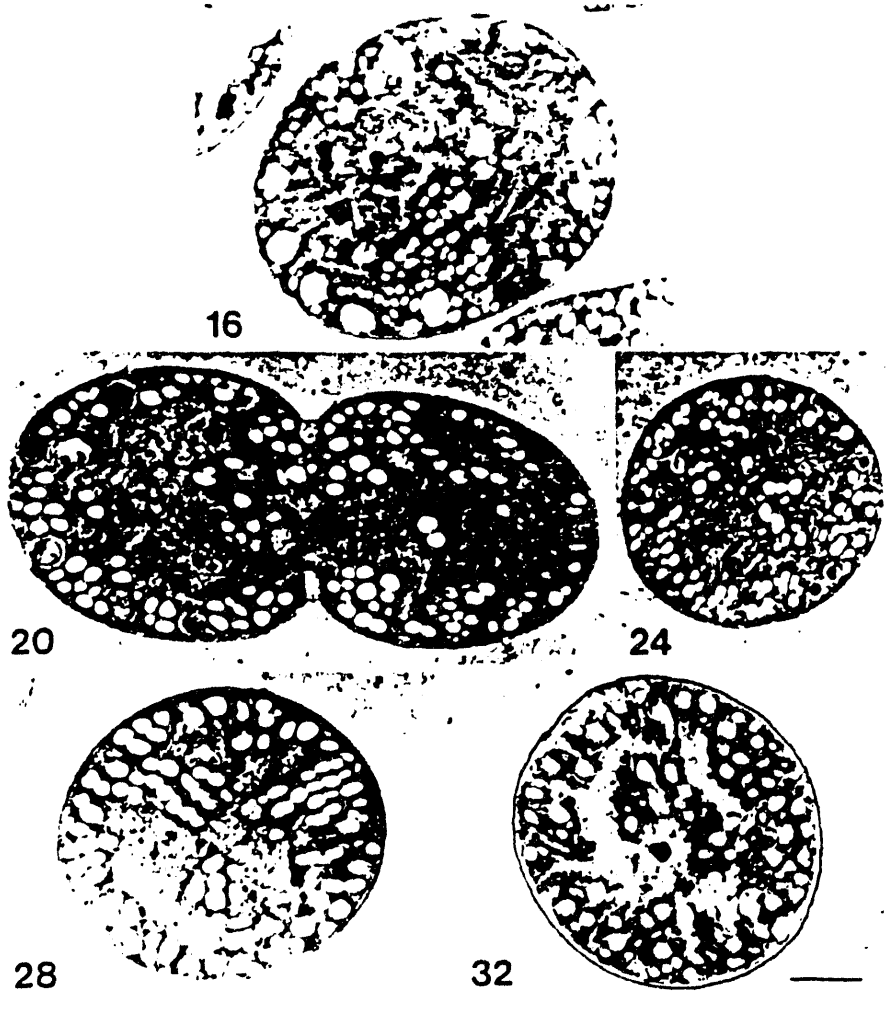

Fig 9 (*continued*)

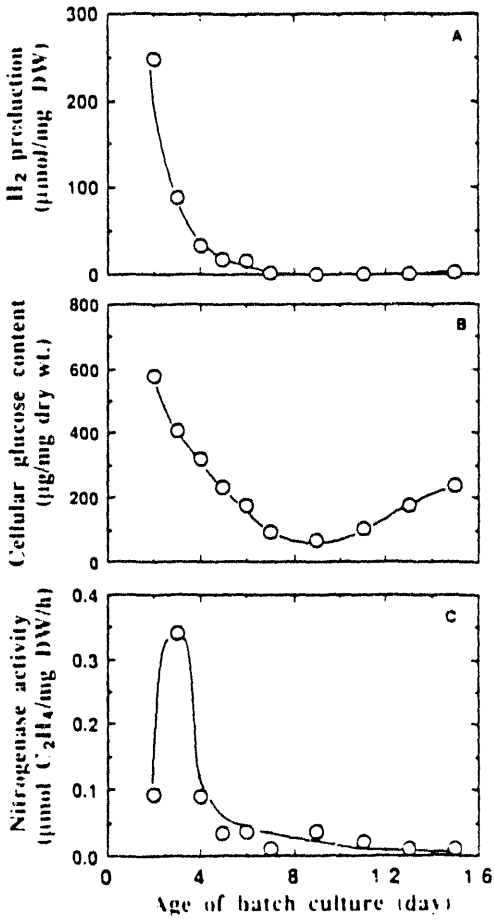

Fig 10 Changes of cellular glucose content, H_2 photoproduction activity and nitrogenase activity in the batch culture of *Synechococcus* sp. strain Miami BG 043511. Luo and Mitsui (1994) submitted.

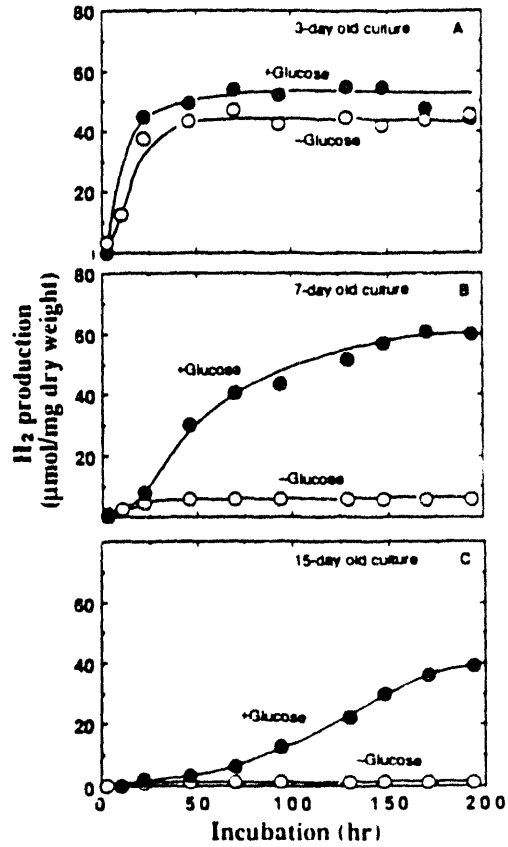

Fig 11 Stimulating effects of glucose (5 mM) on H_2 production in different ages of batch cultures of *Synechococcus* sp. Miami BG 043511. A, 3-day old culture; B, 7-day old culture; C, 15-day old culture. Luo and Mitsui (1994) submitted.

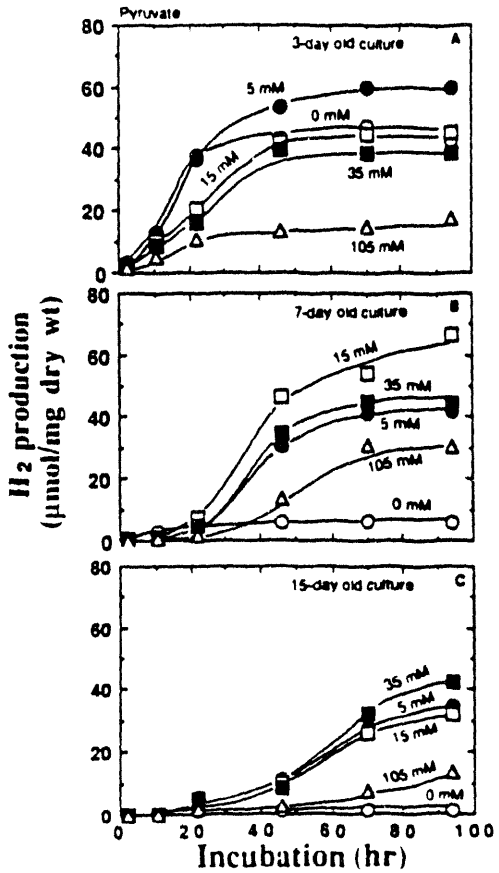

Fig 12 Effects of various concentrations of pyruvate on H_2 production. A, 3-day old culture; B, 7-day old culture; C, 15-day old culture. Luo and Mitsui (1994) submitted.

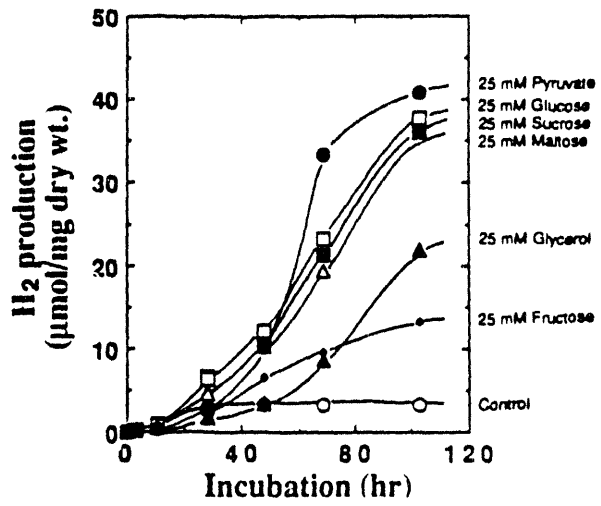

Fig 13 Hydrogen photoproduction with 25 mM of pyruvate, glucose, sucrose, maltose, fructose, glycerol and control (without substrate) using a 6-day old batch culture of *Synechococcus* sp. strain Miami BG 043511. Luo and Mitsui (1994) submitted.

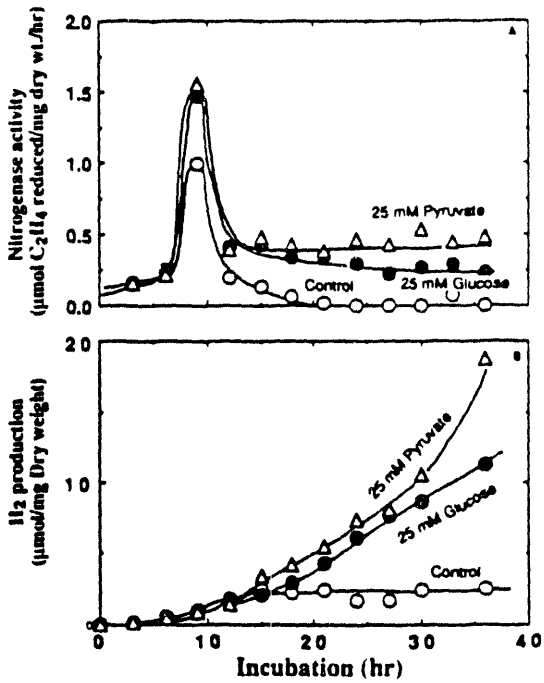

Fig 14 Effects of exogenous glucose (25 mM) and pyruvate (25 mM) on nitrogenase activity and H_2 production in the batch culture of *Synechococcus* sp. Miami BG 043511. Luo and Mitsui (1994) submitted.

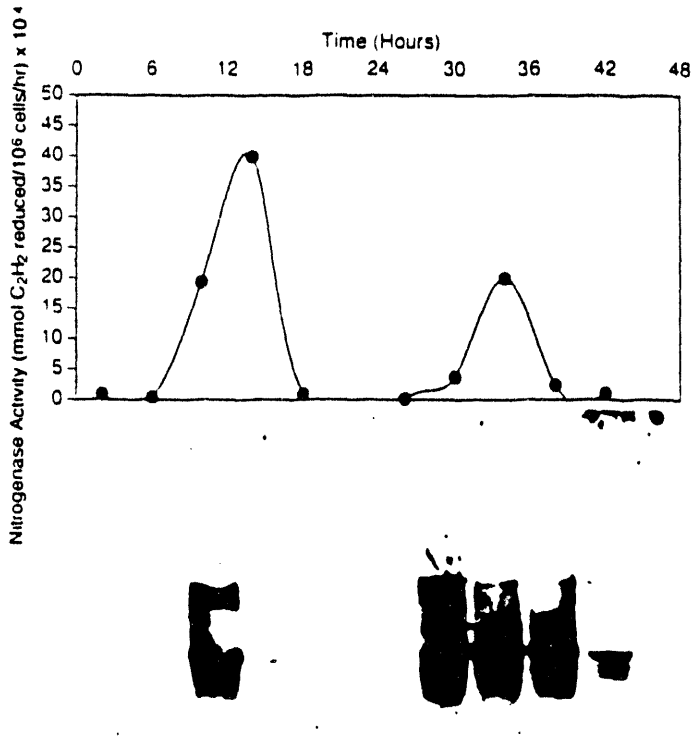

Fig 15 Relationship between the nitrogenase activity and the amout of *nif* H mRNA during the synchronous culture of *Synechococcus* sp. strain Miami BG 043511. Upper part shows the nitrogenase activity and lower part shows Northern analysis of total RNA using PCR product of *nif* H as a probe. Campbell, Takeyama and Mitsui (1994) submitted.

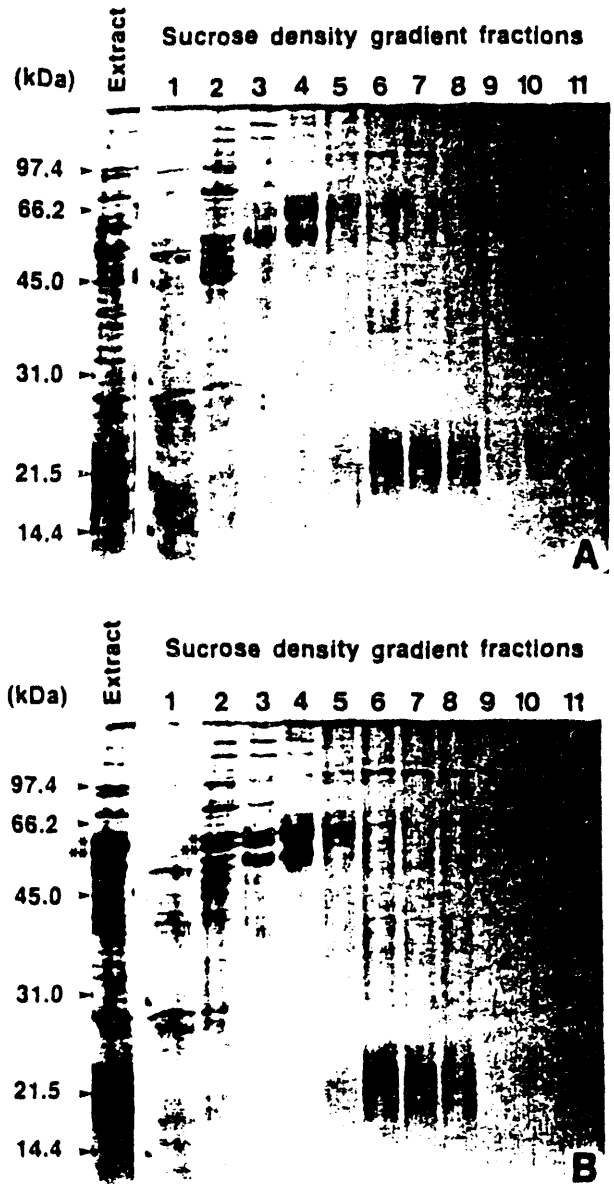

Fig 16 Composition of polypeptide components of sucrose density gradient fractions analyzed by SDS-polyacrylamide gel electrophoresis. (A) Cells of the 0th hour (no nitrogenase activity), and (B) cells of the 12th hour (highest nitrogenase activity) after the onset of synchronous growth. Two polypeptides were found to be specific to the 12th hour cells, one is 57 kDa (*) and the other is 54 kDa (**). Nemoto, Blackwelder and Mitsui (1994) in press.

PHOTOBIOLOGICAL H_2 FROM H_2O

P. Weaver, P.-C. Maness, A. Frank, S. Li, and S. Toon
National Renewable Energy Laboratory
Golden, CO 80401

Abstract

An economic process for producing hydrogen, whether biologically or chemically based, would ideally be (1) H_2O derived, (2) solar driven, (3) highly efficient, (4) durable, (5) insensitive to hydrogen partial pressure, and (6) inexpensive to build and operate. A complete system fulfilling all of these goals is not currently available. Of the biological options, systems employing intact cells of photosynthetic bacteria are the most advanced. Unlike cyanobacteria or algae, however, photosynthetic bacteria do not oxidize water. The desired criterion of sustained hydrogen production based on the photooxidation of water is the most difficult to achieve. Oxygen production is inherent in the oxidation of water, and the hydrogen-evolving enzymes of cyanobacteria and algae are usually rapidly inactivated by oxygen. A number of newly isolated photosynthetic bacterial strains apparently contain O_2-tolerant, evolving hydrogenase enzymes. This hydrogenase has been partially purified from two strains of bacteria, where it is found tightly bound to membrane fractions. The enzymes utilize a ferredoxin-like electron donor for H_2 production. Genetic transfer and expression of an oxygen-tolerant, bacterial hydrogenase enzyme in a cyanobacterial or algal host could provide a method for the linkage of photoreduced ferredoxin to an evolving hydrogenase, even in the simultaneous presence of photoevolved oxygen. Cell-free extracts of cyanobacteria or algae are being examined in mixtures with bacterial preparations containing the O_2-tolerant hydrogenases to ascertain the potential for coupling the processes in intact, genetically modified cells. Alternatively, the water-splitting and H_2-producing enzymes could be reversibly immobilized and linked on electroactive surfaces to generate water-splitting, hydrogen-evolving devices operating at up to 25% solar efficiencies. Whole-cell genetic constructs are considered mid-term, while linked enzyme/electrodes for H_2 production are longer term. The enzyme/electrode work has many potential additional uses in numerous specific biosensors, biological fuel cells, bioelectrochemical syntheses, nanoscale devices, etc., and is partially covered by an NREL patent (1993). Proposals have been written to EPA, DOD, and other agencies of DOE on these proposed technologies. Applications incorporating the novel fermentative hydrogenase of photosynthetic bacteria into a method for solar-enhancement of anaerobic digestion have also been patented (1990).

Introduction

Many microbes, including photosynthetic microbes, evolve and consume hydrogen as a normal part of their metabolism. Several distinct metabolic mechanisms have been examined for their potential for large-scale production of hydrogen from water. The biggest advantages of utilizing photosynthetic micro-organisms for H_2 production is their ease of growth, since they use primarily only sunlight as their energy source, and the eons of evolutionary adaptation that has allowed them to easily synthesize and assemble enzymatic components to perform specific biochemical photoconversions at high rates and efficiencies. In looking to nature to find a photosynthetic microbe that will directly photoproduce H_2 and O_2 from H_2O over long periods of time, it is readily apparent that none exist, since that would provide no direct benefit to the microbe. However, the necessary component enzymes to link water splitting to H_2 production are present in different photosynthetic organisms, or under different environmental conditions, or at different times within a given organism.

Any biological or chemical process for the economic production of H_2 should ideally be: H_2O-derived; solar driven; highly efficient; durable; insensitive to H_2 partial pressure; and inexpensive to build and operate. Obviously, no current system fulfills all of these goals. By combining pertinent enzyme complexes either in genetic constructs or in self-assembling, cell-free organizations, however, it is believed that the above-mentioned ideal criteria can be met. The most difficult criterion to achieve is that of sustained hydrogen production based on water oxidation, which simultaneously produces oxygen. Most of the hydrogen-evolving enzymes of cyanobacteria and algae are rapidly inactivated by oxygen. Some oxygenic microbes have partially solved this incompatibility by temporally or spatially (e.g., nitrogenase found in relatively O_2-impermeable heterocysts) separating O_2 production from H_2 metabolism. A second difficulty with application of intact cell systems is that much of the reductant that they generate goes to other metabolic functions, such as CO_2 reduction, rather than H_2 production, and therefore, solar efficiencies are low. A third potential difficulty is due to an oxyhydrogen reaction that occurs in the presence of many hydrogenases. That is, H_2 and O_2 are recombined by these particular hydrogenase enzymes to produce H_2O, thereby short-circuiting the biophotolytic process. All of these potential difficulties can be overcome by the use of proper genetically constructed strains or by spatially isolating incompatible enzymes in a cell-free matrix.

Results and Discussion

Of the intact cell metabolisms of phototrophs that evolve hydrogen, the nitrogenase-mediated reactions have been the most studied. Nearly all isolates of photosynthetic bacteria have a nitrogenase enzyme complex (Weaver et al. 1975), which, in the absence of ammonium ion or dinitrogen gas and in the presence of oxidizable organic materials, functions to reduce protons and evolve hydrogen. Hydrogen evolution is largely light dependent (Schultz et al. 1985) and strongly exergonic. The hydrolysis of about 4 ATP (largely synthesized in light) is required to generate each H_2 and can drive the gas production to equilibrium pressures in excess of 100 atmospheres. Radiant energy conversion efficiencies (ignoring the chemical energy of the organic substrate) are about 5.3% for the most active strains of photosynthetic bacteria. The best outdoor, solar-driven efficiency is 3.4%. Previous cultures grown on glutamate as the nitrogen source produced H_2 at linear rates for 7-10 days before *nif*$^-$ strains began to dominate the cultures. Experiments with weekly feedings of N_2 maintained the *nif*$^+$ wild-type genotype dominant and active H_2 production could be observed for more than 30 days. Even with the assumption that the best

strains and conditions could be maintained, the maximum solar conversion efficiencies that could be expected are probably less than 10%, however.

Many strains of photosynthetic bacteria also produce hydrogen from organic substrates by way of a fermentative hydrogenase enzyme when grown in darkness, or intermittent or low continuous light (Schultz and Weaver 1982). High, continuous light represses synthesis of the enzyme. The enzyme does not require ATP. It can mediate hydrogen production at rates more than 3-fold those of nitrogenase. However, it equilibrates at low partial pressures of about 0.1 atmospheres of H_2. The active rates of hydrogen production can thus only be maintained by sparging with inert gas, by vacuuming, or by scavenging with a hydrogen-consuming process (e.g., methanogenesis, which has been demonstrated, Weaver 1990). H_2 production from cyanobacterial or algal hydrogenases also may be subject to this same limitation.

A particularly unique hydrogen-evolving enzyme has been found in a group of photosynthetic bacteria that shift CO and H_2O into H_2 and CO_2 (see accompanying manuscript in these proceedings). A sub-set of these bacterial strains were isolated for their ability to shift CO into H_2 in the presence of 2% or more O_2. The only strains capable of growth under these conditions must, therefore, have a functional evolving hydrogenase enzyme even in the presence of O_2. Subsequent testing of some of these isolates showed only small losses of evolving hydrogenase activity over a one or two hour exposure to full air.

The CO-linked bacterial hydrogenase enzyme has maximal activities of about 1.51 mmol H_2 produced/min-g cell dry weight and may be under an energy charge mode of regulation. For comparison, representative rates for the more direct production of H_2 from H_2O in cyanobacteria and algae are each about 30 µmol H_2 produced/min-gram cell dry weight. Both the nitrogenase-based, heterocystous cyanobacterial system (Benemann and Weissman 1977) and the hydrogenase-based, green algal system (Weaver et al. 1980) had to be continuously sparged with inert gas in order to prevent O_2 build-up and inactivation of hydrogen evolution in order to obtain these rates. Equilibrium pressures were not determined.

If the O_2-tolerant hydrogenase enzymes from bacteria could be genetically transferred into cyanobacteria or algae, expressed, integrated into their membranes, and linked to photoreduced ferredoxin in the absence or limitation of CO_2, then a new whole-cell method for the photoproduction of H_2 from H_2O becomes feasible.

The bacterial CO-linked hydrogenase has been examined in extracts of three different strains of photosynthetic bacteria. It is strongly bound to membrane fractions in all three. Several attempts at hydrogenase extraction with ionic or non-ionic detergents resulted in partial release of the enzyme, which degraded relatively rapidly with time. CHAPS was partially effective at solubilizing hydrogenase activity without causing degradation. However, specific activities were only slightly increased, indicating that the membranes were primarily being comminuted into small membrane particles. Further chromatographic methods are being explored.

The question of whether the CO-linked hydrogenase of photosynthetic bacteria would participate in a wasteful oxyhydrogen reaction if it was transferred to a cyanobacterial or algal host was addressed by examining bacterial whole cells and membrane preparations. Bacterial cells can contain three distinct hydrogenase enzymes, so cells or cell-free preparations containing only the CO-linked hydrogenase are difficult to prepare. The uptake hydrogenase enzyme exhibits definite oxyhydrogenase activity, and, while not constitutive, is usually evident when hydrogen is present. Co-induction of the CO-linked hydrogenase

with the uptake hydrogenase does not significantly increase oxyhydrogen activity, highly suggestive that the CO-linked hydrogenase does not participate as an oxyhydrogenase. Definite proof must await experimentation with more purified enzymes, however.

Attempts are being made to couple the O_2-tolerant hydrogenase enzymes from bacteria with the water-splitting enzyme complexes of cyanobacteria, algae, and higher plants. Sub-chloroplast fractions of spinach were prepared that exhibited active photoreduction of $NADP^+$ (and, therefore, must have photoreduced ferredoxin in the process). Also, crude cell-free extracts of a culture actively shifting CO into H_2 were prepared and the extracts were mixed together. Upon illumination, neither oxygen nor hydrogen was produced, suggesting that reduced spinach ferredoxin was unable to reduce the bacterial hydrogenase or its electron donor, possibly because the redox cofactors do not directly interact or because the bacterial hydrogenase was inaccessible and buried within the bacterial membrane. Similar experiments will soon be performed using cyanobacterial preparations that have significantly closer kinship. Successful coupling between water-splitting complexes and bacterial hydrogenase is considered essential before genetic exchange techniques are attempted.

The theoretical maximum efficiency of biological H_2 production from water is about 10-12% (Bolton 1977) assuming that hydrogenase is the mediating enzyme. With a nitrogenase-based mechanism, the maximum efficiency should be decreased by about one-half if the aforementioned ATP requirements observed for photosynthetic bacteria are similar for cyanobacteria. Since the current intact-cell efficiencies of H_2 production from water oxidation are in the 0.1-0.3% range, there is considerable room for improvement if the twin problems of O_2 inactivation of hydrogenase and competition for reductant can be overcome.

A hybrid biological/electrochemical method is being developed that should confront these problems. In this scheme the water-oxidizing enzyme complex (PSII) is adsorbed to a conducting surface derivatized with benzoquinone, an electron acceptor for PSII. Light shining on PSII oxidizes water and liberates O_2 on the anodic side with electrons entering the electrode through quinone. Other photons absorbed either by a biomimetic chlorophyll or by a semiconductor photoelectrode elevate the electron energy sufficiently to reduce a redox mediator, a viologen dye covalently linked to the cathodic surface. Reduced viologen dyes readily couple with hydrogenase enzymes which then reduce protons to produce H_2 as the exclusive product. Our first choice for the hydrogenase enzyme to be used is the O_2-resistant, CO-linked hydrogenase of identified strains of photosynthetic bacteria. If near infrared photons could be used for the PSI component (e.g., by using bacteriochlorophyll), the theoretical efficiency of the device rises to 20-24%.

Negatively charged biological materials will electrostatically bind to positively charged surfaces. By being adsorbed, thermal stability increases. In one case, O_2-inactivation of hydrogenase was decreased more than a thousand-fold when it was bound to an ion-exchange surface (Klibanov et al. 1978). We have also adsorbed O_2-sensitive, purified carbon monoxide dehydrogenase to ion-exchange resins and shown greatly enhanced resistance to O_2 inactivation. Nevertheless, enzymes have finite lifetimes and must be replaced on the electrode surface if the whole apparatus is not to be discarded. To accomplish this, we are adding electroactive groups on the electrode surface that confer a positive surface charge when oxidized, which promotes binding, and a neutral or negative surface charge when electrochemically reduced, which promotes release. Spent enzymes should therefore be readily replaced without replacement of the derivatized electrode.

Singly and in combinations, we have derivatized ITO and graphite electrodes with quaternary amines, ferrocenes, quinones, pyridinium, nickel and ruthenium complexes, and other functional groups to determine their ability to reversibly bind biological materials. As a test system, intact bacterial cells were bound to the oxidized electrode surfaces where they remained metabolically active in monolayer films. Upon reduction of the electrode, the adsorbed cells were released into an effluent stream in a viable state. Multiple cycles of binding and release could be observed with several of the derivatized electrode surfaces.

Polyferrocene-coated electrodes were developed in order to determine the potential for reversible binding and self orientation of proteins on electrode surfaces. An oxidized (positively charged) derivatized electrode will bind proteins that are net anions at neutral pH, such as hemoglobin, bovine serum albumin, glucose oxidase, catalase, or clostridial hydrogenase. A hemoglobin solution was continuously pumped past the oxidized ferrocene surface and was completely adsorbed until the surface became saturated. Calculations indicate that nearly twice the geometrical surface area of the electrode was binding hemoglobin molecules. Upon electrochemical reduction of the surface, or by the addition of high salt concentrations, the majority, but not the total amount, of the hemoglobin, was eluted. Presumably, some surface charge may remain upon electrode reduction or, more likely, some protein may be entrapped in the polymer matrix.

Glucose oxidase was also adsorbed to a polyferrocene-coated electrode. With a constant bias applied and a continuous flow of buffer pumped across the electrode surface, pulse injections of glucose produced a current, reflecting that the enzyme/polymer surface was oxidizing glucose and mediating electron flow into the conducting support. Mannose, galactose, and fructose produced no current. These data indicate the potential for enzyme chromatography and binding site affinity for enzyme orientation on the electrode surface.

Quinone-derivatized electrode surfaces (for PSII binding) and viologen-derivatized electrode surfaces (for hydrogenase binding) are also being developed. PSII particles have been bound to benzoquinone surfaces; however, electron mediation or orientation of the complexes has not been examined.

Future Work

The CO-linked hydrogenase will be further purified from membrane preparations of O_2-tolerant bacterial strains. Their O_2-tolerance, oxyhydrogenase activity, and electron donor can then be further explored. Linkage of water-splitting preparations from cyanobacteria or algae to the purified hydrogenases will allow determinations of the activities, durabilities, and equilibrium concentrations for potential oxygenic strains that could be genetically transformed with the bacterial hydrogenase. Attempts at genetic exchange will follow.

Electrode surfaces will be derivatized with pendant groups of methyl viologen and benzoquinone. Electronegative groups will be included to enhance the release of anionic proteins. Orientation of redox enzymes by active site affinity will be examined. Electron mediation between redox enzymes and electrode surfaces will be improved. Stability of the enzymes in bound states will be compared with those in solutions.

References

Benemann, J.R., and J.C. Weissman. 1977. *Microbial Energy Conversion.* Pergamon Press: Oxford, pp. 413-426.

Bolton, J.R. 1977. *Proc. of the 4th International Congress on Photosynthesis*, pp. 621-634.

Klibanov, A.M., N.O. Kaplan, and M.D. Kamen. 1978. *Proc. Nat. Acad. Sci.*, 75:3640-3643.

Schultz, J.E., and P.F. Weaver. 1982. *J. Bacteriol.*, 149:181-190.

Schultz, J.E., J.W. Gotto, P.F. Weaver, and D.C. Yoch. 1985. *J. Bacteriol.*, 162:1322-1324.

Uffen, R.L. 1976. *Proc. Nat. Acad. Sci.*, 73:3298-3302.

Weaver, P.F. 1990. U.S. Patent 4,919,813, issued April 24, 1990.

Weaver, P.F., J.D. Wall, and H. Gest. 1975. *Arch. Microbiol.*, 105:207-216.

Weaver, P.F., S. Lien, and M. Seibert. 1980. *Solar Energy*, 24:3-45.

BIOLOGICAL WATER-GAS SHIFT ACTIVITY

P. Weaver, P.-C. Maness, A. Frank, S. Li, and S. Toon
National Renewable Energy Laboratory
Golden, CO 80401

Abstract

A unique subgroup of bacteria were isolated that shift CO (plus H_2O) into H_2 (plus CO_2) at near ambient conditions of temperature and pressure. The bacterial cultures performed a similar water-gas shift activity with the CO component of raw synthesis gas obtained from the thermal gasification of wood chips. When starting with 200,000 ppm of CO in the gas phase, less than 18 ppm of CO remained at equilibrium. Hydrogen production stoichiometry appeared to be strain and medium dependent and ranged from 90-100%. Rates of shift activity were as high as 1.51 mmols H_2 produced per min per g cell dry weight from CO in solution. Genetic or cell-free manipulations can be foreseen that could easily increase these rates 100-fold. Currently, however, the rate-limiting step, by far, is in the mass transfer of gaseous CO into the aqueous phase of the microbes. Mass transfer and, therefore, CO shift activity can be significantly enhanced by immobilizing the microbes in monolayer films on high-surface-area particles stacked in columns with the bulk water phase drained away. A CO gas stream passing around the column particles is thereby contacted with high concentrations of bacterial cells and a minimum diffusion distance. Glass beads coated with mussel hold-fast protein electrostatically bound films of bacteria. The bacterial films actively shifted CO into H_2 for periods of at least 10 weeks in the absence of any growth medium or cell growth. Electrochemical methods to reversibly ion exchange bacteria on similar conducting particles hold promise for making the surfaces easily regenerable and, therefore, economic for a relatively near-term, novel technology. Microbial binding to electrochemical surfaces has been patented and has several spin-off applications for disinfection of drinking water, bioremediation of organic and heavy metal pollutants, harvesting of microbes from fermenters or from dilute marine sources, etc. Proposals written on these additional applications have been submitted to EPA and other offices of DOE. The biological assimilation of synthesis and producer gases in light for the production of higher value products, such as polyhydroxyalkanoates, has also been patented and is a currently funded research project through the Office of Industrial Technology.

Introduction

A unique type of hydrogen producing activity was found in a strain of photosynthetic bacteria by Uffen (1976) that functioned only in darkness to shift CO (and H_2O) into H_2O (and CO_2). We have isolated more than 400 strains of photosynthetic bacteria from local sites that perform this shift reaction in darkness, as does the Uffen strain, but will also quantitatively assimilate CO into new cell mass in light, which makes them easy to grow. We have tested many of our strains for CO shift activity and growth with crude (water-scrubbed only) synthesis gas (primarily CO and H_2) generated from thermally gasified wood chips. In light, the novel photosynthetic bacteria assimilate the CO and H_2 components and a portion of the trace gases. In darkness, all of the isolates respond similarly by shifting the CO component into additional H_2, thereby leaving a product gas highly enriched in H_2 (with CO_2 and trace pyrolysis gases). No inhibitory effects of synthesis gas on long-term photosynthetic growth were noted. At ambient temperature and pressure conditions and starting from 200,000 ppm of CO in the gas phase, less than 18 ppm of CO remained at equilibrium. In order to determine the feasibility of using the biological catalysts for large-scale conditioning of synthesis gas, further information is needed on the maximal activities and durabilities of the enzymes involved. From an engineering standpoint, the rate-limiting step by far is in the mass transfer of the gaseous substrate into the aqueous phase of the bacteria.

Results and Discussion

Free energy calculations indicate that the shift conversion of CO into H_2 should release about 6.20 kcal per mol. This may be barely sufficient to generate ATP in an energy conserved reaction, depending on the biochemical mechanism employed by the bacteria. Anaerobic, dark growth on CO as the sole source of both carbon and energy is not readily apparent as an increase in cell mass, although slight increases are observed when CO and low levels of non-fermentable yeast extract are simultaneously present.

Phosphorylation experiments have not yet been performed. However, the addition of 10 µM carbonylcyanide m-chlorophenylhydrazone (un uncoupler of anaerobic respiratory, oxidative, and photosynthetic phosphorylation) increases CO shift rates by 20-40%, suggesting that the pathway may be regulated by the energy state of the cells. Measurements on cultures grown on CO in minimal medium in light and then placed in darkness routinely exhibit stoichiometries of 0.88 to 0.94 mol H_2 per mol CO consumed. These data also imply that the missing portion of the H_2 is going into cell growth, but no increase in optical density is observed. ^{14}C-labelled CO or bicarbonate show only minimal incorporation into cell mass or extra-cellular, non-volatile products. Resolution of the growth versus non-growth data under strictly anaerobic dark conditions is important for determining potential bioreactor designs for the long term shift of synthesis gas into purified H_2 gas streams with or without cell replenishment.

Bacterial catalyzed rates as high as 1.51 mmol H_2 produced from CO per min per g cell dry weight have been obtained in vigorously agitated cultures. Less actively stirred cultures exhibit H_2 production rates of 10-100 µmol per min per g cells, reflecting lower mass transfer rates.

Bioreactor designs utilizing bubble tower, sprinklered, gas-permeable hollow fibers, nebulizers, mat-forming, pressurized, or trickle filters are being adapted from another task to address the problem of increasing mass transfer of the CO component over prolonged periods of time with limiting mechanical and electrical energy input. A counter-current, continuous-flow trickle-filter reactor has been constructed, which can incorporate essential growth nutrients (ammonia, salts, etc.) if necessary and is undergoing

optimization to prevent air leaks. It will be operated in both nutrient-feed and non-feed modes to determine the functional lifetimes of shift activity. Reactivation of cells by intermittent exposure to light can also be assessed.

A simple, low energy method to enhance mass transfer of the gaseous substrate has proven to be at least partially effective. Six-mm polyethylene beads were coated with mussel hold-fast protein. About 25% of the amino acid residues of the protein are lysines, which present positively charged quaternary amines to the surrounding environment. Since microbes in solution at neutral pH have an excess number of negative charges on their surfaces, they electrostatically bind to the coated bead surfaces at high concentrations in monolayer films. When the immobilized bacteria on beads are stacked in a column and the bulk water drained away, passage of gaseous CO through the interstitial zone of the column results in its effective shift into H_2. Batch feeding of the immobilized bacteria with CO over the past ten weeks indicates that the bacterial enzymes remain relatively active with no cell growth or protein turnover and rates of about 0.5 mmol CO shifted per min per g cells.

Depending on the functional lifetimes of reactor designs using immobilized bacterial cells, we will probably have to replace the bacteria periodically. We are developing electrochemically controlled, ion exchange surfaces to accomplish this. Small conducting particles (e.g., graphite) are being surface derivatized with electroactive groups (e.g., ferrocenes or viologens) that in the oxidized state have a positive charge that will electrostatically bind bacterial cells to the surface. Upon reduction of the electroactive groups to a net neutral or negative charge, the bacteria are released into an aqueous void volume and can be washed away. Reoxidation of the surface presents a clean surface for the binding of fresh bacteria to regenerate the water-gas shift activity.

Future Work

Increasing the mass transfer and determining the maximal activities and functional lifetimes of the bacteria are the most pressing areas in need of further evaluation. Mass transfer rates with various reactor designs and methods of cell replacement will be determined. Bacterial strains and conditions exhibiting high rates and long lifetimes will be determined.

This project, to this point, is intended to be relatively near-term in development. If the basic system is proved to be feasible, however, there are a number of ways to improve upon it.

The carbon monoxide dehydrogenase enzyme that is responsible for the initial oxidation of CO represents only about 0.15% of the total cell protein. Assuming that the evolving hydrogenase is present in similar concentrations in the cell (i.e., ~0.15%), relatively straightforward genetic techniques could be used to increase the activity by up to 100-fold.

By utilizing only the carbon monoxide dehydrogenase enzyme and the hydrogenase enzyme purified from cell-free extracts, and reversibly immobilizing them on viologen-derivatized particles, the rate of the shift activity could be significantly increased by several orders of magnitude, provided that mass transfer rates can meet the enzymes' greatly enhanced capabilities.

References

Uffen, R.L. 1976. *Proc. Nat. Acad. Sci.*, 73:3298-3302.

Weaver, P.F., and A.J. Frank. U.S. Patent #5,208,154, Issued May 4, 1993.

Weaver, P.F., and P.-C. Maness. U.S. Patent #5,250,427, Issued Oct. 5, 1993.

Biomass to Hydrogen via Pyrolysis and Reforming

E. Chornet, S. Czernik. D. Wang, C. Gregoire, and M. Mann
National Renewable Energy Laboratory
1617 Cole Boulevard
Golden, CO, 80401-3393

Abstract

Pyrolysis of lignocellulosic biomass and reforming of the pyroligneous oils is being studied as a strategy for the production of hydrogen. New technologies for the rapid pyrolysis of biomass have been developed in the past decade. They provide compact and efficient systems to transform biomass into vapors which are condensed to oils, with yields as high as 75-80% by weight of the anhydrous biomass. This "biocrude" is a mixture of aldehydes, alcohols, acids, oligomers from the constitutive carbohydrates and lignin, and some water produced during the dehydration reactions. Hydrogen can be produced by reforming the biocrude with steam. A process of this nature has the potential to be cost competitive with conventional means of hydrogen production.

The concept of hydrogen from biomass offers significant opportunities for novel research and development. The use of a renewable resource feedstock is an alternative to conventional means of hydrogen production from petroleum and natural gas. As a consequence, the environmental benefit of zero net carbon dioxide emissions facilitates the approach to a pollution-free energy system. An additional benefit is that a regionalized system of hydrogen production can be envisioned using this technology. Small and medium-sized pyrolysis units (<500 Mg/day) could provide the biocrude to a centralized reforming facility to be catalytically converted to the H_2 and CO_2. Therefore, storage and transportation problems associated with hydrogen production become less important in the economics of the process. The reforming facility can be designed to handle alternate feedstocks, such as natural gas and naphtha, if necessary. Additionally, the biocrude can first be refined to yield valuable oxygenates so that only the residue is used for hydrogen production.

Project work is being conducted in five areas: literature reviews on the composition of pyrolysis oils and the technology of steam reforming to hydrogen; thermodynamic modelling to guide experimental design;

experimental research and catalyst testing; process development; economic evaluation; and environmental impact studies. Thermodynamic modelling of the major constituents of the biocrude has shown that reforming is possible within a wide range of steam/compound ratios. Additionally, catalytic reforming of model compounds to hydrogen using a Ni-based catalyst has begun. Existing catalytic data on the reforming of oxygenates has been studied to guide catalyst selection. An initial process diagram for the pyrolysis and reforming operations will also be presented, along with initial production cost estimates.

Introduction

Gasification of solid fuels to yield syngas (a mixture of H_2 and CO), followed by shift conversion to produce H_2 and CO_2, and steam reforming of hydrocarbons are well established processes. Renewable lignocellulosic biomass has been considered as a potential solid fuel feedstock for gasification. Economics of current processes favor the use of hydrocarbons (natural gas, C_2-C_5, and naphtha) and inexpensive coal as feedstocks. An alternative approach to H_2 production begins with fast pyrolysis of biomass.

Recent advances in the understanding of pyrolytic mechanisms and in the technology needed to achieve high heat transfer rates to particles, while controlling secondary cracking reactions responsible for gas and char production, have led to the development of fast pyrolysis routes. These convert biomass materials in high yields (~ 75% wt of dry biomass) into a "pyrolytic oil," or "biocrude." Typically, 85% wt of the biocrude is made of oxygenated organic compounds (Elliott, 1988): acids, alcohols, aldehydes, ketones, furans, substituted phenolics and complex oxygenates derived from biomass carbohydrates and lignin. About 15% wt of the biocrude is water from the dehydration reactions. Very little ash and char are present in the biocrude when appropriate filtration technology is used in the pyrolysis process.

Results from fluid bed fast pyrolysis (Radlein et al., 1991) have shown that a 76% wt yield of biocrude can be obtained from poplar ($CH_{1.47}O_{0.67}$). The organic fraction of the biocrude represents 85% wt and its elemental composition is $CH_{1.33}O_{0.53}$. Table 1 shows the expected yields of hydrogen from two thermochemical routes (pyrolysis and gasification), compared to the theoretical yield of the reaction between wood and steam using externally supplied heat.

Table 1. Comparison of H_2 yields from biomass process routes

Process Routes	Yield of Hydrogen (% wt biomass)	$\frac{\text{Energy Content (HHV) of } H_2}{\text{Energy Content of Biomass}}$
Pyrolysis + Catalytic Reforming	12.6	91%
Gasification + Shift Conversion	11.5	83%
Biomass + Steam + External Heat (Theoretical Maximum)	17.1	124%

Calculations were made using current yields for non-optimized fast pyrolysis (Radlein et al, 1991) and gasification (Probstein and Hicks, 1982) processes. The H_2 production potential for these two routes is similar. However, the pyrolysis process is less severe and does not require an oxygen supply as in gasification. Both options require steam for the reforming and shift conversion steps.

The objectives of our investigation are:

- To determine via thermodynamic simulations the conditions under which the components of the pyrolytic oils can be steam reformed to H_2 and CO_2, including equilibrium yields as a function of steam to carbon ratio and temperature
- To assess the scientific feasibility of catalytically converting the oxygen-rich pyrolytic oil compounds and to select suitable catalysts and conditions to be used

- To conduct an experimental bench scale program to determine real yields as a function of treatment severity, catalyst type and experimental conditions

- To develop a process flow diagram based on the results obtained and conduct economic calculations as a function of plant capacity.

Fast Pyrolysis: Biocrude Yields and Composition

Three technologies appear to be capable of achieving high yields of biocrude by a proper combination of temperature, time and heat transfer rates.

- Fluid beds (Piskorz et al, 1988): 450°C-550°C, < 0.5s

- Entrained beds (Graham and Freel, 1988): ~650°C, < 1.0s

- Ablative reactors, i.e. vortex (Diebold and Scahill, 1988): 450°C-625°C, < 1.0s

In the above technologies, 55-70% wt of mf biomass is the organic fraction of the biocrude, and 5-15% wt is water. A fourth technology (Roy et al, 1990), vacuum pyrolysis, has also demonstrated the ability to produce high biocrude yields. From this process, the organic fraction represents 50-60% wt of mf biomass and water 13-16% wt. Reliable values of oil, water, char and gas yields are difficult to obtain because of unclosed and/or unreported material balances. The composition of typical oils has only been reported in quantitative detail by the University of Waterloo, Canada (Piskorz et al, 1988), and is shown in Table 2.

Table 2: Pyrolytic Oil Composition Derived from Poplar (Radlein et al, 1991)

Yields	wt % mf wood
Oil*	65.8
Water*	12.2
Char	7.7
Gas	10.8
Unaccounted	3.5
Composition	
Acetic Acid	5.4
Formic Acid	3.1
Hydroxyacetaldehyde	10.0
Glyoxal	2.2
Methylglyoxal	0.65
Formaldehyde	1.2
Acetol	1.4
Ethylene Glycol	1.05
Levoglucosan	3.0
1,6-Anhydroglucofuranose	2.4
Fructose (?)	1.3
Glucose	0.4
Cellobiosan	1.3
Oligosaccharides	0.7
Pyrolytic Lignin**	16.2
Unidentified	15.5

*Oil + Water = Biocrude
**Material precipitated by addition of water

Variations in the composition of pyrolysis oil as shown in Table 2, should be expected as a function of raw material, pyrolysis treatment severity (T, t, and dT/dt profiles) and the use of catalysts during the pyrolytic step. However, the information presented in Table 2 clearly indicates that the biocrude is essentially a mixture of two major acids (acetic and formic), aldehydes and alcohols plus a significant fraction of lignin (denoted as pyrolytic lignin), probably present as a low to medium molecular weight material since it precipitates by simple addition of water. Based on the mechanistic works of Antal (1982), Shafizadeh (1982), and Richards (1987), the unidentified compounds should contain a large number of carbohydrate-derived components. Monomeric lignin-derived products having alcohol characteristics should also be present (Elliott, 1988).

The oxygenated biocrude may be an appropriate feedstock for further catalytic steam reforming to H_2 and CO_2 using a conversion strategy paralleling that of catalytic steam reforming of alcohols. Optimization of the pyrolysis conditions to obtain high yields of biocrude having a significant fraction of low molecular weight aldehydes and alcohols is required.

Thermodynamics

Thermodynamic simulations of the reforming reaction were performed in order to guide experimental design and determine equilibrium constraints. These simulations were performed on ASPEN Plus using compounds representative of the oil and a mixture of compounds with the following composition, based on the results obtained by the University of Waterloo and from the vortex reactor at NREL.

Compound	Molar Percent	Weight Percent
hydroxyacetaldehyde	38%	33%
acetic acid	27%	23%
acetol	9.3%	9.8%
guaiacol	3.7%	6.6%
syringol	1.4%	3.3%
formic acid	7.5%	4.8%
coniferol	2.6%	6.6%
phenol	2.4%	3.3%
benzene	2.9%	3.3%
toluene	2.5%	3.3%
furfural	2.4%	3.3%

A three dimensional plotting program was used to graph the production of hydrogen by steam reforming as a function of temperature and the molar ratio of steam to carbon content (R). Figures 1, 2 and 3 show these plots for hydroxyacetaldehyde, syringol and the mixture of model compounds, respectively. These should be viewed as qualitative tools only and not for the determination of optimal operating parameters; the region to work within when designing experimental conditions can be approximated from the plots. It will not be possible to model the thermodynamics of the actual oil because of its complexity and limitations in the ASPEN Plus component data bank.

A more useful method of estimating experimental conditions is to define a practical operating temperature and calculate the yield of hydrogen as a function of R. Because pyrolysis oil vapors are produced at approximately 450°C to 600°C, thermodynamic simulations were performed at a reaction temperature of 500°C. Figures 4, 5 and 6 show the mole fraction of hydrogen in the product as a function of R at 500°C for hydroxyacetaldehyde, syringol and the mixture of compounds, respectively.

Figure 7 shows the approach of many of the model compounds and the mixture of compounds to maximum stoichiometric yields of hydrogen as a function of R. The most important result from this plot is that the necessary amount of steam is dependent only on the carbon content of the compound. Differences in the results between compounds can be attributed to the approximations made in the thermodynamic calculations. Therefore, given the carbon content of the pyrolysis oil, the appropriate amount of steam for high hydrogen yields can be estimated. Approximately 6.5 moles of steam per carbon are needed to achieve 80% of the stoichiometric maximum yield of H_2. For 90% of the maximum, 9.0 - 9.5 moles of steam per carbon are required. This suggests that a wide range of combinations of operating variables is possible to obtain near stoichiometric yields. Simulation results are currently being used to design laboratory experiments.

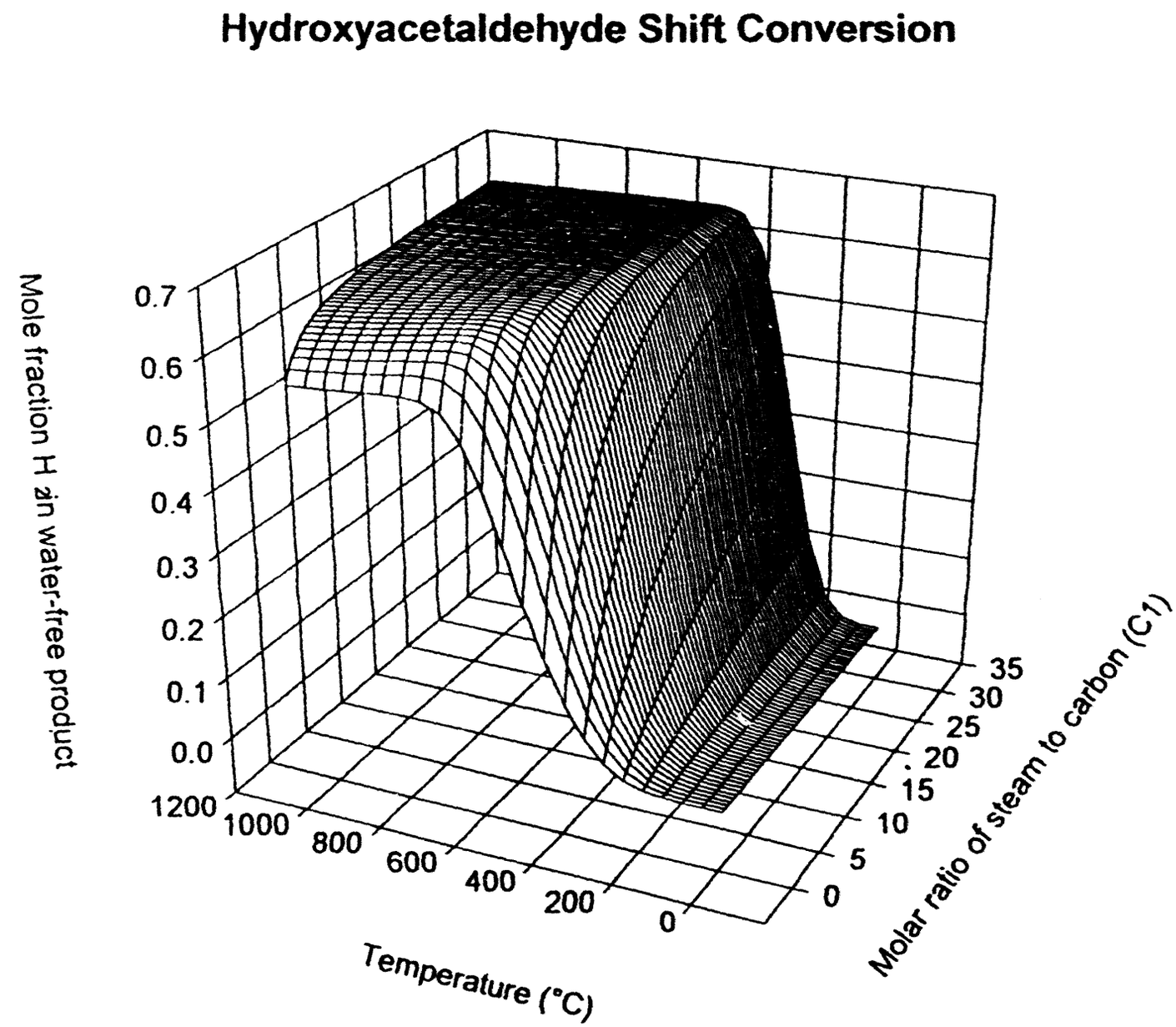
Hydroxyacetaldehyde Shift Conversion
Mole fraction H in water-free product
0.7
0.6
0.5
0.4
0.3
0.2
0.1
0.0
1200
1000
800
600
400
200
0
Temperature (°C)
0
5
10
15
20
25
30
35
Molar ratio of steam to carbon (C1)

Figure 1

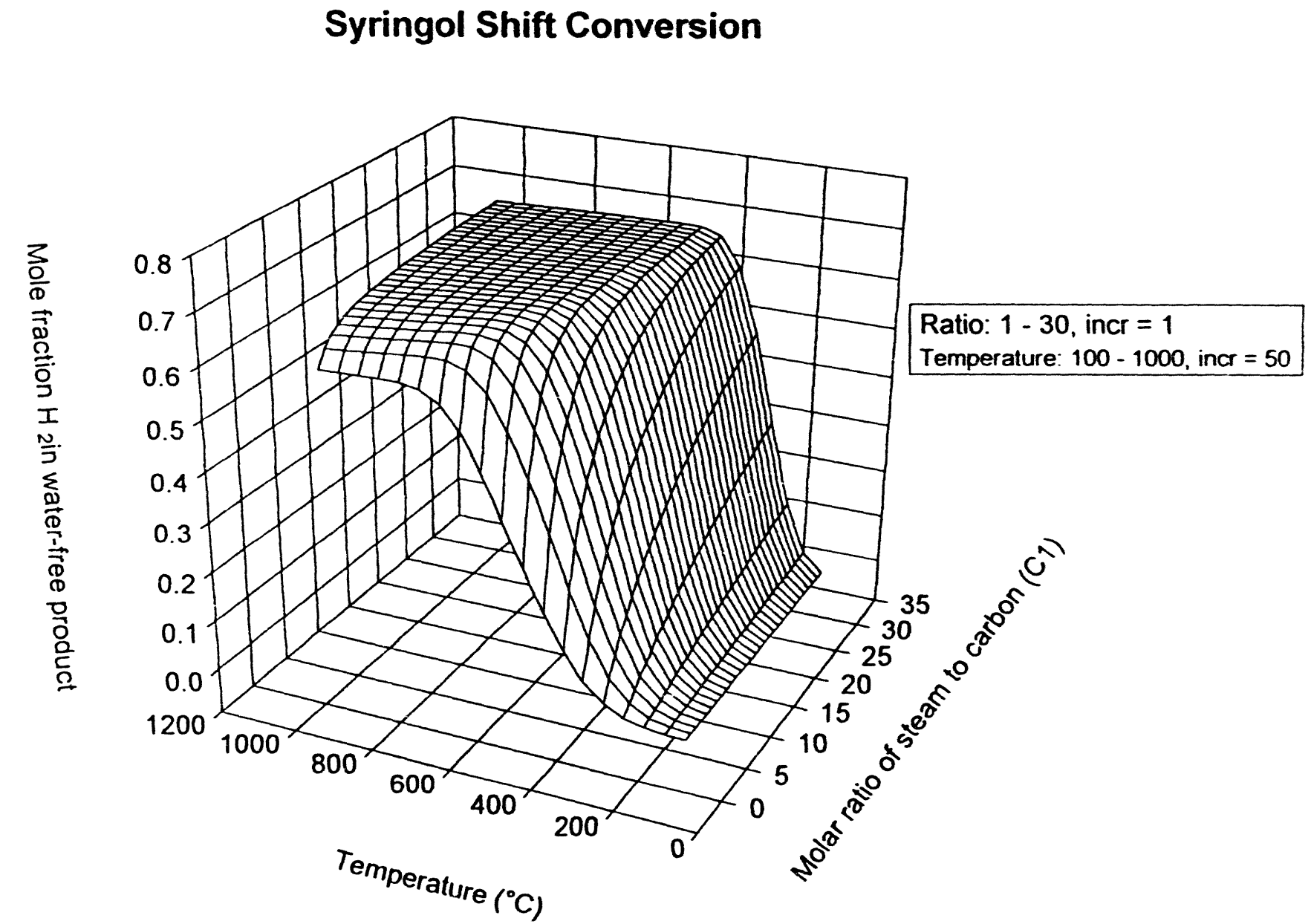
Syringol Shift Conversion
Mole fraction H 2in water-free product
0.8
0.7
0.6
0.5
0.4
0.3
0.2
0.1
0.0
1200
1000
800
600
400
200
0
Temperature (°C)
35
30
25
20
15
10
5
0
Molar ratio of steam to carbon (C1)
Ratio: 1 - 30, incr = 1
Temperature: 100 - 1000, incr = 50

Figure 2

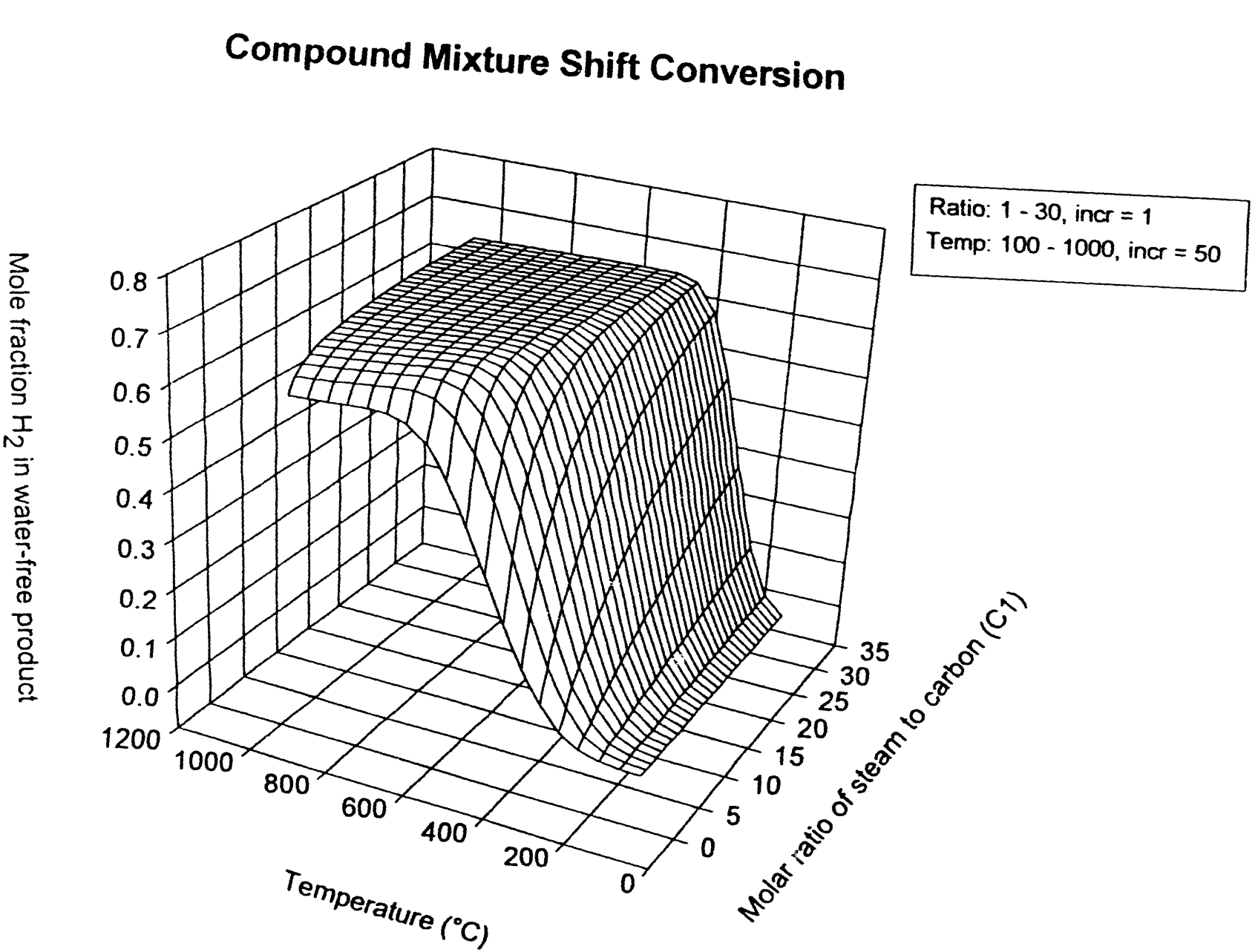
Compound Mixture Shift Conversion
Ratio: 1 - 30, incr = 1
Temp: 100 - 1000, incr = 50
Mole fraction H_2 in water-free product
0.8
0.7
0.6
0.5
0.4
0.3
0.2
0.1
0.0
1200
1000
800
600
400
200
0
Temperature (°C)
0
5
10
15
20
25
30
35
Molar ratio of steam to carbon (C1)

Figure 3

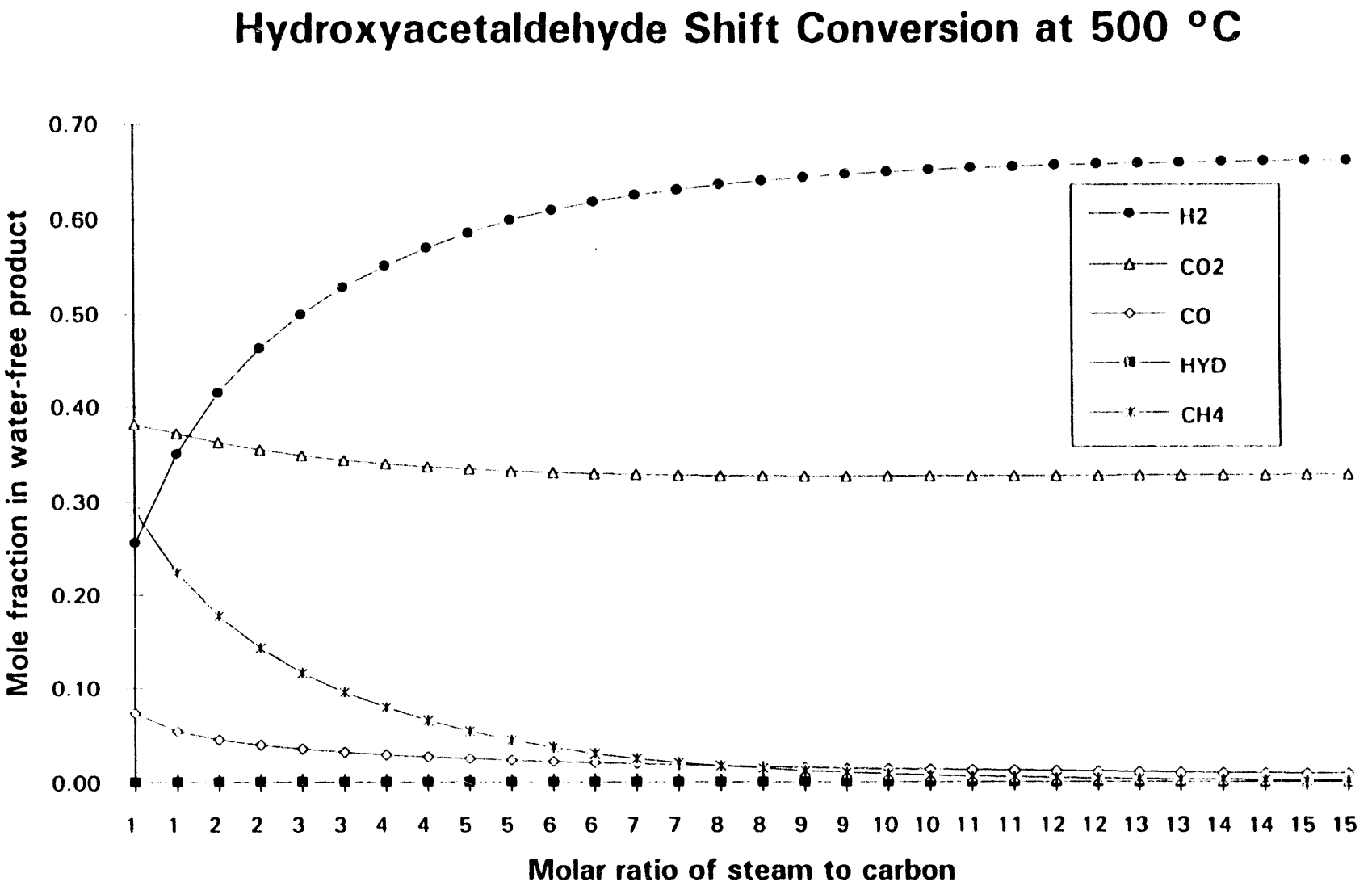
Hydroxyacetaldehyde Shift Conversion at 500 °C
Mole fraction in water-free product
0.70
0.60
0.50
0.40
0.30
0.20
0.10
0.00
H2
CO2
CO
HYD
CH4
1 1 2 2 3 3 4 4 5 5 6 6 7 7 8 8 9 9 10 10 11 11 12 12 13 13 14 14 15 15
Molar ratio of steam to carbon

Figure 4

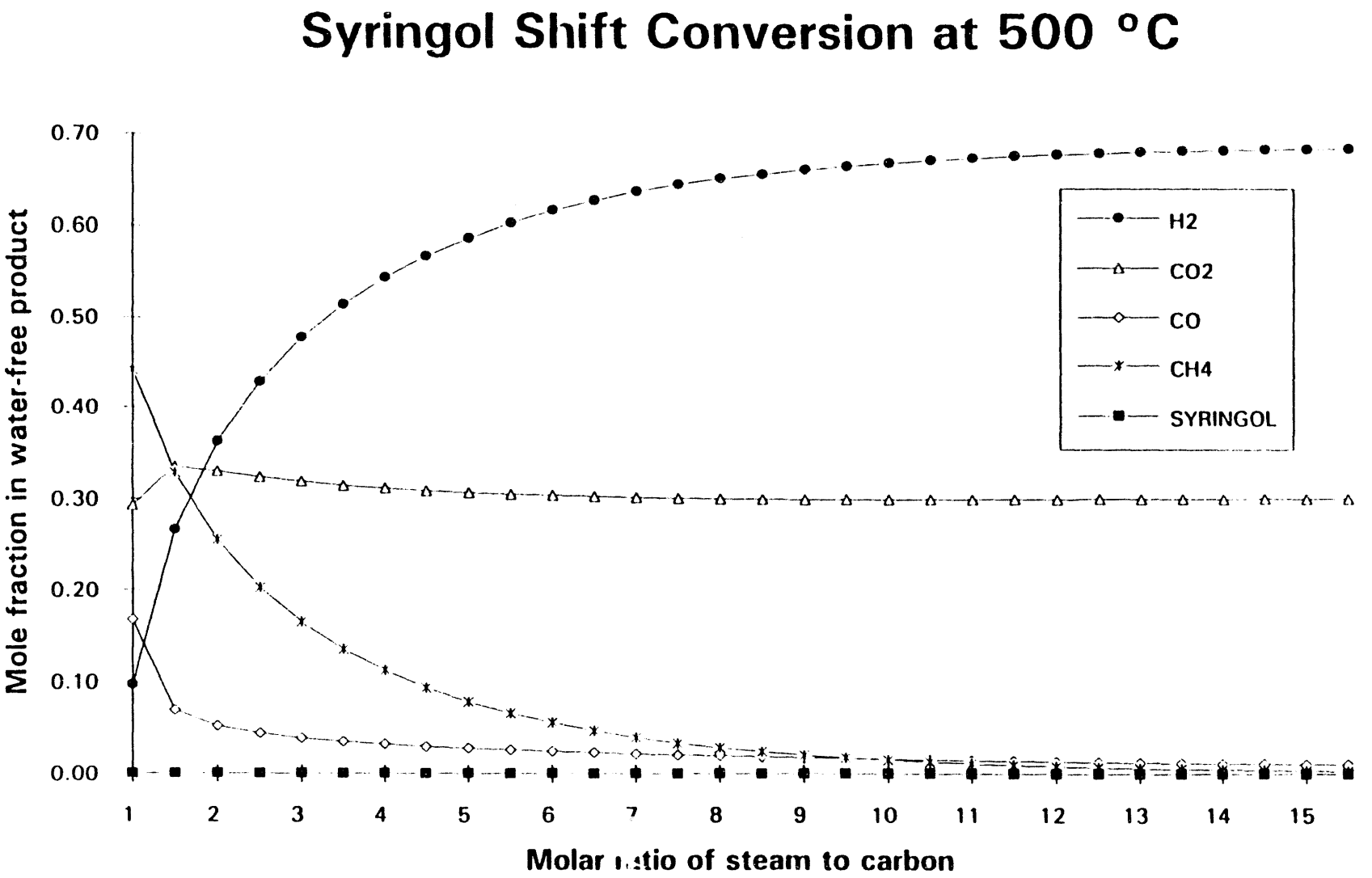
Syringol Shift Conversion at 500 °C
Mole fraction in water-free product
0.70
0.60
0.50
0.40
0.30
0.20
0.10
0.00
1
2
3
4
5
6
7
8
9
10
11
12
13
14
15
Molar ratio of steam to carbon
H2
CO2
CO
CH4
SYRINGOL

Figure 5

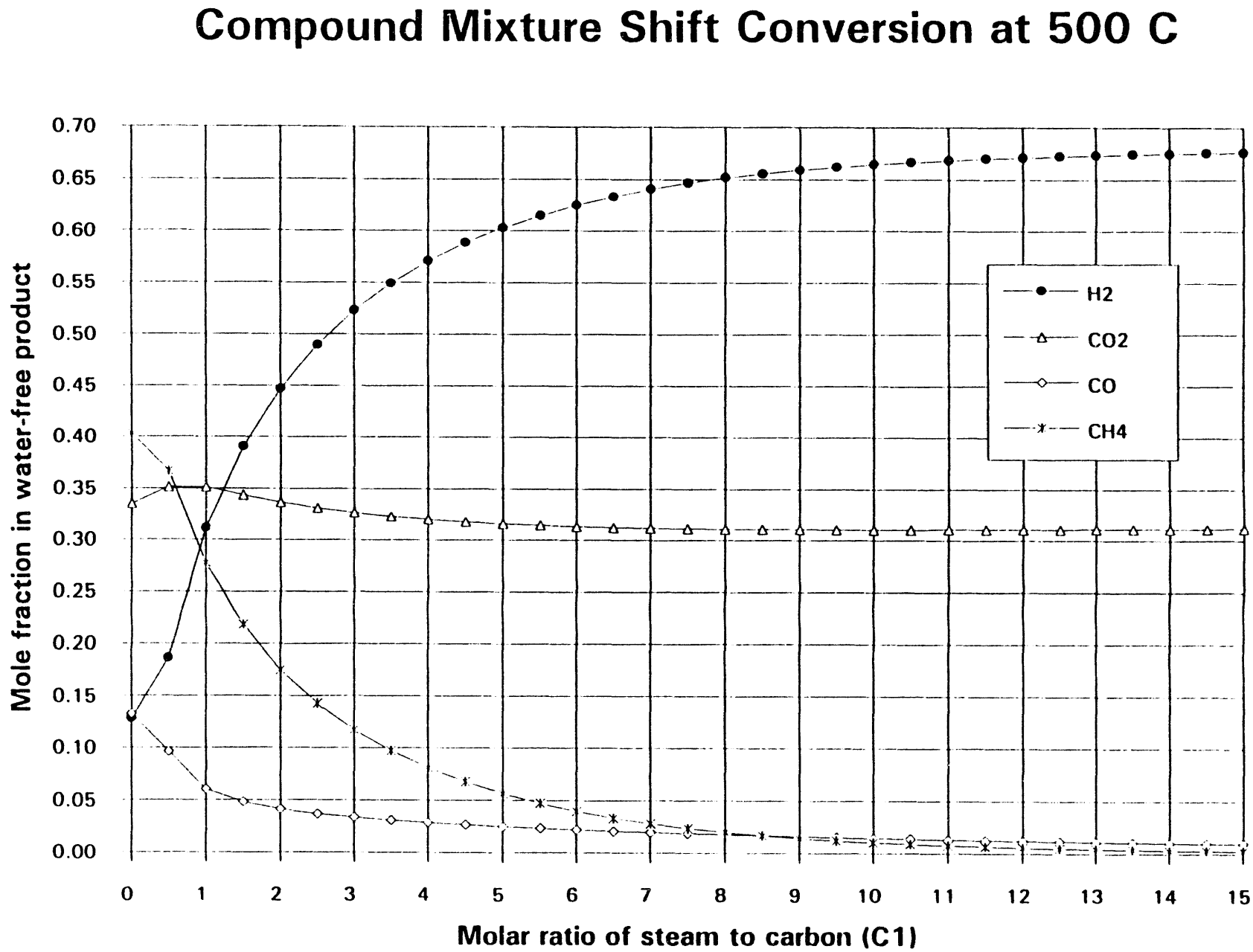
Compound Mixture Shift Conversion at 500 C
Mole fraction in water-free product
0.70
0.65
0.60
0.55
0.50
0.45
0.40
0.35
0.30
0.25
0.20
0.15
0.10
0.05
0.00
0
1
2
3
4
5
6
7
8
9
10
11
12
13
14
15
Molar ratio of steam to carbon (C1)
H2
CO2
CO
CH4

Figure 6

Approach to Maximum Stoichiometric Yield of Hydrogen at 500 °C

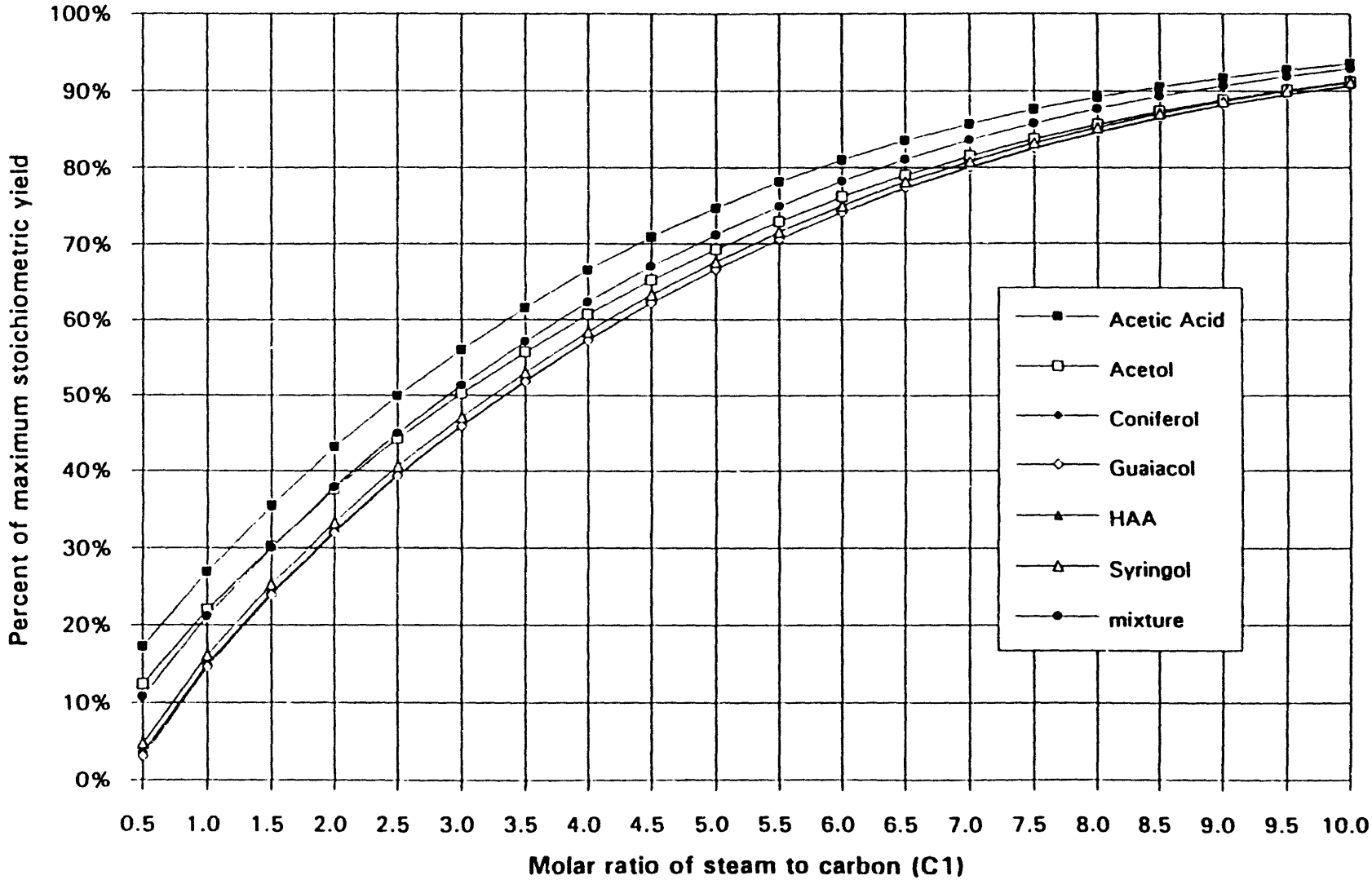

Figure 7

Catalytic Reforming of Oxygenates

Steam reforming C_1-C_5 hydrocarbons, naphtha, gas oils and simple aromatics are commercially practiced, well known processes. When the objective is to maximize the production of H_2 the stoichiometry describing the overall process is:

$$C_n H_m + 2n H_2O = n CO_2 + (2n + m/2) H_2 \quad (1)$$

The simplicity of Equation 1 hides the fact that in a hydrocarbon reformer, the following reactions take place concurrently:

$$C_n H_m + n H_2O = n CO + (n + m/2) H_2 \quad (2)$$

$$CH_4 + H_2O = CO + 3 H_2 \quad (3)$$

$$CO + H_2O = CO_2 + H_2 \quad (4)$$

At normal operating conditions, reforming of higher hydrocarbons (Equation 2) is irreversible (Tottrup and Nielsen, 1982), whereas the methane reforming reaction (Equation 3) and the shift conversion reaction (Equation 4) approach equilibrium. A large molar ratio of steam to hydrocarbon will ensure that the equilibrium for reactions (3) and (4) is shifted towards H_2 production.

The main problem in the steam reforming of hydrocarbons is carbon formation. Three types of carbon may be formed: whiskers, encapsulating deposits ("polymers"), and pyrolytic carbon (Rostrup-Nielsen and Tottrup, 1979). The carbon formation is related to the kinetics, and hence the selectivity, of the catalyst. In steam reforming, adsorption of hydrocarbons on the metal sites (Ni is commonly used) is followed by dehydrogenation and cracking. This results in smaller $C_x H_y$ adsorbed fragments which can polymerize to unwanted intermediates and lead to coke formation. These reactions compete with reactions of the adsorbed water species. The catalyst must then be formulated to supply enough adsorbed H_2O-derived species, mainly OH and H, to overcome the coke formation reactions. This implies that the adsorbed OH and H must have sufficient surface mobility to reach the adsorbed hydrocarbon-derived species and react with them (Rostrup-Nielsen, 1984).

The steam adsorption capability can be significantly improved by promoting the classical Ni-alumina or Ni-silica/alumina formulations with Ca and/or K. An alternative is the use of magnesia as magnesium-aluminum spinel which enhances steam adsorption and can be prepared as high surface area refractory ceramic pellets.

The reforming operation requires relatively high steam/carbon molar ratios (S/C1 = 3.5 - 5.0 for methane), adequate temperature profiles in the tubular reactor (low inlet temperature increased along the tube length to a maximum of 750°C-775°C due to the structural constraints of the Ni-Cr alloys used), and a Ni-based catalyst (20-30 wt% as NiO) on a refractory support having appropriate steam adsorption characteristics as previously discussed. The reforming operation is not very sensitive to pressure which is essentially dictated by the applications of the product H_2 (Patil, 1987). The NiO is reduced to its metal form prior to use. Space velocities used in tubular reformers are typically comprised between 1500-2000 (volume of C_1 equivalent/h/volume of catalyst).

Sulfur is the most severe catalyst poison. Biomass-derived feedstocks, i.e. biocrudes, have only traces of sulfur and thus a desulfurization unit prior to the reformer may not be necessary. However, because of the oxygenated nature of the pyrolysis oil, the catalyst to be used in the reforming process must be able to handle high percentages of oxygen-containing functional groups. Efforts to modify steam reforming catalysts and render them less susceptible to poisoning by heteroatoms, mainly sulfur, have led to the development of novel preparations. Thus, sulfur resistant rare earth promoted catalysts for gas oil feeds have been available since the mid-eighties (Patil, 1987). The unreduced catalyst form is a mixture of NiO, rare earth oxides and Zr_2O_3. The applicability of this family of catalysts to reform oxygenates is not known. However, their satisfactory performance in the presence of sulfur makes such preparations attractive for the reforming of oxygen-containing molecules.

Aznar et al (1993), have clearly demonstrated that steam reforming syngas obtained from the gasification of lignocellulosics is possible using commercially available Ni-based catalysts (Topsoe R-67 and RKS-1), even with rapid deactivation of the catalyst after a few hours. Tars produced during gasification contain a high percentage of polycyclic aromatics, while pyrolysis oil is essentially a mixture of carbohydrate-derived fragments and lignin-derived phenolics (Elliott, 1988).

Literature on the steam reforming of oxygenates follows within two categories:

- Reforming methanol and ethanol
- Reforming oxygenated aromatics, i.e. cresols

Methanol reforming is of interest as a process for the production of H_2 in numerous applications, hydrogenation of organic compounds and fuel cells being the most obvious. A large body of information has thus been accumulated on the catalytic reforming of methanol (the C1 alcohol). The comparison with methane, the analog C_1 hydrocarbon, is thus appropriate. Methane requires high temperatures (> 500°C) to be effectively steam reformed. The mechanism has been proposed as follows (Ross et al, 1978):

- Methane, or any other hydrocarbon, is dissociatively adsorbed on the metal sites
- H_2O is also dissociatively adsorbed on the Al sites, hydroxylating the surfaces
- Metal-catalyzed dehydrogenation takes place creating adsorbed hydrocarbon-derived fragments
- The OH surface groups migrate to the metal sites, activated by the temperature, and they eventually form intermediates leading to carbon oxides.

Methanol can be steam reformed at much lower temperatures (< 300°C) than methane. A variety of catalysts are capable of carrying out the conversion including reduced NiO-based preparations (Mizuno et al, 1986), reduced CuO/ZnO shift preparations (extensive literature cited by Amphlett et al, 1985; Su and Rei, 1991), Cu/SiO_2 and Pd/SiO_2 (Takahashi et al, 1982), Cu/ZrO_2 (Takezawa et al, 1987), and Pd/ZnO (Iwasa et al, 1993). The product slate is markedly affected by the type of catalyst and the experimental conditions used. Two main mechanisms have been proposed (Jiang et al, 1993 a and 1993 b):

- The decomposition-shift mechanism where the chemisorbed methanol is totally

dehydrogenated on the metal surface prior to forming CO. The shift reaction then proceeds with the adsorbed water-derived species.

- The formate mechanism initially proposed by Takahashi et al (1982) is based on the formation of methylformate ester on the catalyst surface between two adsorbed species, H_3CO and HCO. The ester is hydrolyzed to methanol and formic acid. The latter decomposes directly to CO_2 and H_2 with 100% selectivity i.e. no CO is formed.

Ethanol reforming has been studied with two main objectives. Iwasa and Takezawa (1991) have reformed ethanol to study the formation of acetic acid. They have shown that acetaldehyde is the key intermediate when Cu-based catalysts are used. They found that the role of the support is important; Cu alone shows very high selectivity towards acetaldehyde (88% at 250°C), whereas the presence of a support (either Al_2O_3, SiO_2, ZrO_2, or ZnO) markedly affects this selectivity, producing a diversified number of intermediates at significant concentrations. Garcia and Laborde (1991) did a thermodynamic study on the reforming of ethanol to H_2. They concluded that H_2 production requires higher temperatures than those needed for the reforming of methanol and that steam to ethanol ratios higher than 10 (equivalent steam to C_1 ratios higher than 5) were required to prevent carbon formation.

Steam reforming of oxygenated aromatics has been directed towards the dealkylation of cresol. The reaction proceeds at temperatures of 400°-500°C and steam to carbon ratios of 6 using Pd, Rh or Ni on alumina, silica or chromia-alumina. The predominant reaction is degradation to H_2 and CO (Daly, 1980; Duprez, 1992). Assafi and Duprez (1988) proposed a mechanism in which the OH from the aromatic ring participates in the overall reaction process in the same manner as the OH group derived from the dissociation of water. Most important, under the conditions used, the aromatic ring is "cracked" and thus total reforming may be indeed feasible.

From the work on steam reforming of oxygenated aromatics, dehydroxylation proceeds at a significant rate to produce aromatic species on the catalyst surface. Thus, we ought to consider how these aromatic species can be steam reformed. Duprez (1992) discusses the work of a Russian group who reformed mixtures of aliphatic and aromatic hydrocarbons using a combination of Ni and V at 850°C. Work conducted at much lower temperatures, 440°C-480°C, and at steam to compound ratios lower than 10 (equivalent S/C1 ratio close to 1), with complex aromatics on Rh - V on alumina (Kim, 1976) and on Rh, Pt and Ni on alumina and silica (Delahay et al, 1985) showed that with methylnaphthalene as feed, partial degradation to CO and H_2 takes place in competition with ring opening and dealkylation. Delahay and Duprez (1985) concluded that intermediate hydrogenation favors but is not a necessary prerequisite for ring opening.

In summary,

- Reforming of hydrocarbons (C_1-C_5, naphtha and gas oils) is well understood and proceeds readily at steam to C_1 ratios (S/C_1) between 3.5 and 5.0, and temperatures up to 775°C.

- The most commonly used catalyst is Ni on alumina. Ca, K and Mg are often used with the alumina to enhance water adsorption, lower the acidity and favor mobility of the OH species on the surface.

- Alternate catalyst formulations have been developed to increase the resistance of the catalyst to poisoning, particularly by sulfur. These novel catalysts are also Ni-based with

mixtures of rare earth oxides and a refractory support.

- Methanol, a prototype of an oxygenated molecule, is readily steam reformed at low temperatures (< 300°C). Cu-based catalysts and recently developed Pd/ZnO preparations are extremely selective towards the formation of CO_2 and H_2 via the formate ester mechanism.

- Ethanol requires higher reforming temperatures than methanol to be reformed at appreciable rates. The mechanism proceeds through acetaldehyde and ethylacetate intermediates on the same Cu-based catalysts used for the methanol reforming.

- The existing data on oxygenated aromatic compounds, i.e. cresols, suggest that they can be steam reformed using known catalyst preparations. Little is known, however, about optimum experimental conditions that will result in long-term catalyst activity.

When considering the biocrude composition shown in Table 2, it is clear that challenges in catalytic steam reforming will be linked to the ability of the catalyst to handle the "pyrolytic lignin fraction" as well as the carbohydrate-derived fractions: monomeric sugars, anhydrosugars, and oligomers. Our goal is to find a catalyst formulation that can reform both the complex and simple molecules present in the biocrude while limiting undesirable side reactions which will lower the yields of H_2.

If the oxygen in the aldehydes, alcohols and acids could be removed as CO_2, via ester intermediates as in methanol reforming, the production of H_2 would then be maximized. This could be done if, in the pyrolysis operation, a low molecular weight fraction of the biocrude is separated from a high molecular weight fraction during the condensation of the pyrolytic vapors. The low molecular weight fraction (a mixture of simpler compounds like hydroxyacetaldehyde, acetic acid, ethylene glycol, formaldehyde, glyoxal) could be reformed at low temperatures using the Cu-based or the Pd/ZnO catalysts.

An alternate approach is to conduct the steam reforming of the entire biocrude near equilibrium conditions. By an appropriate choice of steam to biocrude ratio, temperature and residence time, the reforming could maximize the H_2 production. This may be possible, according to the literature reviewed, by choosing stable and resistant Ni-based catalysts operating in the 700°-800°C range. An appropriate temperature profile through the reactor will have to be developed experimentally to carefully control coke formation. A favored combination could be: NiO (20-30 wt%), MgO (10-15 wt%), Al_2O_3 (50-65 wt%), rare earth oxides (5-15 wt%), and a promoter like Cr_2O_3, V_2O_5, or WO_3 (5-10 wt%).

Process Design

Two scenarios for the production of hydrogen from pyrolysis oil can be envisioned. One would involve a regionalized system of hydrogen production with small and medium-sized pyrolysis units providing biocrude to a centralized reforming unit. The alternative is to pyrolyze biomass in a large unit and feed the uncondensed vapors directly to the reforming unit. The first case has the advantage of the availability of cheaper feedstocks, perhaps biomass waste. In the integrated system, however, the costs of condensing the vapors to the oil and transporting them to the hydrogen facility are avoided.

A conceptual process design to make hydrogen from pyrolysis oil is shown in Figure 8. Unlike other

Hydrogen From Pyrolysis Oil

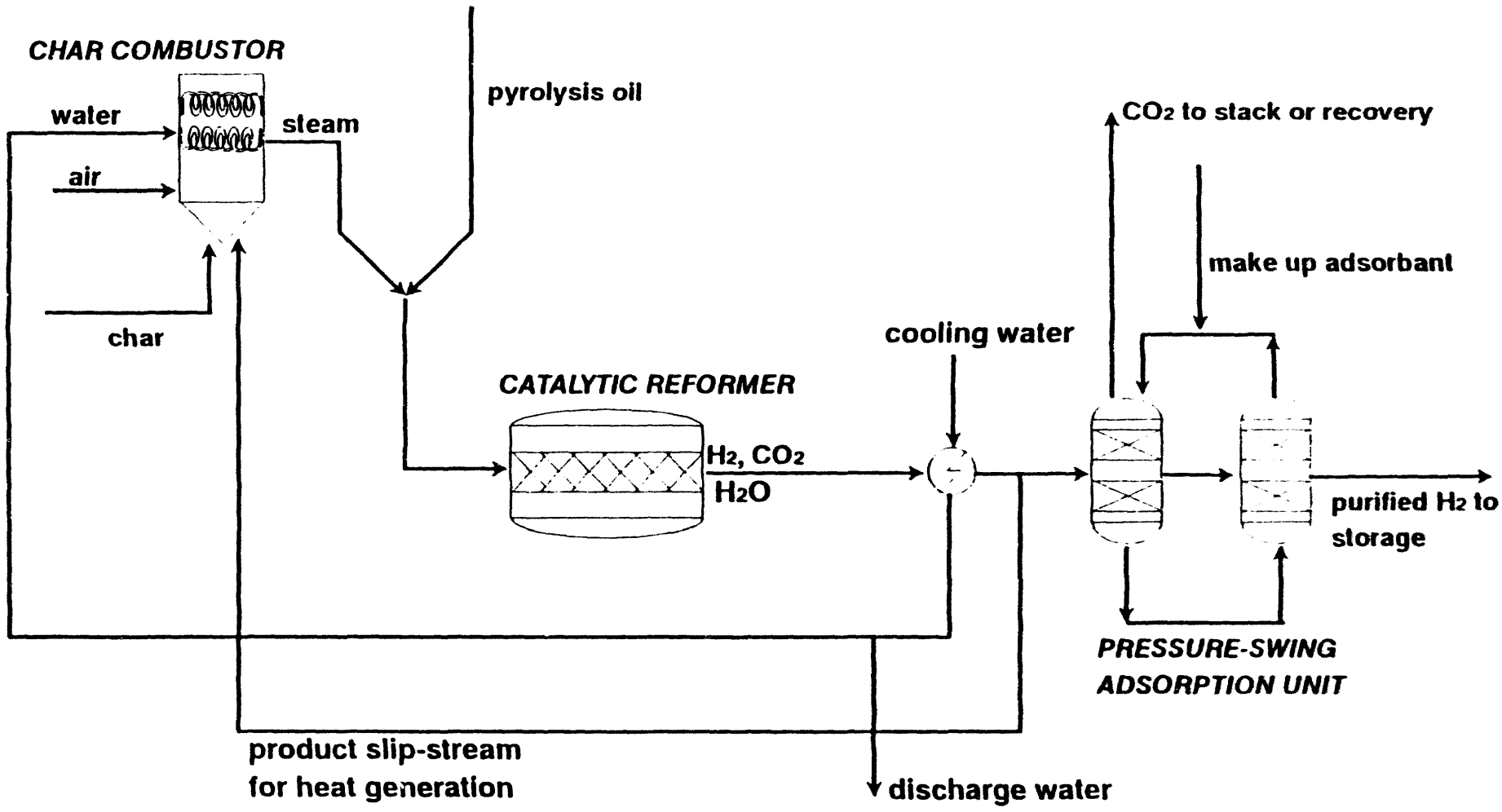

Figure 8

reforming processes, this process involves very few unit operations, which should increase its economic feasibility. Because of the low sulfur content of biomass, a sulfur removal system is not likely to be required,while one is always used in petroleum and methane reforming. Also, according to thermodynamic simulations and current experimental results, only one medium temperature reformer is required; conventional methane reforming uses a furnace-like converter followed by a high temperature reformer and a low temperature reformer.

In the process being evaluated, pyrolysis oil or the uncondensed vapors are fed with steam into a catalytic reactor. Laboratory experiments will choose a suitable catalyst and reactor configuration; the base-case will use a fixed-bed catalytic reactor. The reaction will occur at 500°C, and the ratio of steam to oil will be determined by experimental results and economic optimization. Since the overall reaction of pyrolysis oil to H_2 is endothermic, the char produced in the pyrolysis of the biomass will be burned to produce heat and steam. Preliminary energy balances indicate that a fraction of the oil may also be used as a source of heat, especially in the centralized reformer supplied by satellite pyrolysis units.

In the base-case design, a pressure swing adsorption unit will be used to purify the H_2 produced. This was chosen because of commercially available processes such as the light hydrocarbon reforming process by Foster Wheeler USA, which is designed to purify 1 MM scfd to 95 MM scfd reformed gas. Alternative purification processes include extraction with monoethanolamine and membrane separation.

As information becomes available, the process will be simulated in ASPEN Plus. This will facilitate sensitivity runs and the implementation of process design changes. As an economic model is developed, results from process sensitivity runs will be incorporated into the cost of the project.

Economics

Preliminary calculations were performed in order to determine the boundaries of economic feasibility of the process. To examine these boundaries before plant costs can be figured, the ratio of the current market selling price of H_2 to the pyrolysis oil production cost was calculated. If the ratio is greater than one, the process has the potential to be economically feasible. This method assumes that the process to produce H_2 is completely free of capital and operating costs. The results, therefore, set the minimum limits on the recovery of theoretical hydrogen and product selling price.

The maximum stoichiometric amount of H_2 was calculated as that obtained by reforming all of the carbon in the oil with steam plus the hydrogen in the oil, where the oil was defined to have the formula $CH_{1.33}O_{0.53}$, as described earlier. The equilibrium amount was not used because of the difficulty in simulating the thermodynamics of pyrolysis oil reforming on ASPEN Plus. This is due to lack of reliable thermodynamic data and the complexity of the pyrolysis oil. The current selling price of H_2 in industry is between $5.00/MM Btu and $15.00/MM Btu, depending on the size of the production facility.

For these calculations, the feedstock was considered pyrolysis oil rather than biomass, in order to take into account the cost of the pyrolysis process. The cost of the oil is $0.141/kg, as calculated in an NREL report by C. Gregoire, on producing pyrolysis oil from biomass for power generation. This study used a biomass cost of $2.50/MMBtu, which is equivalent to $42/dry ton.

Tables 3 and 4 show the results of the preliminary economic calculations. Table 3 is the profitability ratio

Table 3: Potential Profitability vs. Hydrogen Selling Price and Cost of Oil

(assumes a no-cost process for producing hydrogen)

wood feed (tons)	1000
wood feed (kg)	907,186
oil cost ($/kg)	0.141
oil produced (kg)	589,671
oil cost ($)	83,144
kg H2/kg oil	0.197
% recovery of stoichiometric maximum	70%

current selling price of H2			
$/MMBtu	**$/kg**	product price ($)	product $/feed $ *
5.00	0.67	54,767	0.66
5.50	0.74	60,244	0.72
6.00	0.81	65,720	0.79
6.50	0.88	71,197	0.86
7.00	0.94	76,674	0.92
7.50	1.01	82,150	0.99
8.00	1.08	87,627	1.05
8.50	1.14	93,104	1.12
9.00	1.21	98,581	1.19
9.50	1.28	104,057	1.25
10.00	1.35	109,534	1.32
10.50	1.41	115,011	1.38
11.00	1.48	120,487	1.45
11.50	1.55	125,964	1.52
12.00	1.62	131,441	1.58
12.50	1.68	136,917	1.65
13.00	1.75	142,394	1.71
13.50	1.82	147,871	1.78
14.00	1.89	153,348	1.84
14.50	1.95	158,824	1.91
15.00	2.02	164,301	1.98

*feed = pyrolysis oil

inputs are in bold

Table 4: Profitability vs. Percent Recovery of Stoichiometric Maximum

(assumes a no-cost process for producing hydrogen)

H2 selling price ($/MMBtu)	**8.8**
H2 selling price ($/kg)	1.19
wood feed (tons)	**1000**
wood feed (kg)	907,186
oil cost ($/kg)	**0.141**
oil produced (kg)	589,671
oil cost ($)	83,144
kg H2/kg oil from reforming	**0.197**

% recovery	H2 produced (kg)	product price ($)	product $/feed $ *
100%	116,165	137,700	1.66
95%	110,357	130,815	1.57
90%	104,549	123,930	1.49
85%	98,740	117,045	1.41
80%	92,932	110,160	1.32
75%	87,124	103,275	1.24
70%	81,316	96,390	1.16
65%	75,507	89,505	1.08
60%	69,699	82,620	0.99
55%	63,891	75,735	0.91
50%	58,083	68,850	0.83
45%	52,274	61,965	0.75
40%	46,466	55,080	0.66
35%	40,658	48,195	0.58
30%	34,850	41,310	0.50
25%	29,041	34,425	0.41
20%	23,233	27,540	0.33
15%	17,425	20,655	0.25
10%	11,617	13,770	0.17
5%	5,808	6,885	0.08
0%	0	0	0.00

*feed = pyrolysis oil

inputs are in bold

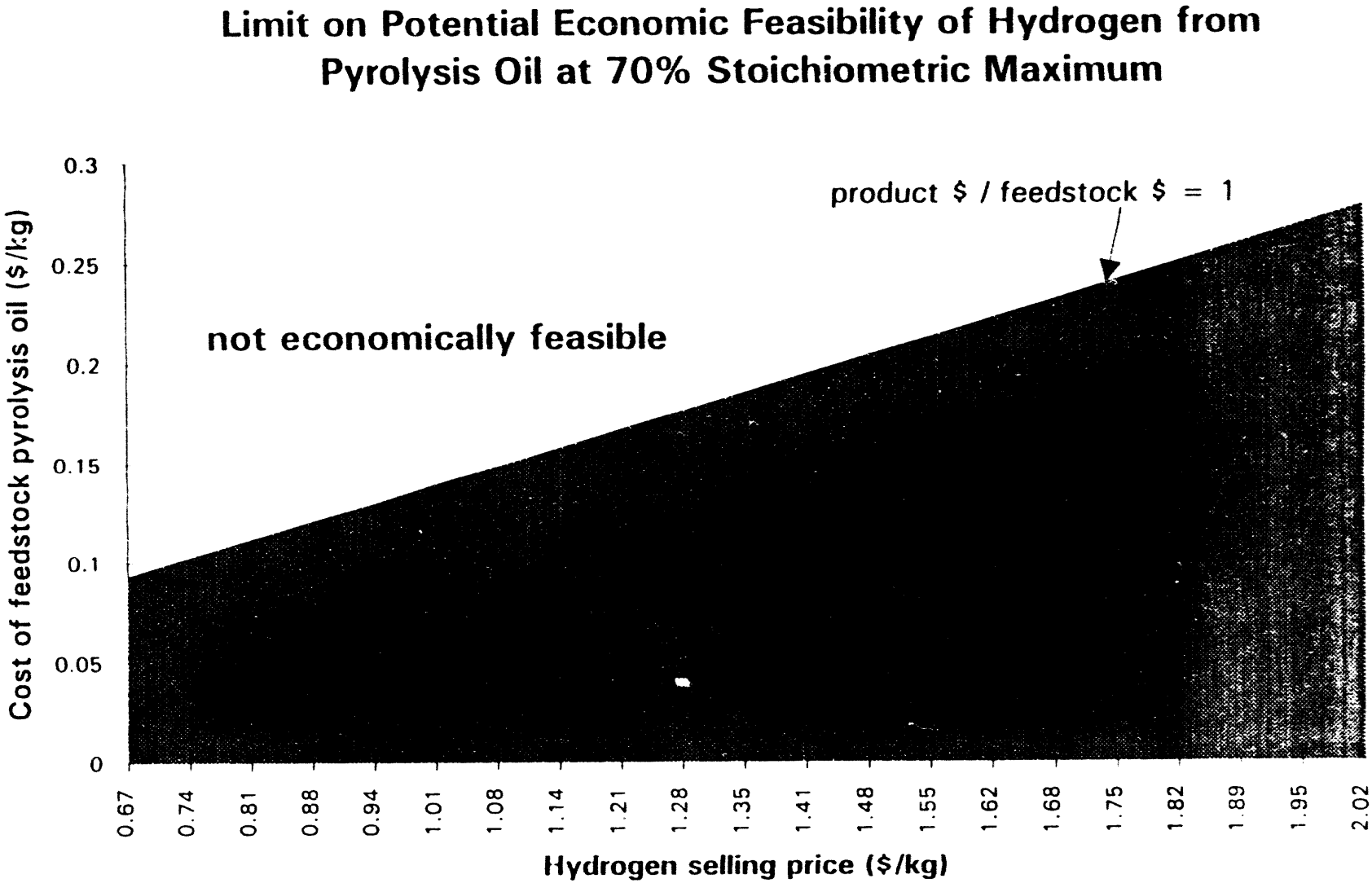
Limit on Potential Economic Feasibility of Hydrogen from Pyrolysis Oil at 70% Stoichiometric Maximum
product $ / feedstock $ = 1
not economically feasible
Cost of feedstock pyrolysis oil ($/kg)
0.3
0.25
0.2
0.15
0.1
0.05
0
0.67
0.74
0.81
0.88
0.94
1.01
1.08
1.14
1.21
1.28
1.35
1.41
1.48
1.55
1.62
1.68
1.75
1.82
1.89
1.95
2.02
Hydrogen selling price ($/kg)

Figure 9

as a function of the selling price of H_2, assuming that 70% of the total hydrogen available in the process can be recovered. From Table 3, if 70% recovery can be achieved, the selling price of H_2 must be at least $7.50/MM Btu. Again, this does not take capital and operating costs into account.

Table 4 shows the profitability ratio as a function of the percentage recovery. For this table, calculations were made based on a H_2 selling price of $8.80/MM Btu, corresponding to a moderate size hydrogen facility of 10 MM scfd. Table 4 shows that if the selling price is $8.80/MM Btu, 60% of the H_2 that is available from reforming pyrolysis oil must be recovered to reclaim the cost of the feedstock; more would be necessary to cover capital and operating expenses.

Figure 9 shows the combinations of H_2 selling price and feedstock cost that will result in a ratio greater than one. Hydrogen from pyrolysis oil has the potential to be economically feasible if costs fall within the shaded region. This graph assumes that 70% of the maximum stoichiometric H_2 will be recovered. The pyrolysis oil cost will depend heavily on the cost of the biomass; a regionalized system to produce oil for a central hydrogen facility could utilize waste biomass which would bring down the cost of the oil considerably.

Conclusions

Fast pyrolysis of biomass is an advanced technology to produce a biocrude in high yields (70-75 wt% of anhydrous biomass). This biocrude is a complex mixture of simple aldehydes, alcohols and acids together with more complex carbohydrate and lignin derived oligomeric materials. Fractional condensation of the pyrolytic vapors could separate the simple monomeric materials, which comprise about one third to one half of the biocrude from the complex oligomeric fraction. Steam reforming of the simple monomeric materials is thermodynamically and chemically feasible. By a proper choice of catalyst esters, intermediates could be favored, which would shift the selectivity to CO_2 and H_2. Little or no CO will be then produced.

Steam reforming of the entire biocrude is thermodynamically feasible. High steam to carbon ratios relative to methane reforming, which requires ~5 moles of steam per mole of carbon, will be needed to ensure that the equilibrium shifts towards H_2 from the analysis of the literature. Thermodynamically, this ratio is dependent on the carbon content of the compounds being reformed. Reforming the complex oxygenates seems chemically possible. The oxygenates rapidly dehydroxylate and aromatics are formed on the surface of the catalyst. Carbon-carbon bonds are then ruptured and a large supply of OH and H species ensure that carbon formation is minimized or even suppressed. This will require modifications of known reforming catalysts and specific temperature profiles which will be developed experimentally. Hydrogenation of the aromatics does not seem to be a prerequisite for low carbon production.

The fast pyrolysis technology options, i.e. fluid beds, entrained beds or ablative reactors, are at a level of advanced development; pilot and demonstration units are in operation and construction respectively. However, the steam reforming of a complex feedstock such as biocrude requires a major effort at the bench scale level to determine how catalysis can direct the surface chemistry towards gas forming pathways rather than undesirable carbon forming reactions, which will lead to coke formation. Modifications of existing catalytic preparations may be needed to reach this goal.

The strategy being studied consists of small- to medium-size regional fast pyrolysis units which will produce the biocrude from either dedicated crops or plantations, or will use waste lignocellulosics as feedstocks. The biocrude produced will be transported to a central reforming unit in a given region where H_2 will be produced. Alternatively, if the biomass supply is abundant in a given region the fast pyrolysis and reforming operations can be conducted at the same site. Condensation of the vapors will not be necessary, giving a significant gain in efficiency. The biocrude is a more condensed form of energy than biomass, however. Thus, the choice between the two strategies will be based on transportation and feedstock costs.

The process concept is extremely simple: a desulfurization unit is not needed, and the biocrude can be atomized in a flow of steam which is then processed through a reforming unit. By a proper choice of conditions the near equilibrium design can be driven to maximize H_2 production. A pressure swing adsorption unit will purify the gas stream.

The preliminary economics, based on input/output calculations (no plant or operating costs considered),with a price of biocrude of \$0.141/kg, suggest that the H_2 cost, at 70% of the maximum stoichiometric yield from biocrude, will be \$7.50/MM Btu. Alternatively, if the H_2 can be sold for \$8.80/MMBtu, at least 65% of the maximum must be recovered. A wide margin thus exists in which to include capital and operating costs and still make hydrogen from biomass pyrolysis economically attractive.

References

Amphlett, J. C.; Evans, M. J.; Mann, R. F. and Weir, R. D., Can. J. Chem. Eng. 63 (1985) 605.

Antal, M. J., in Advances in Solar Energy, Boer, K. W. and Duffield, J. A., eds., Solar Energy Soc., New York (1982) 61.

Assafi, M. and Duprez, D., Bull. Soc. Chim. Fr. (1988) 108.

Aznar, M. P.; Corella, J.; Delgado, J.; and Lahoz, J., Ind. Eng. Chem. Res. 32 (1993) 1.

Daly, F., J. Catal. 61 (1980) 528.

Delahay, G. and Duprez, D., Bull. Soc. Chim. Fr. II (1985) 1245.

Delahay, G.; Bousquet, J. and Duprez, D., Bull. Soc. Chim. Fr. II (1985) 1237.

Diebold, J. and Scahill, J., in Pyrolysis Oils from Biomass: Producing, Analyzing and Upgrading, Soltes, E. J. and Milne, T. A., eds., ACS Symposium Series 376, ACS, Washington, D.C. (1988) 31.

Duprez, D., Applied Catalysis A: General 82 (1992) 111.

Elliott, D.C., in Pyrolysis Oils from Biomass: Producing, Analyzing and Upgrading, Soltes, E. J. and Milne, T. A., eds., ACS Symposium Series 376, ACS, Washington, D.C. (1988) 55.

Garcia, E. Y. and Laborde, M. A., Int. J. Hydrogen Energy 16, 5 (1991) 307.

Graham, R. G.; Freel, B. A. and Bergougnou, M. A., in Research in Thermochemical Biomass Conversion, Bridgwater, A. V. and Kuester, J. L., eds., Elsevier Applied Science, London (1988) 629.

Iwasa, N. and Takezawa, N., Bull. Chem. Soc. Jpn. 64 (1991) 2619.

Iwasa, N.; Kudo, S.; Takahashi, H.; Masuda, S. and Takezawa, N., Catalysis Letters 19 (1993) 211.

Jiang, C. J.; Trimm, D. L.; Wainright, M. S. and Cant, N. W., Applied Catalysis A: General 97 (1993) 145 and 97 (1993) 245.

Kim, C. J., J. Catal. 42 (1976) 323.

Mizuno, K.; Yoshikawa, K.; Wakejima, N.; Takeouchi, Y. and Watanabe, A., Chemistry Letters, The Chem. Soc. Jpn. (1986) 1969.

Patil, K. Z., Chemical Age of India 38, 10 (1987) 519.

Piskorz, J.; Scott, D. S. and Radlein, D., in Pyrolysis Oils from Biomass: Producing, Analyzing and Upgrading, Soltes, E. J. and Milne, T. A., eds., ACS Symposium Series 376, ACS, Washington, D. C. (1988) 167.

Probstein, R. and Hicks, R., Synthetic Fuels, Mc Graw Hill, New York (1982) 235.

Radlein, D.; Piskorz, J. and Scott, D. S., J. Anal. Appl. Pyrolysis 19 (1991) 41.

Richards, G. N., J. Anal. Appl. Pyrolysis 10 (1987) 108.

Rostrup-Nielsen, J. R. and Tottrup, P. B., Proc. Symp. on Science and Catalysis and its Applications in Industry, FPDIL, Sindri, Feb 1979, p. 379.

Rostrupp-Nielsen, J. R., Catalysis Science and Technology, Enderson, J. R. and Boudart, M., eds., Springer-Verlag: Berlin, Heidelberg (1984) vol 5, Ch 1.

Ross, J. R. H.; Steel, M. C. F. and Zeini-Isfahani, A., J. Catal. 52 (1978) 280.

Roy, C.; de Caumia, B. and Plante, P., in 5th European Conference on Biomass for Energy and Industry, Grassi, G.; Goose, G. and dos Santos, G., eds., Elsevier Applied Science, London (1990) 2595.

Shafizadeh, F., J. Anal. Appl. Pyrolysis 3 (1982) 283.

Su, Tien-Bau, and Rei, Min-Hon, J. Chinese Chem. Soc. 38 (1991) 535.

Takahashi, K.; Takezawa, N. and Kobayashi, H., Applied Catalysis 2 (1982) 363.

Takezawa, N.; Shimokawabe, M.; Hiramatsu, H.; Sugiura, H.; Asakawa, T. and Kobayashi, H., React. Kinet. Catal. Lett. 33, 1 (1987) 191.

Tottrup, P. B. and Nielsen, B., Hydrocarbon Processing, March 1982, p. 89.

MSW TO HYDROGEN

A. D. Pasternak, J. H. Richardson, R. S. Rogers, C. B. Thorsness, and H. Wallman
Lawrence Livermore National Laboratory
Livermore, CA 94550

G. N. Richter and J. K. Wolfenbarger
Montebello Research Laboratory
Texaco Inc
Montebello, CA 90640

Abstract

LLNL and Texaco are cooperatively developing a physical and chemical treatment method for the preparation and conversion of municipal solid waste (MSW) to hydrogen by gasification and purification. The laboratory focus will be on pretreatment of MSW waste in order to prepare a slurry of suitable viscosity and heating value to allow efficient and economical gasification and hydrogen production. Initial pretreatment approaches include 1) hydrothermal processing at saturated conditions around 300 °C with or without chemical / pH modification and 2) mild dry pyrolysis with subsequent incorporation into an appropriate slurry. Initial experiments will be performed with newspaper, a major constituent of MSW, prior to actual work with progressively more representative MSW samples. Overall system modeling with special attention to energy efficiency and waste water handling of the pretreatment process will provide overall guidance to critical scale-up parameters. Incorporation of additional feed stock elements (e.g., heavy oil) will be evaluated subject to the heating value, viscosity, and economics of the MSW optimal slurry for hydrogen production. Ultimate scale-up of the optimized process will provide sufficient material for demonstration in the Texaco pilot facility; additional long term objectives include more detailed economic analysis of the process as a function of technical parameters and development of a measurement/control system to ensure slagging ash for variable MSW feed stocks. Details of the overall project plan and initial experimental and modeling results are presented.

Introduction

Municipal Solid Waste (MSW) is a large, growing, and little-used by-product resource of the United States. Approximately 200 million tons of MSW are produced annually in the United States, and the vast majority of this eventually winds up in landfills (Khan, 1993). Environmental concern over air pollution and the ash by-product has limited incineration as a disposal method, current landfills are becoming full, and concern over water pollution makes siting of future landfills difficult and expensive.

MSW is predominantly composed of carbon, hydrogen and oxygen, and as such is a potential energy source. Thus, development of the technology necessary for gasification of MSW to hydrogen has the potential to address a number of economic, environmental, societal and resource issues. A path for the conversion of MSW to hydrogen has the potential to be economically advantageous because management and disposal of MSW is expensive, and the fees otherwise required to dispose of MSW become a credit against the cost of the produced hydrogen. The economics of MSW to hydrogen conversion relative to other sources will depend on tipping fees, the cost of alternate feed stocks such as coal or natural gas, and the differential processing costs. Conversion of MSW to hydrogen has the environmental advantage of decreasing the number of future landfills needed with the concomitant decrease in the associated water pollution issues. Furthermore, as gasification of MSW involves recycling of what is predominantly biomass, it introduces virtually no new carbon into the atmosphere. Finally, the energy content of one ton of MSW is comparable to a barrel of oil. Recovery of that energy through gasification would eliminate importing approximately 200 million barrels of oil, or ≈ 3-4 B$. Thus, even recovery of only a substantial fraction of the energy in MSW would have significant environmental and fiscal impact on the United States.

This report describes work intended to be done jointly between Lawrence Livermore National Laboratory (LLNL) and Texaco. The objective of this work is to capitalize on the proven gasifier technology developed and marketed by Texaco for the purpose of generating hydrogen from MSW. The primary technical problem is the pretreatment of MSW into a form suitable to use as a feed stock to the Texaco gasifier. LLNL will focus its efforts on the effects of MSW pretreatment on the heating value and viscosity properties of slurries suitable for injection into the gasifier. Supplemental feed stocks would be considered as needed (e.g., coal; heavy oils, which are of particular interest in California). The scope of this project did not include initial MSW classification; hence and as appropriate, additional industrial partnerships in the realm of MSW classification would be explored in order to address as fully as possible all the technical and economic issues.

The Texaco gasifier has been successfully developed and commercially employed for gasification of coal, heavy oils, and petroleum coke with subsequent shift and hydrogen separation. The Texaco gasifier has many advantages: 1) oxygen can be utilized as the oxidant, resulting in no dilution and few nitrogen impurities; 2) hazardous metals are encapsulated in the slag; 3) the high temperatures insure the complete destruction of hazardous organics; 4) the Texaco gasifier represents proven technology. Texaco will perform laboratory gasification runs of MSW feed stocks prepared by LLNL during the initial phase of pretreatment parameters optimization. Texaco and LLNL will jointly perform a system analysis of the feed preparation/gasification process in order to allow process tradeoffs to be evaluated on an economic as well as a technical basis. Slagging is both a proven asset and potential issue with respect to gasification of MSW. Consequently, another goal of this project is the development of a measurement/control system to ensure slagging ash for variable MSW feeds. Finally, it is intended that the project will conclude with the demonstration of MSW slurrying and subsequent gasification at the pilot scale size.

Subsequent work may deal with alternate biomass and waste feed stocks which potentially represent major energy resources; e.g., there are approximately 7 million tons of dry sewage sludge produced daily in the United States (Khan, 1993). MSW in particular and biomass/waste in general are predicted to have the greatest potential for annualized growth of electricity generation and displacement among renewable energy resources during the next 20 years (US Department of Energy, 1991). The development of technically and economically successful pretreatment processes for biomass waste suitable for subsequent gasification and hydrogen separation will make a major contribution towards the realization of this major renewable resource.

Discussion

Composition and Heating Value

Table 1 summarizes the average composition of MSW in the United States (AIChE, 1994).

Table 1. Typical MSW by material (U.S. average)

Material	Percentage by Weight
Paper & paperboard	37.5
Glass	6.7
Ferrous metals	6.3
Aluminum	1.4
Plastics	8.3
Rubber & leather	2.4
Textiles	2.8
Wood	6.3
Food wastes	6.7
Yard wastes	17.9*
Other	3.7

* Yard waste constitutes 30% in California

This data is similar to that reported from earlier surveys (Khan, 1993). Consequently, the major component in MSW is derived from biomass and consists predominantly of cellulose-like material. Typical heating values of MSW range from 3,500 to nearly 6,000 Btu/pound. Reducing either the water content (i.e., increasing the solids loading) or decreasing the percentage of inert components will increase the heat content (Hecht, 1983). Refuse Derived Fuel (RDF) results when MSW is pretreated to remove some of the water and inert components while leaving the combustible components. Heating values for RDF of nearly 6,000 to over 8,000 Btu/pound can be achieved, thus approaching the heating value of medium ranked coals. RDF is generally categorized as fluff or densified (e.g., powder or pellets), and is more homogeneous and has a longer "shelf life" than MSW (Alter, 1983). However, conventional RDF would not form a high solids slurry, and hence is not suitable for direct injection into the Texaco gasifier. Typical atomic compositions and heating values for previously characterized MSW and RDF are presented in Table 2 (Ferraro, 1988; and General Electric, 1976).

Table 2. Atomic Percent Composition and Heating Values for Representative MSW and RDF

RDF	Maine MSW			GE MSW	GE
	As Received	Dry	Dry-Ash-Free		
Moisture	29.2	0	0	25	23.8
Carbon	32.2	45.5	52.5	26.2	33.1
Oxygen	24.2	34.2	39.5	22.1	28.7
Hydrogen	4.2	5.93	6.85	3.5	4.5
Nitrogen	0.4	0.6	0.7	0.6	0.6
Chlorine	0.1	0.14	0.16	0.1	0.1
Sulfur	0.2	0.28	0.32	0.1	0.1
Ash	9.5	13.4	0	22.5	9.2
Heating value (BTU/pound)	5800 4700	8230 5870	9480		

For comparison, sewage sludge typically varies from a primary sludge value of ≈ 7000 BTU/pound to 4000 BTU/pound after biological treatment and formation of secondary sludge (Khan, 1993).

Hydrothermal Treatment

Initially two pretreatment methods were considered: 1) hydrothermal treatment (at steam saturated conditions around 300°C) with and without chemical or pH modification and 2) mild dry pyrolysis. In each case pretreatment conditions were to be varied and the outcome evaluated primarily on the basis of the heating value and viscosity of the resulting aqueous slurry. Additional experiments involving kinetic measurements of starting material modification, rate and speciation of gas evolution, and effects of simultaneous mechanical agitation/shearing would be performed as appropriate. Because MSW is predominantly cellulose, initial experiments would be done with a primarily cellulose material: newspaper.

Initial efforts to form a slurry from newspaper material subjected to dry pyrolysis were not particularly successful. In contrast, initial experiments using hydrothermal treatment at temperatures up to 300°C of newspaper, cellulose or tissue paper did result in the formation of slurries with almost 50% solids loading (by weight). However, water:solid ratios of at least 2:1 were required for complete immersion of the solid in water during the pretreatment. Not surprisingly, and although the detailed chemistry has not been elucidated, the excess water is a reactant which results in a product being formed which is more amenable to slurrying than the product resulting from dry pyrolysis.

Additional factors and considerations also led to a preference being given to hydrothermal treatment versus dry pyrolysis. 1) Although several different gasifiers are being developed suitable for handling biomass with or without a supplemental feed stock line in order to boost the heating value (Feldmann, 1986; Larson, 1992; Litt, 1990), the Texaco gasifier is a proven technology which has enjoyed widespread commercialization (Robin *et al*, 1989 and 1993). The Texaco gasifier offers several advantages. It uses pure oxygen; hence, there is no nitrogen dilution of the produced synthesis gas. The slagging in the Texaco gasifier also provides an environmental advantage, as non-combustible inorganics are effectively encapsulated and hazardous organics are completely destroyed. This gasifier requires a liquid slurry as an input feed stock. Hydrothermal treatment integrates well with slurry feed gasifiers; only dewatering or concentrating of the treated MSW is required. Conversely, dry pyrolysis requires an initial drying step. Because of the high water content in MSW, this would be accompanied by a large energy penalty. 2) Reports of similar hydrothermal treatment of classified MSW do result in an aqueous slurry with solids loading of up to 42% by weight and with heating values of over 6,000 Btu/pound (Klosky, 1994). 3) Initial classification of MSW, ultimately to form a RDF, involves aqueous shredding, settling, and separations processing. Also called wet resource recovery, this process is being prototyped at several facilities throughout the United States (e.g., San Leandro, CA and Reno, NV). It would be a natural integration step to incorporate hydrothermal treatment into the wet resource recovery process before the final RDF is dried and formed (Gugliamo, 1994; Klosky, 1994). 4) Hydrothermal treatment is well established in the pulp and paper industry. Consequently, the future focus of the experimental pretreatment processing will be on hydrothermal treatment.

Hydrothermal treatment of cellulose results in a carbonization of the starting materials, as represented by the following reaction (Schuhmacher *et al*, 1960):

$$(C_6H_{10}O_5)_4 \text{ fi } C_{21}H_{16}O_2 + 3\ CO_2 + 12\ H_2O + 1.19\ MJ$$

The solid component of the products is 47 % by weight of the starting cellulose. Table 3 represents the evolution of cellulose and wood into a more carbonaceous material as a function of processing temperature for a total of 3 hours processing (Schuhmacher *et al*, 1960).

Table 3. Carbonization of Cellulose and Wood After Processing for 3 Hours

	Cellulose		Wood	
T°C	H/C	O/C	H/C	O/C
Unreacted	1.67	0.83	1.46	0.65
225	1.67	0.83	0.8	0.65
275	1.27	0.55	0.86	0.19
340	0.75	0.19	0.72	0.22
360	--	--	0.63	0.077
370	0.69	0.1	--	--
390	0.71	0.073	--	--

Assuming that MSW decomposes in the hydrothermal process to the same final solid product as cellulose

(a reasonable assumption considering that cellulose is the dominant component of MSW, especially after preliminary classification), the following reaction, expressed on a per carbon basis, approximates the carbonization of MSW (using the average composition of Table 1 for Maine MSW/RDF):

$$CH_{1.57}O_{0.56} \rightarrow 0.97\ CH_{0.76}O_{0.095} + 0.03\ CO_2 + 0.41\ H_2O + 21.4\ kJ$$

This solid product, 61% by weight of the starting ash-free MSW, has an estimated heating value of 14,400 Btu/pound; the dry Maine MSW carbonized product, now containing 20% ash by weight, would have a heating value of 11, 500 Btu/pound. Thus the hydrothermal treatment of MSW results in a solid product with a heating value comparable to a good coal (Probstein, 1982). For comparison, a similar hydrothermal treatment of MSW resulted in a solid product comprising 79 % by weight of the starting material, including ash (Klosky, 1994).

Process Modeling

A rudimentary overall process model has been constructed using ASPEN PLUS (a commercial process simulator from Aspen Technology Inc.). Figure 1 summarizes the overall division of the process into discrete modules: pretreatment, gasification, quench, cleanup, shift and separation. This model was used to provide an initial evaluation of the overall process with respect to major technical and economic inputs and outputs (e.g., steam requirements, shift temperatures, operating pressure, primary heat exchanger requirements, oxygen input, water recycling, hydrogen production rates, waste gas and water rates, batch vs. continuous MSW pretreatment processing). Furthermore, without requiring proprietary details, this model is also sufficient, to a first approximation, to model the overall gasification/shift/separation process, and the interaction between the energy/material flows in the overall process and those associated with the pretreatment steps.

All of the modules will not be described in detail. However, Figure 2 illustrates the level of detail currently existing in the model for a continuous hydrothermal pretreatment. Provision is made for a recycled water stream as well as a small slipstream of waste water to control, if necessary, any buildup of problem constituents. One conclusion is, therefore, that given recycle of water as desirable in the pretreatment, there is no absolute need to limit considerations to systems where high solids loading in the slurry are present after and prior to MSW decomposition (e.g., in a batch mode with steam heating and the associated uncertainties of uniform heating). Figures 3 and 4 illustrate overall process material/energy/water requirements for a 1600 ton/day plant (typical of a large landfill site). From such an overall model the ability to balance downstream processing outputs with pretreatment inputs is apparent. For example, the steam generated in the shift reaction is approximately that required in the hydrothermal pretreatment. Similarly, the heating value of the fuel gas generated during the hydrogen separation process is approximately equivalent to the heating value required for the overall shift processing. Separation is done by a 3 stage pressure swing adsorption process (Katofsky, 1993). Figure 4 corresponds to the solids loading previously demonstrated for carbonization of MSW (Klosky, 1994); the viscosity for this slurry was $\approx$ 1000 cp, well within Texaco's gasifier experience.

Consideration of the overall process is necessary in order to understand requirements on the initial classification and hydrothermal treatment of MSW. For example, current shift catalysts require some sulfur in the feed stock. Ironically, MSW is generally of such low sulfur content that sulfur may need to be added for the high temperature shift stage, with removal of H_2S prior to the low temperature shift catalyst bed. The capability of the Texaco gasifier to accommodate a large variability in ash content (species as well as quantity) decreases the initial classification restrictions on MSW. The slag is relatively

unleachable, hence providing additional environmental advantages and decreasing restrictions on type and quantities of impurities in the MSW inorganic components. The process model permits consideration of different delivery pressures of the produced hydrogen. Finally, halides are effectively converted to inorganic forms in the gasifier and removed in the water quench, thereby removing a potential requirement on the hydrothermal pretreatment.

Even this initial process model provides some economic insight into the overall viability of the conversion of MSW to hydrogen. For example, the process depicted in Figure 3 has a very large requirement for heat exchangers, particularly in the hydrothermal treatment module. Figure 5 illustrates the dependence on this heat exchanger area and the additional plant process heating and cooling requirements as a function of approach temperature. Figure 6 uses a standard ASPEN PLUS cost for heat exchangers to calculate a minimum in the amortized cost for heat exchangers as a function of approach temperature. However, additional process modeling is still required, both from an economic, technical, and environmental standpoint (e.g., ammonia as a waste stream needs to be considered, there is considerable swing in the cost of heat exchanger materials).

The overall goal of this project is the production of hydrogen from MSW using the Texaco gasifier. Consequently, this initial process model was used to evaluate the performance of the gasifier as a function of solids loading. Figure 7 illustrates the ratio of synthesis gas (carbon monoxide and hydrogen) produced by the gasifier to oxygen input as a function of slurry concentration. Table 4 represents some preliminary estimates of selected operating costs for the gasification of MSW to produce hydrogen. The costs of hydrogen from coal and natural gas are taken from the literature (Katofsky, 1993).

Table 4. Selected Operating Costs for the Production of Hydrogen from MSW.

	Unit Cost	$/kmol
Hydrogen (coal)	12/GJ	3.07
Hydrogen (NG)	6.5/GJ	1.86
Dilute slurry w heat exchanger		
Capital costs, 5000 m^2	*	0.02
10 MW Heating	3.0/GJ	0.03
35 MW Cooling	1.3/GJ	0.05
Dilute slurry w/o heat exchanger		
200 MW Heating	3.0/GJ	0.60
200 MW Cooling	1.3/GJ	0.26
Classification/shredding	25/tonne	0.75
Oxygen (12 kg/s)	36/tonne	0.43
Tipping (30 kg/s)	55/tonne	1.65

*$500/$m^2$, 20% amortization rate

The capital costs for the heat exchanger were obtained from estimates made by ASPEN PLUS cost module ($500/m^2) and probably represent a lower bound. Oxygen values reflect a dedicated plant, and the classification/shredding are taken from estimates of RDF costs (Office of Technology Assessment, 1979) which have been brought forward to 1993 dollars. Tipping fees vary greatly within the United States, ranging from lows of approximately $20/ton to highs of over $100/ton; $55/ton was a recently quoted average (Klosky, 1994). Obviously many components have not been estimated in Table 4 (e.g., the cost of the gasifier and downstream shift and separation). However, the avoidance cost, represented by the tipping fee, is a large off-set against what might be potentially significant costs associated with MSW pretreatment, and it is certain that tipping fees are only going to increase.

Conclusions

Preliminary experiments plus overall process considerations have led to the initial conclusion that hydrothermal treatment is preferable to dry hydrolysis for the pretreatment of MSW. An initial process model has been built consisting of six primary modules: pretreatment, gasification, quench, cleanup, shift and separation. This model has been used to estimate the overall gasifier performance as a function of the solids loading in the aqueous slurry feed stock. While by no means conclusive, the model indicates that production of hydrogen from MSW might be economically competitive with coal or natural gas derived hydrogen. The reason for this somewhat surprising result is the relatively large influence of tipping fees in comparison to the preliminary estimates of the major additional costs associated with MSW pretreatment (e.g., heat exchangers, initial classification). Additional factors need to be considered (e.g., autoclave equipment) and a much more refined economic analysis needs to be completed. However, the initial results support the idea that hydrothermal treatment of MSW and its subsequent gasification is supportable from a technical, economic, and environmental basis.

Future Work

As this project is in its very early stages, significant future work is planned. A series of laboratory - scale experiments are planned over the next 6 months in order to optimize the hydrothermal treatment conditions necessary to produce a slurry suitable for injection into the Texaco gasifier. These experiments will be batch Parr bomb experiments, using newspaper as the initial material and varying the time, temperature and pH. Viscosities and heating values will be measured; the viscosities will be correlated with measurements at Texaco on slurries previously successfully injected into the pilot gasifier. In addition, the chemical composition of the hydrothermal process gas and water will be characterized.

It is our intention to move quickly into providing sufficient material for laboratory-scale and then pilot scale gasifier experiments at the Montebello Research Laboratory. Texaco has a portable 6 ton/day hydrothermal treatment facility which can be modified and upgraded for these experiments. LLNL is discussing mutual collaboration with an upstream MSW classifier as well as a small business involved in carbonization and wet oxidation of MSW. Material from the 6 ton/day hydrothermal plant will be evaluated by Texaco using a laboratory-scale gasifier. Ultimately enough material will be produced, using optimized parameters based on the process modeling, heating value and viscosity, for the Montebello pilot facility. It is expected that this data will be the basis for the design of a 100 ton/day hydrothermal facility. The overall process facility and process model should be sufficiently robust to entertain alternate feed stocks, accomplishing hydrogen production and waste destruction from a multiplicity of sources (e.g.,

sewage sludge, biomass, energetic materials, fossil fuel co-feeds).

Acknowledgements

This work was performed under the auspices of the U. S. Department of Energy by Lawrence Livermore National Laboratory under contract No. W-7405-Eng-48.

References

AIChE, **1994**. *Garbage- The Story of Waste Management and Recycling*, American Institute of Chemical engineers, 345 East 47th Street, New York, N.Y. 10017.

Alter, H. **1983**. *Material Recovery from Municipal Solid Waste*. New York: Marcel Dekker.

Feldman, H. G., M. A. Paisley, and H. R. Appelbaum. **1986**. *Conversion of Forest Residues to a Methane-Rich Gas*. Report Number PNL-5798-3 DE 86 008521, prepared for Pacific Northwest Laboratories by Battelle Columbus Laboratories, Columbus, Ohio.

Ferraro, F. A. **1988**. *Results of Emissions and Ash Testing at a Modern Refuse-Derived Fuel Plant*. AIChE Symposium Series - Resource Recovery of Municipal Sold Wastes, 265 Vol 84. pg 36-43.

General Electric Company, **1975**. *Solid Waste Management Technology*. New York: Van Nostrand Reinhold Company.

Gugliamo, J. **1994**. Private communication. Biomass Systems, Inc wet resource recovery system is described in *A Brief Description of the Newest Resource Recovery System*, Resource Recovery Report Volume XVII, No. 7, June, 1992.

Hecht, N. **1983**. *Design Principles in Resource Recovery Engineering*. Boston: Butterworth Publishers.

Katofsky, R. E. **1993**. *The Production of Fluid Fuels from Biomass*. Princeton University/Center for Energy and Environmental Studies Report No. 279. Princeton, NJ.

Khan, M. R. **1993**. *Clean Energy from Waste and Coal. ACS Symposium Series 515*. Washington, D.C.: American Chemical Society.

Klosky, M., N. Dickinson, and C. Anderson. **1994**. *Chlorine, Sulfur, and Soluble Slag Extraction with Energy Density Improvements of a MSW Slurry*. in Proceedings of the 19th International Conference on Coal Utilization & Fuel Systems, Clearwater, Florida.

Larson, E. D. and R. E. Katofsky. **1992**. *Production of Methanol and Hydrogen from Biomass*. Princeton University/Center for Energy and Environmental Studies Report No. 271. Princeton, NJ.

Litt, R. D., M. A. Paisley, and T. L. Tewksbury. **1990.** *Experimental Development of a Multi-Solid Fluidized Bed Reactor Concept.* Report Number DOE/MC/23293-2856, prepared for Morgantown Energy Technology Center by Battelle Columbus Laboratories, Columbus, Ohio.

Office of Technology Assessment, Congress of the United States. **1979.** *Volume I: Materials and Energy from Municipal Waste - Resource Recovery and Recycling from Municipal Solid Waste and Beverage Container Deposit Legislation.*

Probstein, R. F. and R. E. Hicks, **1982.** *Synthetic Fuels.* New York: McGraw-Hill.

Robin, A.M., Wu, C.M, and Kassman, J.S. **1989.** *Integration and Testing of Hot Desulfurization and Entrained-flow Gasification for Power Generation Systems., Phase I, Preliminary Report for Period Oct. 1, 1987 - Jan. 1, 1989, Volume I - Program Summary and PDU Operations.* Montebello Research Laboratory, Texaco, prepared for Morgantown Energy Technology Center.

Robin, A.M., Leininger, T.F., Davis, L.A., Junjg D.Y., Kassman, J.S., Lafferty, W.L., Stevenson, J.S., Wolfenbarger, J.K., Wu, C.M., and Yang, P.P. **1993.** *Integration and Testing of Hot Desulfurization and Entrained-flow Gasification for Power Generation Systems., Fianl Report, Volume I - Program Summary and Summary of PDU Operations and Process Economics for the Period January 1, 1991 - September 30, 1992.* Montebello Research Laboratory, Texaco, prepared for Morgantown Energy Technology Center.

Schuhmacher, J.P., Hutjens, F.J. and van Krevelen. **1960.** Ch*emical Structure and Properties of Coal XXVI - Studies of Artificial Coalification.* Fuel, 14: 223.

US Department of Energy, **1991.** Energy Information Administration/Annual Energy Outlook.

Figure Captions

Figure 1. Overall process block diagram modeled by ASPEN PLUS, showing principle modules with corresponding major material and energy inputs and outputs.

Figure 2. Detailed processing steps included in the hydrothermal pretreatment module for a continuous MSW slurry reactor, with *circa* 15% by weight solids input, *circa* 50% by weight output, recycling of the majority of the water, and associated energy inputs/outputs.

Figure 3. Overall process block diagram for 1600 tons/day MSW (30 kg/s corresponding to 18.3 kg/s dry ash free), 55% solids slurry to gasifier, hydrothermal treatment at 275°C and 6.5 MPa, gasifier at 1300°C and 4 MPa.

Figure 4. Overall process block diagram for 1600 tons/day MSW (30 kg/s corresponding to 18.3 kg/s dry ash free), 42% solids slurry to gasifier, hydrothermal treatment at 275°C and 6.5 MPa, gasifier at 1300°C and 4 MPa.

Figure 5. Heating-cooling trade-offs as a function of approach temperature for the large pretreatment heat exchanger; as the approach temperature (temperature difference between the input of the cooling stream and the output of the counterflowing heating stream) increases, the heat exchanger area decreases but the additional plant process heating and cooling requirements (MW) increase.

Figure 6. Economic trade-offs for the large pretreatment heat exchanger as a function of approach temperature; as the approach temperature (temperature difference between the input of the cooling stream and the output of the counter flowing heating stream) increases, the heat exchanger area decreases. At an average heat exchanger cost of \$ 500/m^2 (stainless steel, ASPEN PLUS estimate), the total cost consisting of 20 % amortized heat exchanger capital cost and additional heating/cooling costs goes through a minimum at an approach temperature between 35-45 C.

Figure 7. Estimated gasifier performance (1300°C, 4 MPa), as measured by produced synthesis gas per unit oxygen input, and calculated slurry heating values as a function of solids loading of the slurry feed.

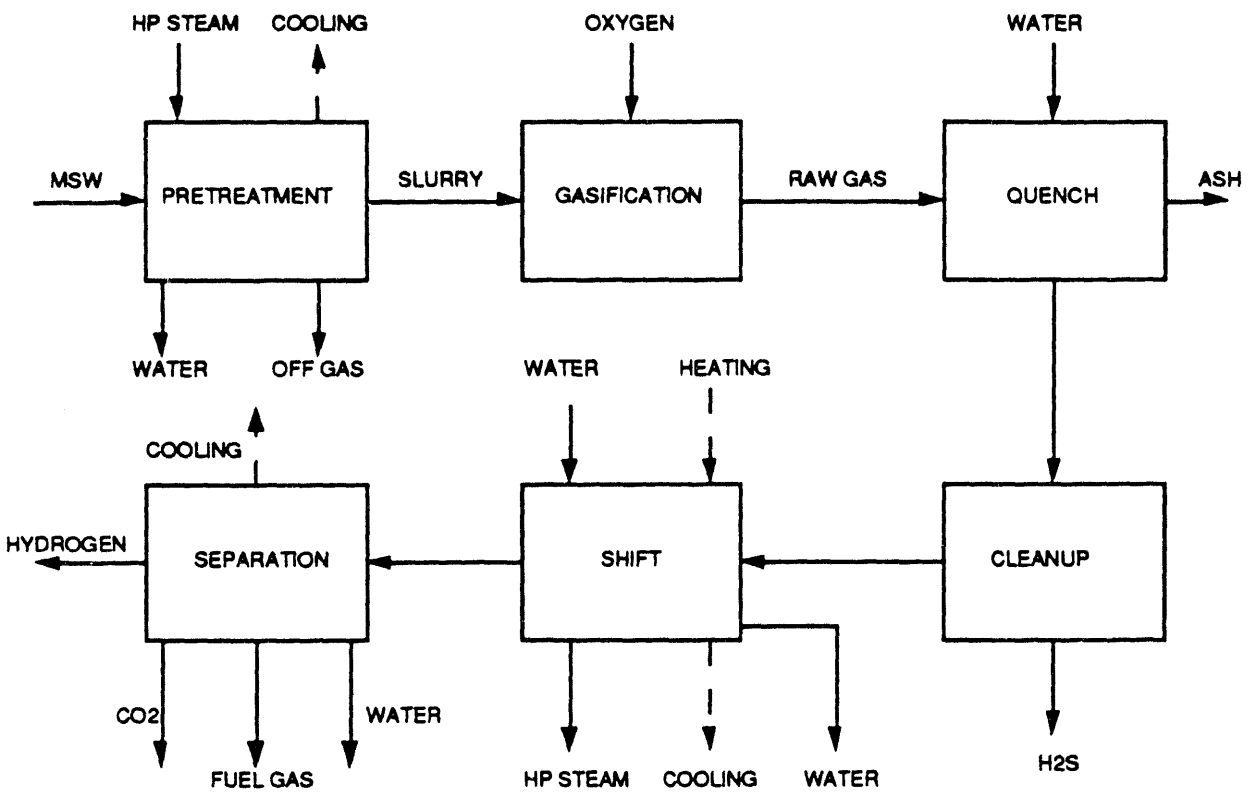
HP STEAM
COOLING
OXYGEN
WATER
MSW
PRETREATMENT
SLURRY
GASIFICATION
RAW GAS
QUENCH
ASH
WATER
OFF GAS
WATER
HEATING
COOLING
HYDROGEN
SEPARATION
SHIFT
CLEANUP
CO2
WATER
FUEL GAS
HP STEAM
COOLING
WATER
H2S

FIGURE 1

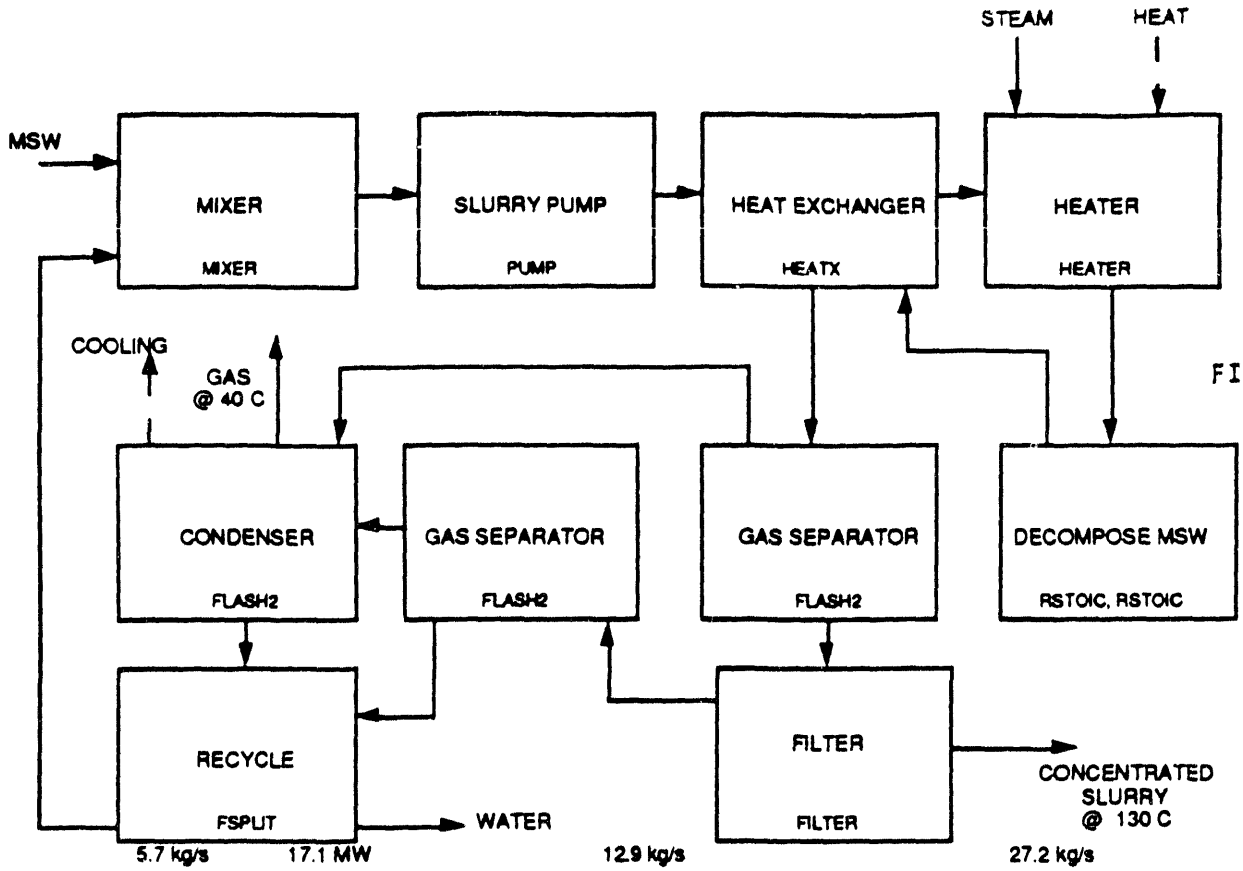

FIGURE 2

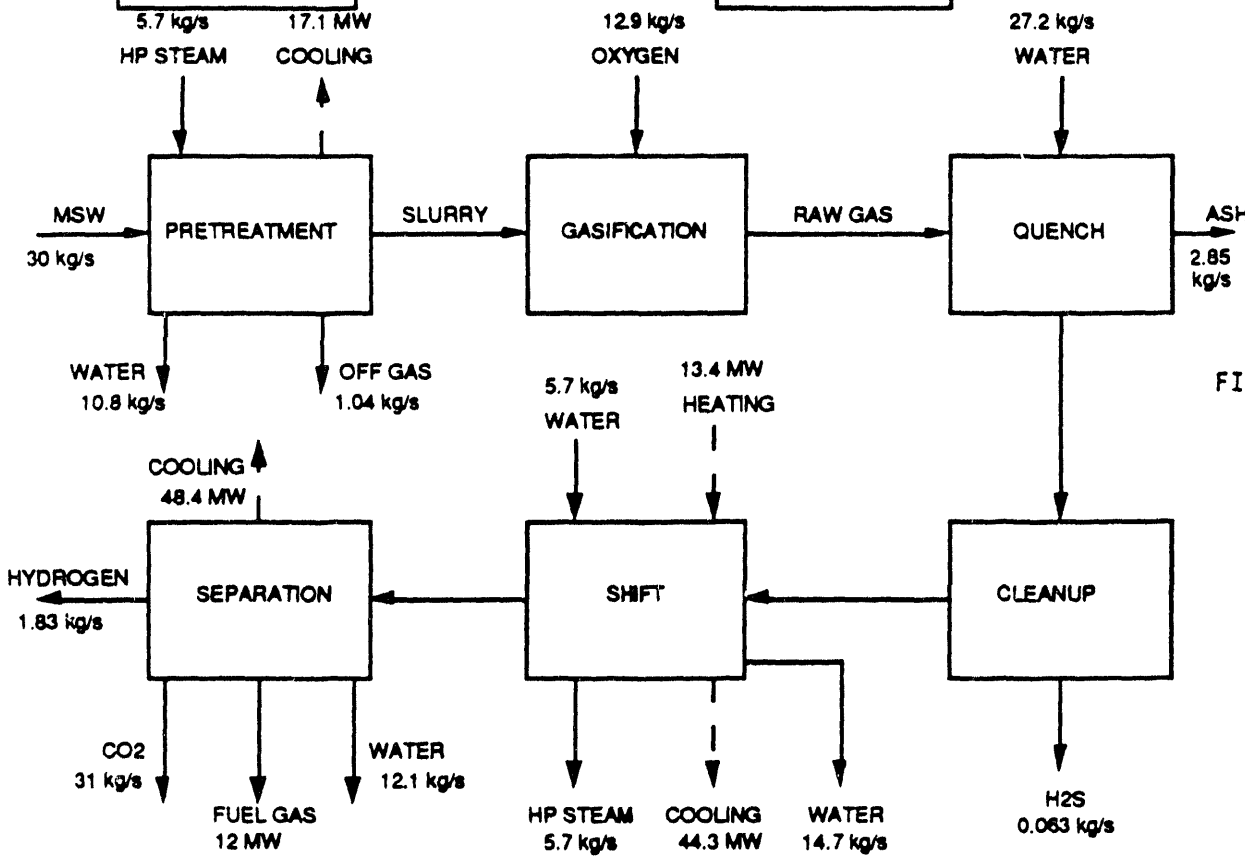

FIGURE 3

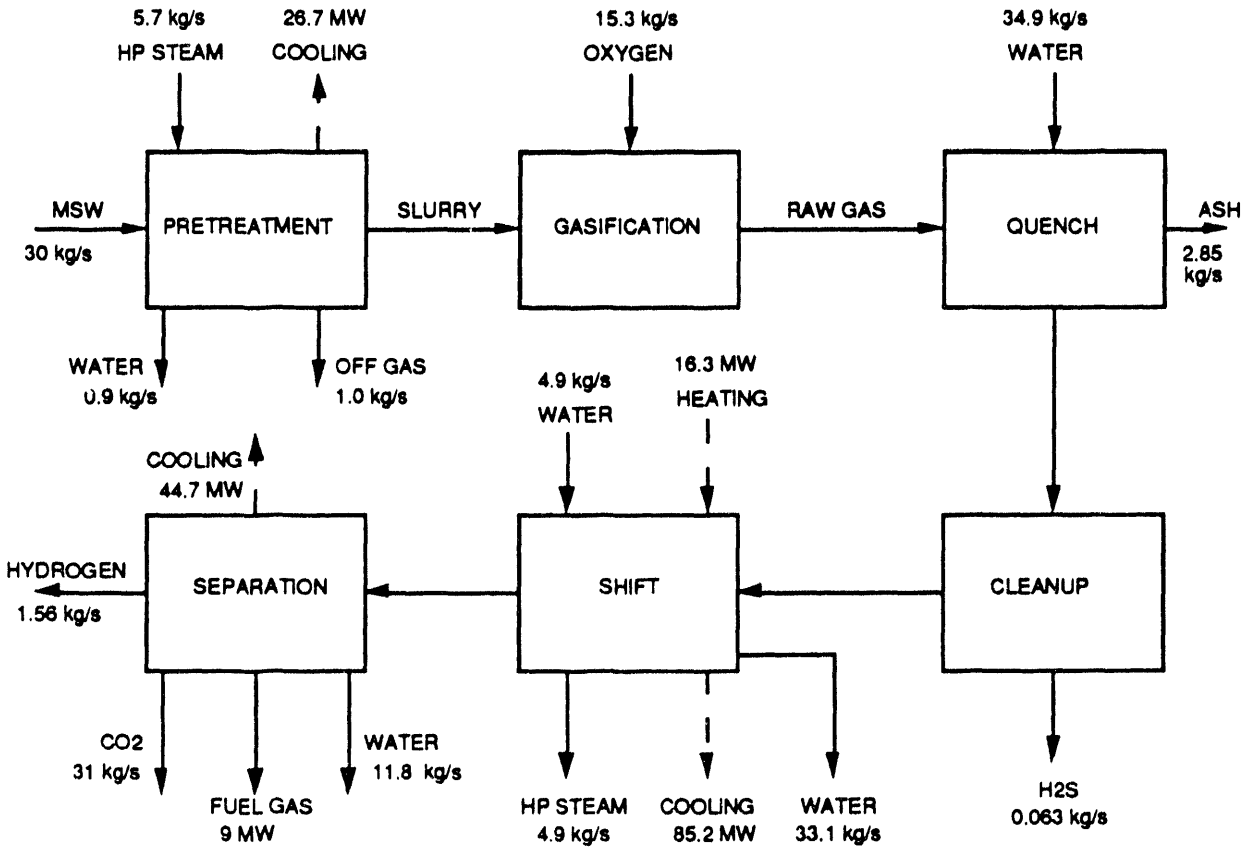
5.7 kg/s
HP STEAM
26.7 MW
COOLING
15.3 kg/s
OXYGEN
34.9 kg/s
WATER
MSW
30 kg/s
PRETREATMENT
SLURRY
GASIFICATION
RAW GAS
QUENCH
ASH
2.85
kg/s
WATER
0.9 kg/s
OFF GAS
1.0 kg/s
4.9 kg/s
WATER
16.3 MW
HEATING
COOLING
44.7 MW
HYDROGEN
1.56 kg/s
SEPARATION
SHIFT
CLEANUP
CO2
31 kg/s
FUEL GAS
9 MW
WATER
11.8 kg/s
HP STEAM
4.9 kg/s
COOLING
85.2 MW
WATER
33.1 kg/s
H2S
0.063 kg/s

FIGURE 4

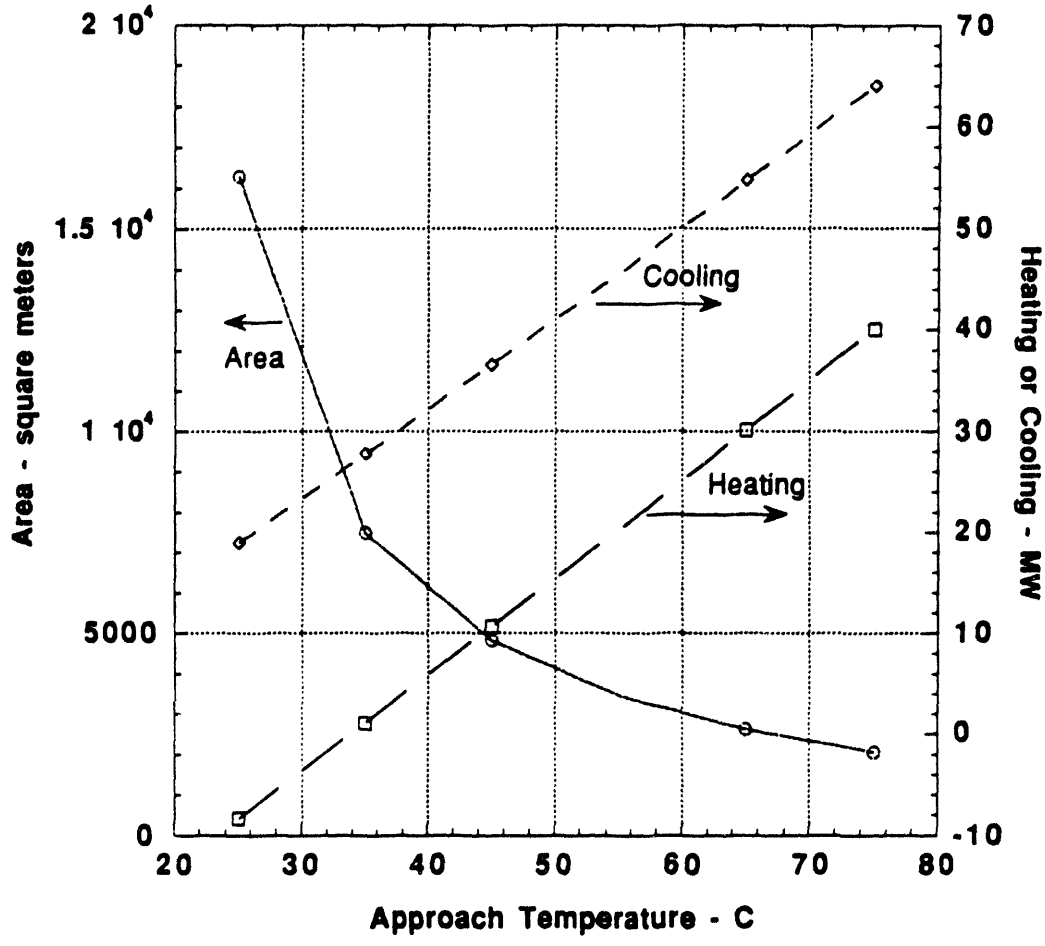
2 10^4
1.5 10^4
1 10^4
5000
0
Area - square meters
70
60
50
40
30
20
10
0
-10
Heating or Cooling - MW
Cooling
Area
Heating
20
30
40
50
60
70
80
Approach Temperature - C

FIGURE 5

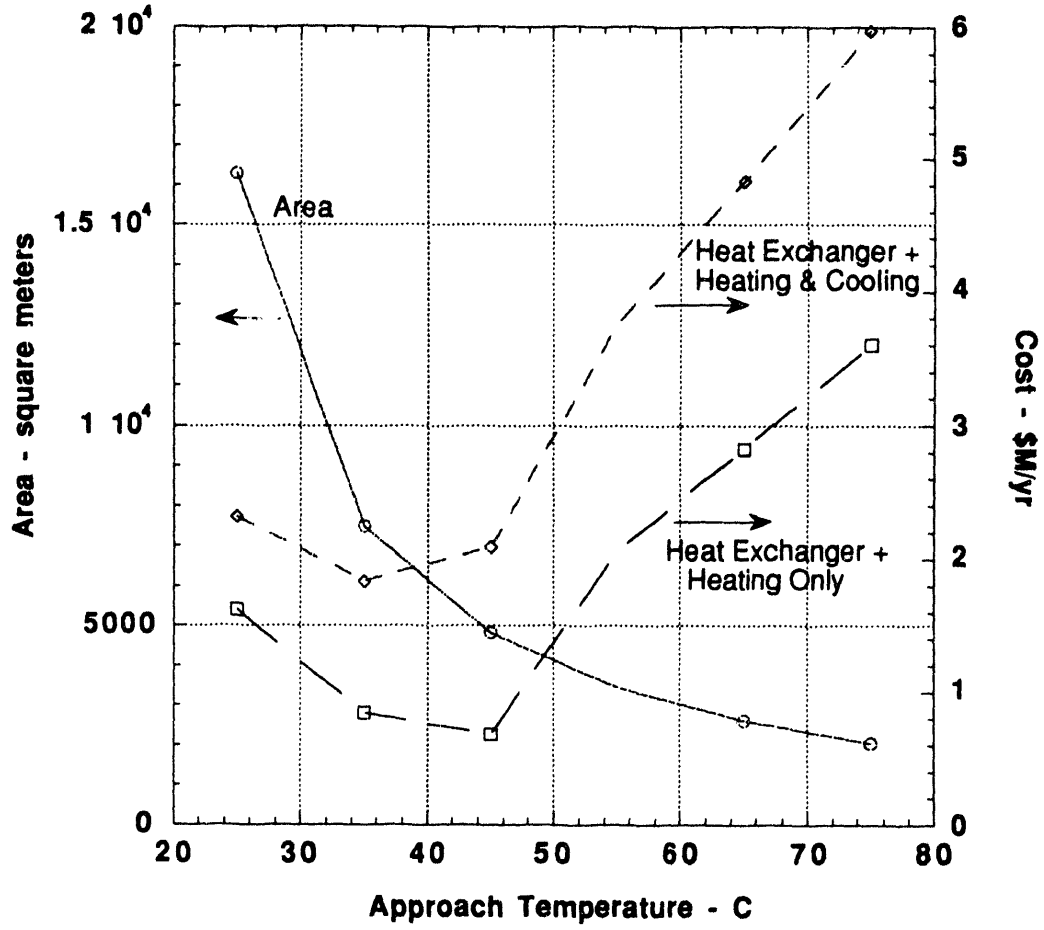
2 10^4
1.5 10^4
1 10^4
5000
0
Area - square meters
Area
Heat Exchanger +
Heating & Cooling
Heat Exchanger +
Heating Only
6
5
4
3
2
1
0
Cost - $M/yr
20
30
40
50
60
70
80
Approach Temperature - C

FIGURE 6

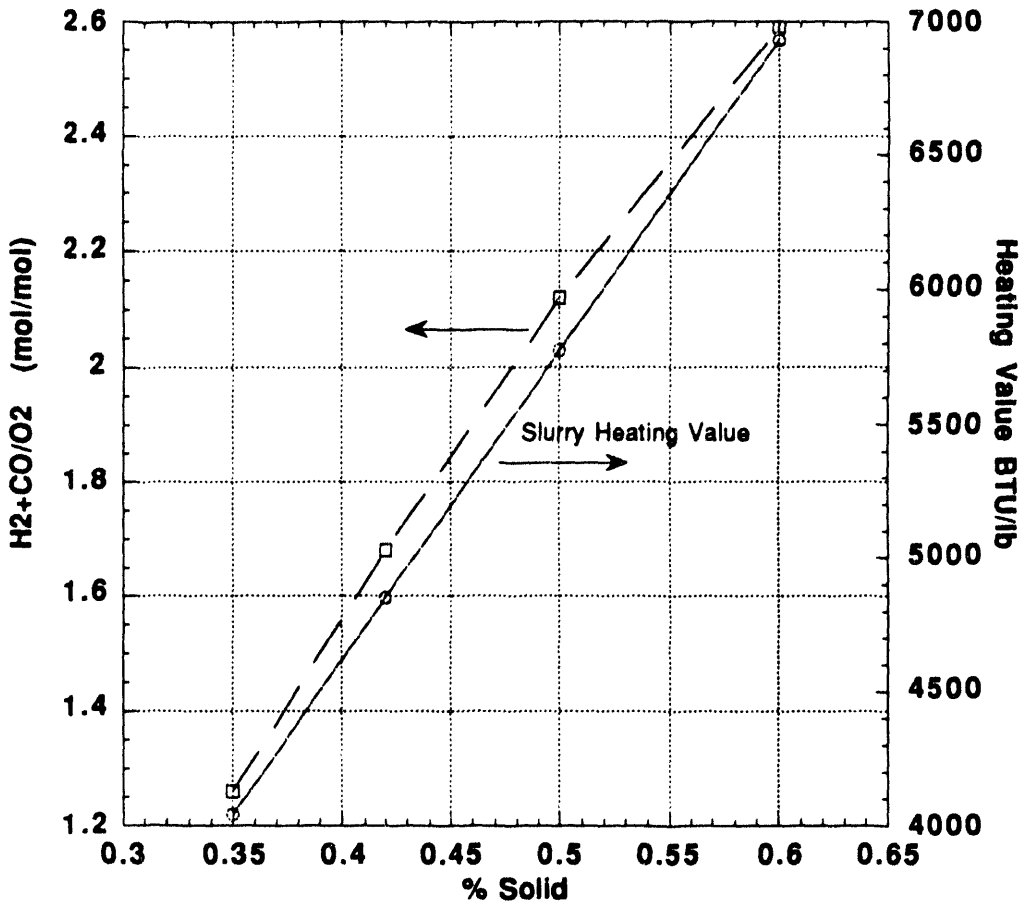
2.6
2.4
2.2
2
1.8
1.6
1.4
1.2
H2+CO/O2 (mol/mol)
7000
6500
6000
5500
5000
4500
4000
Heating Value BTU/lb
Slurry Heating Value
0.3
0.35
0.4
0.45
0.5
0.55
0.6
0.65
% Solid

FIGURE 7

HYDROGEN PRODUCTION FROM HIGH-MOISTURE CONTENT BIOMASS IN SUPERCRITICAL WATER

Michael Jerry Antal, Jr., Xiaodong Xu, and Jonny Stenberg
Hawaii Natural Energy Institute and
the Department of Mechanical Engineering
University of Hawaii at Manoa
Honolulu, HI 96822

Abstract

Wet biomass (water hyacinth, banana tree, cattails, green alga, kelp, etc.) grows rapidly and abundantly around the world. As a biomass crop, these aquatic species are particularly attractive because their cultivation does not compete with land based agricultural activities designed to produce food for local consumption or export. Many of these species possess other peculiar, desirable features. For example, water hyacinth is used to remove pollutants from water. The banana tree bears only one crop of fruit, after which it produces no more and must be cut down. Consequently, the stem is available for only the cost of its collection. In spite of these many attractive features, wet biomass is not regarded to be a promising feed for conventional thermochemical conversion processes because the cost associated with drying the feed is too high. This research seeks to circumvent this problem by employing water as the gasification medium. Prior work has shown that low concentrations of glucose (a model compound for whole biomass), and various wet biomass species (water hyacinth, algae) can be completely gasified in supercritical water at 600 °C and 34.5 MPa after a 30 s reaction time. Higher concentrations of glucose (up to 22% by weight) evidenced high (but somewhat incomplete) conversion to gas at these conditions. The gas contained hydrogen, carbon dioxide, carbon monoxide, methane, ethane, propane, and traces of other hydrocarbons. The carbon monoxide and hydrocarbons are easily converted to hydrogen by commercial technology available in most refineries. This prior work utilized capillary tube flow reactors that could not accommodate slurry feeds of wet biomass. Nor could these reactors accommodate a packed bed of catalysts, which we believed were necessary to achieve complete conversion of high concentration biomass slurries. For these reasons, we proposed to fabricate a completely redesigned, larger reactor system and initiate studies of heterogeneous catalysis of the gasification reactions.

During the past year a 0.375" O.D. Inconel 625 reactor system was assembled. This reactor has been

operating six hours per day, two days per week during the past 5 months at temperatures as high as 700 °C (or more) and pressures of 34.5 MPa (or less) without significant problems. Gasification results from this reactor reproduced earlier work reasonably well. During February we initiated studies of catalytic gasification employing solid catalyst X. Catalyst X is not expensive, survives well in supercritical water, and is extremely effective. Complete conversions of glucose (18% by weight in water) to gas are obtained at a weight hourly space velocity (WHSV) as high as 13.5 hr^{-1}. Complete conversions of low concentration water hyacinth in water have also been achieved. We are now modifying the feed system to study gasification of high concentration wet biomass feeds. We are also initiating fundamental studies of the heterogeneous catalytic gasification chemistry. A patent disclosure has been prepared and submitted to the University. The identity of catalyst X will be revealed after the University determines its position concerning a patent application.

An economic study of this process by F.S. Frenduto of Air Products Corp. dated 17 March 1992 projected economic feasibility if complete gasification of 18% by weight biomass in water could be achieved. We have realized this goal, which defines success for our work. We invite industrial participation in the design of a pilot plant to prove this process on a larger scale.

Introduction

A pressurized catalytic gasification process, operated at 600°C, 34.5 MPa, is effective for hydrogen production from high-moisture content biomass. In the first part of this work, focus has been placed on the catalytic gasification of glucose as a model compound for whole biomass and the evaluation of the catalyst. In the second part of this work, whole biomass feed will be used with the identified catalyst.

This paper presents the experimental results for the gasification of glucose with catalyst X. Effects of temperature, Pressure, weight hourly space velocity (WHSV), and reactant concentration are discussed.

Apparatus and Experimental Procedures

The reactor system scheme is presented in Figure 1. The reactor is made of Inconel 625 tubing with 0.375" OD and 0.187" ID. The temperature of the reactant flow is abruptly brought up to a desired value by an entry heater (ARi Industries)/cooling water jacket. The reactor is maintained at isothermal conditions by a furnace (Mellen Company) and a down stream heater (ARI Industries)/cooling water jacket combination. To improve the heat transfer from the heaters to the fluids inside the reactor, the heaters are coiled on stainless steel rods which are in direct contact with the Inconel reactor. A unique feature of this reactor is that different sizes of annuli (made of Inconel 625) can be easily installed, giving different residence times. Moreover, different amounts of solid catalyst can be packed inside the reactor, giving desired WHSV (weight hourly space velocity). For the experiments reported in this paper, about 2/3 of the heated zone of the reactor is packed with catalyst X. The axial temperature profile along the reactor's functional length of approximately 0.48 m is measured with 15 fixed, type K thermocouples. Furthermore, a movable type K thermocouple inside the annulus (Inconel 625) provides a temperature profile inside the reactor. Pressure in the reactor system is measured using an Omega PX302 pressure transducer. A Grove Mity-Mite model 91 back pressure regulator (Grove Valve and Regulator Company) reduces the working pressure from 34.5 MPa to atmospheric pressure. After passing through the back pressure regulator, the reactor effluent goes through an in-house fabricated glass gas-liquid separator. The gas flow rate is

measured using a Wet Test Meter (Precision Scientific).

A new feeding system for wet biomass slurries is being developed. Currently, a balloon feeding system is employed to feed the wet biomass slurry into the reactor. Wet biomass is first ground with a Speed Blender (Hamilton Beach, Inc.) and then with a Brinkmann Homogenizer (Brinkmann Instruments, Inc.). The heterogeneous biomass slurry fills the 500 ml high pressure/temperature vessel (series 4570/80) equipped with a A1120HC magnetic drive (Parr Instrument Company). A 10 gram Weather Measure meteorological balloon (Weather Measure Corp.) is placed in the vessel together with the biomass slurry. Water is pumped into the balloon, and as the balloon expands the biomass slurry is forced into the reactor.

The analysis of the gaseous products is accomplished on a Hewlett-Packard GC (model 5890) equipped with flame ionization and thermal conductivity detectors. A 800/100 mesh Carbosphere molecular sieve packed column is used, operating at 35°C for 4.2 min, followed by a 15°C/min ramp to 227°C, a 70°C/min ramp to 350°C, and a 5.3 min hold at 350°C. A standard gas mixture used for calibration is obtained from AIRCO. The following gases are detected as the products of glucose gasification: H_2, CO, CO_2, CH_4, C_2H_4, C_2H_6 , C_3H_6, C_3H_8.

Results and Discussion

When 0.2 M glucose is gasified without solid catalyst X at about 30 s residence time in supercritical water at 600°C, 34.5 MPa, complete carbon conversion is observed. The liquid sample is clear. As the reactant glucose concentration increases, the carbon conversion decreases. With 0.8 M glucose reactant, the conversion drops to 88%, and a dark brownish oil layer is present in the liquid sample.

As indicated in Table 1, the presence of solid catalyst X (2.77 g packed in the heated zone of the reactor) effects complete conversion of the 0.8 M glucose feed. The liquid effluent is clear. Gas yields of hydrogen, monoxide, methane, dioxide increase significantly with catalyst X over that without catalyst.

When the glucose reactant concentration increases from 0.8 M to 1.0 M, with catalyst X the gasification remains complete, as shown in Table 2. The liquid sample is still clear.

For this heterogeneous catalytic reactor, the WHSV (weight hourly space velocity) is defined as the ratio of the mass flow rate of the feed to the mass of catalyst X used in the heated zone.

$$MHSV = \frac{C_o v \dot{m}}{W}$$

where

C_o = reactant concentration at NTP, g of reactant/cm^3

$\dot{m}$ = inlet mass flow rate at NTP, g/hr

v= specific volume of reactant at NTP, cm^3/g

w= weight of catalyst X, g

By changing the inlet mass flow rate, we can vary the WHSV. The effect of WHSV on the gasification

of glucose is shown in Table 3. Although the WHSV increases by a factor of four, the carbon conversion remains at effectively 100%.

The effect of temperature on the gasification of glucose in the presence of catalyst X is shown in Table 4. Complete carbon conversion is observed at 600°C, however, as temperature drops conversion decreases drastically. When the reaction temperature is below 580°C the gasification reaction begins to become incomplete, the liquid effluent becomes yellowish and there is a thin layer of a dark brown, oil-like tar. We dried 10 ml samples of the liquid effluent from the experiments at 500°C, 550°C, and 600°C in small beakers in an oven and measured the weight gain. After the samples were dried, only a dark tar deposit remains on the bottom of the beaker. Figure 2 illustrates the amount of tar present in the liquid sample as a function of reaction temperature.

The effect of pressure on the gasification experiment is shown in Table 5. As pressure increases, the yield of methane increases. This confirms Elliott et al's (Elliott et al, 1993; Baker et al, 1989; Sealock et al, 1993) results.

Conclusion

As high as 18 % (by weight in water) glucose can be completely gasified to hydrogen rich gas with catalyst X at a WHSV as high as 13.5 hr^{-1} in supercritical water at 600°C, 34.5 MPa. Complete conversions of low concentration of water hyacinth (0.24% by weight in water) have also been achieved. No deactivation of catalyst X has been observed.

Future Work

Future work will be focused on the heterogeneously catalyzed gasification of high concentration whole biomass and the treatment of waste materials such as sewage sludge to address both the energy recovery and environmental cleanup goals. Fundamental studies of the heterogeneous catalysis chemistry including effects of external mass transfer and intraparticle diffusion on the conversion rate will be initiated.

References

Elliott, D.C., E.G. Baker, R.S. Butner, and L.J. Sealock, Jr.. 1993. "Bench-Scale Reactor Tests of Low Temperature, Catalytic Gasification of Wet Industrial Wastes." *Journal of Solar Energy Engineering*, 115:52-56.

Baker, E.G., L.J. Sealock, Jr., R.S. Butner, D.C. Elliot, and G.G. Neuenschwander. 1989. "Catalytic Destruction Of Hazardous Organics in Aqueous Wastes: Continuous Reactor System Experiments." *Hazardous Waste & Hazardous Materials*, 6:87-94.

Sealock, L.J. Jr., D.C. Elliott, E.G. Baker, and R.S. Butner. 1993. "Chemical Processing in High-Pressure Aqueous Environments. 1. Historical Perspective and Continuing Developments." *Industrial & Engineering Chemistry Research*, 32:1535-1541.

Elliott, D.C., L.J. Sealock, Jr., and E.G. Baker. 1993. "Chemical Processing in High-Pressure Aqueous Environments. 2. Development of Catalysts for Gasification." *Industrial & Engineering Chemistry Research*, 32· 1542-1548.

Table & Figure Captions

Table 1: Glucose gasification in supercritical water at 600°C, 34.5 MPa with and without catalyst X.

Table 2: Reactant concentration effect on glucose gasification in supercritical water at 600°C, 34.5 MPa.

Table 3: WHSV effect on glucose gasification in supercritical water at 600°C, 34.5 MPa (1.0 M glucose reactant).

Table 4: Temperature effect on glucose gasification in supercritical with 1.0 M glucose reactant (WHSV[a] = 13.5 (g/hr)/g).

Table 5: Pressure effect on glucose gasification in supercritical water at 600°C.

Figure 1: Supercritical flow reactor scheme.

Figure 2: Tar yield vs reaction temperature for gasification of glucose (1.0 M glucose reactant, WHSV=13.5 (g/hr)/g).

Table 1: Glucose gasification in supercritical water at 600°C, 34.5 MPa with and without catalyst X

Product	0.8 M glucose (with 2.77 g catalyst X) WHSV[a] = 2.5 (g/hr)/g	0.8 M glucose (no catalyst) res. time=28 s
	yield[b]	yield[b]
H2	2.13	0.70
CO	2.04	1.63
CO2	2.64	2.01
CH4	1.29	0.75
C2H4	0.0	0.04
C2H6	0.37	0.22
C3H6	0.0	0.04
C3H8	0.13	0.09
Carbon conversion[c]	119%	88%

[a] WHSV = weight hourly space velocity

[b] yield = mole of gas/ mole of reactant

[c] carbon conversion = mole of carbon in the gas/ mole of carbon in the reactant

Table 2: Reactant concentration effect on glucose gasification in supercritical water at 600°C, 34.5 MPa

Product	0.8 M glucose (with 2.77 g catalyst X) WHSV[a] = 2.5 (g/hr)/g	1.0 M glucose (with 2.77 g catalyst X) WHSV[a]= 3.7 (g/hr)/g
	yield[b]	yield[b]
H2	2.13	1.73
CO	2.04	1.32
CO2	2.64	2.54
CH4	1.29	1.10
C2H4	0.0	0.001
C2H6	0.37	0.33
C3H6	0.0	0.005
C3H8	0.13	0.19
Carbon conversion[c]	119%	103 %

[a] WHSV = weight hourly space velocity

[b] yield = mole of gas/ mole of reactant

[c] carbon conversion = mole of carbon in the gas/ mole of carbon in the reactant

Table 3. WHSV effect on glucose gasification in supercritical water at 600°C, 34.5 MPa (1.0 M glucose reactant)

Product	WHSV=3.7 (g/hr)/g	WHSV=6.6 (g/hr)/g	WHSV=13.5 (g/hr)/g
	yield[b]	yield[b]	yield[b]
H2	1.73	1.57	1.97
CO	1.32	2.33	2.57
CO2	2.54	1.42	1.54
CH4	1.10	1.01	0.90
C2H4	0.001	0.003	0.008
C2H6	0.33	0.29	0.25
C3H6	0.005	0.001	0.009
C3H8	0.19	0.14	0.11
Carbon conversion[c]	103 %	96 %	98 %

[a] WHSV = weight hourly space velocity

[b] yield = mole of gas/ mole of reactant

[c] carbon conversion = mole of carbon in the gas/ mole of carbon in the reactant

Table 4: Temperature effect on glucose gasification in supercritical with 1.0 M glucose reactant (WHSV[a] = 13.5 (g/hr)/g)

Product	600°C 34.5 MPa	550°C 34.5 MPa	500°C 34.5 MPa
H2 yield[b]	1.97	0.62	0.46
CO yield	2.57	1.67	1.57
CO2 yield	1.54	0.73	0.85
CH4 yield	0.90	0.37	0.25
C2H4 yield	0.008	0.01	0.016
C2H6 yield	0.25	0.10	0.07
C3H6 yield	0.009	0.03	0.04
C3H8 yield	0.11	0.05	0.036
Tar yield[c]	0.013	0.009	0.001
Carbon conversion[d]	98 %	54%	51%

[a] WHSV = weight hourly space velocity

[b] gas yield = mole of gas/ mole of reactant

[c] Tar yield = gram of residue after drying the liquid sample/ gram of reactant

[d] carbon conversion = mole of carbon in the gas/ mole of carbon in reactant

Table 5: Pressure effect on glucose gasification in supercritical water at 600°C

Product	1.0 M glucose WHSV[a]= 3.7 (g/hr)/g	1.0 M glucose WHSV[a]= 8.3(g/hr)/g
Pressure	34.5 MPa	25.5 MPa
	yield[b]	yield[b]
H2	1.73	1.18
CO	1.32	2.47
CO2	2.54	1.30
CH4	1.10	0.86
C2H4	0.001	0.0081
C2H6	0.33	0.25
C3H6	0.005	0.014
C3H8	0.19	0.012
Carbon conversion[c]	103%	92%

[a] WHSV = weight hourly space velocity

[b] yield = mole of gas/ mole of reactant

[c] carbon conversion = mole of carbon in the gas/ mole of carbon in the reactant

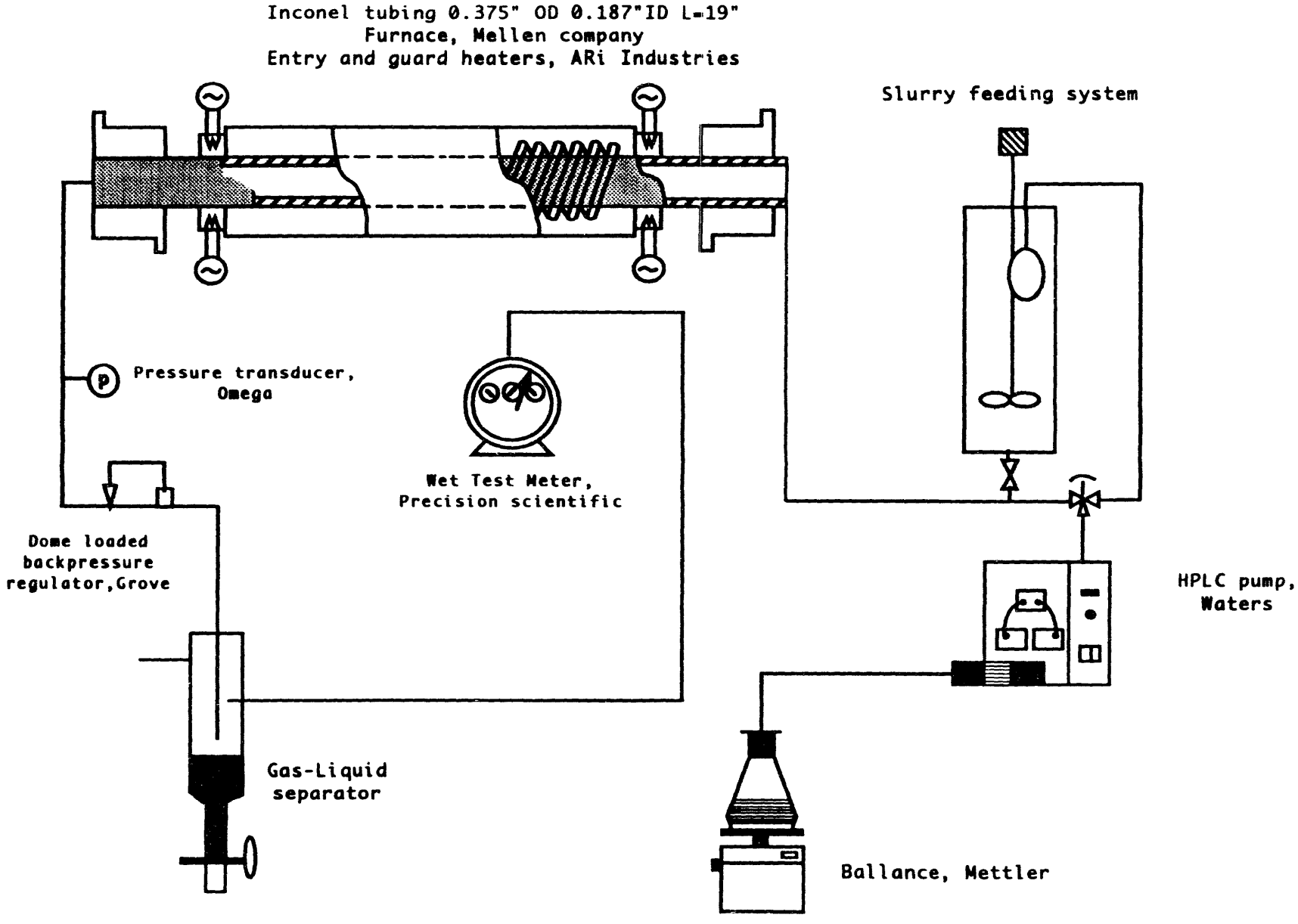

Figure 1. Supercritical Flow Reactor Scheme

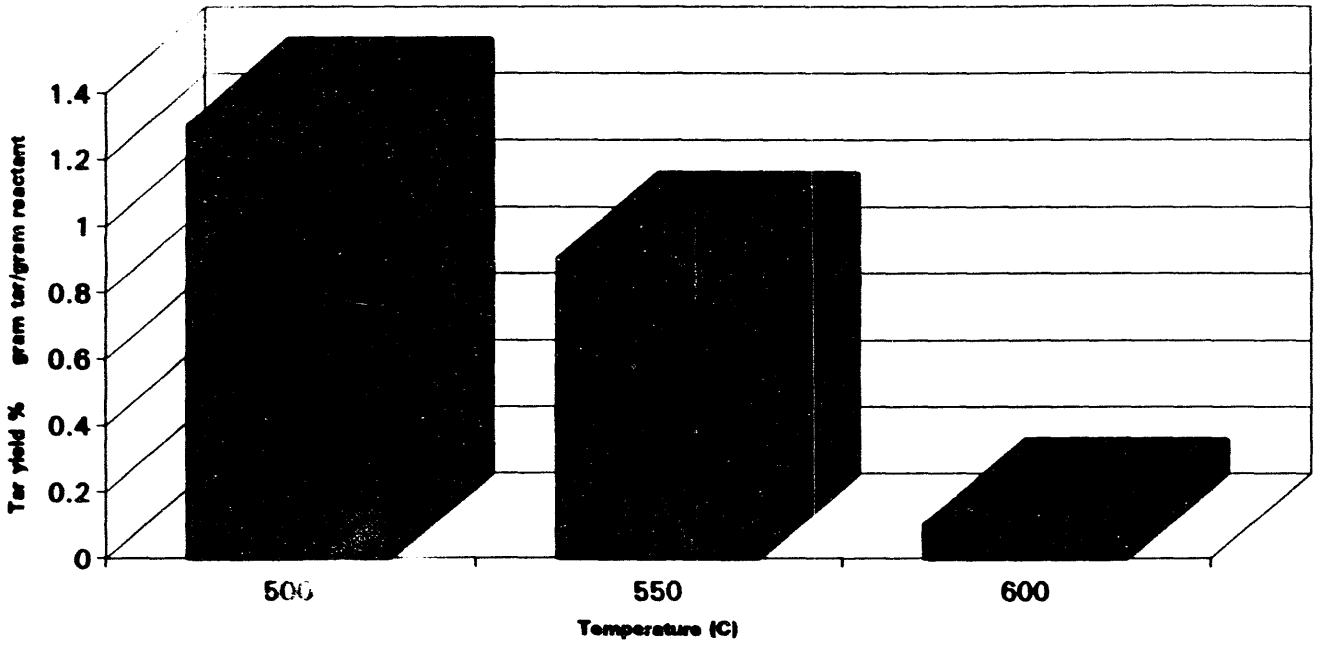

Figure 2. Tar Yield vs Reaction Temperature for Gasification of Glucose (1.0 M glucose reactant, WHSV=13.5 (g/hr)/g)

SOLAR ENERGY CONVERSION WITH CYANOBACTERIA

Edward J. Bylina
Pacific Biomedical Research Center
University of Hawaii at Manoa
Honolulu, HI 96822

Abstract

Hydrogen production in cyanobacteria is particularly attractive because these organisms are able to generate their own source of organic substrates using light energy and use water as their ultimate source of reductant. Molecular biology approaches are being applied to understanding and increasing hydrogen production in filamentous strains of cyanobacteria. *Spirulina* produces hydrogen under anaerobic conditions in the dark. Experiments have continued towards the development of a genetic system for the cyanobacterium, *Spirulina pacifica* . These include (1) the identification of three unique restriction enzymes , (2) determining the levels of natural resistance to antibiotics, (3) PCR amplification of the gene encoding the 16S ribosomal RNA in this strain, (4) constructing a library of *Spirulina* chromosomal DNA, (5) developing DNA vectors for use in *Spirulina*, and (6) establishing conjugation conditions for DNA transfer into *Spirulina*. Once this genetic system is completed, it will be used to elucidate the molecular basis of hydrogen metabolism in *Spirulina* in order to redirect the metabolic energies of cyanobacteria toward the production of hydrogen.

Introduction

The goals of this subtask of the Hydrogen from Renewable Resources Program are to investigate the molecular basis of hydrogen metabolism and evolution in cyanobacteria and to develop enhancement methodologies for the production of improved strains of hydrogen producers. The use of hydrogen production in cyanobacteria to convert solar energy to useful energy is particularly attractive because these organisms are able to generate their own source of organic substrates using light energy and use water as their ultimate source of reductant. Three basic enzyme systems are involved in hydrogen metabolism in cyanobacteria: nitrogenase, uptake hydrogenase, and reversible hydrogenase (Houchins 1984).

In order to capitalize on this photosynthetic production of hydrogen, one must gain a better understanding of the mechanisms and regulation of the systems involved. This is especially important in view of the fact that competition for reductant by various enzyme systems appears to be one of the limiting factors on the evolution of hydrogen gas in cyanobacteria. While much attention has been directed at the nitrogenase system in cyanobacteria, the hydrogenase systems have not been as well characterized. Hydrogenases have been purified to varying degrees of homogeneity and studied from a number of cyanobacteria (Houchins & Burns, 1981; Kentemich et al., 1989; Ewart & Smith, 1989; Rao & Hall, 1988; Gu and Zhou, 1987), but molecular biological studies of cyanobacterial hydrogenase systems are only beginning (Ewart et al., 1990).

Characterization of hydrogen evolution in *Spirulina* is important, since this species is already cultivated on an industrial scale. Although *Spirulina* species do not form heterocysts and do not fix nitrogen (Durand-Chastel, 1982), these organisms are capable of hydrogen evolution (Gu and Wang, 1984). While hydrogen production in a number of cyanobacterial species is predominantly formed by nitrogenase, hydrogen evolution is catalyzed by hydrogenase in *Spirulina*. Under anaerobic conditions in the dark, *Spirulina* produces hydrogen. There appears to be competition for reductant between the hydrogenase and nitrate reductase in *Spirulina*. The hydrogenase from *Spirulina platensis* has been partially purified (Gu and Zhou, 1987). The biological electron donor to hydrogenase has not yet been identified in *Spirulina*. No hydrogenase activity was observed using *Spirulina* ferredoxin, NADH, NADPH or FMNH as electron donors. While no genetic system has yet been described for these organisms, a library of *Spirulina* chromosomal DNA has been constructed (DeRossi et al., 1985) and a number of genes have been cloned and sequenced (Bini et al., 1992; Riccardi et al., 1991).

In this report, we will summarize our experiments using the commercially important cyanobacterial species *Spirulina pacifica*. Our progress in developing a genetic system for *Spirulina* will be discussed. We are currently concentrating our efforts with *Spirulina pacifica* to elucidate the molecular mechanisms of hydrogen metabolism in these organisms.

Results and Discussion

Requirements for the establishment of a genetic system in *Spirulina pacifica* include: (a) characterizing the DNA restriction-modification system present in the strain, (b) determining the levels of natural resistance to antibiotics in the strain, (c) constructing a library of *Spirulina* chromosomal DNA, (d) designing a DNA vector which will be stably maintained in *Spirulina*, and (e) developing either physical or biological methods for introducing foreign DNA into *Spirulina* cells. Progress has been made in each of these areas.

One genetic system requirement is the characterization of the DNA restriction-modification system present in *Spirulina pacifica*. Three restriction enzymes were identified in *Spirulina platensis* subspecies *siamese* (Kawamura et al., 1986). The same enzyme purification protocol was used with cell extracts of *Spirulina pacifica*. Three different restriction enzyme activities in the cell extract from *Spirulina pacifica* have been found and the recognition sites for each of the enzymes have been identified. All three enzymes are isoschizomers of known enzymes. However, only one of the three enzyme activities is found in both *Spirulina* species. We have also determined that DNA from *Spirulina pacifica* is dam methylated, but a Sau3A isochizomer has not been identified in cell extracts from this strain.

Bacterial species use their restriction systems to differentiate between foreign DNA and their own DNA, destroying foreign DNA molecules in the process. Once the restriction systems present in *Spirulina* have been identified, we can modify our genetically engineered DNA constructs the same way that *Spirulina* modifies its own DNA. This will prevent our genetically engineered DNA constructs from being destroyed by the *Spirulina* restriction system when we introduce these constructs into *Spirulina* cells.

Levels of resistance to various antibiotics on solid media have been determined for *Spirulina pacifica* (see Table 1). Varying amounts of *Spirulina* culture were spotted on filter paper, and these filters were placed on solid Z medium containing varying amounts of antibiotics. *Spirulina* appears to be most sensitive to chloramphenicol and erythromycin. Even at levels of 0.1 mg/ml of each of these antibiotics, no *Spirulina* growth was observed. *Spirulina* showed a relatively high natural resistance to the other antibiotics tested. Genes conveying resistance to chloramphenicol and erythromycin will be used as selectable markers in *Spirulina*.

The presence of gas vacuoles in *Spirulina* causes the organism to float in liquid media. Harvesting by centrifugation is inefficient, since only a portion of the cells actually pellet after attempts to spin them down. A rapid method of harvesting these cultures has been established. Silk screen material obtained from a commercial art supply store is used as the filter material in a reusable filter holder with receiver device from Nalgene. If necessary, cells can also be washed in this device. After filtering, the device is taken apart and the *Spirulina* paste is scraped off the filter. The large size of *Spirulina* filaments allows us to use the silk screen material as the material for the filter.

Table 1. *Spirulina pacifica* Natural Resistance to Various Antibiotics

Antibiotic	Resistance Level (mg/ml)*
chloramphenicol	<0.1
erythromycin	<0.1
spectinomycin	5-10
gentamycin	10-50
streptomycin	25-100
G-418	50-100
tetracycline	100-500
neomycin	200-300
ampicillin	500-1000
kanamycin	500-1000

*The lower value in the resistance level range corresponds to the highest amount of antibiotic tested which still supported growth. The higher value in the resistance level range corresponds to the lowest amount of antibiotic tested which inhibited growth.

The construction of the *Spirulina* genomic DNA cosmid library has been completed. Large scale (1-2 g wet cells) chromosomal DNA preparations from axenic *Spirulina* cultures have been performed. This protocol included lysozyme treatment, incubation with SDS/proteinase K, and phenol/chloroform extraction. The resulting aqueous phase was mixed with ethanol, and the chromosomal DNA was spooled on a glass loop. This purified chromosomal DNA can be digested by a variety of restriction enzymes. After partial digest conditions with the enzyme Sau3A were established to obtain DNA fragments of 30-40 kb in size, this information was used to scale up the partial digestion of ~200 mg of *Spirulina* genomic DNA. Two digestion conditions were used and the resulting digested DNA was fractionated on a 10-40% sucrose gradient. Fractions were collected and analyzed by agarose gel electrophoresis. Fractions containing fragments in the 10-15 kb, 15-20 kb, 20-30 kb, 30-40 kb and 40-50 kb ranges were pooled, concentrated, precipitated and resuspended. The resulting samples were again checked by agarose gel electrophoresis to determine DNA size, quality and concentration. Cosmid vector pLAFR3 DNA (Staskawicz et al., 1987) was linearized with BamHI and treated with shrimp alkaline phosphatase. The 20-30 kb sized DNA fraction was ligated into this cosmid vector. A commercially available l in vitro packaging kit (Stratagene Giga-Pack Gold) was used to produce the library. This library will be used to isolate structural genes of proteins involved in hydrogen metabolism.

Using chromosomal DNA isolated from *Spirulina*, PCR was used (Weisburg et al., 1991) to amplify the 16S RNA gene of *Spirulina pacifica*. Eubacterial specific 16S rRNA oligonucleotides were used for the

amplification of this *Spirulina* gene. A distinct fragment of expected size (~1500 bp) was observed after PCR amplification. Characterization of the PCR-amplified 16S RNA gene of Spirulina is in progress. We have subcloned the amplified DNA fragment first into the plasmid vector pRL498 (Elhai and Wolk, 1988) and then into M13. The correct constructions were verified by agarose gel electrophoresis. Single stranded M13 DNA containing the amplified DNA fragment has been purified and will be used for sequencing. This strain originated from the UTEX strain collection (UTEX 1926), however little work has been published on the strain. Determination of the 16S RNA sequence will allow us to determine the phylogenetic relationship between *Spirulina pacifica* and other cyanobacterial species. Techniques developed in our *Spirulina* species can be applied to related species (either known or yet to be discovered) that show high natural levels of hydrogen production.

A DNA vector which is stably maintained in *Spirulina pacifica* must be identified. We have obtained a plasmid vector containing an origin of replication from the cyanobacterium *Fremyella diplosiphon* (Cobley et al., 1993) from John Cobley at the University of San Francisco. This replication origin will be tested to determine whether it functions in *Spirulina*. Once such a vector has been identified, it will be used to introduce genes (either foreign genes or altered *Spirulina* genes involved in hydrogen metabolism) into *Spirulina* in order to alter the hydrogen production of the cyanobacterium.

One possible method of DNA transfer into *Spirulina* is conjugation using *E. coli*. Unfortunately, most *E. coli* strains cannot tolerate the high salt concentrations required for *Spirulina*. Growth conditions for conjugation on solid media have been established by determining the growth conditions under which both *Spirulina* and *E. coli* can survive. Conjugations between two strains of *E. coli* have been demonstrated by mating on Z medium for 4 hours. The conjugating *E. coli* strain S17-1 appears to be relatively sensitive to the high salt Z medium. Efforts are under way to make this strain more tolerant to Z medium. The high salt Z media has been diluted to determine the minimum dilution on which *Spirulina* can be propagated. This may make conditions more favorable for *E. coli* survival. Our initial experiments suggest that *Spirulina* can grow on 1/4 Z media in liquid and as low as 1/16 Z media on agar plates. Plates containing 5% LB + 1/2 Z media will be used for conjugation experiments to introduce genes into *Spirulina*.

Future Work

Continuing the work of the on-going program, we are pursuing several research goals with respect to *Spirulina*. Since *Spirulina* species are probably the most commercially exploited cyanobacteria, experimental successes will likely result in early practical applications. The sequence of the 16S rRNA gene of *Spirulina pacifica* will be determined. Isolated single strand DNA from a number of independent clones will be used in DNA sequencing experiments with sequencing primers from conserved regions of the 16S RNA gene that have been obtained from Craig Moyer at the University of Hawaii.

Growth conditions for maximal hydrogen production in *Spirulina pacifica* will be established. The *Spirulina* hydrogenase will be purified to homogeneity from cultures grown under these conditions. The hydrogenase from *Spirulina platensis* has already been partially purified (Gu and Zhou, 1987). Once this enzyme complex has been isolated, the amino-terminal sequence of the protein subunits shall be determined. Our DNA library of *Spirulina* chromosomal DNA will be used to isolate the hydrogenase genes. Degenerate oligonucleotide probes based on the amino acid sequence of the hydrogenase will be synthesized. These probes will be used in hybridization studies to identify the *Spirulina* DNA fragments which contain the hydrogenase genes.

Characterization of the *Spirulina* hydrogenase genes will allow us to (1) investigate structure-function relationships in the hydrogenase enzyme, (2) determine the regulation of hydrogenase expression and (3) better understand the molecular mechanisms of hydrogen production.

We will continue our efforts to develop a genetic system for *Spirulina pacifica*. With the identification of the restriction enzymes present in this strain, the genes for the DNA modification enzymes corresponding to these restriction enzymes can be isolated and characterized. These modification enzymes will be used to modify DNA that will be introduced into *Spirulina*. These modifications will make the introduced DNA resistant to cleavage inside the *Spirulina* cell, thereby increasing DNA transformation efficiencies. We will use a variation of the genomic DNA library enrichment strategy (Renbaum et al., 1990) that was used to isolate the CpG methylase gene from *Spiroplasma*. Other requirements of a genetic system include: (1) establishing conditions to reproducibly regenerate *Spirulina* filaments from fragments containing only a few cells, (2) designing a DNA vector which will be stably maintained in *Spirulina* (either in plasmid form or integrated into the chromosome), and (3) developing either physical or biological methods for introducing foreign DNA into *Spirulina* cells. Conjugation, electroporation and particle gun technologies will be investigated.

The future of genetic engineering approaches to hydrogen production in cyanobacteria is bright. Rapid advances are taking place in the ability to manipulate cyanobacterial strains. As we learn more about the molecular basis of hydrogen metabolism in cyanobacteria, these advances can be used to redirect the metabolic energies of cyanobacteria toward the production of hydrogen for man's benefit.

Acknowledgments

This work supported under contract to the U.S. Department of Energy via the National Renewable Energy Laboratory (XAR-3-13514-01). I would like to acknowledge Jianguo Xiao for his contributions to the work described in this report.

References

Bini, F., E. DeRossi, L. Barbierato, and G. Riccardi. 1992. "Molecular cloning and sequencing of the b-isopropylmalate dehydrogenase gene from the cyanobacterium *Spirulina platensis*." *J. Gen. Microbiol.* 138:493-498.

Cobley, J.G., E. Zerweck, R. Reyes, A. Mody, J.R. Seludo-Unson, H. Jaeger, S. Weerasuriya, and S. Navankasattusas. 1993. "Construction of shuttle plasmids which can be efficiently mobilized from *Escherichia coli* into the chromatically adapting cyanobacterium, *Fremyella diplosiphon*." *Plasmid*, 30: 90-105.

DeRossi, E., G. Riccardi, A.M. Sanangelantoni, and O. Ciferri. 1985. "Construction of a cosmid library of *Spirulina platensis* as an approach to DNA physical mapping." *FEMS Microbiol. Lett.*, 30:239-244.

Durand-Chastel, H. 1982. "General characteristics of blue-green algae (cyanobacteria): *Spirulina*." In: *C.R.C. Handbook of Biosolar Resources*, Vol.1, part 2, 19-23.

Elhai, J., and C.P. Wolk. 1988. "A versatile class of positive-selection vectors based on the nonviability of palindrome containing plasmids that allows cloning into long polylinkers."*Gene*. 68:119-138.

Ewart, G.D., and G.D. Smith. 1989. "Purification and properties of soluble hydrogenase from the cyanobacterium *Anabaena cylindrica*" *Arch. Biochem. Biophys.* 268:327-337.

Ewart, G.D., K.C. Reed, and G.D. Smith. 1990. "Soluble hydrogenase of *Anabaena cylindrica*. Cloning and sequencing of a potential gene encoding the tritium exchange subunit." *Eur. J. Biochem.*, 187:215-223.

Gu, T. and F. Wang. 1984. "Studies on H_2 evolution by *Spirulina platensis*." *Hydrobiologia*, 116/117:467-470.

Gu, T. and P. Zhou. 1987. "Isolation and characterization of hydrogenase from *Spirulina platensis*." *Hydrobiologia*, 151/152:557-561.

Houchins, J.P. 1984. "The physiology and biochemistry of hydrogen metabolism in cyanobacteria" *Biochim. Biophys. Acta*. 768:227-255.

Houchins J.P., and R.H. Burns. 1981. "Comparative characterization of two distinct hydrogenases from *Anabaena* sp. strain 7120" *J. Bacteriol.* 146:215-221.

Kawamura, M., M. Sakakibara, T. Watanabe, K.Kita, N. Hiraoka, A. Obayashi, M. Takagi, and K. Yano. 1986. "A new restriction endonuclease from *Spirulina platensis*." *Nucleic Acids Res.*, 14:1985-1989.

Kentemich, T., M. Bahnweg, F. Mayer, and H. Bothe. 1989. "Localization of the reversible hydrogenase in cyanobacteria" *Z. Naturforsch.* 44c:384-391.

Rao, K.K., and D.O. Hall. 1988. "Hydrogenases: isolation and assay" *Methods Enzymol.* 167:501-509.

Renbaum, P., D. Abrahamove, A. Fainsod, G.G. Wilson, S. Rottem, and A. Razin. 1990. "Cloning,

characterization, and expression in *Escherichia coli* of the gene coding for the CpG DNA methyiase from *Spiroplasma* sp. strain MQ1 (M-SssI)." *Nucleic Acids Res.*, 18:1145-1152.

Riccardi, G., E. DeRossi, A. Milano, G. Forlani, and M. DeFelice. 1991. "Molecular cloning and expression of Spirulina platensis acetohydroxy acid synthase genes in *Escerichia coli*." *Archives Microbiology*, 155:360-365.

Staskawicz, B., D. Dahlbeck, N. Keen, and C. Napoli. 1987. "Molecular characterization of cloned avirulence genes from race 0 and race 1 of *Pseudomonas syringae* pv. *glycinea*." *J. Bact.* **169**, 5789-5794.

Weisburg, W.G., S.M. Barns, D.A. Pelletier, and D.J. Lane. 1991."16S ribosomal DNA amplification for phylogenetic study." *J. Bacteriology*, 173:697-703.

REPORT DOCUMENTATION PAGE

Form Approved
OMB NO. 0704-0188

1. AGENCY USE ONLY (Leave blank)	2. REPORT DATE	3. REPORT TYPE AND DATES COVERED
	July 1994	Conference Proceedings (FY 1994)

4. TITLE AND SUBTITLE
Proceedings of the 1994 DOE/NREL Hydrogen Program Review, April 18-21, 1994, Livermore, California

5. FUNDING NUMBERS
(TA) HY41.1010

6. AUTHOR(S)
National Renewable Energy Laboratory

7. PERFORMING ORGANIZATION NAME(S) AND ADDRESS(ES)
National Renewable Energy Laboratory
1617 Cole Boulevard
Golden, CO 80401-3393

8. PERFORMING ORGANIZATION REPORT NUMBER
DE94011835

9. SPONSORING/MONITORING AGENCY NAME(S) AND ADDRESS(ES)
National Renewable Energy Laboratory
1617 Cole Boulevard
Golden, CO 80401-3393

10. SPONSORING/MONITORING AGENCY REPORT NUMBER
NREL/CP-470-6431

11. SUPPLEMENTARY NOTES
Hydrogen Program Review was hosted by NREL and sponsored by the Advanced Utility Concept Division, Office of Energy Management, U.S. Department of Energy

12a. DISTRIBUTION/AVAILABILITY STATEMENT
National Technical Information Service
U.S. Department of Commerce
5285 Port Royal Road
Springfield, VA 22161

12b. DISTRIBUTION CODE
UC Category 1360

13. ABSTRACT

The U.S. Department of Energy has conducted programs of research and development in hydrogen and related technologies since 1975. The current program, conducted in accordance with the DOE *Hydrogen Program Plan FY 1993 - FY 1997* published in June 1992, establishes program priorities and guidance for allocating funding. The core program, currently under the Office of Energy Management, supports projects in the areas of hydrogen production, storage, and systems research. At an annual program review, each research project is evaluated by a panel of technical experts for technical quality, progress, and programmatic benefit. This *Proceedings* of the April 1994 Hydrogen Program Review compiles all research projects supported by the Hydrogen Program during FY 1994. For those people interested in the status of hydrogen technologies, we hope that the *Proceedings* will serve as a useful technical reference.

14. SUBJECT TERMS
Hydrogen; hydrogen production; hydrogen storage; hydrogen system studies

15. NUMBER OF PAGES
478

16. PRICE CODE
A21

17. SECURITY CLASSIFICATION OF REPORT	18. SECURITY CLASSIFICATION OF THIS PAGE	19. SECURITY CLASSIFICATION OF ABSTRACT	20. LIMITATION OF ABSTRACT

DATE
FILMED
9/26/94
END